Making Light Work Lighter

General Photonics Corporation

YOUR PARTNER IN INNOVATION

Navigation

Telecom

Remote Sensing

Laser Systems

Optical Imaging

Fiber Optic Distributed Sensing

MESSAGE FROM THE PRESIDENT

Dr. Steve Yao
President

Welcome to the 2017 edition of the General Photonics catalog. I am excited to announce that with the efforts in the past two years, we have added multiple advanced products to expand our product portfolio, including the Optical Component Analyzer for characterizing the performances of multi-port optical components, the polarization analyzing OFDR to measure the stresses along an optical path with high spatial resolution, and the 3D optical non-destructive evaluation (NDE) system for composite material inspection. We have also added the capability to measure the circular birefringence of spun fibers for the current sensing market. Finally, we have developed a full array of optical fiber coil products with the highest performance for fiber optic gyros, current sensors, acoustic sensors, and microwave photonics systems, thanks to our unparalleled capabilities in, and deep understanding of, polarization measurements. With more than 52 issued US patents, numerous pending applications, and an array of innovative products, General Photonics is proud to maintain its lead in the fields of polarization management and delay/timing control, and expand our product offerings in the composite industry and sensing systems. I am confident that you will find this catalog and the products included herein of great value to your endeavors in product development, production, quality control, system integration, and advanced research.

In recognition of the merit of our technology and products, the Photonics Circle of Excellence Award - an honor conferred only on the 25 most innovative products in the industry - has been awarded to our dynamic polarization controller module and dynamic differential group delay module in 2000 and 2001, respectively. In addition, our PMD-1000 received the 2010 CLEO/Laser Focus World Innovation Award and the 2009 Frost & Sullivan PMD Test Equipment Emerging Company of the Year Award.

All of us at General Photonics are committed to quality, performance, innovation, and customer satisfaction. Please feel free to contact us if you have any issues regarding polarization or timing management and measurement. Chances are you will find satisfactory solutions here at General Photonics. Thank you for considering us.

Dr. Wilson Lin
CEO

For 20 years, under the visionary leadership of Dr. Steve Yao, General Photonics has been a pioneer in the field of polarization related phenomena in fiber optics. During this time, we have developed and integrated several key photonics technologies in innovative ways to measure and control most polarization-related properties of light. Our product portfolio has expanded from simple but effective manual polarization controllers to more and more complex and specialized devices and measurement systems that include several products that are unique in the market.

Along the way, we have maintained a philosophy of flexibility and responsiveness to customer needs that has allowed us not only to develop custom subsystems for customers in areas as varied as Lidar, medical imaging, and telecom, but also to anticipate and develop products to satisfy measurement needs in emerging fields.

Going forward, General Photonics continues to embrace its entrepreneurial spirit and sustain its legacy of intellectual curiosity, dedication to customer needs, and excitement in exploring new ideas and new markets. We welcome ideas for new products and applications from our customers.

To respond quickly and effectively to the market, General Photonics will incorporate lean manufacturing and six-sigma processes to build a tier-one manufacturing operation that can guarantee low cost, high quality products to our customers. We will also partner with key niche players in emerging markets around the world. With these resources at hand, we will grow our business beyond our current market positions to serve adjacent markets such as navigation, sensing, defense, medical imaging, and robotics. With a strong internal team of engineering, operations, and sales staff, as well as a robust network of regional support, we will expand our business footprint globally and provide all of our customers with the best products and support.

TABLE OF CONTENTS

Corporate Profile 9
Ordering Information 10
Customer Service 11
Awards 12
- **The 2010 CLEO/LFW Innovation Award** 12
- **The 2001 Photonics Circle of Excellence Award** 13
- **The 2000 Photonics Circle of Excellence Award** 14

OEM Capability Showcase 15
Instruments 16
- **Measurement and Characterization** 17
  - Polarization Measurement System - PolaWise™ (PSGA-101A) 18
  - Polarization Analyzing Optical Domain Reflectometer - PolaMagic™ (OFDR-1000A) 20
  - Distributed Polarization Crosstalk Analyzer - PolaX™ (PXA-1000) 22
  - Polarization Synthesizer/Analyzer - PolaFlex™ (PSY-201) 24
  - Polarimeter - PolaDetect™ (POD-201) 26
  - Optical Component Analyzer (OCA-1000) 28
  - Polarization Dependent Loss Multimeter - PolaChex™ (PDL-201) 30
  - Degree of Polarization Meter (DOP-201) 32
  - Polarization Extinction Ratio Meter (ERM-202) 33
  - 3D Optical NDE System (OIS-1000) 34
  - Distributed Vibration Sensor - OptiEar™ (DVS-1000) 36
- **Impairment Emulation and Polarization Control** 37
  - Polarization Optimized PMD Source - PMDPro™ (PMD-1000) 38
  - Polarization Dependent Loss Source/Emulator - PDLPro™ (PDLE-101) 40
  - Advanced Multifunction Polarization Controller - PolaMight™ (MPC-202) 42
  - Multifunction Polarization Controller - PolaMight™ (MPC-201) 44
  - Programmable Optical Delay Generator - TimeRITE™ (ODG-101) 46
  - Polarization Scrambler - PolaMix™ (PCD-104) 47
  - Reset-Free Polarization Stabilizer - PolaStay™ (POS-20X) 48
- **Light Sources** 51
  - Superluminescent Diode Light Source (SLD-101S) 52
  - Tunable Laser Source (TLS-101) 53

Modules 54
- **Active Polarization Modules** 55
  - Reset-Free Polarization Tracker - PolaStay™ (POS-002) 56
  - Polarization Scrambler Module with Microprocessor Controller (PCD-005) 59
  - Polarization Scrambler Module (PCD-003) 61
  - Miniature Polarization Scrambler Module (PSM-002) 62
  - Micro Polarization Controller (PSM-003-C) 63
  - Micro Polarization Scrambler (PSM-003-S) 64
  - High Speed In-line Polarimeter - PolaDetect™ (POD) 65
  - High-Speed Polarization State Generator - PolaPal™ (PSG-001) 67
  - Dynamic Polarization Controller with Miniature Piezo Driver Card (PCD-M02) 68
  - Multimode Scrambler - SpeckleFree™ (MMS-201) 69
  - Mini Dynamic Polarization Controller - PolaRITE™ III (MPC-3/4X) 72

TABLE OF CONTENTS

Polarization Switch - PolaSwitch™ (PSW-002) ... 75
Pigtailed Polarization Controller - PolaRITE™ (PLC-002/M02) ... 76
Drop-in Polarization Controller - PolaRITE™ (PLC-003/006) ... 77
Fully Connectorized Polarization Controller - PolaRITE™ (PLC-004/005) ... 78
Passive Polarization Modules ... 79
Fiber Optic Depolarizer - PolaZero™ (DEP) ... 80
PMD and PDL Calibration Standards (CS-DGD/PDL/SOPMD) ... 82
Fixed Differential Group Delay- PolaDelay™ (FDE-002) ... 84
Active Timing/ Delay Modules ... 85
Motorized Variable Optical Delay Line - VariDelay™ II (MDL-002) ... 86
Miniature Motorized Variable Optical Delay Line - VariDelay™ II (MDL-003) ... 88
Manual Variable Optical Delay Line - VariDelay™ I (VDL-001) ... 89
Miniature Manual Variable Optical Delay Line - VariDelay™ I (VDL-002) ... 91
Fiber Stretcher (FST-001) ... 92
Fiber Phase Shifter (FPS-001) ... 93
Fiber Phase Shifter (FPS-002) ... 94
Fiber Phase Shifter (FPS-003) ... 95
Passive Timing/ Delay Modules ... 96
Compact Time Delay Coil (TDC) ... 97
Fiber Gyro Coils (FC series) ... 98
Specialty Fiber Coils ... 100
Detectors ... 103
Balanced Photodetector (BPD-002) ... 104
OEM Balanced Detector (BPD-003) ... 105
Polarization Diverse Balanced Photodetector (PBPD-001) ... 107
Polarization Diversity Detector (PDD-001) ... 108
Miniature Polarization Diversity Detector (PDD-003) ... 109
Fiber Pigtailed Free Space Interferometer (MZI-001) ... 110
Passive Components ... 111
NoTail™ Components (Summary Sheet) ... 112
NoTail™ Drop-in Coupler (NTC) ... 113
Polarization Maintaining Coupler (PMC & NPMC) ... 114
Polarization Beam Combiner/Splitter (PB & NPB) ... 116
Faraday Rotator Mirror (FRM & NFRM) ... 117
In-line Polarizer (POL & NPOL) ... 119
In-line Isolator (ISO & NISO) ... 120
3-Port Fiber Optic Circulator (CIR & NCIR) ... 122
Accessories ... 124
Bare Fiber Adapter - PolaEZ™ (PEZ-001) ... 125
Rack Mount Kit (RCK-001) ... 126
Application Guide ... 127
White Papers ... 128
What is Polarization? ... 129
Polarization in Fiber Systems: Squeezing out More Bandwidth ... 131
Combat Polarization Impairments with Dynamic Polarization Controllers ... 136
Scrambling to Minimize Polarization Related Impairments ... 140

TABLE OF CONTENTS

Polarization Related Tests for Coherent Detection Systems ... 143
Practical 4-Stage Optical PMD Compensator for Mitigating 1st-and 2nd-Order PMD Impairments on 40-Gbit/s RZ-D(Q)PSK Signals ... 150
Polarization Crosstaik in PM Fiber ... 153
Distributed Polarization X-talk Measurement for the Production of Polarization-Maintaining Fiber Coils ... 156
Complete characterization of polarization-maintaining fibers using distributed polarization analysis ... 162
Journal Papers ... 171
In-service light path PMD (polarization mode dispersion) monitoring by PMD compensation ... 172
High accuracy polarization measurements using binary polarization rotators ... 185
Highly Repeatable All Solid-State Polarization State Generator ... 204
Self-calibrating Binary Polarization Analyzer ... 207
A novel scheme for achieving quasi-uniform rate polarization scrambling at 752 krad/s ... 210
Automatic Maximum-Minimum Search Method for Accurate PDL and DOP Characterization ... 219
Real-Time Optical Spectrum Analysis of a Light Source Using a Polarimeter ... 226
Programmable optical delay generator with uniform output and double-delay capability ... 236
Distributed Transverse Stress Measurement Along an Optic Fiber Using Polarimetric OFDR ... 242
A Novel Method for Determining and Improving the Quality of a Quadrupolar Fiber Gyro Coil under Temperature Variations ... 246
Method for Improving the Resolution and Accuracy against Birefringence Dispersion in Distributed Polarization Cross-Talk Measurements ... 256
Accurate Method for Measuring the Thermal Coefficient of Group Birefringence of Polarization-Maintaining Fibers ... 259
Tomographic Inspection of Fiber Coils Using Optical Coherence Tomography ... 262
Application Notes ... 266
Polarization Optimized PMD Source Applications ... 267
PolaRITE™ Polarization Controllers ... 272
PolaRITE™ II/III Polarization Controllers/Scramblers ... 275
Faraday Rotator Mirror ... 278
Application Note for PDL Measurement ... 279
Accurate DOP Characterization with Less Effort ... 282
Optical Coherence Tomography Technologies ... 285
FAQs ... 286
Dynamic Polarization Controllers ... 287
Polarization Scramblers ... 291
Depolarizers ... 294
Polarization Stabilizers ... 295
ER Measurement ... 296
Polarimeters ... 298
Phase Shifters ... 300
Delay Lines (MDL/VDL, ODG) ... 301
Fiber Coils ... 303
Other Products ... 304
Glossary and Acronyms ... 305
Distributors & Representatives ... 307
Asia Distributors ... 307
Europe Distributors ... 308
North America Distributors & Reps ... 309

Fiber Optic Distributed Sensing

Sensing Instruments

- Distributed Polarization Crosstalk Analyzer (PXA-1000)
- Polarization Analyzing OFDR (OFDR-1000A)
- Distributed Vibration Sensor (DVS-1000)

Detectors

- Polarization Diversity Detectors (PDD-001, PDD-003)
- Balanced Detectors (BPD-002, BPD-003)

Polarization Management

- Depolarizer (DEP)
- Polarization Switch (PSW-002)
- Polarization Controller/Scrambler (PSM-002, PCD-M02)

Optical Components

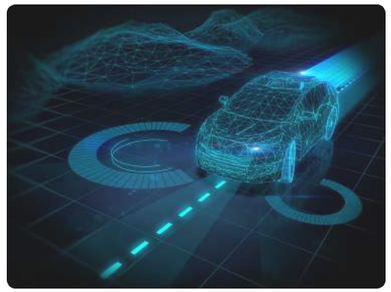

Lidar

Detectors

- Polarization Diversity Detectors (PDD-001, PDD-003)
- Balanced Detectors (BPD-002, BPD-003, PBPD-001)

Polarization Management

- Depolarizer (DEP)
- Polarization Switch (PSW-002)
- Polarization Controller/Scrambler (PSM-002, PCD-M02)

Optical Delay

- Time Delay Coils (TDC)

Optical Components

Fiber Optic Gyros (FOG)

Measurement Instruments

- Distributed Polarization Crosstalk Analyzer (PXA-1000)
- Polarization Analyzing OFDR (OFDR-1000A)
- Polarization Measurement System (PSGA-101A)
- Polarization Extinction Ratio Meter (ERM-202)
- DOP Meter (DOP-201)
- PDL Multimeter (PDL-201)
- SLD Source (SLD-101)

Fiber Gyro Coils

- FC series specialty coils

Subsystem Assembly Services

Contact General Photonics to discuss your application

PRODUCT GUIDE BY APPLICATION

Fiber Optic Communications

Emulation Instruments

- PMD Source/Emulator (PMD-1000)
- PDL Source/Emulator (PDLE-101)
- Advanced Multifunction Polarization Controller (MPC-202)

Test/Measurement Instruments

- Optical Component Analyzer (OCA-1000)
- Polarization Analyzing OFDR (OFDR-1000A)
- Polarization Measurement System (PSGA-101A)
- Polarization Synthesizer/Analyzer (PSY-201)
- High Speed Polarimeter (POD-201)

Fiber Health Monitoring

- Polarization Analyzing OFDR (OFDR-1000A)
- Distributed Vibration Sensor (DVS-1000)

PMD/PDL Modules

- Fixed DGD (FDE-002)
- PMD/PDL Calibration Standards (CS-DGD/PDL/SOPMD)

Polarization Control

- Polarization Controller (PCD-M02)

Medical Imaging

Detectors

- Polarization Diversity Detector (PDD-001)
- Balanced Detectors (BPD-002, BPD-003)
- Free-Space Mach-Zehnder Interferometer (MZI-001)

Optical Delay Lines

- Motorized Delay Lines (MDL-002, MDL-003)
- Manual Delay Lines (VDL-001, VDL-002)

Polarization Management

- Polarization Switch (PSW-002)
- Polarization Scrambler (PCD-005, PSM-002)
- Polarization Controller (PCD-M02)
- Manual Polarization Controller (PLC-003/006)

Optical Components

Subsystem Assembly Services

Contact General Photonics to discuss your application

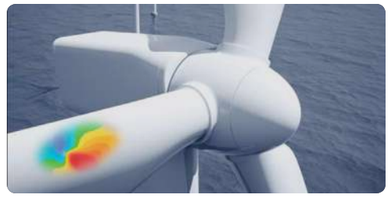

Nondestructive Testing (NDT)

Measurement Instruments

- 3D Optical NDE System (OIS-1000)
- Polarization Analyzing OFDR (OFDR-1000A)
  For structural health monitorning and stress analysis.

PRODUCT GUIDE BY APPLICATION

Laser Systems

Test/Measurement Instruments

- Polarization Extinction Ratio Meter (ERM-202)
- DOP Meter (DOP-201)

Optical Delay

- Motorized Delay Lines (MDL-002, MDL-003)
- Manual Delay Lines (VDL-001, VDL-002)
- Fiber Stretcher (FST-001)
- Phase Shifters (FPS-001, FPS-002, FPS-003)

Polarization Control

- Polarization Tracker (POS-002)
- Polarization Controller (PCD-M02)
- Manual Polarization Controller (PLC-003/006)
- Depolarizer (DEP)

Optical Clock

- Free-Space Mach-Zehnder Interferometer (MZI-001)

Optical Components

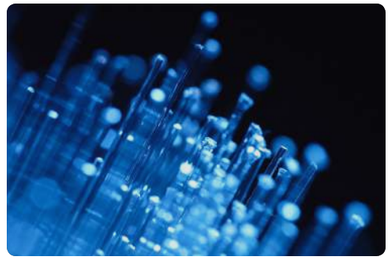

Specialty Optical Fiber Characterization

Measurement Instruments

- Distributed Polarization Crosstalk Analyzer (PXA-1000)
  PER and polarization crosstalk in PM fiber
- Polarization Analyzing OFDR (OFDR-1000A)
  Stress and birefringence in SM fiber
- Polarization Measurement System (PSGA-101A)
  PMD, PDL, and birefringence in SM and spun fiber
- Polarization Extinction Ratio Meter (ERM-202)

Optical Delay/Timing Control

Long Range Delay System

- Programmable Optical Delay Generator (ODG-101)

Optical Delay

- Motorized Delay Lines (MDL-002, MDL-003)
- Manual Delay Lines (VDL-001, VDL-002)
- Fiber Stretcher (FST-001)
- Phase Shifters (FPS-001, FPS-002, FPS-003)

Fiber Coils

- Timing Coils (TDC)
- Specialty Coils

CORPORATE PROFILE

Our Mission

At General Photonics, we develop and build innovative optical instruments and modules to fuel the growth of optical networks, sensor systems, and biomedical diagnosis systems. Our philosophy is to seek simple solutions to complicated problems. Our focus is on dynamic polarization management and measurement, and on optical delay/timing control. Our practice is to build high quality products that surpass customer expectations.

Our Track Record

- More than 50 issued and numerous pending US and international patents
- 2010 CLEO/Laser Focus World Innovation Award
- 2009 Frost & Sullivan North America PMD Test Equipment Emerging Company of the Year Award
- Photonics Circle of Excellence Award (2001)
- Photonics Circle of Excellence Award (2000)
- OFC New Product Award (1999)

13 FIRSTS in reaching the market:

1. The first manual fiber-squeezer based polarization controller (1996)
2. The first electrically activated fiber-squeezer based polarization controller (2000)
3. The first programmable differential group delay based on polarization switching (2001)
4. The first commercial in-line polarimeter (2001)
5. The first fiber-squeezer based polarization scrambler (2002)
6. The first depolarizer with working coherence length longer than 10 meters (2002)
7. The first reset free polarization stabilizer (2003)
8. The first all-order PMD emulator with digitally variable and selectable DGD (2004)
9. The first binary magneto-optic polarization state generator/analyzer (2004)
10. The first PMD source with polarization optimization (2009)
11. The first distributed polarization crosstalk analyzer for PM fiber and waveguides (2010)
12. The first multistage optical PMD compensator (2010)
13. The first polarization analyzing OFDR (2016)

Our Markets

- Fiber optic communications networks
- Fiber optic equipment and component manufacturers
- Fiber optic sensor manufacturers, including fiber optic gyro (FOG) manufacturers
- Biomedical imaging equipment manufacturers, including OCT system manufacturers
- Research & development laboratories and universities

Our Products

General Photonics provides the most complete line of products for dynamic polarization and timing management in the industry, with products ranging from instruments to modules and components.

Our Quality Policy

General Photonics is committed to consistently providing superior products and services by rigorously following, and continually improving, our quality management system; continuously improving products and processes; setting and reviewing our quality objectives; focusing on customer needs; and meeting or exceeding customer expectations.

Our Locations

General Photonics' headquarters and manufacturing facilities are conveniently located in Chino, California, a city bordering Los Angeles County, Orange County, and Riverside County. There are many universities within a 30-mile radius, including the California Institute of Technology, University of Southern California, UC Irvine, UC Riverside, Cal Poly Pomona, the Claremont Colleges, CSU Fullerton, and CSU LA. The company is easily accessible from Ontario International Airport (10 miles), John Wayne International Airport (35 miles), and Los Angeles International Airport (60 miles).

General Photonics maintains an Engineering Center of Excellence in the Haidian District of Beijing, China. General Photonics also maintains a Technical Support and Marketing Center in Beijing. Throughout the world, our customers can receive personal attention through our network of distributors and representatives.

Our Employees

General Photonics is fortunate to have employees that take pride in the job we are doing. Our products are made up of a continuous series of individual employee contributions, and our sense of pride comes from knowing that we have all contributed to our customers' success. Our employees constantly monitor our processes with an eye to consistency, quality and efficiency.

Our Ownership

General Photonics is a privately held, VC funded high-technology company.

ORDERING INFORMATION

Product and technical information, are available 24 hours a day on our website: www.generalphotonics.com To request additional information or quotes, please call us Monday through Friday, from 8:30 AM to 6:00 PM Pacific Time, or send an email to sales@generalphotonics.com.

Note: Specifications are subject to change without notice.

How to contact us:

General Photonics Corp.
5228 Edison Avenue Chino, CA 91710
Phone: 909-590-5473 Fax: 909-902-5536
Email: sales@generalphotonics.com or info@generalphotonics.com
Web: www.generalphotonics.com

Orders:

General Photonics Corporation accepts orders by telephone (909-590-5473), fax (909-902-5536), e-mail, or mail. Telephone orders must be followed with a hard copy by email, mail or fax. Purchase orders must include:

- Name and telephone/fax numbers of the customer contact.
- Billing and shipping address.
- Product number, quantity, and description.
- General Photonics Corp. quoted price. Please reference the quote number, if possible.

Payment options:

Domestic orders: Net 30 days after establishing credit with General Photonics. We also accept credit cards (Visa or MasterCard) and C.O.D. All bank and document fees are the responsibility of the customers.

International orders: All international orders must be prepaid by the following methods: credit card (Visa or MasterCard), wire transfer, cashier's check, or money order.

To place a credit card order, simply call or fax us the name of the card, the name of the cardholder, the credit card number and the expiration date.

For Wire Transfer, please contact us at any of the contact numbers or methods above.

CUSTOMER SERVICE

Satisfaction:

At General Photonics, customer satisfaction is our first priority. Our commitment does not end with providing the best products, technology, and solutions. We are here to support you in the use of our products in your products or projects.

Convenience:

Send your inquiries or orders at any time of the day or night via email or fax. Or visit our Web site at www.generalphotonics.com for specifications, answers to frequently asked questions, application notes, copies of our manuals, or mechanical drawings.

Responsiveness:

General Photonics' sales staff is available to answer your questions from 8:30 AM to 6:00 PM Pacific Time. You may email or fax your questions at any time. We will typically respond within one business day.

Technical Support:

Our support team of engineers and sales staff are pleased to help you to find the solutions you need. They are highly trained professionals with in-depth knowledge of our products. They will go the extra mile to help you with your design challenge, both before and after the sale.

OEM Solutions:

The products listed in this catalog are our standard products, representing our understanding of general market requirements. However, we will be happy to tailor our products to the specific requirements of your applications. Please let us know what you need, and we will give you an honest opinion about the feasibility of the modification you suggest or the specification you require. We will also be happy to enter into mutual non-disclosure agreements to keep the information exchange confidential if needed.

Product Warranty:

General Photonics warrants that standard products will be free from defects in materials or workmanship for a period of one year from the date of shipment. A product found to be defective during the warranty period will be repaired or replaced, at no charge, at General Photonics' option.

If a problem is found, please contact General Photonics at (909) 590-5473 or info@generalphotonics.com. You will be provided with a problem report form. Please complete the form with as complete a description of the problem and the conditions under which it occurred as possible. If the product is found to require factory repair, General Photonics will issue an RMA number for the return. Please label the product clearly with the RMA number. Failure to follow this procedure may delay the evaluation and repair of the product.

The above warranty specifically excludes products that have been repaired or modified by non-manufacturer-authorized personnel, products with a broken warranty seal or opened enclosure, and damage caused by misuse, abuse, improper storage or handling, or acts of nature. This warranty is in lieu of all other warranties, expressed or implied. General Photonics will not be liable for any indirect or consequential damages or losses resulting from the use of its products.

Delivery and Shipment:

Most orders are shipped via Federal Express or UPS. For domestic shipments: shipping and handling charges and sales tax are included in our invoice. For international shipments: the carrier bills delivery charges, duties and taxes to you separately. Upon request, we will ship via the carrier of your choice with a valid account number. All orders are shipped F.O.B our warehouse. All duties and taxes are the responsibility of the customer.

Returns:

A Return Material Authorization Number must accompany all returns. Contact our sales or technical support staff for an RMA number.

Billing Questions:

If you ordered directly from General Photonics and have a question regarding your billing, please contact your sales staff at General Photonics.

Special Note:

All statements, technical information, and recommendations related to the products herein are based upon information believed to be reliable or accurate. However, the accuracy or completeness thereof is not guaranteed, and no responsibility is assumed for any inaccuracies. The user assumes all risks and liability whatsoever in connection with the use of a product or its application. General Photonics reserves the right to change at any time, without notice, the design, specifications, function, fit or form of its products described herein, including withdrawal at any time of a product offered for sale herein.

CLEO/*Laser Focus World*
Innovation Award
2010 Honorable Mention

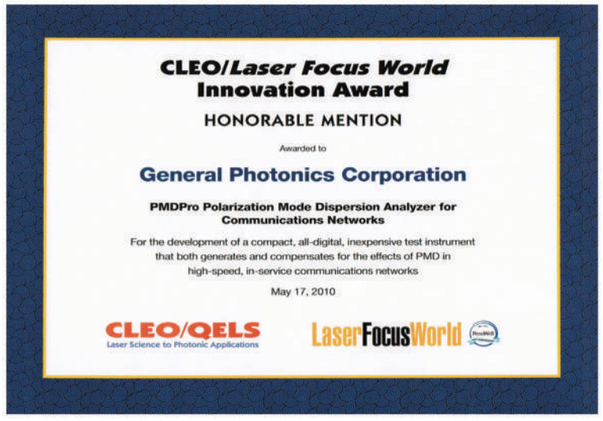

Each year, the CLEO/Laser Focus World Innovation Awards Program honors the most timely, ground-breaking products in the field of laser science. Designed to showcase some of the most significant new products in the field, Innovation Award entries are evaluated on criteria critical to product success: impact, functionality, life expectancy, effect on the optics industry, innovation and patents or trademarks.

The PMDPro™ Polarization Optimized PMD Source precisely generates 1st order PMD up to 180 ps and 2nd order PMD up to 8100 ps^2 in as fast as 1ms, orders of magnitude faster than other technologies. Its speed and built-in emulation functions make PMD tolerance testing easy. This is the only PMD source with automatic polarization optimization for worst-case PMD effects and PMD compensation, as well as a built-in scrambling function for testing polarization multiplexed signals. It is the only available instrument for monitoring the PMD in in-service links.

The 2001 Photonics Circle of Excellence Award Winners

The Photonics Circle of Excellence Awards:
Recognizing the 25 Most Technically Innovative New Products of the Year

For more than a decade, these annual awards have recognized the enterprising companies and individuals who have refused to accept the status quo and have instead pushed the limits of technology to develop new photonic products and processes.

This year's 25 winning products, described on the following pages, were chosen from among the hundreds of entries submitted from around the world. They have survived the toughest scrutiny: judgment by the members of *Photonics Spectra*'s Editorial Advisory Board — a panel of recognized experts in a variety of disciplines.

To be eligible, products had to be commercially available between June 1, 2000, and May 31, 2001.

The ceremony honoring this year's Distinction in Photonics and Circle of Excellence award winners will take place Jan. 21 in San Jose, Calif., at the Fairmont Hotel, concurrently with Photonics West.

General Photonics Corp.
• Dynamic Differential Group Delay Module •

The dynamic differential group delay module from General Photonics Corp. is designed to provide programmable, low-insertion-loss, high-speed, compact and low-cost management of the delay variations of two polarization components, thus offering an essential building block for polarization-mode-dispersion compensation for next-generation optical networks.

The Dyna-Delay 111-002 module consists of multiple birefringent crystal segments with 90° polarization rotators sandwiched between them to achieve fast differential delay variations. The Chino, Calif., company says the construction helps compensate for unpredictable dispersion penalties by allowing the amount of differential group delay to be digitally switched in just 150 µs from −45 to 45 ps with six-bit resolution.

The insertion loss for the 112 × 24 × 15-mm device is lower than 1.2 dB. The module is integrated with a microprocessor-based control circuit, allowing the delay to be controlled via a high-speed parallel port.

A typical solution for polarization-mode-dispersion compensation consists of at least four functions: a polarimeter to detect the state or degree of polarization; a polarization controller to change any state of polarization to any other state; a differential group delay to realign two orthogonal polarization components of a signal; and a feedback loop to form an automatic control system.

General Photonics says that its module is ideal for use in compensation solutions that must be provided before widespread deployment of 40-Gb/s optical transmission systems will be possible.

Making Light Work Lighter
General Photonics Corporation
5228 Edison Avenue, Chino, CA 91710, U.S.A.
Website: www.generalphotonics.com Email: info@generalphotonics.com
Tel: (909) 590-5473 Fax: (909) 902-5536

Reprinted from the January 2002 issue of PHOTONICS SPECTRA © Laurin Publishing

The 2000 Photonics Circle of Excellence Award Winners

The Photonics Circle of Excellence Awards:
Recognizing the 25 Most Technically Innovative New Products of the Year.

For more than a decade, these annual awards have recognized the enterprising companies and individuals that have refused to accept the status quo and have instead pushed the limits of technology to develop new photonic products and processes.

This year's 25 winning products, described on the following pages, were chosen from among the hundreds of entries submitted from around the world. They have survived the toughest scrutiny: judgment by the members of *Photonics Spectra*'s Editorial Advisory Board — a true panel of recognized experts in a variety of disciplines.

To be eligible, products had to be commercially available between October 1, 1998, and May 31, 2000.

The ceremony honoring this year's Distinction in Photonics and Circle of Excellence award winners will take place in San Jose, Calif., at the Fairmont Hotel concurrently with Photonics West.

General Photonics Corp.
• Dynamic Polarization Controller •

General Photonics Corp. of Chino, Calif., has produced a multiaxis, fiber-squeezer-based dynamic polarization controller/scrambler that promises to solve the polarization-related afflictions of fiber optic communications systems when the bit rate climbs to 10 Gb/s.

Penalties such as polarization mode dispersion in optical fibers, polarization-dependent loss in passive optical components, polarization-dependent gain in optical amplifiers and polarization-dependent modulation in electro-optic modulators are unpredictable and require solutions that are dynamic in nature and adaptable to random time variations. The PCS-3× Dynamic Polarization Controller is designed to be integrated into control modules for mitigation of these impairments as well as for polarization stabilization and polarization-dependent-loss measurements.

The device contains multiple retardation plates with varying angles of orientation. The plates are generated by squeezing a section of fiber with a piezoelectric transducer actuator; their retardation can be changed by varying the voltage applied to the actuator.

The company says the controller has almost no insertion loss, no backreflection, no wavelength dependence and no polarization dependent loss. It has a response time of less than 35 µs. Activation-induced loss can be less than 0.002 dB, making it suitable for compensating polarization induced penalties in a feedback loop and polarization-dependent-loss measurement.

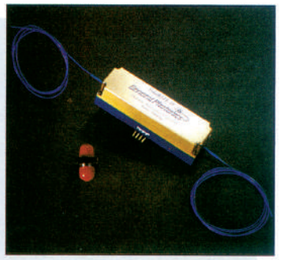

The device's voltage requirements are less than 35 volts so that it can be driven and controlled with low-cost electronics. It can also be used as a polarization scrambler to randomize the light signal's polarization state.

Making Light Work Lighter
General Photonics Corporation

13766 Arapahoe Place, Chino, CA 91710
Website: www.generalphotonics.com Email: info@generalphotonics.com
Tel: (909) 590-5473 Fax: (909) 902-5536

Reprinted from the January 2001 issue of PHOTONICS SPECTRA © Laurin Publishing Co. Inc.

OEM CAPABILITY SHOWCASE

General Photonics has extensive experience in the polarization and timing management fields, and has pioneered a variety of advanced technologies in these areas. Our portfolio of standard products reflects this history, covering a wide range of functions that satisfies the requirements of most general polarization and timing applications. However, we recognize that some of our customers have very specialized needs that require custom solutions. General Photonics has the expertise and manufacturing flexibility to tailor solutions for special applications in many different fields. Below are examples of custom solutions to three very different problems, based on General Photonics patented technologies.

Case 1: Telecommunications (PMD Compensation)

A network developer needed a compact, fast variable differential group delay generator that could withstand constant switching and had to fit between existing components in their chassis.

General Photonics successfully packaged a DGD in a very small stainless steel chassis. The circuitry utilized magneto-optic crystals for precise control, a technique documented in papers published by General Photonics.

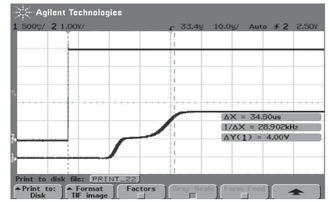

DGD switching time 34.6µs.

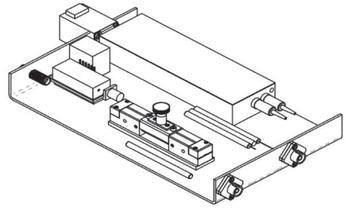

A 3D model of an OCT assembly design.

Case 2: Medical Imaging

Optical coherence tomography (OCT) systems require the integration of several diverse elements, including interferometers, polarization controllers, optical delay lines, and balanced detectors. This integration requires precise path and loss matching, as well as interface compatibility of each component part.

General Photonics has made several specialized modules for such systems, including dual-stage delay lines, custom balanced detectors, and integrated subsystems such as the one pictured here.

Case 3: Astronomical Imaging

The Atacama Large Millimeter/submillimeter Array (ALMA) is composed of 80 high-precision antennas located on the Chajnantor plain of the Chilean Andes, 5000 meters above sea level. Using ALMA, astronomers have unprecedented visibility into deep space. The antennas are up to several kilometers away from the control center, so the receivers must be synchronized to femtoseconds; otherwise the images will be blurred.

Their solution is a General Photonics long range polarization-stabilized fiber stretcher assembly that combines several of General Photonics' patented technologies. The custom module developed by General Photonics generates up to 4 mm of optical delay at up to 100Hz. The precise control is enabled by custom polarization control an monitoring circuits.

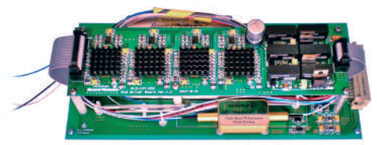

INSTRUMENTS

Measurement and Characterization

Impairment Emulation and Polarization Control

Light Sources

Measurement and Characterization

Polarization Measurement System - PolaWise™ (PSGA-101A) 18
Polarization Analyzing Optical Domain Reflectometer - PolaMagic™ (OFDR-1000A) 20
Distributed Polarization Crosstalk Analyzer - PolaX™ (PXA-1000) 22
Polarization Synthesizer/Analyzer - PolaFlex™ (PSY-201) 24
Polarimeter - PolaDetect™ (POD-201) 26
Optical Component Analyzer (OCA-1000) 28
Polarization Dependent Loss Multimeter - PolaChex™ (PDL-201) 30
Degree of Polarization Meter (DOP-201) 32
Polarization Extinction Ratio Meter (ERM-202) 33
3D Optical NDE System (OIS-1000) 34
Distributed Vibration Sensor - OptiEar™ (DVS-1000) 36

Polarization Measurement System - PolaWise™ (PSGA-101A)

PolaWise™ is an advanced polarization measurement system for accurate measurement of all polarization related properties of light sources and optical materials. Based on General Photonics' patented magneto-optic polarization generation and analysis technology, the PSGA-101-A is specially designed for fiber optic applications and can effortlessly accomplish multiple functions, including polarization state generation (PSG), polarization state analysis (PSA), polarization extinction ratio (PER) measurement, polarization dependent loss (PDL) measurement, and polarization mode dispersion (PMD) measurement, as well as birefringence measurement in spun fiber. Another attractive feature of the instrument is its large flip-top LCD graphic display design, an industry first that allows large viewing area on a compact, portable enclosure. Furthermore, a 2x20 character LCD is also included on the front panel for easy operation of the instrument for applications that do not require a graphic display. The instrument comes with an internal tunable laser for PDL and PMD measurement up to 10ps. It can also control tunable lasers from third parties via a GPIB port for measurement of larger PMD values. The instrument also comes with a VGA port for use with an external LCD graphic display of the user's choice. PolaWise™ : a wise instrument and a smart choice!

Specifications:

Operating Wavelength Range		1440 to 1620 nm	1280 to 1340 nm
SOP Generation Accuracy[1]		±1° on Poincaré Sphere	±1° on Poincaré Sphere
SOP Repeatability		±1°	±1°
Azimuth & Ellipticity Angle Accuracy[1]		< 0.25°	< 0.25°
Stokes Vector Accuracy[1]		±0.5%	±0.5%
DOP Measurement Accuracy[1,2]		±1%	±1%
PER Dynamic Range		> 40 dB (Input Power > -10 dBm)	> 40 dB (Input Power > -10 dBm)
PER Axis Accuracy[1]		±1°	±1°
PMD Measurement Range		1 fs to 10 ps (Internal tunable laser)	
		1 fs to 400 ps (External laser, 0.01 nm < λ_{step} < 10 nm)	1 fs to 400 ps (External laser, 0.01 nm < λ_{step} < 10 nm)
PDL Measurement Range		0 to 40 dB (Input power > -10 dBm)	0 to 40 dB (Input power > -10 dBm)
Accuracy:	DGD SOPMD PDL	± (1 fs + DGD * 0.5%) ± (SOPMD * 1%) ± (0.05 dB + PDL * 2%)	± (5 fs + DGD * 1%) ± (SOPMD * 2%) ± (0.05 dB + PDL * 2%)
Repeatability:	DGD[3] SOPMD[3] PDL[4]	0.03 fs 0.3 ps^2 0.04 dB	0.05 fs 0.3 ps^2 0.05 dB
Resolution:	DGD SOPMD PDL	1 fs (1550 nm, λ_{step} = 2 nm) 0.005 ps^2 (1550 nm, λ_{step} = 2 nm) 0.01 dB	1 fs (1310 nm, λ_{step} = 2 nm) 0.005 ps^2 (1310 nm, λ_{step} = 2 nm) 0.01 dB
Internal Tunable Laser		1528 to 1563 nm	Not available
Wavelength Tuning Step		50 GHz minimum for internal tunable laser	N/A
Operating Power Range		-40 dBm to + 2 dBm	-40 dBm to + 2 dBm
Optical Power Accuracy[1]		± 0.25 dB	± 0.25 dB
Optical Power Damage Threshold		300 mW	300 mW
Operating Temperature		5 °C to 40 °C	5 °C to 40 °C
Storage Temperature		-20 °C to 60 °C	-20 °C to 60 °C
Communication Interfaces		GPIB, Ethernet	GPIB, Ethernet
Displays		8" flip-top graphic LCD & 2x20 character front panel LCD	8" flip-top graphic LCD & 2x20 character front panel LCD
External Storage		USB removable storage media, such as compact flash	USB removable storage media, such as compact flash
Power Supply		100 – 240 VAC, 50 – 60 Hz	100 – 240 VAC, 50 – 60 Hz
Software		Control/display program (included)	Control/display program (included)
Dimensions		2U, 3/4 of 19" rack width 14" (L) x 14" (W) x 3.5" (H)	2U, 3/4 of 19" rack width 14" (L) x 14" (W) x 3.5" (H)

Notes:
1. At 23 ° ± 5°C.
2. DOP measurement accuracy for C and L bands or for O band, depending on version.
3. Averaged over 10 steps, with wavelength step size = 2 nm for DGD, 0.1 nm for SOPMD.
4. Measured by Mueller Matrix method.

MEASUREMENT AND CHARACTERIZATION

Polarization Measurement System - PolaWise™ (PSGA-101A)

Features:

- Multiple operation modes
- Flip-top graphic display
- Front panel character LCD display
- External LCD monitor enabled
- USB removable data storage
- Compact and portable
- Ethernet for remote operation

Applications:

- PMD measurement
- PDL measurement
- Polarization state generation (PSG)
- PER measurement
- PM fiber connector key alignment
- Connector stress evaluation of PM fiber connector
- SOP measurement
- Source DOP measurement
- Birefringence measurement of spun fiber

Related Products:

- PMD/PDL Calibration Standards (CS-DGD/PDL/SOPMD)
- Components
- Bare Fiber Adapter (PEZ)

Tech Info:

- What is Polarization?
- Polarization Related Tests for Coherent Detection Systems
- High accuracy polarization measurements using binary polarization rotators
- Highly Repeatable All Solid-State Polarization State Generator
- Self-calibrating Binary Polarization Analyzer

Measurement Examples:

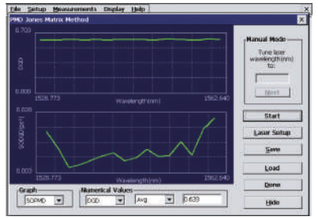

1st and 2nd order PMD measurement (Jones Matrix) of 20mm quartz crystal. Specified DGD=0.627ps, Measured DGD=0.628ps

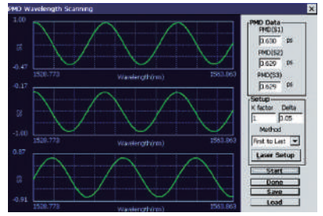

DGD measurement (Wavelength Scanning Method) of 20mm quartz crystal. Specified DGD=0.628ps, Measured DGD=0.629ps

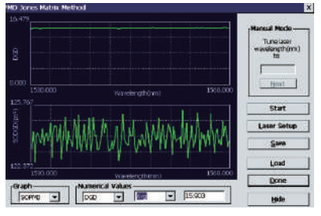

1st and 2nd order PMD measurement (Jones Matrix Eigenanalysis) of two 15.75 mm YVO_4 crystals with 45° alignment. Specified DGD=15.90ps, SOPMD=126.46ps^2, Measured DGD=15.903ps, SOPMD=124.03ps^2

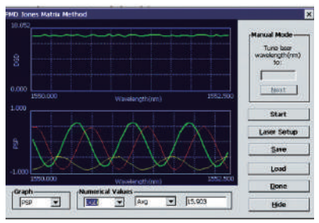

DGD and PSP measurement (Jones Matrix Eigenanalysis) of two 15.75 mm YVO_4 crystals with 45° alignment. Specified DGD=15.90ps, SOPMD=126.46ps^2, Measured DGD=15.903ps

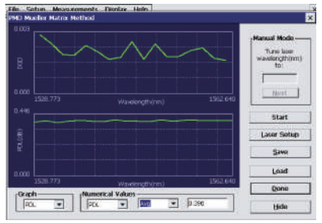

DGD and PDL measurement (Mueller Matrix Method) of PDL standard. Specified PDL=0.389dB, Measured PDL=0.396dB

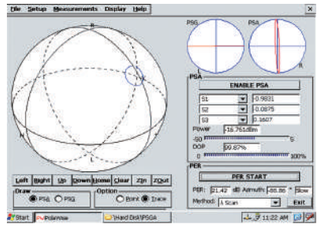

PER measurement example. The PM fiber under test has a PER of 21.42 dB, and the key of the PM output connector is aligned 1.1° from the slow axis of the fiber.

Ordering Information:

PSGA — 101 — A — ☐☐ **—** ☐ **—** ▭

Wavelength:
13 = 1310nm
15 = 1550nm

Options:
1 = with internal tunable laser
2 = without internal tunable laser

Connector Type:
(PSG input/output and laser output,if applicable)
FC/PC, FC/APC

Notes:
Please specify Connector Types for laser and PSG input/output when ordering.

PSA input is FC free-space adapter. Internal tunable laser available only for 1550nm version.

MEASUREMENT AND CHARACTERIZATION

Polarization Analyzing Optical Domain Reflectometer - PolaMagic™ (OFDR-1000A)

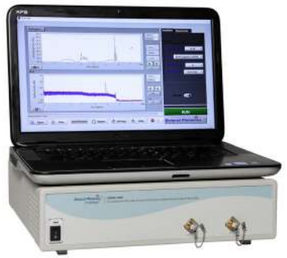

The OFDR-1000A is a polarization analyzing optical frequency domain reflectometer (PA-OFDR), a breakthrough instrument capable of analyzing polarization evolution along an optical fiber. The patent-pending technology obtains space-resolved reflection as well as birefringence or polarization mode dispersion (PMD) information for optical paths consisting of optical fibers, micro-optical components, and waveguides.

Users can measure and record stress levels as well as reflected energy and do predictive analysis of reliability. The data gathered by the OFDR-1000A is independent of temperature; therefore, data gathered over time does not require temperature normalization.

The OFDR-1000A can be used with various tunable lasers, such as those from Keysight, Newport, Yenista, or Santec. This flexibility offers the user the opportunity to make full use of his laser resources and reduce the cost of making OFDR measurements.

Specifications:

Operation Wavelengths[1]	C/ L band
Maximum DUT Distance	100 m
Spatial Resolution[2]	10 µm
Distance Uncertainty	± (0.0005 +0.01% x distance) (m)
Dead Zone	See spatial resolution
Return Loss Dynamic Range	70 dB (for laser input power >5dBm)
Return Loss Measurement Range	0 to – 120 dB
Return Loss Sensitivity[4,5]	−130 dB
Return Loss Resolution[5]	±0.05 dB
Return Loss Uncertainty[5]	±0.2 dB
Birefringence Spatial Resolution[2]	250 µm
Birefringence Resolution[6]	$2x10^{-7}$
Birefringence Sensitivity[6]	$2x10^{-7}$
Maximum Birefringence	$2x10^{-4}$
Insertion Loss Dynamic Range[4,5,7]	18 dB
Insertion Loss Resolution[5]	±0.05 dB
Insertion Loss Uncertainty[5]	±0.1 dB
Wavelength Range	Refer to user laser specs[1,3]
Wavelength Uncertainty	Refer to user laser specs[3]
Center Wavelength	Refer to user laser specs[3]
Optical Power	Refer to user laser specs[3]
Operating Temperature	10 to 40 °C
Storage Temperature	−20 to 60 °C
Power Supply	100-240VAC, 50-60 Hz
Communications Interface	USB 2.0
Display	Notebook computer with USB connection
Connector Type	FC/APC standard
Dimensions	2U, ¾ 19" rack width 3.5" (H) x 14" (W) x 14" (D)

Notes:
1. Typical. The user's tunable laser must be a single mode tunable laser without any mode hopping, with a wavelength scanning speed of 10 nm/s.
2. Highest spatial resolution for DUT fiber length <40m.
3. Refer to technical specifications of user's laser. The laser wavelength must be in the C or L bands.
4. This is a typical range for a two-way value between a strongest reflection greater than −30dB and the noise floor, averaged over ten (10) measurements. Without averaging, the range is reduced by 5 dB.
5. Measured with 0.5 m integrated width.
6. When birefringence spatial resolution is set to 10 cm.
7. Two-way loss before backscatter reaches the noise floor and insertion loss (IL) measurements are no longer possible.

Features:

- High spatial resolution for reflection: 10 µm
- High spatial resolution for stress: 250 µm
- −130 dB measurement sensitivity

Applications:

- Fiber optic component quality inspection
- Fiber optic module/system QA
- Distributed stress sensing
- Structural health monitoring
- Fiber optic component troubleshooting
- Photonic Integrated Circuit (PIC) characterization

Tech Info:

- Distributed Transverse Stress Measurement Along an Optic Fiber Using Polarimetric OFDR

Video:

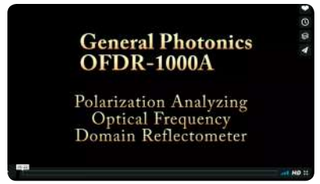

Ordering Information:

OFDR — 1000A — [ ]

Connector Type:
FC/APC standard
FC/PC available

MEASUREMENT AND CHARACTERIZATION

Polarization Analyzing Optical Domain Reflectometer - PolaMagic™ (OFDR-1000A)

Typical Performance Data:

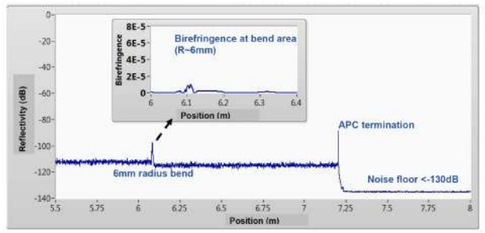

Figure 1 SMF-28 fiber test results

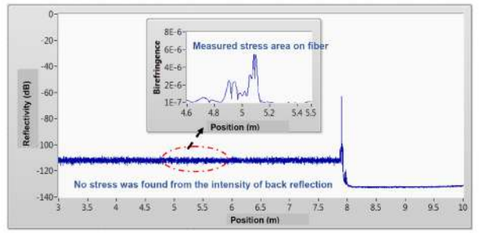

Figure 2 Bend insensitive fiber test results

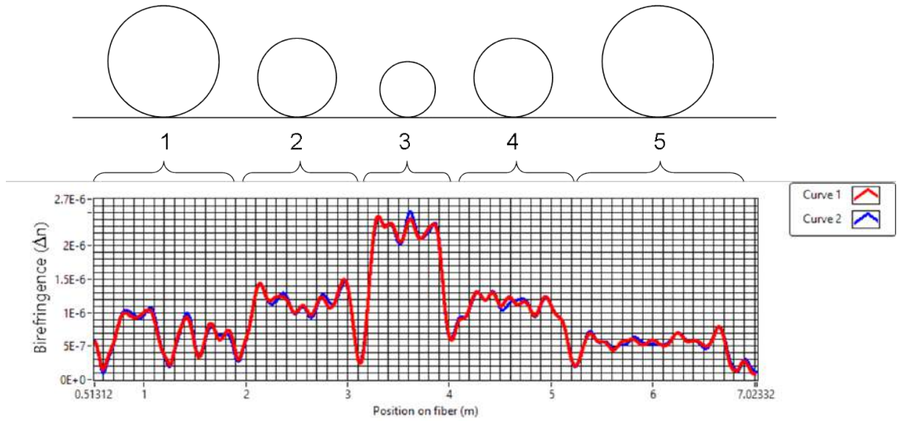

Figure 3 Birefringence measurement of a length of SMF-28 fiber in which different sections are coiled at different bend radii, resulting in different levels of bend-induced birefringence. It is clear that as the bend radius increases by a factor of √2, the induced birefringence increases by a factor of 2. In addition to the bend-induced birefringence, the beginning of section 1 shows slightly higher birefringence at the end of a fiber protection tube.

Curve 1 and curve 2 are consecutive measurements of the same fiber, illustrating the repeatability of the measurement.

Section	Fiber Length (m)	Bend Radius (mm)	Average Birefringence
1	1.5	40	~$6x10^{-7}$
2	1.1	28	~$1.2x10^{-6}$
3	0.8	20	~$2.4x10^{-6}$
4	1.1	28	~$1.2x10^{-6}$
5	1.5	40	~$6x10^{-7}$

MEASUREMENT AND CHARACTERIZATION

Distributed Polarization Crosstalk Analyzer - PolaX™ (PXA-1000)

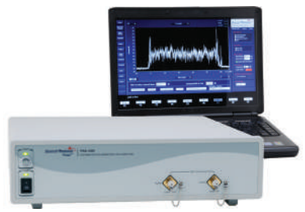

The Distributed Polarization Crosstalk (X-Talk) Analyzer (PXA-1000) is an enhanced version of a white light interferometer designed to obtain space-resolved stress information by analyzing stress-induced polarization cross-coupling along a length of polarization maintaining (PM) fiber. Its patented (US 8,599,385) optical design eliminates the strong zero-order interference and reduces the multi-coupling interference common in traditional white light interferometers, both of which can cause "ghost" peaks in the measured signal. The removal of the "ghost" peaks enables the PXA-1000 to unambiguously identify the magnitudes and locations of actual x-talk peaks, resulting in higher measurement sensitivity, higher dynamic range, and higher spatial measurement accuracy than traditional white light interferometers. The PXA-1000 also enables the use of the PM fiber itself as the sensing medium, eliminating the need to place multiple fiber gratings along the fiber. It can therefore obtain higher spatial resolution of the stress distribution than grating-based systems. Because no discrete sensing elements are required, the system is easy to install and calibrate, making it ideal for monitoring space-resolved structural changes along bridges, tunnels, dams, oil pipes, or buildings. It can also be used as an intrusion detection system, because any mechanical disturbances to the PM fiber will cause polarization coupling. Another important application is PM fiber quality inspection. The PXA-1000 easily identifies defective sections of PM fiber, enabling the manufacturers or users to remove them. Furthermore, the PXA-1000 is ideal for quality inspection and screening of PM fiber coils, since it can pinpoint the locations of imperfections or areas of local stress on the fiber coil induced during the fiber winding process. The PXA-1000 comes with a notebook computer equipped with PolaXView™ software, which displays the location and polarization coupling ratio of each stress point as a function of distance, and identifies stress points with polarization coupling above a user defined threshold level, with a list of the locations and polarization coupling strengths of all stress points. Other applications of the instrument include measuring the extremely high polarization extinction ratio of a polarizing waveguide, obtaining the autocorrelation function of a light source, measuring the birefringence of a PM fiber and the lengths of PM and SM fibers, and matching the optical path lengths of an interferometer.

Specifications:

Operation Wavelengths[1]	1310 or 1550 nm
Polarization X-talk Measurement Sensitivity	-75 dB (for DUT output power >5dBm) -80 dB typical
Polarization X-talk Measurement Noise Floor[2]	-95 dB
Polarization X-talk Resolution	0.25 dB
Polarization X-talk Repeatability[3]	±0.5 dB
Polarization X-talk Accuracy[4]	±0.5 dB
Measurement or Sensing Range (Assuming PM Fiber Δn of 5 $\times 10^{-4}$)	1.3 km or 2.6 km standard 3.1 km available
Measurement Speed[5]	8 s/100m (with fiber $\Delta n = 5 \times 10^{-4}$)
Spatial Resolution[6]	6 cm (assuming no fiber dispersion, birefringence $\Delta n=5\times10^{-4}$)
PER Measurement Range	> 30 dB
Spatial Accuracy[7]	±20 cm (with fiber $\Delta n = 5\times10^{-4}$)
Waveguide Polarization Dependent Attenuation	up to 75dB (for DUT output power > 5dBm)
$LiNbO_3$ Waveguide Spatial Resolution	0.75 mm
SLD Power	> 10 dBm
SLD Bandwidth	> 30 nm
SLD PER	> 20 dB
Software	PolaXView™ data analysis/display software
Operating Temperature	10 to 50 °C
Storage Temperature	-20 to 60 °C
Power Supply	100 – 240 VAC, 50 – 60 Hz
Communications Interface	USB 2.0
Display	Notebook computer with USB connection
Connector Type	PM narrow key FC/PC standard
Dimensions	2U, ¾ 19" rack width 14" (L) x 14" (W) x 3.5" (H)

Notes:
1. Shorter wavelengths around 850 nm and 1060 nm available upon request.
2. Defined as the system noise displayed on the polarization X-talk curve when input light is turned off during a measurement for which the DUT output power >5 dBm (See Fig. 1).
3. Defined as the standard deviation of twenty successive measurements of the amplitude of an X-talk peak between -15 and -40 dB.
4. At 23 ± 5 °C. Guaranteed by design and calibration in manufacturing process.
5. Average speed for full-length scan.
6. Defined as the minimum resolvable distance between two polarization X-talk points of equal amplitude, based on Sparrow Criterion (two peaks of equal height overlap at 3dB point, resulting in a flat-top curve) and measured when the peaks are between -15 and -40 dB.
7. Defined as the standard deviation of twenty successive measurements of the distance of an X-talk peak of height between -15 and -40 dB from the X-talk peak induced by the input connector (zero position).

Features:

- High spatial resolution: 6 cm
- PM fiber as intrinsic sensing element
- - 80 dB polarization X-talk sensitivity
- 30 dB PER measurement range
- Large fiber measurement range: 2.6 km
- Remote control option available for automated testing applications

Applications:

- Distributed stress sensing
- Structural change monitoring in bridges, tunnels, dams, and buildings
- PM fiber quality inspection
- PM fiber coil winding in-process monitoring
- PM fiber coil quality inspection
- Quality inspection of polarizing waveguides
- Intrusion detection

Related Products:

- Components
- Fiber Gyro Coils (FC series)

Tech Info:

- Polarization Crosstalk in PM Fiber
- Distributed Polarization X-talk Measurement for the production of Polarization-Maintaining Fiber Coils
- Complete Characterization of Polarization-Maintaining Fibers Using Distributed Polarization Analysis
- A Novel Method for Determining and Improving the Quality of a Quadrupolar Fiber Gyro Coil under Temperature Variations
- Method for Improving the Resolution and Accuracy against Birefringence Dispersion in Distributed Polarization Cross-Talk Measurements
- Accurate Method for Measuring the Thermal Coefficient of Group Birefringence of Polarization-Maintaining Fibers

MEASUREMENT AND CHARACTERIZATION

Distributed Polarization Crosstalk Analyzer - PolaX™ (PXA-1000)

Typical Performance Data:

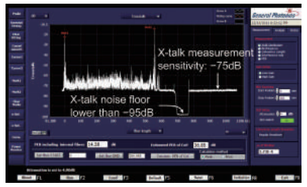

Figure 1. Instrument display showing the x-talk measurement sensitivity and x-talk measurement noise floor.

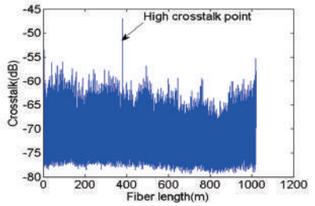

Figure 2. PM fiber quality inspection: Polarization x-talk measurement of 1000 m of raw fiber. High x-talk (-47 dB) is observed at 381 m.

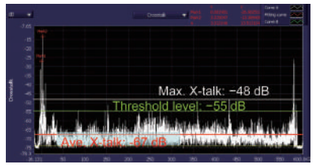

Figure 3. PM fiber coil quality inspection: Average and maximum polarization x-talk can be easily identified. In addition, the total number of x-talk peaks above a certain level (-55 dB in the graph) can be identified and their magnitudes and locations listed in a table.

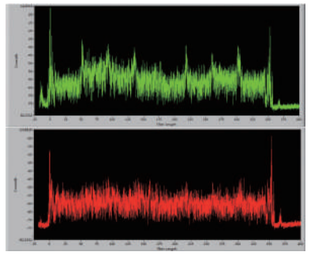

Figure 4. PM fiber coil manufacturing in-process monitoring.
Green: In-line polarization x-talk measurement of a PM coil with quadrupole winding pattern from an initial winding trial.
Red: In-line x-talk measurement of the same PM coil after adjusting winding procedure. The high x-talk peaks at cross-over points have been eliminated.

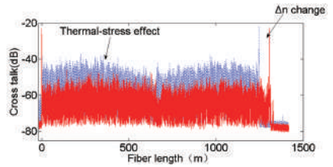

Figure 5. Measurement of thermal stress-induced polarization x-talk in PM fiber coils with quadrupole winding patterns. The temperature dependence of the fiber birefringence or beat length can also be determined from this measurement.

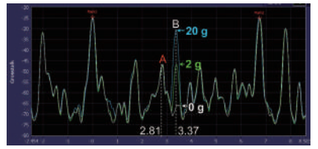

Figure 6. A 2 gram weight is placed on a straight PM fiber at position 2.81 m to induce an x-talk peak at point A. A second weight of varying mass is placed on the same PM fiber at position 3.37 m to induce an x-talk peak at point B. Three curves corresponding to 0, 2g, and 20g weights at point B are superposed in this figure to show that the instrument correctly identifies the stress induced x-talk at point B.

Video:

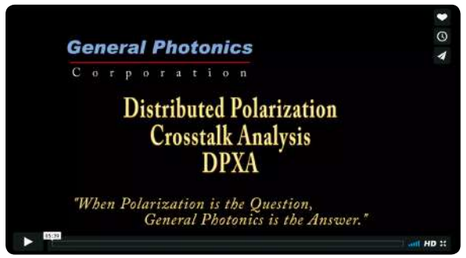

Ordering Information:

PXA — 1000 — □ □ — □ □ — □

Wavelength:
13 = 1310 nm
15 = 1550 nm

Range:
13 = 1.3km
26 = 2.6km

Connector Type:
FC/PC standard
FC/APC available

Polarization Synthesizer/Analyzer - PolaFlex™ (PSY-201)

The PSY-201 is a deterministic polarization controller that can generate and maintain any state of polarization (SOP), regardless of the input SOP. It combines General Photonics' patented polarization controller, in-line polarimeter, and control algorithm into an instrument that functions as both a polarization state generator and a polarization analyzer. The generated SOP and the corresponding Poincaré Sphere representation can be displayed on a computer screen via USB interface. The output SOP can be specified by inputting Stokes parameters using the front panel keypad or by manually tuning the SOP to reach a specific point on the Poincaré sphere or to reach an optimum value of a polarization-dependent metric. Once a desired output SOP is found, the instrument can automatically maintain this SOP against input SOP fluctuations. Another attractive feature is that the user can generate any of 6 distinct SOPs (0°, 90°, ± 45°, RHC and LHC) for Mueller matrix calculations, or select any of the 6 states at the touch of a button. Furthermore, the instrument can generate several preprogrammed SOP traces that emulate certain common polarization variations. The instrument can also function as a polarization scrambler, generating SOP scans with user-defined pattern and speed. Finally, with the internal polarization controller disabled, PolaFlex™ can function as an in-line polarimeter, displaying the instantaneous SOP and DOP of the input light beam. Features include long-term SOP monitoring, SOP markers for angle measurement, and a "SOP replay" function in sphere display mode, as well as extended triggering capability in oscilloscope mode. It puts all of the tools necessary for polarization management at your fingertips.

Specifications:

Operating Wavelength Range	1480 to 1620 nm or 1280 to 1340 nm
Sampling Rate (max.)	4.0M SOP samples/s
Analog Bandwidth[1]	1MHz
SOP Settling Time	1ms at stable input SOP
SOP Stability (Input Power > -25 dBm, DOP > 95%)	0.1° with stable input SOP 0.5° with input SOP variation < 2 π/s 2° with input SOP variation < 10 π/s
SOP Measurement/Generation Uncertainty	±0.25° after user calibration, with input > -25 dBm
DOP Uncertainty	±2% using built-in calibration, with input > -25 dBm ±0.5% after user calibration, with input > -25 dBm
Input Stokes Parameter Resolution	0.001
Optical Power Uncertainty	±0.25 dB
Insertion Loss	1.6 dB max. at center wavelength
Return Loss	55 dB (APC connector), 45 dB (PC connector)
PDL	< 0.25 dB
PMD	< 0.1 ps
Operating Power Range	-35 dBm to +10 dBm
Optical Power Damage Threshold	300 mW
Operating Temperature	0 °C to 40 °C
Storage Temperature	-20 °C to 60 °C
Front Panel Display	Graphic OLED
Communication Interfaces	High Speed USB 2.0 (30 MB/s data rate) for PolaView software, RS-232, Ethernet, GPIB
Analog Output	0 to 5 V max range, user configurable Monitor voltage for DOP, S1, S2, S3, power or dREF
Power Supply	100 – 240 VAC, 50 – 60 Hz
Software	PolaView™ (included)
Dimensions	2U, 19" half rack width 14" (L) x 8.5" (W) x 3.5" (H)

Notes:
Loss specifications are referenced without connectors. Unless otherwise noted, specifications listed in table apply for standard 1480-1620nm or 1280-1340nm operation at 23±5°C, at power levels >-25 dBm.

1. For input power > -10 dBm. At lower power levels, bandwidth may change due to automatic gain control.

Features:

- 4 MHz SOP sampling rate
- 1 MHz analog bandwidth
- 45 dB input power dynamic range
- Real-time Poincaré Sphere display
- High-speed SOP generation and tracking
- High speed analog output of SOP & DOP

Applications:

- Receiver polarization sensitivity analysis
- System SOP/DOP monitoring
- PER measurement
- Polarization generation and stabilization
- Sensor system characterization
- 100G system polarization characterization

Related Products:

- Polarization Measurement System (PSGA-101)
- Multifunction Polarization Controller (MPC-202, MPC-201)
- Polarimeter (POD-201)
- Rack Mount Kit (RCK-001)
- Components

Tech Info:

- What is Polarization?
- Combat Polarization Impairments with Dynamic Polarization Controllers
- Polarization Related Tests for Coherent Detection Systems

FAQ:

- Dynamic Polarization Controllers
- Polarimeter

MEASUREMENT AND CHARACTERIZATION

Polarization Synthesizer/Analyzer - PolaFlex™ (PSY-201)

Application Example:

Coherent Receiver Polarization Sensitivity Test

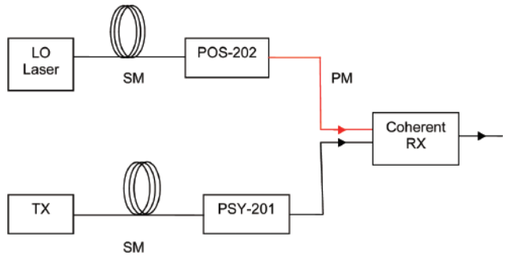

Sample setup for a coherent receiver performance test using a polarization stabilizer (POS-202) and a polarization synthesizer (PSY-201).

1. Use polarization stabilizer (POS-202) to lock the polarization of one receiver input (local oscillator input).
2. Use polarization synthesizer (PSY-201) to control the polarization of the other receiver input to find the SOP that maximizes the receiver power reading.
3. Lock the PSY-201 output at that SOP to eliminate polarization fluctuations in the SM fiber. Test receiver performance.
4. Use PSY-201 to find or switch to the orthogonal SOP (minimize receiver power reading).
5. Lock PSY-201 output at that SOP to eliminate polarization fluctuations. Test receiver performance.

Typical Performance Data:

Polarization stabilization

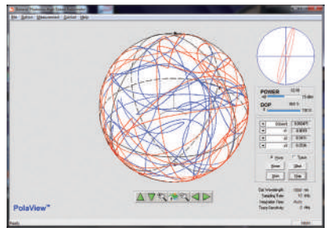

Figure 1. Input polarization pattern: triangle wave scramble at 1 Hz, taken over 20 sec

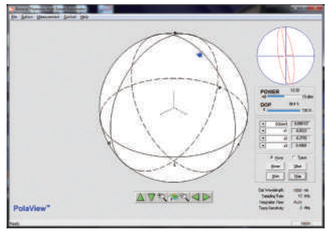

Figure 2. Output polarization stabilized by PSY-201 against the same polarization-scrambled input, taken over 20 sec

Special polarization state/trace generation

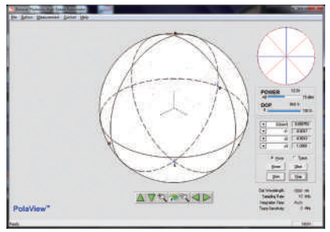

Figure 3. Poincaré sphere pole state generation

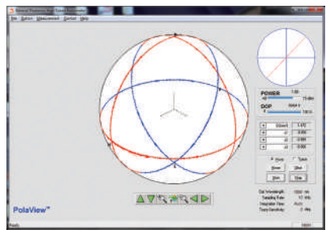

Figure 4. Trace Scans

Scrambling

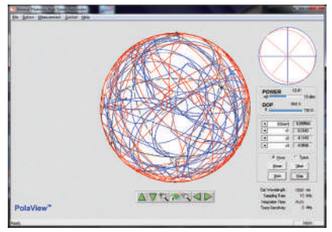

Figure 5. Triangle scrambling trace, 1 Hz after 1 minute

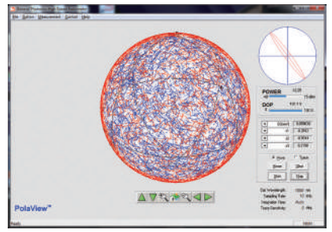

Figure 6. Discrete scrambling, 100 Hz after 1 minute

Video:

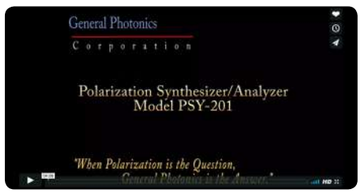

Ordering Information:

PSY — 201 — □ □ — □

Wavelength:
15=1550nm
13=1310nm

Connector Type:
FC/PC, FC/APC
SC/PC, SC/APC

Polarimeter - PolaDetect™ (POD-201)

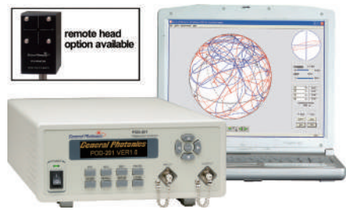

The POD-201 is an FPGA powered polarimeter specially designed for high-speed polarization analysis and monitoring. The instrument uses four channels to simultaneously obtain the four Stokes parameters and measure the instantaneous state of polarization (SOP) and degree of polarization (DOP) of an input light beam. A USB 2.0 interface enables data to be transferred directly to a computer at a rate up to 30 MB/s. Thanks to the high speed FPGA electronics, this polarimeter easily monitors and analyzes fast polarization changes with a sampling rate of up to 4MS/s. The POD-201 comes with PolaView™ software for real-time graphic display of polarization state either on a Poincaré Sphere window for viewing SOP traces or on an oscilloscope window for monitoring polarization changes over time. It can be quickly and easily calibrated using its built-in self-calibration program to optimize DOP and SOP accuracies at special wavelengths and temperatures. With a suitable light source and measurement techniques, it can be used to measure polarization extinction ratio (PER) to aid in aligning PM fiber to laser sources. Features include long-term SOP monitoring, SOP markers for angle measurement, a "SOP replay" function in sphere display mode, extended triggering capability in oscilloscope mode, an OLED display for easy setup and data display and a configurable analog SOP/DOP/power output for easy integration with automated test systems. The standard configuration is a two-port inline version, to monitor a signal without interruption; a one-port remote head option that can accommodate free-space inputs is also available.

Specifications:

Operating Wavelength Range[1]	1480 to 1620 nm or 1280 to1340 nm
Analog Bandwidth[2]	1 MHz
Sampling Rate (max)	4.0M SOP samples/s
SOP Uncertainty[3]	±0.25° after user calibration
DOP Uncertainty[3]	±2% using built-in calibration ±0.5% after user calibration
PER Measurement Range[3]	0 to 40 dB
PER Resolution	0.1 dB
Insertion Loss	1.2 dB max. at center wavelength
Return Loss	55 dB (APC connector) 45 dB (PC connector)
PDL	< 0.25 dB
PMD	< 0.1 ps
Aperture Size (Remote Head)	2.5 mm
Operating Power Range	-35 to +10 dBm (2-port in-line) -40 to +2 dBm (remote head)
Optical Power Uncertainty[3]	± 0.25 dB
Optical Power Damage Threshold	300 mW
Operating Temperature	0 °C to 40 °C
Storage Temperature	-20 °C to 60 °C
Front Panel Display	Graphic OLED
Communication Interfaces	High Speed USB 2.0 (30 MB/s data rate) for PolaView software RS-232, Ethernet, GPIB
Analog Output	0 to 5 V max range, user configurable Monitor voltage for DOP, S1, S2, S3, power or dREF
Electrical Power Supply	100 – 240 VAC, 50 – 60 Hz
Software	PolaView™ (included)
Dimensions	2U 19" half rack width 14" (L) x 8.5 " (W) x 3.5" (H)

Notes:
Unless otherwise noted, specifications listed in table apply for standard fiber-coupled in-line configurations with 1480 - 1620nm or 1280-1340nm operation at 23±5 °C. Specs for one-port remote head may be slightly different. Loss specifications are referenced without connectors.

1. Other wavelengths may be possible. Contact General Photonics for details.
2. For input power > -10 dBm for 2-port in-line version. At lower power levels, bandwidth may change due to automatic gain control.
3. For input power > -25 dBm for 2-port in-line version.

Polarimeter - PolaDetect™ (POD-201)

PolaView™ Display Interfaces:

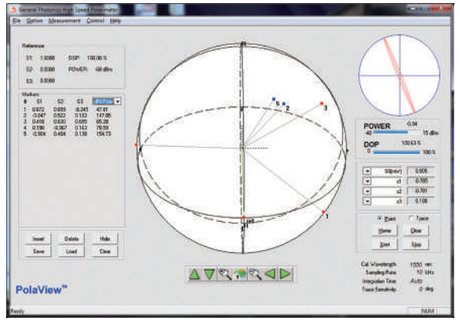

Figure 1. Poincaré sphere display with markers

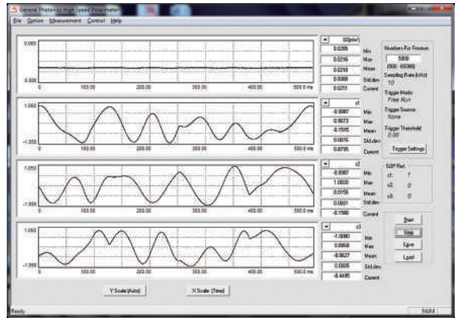

Figure 2. Oscilloscope display

Features:

- 4 MHz polarization sampling rate
- Up to 1 MHz analog bandwidth
- Real time Poincaré Sphere display
- Continuous measurement
- External trigger
- Long term polarization monitoring
- PER measurement

Applications:

- 100G system polarization test
- SOP/DOP monitoring
- Polarization analysis
- Scrambler DOP characterization
- SOP statistics
- PM fiber alignment to light sources

Related Products:

- Multifunction Polarization Controller (MPC-202, MPC-201)
- Polarization Scramblers (PCD-104, PSM-002)
- Polarization Synthesizer (PSY-201)
- Rack Mount Kit (RCK-001)
- Components

Tech Info:

- What is Polarization?
- Polarization Related Tests for Coherent Detection Systems
- Real-Time Optical Spectrum Analysis of a Light Source Using a Polarimeter

FAQ:

- Polarimeter

Ordering Information:

POD — 201 — □ — □□ — □

Configuration:
I = 2-port in-line
R = 1-port, remote head*

Wavelength:
15 = 1550 nm
13 = 1310nm
Others specify

Connector Type:
FC/PC, FC/APC
SC/PC, SC/APC
(only for in-line version)

Note:
* Contact General Photonics for details.

Optical Component Analyzer (OCA-1000)

The OCA-1000 is a multi-channel optical component analyzer capable of performing simultaneous insertion loss (IL), polarization dependent loss (PDL), and optical power (P) measurements on multiple optical paths. The measurement is based on the Mueller Matrix method, which offers fast characterization of wavelength dependent optical parameters that are critical in today's optical communication systems. The base model can have up to 8 channels, and the system is expandable to additional sets of channels for maximum flexibility.

The instrument comes with a user-friendly control program with built-in functions to display measured power, IL, and PDL vs. wavelength or to monitor the time variation of power/IL for all channels simultaneously to determine their stability. Other functions available after post processing the data include calculation of the isolation between wavelength channels (adjacent and distant), pass band center frequency, bandwidth, and ripple as well as noise floor.

The OCA-1000 is an ideal solution for easy, accurate characterization of components and modules with multiple outputs, including DWDMs, ROADMs, AWGs and PLCs. It can be used with various tunable lasers, such as those from Keysight or Santec. This flexibility offers the user the opportunity to make full use of his/her laser resources and reduce the cost of making such measurements. Its fast measurement speed reduces the time required to characterize devices with large numbers of ports, enabling higher production throughput.

Specifications:

Number of channels	8 channels in base unit; Can be expanded to more channels
Wavelength range	1260 ~1360 nm (O-band) and 1480 ~ 1620 nm (C + L bands)
Optical power range[1]	−60 dBm to +8 dBm
Optical power accuracy[1]	± 0.5 dB
Optical power variation for different channels[1]	± 0.1 dB
Integration time of power meter	0.5 ~ 1000 ms
PDL measurement range[2]	0 ~ 20 dB
PDL measurement uncertainty[2]	± (0.02 + 2% of PDL) dB @PDL<10dB ± (0.02 + 5% of PDL) dB @10<PDL<20dB
PDL resolution	0.01 dB
PDL repeatability[2]	± 0.02 dB
IL measurement range[3]	0 to 60 dB (single point or stepped wavelength sweep mode) 0 to 55 dB (continuous wavelength sweep mode)
IL measurement uncertainty[3]	± (0.01 + IL× 0.5%) dB
IL resolution	0.002 dB
IL repeatability[2]	± 0.005 dB
Sweep period of 6-state PDL/IL measurement (typ.)	(2+wavelength sweep range (nm)/40)×6 seconds when laser sweep speed is 40 nm/s
Fiber type	1550nm PSG in: PM 1550 Panda fiber 1310nm PSG in: PM 1300 Panda fiber PSG outputs: SMF-28
Optical Connector Type	PSG in/out: FC/APC standard Detector inputs: FC free space
Communication	USB (USB 2.0), GPIB (IEEE 488.2)
Operating temperature	10 ~ 40 °C
Storage temperature	-20 ~ 60 °C
Operating humidity	< 80 %, non-condensing
Mechanical Dimensions (One unit)	1U 19" rack mountable enclosure, 12" depth

Notes:
1. At 23 ± 5 °C.
2. With DUT input power >−10dBm, DUT IL <20dB, and integration time = 10ms.
3. With DUT input power >5dBm, integration time = 100ms.
4. Recommended laser brands:
   - Any Keysight/Agilent tunable laser with trigger output.
   - Santec 5 and 7 series tunable lasers with trigger output (confirm with GP)

Features:

- Wide wavelength range
- High PDL accuracy
- High channel-to-channel uniformity
- User-friendly control program

Applications:

- PDL vs. wavelength measurement
- IL vs. wavelength measurement
- IL/Power vs. Time
- Pass band parameters: center frequency, BW, ripple, noise floor
- Fiber optic component characterization
- Network component characterization (e.g. DWDM, ROADM.)
- Planar Lightwave Circuits (PLC)
- Photonic Integrated Circuit (PIC)

Related Products:

- PDL Meter (PDL-201)
- PDL Calibration Artifact (CS-PDL)
- Polarization Measurement System (PSGA-101)
- Bare Fiber Adapter (PEZ-001)

Tech Info:

- What is Polarization?
- Application Note for PDL Measurement

Order Information:

OCA — 1000 — □ □

# of Channels:
8 standard

MEASUREMENT AND CHARACTERIZATION

Optical Component Analyzer (OCA-1000)

Typical Performance Data:

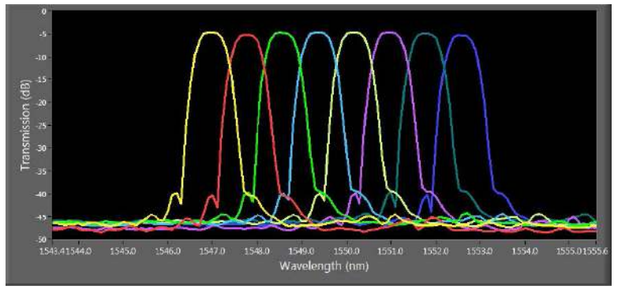

Figure 1. Transmission vs. wavelength for 8 channels of an arrayed waveguide grating (AWG). Pass bands for each channel are clearly visible.

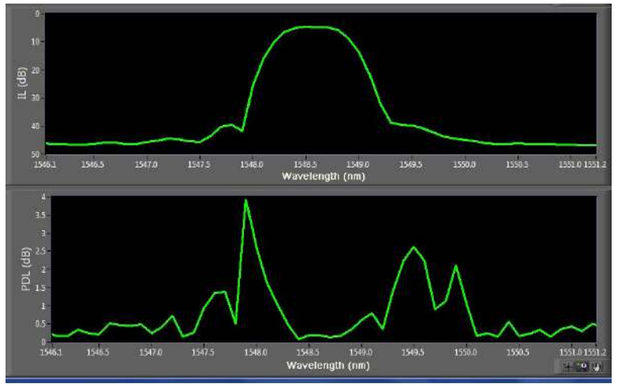

Figure 2. IL and PDL vs. wavelength for one channel of the AWG. PDL is relatively flat over the passband of this channel.

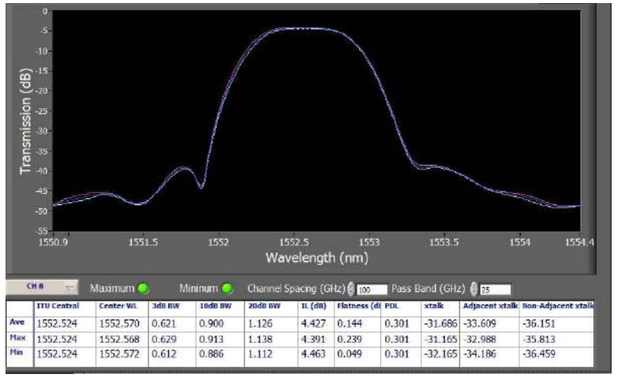

Figure 3 Detailed transmission vs. wavelength data for one channel of the same AWG. The plot shows the maximum, minimum, and average transmission vs. wavelength. The difference between maximum and minimum is an indication of the polarization dependent behavior for this device. The table shows the passband, flatness, and crosstalk information for this channel.

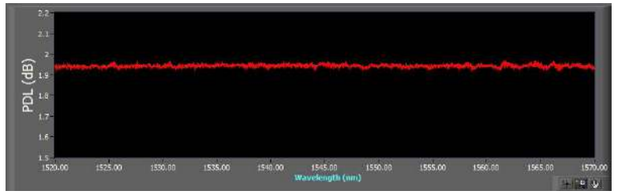

Figure 4. PDL vs. wavelength for a 1.96dB PDL artifact. The data indicates that the PDL of this device is relatively flat over the tested wavelength range.

Polarization Dependent Loss Multimeter - PolaChex™ (PDL-201)

Using a patented maximum and minimum search method (compliant with TIA/EIA-455-198; ref. "Automatic Maximum-Minimum Search Method for Accurate PDL and DOP Characterization"), General Photonics' PDL multimeter simultaneously measures the Polarization Dependent Loss (PDL), Insertion Loss (IL), and optical power of a device under test (DUT) in just 30 ms. Unlike PDL meters that use the polarization scrambling method, which has large measurement uncertainty, PolaCHEX™ systematically searches for the maximum and minimum transmissions to assure measurement accuracy at all times for devices with both low and high PDL values. It is therefore the most accurate PDL meter available. Even more impressively, PolaCHEX covers a wide wavelength range from 1260 to 1620 nm without wavelength calibration, a clear advantage over PDL meters based on the Mueller Matrix method. PolaCHEX comes with USB, Ethernet, GPIB and RS-232 interfaces for PC control and is ideal for fast, accurate characterization of the wavelength dependence of passive devices, especially DWDM and fiber sensor components, in manufacturing environments as well as in laboratories. The PDL-201 features fast measurement, large measurement dynamic range, bright OLED display, and an analog output port for easy integration in automated measurement stations.

Specifications:

Wavelength Range	1260 to 1620 nm
Resolution	0.01 dB
PDL Accuracy[1, 2, 3]	± (0.01 + 5% of PDL) (dB)
PDL Repeatability[1]	± (0.005 + 2% of PDL) (dB)
PDL Dynamic Range[4]	0 to 45 dB
IL Accuracy[1, 5]	± (0.01 + 5% of IL) (dB)
IL Repeatability[1]	± (0.005 dB + 2% of IL) (dB)
IL Dynamic Range[4]	0 to 45 dB
Optical Power Range (at DUT output port)	-40 to +6 dBm
Optical Power Accuracy	±0.25 dB
Wavelength Calibration for Power Measurement	1260 to 1360 nm and 1440 to 1620 nm
Measurement Speed	30 ms/measurement for input > -30 dBm
Operating Temperature	0 to 50 °C
Storage Temperature	-20 to 70 °C
Front Panel Display	OLED graphic display
Optical Connector Type	Light source and DUT input: APC DUT output: Free space adapter
Analog Output	0 to 4V PDL monitor voltage (0 to 3.5V linear with PDL, 4V indicates power low) User-configurable PDL range
Power Supply	100 – 240 VAC, 50 – 60 Hz
Communication Interfaces	USB, Ethernet, RS-232, and GPIB
Dimensions	2U, 19" half rack width 14" (L) x 8.5" (W) x 3.5" (H)

Notes:
1. For 10 sample average.
2. At 23 ± 5°C.
3. Accurate PDL measurement also depends on test setup. Optimize your test environment with suggestions from General Photonics' PDL measurement application note.
4. For input power ≥0 dBm.
5. In power meter measurement mode with user-defined reference

Features:

- 30 ms measurement speed
- Wide wavelength range
- High PDL accuracy
- Analog PDL output
- Bright OLED display
- Power meter function

Applications

- PDL vs. wavelength measurement
- DWDM device characterization
- Fiber sensor component characterization

Related Products:

- Optical Component Analyzer (OCA-1000)
- DOP Meter (DOP-201)
- ER Meter (ERM-202)
- Rack Mount Kit (RCK-001)
- Components
- Bare Fiber Adapter (PEZ-001)

Tech Info:

- What is Polarization?
- Automatic Maximum-Minimum Search Method for Accurate PDL and DOP Characterization
- Application Note for PDL Measurement

Ordering Information:

PDL — 201 — ☐

Connector Type:
FC
SC

Note:
A NoTail isolator is recommended at the light input port to minimize back reflections.

MEASUREMENT AND CHARACTERIZATION
Polarization Dependent Loss Multimeter - PolaChex™ (PDL-201)

Typical Performance Data:

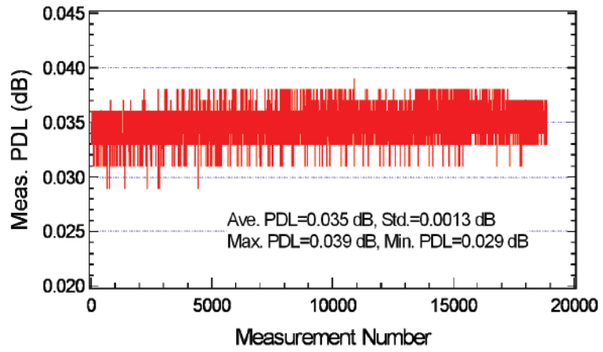

Figure 1. Measurement of a low PDL sample: APC Connector

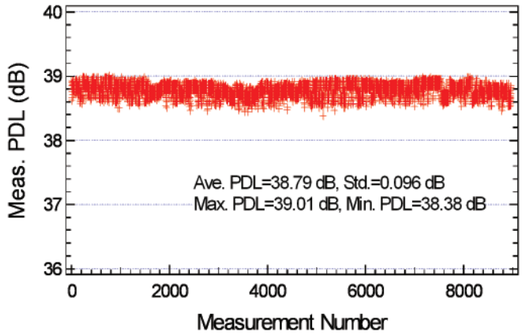

Figure 2. Measurement of high PDL sample: Polarizer

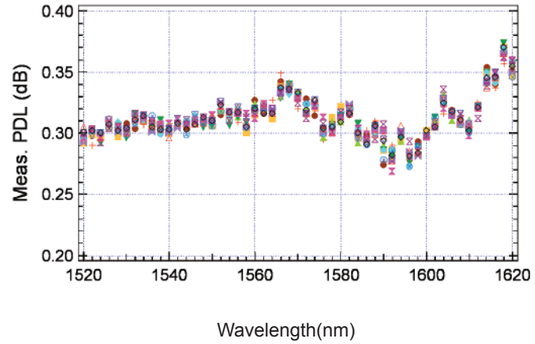

Figure 3. Wavelength scan and multiple (12) scan repeatability

Video:

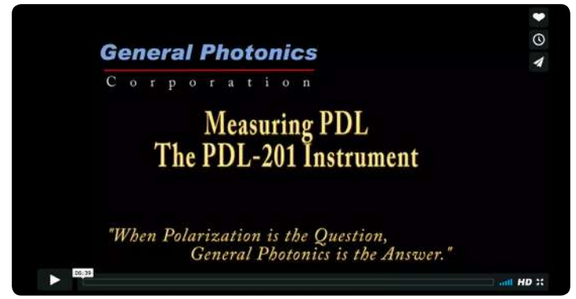

Degree of Polarization Meter (DOP-201)

Using a patented maximum & minimum search technique (ref. "Automatic Maximum-Minimum Search Method for Accurate PDL and DOP Characterization"), the DOP-201 measures and displays the Degree of Polarization (DOP) of a light source in real time with high accuracy and wide dynamic range. While polarimeter-based systems are expensive and can be inaccurate for low-DOP sources, and polarization scrambler-based instruments are less accurate for high DOP sources, the DOP-201 accurately measures both low and high DOP. It is ideal for characterizing the performances of depolarizers and depolarized light sources, such as ASE and SLED sources and the pumps for Raman amplifiers. It can also be used to monitor the OSNR and PMD of optical signals, and to measure the noise figure of optical amplifiers. The instrument can cover a wide operating wavelength range, including the S, C and L bands, without calibration. Its simultaneous measurement of DOP and optical power level of the light source under test can be used to obtain DOP power dependence and to ensure low insertion loss during depolarizer manufacturing. The DOP-201 features fast measurement, high accuracy and resolution, a wide operating power range, a bright OLED display, and an analog output port for easy integration in automated depolarizer manufacturing stations.

Specifications:

Operating Wavelength Range	1260 to 1620 nm standard
DOP Resolution	0.01%
DOP Accuracy[1]	±0.5% (single sample) ±0.2% (10 sample average)
Repeatability	±0.2% (10 sample average)
DOP Range	0 – 100%
Measurement Speed	30 ms/measurement for input > -30 dBm
Operating Power Range	-40 to 6 dBm
Optical Power Accuracy	±0.25 dB
Wavelength Calibration for Power Measurement	1260 to 1360 nm and 1440 to 1620 nm
Operating Temperature	0 to 50 °C
Storage Temperature	-20 to 70 °C
Front Panel Display	OLED graphic display
Analog Output	0 to 5 V max range, user configurable Monitor voltage for DOP
Power Supply	100 – 240 VAC, 50 – 60 Hz
Communication Interfaces	USB, Ethernet, RS-232, and GPIB
Dimensions	2U 19" half rack width 14" (L) x 8.5" (W) x 3.5" (H)

Note:
1. At 23 ± 5°C.

Video:

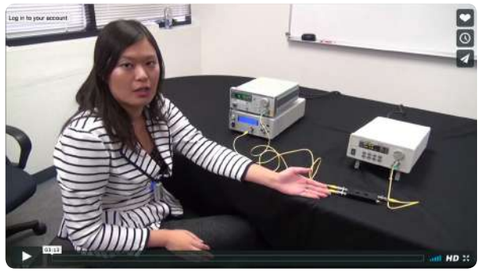

Features:

- Rapid measurement
- DOP is wavelength independent
- High accuracy
- Front panel real time display
- Analog output

Applications:

- Depolarizer manufacturing and QC
- Fiber gyro coil characterization
- ASE & SLED source characterization
- Raman amplifier block manufacturing
- ROADM manufacturing
- Amplifier noise figure measurement

Related Products:

- Polarization Scramblers (PCD-104, PSM-002)
- Polarimeter (PSY-201, POD-201)
- PDL Meter (PDL-201)
- ER Meter (ERM-202)
- Rack Mount Kit (RCK-001)
- Components

Tech Info:

- What is Polarization?
- Automatic Maximum-Minimum Search Method for Accurate PDL and DOP Characterization
- Accurate DOP Characterization with Less Effort

Ordering Information:

DOP — 201 — □ — □

Wavelength:
1 = 1260 - 1620nm

Connector Type:
FC/PC, FC/APC
Others specify

Polarization Extinction Ratio Meter (ERM-202)

The ERM-202 is a dual channel polarization extinction ratio (PER) meter specifically designed to simultaneously measure the PER and power ratio of a device with two polarization maintaining (PM) outputs, such as a Y-branch fiber gyro IOC, PM coupler (PMC), or polarization beam splitter (PBS), as well as evaluate the performance (output DOP) of depolarizers. A lower-cost single-channel version, which can later be upgraded to dual-channel, is also an option. An analog electrical PER output for each channel is provided. With a PER dynamic range of 50 dB and an angular resolution of 0.06°, this instrument outperforms all competitors in its class. Its bright graphic OLED display allows information to be comfortably seen at large viewing angles and at a distance. The instrument has 4 measurement speeds ranging from 0.1 to 1 second/cycle, with the high speed for live alignment and the low speed for accuracy. PER, axis angle, power ratios, and optical power are automatically measured and displayed on the OLED screen. The measurement data can also be stored and recalled at the touch of a button for comparison purposes. The ERM-202 is ideal for PM fiber pigtailing of modulators, waveguides, and laser diodes, as well as for PMC and PBS manufacturing, PM fiber connectorization, depolarizer characterization, PM fiber fusion splicing, PM fiber coil production and quality assurance for fiber gyros.

Specifications[1]:

Operating Wavelength Range[2]	1260 to 1620 nm	960 to 1160 nm	600-850 nm
Calibrated Wavelengths[2]	1550 and 1310 nm	980 and 1064 nm	630 and 830 nm
PER Dynamic Range	> 50 dB	> 40 dB	> 40 dB
PER Ranges[3]	0 to 50 dB for input power -5 to 10 dBm 0 to 30 dB for input power -25 to -5 dBm	0 to 40 dB for input power 0 to 10 dBm 0 to 30 dB for input power -20 to 0 dBm	0 to 40 dB for input power 0 to 10 dBm 0 to 30 dB for input power -20 to 0 dBm
Input Optical Power Range	-30 dBm to 10 dBm	-20 dBm to 10 dBm	-20 dBm to 10 dBm
PER Resolution	0.1 dB		
PER Accuracy	±0.15 dB for ER < 30 dB		
Angular Resolution	0.06°		
Angular Accuracy	±1°		
Power Measurement Accuracy	±0.5 dB		
Power Resolution	0.02 dB (PER < 30 dB) 0.2 dB (PER > 30 dB)		
Measurement Speeds	0.1, 0.2, 0.4, 1 seconds (Single channel version also has 10s measurement speed and manual polarizer control mode)		
Connector Type[2]	Free space adapter for FC connector		
Optical Power Damage Threshold	300 mW		
Operating Temperature	0 °C to 40 °C		
Storage Temperature	-20 °C to 60 °C		
Display	OLED graphic display		
Communication Interfaces	USB, RS-232, Ethernet, and GPIB		
Analog Output	0-5V (max range) monitor voltage scales with log of instantaneous power after rotating polarizer.		
Electrical Power Supply	100 – 240 VAC, 50 – 60 Hz		
Dimensions	2U 19" half rack width 14" (L) x 8.5 " (W) x 3.5" (H)		

Notes:
1. Specifications given at 23±5 °C.
2. Other wavelength ranges and connector types may be available.
3. Other calibrated wavelengths available.
4. For measurement at or slower than 0.4 s/cycle

Features:

- Two measurement channels
- Simultaneous PER & power ratio testing
- > 50 dB PER range
- Bright OLED display
- High angular resolution
- Store and recall functions

Applications:

- IOC PER & coupling ratio tests
- PMC & PBS PER & coupling ratio tests
- Laser diode PM fiber pigtailing
- PM fiber patch cord production
- PM fiber fusion splicing QA
- PM fiber coil and fiber gyro QA monitoring / measurement

Related Products:

- Distributed Polarization Crosstalk Analyzer (PXA-1000)
- Polarimeter (PSY-201, POD-201)
- Bare Fiber Adapter (PEZ)
- Rack Mount Kit (RCK-001)

FAQ:

- ER Measurement

Ordering Information:

ERM — 202 — □ — □ — □

Channel Option:
1 = Single channel
2 = Dual channel

Wavelength:
13/15 = 1260 - 1620nm
98/10 = 960 - 1160nm
63/83 = 600 - 850nm

Connector Type:
FC = FC
free space adapter

3D Optical NDE System (OIS-1000)

The OIS-1000, also known as the Acute Detection for Advanced Materials (ADAM™) system, is a high speed, high resolution 3D optical non-destructive evaluation (NDE) system for the inspection of advanced materials. A laser and optical detection circuitry combine to present the operator with a 3 mm deep view inside semiopaque materials such as plastics and composites. Powerful software processes the optical signals to present the operator with clear visualization of the object under test.

The resulting images allow identification of internal inhomogeneities, boundaries, air bubbles, and cracks. Testing and validation processes are faster and easier than ever with ADAM™.

Specifications[1]:

Central Wavelength[2]	1305 nm
A-Scan Rate[3]	100 kHz
B-Scan Rate[4]	99.4 Hz
Average Output Power	≥10 mW
Sensitivity	105 dB
Axial resolution (in air)	≤20 µm
Imaging depth (in air)	6 mm
Depth of penetration	1-3 mm
Probe lateral resolution[4]	≤20 µm
Probe field of view[4]	5 × 5 mm
Probe length[4]	2 m
Dimensions, Optical module	53.5 (L) × 48.3 (W) × 13.2 (H) cm
Operating Temperature	10-35 C°
Storage Temperature	10-45 C°
Humidity	10-90% relative humidity

Notes:
1. Typical values for 1305 nm and 100 kHz A-Scan Rate. Specifications may vary based on the system configuration.
2. Other wavelengths available such as 1060 nm.
3. 200 kHz A-Scan Rate is available for 1060 nm option.
4. With standard probe.

Features:

- Non-Contact Measurement
- 100,000 A-Scans per Second
- 20 µm Depth Resolution
- 3 mm Depth Penetration
- Mitigated shadowing effect

Applications:

- NDE of Plastics and Composites
- Quality Control
- Failure Analysis

Order Information:

OIS — 1000 — □ — □□ — □

Probe Option:
00 = Without probe
HP = With handeld probe

Wavelength:
13 = 1310 nm
10 = 1060 nm

A-Scan Rate:
100 = 100 KHz
200 = 200 KHz*

Notes:
* Available in 1060nm version only.

MEASUREMENT AND CHARACTERIZATION

3D Optical NDE System (OIS-1000)

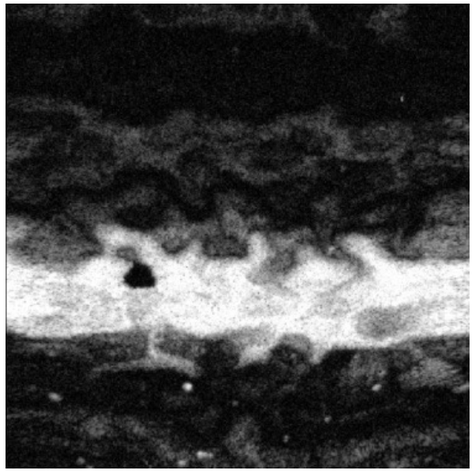

Figure 1. Image of the surface of a composite material showing surface roughness and bubbles.

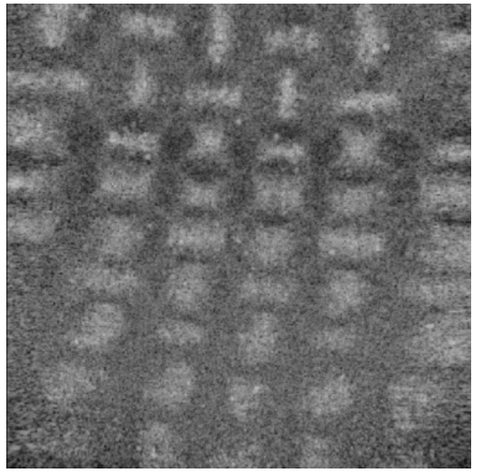

Figure 2. Subsurface image showing the internal structure of a composite material, including the plain weave glass fiber reinforcement.

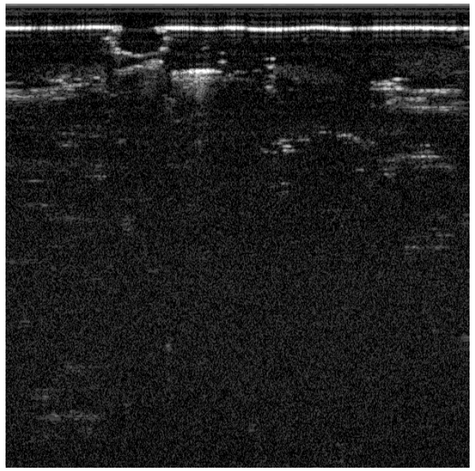

Figure 3. Cross sectional view of a material showing an air bubble at the top.

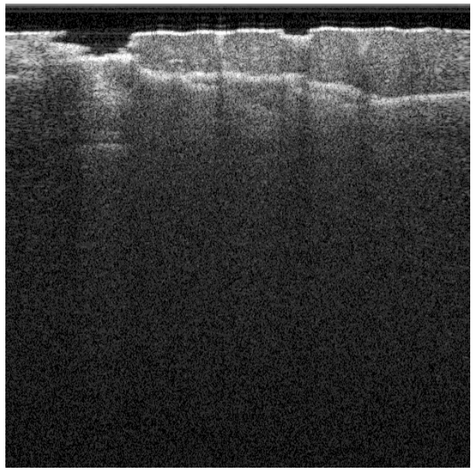

Figure 4. Cross sectional view of composite material showing defects (cracks) at different depths.

Distributed Vibration Sensor - OptiEar™ (DVS-1000)

The DVS-1000 is a versatile distributed vibration sensor system, capable of monitoring both buried installations (pipelines, borders, optical cables, etc.) and above ground fence and wall mounted systems. Based on single fiber optic sensing cable, the DVS-1000 is able to create a distributed acoustic (or vibration) measurement along the entire length of the fiber, effectively turning the telecom cable into a continuous series of microphones. The system features a long measurement range of up to 100km per unit. In addition, the built-in intelligent classification engines with motion recognition allow accurate location of intrusion events with minimal nuisance events and false alarms. The DVS-1000 is an ideal solution, both as a Perimeter Intrusion Detection System (PIDS) and as a Third Party Interference (TPI) system. The system is easy to install and offers low cost of ownership with low ongoing maintenance costs. The system comes with integration software which is a proven solution to provide advanced visualization and integration with existing security technologies deployed on site. It provides a system mapping function, along with real time event management. The Interprocess Communication (IPC) units also provide alarm management capabilities by the use of event database management and seamless integration with other security technologies including DCS, CCTV and access control, to provide an effective integrated security solution.

Specifications:

Smart Zones	1000+ zones, fully configurable, independent of each other
Intelligent Classification Engines	Fence related intrusions alerts Environmental noise reduction
Range (per unit)	20 Km, 40 Km, 50 Km, or 100 Km
Positional Accuracy	± 5 m
Number of Channels	1, or 2 channels
Optical Fiber Type	G.652/ G.654 Single Mode Optical Fiber
Frequency Range	1 Hz ~ 2.5 KHz
Response Time	2 to 10 seconds
Data Export	TCP/IP, RS232/RS485, Modbus, DCS (Honeywell, Siemens, ABB…….)
Power Consumption	75 W
Operation Temperature	10 to 50° C
Storage Temperature	−20° to 60° C
Power Supply	100 – 240 VAC, 50 – 60 Hz
Dimensions	19” rack mount, 20” depth; 3U height

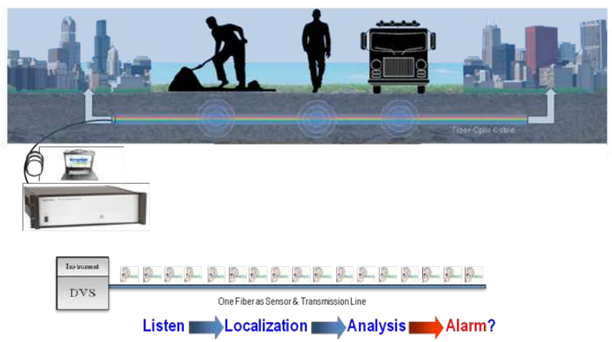

Features:

- Long distance monitoring – up to 100km per unit
- Location of intrusion event to within 5m over long distances
- Intelligent classification engine with motion recognition
- Based on single fiber optic sensing cable
- Robust and reliable with no moving parts

Applications:

- Asset monitoring (Pipeline, Optical Cables, Fence)
- 3rd party interference
- Intrusion detection

Order Information:

DVS — 1000 — ☐ — ☐☐ — ☐☐

Measurement Range:	Number of Channels:	Fiber Type:
020 = 20 Km	01 = 1 Channel	52 = G.652
040 = 40 Km	02 = 2 Channels	54= G.654
050 = 50 Km		
100 = 100 Km		

Impairment Emulation and Polarization Control

Polarization Optimized PMD Source - PMDPro™ (PMD-1000) 38
Polarization Dependent Loss Source/Emulator - PDLPro™ (PDLE-101) 40
Advanced Multifunction Polarization Controller - PolaMight™ (MPC-202) 42
Multifunction Polarization Controller - PolaMight™ (MPC-201) 44
Programmable Optical Delay Generator - TimeRITE™ (ODG-101) 46
Polarization Scrambler - PolaMix™ (PCD-104) 47
Reset-Free Polarization Stabilizer - PolaStay™ (POS-20X) 48

Polarization Optimized PMD Source - PMDPro™ (PMD-1000)

The PMD-1000 (PMDPro™) is a breakthrough PMD source that can deterministically generate precise 1st order PMD up to 180 ps and 2nd order PMD up to 8100 ps^2. Its quasi-continuous operation mode enables independent generation of first order and wavelength independent second order PMD for uniform coverage of the PMD space. It contains an automatic polarization controller and two polarimeters that monitor the state of polarization (SOP) and degree of polarization (DOP) before and after the PMD generating elements. The polarization controller can be used with the front polarimeter to automatically align and maintain the input SOP at 45° from the principal axis of the DGD element to obtain the worst-case first order PMD effect. Alternatively, the controller can automatically adjust and maintain the input SOP using the feedback from the rear polarimeter to either minimize or maximize the output DOP for each PMD setting. Minimizing the output DOP enables testing of the worst-case total PMD effect, while maximizing the DOP turns the PMDPro™ into a PMD compensator, allowing the user to obtain optimized PMD values for PMD compensation. PMDPro™ can also perform PMD emulation by generating statistical PMD distributions. Finally, the polarization controller and polarimeters enable variable rate scrambling and deterministic polarization control functions, including trace generation and polarization stabilization at any SOP. PMDPro™ makes your PMD related systems testing simple, fast, and professional.

Specifications:

Operating Wavelength Range[1]	C band or L band		
Insertion Loss	5.0 dB (90 ps version) 5.5 dB (180 ps version)		
Input Power Range	-10 to 10 dBm		
Return Loss	50 dB		
PDL	0.45 dB typical (90 ps version) 0.5 dB typical (180 ps version)		
1st Order PMD Range	0 to 91 ps or 0.36 to 182.4 ps		
1st Order PMD Resolution		90 ps range	180 ps range
	Discrete mode	0.357 ps	0.714 ps
	Quasi-continuous mode	0.1 ps	0.2 ps
2nd Order PMD Range	2000 ps^2 (90 ps range) or 8100 ps^2 (180 ps range)		
PMD Variation Time	1 ms min.		
SOP Alignment Accuracy[2]	± 2°		
SOP Tracking Speed	10 π/s		
DOP Accuracy[2]	± 2%		
Optical Power Handling	300 mW min.		
Operating Temperature	10 to 50 °C		
Storage Temperature	-20 to 60 °C		
Communications Interfaces	USB, RS-232, Ethernet, and GPIB		
Front Panel Display	2 x 20 character LCD		
Power Supply	100 – 240 VAC, 50 – 60 Hz		
Dimensions	2U, 3/4 of 19" rack width 14" (L) x 14" (W) x 3.5" (H)		

Notes:
1. Standard option: C band.
2. At 23 ± 5°C.

Ordering Information:

PMD — 1000 — □ □ — □ — □

DGD Range:	Wavelength:	Connector Type:
90 = 90 ps	C = C band	FC/PC, FC/APC
18 = 180 ps	L = L band	SC/PC, or SC/APC

Features:

- 1st & 2nd order PMD source
- 1st & 2nd order PMD emulator
- Automatic polarization alignment
- Polarization scrambling
- PMD compensation
- Rapid PMD switching: 1 ms

Applications:

- System PMD tolerance test
- PMD compensator evaluation
- System PMD emulation
- Optimizing PMD values for PMDC
- PMD measurement instrument calibration

Related Products:

- PDL Source (PDLE-101)
- DGD and SOP Calibration Artifacts (CS-DGD/SOPMD)
- Polarization Measurement System (PSGA-101)
- Multifunction Polarization Controller (MPC-202, MPC-201)
- Polarimeter (PSY-201, POD-201)
- Fixed DGD (FDE-002)
- Rack Mount Kit (RCK-001)

Tech Info:

- Polarization Related Tests for Coherent Detection Systems
- In-service light path PMD (polarization mode dispersion) monitoring by PMD compensation
- Polarization Optimized PMD Source Applications
- Why Coherent Detection Systems May Fail at Compensating for Polarization Mode Dispersion

IMPAIRMENT EMULATION AND POLARIZATION CONTROL

Polarization Optimized PMD Source - PMDPro™ (PMD-1000)

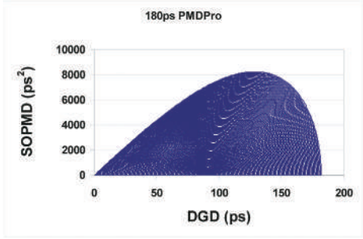

Figure 1. DGD and wavelength independent SOPMD range (180 ps PMDPro™)

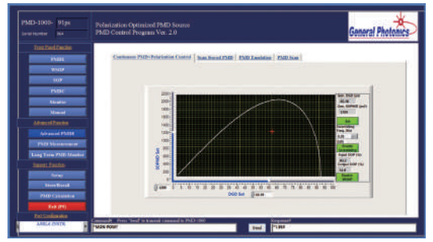

Figure 2. Quasi-continuous PMD control

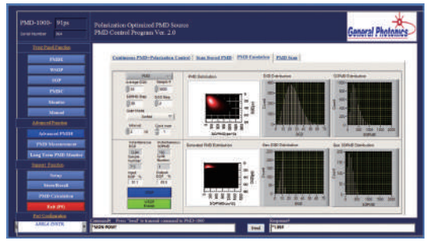

Figure 3. Maxwellian PMD emulation

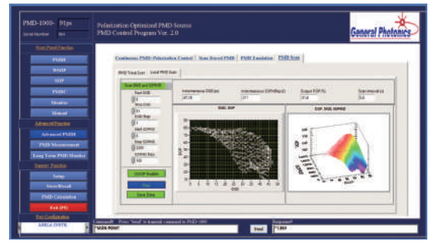

Figure 4. 3D graph display of a DGD/SOPMD scan

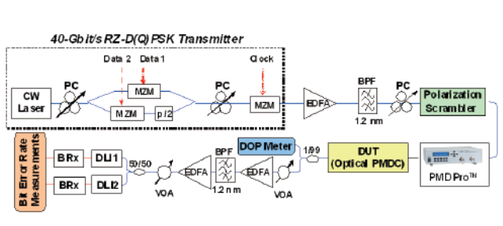

Figure 5. Experimental setup for PMD compensator performance test, using PMDPro™ as a PMD source to add DGD and SOPMD to the signal.

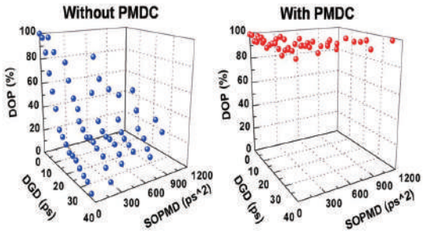

Figure 6. Measured DOP (without PMDC and with PMDC) of a 40-Gbit/s RZ-DQPSK signal versus DGD and SOPMD.

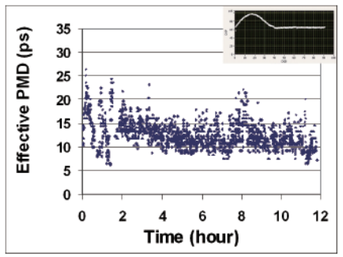

Figure 7. Long-term monitoring of PMD in an in-service link by PMDC. Instantaneous PMD vs. time.
Inset: DOP vs. DGD plot for a single measurement.

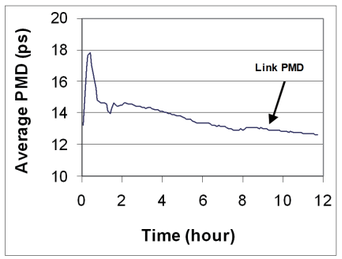

Figure 8. Long-term monitoring of PMD in an in-service link by PMDC. Average PMD vs. time.

IMPAIRMENT EMULATION AND POLARIZATION CONTROL

Polarization Dependent Loss Source/Emulator - PDLPro™ (PDLE-101)

High speed fiber optic transceivers, including those deploying coherent detection technology for 40Gb/s and 100Gb/s data transmission, must meet stringent PDL tolerance specifications. In addition, the PDL tracking speed and response time of the PDL mitigation algorithm of a coherent detection receiver must be quantified. The PDLE-101 is specially designed for such PDL-related tests. This PDL source/emulator can generate individual PDL values between 0 dB and 20 dB, with a resolution of 0.1 dB for PDL tolerance testing. It can also generate variable PDL with user defined range, waveform, and speed for PDL tracking speed and recovery time tests. The instrument can be controlled via the front panel keypad or by remote control via USB, RS-232, GPIB, or Ethernet interfaces. The residual PMD of the unit is less than 0.1 ps.

Specifications:

Wavelength Range[1]	C band or L band
Insertion Loss (max.)	2 dB at PDL = 0, excluding connectors
PDL Dynamic Range[2]	0.1 to 20 dB
PDL Resolution[2]	0.1 dB
PDL Accuracy[2]	± (0.1 dB +1% of PDL)
PDL Switching Time[3]	5 ms max., 1 ms typical
Residual PMD	< 0.1 ps at PDL = 0
Return Loss	> 50 dB
PDL Control	Front panel control or remote control with communication interface
PDL Waveforms	Sine, square, triangle, random
Fiber Type	SMF-28
Optical Connector Type	FC/PC, FC/APC, SC/PC, or SC/APC
Optical Power Damage Threshold	500 mW
Display	2 x 20 character LCD
Communication Interface	USB, RS-232, Ethernet, and GPIB
Operating Temperature	0 to 40 °C
Storage Temperature	-20 to 60 °C
Electrical Power Supply	100 – 240 VAC, 50 – 60 Hz (16W)
Dimensions	2U, 19" half rack width, 14" (L) x 8.5" (W) x 3.5" (H)

Notes:
1. Other wavelength ranges available upon request.
2. At 23 ± 5°C.
3. Rise time for square wave transition.

Features:

- Large PDL range
- High speed
- High PDL resolution
- Low residual PMD
- PDL scanning
- Random PDL generation

Applications:

- PDL tolerance test
- PDL tracking speed test
- PDL recovery time test
- PDL emulation
- Code development for PDL compensation in coherent systems
- System PDL response test

Related Products:

- PMD Source (PMD-1000)
- Polarization Measurement System (PSGA-101)
- Multifunction Polarization Controller (MPC-202, MPC-201)
- Polarimeter (PSY-201, POD-201)
- PDL Meter (PDL-201)
- Rack Mount Kit (RCK-001)
- PDL Calibration Artifact (CS-PDL)

Tech Info:

- Polarization Related Tests for Coherent Detection Systems

Ordering Information:

PDLE — 101 — □ — □

Wavelength Range:
C = C band
L = L band

Connector Type:
FC/PC, FC/APC,
SC/PC, SC/APC
Others specify

IMPAIRMENT EMULATION AND POLARIZATION CONTROL

Polarization Dependent Loss Source/Emulator - PDLPro™ (PDLE-101)

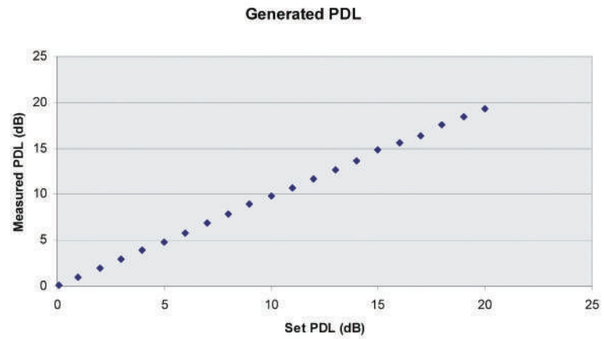

Figure 1. PDL generation accuracy: PDL generated by the PDLE-101 PDL Source/Emulator, measured using a PDL-101 PDL meter.

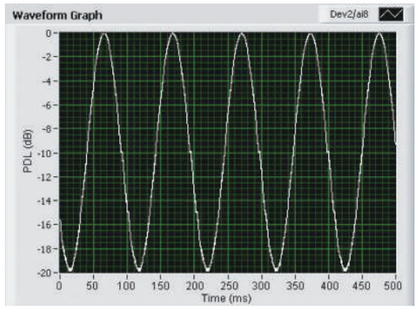

(a)

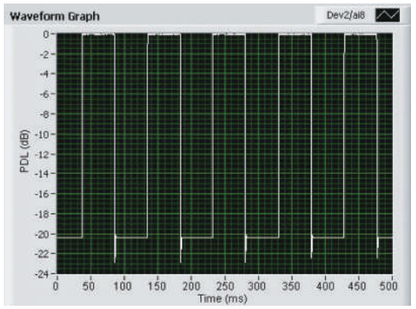

(b)

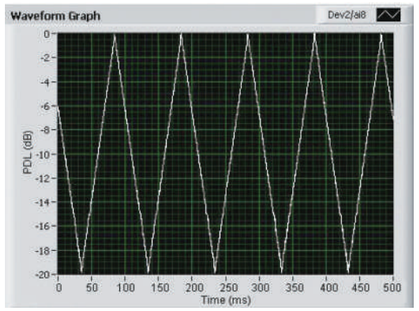

(c)

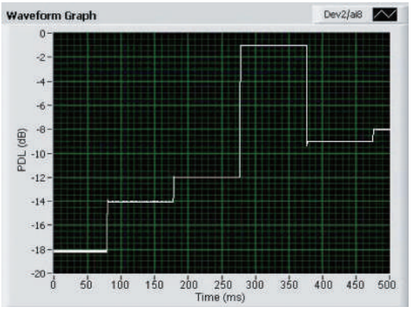

(d)

Figure 2. PDL variation functions for PDL tracking speed and recovery time tests: (a) Sine wave PDL variation (b) Square wave variation.(c) Triangle wave variation (d) Random-amplitude square wave variation.

IMPAIRMENT EMULATION AND POLARIZATION CONTROL

Advanced Multifunction Polarization Controller - PolaMight™ (MPC-202)

The MPC-202 is an advanced Multifunction Polarization Controller specially designed to meet the requirements of coherent receiver performance tests. It combines General Photonics' award winning PolaRite™ III polarization controller with proprietary polarization control algorithms to achieve a wide range of polarization control functionalities, including high speed quasi-uniform rate polarization scrambling, random-rate polarization scrambling with Rayleigh rate distribution, discrete-state polarization scrambling, sine, square, and triangle-wave SOP modulation, and manual polarization control functions. In particular, the "Tornado" quasi-uniform rate polarization scrambling function can achieve a high SOP scrambling rate of up to 60,000 revolutions/s (more than 360 krad/s) with a narrow rate distribution clustered around the highest rate. In short, the MPC-202 is an ideal tool for production or laboratory testing of polarization related functions and parameters, including passive/active component characterization, performance tests of fiber optic interferometers, sensor systems, RF photonics systems, etc. The quasi-uniform rate high speed scrambling function is particularly useful for SOP tracking speed testing of coherent receivers. The square wave SOP modulation function is ideal for SOP recovery time tests.

Specifications:

Operating Wavelength Range	1260 to 1620nm (standard) or 980 to 1310nm
Polarization Scrambling	Tornado (quasi-uniform rate distribution): 0.00 to 60,000 revolutions/s. Rayleigh rate distribution: 0.00 to 2000 rad/s (mean) Triangle: 0.00 to 2000 × 2π rad/s Discrete random states: 0.00 to 20,000 points/s
Agilent 11896A Scrambling Emulation	Speed settings 1-8, matched to Agilent 11896A settings
Manual polarization Control	# of channels: 4 Range: 0 – 4π each channel
Polarization Modulation (Each Channel)	Waveforms: Sine, Triangle, Square Frequency: 0.00 to 1000 Hz Amplitude: 0 to 3π peak-to-peak
Slew Rate for Square Wave SOP Modulation	360 krad/s (10% to 90%, channel 3)
External Trigger Mode	Random SOP per TTL trigger pulse, up to 20,000 points/s
Insertion Loss	< 0.6 dB with connectors (< 0.15 dB intrinsic)
PDL	< 0.1 dB with connectors (< 0.02 dB intrinsic)
Activation Loss	< 0.1 dB with connectors
Return Loss	> 50 dB with connectors (> 65 dB intrinsic)
PMD	< 0.2 ps with connectors
Optical Power Handling	1000 mW
Operating Temperature	0 °C to 50 °C
Storage Temperature	-20 °C to 70 °C
Communication Interfaces	USB, Ethernet, RS-232, and GPIB
Electrical Triggers	Connectors: BNC Output trigger: TTL pulse per SOP generated in discrete scrambling mode Input trigger: One random SOP generated per TTL pulse received in trigger mode
Front Panel Display	OLED graphic display
Power Supply	100 – 240 VAC, 50 – 60 Hz
Dimensions	2U, ¾ 19" rack width 14" (L) x 14" (W) x 3.5" (H)

Note:
Specifications in this table apply for the standard 1260 to 1620nm version over a temperature range of 23 ± 5°C.

Features:

- Quasi-uniform rate SOP scrambling with SOP change rate up to 360 krad/s
- Scrambling with Rayleigh rate distribution
- Discrete SOP scrambling
- SOP modulation
- Low IL, PDL, PMD, and AL
- Bright OLED display

Applications:

- SOP response test of coherent receivers
- SOP tracking speed test
- SOP recovery time test
- Polarization deMux performance test
- PMD and PDL related tests

Related Products:

- PMD Source (PMD-1000)
- PDL Source (PDLE-101)
- Polarization Measurement System (PSGA-101)
- Multifunction Polarization Controller (MPC-201)
- Polarimeter (PSY-201, POD-201)
- Rack Mount Kit (RCK-001)
- Components

Tech Info:

- Combat Polarization Impairments with Dynamic Polarization Controllers
- Polarization Related Tests for Coherent Detection Systems
- A novel scheme for achieving quasi-uniform rate polarization scrambling at 752 krad/s

FAQ:

- Dynamic Polarization Controllers

IMPAIRMENT EMULATION AND POLARIZATION CONTROL
Advanced Multifunction Polarization Controller - PolaMight™ (MPC-202)

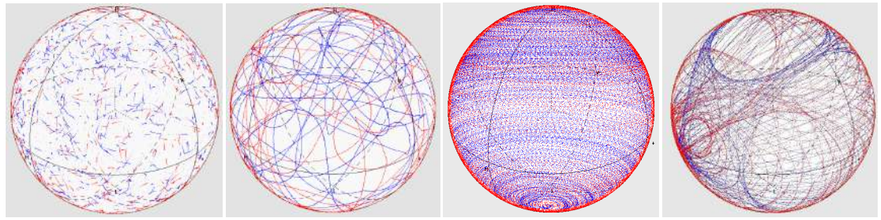

(a) (b) (c) (d)

Figure 1. Poincaré sphere SOP traces for four different scrambling methods: (a) Discrete, (b) Typical Rayleigh or Triangle trace, (c) Tornado (fixed axis), and (d) Tornado (rotating axis).

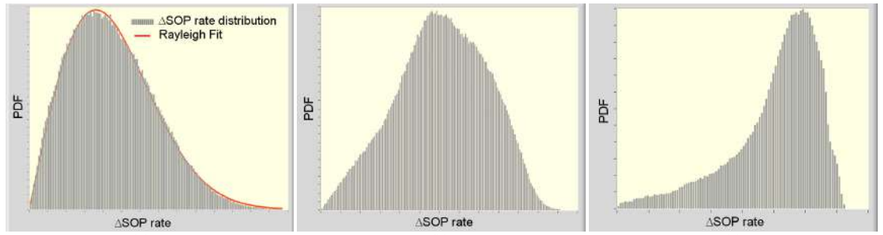

(a) (b) (c)

Figure 2. SOP variation rate distributions for (a) Rayleigh, (b) Triangle, and (c) Tornado scrambling methods.

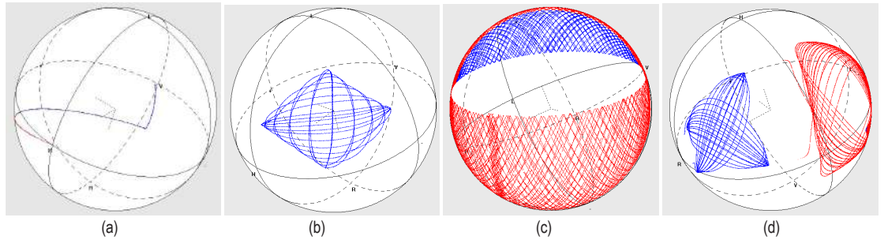

(a) (b) (c) (d)

Figure 3. (a) Manual adjustment of SOP from H to V state. (b-d) SOP patterns generated in polarization modulation mode using different combinations of waveforms on different channels of the polarization controller.

Ordering Information:

MPC — 202 — □ — □

Wavelength Range:
1 = 1260 – 1620nm
2 = 980 – 1310nm

Connector Type:
FC/PC
FC/APC
Others specify

Video:

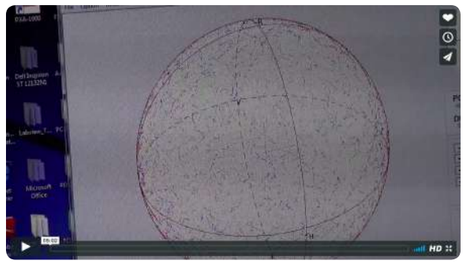

Multifunction Polarization Controller - PolaMight™ (MPC-201)

Controlling the state of polarization (SOP) of an optical signal has never been easier: This multifunction polarization controller has four operational modes for complete polarization control: variable rate polarization scrambling, manual polarization adjustment, polarization modulation, and externally triggered random SOP generation. Four different polarization scrambling methods enable the SOP to a) trace out a spiral pattern about a static or rotating axis with a nearly uniform SOP variation rate for system stress tests (Tornado scrambling); b) generate a continuous trace with a Rayleigh distribution of SOP variation rate, for emulation of the SOP variation in a fiber link (Rayleigh scrambling); c) generate a continuous trace with uniform sphere coverage for PDL measurement (Triangle scrambling); or d) evenly cover the Poincaré sphere with discrete, random points at a uniform rate (Discrete scrambling). In the SOP modulation mode, each polarization control axis can be selectively controlled with a sine, square, or triangle wave of user defined frequency and amplitude. Each polarization control axis can also be controlled manually, by setting the input voltage either from the front panel controls or through a remote control interface. In externally triggered scrambling mode, discrete, random SOPs are generated in response to a trigger input, a feature desirable for recirculating loop applications or other applications requiring synchronization with other devices. Finally, the MPC-201 can emulate the Agilent 11896A polarization scrambler function, allowing it to act as a plug-in replacement for this popular but discontinued device, while offering many more advanced features. PolaMight puts the user in control.

Specifications:

Operating Wavelength Range	1260 to 1620 nm (standard) or 980 to 1310 nm
Polarization Scrambling	Discrete random states: 0.00 to 20,000 points/s Triangle: 0.00 to 2000 x 2π rad/s Rayleigh rate distribution: 0.00 to 2000 rad/s (mean) Tornado (quasi-uniform rate distribution): 0.00 to 2000 revolutions/s.
Agilent 11896A Scrambling Emulation	Speed settings 1 – 8, matched to Agilent 11896A settings
Manual Polarization Control	# of channels: 4 Range: 0 – 4π each channel
Polarization Modulation (Each Channel)	Waveforms: Sine, Triangle, Square Frequency: 0.00 to 1000 Hz Amplitude: 0 to 3π peak-to-peak
External Trigger Mode	Random SOP per TTL trigger pulse, up to 20,000 points/s
Insertion Loss	< 0.5 dB with connectors (< 0.1 dB intrinsic)
PDL[1]	< 0.05 dB with connectors
Activation Loss[1]	< 0.05 dB with connectors
Return Loss	> 50 dB with connectors (> 65 dB intrinsic)
PMD	< 0.1 ps with connectors
Optical Power Handling	1000 mW
Operating Temperature	0 °C to 50 °C
Storage Temperature	-20 °C to 70 °C
Communication Interfaces	USB, Ethernet, RS-232, and GPIB
Electrical Triggers	Connectors: BNC Output trigger: TTL pulse per SOP generated in discrete scrambling mode Input trigger: One random SOP generated per TTL pulse received in trigger mode
Front Panel Display	OLED graphic display
Power Supply	100 – 240 VAC, 50 – 60 Hz
Dimensions	2U, 19" half rack width 14" (L) x 8.5" (W) x 3.5" (H)

Notes:
Specifications in this table apply for the standard 1260 to 1620nm version over a temperature range of 23 ± 5 °C.
1. A low PDL/activation loss version (0.01 dB intrinsic) is available upon request for PDL measurement applications.

Features:

- Multiple polarization control modes
- Tornado scrambling (quasi-uniform rate distribution)
- Real fiber SOP variation emulation (Rayleigh rate distribution)
- Discrete SOP scrambling
- Agilent 11896A scrambling emulation
- SOP modulation
- Low IL, PDL, PMD, and AL
- Bright OLED display

Applications:

- SOP variation emulation
- PMD emulation
- Polarization scrambling
- System polarization studies
- PDL/DOP measurement
- Recirculating loop studies

Related Products:

- Polarization Measurement System (PSGA-101)
- Multifunction Polarization Controller (MPC-202)
- Polarimeter (PSY-201, POD-201)
- Rack Mount Kit (RCK-001)
- Components

Tech Info:

- What is Polarization?
- Polarization in Fiber Systems: Squeezing out More Bandwidth
- Combat Polarization Impairments with Dynamic Polarization Controllers

FAQ:

- Polarization Controllers

IMPAIRMENT EMULATION AND POLARIZATION CONTROL

Multifunction Polarization Controller - PolaMight™ (MPC-201)

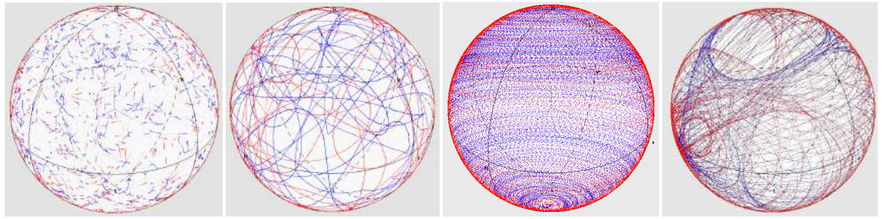

Figure 1. Poincaré sphere SOP traces for four different scrambling methods: (a) Discrete, (b) Typical Rayleigh or Triangle trace, (c) Tornado (fixed axis), and (d) Tornado (rotating axis).

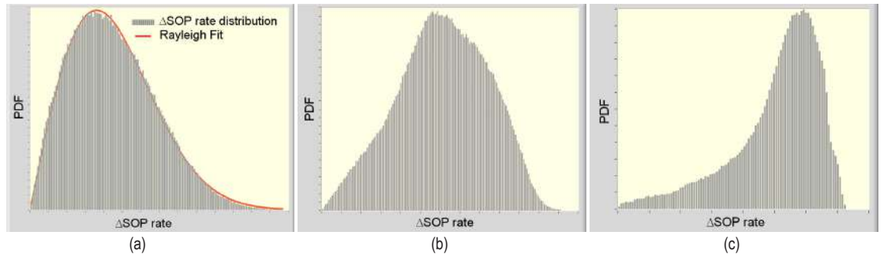

Figure 2. SOP variation rate distributions for (a) Rayleigh, (b) Triangle, and (c) Tornado scrambling methods.

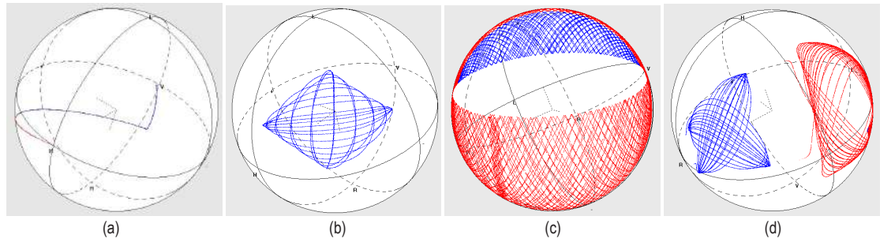

Figure 3. (a) Manual adjustment of SOP from H to V state. (b-d) SOP patterns generated in polarization modulation mode using different combinations of waveforms on different channels of the polarization controller.

Ordering Information:

MPC — 201 — □ — □

Wavelength Range:
1 = 1260 – 1620nm
2 = 980 – 1310nm

Connector Type:
FC/PC
FC/APC

IMPAIRMENT EMULATION AND POLARIZATION CONTROL

Programmable Optical Delay Generator - TimeRITE™ (ODG-101)

Generating programmable time delay from nanoseconds to milliseconds is important for various applications ranging from data center testing to wireless communications to radar, optical communications, and measurement systems. General Photonics' TimeRITE™ programmable optical delay generator is the first such product on the market. With a total delay range up to 2 ms (600 km) and a delay resolution up to 12 bits, this easy-to-use instrument features low insertion loss (~0.6 dB per bit), low delay dependent loss (DDL<0.2 dB), low polarization dependent loss, and fast delay changing speed (<10 ms). When operating in manual mode, different delay values can be selected and stepped up and down using the front panel thumb wheel. When in auto mode, the instrument scans through a set of delays with user-defined range, starting and stopping values, step size, and time interval between delay changes. The instrument also features double-pass and quadruple pass modes to increase the total delay range by passing light through the optical path multiple times. A polarization maintaining option is also available for the double-pass input and output ports. Access ports for connecting to optical amplifiers are available upon request. By connecting a fiber optic RF or digital transmitter at the input and a fiber optic RF or digital receiver at the output, programmable delay for RF or digital signals can be readily obtained. This instrument can also be used to emulate signal delay and chromatic dispersion in fiber communication systems. At General Photonics, we manage delay to make your timing right.

Specifications:

Operating Wavelength Range	1310 ± 30 or 1550 ± 30nm
Optical Delay Range[1]	Up to 2 ms or 600 km in vacuum for quadruple pass (150km single-pass). User selectable at time of purchase.
Optical Delay Resolution	4 to 12 bits, user selectable at time of purchase
Minimum Delay Step Size	1 ns or 30 cm in vacuum, single pass
Optical Delay Accuracy[2]	±5 meter in vacuum, single pass
Delay Change Speed	10 ms
Delay Switching Frequency	< 50 Hz
Residual Optical Delay	2m + 0.5m per bit
Insertion Loss[3,4,5]	0.6 dB per bit plus 0.3 dB/km for single pass ports 2x single pass IL + 1.5 dB for double pass option 4x single pass IL + 5.5 dB for quadruple pass option
Delay Dependent Loss	0.2 dB, single pass
PDL	0.2 dB single pass, less for double & quadruple pass
Return Loss	55 dB, excluding contributions from fiber Rayleigh and Brillouin scatterings (for transmission mode)
Extinction Ratio	> 18 dB for double-pass ports with PM option
Optical Power Damage Threshold	300 mW
Operating Temperature	0 to 40 °C
Storage Temperature	-20 to 60 °C
Fiber Type (Delay Fiber)	SMF-28 compatible
Fiber Type (Double Pass Port Input/Output Fiber)	SMF-28 or PM Panda fiber
Power Supply	100 – 240 VAC, 50 – 60 Hz
Control Interface	USB, RS-232, Ethernet, DB25
Dimensions	19" rack mount, 20" depth; height depends on delay length (3U height for up to 0.125 ms delay, single pass)

Notes:
1. Double-pass option can use both single and double-pass optical paths. Quadruple-pass option is intended for applications that require extremely long delays, and includes quadruple-pass optical path only.
2. For total delay less than 20 km.
3. With SMF-28 fiber for delay path.
4. Double pass: input can be SM or PM.Quadruple pass: PM input only.
5. Excluding connectors.

Features:

- Data rate & data format independent
- Compact size & high resolution
- Large delay range
- Low insertion loss
- Fast delay switching speed
- Low delay dependent loss

Applications:

- Data center time delay & jitter impact testing
- Cloud computing delay & jitter impact testing
- Wireless base station delay test & calibration
- Radar range calibration
- RF link emulation
- Laser linewidth & phase noise measurement

Related Products:

- Components

Tech Info:

- Programmable optical delay generator with uniform output and double-delay capability

FAQ:

- Delay Lines

Ordering Information:

ODG — 101 — □□ — ▭ — □ — □□ — □□ — □□ — ▭

- **Resolution (# bits):** 4 - 12
- **Delay Range:** (single pass, in µs): 0 - 500
- **Multi-Pass Option:** 1 = single, 2 = double, 4 = quadruple
- **Wavelength:** 13 = 1310, 15 = 1550
- **Fiber Type:** (double pass input/output fiber): SS = SM, PP = PM, 00 = no double-pass
- **Connector Type:** FC/PC, FC/APC

IMPAIRMENT EMULATION AND POLARIZATION CONTROL

Polarization Scrambler - PolaMix™ (PCD-104)

General Photonics' Polarization Scrambler uses a breakthrough all-fiber technology to effectively randomize polarization states. Depolarizing by polarization scrambling has many important applications. Scrambling the input polarization can eliminate measurement uncertainties caused by the polarization sensitivity of the testing device. Performance degradation due to polarization dependent gain (PDG) induced in optical amplifiers can also be suppressed by polarization scrambling. In addition, polarization scrambling can be used in systems to facilitate and simplify PMD monitoring. Based on a patented, award-winning all-fiber technology, the PCD-104 delivers superior performance, including extremely low insertion loss, back reflection, and residual phase and amplitude modulation.

Specifications:

Insertion Loss[1]	< 0.05 dB (without connectors) < 0.6 dB (with connectors)
Center Operating Wavelength[2]	λ range 1: 1310, 1480, 1550, 1600nm λ range 2: 980, 1060, 1310nm
Operating Wavelength Range[3]	> 100 nm
Output Degree of Polarization[4,5]	< 5%
Average PMD	< 0.05 ps
Intrinsic PDL	< 0.05 dB
Optical Return Loss	> 65 dB (without connectors)
Optical Power Handling	> 1000 mW
Residual Amplitude Modulation	< ±0.01 dB
Residual Phase Modulation	< 0.1π
Power Supply	100 – 240 VAC, 50 – 60 Hz
Power Consumption	12 W typical
Scrambling Frequencies[4]	Factory set 4 fixed frequencies distributed between DC and > 700 kHz
Communication Interfaces	RS-232, Ethernet, GPIB
Operating Temperature	10 to 45 °C
Storage Temperature	-10 to 50 °C
Dimensions	2U, 19" half rack width, 14" (L) x 8.5" (W) x 3.5" (H)

Notes:
1. For SMF-28 compatible fiber. Other fibers may have higher loss, especially wtih connectors.
2. Please note that the fiber used determines the operating wavelength range. The standard fiber covers wavelengths in the 1260 to 1620 nm range. The PCD-104 can also be configured to cover the 980 to 1310 nm range using a different fiber. This fiber can handle wavelengths up to 1650nm, but if it is coupled to SMF-28 fiber, the performance may not be quite as good as normal due to mode mismatch. Please contact General Photonics for details.
3. Center wavelength ±50 nm.
4. At 500Hz detection bandwidth.
5. Measured by a photodetector at the PCD-104 output using a spectrum analyzer. A polarizer is placed in front of the photodetector to convert polarization modulation to amplitude modulation.

Features:

- Minimal Insertion Loss and Back Reflection
- Low Residual Phase and Amplitude Modulation
- Built-in RS-232,GPIB and Ethernet ports
- Remote Operation Wavelength Control

Applications:

- PDG Mitigation
- Elimination of Polarization Sensitivity
- Facilitating PMD Emulation
- Facilitating PMD Compensation
- Facilitating PDL Measurement

Related Products:

- Polarization Scrambler Modules (PCD-003, PCD-005)
- Rack Mount Kit (RCK-001)
- Components

Tech Info:

- Scrambling to Minimize Polarization Related Impairments

FAQ:

- Scramblers

Ordering Information:

PCD — 104 — □ — ▭

- **Wavelength Range:** 1 = 1260 - 1620nm, 2 = 980 - 1310nm
- **Connector Type:** FC/PC, FC/APC, SC/PC, SC/APC, Others specify

Note:
See PCD-005 spec sheet for typical performance data.

Reset-Free Polarization Stabilizer - PolaStay™ (POS-20X)

PolaStay™ polarization stabilizers actively maintain a stable output state of polarization (SOP) against rapid input SOP fluctuations, compensating for an input polarization discontinuity in as fast as 5 ms, or tracking without resets against a continuous input SOP rotation of up to 32π/s. This unique family of products combine General Photonics' polarization controller, in-line polarization monitor, and proprietary algorithm to find and maintain the target SOP. The instrument's output fiber can be either single mode fiber or PM fiber with the output polarization aligned to its slow axis. When a polarizer is placed at the output, the maximum power fluctuation caused by input polarization fluctuation is less than 0.1 dB. These instruments can be used to eliminate polarization fluctuations in fiber systems, suppress noise figure in optical amplifiers, reduce PDL effects, demultiplex polarization division multiplexed channels, and eliminate polarization fading in coherent communication and fiber sensor systems. The POS-20X features a bright OLED display for easy setup and optimization of operation parameters such as control step size, feedback delay, activation threshold, and minimum or maximum search. It can accept either optical or electrical feedback. The POS-20X line includes 3 different configurations (X=2, 3, or 4) to meet different application requirements.

Specifications:

Operating Wavelength Range[1]	calibrated wavelength ± 50nm standard
Calibrated Wavelengths	1550, 1310, 1060nm
SOP Recovery Time	< 5 ms (1.5 ms typical)
SOP Rotation Tracking Speed[2]	32 π/s, endless tracking & reset free
SOP Accuracy[3]	< 0.1 dB (PM output fiber)
Repeatability[3]	< 0.1 dB
Insertion Loss	0.8 dB typical, 1.2 dB max. (POS-202) 0.1 dB intrinsic, < 0.5 dB with connectors (POS-203 polarization controller optical path)
Return Loss	> 50 dB
Isolation in Orthogonal Polarization	20 dB
Minimum Optical Input	-30 dBm (POS-202) -35 dBm (POS-203 optical feedback)
Optical Power Handling[4]	20 dBm (POS-202) 30 dBm (POS-203 polarization controller input) 6 dBm (POS-203 optical feedback input)
Operating Temperature	0 to 50 °C
Storage Temperature	-20 to 70 °C
Front Panel Display	OLED graphic display
Electrical Feedback	BNC connector to accept 0 – 4.5 V analog voltage
Power Supply	100 – 240 VAC, 50 – 60 Hz
Communication Interfaces	USB, Ethernet, RS-232, and GPIB
Dimensions	2U 19 inch half rack width 14" (L) x 8.5" (W) x 3.5" (H)

Notes:
Specifications listed in table apply for standard 1310 or 1550nm operation at 23±5 °C.

1. For standard versions with PM outputs. Other wavelength ranges are available. Specifications may be different for instruments with different wavelength or power ranges or different output fibers.
2. For input power >-25 dBm for POS-202, or optical feedback signal >-35 dBm for POS-203 and POS-204.
3. The output power fluctuation caused by SOP fluctuation after passing through a polarizer.
4. Standard version. Higher power ranges may be possible by special request.

Ordering Information:

POS — 20 — □ — □ □ — □

# Ports:	Calibrated Wavelength:	Connector Type:
2	15 = 1550nm	FC/PC
3	13 = 1310nm	FC/APC
4	10 = 1060nm	Others Specify

Features:

- Reset free operation
- 5 ms recovery time
- 32π/s tracking speed
- Front panel control parameter setup
- Low insertion loss

Applications:

- Optical amplifier polarization stabilization
- Polarization demultiplexing
- Elimination of polarization fading
- Coherent communication

Related Products:

- Polarization Tracker Module (POS-002)
- Rack Mount Kit (RCK-001)
- Components

Tech Info:

- What is Polarization?
- Combat Polarization Impairments with Dynamic Polarization Controllers

FAQ:

- Stabilizer

IMPAIRMENT EMULATION AND POLARIZATION CONTROL

Reset-Free Polarization Stabilizer - PolaStay™ (POS-20X)

Function Diagrams:

POS-202 (2 optical ports)

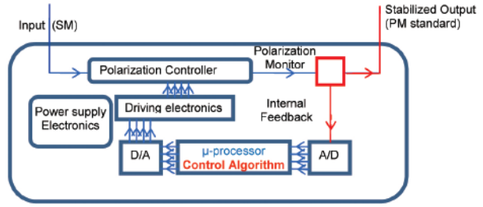

POS-202: The instrument has two optical ports on the front panel for input and output. It has an internal polarization monitor. It stabilizes output polarization to its internal reference state (linear, aligned to slow axis of output PM fiber).

POS-203 (3 optical ports)

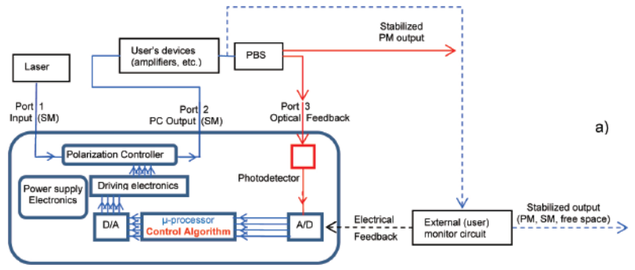

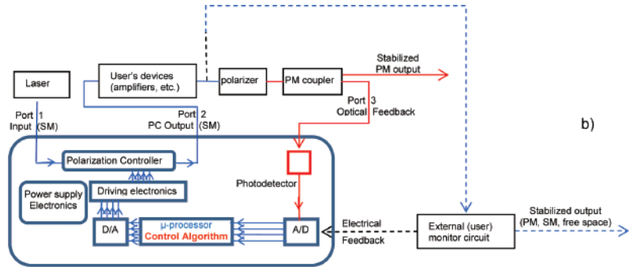

POS-203: The instrument has three optical ports on the front panel for input, output, and an external optical feedback signal. It also has an electrical port to accept an external electrical feedback signal. Either the optical or electrical feedback signal can be used for stabilizer control. The polarization controller tunes the output polarization to maximize or minimize the selected feedback signal. Diagram a) shows a sample setup for minimum search, in which a PBS is used to monitor the output polarization from the user device. Diagram b) shows a sample setup for maximum search, in which a polarizer followed by a PM coupler is used to monitor the output polarization from the user device. In both cases, the resulting optical monitor signal is fed back to port 3 on the front panel of the stabilizer. The user can also use his own optical/electrical polarization monitoring circuit to generate an electrical feedback signal to control the stabilizer. In this case, the optical path follows the blue dotted line, and the electrical feedback signal is connected to the corresponding BNC connector on the rear panel of the stabilizer.

POS-204 (4 optical ports)

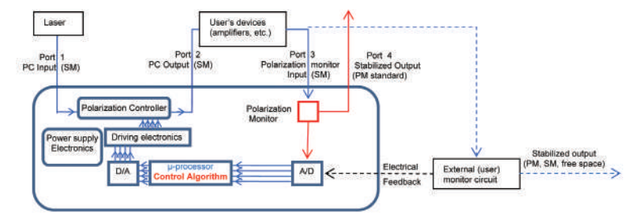

POS-204: The instrument has four optical ports on the front panel for polarization controller input and output, and for polarization monitor input and output. As with the POS-203, there is also an electrical port to accept an external electrical feedback signal from a user's own external monitor circuit. In this case, the optical path follows the blue dotted line, and the electrical feedback signal is connected to the corresponding BNC connector on the rear panel of the stabilizer. Either the optical or electrical feedback signal can be used for stabilizer control. The polarization controller tunes the output polarization to maximize or minimize the selected feedback signal.

Reset-Free Polarization Stabilizer - PolaStay™ (POS-20X)

Typical Performance Data:

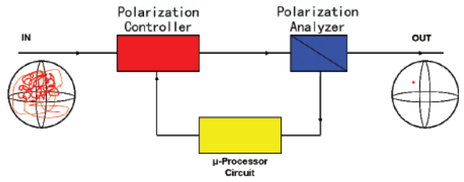

Figure 1. PolaStay™ polarization stabilizer function diagram.

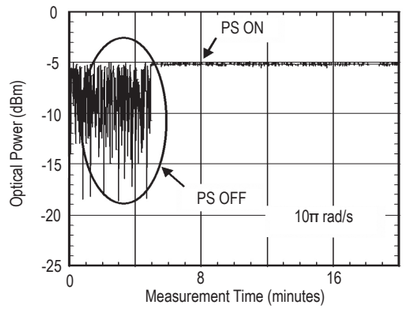

Figure 2. Polarization stabilization against endless half-wave plate rotation at 10π rad/s

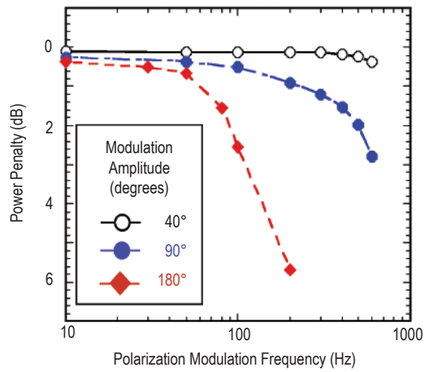

Figure 3. Polarization stabilization against sinusoidal polarization modulation.

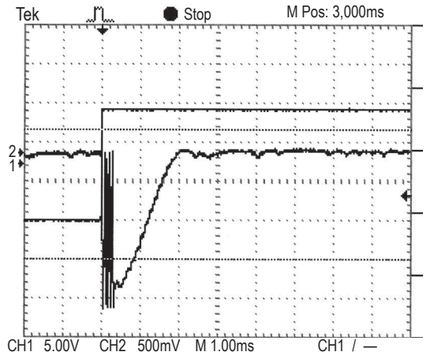

Figure 4. Polarization stabilization against a step polarization change.

Light Sources

Superluminescent Diode Light Source (SLD-101S) 52
Tunable Laser Source (TLS-101) 53

LIGHT SOURCES

Superluminescent Diode Light Source (SLD-101S)

The SLD-101S is a highly stable superluminescent light source designed specifically for OCT, sensor and test & measurement applications. During operation, both the current and temperature are accurately controlled for superb power and spectral stabilities. The output power and diode temperature are stabilized to 0.02 dB and 0.05°C respectively. The light source has three available operation modes: constant current, constant power (optional), and modulated power. The modulation can be either external or internal, with different waveforms (sine or square) and different speeds (up to 100 kHz). One unique feature is that users can select either low or high degree of polarization (DOP) options for specific applications. Other user-selectable options include output fiber type (SM or PM), center wavelength, spectral width, and output power. Finally, the SLD-101S comes with USB, RS-232, Ethernet, and GPIB communication ports for easy, flexible interface with computers and other instruments. It is an ideal source for OCT, fiber sensors, fiber gyros, PM patch cord extinction ratio (ER) measurement, and general-purpose test and measurement.

Specifications:

Center Wavelengths[1]	1310 nm	1550 nm
Output Power[1]	10 mW typical	10 mW typical
Spectral Width[1]	> 30 nm	> 40 nm
Short Term Optical Power Stability[2] Long Term Stability	±0.02 dB over one hour ±0.05 dB over 8 hours	
DOP	Low DOP option: < 5%, 2% typical High DOP option: > 95% Neutral: no specific DOP requirement	
PER[3]	> 18 dB for PM output option with high DOP	
Temperature Stability	0.05 °C	
Temperature Setting Range	10 to 40 °C	
Internal Modulation Waveforms & Speed	Sine: 0 – 200 Hz Square: 0 – 2 kHz	
External Modulation Speed	DC to 100 kHz	
External Modulation Connector	BNC	
Display	2 x 20 character LCD display	
Connector Type	FC/PC, FC/APC, SC/PC, SC/APC	
Operating Temperature	0 to 50 °C	
Storage Temperature	-20 to 65 °C	
Communication Interface	USB, Ethernet, RS-232, and GPIB	
Electrical Power Supply	100 – 240 VAC, 50 – 60 Hz	
Dimensions	2U 19" half rack width 14" (L) x 8.5" (W) x 3.5" (H)	

Notes:
1. Other options available. Contact General Photonics for details.
2. Stability specs listed apply to standard configuration with neutral DOP at an output larger than 80% of the maximum output power or driving current. Other options, such as low DOP, high DOP or high PER, may degrade stability.
3. High ER polarizer (ER > 35 dB) with long PM pigtails available. Contact General Photonics for details.

Features:

- Extremely power stable
- Extremely temperature stable
- Internal and external modulation options
- Low and high DOP options

Applications:

- Optical coherence tomography (OCT)
- Fiber sensors
- Fiber gyros
- Test and measurement
- Component and system QA
- R&D

Related Products:

- Rack Mount Kit (RCK-001)
- Components

Tech Info:

- Optical Coherence Tomography Technologies

Ordering Information:

SLD — 101S — □ — □□ — □□ — □□ — □□ — □□ — □□

DOP Option:	Wavelength:	Bandwidth (nm)	Power (mW)	Output Fiber Type:	Connector Type:
1 = low DOP 2 = high DOP 3 = neutral	13 = 1310 nm 15 = 1550 nm			SM PM	FC/PC, FC/APC SC/PC, SC/APC

LIGHT SOURCES

Tunable Laser Source (TLS-101)

The TLS-101 is a compact tunable laser source for daily test and measurement applications. The laser can be step-tuned across the C or L band communication channels with a tuning resolution of 50 GHz in less than 20 ms. The internal wavelength locker assures that the wavelengths or frequencies of the output light are exactly on the ITU grid of the DWDM channels. The light source has three operation modes: fixed wavelength output for the user to select a static wavelength or frequency output, single-trip wavelength (frequency) scan with a user-set range, step, and speed, and round-trip frequency scan. Finally, the TLS-101 comes with USB, RS-232, Ethernet, and GPIB communication ports for easy, flexible interface with computers and other instruments. In particular, the Ethernet port allows the instrument to be controlled remotely, from home, office or a hotel room when on travel. The TLS-101 is an ideal source for WDM component testing, sensor interrogation, optical coherence tomography (OCT), PMD and PDL characterization, and for use in general purpose test and measurement applications.

Specifications:

Wavelength/Frequency Tuning Range		C band 1528.77 to 1563.86nm 191.7 to 196.1THz	L band 1568.77 to 1607.47 nm 186.5 to 191.1 THz
Number of ITU Channels		89	93
Tuning Resolution (Minimum Tuning Step)		50 GHz	50 GHz
Optical Power		13 dBm	10 dBm
Power Ripple		0.3 dB typical 0.5 dB max. } over tuning range	
Side Mode Suppression Ratio (SMSR)		> 40 dB	
Output Linewidth (Lorentz)		< 5 MHz (1MHz typical)	
Average Relative Intensity Noise (RIN)	(10 MHz -1GHz)	< -110 dB/Hz	
	(1-10GHz)	< -145 dB/Hz	
OSNR (0.1nm Bandwidth)		> 50 dB	
Polarization Extinction Ratio		> 20 dB	
Return Loss		> 40 dB	
Locked Frequency Accuracy		-1.8 to 1.8 GHz	
Shuttered Output Power		< -30 dBm	
Tuning Speed		20 ms for adjacent channels	
Operating Mode		Single wavelength output; Single trip & round trip wavelength scanning	
Operating Temperature		5 to 50 °C	
Storage Temperature		0 to 70 °C	
Output Optical Interface		PM, FC/APC connector	
Communication Interface		USB, Ethernet, RS-232, and GPIB	
Electrical Power Supply		100 – 240 VAC, 50 – 60 Hz	
Dimensions		2U 19" half rack width 14" (L) x 8.5" (W) x 3.5" (H)	

Features:

- Fast tuning speed (20 ms)
- High output power
- ITU grid locking
- Ethernet interface for remote control
- GPIB, USB, and RS-232 interfaces for flexibility

Applications:

- WDM component testing and QA
- Fiber sensors
- PMD and PDL measurement
- Test & measurement
- Optical coherence tomography (OCT)
- R&D

Related Products:

- Rack Mount Kit (RCK-001)
- Components

Ordering Information:

TLS — 101 — □

Wavelength:
C = C band
L = L band

MODULES

Active Polarization Modules

Passive Polarization Modules

Active Timing/Delay Modules

Passive Timing/Delay Modules

Detectors

Active Polarization Modules

Reset-Free Polarization Tracker - PolaStay™ (POS-002) 56

Polarization Scrambler Module with Microprocessor Controller (PCD-005) 59

Polarization Scrambler Module (PCD-003) 61

Miniature Polarization Scrambler Module (PSM-002) 62

Micro Polarization Controller (PSM-003-C) 63

Micro Polarization Scrambler (PSM-003-S) 64

High Speed In-line Polarimeter - PolaDetect™ (POD) 65

High-Speed Polarization State Generator - PolaPal™ (PSG-001) 67

Dynamic Polarization Controller with Miniature Piezo Driver Card (PCD-M02) 68

Multimode Scrambler - SpeckleFree™ (MMS-201) 69

Mini Dynamic Polarization Controller - PolaRITE™ III (MPC-3/4X) 72

Polarization Switch - PolaSwitch™ (PSW-002) 75

Pigtailed Polarization Controller - PolaRITE™ (PLC-002/M02) 76

Drop-in Polarization Controller - PolaRITE™ (PLC-003/006) 77

Fully Connectorized Polarization Controller - PolaRITE™ (PLC-004/005) 78

Reset-Free Polarization Tracker - PolaStay™ (POS-002)

The PolaStay™ polarization tracker automatically adjusts the state of polarization (SOP) towards a reference SOP, counteracting continuous input SOP variations as fast as 0.9 ms with no resets. The reference SOP is determined by a feedback signal which can be provided either internally or externally. The internal feedback version (POS-002-I) consists of a fiber squeezer polarization controller, in-line polarization monitor, digital and analog circuits, and proprietary algorithm. The error signal from the polarization monitor is fed back to the polarization controller to maintain a linear SOP at the output. The external feedback version (POS-002-E) replaces the internal polarization monitor with an external analog electrical feedback signal of the user's choice, such as a voltage proportional to the degree of polarization (DOP) measured by a polarimeter, the bit-error rate (BER) from a BER chip, the RF spectrum of a detected signal, or the optical power after a polarizer. Depending on the version chosen, the output fiber is either single mode fiber (POS-002-E) or PM fiber with the SOP aligned to its slow axis (POS-002-I). This module can be used for PMD compensation, polarization division demultiplexing, elimination of polarization fading in coherent detection and fiber sensor systems, suppression of noise figure in optical amplifiers, and reduction of PDL effects.

Specifications:

Operating Wavelength Range[1]	1060, 1310 or 1550 ± 50 nm
SOP Recovery Time	< 3 ms (0.9 ms typical)
SOP Rotation Tracking Speed (Reset Free)	47 π/s
SOP Accuracy[2]	< 0.1 dB
Repeatability[2]	< 0.1 dB
Insertion Loss	Internal feedback: 0.8 dB typical, 1.2 dB max. External feedback: < 0.1 dB
Return Loss	> 50 dB
Isolation in Orthogonal Polarization	20 dB
Optical Input Power	-20 dBm to 20 dBm standard for 1310 or 1550nm internal feedback version, -18 to 20 dBm for 1060nm internal feedback version (low power option available)
External Feedback Voltage	0 to 4.6 volts for external feedback version
Optical Power Handling	20 dBm max., higher possible
Optical Power Damage Threshold	300 mW
Operating Temperature	0 to 70 °C
Storage Temperature	-20 to 70 °C
Power Supply	+12 VDC / 0.5A -12 VDC / 0.15A
Communications Interface[3]	RS-232
Dimensions	184 (L) x 98 (W) x 19.1 (H) mm

Notes:
Unless otherwise noted, specifications listed above are for the standard configuration with internal feedback option without connectors; specs may be different for instruments with different wavelength or input power ranges.

1. Other wavelengths and control algorithms may be available upon request.
2. The output power fluctuation caused by SOP fluctuation after passing through a polarizer.
3. Requires a special cable (included).

Features:

- Reset free operation
- 0.9 ms recovery time
- 47 π/s tracking speed
- Plug and play

Applications:

- PMD compensation
- Polarization demultiplexing
- Elimination of polarization fading
- Coherent detection

Related Products:

- Polarization Stabilizer (POS-20X)
- Components

Tech Info:

- What is Polarization?
- Combat Polarization Impairments with Dynamic Polarization Controllers

FAQ:

- Stabilizer

Ordering Information:

POS — 002 — □ — □ □ — □ □ — □

Feedback Option:	Output Fiber:	Wavelength:	Connector Type:
I = internal	SM	13 = 1310 nm	FC/PC, FC/APC,
E = external	PM	15 = 1550 nm	SC/PC, SC/APC
		10 = 1060 nm	Others specify

Note:
Standard fiber types are SM in, PM out for internal feedback version, and SM in, SM out for external feedback version.

Reset-Free Polarization Tracker - PolaStay™ (POS-002)

Typical Performance Data:

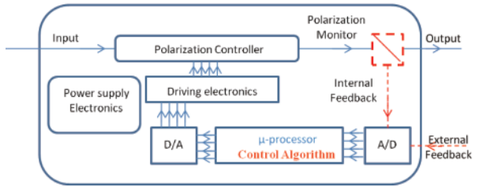

Figure 1. PolaStay™ polarization tracker function diagram. Either internal or external feedback can be used. Diagram shows structure for internal feedback.

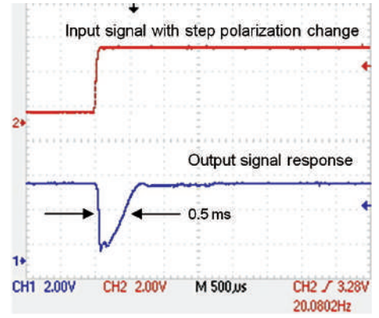

Figure 2 POS-002-I compensation for a step polarization change.

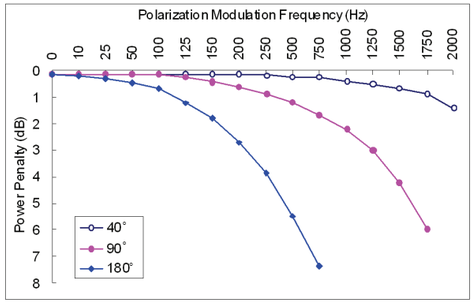

Figure 3. POS-002-I tracking of sinusoidal polarization modulation.

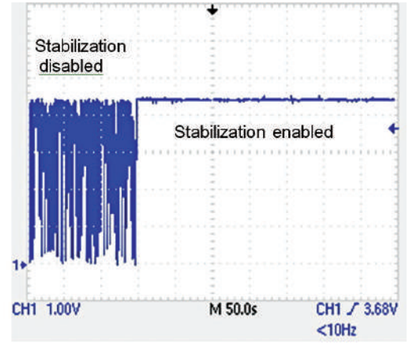

Figure 4. POS-002-I tracking of half-wave plate rotation at 45π rad/s.

Dimensions (in mm):

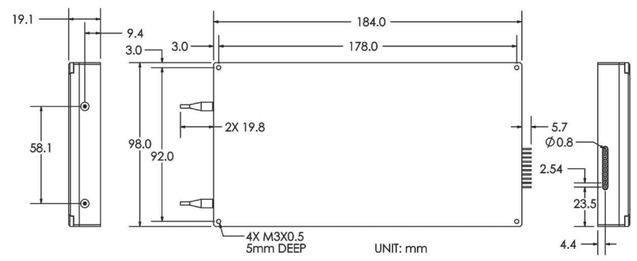

Reset-Free Polarization Tracker - PolaStay™ (POS-002)

Application Examples:

PMD compensation

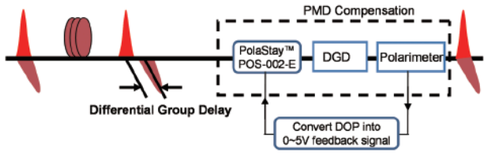

Scheme 1: Using a polarimeter to obtain feedback signal. In this scheme, a polarimeter is used to detect the degree of polarization (DOP) of the signal to indicate the PMD effect on the signal. The DOP will be maximized when the PMD is properly compensated. The user constructs a simple circuit to convert DOP into an analog signal between 0~5V and feeds this signal back to the POS-002-E. The polarization tracker then automatically maximizes DOP to achieve PMD compensation.

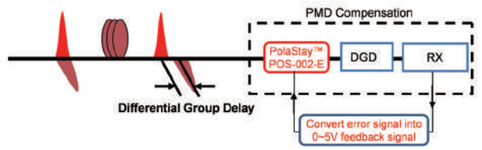

Scheme 2: Using the receiver to obtain the feedback signal. In this scheme, the error signal indicating the PMD effect can be a clock signal from the receiver's photodetector or a BER detected before FEC inside the receiver. The user converts the error signal into an analog signal between 0~5 volts and feeds it back to the POS-002-E. The polarization tracker then either maximizes or minimizes the error signal to achieve PMD compensation.

Polarization Demultiplexing

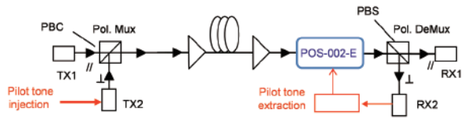

Scheme 1: Pilot tone detection. A low frequency pilot tone around 100 kHz is injected at one of the transmitters. At the receiving end, a pilot tone extraction circuit can be used to detect the strength of the pilot tone and convert it into a 0~5V feedback signal for the POS-002-E. The detected pilot tone will be maximized when the two polarization channels are properly separated. The polarization tracker then automatically maximizes the feedback signal to separate the two polarization channels.

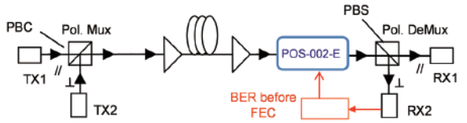

Scheme 2: BER detection. The bit-error rate (BER) before the forward error correction (FEC) in the receiver is detected as the error signal for polarization demultiplexing. The BER will be minimized when the two polarization channels are properly separated. A simple circuit can be used to convert the BER into a 0~5V feedback signal for the POS-002-E: the bigger the voltage, the smaller the BER. The polarization tracker then automatically maximizes the feedback signal to effectively separate the two polarization channels.

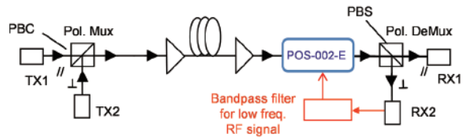

Scheme 3: Low frequency RF detection. The low frequency correlation noise between two polarization channels is an indication of the channel crosstalk. The noise will be minimized when the two polarization channels are properly separated. A low frequency photodetector followed by a bandpass filter can be used to detect the noise level. A simple circuit can be used to convert the noise level into a 0~5V feedback signal for the POS-002-E: the bigger the noise, the smaller the feedback signal. The polarization tracker then automatically maximizes the feedback signal to effectively separate the two polarization channels.

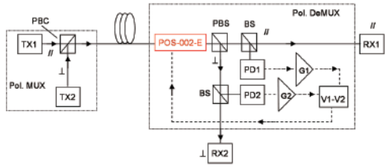

Scheme 4: Power imbalance detection. The two polarization channels are set at different power levels and the detected power difference is an indication of polarization channel separation. A simple circuit can be used to convert the noise channel power difference into a 0~5V feedback signal for the POS-002-E. The polarization tracker then automatically maximizes the feedback signal to effectively separate the two polarization channels.

Coherent Detection

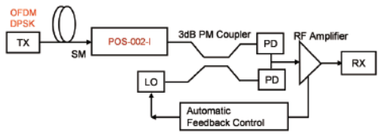

In a coherent detection system, the states of polarization of the signal and local oscillator must be the same in order to maximize signal to noise ratio. A POS-002-I can be used to stabilize the SOP of the signal after it propagates through the transmission fiber. The SOP of the output of the polarization tracker is linear and aligned with the slow axis of the PM fiber pigtail and will beat with the local oscillator.

Polarization Tracking for Sensor System

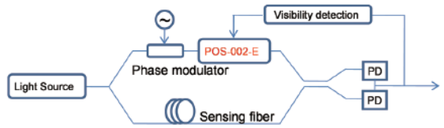

In an interferometric sensor system, the detection sensitivity is directly related to the SOPs of the two interfering signals. A POS-002-E can be used to obtain the maximum detection sensitivity. In this application, the visibility of the sensor can be monitored with a phase modulator and can be converted into an analog signal of 0-5 volts to be fed back to the POS-002-E. The polarization tracker then automatically maximizes the visibility for stable, optimized detection sensitivity.

Polarization Scrambler Module with Microprocessor Controller (PCD-005)

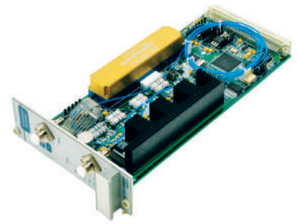

General Photonics' Polarization Scrambler module uses a breakthrough all-fiber technology to effectively randomize polarization states. This module is designed to be easily plugged into sensor equipment or measurement instruments with minimal development effort. Its advanced digital circuitry delivers uniform SOP distribution over a wide operation temperature range, making it a good choice for sensor field applications. The PCD-005 can be remote controlled via RS-232 to set the operation wavelength or enable/disable the scrambling operation.The PCD-005 delivers superior performance with extremely low insertion loss, back reflection, and residual phase and amplitude modulation.

Specifications:

Insertion Loss[1]	< 0.05 dB (without connectors) < 0.6 dB (with connectors)
Center Operating Wavelength[2]	λ range 1: 1310, 1480, 1550, 1600nm λ range 2: 980, 1060, 1310nm
Operating Wavelength Range[3]	> 100 nm
Output Degree of Polarization[4,5]	< 5%
Average PMD	< 0.05 ps
Intrinsic PDL	< 0.05 dB, 0.01dB typical
Return Loss	> 65 dB (without connectors)
Optical Power Handling	> 1000 mW
Residual Amplitude Modulation	< ± 0.01 dB
Residual Phase Modulation	< 0.1π
Power Supply	±12 VDC / 1A to ±15 VDC / 1A, +5 VDC / 0.2A
Power Consumption	12 W typical
Scrambling Frequencies	Factory set 4 fixed frequencies, distributed between DC to > 700 kHz
Operating Temperature	Standard: 10 to 45°C Extended: -5 to 65°C
Storage Temperature	-20 to 75 °C
Board Dimensions	220 × 100 × 30 mm (L × W × H)

Notes:
1. For SMF-28 compatible fiber. Other fibers may have higher loss, especially with connectors.
2. Please note that the fiber used determines the operating wavelength range. The standard fiber covers wavelengths in the 1260-1620nm range. The PCD-005 can also be configured to cover the 980-1310nm range using a different fiber. This fiber can handle wavelengths up to 1650nm, but if it is coupled to SMF-28 fiber, the performance may not be quite as good as normal due to mode mismatch. Please contact General Photonics for details.
3. Center Wavelength ± 50 nm
4. At 500 Hz detection bandwidth
5. Measured from a photodetector at PCD-005 output using a spectrum analyzer. A polarizer is placed in front of the photodetector to convert polarization modulation to amplitude modulation.

Ordering Information:

PCD — 005 — □□ — □□ — □□□

Wavelength Range:
01 = 1260 - 1650 nm
02 = 980 - 1310 nm

Temperature Range:
ST = standard
ET = Extended

Connector Type:
FC/PC, FC/APC, SC/PC, SC/APC, or
NC = no connectors
Others specify

Features:

- Minimal insertion loss and back reflection
- Low residual phase and amplitude modulation
- RS-232 control option
- Remote operation wavelength control

Related Products:

- Polarization Scrambler Instrument (PCD-104)
- Polarization Scrambler Modules (PCD-003, PSM-002)
- Depolarizer (DEP)

Tech Info:

- Scrambling to Minimize Polarization Related Impairments

FAQ:

- Scramblers

Accessories:

ADB — 001 (RS-232 adapter board)

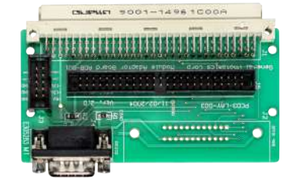

Polarization Scrambler Module with Microprocessor Controller (PCD-005)

Applications:

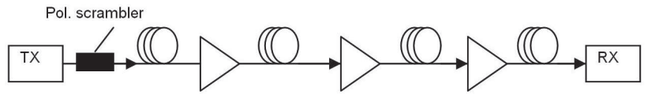

PDG (polarization dependent gain) mitigation

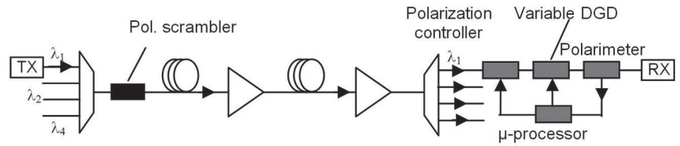

Facilitating PMD compensation

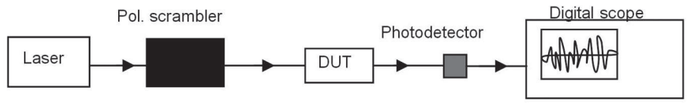

Facilitating PDL measurement

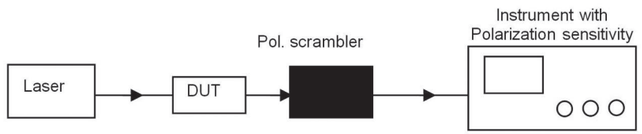

Polarization sensitivity elimination
in fiber sensor systems and in measurement systems

Typical Performance Data:

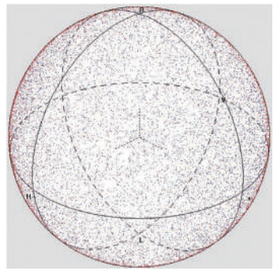

Figure 1. PCD-005 SOP distribution measured by a POD-101D polarimeter using a sampling rate of 625 kS/s over a measurement period of 1 second.

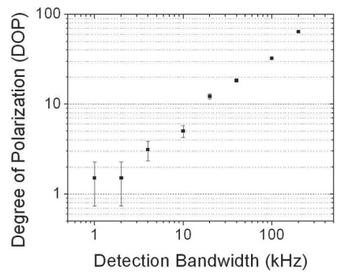

Figure 2. Degree of Polarization (DOP) as a function of detection bandwidth.

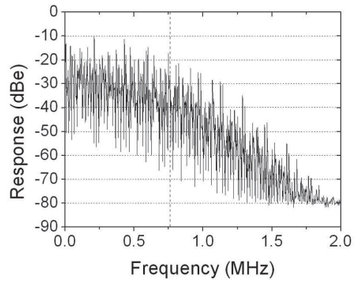

Figure 3. Effective scrambling bandwidth.

Polarization Scrambler Module (PCD-003)

General Photonics' 4-axis Polarization Scrambler Module uses a breakthrough all-fiber technology to effectively randomize polarization states. Depolarizing by polarization scrambling has many important applications: Scrambling the input polarization can remove measurement uncertainties caused by the polarization sensitivity of the device under test. Performance degradation due to polarization-dependent-gain (PDG) induced in optical amplifiers can be suppressed by scrambling the State of Polarization (SOP). Polarization scrambling can also be used in systems to facilitate and simplify PMD monitoring. Based on a patented, award-winning all-fiber technology, the PCD-003 delivers superior performance with extremely low insertion loss, back reflection and residual phase and amplitude modulation. In addition, the total power consumption is typically less than 10W.

Specifications:

Insertion Loss	< 0.05 dB
Center Operating Wavelength	1550 nm standard
Operating Wavelength Range[1]	> 100 nm
Output Degree of Polarization[2,3]	< 5%
Average PMD	< 0.05 ps
Intrinsic PDL	< 0.05 dB, 0.01 dB typical
Return Loss	> 65 dB
Optical Power Handling	> 1000 mW
Residual Amplitude Modulation	< ± 0.01 dB
Residual Phase Modulation	< 0.1π
Power Supply	± 12 VDC/1A to ± 15 VDC/1A
Power Consumption	10 W typical
Scrambling Frequencies	Factory set 4 fixed frequencies, distributed between DC to > 700 kHz
Operating Temperature	10 ~ 40 °C
Storage Temperature	-10 ~ 50 °C
Board Dimension	220 × 100 × 30 mm (L × W × H)

Notes:
Values are referenced without connectors

1. Center Wavelength ± 50 nm
2. At 500 Hz detection bandwidth
3. Measured from a photodetector at PCD-003 output using a spectrum analyzer. A polarizer is placed in front of the photodetector to convert polarization modulation to amplitude modulation.

Features:

- Minimal insertion loss and back reflection
- Low residual phase and amplitude modulation
- Low power consumption

Applications:

- PDG (polarization dependent gain) mitigation
- Polarization sensitivity elimination
- Facilitating PMD emulation
- Facilitating PMD compensation
- Facilitating PDL measurement

Related Products:

- Polarization Scrambler Instrument (PCD-104)
- Polarization Scrambler Modules (PCD-005, PSM-002)
- Depolarizer (DEP)

Tech Info:

- Scrambling to Minimize Polarization Related Impairments

FAQ:

- Scramblers

Ordering Information:

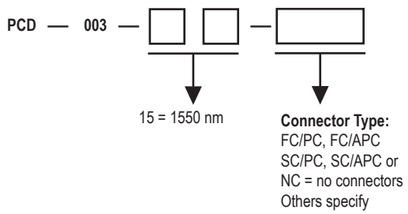

Miniature Polarization Scrambler Module (PSM-002)

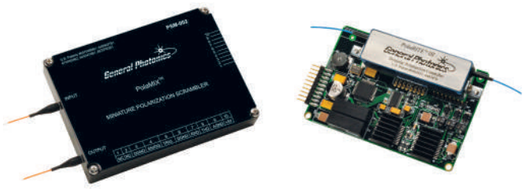

General Photonics' miniature polarization scrambler module, the PSM-002, is specially designed for integration into sensor and communication systems that need to work in extreme environmental conditions. The module uses General Photonics' patented fiber squeezer technology to effectively randomize polarization states. Unlike that of the PCD-005, the scrambling rate of this miniature scrambler is user selectable via an RS-232 command. Another attractive feature is that the scrambling function can also be enabled and disabled by a TTL trigger signal. The PSM-002 is available either as a standard board for lab applications or fully enclosed in a water-tight enclosure for applications in high humidity environments. It also comes in either standard or extended temperature versions.

Specifications:

Insertion Loss[1]	< 0.05 dB (without connectors) < 0.6 dB (with connectors)
Operating Wavelength[2]	1260 to 1650 nm and 980 to 1310 nm standard
Output Degree of Polarization (DOP)[3]	< 5%, 2.5% typical
Average PMD	< 0.05 ps
Intrinsic PDL	< 0.05 dB, 0.01 dB typical
Return Loss	> 65 dB (without connectors)
Optical Power Handling	> 300 mW
Power Supply	5.0 – 5.5 VDC / 9 W max.
Power Consumption	0.5 – 9 watts, depending on the scrambling rate
Scrambling Rate	User selectable from 0.01 to 20,000 points/s
Operating Temperature	Standard: 0 to 65°C Extended: -35 to 70°C
Storage Temperature	-40 to 85 °C
Dimensions	96 (L) x 63.5 (W) x 18 (H) mm (board version) 115 (L) x 82.6 (W) x 19 (H) mm (enclosure)

Notes:
1. For SMF-28 compatible fiber. Other fibers may have higher loss, especially wtih connectors.
2. Standard calibrated wavelengths are 1550nm (1260-1650nm version) and 1310nm (980-1310nm version). Others available.
3. DOP specification is < 5% (to within 2σ) when averaged over 4000 or more points.

Features:

- Works in extreme environmental conditions
- Minimal insertion loss and back reflection
- Low residual phase and amplitude modulation
- Selectable scrambling frequencies
- Small size

Applications:

- Sensor and communication systems
- Polarization sensitivity elimination
- Facilitating PMD emulation
- PMD monitoring for PMD compensation
- Facilitating PDL measurement

Related Products:

- Polarization Scrambler Modules (PCD-005, PCD-003)
- Depolarizer (DEP)
- Multifunction Polarization Controller (MPC-201)

Tech Info:

- Scrambling to Minimize Polarization Related Impairments

FAQ:

- Scramblers

Dimensions (in mm):

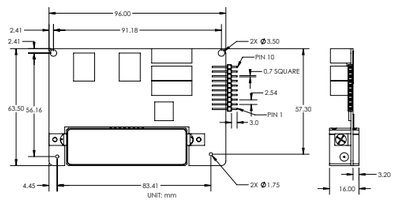

board

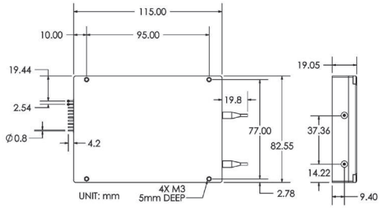

enclosure

Ordering Information:

PSM — 002 — □□ — □ — □□ — □

Wavelength Range:
01 = 1260 - 1650 nm
02 = 980 - 1310 nm

0 = without enclosure
E = with enclosure

Temperature Range:
ST = Standard
ET = Extended

Connector Type:
FC/PC, FC/APC, SC/PC, SC/APC, or
NC = no connectors
Others specify

Micro Polarization Controller (PSM-003-C)

This OEM micro polarization controller integrates General Photonics' all-fiber dynamic polarization control technology with miniature electronic drive/control circuitry into a compact, self-contained device that provides full polarization control functionality while minimizing volume, power consumption, and cost. The state of polarization (SOP) of the output signal can be controlled via three analog 0 to 5V control voltages. This device is ideal for integration into OCT or sensor systems to maximize signal output. It requires only ±12VDC power supplies, and its low power consumption enables use in battery-powered handheld devices.

Specifications:

Operating Wavelength Range	1260 to 1650 nm standard, others specify
Number of Control Waveplates	× 3
Control Voltage	0 – 5V
Rise and Fall Time	< 5 ms/V (or 12.5 ms / V_π)
V_π	2.5 V (typical), 3 V (max) @1550 nm
Frequency of Input Sine Wave	10 Hz max.
Insertion Loss	Control grade: 0.1 dB, excluding connectors Measurement grade: 0.05 dB, excluding connectors
Return Loss	> 65 dB excluding connectors
Activation Loss	Control grade: 0.1 dB Measurement grade: 0.01 dB
PDL	Control grade: < 0.1 dB Measurement grade: < 0.01 dB
PMD	< 0.05 ps
Optical Power Handling	300 mW
Fiber Pigtail	9/125 µm single mode fiber standard, others specify
Electrical Interface	8-wire flat cable
Power Supply	±12 VDC/25 mA
Power Consumption[1]	< 0.6 W typical
Operating Temperature	-10 to 70 °C
Storage Temperature	-40 to 85 °C
Dimensions	2.58"(L) × 1.25"(W) × 0.63"(H)

Notes:
1. 5 V input on all 3 axes at 25 °C.

Features:

- Compact
- Low power consumption
- Low cost
- Plug and play

Applications:

- Polarization control in OCT systems
- Polarization control in sensor systems
- Polarization control in measurement systems

Related Products:

- Polarization Controllers (PCD-M02, MPC-3/4X)
- Components

Tech Info:

- What is Polarization?

FAQ:

- Polarization Controllers

Dimensions (in inches):

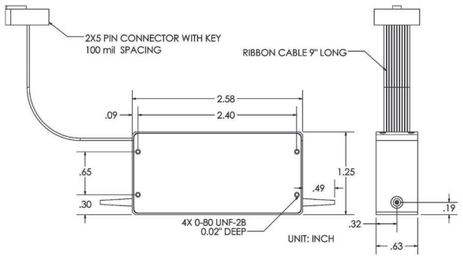

Ordering Information:

PSM — 003 — C — □ — □ — □

Wavelength:
7 = 1260 - 1650nm
6 = 980 - 1310nm

Grade:
C = Control
M = Measurement

Connector Type:
FC/PC, FC/APC
SC/PC, SC/APC
NC = no connector

ACTIVE POLARIZATION MODULES

Micro Polarization Scrambler (PSM-003-S)

This OEM micro polarization scrambler integrates General Photonics' all-fiber dynamic polarization control technology with miniature electronic drive/control circuitry into a compact, self-contained device that provides full polarization control functionality while minimizing volume, power consumption, and cost. Two polarization scrambling options are available: random scrambling at a rate of up to 5 discrete points/s or smooth trace scrambling at a rate of up to 60π rad/s. Scrambling can be disabled with a 5-volt TTL high and enabled with a TTL low. This module is ideal for integration in a PDL measurement instrument or in a sensor system to minimize polarization related measurement uncertainties. It requires only ±12VDC power supplies, and its low power consumption enables use in battery-powered handheld devices.

Specifications:

Operating Wavelength Range	1260 to 1650 nm standard, others specify
Smooth Trace Scrambling Rate	0.0192π, 0.096π, 0.48π, 2.4π, 12π, 60π rad/s, please specify when ordering.
Discrete Scrambling Rate	0.1, 0.2, 1, 5 points/s; please specify when ordering.
Insertion Loss	Measurement grade: 0.05 dB, excluding connectors Control grade: 0.1 dB, excluding connectors
Return Loss	> 65 dB excluding connectors
Activation Loss	Measurement grade: 0.01 dB Control grade: 0.1 dB
PDL	Measurement grade: < 0.01 dB Control grade: < 0.1 dB
PMD	< 0.05 ps
Optical Power Handling	300 mW
Fiber Pigtail	9/125 μm single mode fiber standard, others specify
Electrical Interface	8-wire flat cable
Power Supply	±12 VDC/25 mA
Power Consumption[1]	< 0.6W typical
Operating Temperature	-10 to 70 °C
Storage Temperature	-40 to 85 °C
Dimensions	2.58" (L) × 1.25" (W) × 0.63" (H)

Note:
1. Continuous scrambling, 12π rad/s, at 23 °C.

Features:

- Compact
- Low power consumption
- Low cost
- Plug and play

Applications:

- Minimize polarization related fluctuation in sensor systems
- Minimize polarization related fluctuation in measurement systems
- PDL or DOP measurement

Related Products:

- Polarization Controllers (PCD-M02, MPC-3/4X)
- Polarization Scrambler (PSM-002)
- Components

Tech Info:

- What is Polarization?

FAQ:

- Polarization Controllers
- Scramblers

Ordering Information:

PSM — 003 — S — □ — □ — □□□ — □ — ▭

Wavelength:
7 = 1260 - 1650nm
6 = 980 - 1310nm

Scrambling Type:
R = random
C = continuous

Scrambling Rate:
Continuous: see key*
Random: see key**

Grade:
M = Measurement
C = Control

Connector Type:
FC/PC, FC/APC
SC/PC, SC/APC
NC = no connector

*Continuous Scrambling Rate Key:

000 = 0.0192 π rad/s
001 = 0.09 π rad/s
005 = 0.48 π rad/s
024 = 2.4 π rad/s
120 = 12 π rad/s
600 = 60 π rad/s

**Random Scrambling Rate Key:

001 = 0.1 points/s
002 = 0.2 points/s
010 = 1 point/s
050 = 5 points/s

Dimensions (in inches):

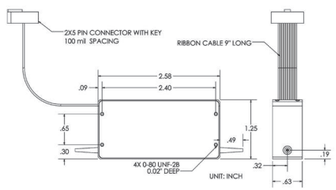

High Speed In-line Polarimeter - PolaDetect™ (POD)

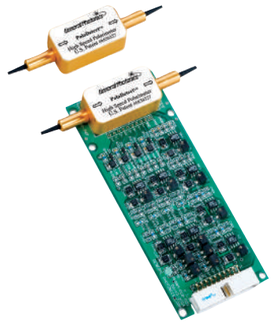

General Photonics' in-line polarimeter is specially designed for low cost, high-speed polarization characterization without interrupting data traffic. It outputs four voltage signals for calculating both the degree of polarization (DOP) and the state of polarization (SOP) of the light passing through the device in microseconds. PolaDetect™ is ideal for integration into polarization monitoring and polarization stabilization modules, or in polarization characterization instruments. It comes with a preamplification board to provide analog signals for SOP/DOP calculation, feedback control, and computer interface. Calibration matrices are provided with every device for the calculation. Devices without preamplification board and calibration matrix are also available for OEM purposes.

Specifications:

Insertion Loss	0.8 dB typical, 1.2 dB max.
Return Loss	55 dB
PDL	< 0.25 dB
PMD	< 0.1 ps
Wavelength Dependent Loss	0.15 dB over C band or 1310 ± 15nm, depending on version
Optical Power Sensitivity	5 μW
Max. Optical Input Power	5 mW
Optical Damage Power	300 mW min.
Measurement Bandwidth	50 kHz with preamplifier board Analog bandwidth for optical head alone is 1.5 MHz
SOP Uncertainty (At Calibration Wavelength)	1% max.
DOP Uncertainty (At Calibration Wavelength)	±2% max
Wavelength Range[1]	1550 ± 50 nm standard, 1310 ± 30nm available
Calibrated Wavelengths	1550nm version: 1520, 1530, 1540, 1550, 1560nm 1310nm version: 1310nm, others user specified
Operating Temperature	0 to 40 °C
Storage Temperature	-40 to 85 °C
Fiber Type	SMF - 28
Electrical Interface	10 pin w/o preamplifier board 20 pin w/preamplifier board
Electrical Power Supply	-5 V to -10 V w/o preamplifier board ±12 V w/preamplifier board
Dimensions	1.45" (L) x 0.8" (W) x 0.58" (H) (optical module) 4.91" (L) x 1.95" (W) x 0.65" (H) (with board)

Note:
Values are referenced without connectors.
1. Contact General Photonics regarding other wavelengths.

Features:

- High speed and low loss
- Compact size
- No moving parts

Related Products:

- Polarimeter Instruments (PSY-201, POD-201)

Tech Info:

- What is Polarization?
- Real-Time Optical Spectrum Analysis of a Light Source Using a Polarimeter

FAQ:

- Polarimeter

Ordering Information:

POD — □□ — □□ — □□ — ▭

Wavelength:
15 = 1550 nm
13 = 1310 nm

Fiber Type:
SS = SM in / SM out

Preamplifier Board:
01 = w/o preamplifier
02 = with preamplifier

Connector Type:
FC/PC, FC/APC
SC/PC, SC/APC or
NC = no connectors
Others specify

Notes:
* Standard version is POD with board (02).
POD without board (01) is available for custom OEM applications. Contact General Photonics for details.

High Speed In-line Polarimeter - PolaDetect™ (POD)

Typical Performance Data:

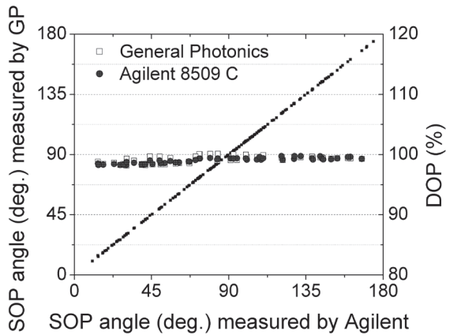

Figure 1. SOP and DOP accuracy compared with Agilent 8509C polarization analyzer.

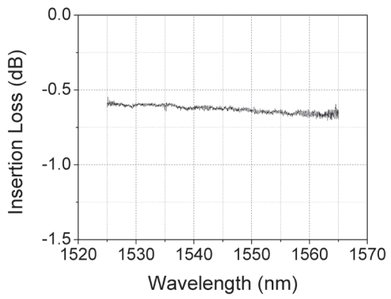

Figure 2. Insertion loss vs. wavelength

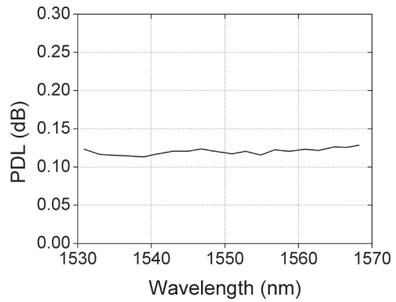

Figure 3. Polarization dependent loss (PDL) vs. wavelength

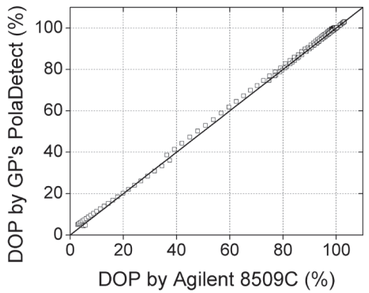

Figure 4. Partial polarized light DOP measurement compared with Agilent 8509C

Dimensions (in inches):

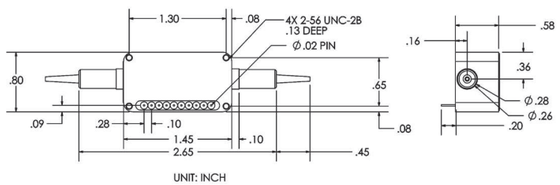

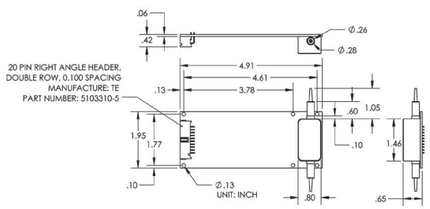

High-Speed Polarization State Generator - PolaPal™ (PSG-001)

General Photonics' high-speed polarization state generator (PSG) module provides the ability to generate 6 states of polarization (-45°, 0°, 45°, 90°, RHC & LHC) across the Poincaré Sphere in less than 250 µs, with an impressive repeatability of less than 0.1 degrees. In addition, it comes as a compact module ideal for integration into systems that require precise generation of these 6 polarization states or precise 90° polarization rotation. Applications include Mueller matrix-based measurements, polarization OTDR, performance monitoring, and swept frequency component measurement systems. The PSG is easily controlled with a 6-bit TTL signal either from a microcontroller or a computer.

Specifications:

Wavelength Range	1480 to 1620 nm[1]	1260 to 1340nm
Insertion Loss	1.0 dB typical	1.2 dB typical
Wavelength Dependent Loss	0.3 dB typical across C band	< 0.3 dB
Maximum Optical Power	300 mW min.	
Insertion Loss Variation	0.1 dB max. for all SOP states	
Return Loss	55 dB min.	
SOP Repeatability	± 0.1 degrees on Poincaré Sphere	
Rotation Angle Wavelength Dependence	-0.068 deg./ nm	
Rotation Angle Temperature Dependence	-0.1 deg./ °C	
Angle Between SOP States	90 ± 10 degrees on Poincaré Sphere	
Transient Loss	0.6 dB per bit max.	
Number of Control Bits	6	
SOP Switching Speed	250 µs max.	
Electrical Interface	10-pin digital port to accept any 6 bit TTL control signal, with +12 V power supply	
Software	None	
Operating Temperature	0 to 50 °C	
Storage Temperature	-40 to 80 °C	
Board Dimensions	5.30" (L) x 2.74" (W) x 0.75"(H)	

Note:
Values are referenced without connectors.

1. Calibrated over 1500 to 1580 nm. Please contact General Photonics for information on other wavelength options.

Features:

- Digitally Switched SOP
- Switching Speed 250 µs or less
- 0.1 degree SOP Repeatability
- 6-bit TTL Control
- Compact

Applications:

- Polarization OTDR
- Polarization Rotation
- Mueller Matrix-based Polarization Analysis
- Swept-Frequency Measurement

Tech Info:

- What is Polarization?
- High accuracy polarization measurements using binary polarization rotators
- Highly Repeatable All Solid-State Polarization State Generator
- Self-calibrating Binary Polarization Analyzer

Ordering Information:

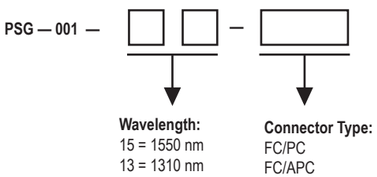

Dimensions (in inches):

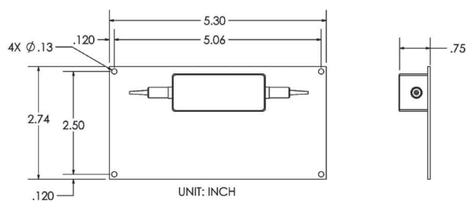

ACTIVE POLARIZATION MODULES

Dynamic Polarization Controller with Miniature Piezo Driver Card (PCD-M02)

This module integrates a General Photonics all-fiber dynamic polarization controller with miniature piezo driver card, so that the SOP of the signal can be directly controlled either by a 0-5V analog control signal or a 12-bit TTL digital control signal. Because there is an on-board HV DC/DC converter, no external high voltage power supply is required. The card can be configured to accept either a ±12 volt power supply or an external 160-volt power supply. As a polarization controller, the PCD-M02 can convert any input polarization state to any desired output polarization state. As a scrambler, it can randomize the output polarization state. This module offers the low insertion loss, low back reflection, and low activation loss needed for test and measurement applications, combined with the compact size needed for system integration or handheld devices.

Specifications[1]:

Operating Wavelength	1260-1650nm or 980-1310nm standard Others available
Insertion Loss[2]	< 0.05 dB (without connectors) < 0.6 dB (with connectors)
Return Loss	>65 dB
Activation Loss	0.01 dB (P grade), 0.05 dB (A grade)
Polarization Mode Dispersion	0.05 ps
Polarization Dependent Loss	0.05 dB
Optical Power Handling	1000 mW
Polarization Control Range	0-4π each channel (Optical head Vπ per channel ≤35V)
Number of Channels	3 or 4
Power Supply	+12VDC/1.2A, −12VDC/0.1A (standard) or +12VDC/1.2A, −12VDC/ 0.1A, +160V/100 mA (ext)
External Analog Input	10 pin
Analog Control Voltage	0-5V
Input Impedance (Analog)	≥20 kΩ
Analog Input Gain	30V/V ±1 %
External Digital Input	20 pin
Digital Control	TTL, 12-bit data, 4-bit control
Output Voltage Range	0-140V
Max. Output Current	20 mA / channel all channels (continuous) 60 mA single channel (continuous) 60 mA per channel (peak)
Output Impedance	50 Ω
140V Output Rise/Fall Time	<30 µs (MPD-001, no load), <400µs (PCD-M02)
15V Output Rise/Fall Time	10 µs (MPD-001, no load), 65µs (PCD-M02)
Noise[3]	<40 mV (RMS)
Operating Temperature	0° to 40° C
Storage Temperature	−20° to 60°C
Board Dimensions	3.94" (L) x 3.94"(W) x 0.69" (H)

Notes:
1. Optical specifications are referenced without connectors.
2. For SMF-28 compatible fibers. Other fibers may have higher loss, especially with connectors.
3. The noise is measured with the output set to 140V and an output capacitance of 0.18µF (capacitance of piezoelectric actuator used in PolaRITE II/III). It may decrease with higher output capacitance and increase with no output capacitance.

Features:

- Minimal Insertion Loss
- Low Activation Loss
- Fast Response
- Digital and Analog Control
- Compact

Applications:

- Polarization Control
- Polarization Scrambling
- PDL Measurement
- PMD Compensation/Emulation
- Fiber Sensor

Related Products:

- Polarization Controller Module (MPC-3/4X)
- Multifunction Polarization Controller (MPC-201)
- Components

Tech Info:

- What is Polarization?
- Polarization in Fiber Systems: Squeezing out More Bandwidth
- Combat Polarization Impairments with Dynamic Polarization Controllers
- PolaRITE™ II/III Polarization Controllers/ Scramblers Application Note

FAQ:

- Polarization Controllers

Dimensions (in inches):

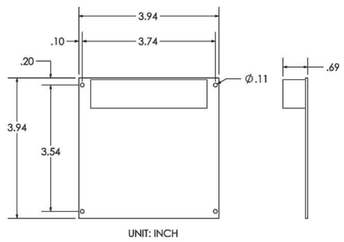

Ordering Information:

PCD — M02 — □ □ — □ — ▭

 # Channels:
3X = 3 Channel
4X = 4 Channel

Operation Wavelength:
1 = 480 nm
2 = 633 nm
3 = 780 nm
4 = 820 nm
6 = 980 - 1310 nm*
7 = 1260 - 1650 nm

Connector Type:
FC/PC, FC/APC,
or NC = No Connectors

MPD — 001 — 4X
(driver board alone, without polarization controller)

ACTIVE POLARIZATION MODULES

Multimode Scrambler - SpeckleFree™ (MMS-201)

Speckle patterns from a multimode fiber can cause problems in many applications that require uniform, stable light distributions at the fiber output. The MMS-201 multimode scrambler, a superior replacement for the MMS-101, is specially designed to solve this problem. Based on a General Photonics proprietary technology, the MMS-201 effectively randomizes multimode speckle patterns over time at a high frequency over 20kHz. The light distribution at the output appears uniform and stationary when viewed by cameras or detectors with averaging times >80 ms. In addition, the all-fiber optical path minimizes the scrambler's insertion loss. The fiber used for this device undergoes a special surface treatment to prevent breakage under stress, ensuring high device reliability. The MMS-201 can improve performance in various applications including DNA sequencing, multimode fiber sensing and test and measurement of multimode fiber devices.

Specifications:

Operating Wavelength Range	530 to 1630 nm
Fiber Type	50/125 µm step index standard, others optional
Fiber NA	0.2
Scrambling Frequency	22 ±1 kHz
Insertion Loss	≤1 dB at 635nm, including connectors
Return Loss	>50 dB (with PC connector) >55 dB (with APC connector)
Scrambling Efficiency[1, 2]	> 80% (effective power)
Flatness[3]	< 20% typical
Ripple[4]	< 10% typical
Optical Power Handling	400 mW
Power Supply	+24VDC/1.5A
Enable/Disable Signal	TTL high = enabled TTL low = disabled
Operating Temperature	10 to 40°C
Storage temperature	−20 to 70°C
Dimensions	23 (L) x 10.5 (W) x 6.5 (H) cm

Notes:
Specifications in this table apply for an MMS-201 made with 50µm step index multimode fiber.
1. Scrambling efficiency is defined as (Light energy ≥ 80% of maximum intensity/Total energy)* (area over which intensity is ≥ 80% of maximum intensity /total core area).
2. Measured over 80 ms integration time at 635 nm.
3. Flatness is defined as (maximum intensity – minimum intensity) expressed as a percentage of maximum intensity, where the maximum and minimum are defined over the center 80% of the fiber core area.
4. Ripple is defined as the maximum peak-to valley difference of intensity fluctuations, expressed as a percentage of maximum intensity, where the fluctuation differences and maximum intensity are measured within the center 80% of the fiber core area.

Features:

- Compact
- Reliable
- High speed
- Efficient
- Can be made with custom fiber

Applications:

- DNA sequencing
- Multimode fiber sensing
- Test and measurement
- MM to SM coupling
- Free-space optical communication

Order Information:

MMS – 201 — □ — □ — □ — ▭

Fiber Type:
50S = 50µm
core step index

Jacket Type:
3 = 3mm
2 = 2mm
9 = 900µm

Pigtail Length:
1 = 1 m
Others specify

Connector Type:
FC/PC, FC/APC,
SC/PC, SC/APC or
NC = no connectors

Multimode Scrambler - SpeckleFree™ (MMS-201)

Typical Performance Data:

SCRAMBLING DISABLED

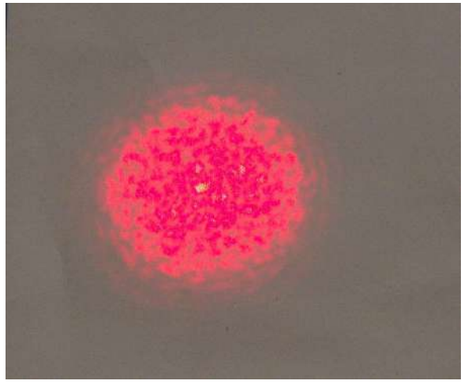

Figure 1. Far-field illumination pattern with scrambler disabled.

SCRAMBLING ENABLED

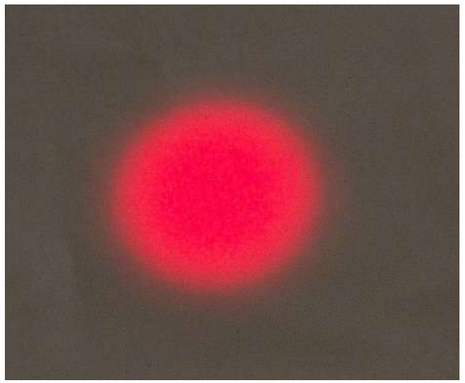

Figure 2. Far-field illumination pattern with scrambler enabled.

2-D Beam Profile

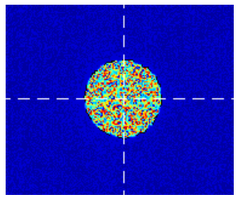

2-D Beam Profile

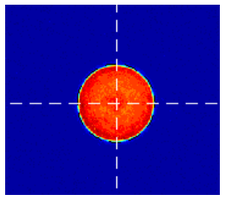

3-D Beam Profile

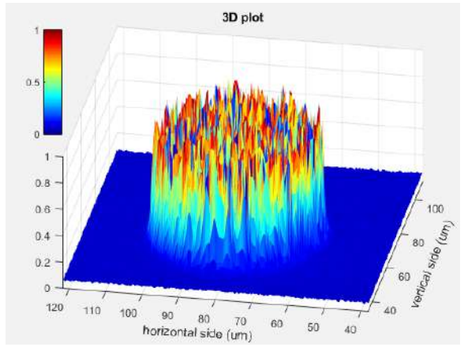

Figure 3. 2D and 3D beam profiles with scrambler disabled.

3-D Beam Profile

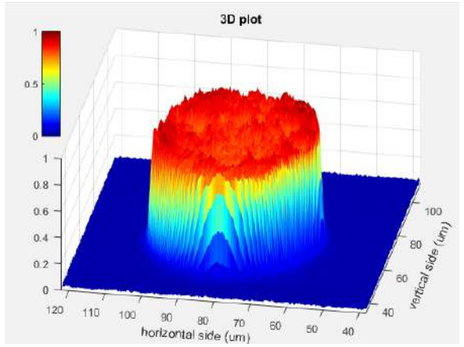

Figure 4. 2D and 3D beam profiles with scrambler enabled

ACTIVE POLARIZATION MODULES
Multimode Scrambler - SpeckleFree™ (MMS-201)

SCRAMBLING DISABLED

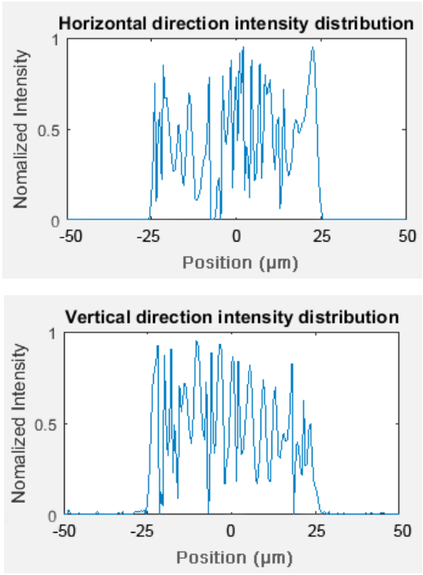

Figure 5. X and Y cross-sectional beam profiles with scrambler disabled.

SCRAMBLING ENABLED

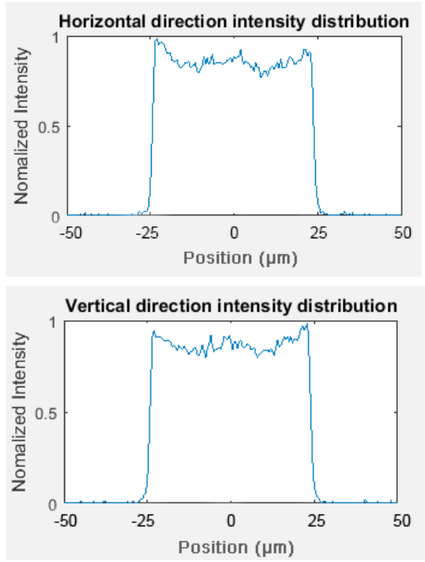

Figure 6. X and Y cross-sectional beam profiles with scrambler enabled.

Note: Data in Figures 3-6 taken at 635nm with 80 ms integration time.

Mechanical Dimensions (in inches):

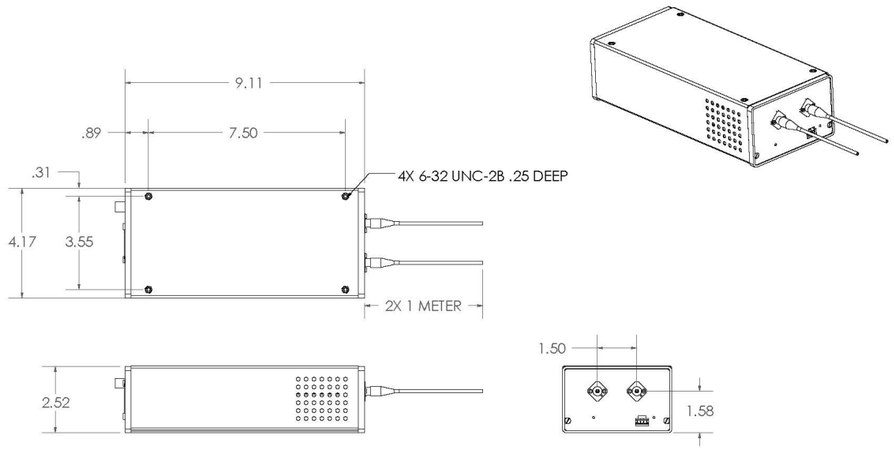

Mini Dynamic Polarization Controller - PolaRITE™ III (MPC-3/4X)

In response to customer requests for low profile polarization controllers for system integration, General Photonics made a special effort in designing this third generation polarization controller, the PolaRITE™ III, with significantly reduced height and size. The height reduction is especially advantageous for integration in test equipment, fiber sensors, fiber lasers and optical network modules. Due to a special athermal design, the temperature stability is also significantly improved over our earlier version PolaRITE™ II. Like the other products in the PolaRITE™ family, PolaRITE™ III essentially eliminates insertion loss and back reflection with its unique all fiber construction. Combined with General Photonics' miniature piezo driver card, it can be controlled either by a digital or analog signal to obtain any desired polarization output from an arbitrary input polarization state.

Specifications:

Intrinsic Insertion Loss	0.05 dB
Return Loss	> 65 dB
Wavelength	1260 to 1650 nm standard, others specify
Rise and Fall Time[1]	30 µs max.
Vπ at DC (at 23 °C)	35 volts max. @ 1550nm
Max. Activation Loss	0.01 dB (P grade), 0.05 dB (A grade) with 0 – 150VDC applied to all axes
Polarization Mode Dispersion	0.05 ps
Operating Temperature	-25 to 80 °C
Storage Temperature	-40 to 85 °C
Fiber Pigtail	9/125 µm single mode fiber standard, others specify
Electrical Interface	8 pin 0.03 inch square, with 0.098 inch pitch
Dimensions	2.58" × 0.80" × 0.63" (3 axes) 3.27" × 0.80" × 0.63" (4 axes)
Maximum Applied Voltage	150 volts

Note:
Values are referenced without connectors

1. 10 to 90% transition for a voltage change of V_{π},

Features:

- No intrinsic insertion loss
- No intrinsic back reflection
- Fast response
- Compact size

Applications:

- PMD compensation
- Polarization stabilization
- Polarization demultiplexing
- Fiber sensor
- Fiber laser
- Testing equipment

Related Products:

- Polarization Controller with Driver Card (PCD-M02)
- Components

Tech Info:

- What is Polarization?
- Polarization in Fiber Systems: Squeezing out More Bandwidth
- Combat Polarization Impairments with Dynamic Polarization Controllers
- PolaRITE™ II/III Polarization Controllers/ Scramblers Application Note

FAQ:

- Polarization Controllers

Dimensions (in inches):

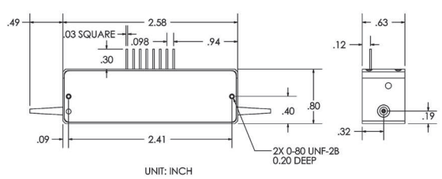

3 axis version

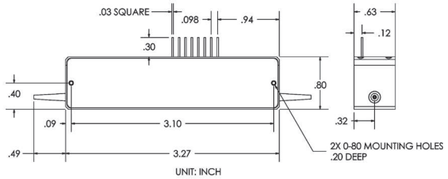

4 axis version

ACTIVE POLARIZATION MODULES
Mini Dynamic Polarization Controller - PolaRITE™ III (MPC-3/4X)

Applications:

Polarization Mode Dispersion (PMD) compensation

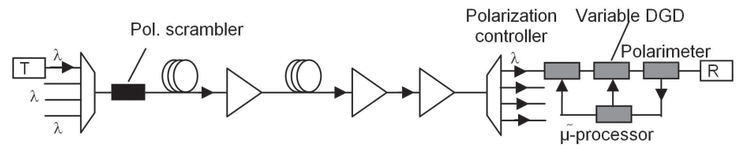

Polarization stabilization

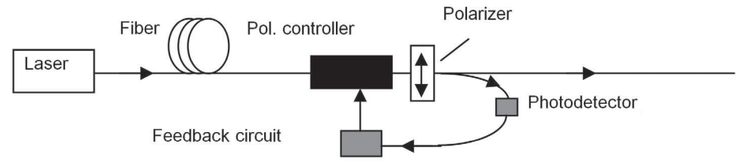

Polarization demultiplexing

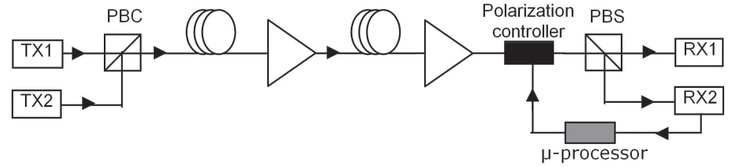

Coherent communications

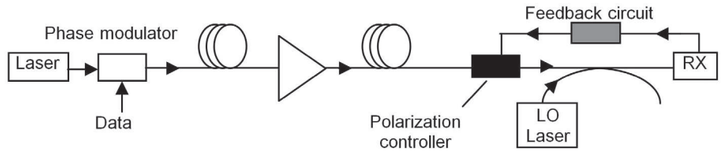

- PMD emulation
- PDL (polarization dependent loss) measurement
- PDL elimination in optical instruments, such as optical spectrum analyzers
- Automatic polarization stabilization for E/O modulator and interferometers
- Reduction of EDFA polarization dependent gain
- Improvement of signal-to-noise ratio in long-haul transmission systems
- Output stabilization in fiber laser systems

ACTIVE POLARIZATION MODULES

Mini Dynamic Polarization Controller - PolaRITE™ III (MPC-3/4X)

Typical Performance Data:

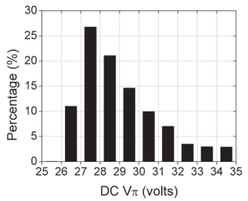

Figure 1. Histogram of DC V_π. In most cases, DC V_π is less than 30 volts

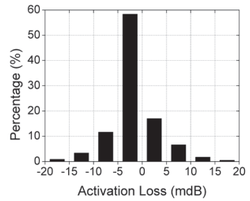

Figure 2. Histogram of activation loss. In most cases, activation loss is less than 0.01 dB.

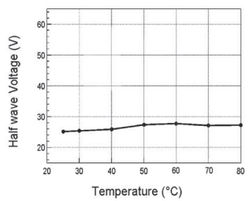

Figure 3. DC V_π as function of operating temperature.

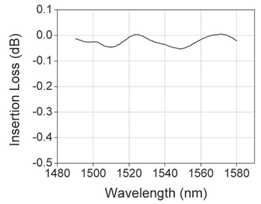

Figure 4. Insertion loss vs wavelength

Ordering Information:

MPC — □□ — □ — □ — □

 # Channels:
3X = 3 Channel
4X = 4 Channel

Operation Wavelength:
1 = 480 nm
2 = 633 nm
3 = 780 nm
4 = 820 nm
6 = 980 - 1310 nm*
7 = 1260 - 1650 nm

P = P grade
A = A grade

Connector Type:
FC/PC, FC/APC,
SC/PC, SC/APC
NC = no connectors
Others specify

Notes:
1260-1650nm and 980-1310 nm are the standard wavelength ranges for this product.
Please contact General Photonics for information on other wavelength options.
Please specify P grade or A grade if activation loss is important for your application.

*This fiber can handle wavelengths up to 1650nm, but if it is coupled to SMF-28 fiber, the performance may not be quite as good as normal due to mode mismatch.

ACTIVE POLARIZATION MODULES

Polarization Switch - PolaSwitch™ (PSW-002)

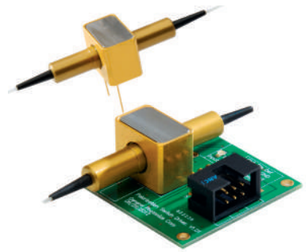

General Photonics' all solid-state polarization switch can quickly and repeatably rotate the SOP of incoming light by a fixed angle, either 45 or 90 degrees. Both single mode and PM fiber pigtailed versions are available. With the PM option, the device functions as a TE to TM converter, switching the SOP between being aligned with the slow and fast axes of the PM fiber, or between the slow axis and 45 degrees from the slow axis. With the SM option, the device simply rotates the polarization ellipse either 45 or 90 degrees. The device can be used for polarization sensitive OCT, polarization sensitive OTDR or OFDR, PMD monitoring, polarization modulation, polarization detection, and polarization metrology. An optional driver board simplifies switch control by allowing the user to control the output SOP using TTL levels.

Specifications:

Operation Wavelength	1550 ± 30nm or 1310 ± 30nm
Polarization Rotation (at λc, 23° C)	45 ± 0.5° or 90 ± 0.5°
Polarization Rotation (All Wavelengths, All Temp.)	45 ± 5° or 90 ± 5°
Rotation Angle Temperature Dependence	-0.1 degree / °C for 45° version -0.2 degree / °C for 90° version
Insertion Loss	< 0.5 dB
Return Loss	> 55 dB
Switching Current	< 130 mA
Switching Voltage	2.5 V
Latching Current	~ 80 mA
Latching Voltage	1.5 to 2 V
Switching Time	100 µs typical
Extinction Ratio[1]	> 18 dB for PM model
Operating Temperature	0° to 50 °C
Storage Temperature	-40° to 85 °C
Fiber Type	PM Panda, SMF-28 or compatible
Dimensions	Optical head: 1.57" (L) x 0.69" (W) x 0.53" (H) Board: 1.50" (L) x 1.50" (W) x 0.58" (H)

Note:
Values referenced without connectors.
1. Both output states of 90° PM PSW with input polarizer at 23 °C.

Features:

- Fast
- No moving parts
- Low insertion loss
- Compact

Applications:

- Polarization diversified detectors and sensors
- Polarization sensitive OCT
- Polarization metrology
- Polarization sensitive OTDR or OFDR
- PMD monitoring

Related Products:

- Polarization State Generator (PSG-001)
- Polarization Synthesizer (PSY-201)

Tech Info:

- What is Polarization?

FAQ:

- Other products

Dimensions (in inches):

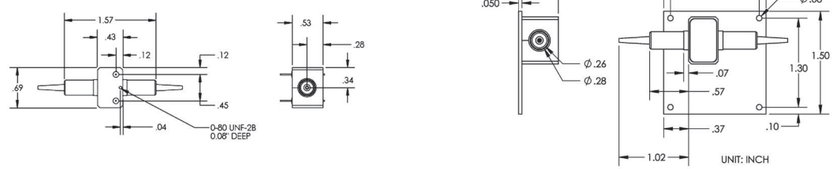

Ordering Information:

PSW — 002 — □□ — □□ — □□ — □ — □ — □

Wavelength:
15 = 1550
13 = 1310

Polarization Rotation:
90 = 90°
45 = 45°

Fiber Type:
SS = SM to SM
PP = PM to PM

Input Polarizer (for PM PSW):
0 = no polarizer
P = Input polarizer (slow axis)

Connector Type:
FC/PC, FC/APC or
NC = No Connectors
Others specify

Board:
D = with driver board
No character here if without driver board

ACTIVE POLARIZATION MODULES

Pigtailed Polarization Controller - PolaRITE™ (PLC-002/M02)

This version of the PolaRITE™ manual polarization controller is conveniently pigtailed with or without connectors. It can be spliced to other components with minimal loss, and is ideal for controlling the polarization state of light in any single mode fiber optic system. It is available in a regular (PLC-002) or miniature (PLC-M02) size for maximum flexibility.

Specifications:

Intrinsic Insertion Loss	< 0.05 dB
Return Loss	> 65 dB
Operating Wavelength[1]	480 nm, 633 nm, 780 nm, 820 nm, 980 to 1310 nm, 1260 to 1650 nm
Extinction Ratio	> 40 dB
Operating Temperature	-40 to 85 °C
Storage Temperature	-40 to 85 °C
Dimensions	PLC - 002: 4.00" (L) x 1.00" (W) x 1.06" (H) PLC - M02: 3.00" (L) x 1.00" (W) x 1.09" (H)

Note:
Values are referenced without connectors

1. 1260 to 1650nm and 980 to 1310 nm are the standard wavelength ranges for this product. Please contact General Photonics for information on other wavelength options.

Features:

- Low Loss
- Low back reflection
- Compact
- Easy to connect
- Low cost
- Insensitive to wavelength variations

Applications:

- High speed telecommunication systems
- WDM systems
- CATV systems
- Fiber laser
- Fiber sensor systems
- PM fiber systems
- Antenna remoting systems

Related Products:

- Polarization Controllers (PLC-003/006, PLC-004/005)
- Components

Tech Info:

- What is Polarization?
- Polarization in Fiber Systems: Squeezing out More Bandwidth
- PolaRITE™ Polarization Controllers Application Note

Dimensions (in inches):

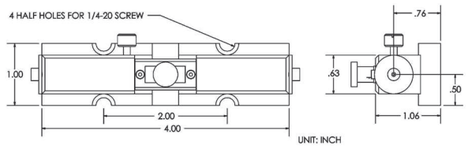

PLC-002

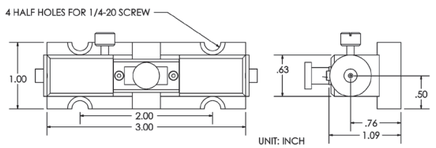

PLC-M02

Ordering Information:

PLC — □ □ □ — □ — □

Configuration:
002 = regular size 900 µm jacket
M02 = miniature version 900 µm jacket

Operation Wavelength:
1 = 480 nm
2 = 633 nm
3 = 780 nm
4 = 820 nm
6 = 980 - 1310 nm*
7 = 1260 - 1650 nm

Connector Type:
FC/PC, FC/APC
SC/PC, SC/APC,
or NC = no connectors
Others specify

Notes:
*This fiber can handle wavelengths up to 1650nm, but if it is coupled to SMF-28 fiber, the performance may not be quite as good as normal due to mode mismatch.

ACTIVE POLARIZATION MODULES

Drop-in Polarization Controller - PolaRITE™ (PLC-003/006)

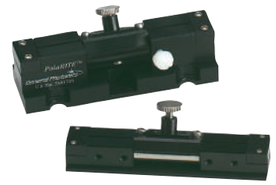

This is the in-line version of the PolaRITE™ polarization controller. It can be inserted into a fiber optic system to control the polarization state of light without having to disconnect any part of the system. It can be used by simply inserting a length of fiber into the slot located on top of the device. The miniature version can be inserted in even tighter spaces in a fiber optic module.

Specifications:

Intrinsic Insertion Loss	< 0.05 dB
Return Loss	> 65 dB
Operating Wavelength	480 nm, 633 nm, 780 nm, 820 nm, 980 nm, 1064 nm, 1260 to 1650 nm
Extinction Ratio	> 40 dB
Operating Temperature	-40 to 85 °C
Storage Temperature	-40 to 85 °C
Dimensions	PLC - 003: 3.00" (L) x 1.00" (W) x 1.09" (H) PLC - 006: 3.00" (L) x 0.63"(W) x 0.67" (H)

Features:

- Low Loss
- Low back reflection
- Compact
- Easy to connect
- Low cost
- Insensitive to wavelength variations
- Works with fibers of any size

Applications:

- High speed telecommunication systems
- WDM systems
- CATV systems
- Fiber laser
- Fiber sensor systems
- PM fiber systems
- Antenna remoting systems

Related Products:

- Polarization Controllers (PLC-002/M02, PLC-004/005)
- Components

Tech Info:

- What is Polarization?
- Polarization in Fiber Systems: Squeezing out More Bandwidth
- PolaRITE™ Polarization Controllers Application Note

Dimensions (in inches):

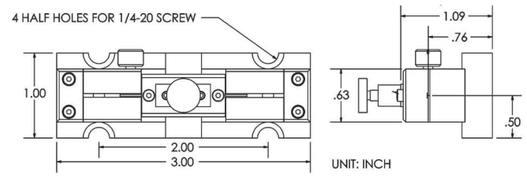

PLC-003

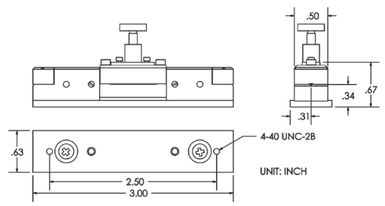

PLC-006

Ordering Information:

PLC — 00 □ — □ — □ □

Configuration:
3 = Lab. version
6 = Miniature version

Clamp Type:
S = Fiber clamp with screws
M = Fiber clamp with magnets

Fiber Size:
25 = 250 µm jacket
90 = 900 µm jacket

Notes:
PLC-006 has no 900 µm jacket option
Magnet clamp available only for PLC-003 for 250µm fiber
900µm fiber version should be used with tight-buffered fiber.

ACTIVE POLARIZATION MODULES

Fully Connectorized Polarization Controller - PolaRITE™ (PLC-004/005)

This is a fully connectorized polarization controller that comes with either male (PLC-005) or female (PLC-004) connectors, thus eliminating the headaches of fiber pigtails. Customers can use the bulkhead connectors of their choice. Although the unit comes with FC type connectors, it can interface with ST and SC type connectors with industry standard FC/ST or FC/SC adapters. The device is especially suitable for interconnecting polarization maintaining (PM) fibers using standard connectors without having to align the birefringent axes of the PM fibers. Optional scales allow easy replication of earlier settings, a feature highly desirable in laboratories for repeating polarization adjustments.

Specifications:

Insertion Loss	< 0.5 dB with connectors
Return Loss	> 55 dB for APC connectors, > 45 dB for PC connectors
Operating Wavelength[1]	480 nm, 633 nm, 780 nm, 820 nm, 980 to 1310 nm, 1260 to 1650 nm
Extinction Ratio	> 40 dB
Operating Temperature	-40 to 85 °C
Storage Temperature	-40 to 85 °C
Dimensions	4.00" (L) x 1.00" (W) x 1.09" (H)

Notes:
1. 1260 to 1650nm and 980 to 1310 nm are the standard wavelength ranges for this product. Please contact General Photonics for information on other wavelength options.

Ordering Information:

PLC — 00 □ — □ — □

Configuration:
4 = Female connectors
5 = Male connectors

Operation Wavelength:
1 = 480 nm
2 = 633 nm
3 = 780 nm
4 = 820 nm
6 = 980 - 1310 nm*
7 = 1260 - 1650 nm

Connector Type:
FC/PC, FC/APC

Notes
*This fiber can handle wavelengths up to 1650nm, but if it is coupled to SMF-28 fiber, the performance may not be quite as good as normal due to mode mismatch.

Dimensions (in inches):

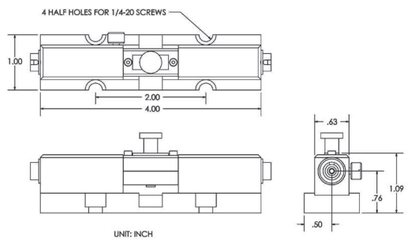

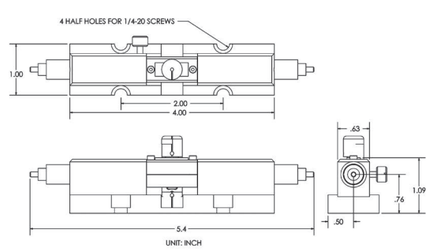

Features:

- Low loss
- Low back reflection
- Compact
- Easy to connect
- Low cost
- Insensitive to wavelength variations

Applications:

- High speed telecommunicationsystems
- WDM systems
- CATV systems
- Fiber laser
- Fiber sensor systems
- PM fiber systems
- Antenna remoting systems

Related Products:

- Polarization Controller (PLC-003/006, PLC-002/M02)
- Components

Tech Info:

- What is Polarization?
- Polarization in Fiber Systems: Squeezing out More Bandwidth
- PolaRITE™ Polarization Controllers Application Note

Passive Polarization Modules

Fiber Optic Depolarizer - PolaZero™ (DEP) 80
PMD and PDL Calibration Standards (CS-DGD/PDL/SOPMD) 82
Fixed Differential Group Delay- PolaDelay™ (FDE-002) 84

Fiber Optic Depolarizer - PolaZero™ (DEP)

Capable of depolarizing lasers with coherence lengths of kilometers, General Photonics' passive depolarizer is miles ahead of the competition. This patented device comes in a package as small as 85 × 60 × 10 mm for lasers with coherence lengths less than 10 meters. Devices for coherence lengths in the kilometer range can be custom made in a larger package, with nominal customization fees. This device is ideal for minimizing the polarization sensitivity of fiber optic sensor systems such as systems for quasi-distributed temperature and strain sensing based on fiber Bragg gratings (FBG), systems for distributed temperature and strain sensing based on Brillouin or Raman scattering, and systems for distributed acoustic sensing based on Rayleigh scattering. It can also help to eliminate the effects of PDL or polarization sensitivity of optical components and instruments. Equally important, it can be used for depolarizing pump lasers to eliminate the polarization sensitivity of Raman amplifiers. The rugged package provides high performance and superb environmental stability. The internal structure and package size may be different depending on the coherence length or spectral width of the light signal to be depolarized (see standard package drawings below). Contact General Photonics for an optimized configuration for your intended applications.

Specifications:

Center Operating Wavelength[1]	1310 nm, 1550 nm
Operating Wavelength Range	± 50 nm
Coherence Length of Light Source	DEP-002: 0 to 30mm (for broadband sources) DEP-003: 0 to 300m (for narrowband sources)
Output Degree of Polarization	< 5%
Insertion Loss[2]	1.0 dB typical, 1.4 dB max.
Residual Extinction Ratio	< 0.5 dB
Return Loss[2]	55 dB
Optical Power Handling	300 mW min.
Operating Temperature	0 to 70 °C
Storage Temperature	-40 to 85 °C
Fiber Type[3]	Input: PM Panda fiber, Output: SMF-28
Dimensions	85 × 85 × 15 mm for DEP-003 85 × 60 × 10 mm or 85 × 85 × 15 mm for DEP-002, depending on the coherence length of the light source Note: Depolarizers with coherence lengths >10 mm (DEP-002) or 200m (DEP-003) may not fit in the standard enclosures.

Notes:
Values are referenced without connectors

1. Contact General Photonics regarding other wavelengths.
2. For DEP-003 with 10m coherence length.
3. DEP-002 can be built for an SM output light source. Please specify that requirement when ordering.

Ordering Information:

DEP — 00 □ — □ □ — □ □ — □

Type*:	Wavelength:	Coherence Length:	Connector Type:
2	15 = 1550 nm	10 = 10 m	FC/PC, FC/APC, or
3	13 = 1310 nm	Others specify	NC = no connectors
			Others specify

Notes:
To be determined by General Photonics depending on customer requirements

Features:

- For lasers with coherence length up to and beyond 10m
- Low degree of polarization
- Wide operating wavelength range
- Low insertion loss
- Compact size

Applications:

- Minimize polarization sensitivity of FBG based fiber sensor systems
- Reduce polarization sensitivity of Brillouin, Raman, or Rayleigh scattering based distributed fiber sensor systems
- Remove polarization sensitivity of Raman amplifiers
- Eliminate polarization sensitivity of optical instruments
- Reduce PDL effects of optical components

Related Products:

- Polarization Scrambler Modules (PCD-005, PCD-003, PSM-002)

Tech Info:

- Scrambling to Minimize Polarization Related Impairments

FAQ:

- Depolarizers

PASSIVE POLARIZATION MODULES

Fiber Optic Depolarizer - PolaZero™ (DEP)

Typical Performance Data:

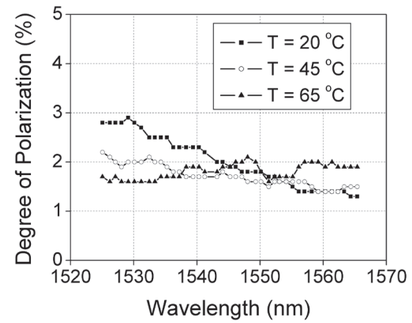

Figure 1. Degree of Polarization (DOP) as function of wavelength and temperature.

Dimensions (standard packages in mm):

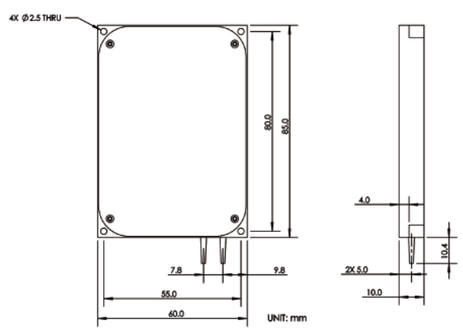

Alternate smaller package for depolarizers with small coherence lengths

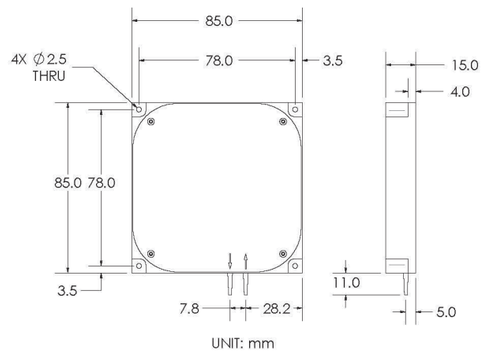

Standard package for DEP-003

PMD and PDL Calibration Standards (CS-DGD/PDL/SOPMD)

PMD and PDL are important considerations in many applications, especially high data-rate communications. With the development of high precision test equipment and tighter-tolerance systems, a need has arisen for extremely precise calibration standards. General Photonics offers a range of calibration standards for DGD, second order PMD, and PDL. The accuracy of the standards is assured by the intrinsic optical and birefringence properties of the materials used in their construction.

Specifications:

DGD Calibration Standard	
Mean DGD (1500 to 1600nm)	0.314 or 0.628 ps
Material	Quartz
Calibration Wavelength Range	1460 to 1620nm
DGD Uncertainty	±1.5 fs over 1460 to 1620 nm
PDL	< 0.05 dB typical, 0.1 dB max.
Insertion Loss	< 0.5 dB typical, 0.7 dB max w/o connectors
Return Loss	50 dB without connectors
Temperature Stability	DGD value × 0.0003/°C
Fiber Type	SMF-28
Power Handling	300 mW
Operating Temperature	23 ± 5 °C
Storage Temperature	-40 to 80 °C
Package Dimensions	2.28" (L) × 0.31" (W) × 0.31" (H)

Second Order PMD (SOPMD) Calibration Standard[1]	
Mean SOPMD (1500 to 1600nm)	2.04 ps^2 (Mean DGD 2.02 ps) 8.16 ps^2 (Mean DGD 5.89 ps) 16.31 ps^2 (Mean DGD 11.51 ps) 32.63 ps^2 (Mean DGD 8.08 ps)
Material	YVO_4
Polarization Dependent Chromatic Dispersion (PDCD)	0
Calibration Wavelength Range	1460 to 1620nm
SOPMD Uncertainty	±1% over 1460 to 1620 nm
PDL	< 0.05 dB typical, 0.1 dB max.
Insertion Loss	< 0.5 dB typical, 0.7 dB max w/o connectors
Return Loss	50 dB without connectors
SOPMD Temperature Stability	SOPMD value × 0.0006/°C
Fiber Type	SMF - 28
Power Handling	300 mW
Operating Temperature	23 ± 5 °C
Storage Temperature	-40 to 80 °C
Package Dimensions	2.28" (L) x 0.43" (W) x 0.36" (H)

Note:
1. Values listed in this table are nominal values. Exact specifications will be provided with individual units.

PASSIVE POLARIZATION MODULES

PMD and PDL Calibration Standards (CS-DGD/PDL/SOPMD)

PDL Calibration Standard	
PDL	0.05, 0.1, 0.2, 0.4, 0.5, 1.0, 1.5 or 2.0 dB
Calibration Wavelength Range	1520 to 1620 nm or 1260 to 1360 nm
Insertion Loss	PDL + 0.5 dB w/o connectors
Return Loss	50 dB without connectors
Temperature Stability	0.001 dB / °C
PDL Uncertainty	± (0.005 dB + PDL * 1%)
Fiber Type	SMF-28
Power Handling	300 mW
Operating Temperature	23 ± 5°C
Storage Temperature	-40 to 80 °C
Dimensions	2.28" (L) × 0.43" (W) × 0.36" (H)

Features:

- Compact size
- Accurate and precise
- Large range of values available

Applications:

- Measurement equipment testing and calibration
- System testing

Related Products:

- Polarization Measurement System (PSGA-101A)
- Fixed DGD (FDE-002)

Tech Info:

- High accuracy polarization measurements using binary polarization rotators

Typical Performance Data:

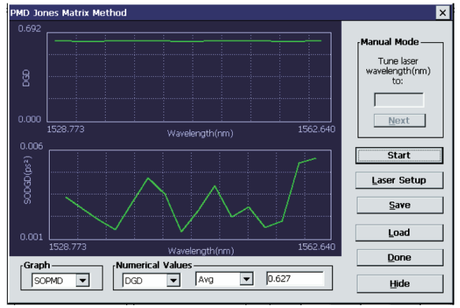

DGD (1st order PMD) calibration standard: 1st and 2nd order PMD measurement of 20mm quartz crystal. Specified DGD=0.628ps, SOPMD = 0 ps^2, Measured DGD=0.627ps, SOPMD <0.006 ps^2

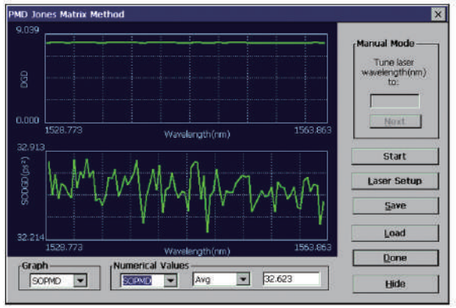

2nd order PMD calibration standard: 1st and 2nd order PMD measurement of two 8mm YVO_4 crystals with 45° relative orientation. Specified DGD=8.078 ps, SOPMD=32.627ps^2, Measured DGD=8.180 ps, SOPMD = 32.623 ps^2

Dimensions (in inches):

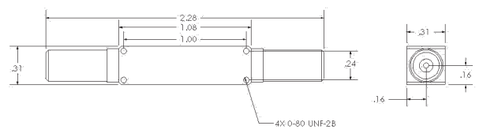

DGD/SOPMD standards

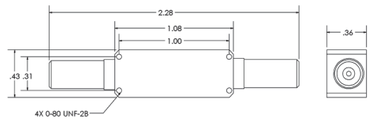

PDL standards

Ordering Information:

Calibration standards are customized to user requirements. Contact General Photonics for details.

Fixed Differential Group Delay- PolaDelay™ (FDE-002)

General Photonics' fixed differential group delay lines eliminate the need for precise measurement of PM fiber lengths to add defined amounts of first order PMD to a system. DGD values of up to 45 ps are available in the standard size package. Larger DGD values are also available by special request.

Specifications:

Operating Wavelength	1550 ± 50 nm
Insertion Loss	0.8 dB typical, 1.0 dB max
DGD Value[1]	0 ps to 45 ps standard
DGD Calibration Accuracy	± (1 fs + DGD x 0.5%)
2nd Order PMD[2]	< 30 ps[2]
PDL	< 0.2 dB
Return Loss	55 dB
Operating Temperature	0 to 70 °C
Storage Temperature	-40 to 85 °C
Optical Power Handling	300 mW min.
Fiber Type	SMF - 28
Dimensions[3]	4.25" (L) × 0.31" (W) × 0.31" (H)

Note:
Values are referenced without connectors

1. DGD values cannot be continuously specified. Contact General Photonics for available values.
2. 2nd order PMD depends on DGD value.
3. Dimensions listed are for the standard package for DGD ≤ 45 ps. Package size may vary with DGD value.

Features:

- Large 1st order PMD up to 45 ps
- Compact size
- Low insertion loss

Applications:

- PMD emulation
- PMD compensation
- TDM bit alignment

Related Products:

- Polarization Measurement System (PSGA-101A)
- PMD Source (PMD-1000)

Tech Info:

- High accuracy polarization measurements using binary polarization rotators

Ordering Information:

FDE — 002 — □ □ — □

DGD Value:
01 = 1 ps
xx = xx ps

Connector Type:
FC/PC, FC/APC
SC/PC, SC/APC or
NC = no connectors
Other specify

Dimensions (in inches):

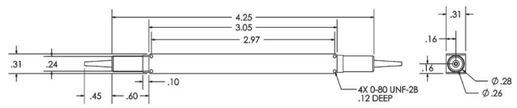

UNIT: INCH

Active Timing/Delay Modules

Motorized Variable Optical Delay Line - VariDelay™ II (MDL-002) 86
Miniature Motorized Variable Optical Delay Line - VariDelay™ II (MDL-003) 88
Manual Variable Optical Delay Line - VariDelay™ I (VDL-001) 89
Miniature Manual Variable Optical Delay Line - VariDelay™ I (VDL-002) 91
Fiber Stretcher (FST-001) 92
Fiber Phase Shifter (FPS-001) 93
Fiber Phase Shifter (FPS-002) 94
Fiber Phase Shifter (FPS-003) 95

Motorized Variable Optical Delay Line - VariDelay™ II (MDL-002)

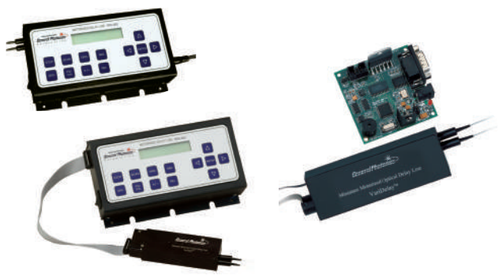

General Photonics' motorized variable optical delay line provides precision optical path length adjustment of up to 560 ps, single-pass. Driven by a DC motor with an integrated encoder, the MDL-002 has a resolution of less than 0.3μm (1 fs). In addition, its advanced motion design guarantees longevity for long-term continuous operation. Low insertion loss and high reliability make this device ideal for integration in optical coherence tomography (OCT) systems, network equipment and test instruments for precision optical path length control or timing alignment. The MDL-002 is available in three configurations: 1) an integrated unit for use as a bench-top instrument for laboratory applications, 2) with the optical head and control unit separated for easy incorporation into other equipment, and 3) an OEM version with a miniature controller board. All three versions can be remote controlled by a PC or a micro-processor through an RS-232 interface. The delay line is available with either single mode or PM fiber pigtails.

Specifications:

Operating Wavelength[1]	SM: 1260 to 1650 nm PM or double-pass: 1310 ± 50 or 1550 ± 50 nm	1060 ± 50nm
Optical Delay Range[2]	0 – 330 ps (single-pass model) 0 – 560 ps (single-pass model) 0 – 1120 ps (double-pass model)	0 – 330 ps (single-pass model) 0 – 560 ps (single-pass model)
Position Accuracy[3]	±3 μm (single-pass) ±6 μm (double-pass)	±3 μm (single-pass)
Position Repeatability[3]	±3 μm (single-pass) ±6 μm (double-pass)	±3 μm (single-pass)
Insertion Loss	1.0 dB nominal (single-pass) 1.5 dB nominal (double-pass)	1.5 dB nominal (single-pass)
Insertion Loss Variation	±0.3 dB over entire range for 330 ps model ±0.5 dB over entire range for 560 ps model ±0.7 dB over entire range for 1120 ps model	±0.3 dB over entire range for 330 ps model ±0.5 dB over entire range for 560 ps model
Optical Delay Resolution	0.3 μm or 1 fs per encoder count (single-pass) 0.6 μm or 2 fs per encoder count (double-pass)	
PDL	0.1 dB max for single-mode fiber	
Return Loss	50 dB	
Extinction Ratio	> 18 dB for PM model	
Optical Damage Power Threshold	300 mW	
Power Supply	12 VDC / 1A max.	
Control Mode	Panel keypad and RS-232 interface	
Display	2 x 16 character LCD	
Operating Temperature	0 °C to 40 °C	
Storage Temperature	-20 °C to 60 °C	
Fiber Type	SMF-28 or PM Panda fiber	HI1060 or PM 980 Panda fiber
Dimensions (Control Unit/Integrated Version)	330 ps model: 7" (L) × 4" (W) × 1.6" (H) 560 ps or 1120 ps models: 9" (L) × 4.4" (W) × 1.6" (H)	330 ps model: 7" (L) × 4" (W) × 1.6" (H) 560 ps model: 9" (L) × 4.4" (W) × 1.6" (H)
Dimensions (Optical Head)	330 ps model: 5.20" (L) x 1.46" (W) × 0.7" (H) 560 ps or 1120 ps models: 6.18" (L) x 1.46" (W) x 0.7" (H)	330 ps model: 5.20" (L) x 1.46" (W) × 0.7" (H) 560 ps model: 6.18" (L) x 1.46" (W) x 0.7" (H)
Dimensions (Mini Controller Board)	2.56" (L) × 2.56" (W) × 0.85" (H)	

Notes:

Values in table are valid over a 1060 ± 50, 1310 ± 50 or 1550 ± 50nm range for a device without connectors.

1. Other wavelengths, also available.
2. The 1120 ps model is a double-pass device. Since input and output signals travel on the same pigtail, a circulator or PBS may be necessary to separate input and output signals for some applications. Double-pass versions not available for 1060nm.
3. Accuracy and repeatability specifications given for mechanical position of reflector at static position setting.

ACTIVE TIMING/ DELAY MODULES

Motorized Variable Optical Delay Line - VariDelay™ II (MDL-002)

Features:

- Compact
- High resolution
- Low backlash
- Low insertion loss
- High stability
- Highest delay to length ratio
- Long delay: more than 560 ps

Applications:

- Optical Coherence Tomography (OCT)
- Optical Fourier spectrum analysis
- Optical interferometry
- Delay generation and measurement
- Optical time division multiplexing (OTDM)
- Fiber sensors

Related Products:

- Miniature Motorized Delay Line (MDL-003)
- Manual Delay Lines (VDL-001, VDL-002)
- Components

Tech Info:

- Optical Coherence Tomography Technologies

FAQ:

- Delay Lines

Typical Performance Data:

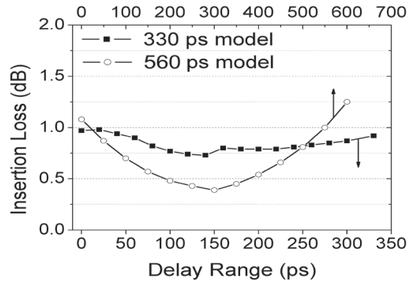

Figure 1. Insertion loss vs. optical delay.

Dimensions: (Representative drawings: 560 ps version, in inches)

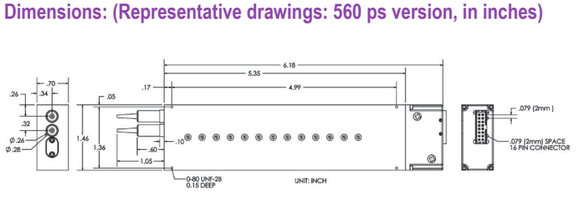

Optical head:

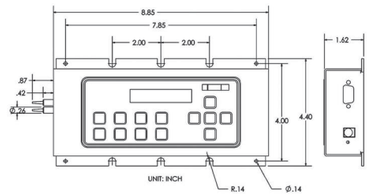

Integrated version/control unit

Ordering Information:

MDL — 002 — □ – □□ – □□ – □□ – □□ – □□□□

Configuration:	Wavelength:	Delay Range:	Fiber Type:	Connector Type:
I = integrated	10 = 1060 nm	33 = 330 ps	SS = SM	FC/PC, FC/APC
D = Remote head/ standard controller	13 = 1310 nm	56 = 560 ps	PP = PM Panda	SC/PC, SC/APC or
O = Remote head/ mini controller board	15 = 1550 nm	11 = 1120 ps		NC = no connectors
	35 = 1310 & 1550 nm			Others specify

Configuration Notes:

1. For SM pigtails, the default configuration is 3mm jacketed. For PM pigtails, the default configuration is 900μm loose tube jacketed.
2. Wavelength: 35 option (dual window 1310/1550nm) is available only for SM single-pass devices (330 and 560 ps). PM or double-pass devices are single-window (1310 or 1550nm) only.
3. Double-pass only available with SM fiber.
4. Double-pass not available for 1060nm.

ACTIVE TIMING/ DELAY MODULES

Miniature Motorized Variable Optical Delay Line - VariDelay™ II (MDL-003)

General Photonics' motorized variable optical delay line provides low cost, precision optical path length adjustment and delay scanning functionality. This addition to the MDL product line is specifically designed for OEM applications that require continuous scanning capability and a small footprint. The standard device has a delay range of 100 ps. An internal mirror can also be installed to cause light to double pass the device, doubling the delay range. A stepper motor and two position sensors ensure precise delay control. Low insertion loss and high reliability make this device ideal for integration in optical coherence tomography (OCT) systems, network equipment and test instruments for precision optical path length control or timing alignment. A mini controller board is available as an accessory.

Specifications[1]:

Operating Wavelength[2]	SM: 1260 to 1650 nm PM: 1310 or 1550 ± 50 nm
Optical Delay Range[3]	0 to 100 ps, single-pass
Optical Delay Resolution	30 µm, single-pass at maximum speed
Optical Delay Accuracy	±40 µm, single-pass at maximum speed
Optical Delay Repeatability	±40 µm, single-pass at maximum speed
Insertion Loss	1 dB
Insertion Loss Variation	±0.3 dB over entire range
PDL	0.15 dB for single mode fiber
Return Loss	55 dB
Extinction Ratio	> 18 dB for PM model
Actuation Speed	50 ps/s (single-pass) max.
Optical Damage Power Threshold	100 mW
Electrical Interface	2 - phase stepper motor drive signal 2 sensor connections
Operating Temperature	0 to 50 °C
Storage Temperature	-20 to 60 °C
Fiber Type	SMF-28 or PM Panda fiber
Dimensions	2" (L) x 1.4" (W) × 0.55" (H)

Notes:
1. Specifications in table apply for a single-pass device without connectors, measured over 1310 ± 50 nm or 1550 ± 50 nm. The output pigtail can also be replaced with a Faraday mirror to create a double pass device with a total range of 200 ps. Some specifications will change for this case.
2. Other wavelengths, such as 1064 nm, also available.
3. Double pass device has 200 ps delay range. Since input and output signals travel on the same pigtail, a circulator or PBS may be necessary to separate input and output signals for some applications.

Features:

- Compact
- Low insertion loss
- High stability
- High reliability
- Low cost

Applications:

- Optical Coherence Tomography (OCT)
- Optical Fourier spectrum analysis
- Optical interferometry
- Delay generation and measurement
- Optical time division multiplexing (OTDM)
- Fiber sensors

Related Products:

- Motorized Delay Line (MDL-002)
- Manual Delay Lines (VDL-001, VDL-002)
- Components

Tech Info:

- Optical Coherence Tomography Technologies

FAQ:

- Delay Lines

Ordering Information:

MDL — 003 — □□ — □□ — □ — □□ — □

Wavelength:
13 = 1310 nm
15 = 1550 nm
35 = 1310 & 1550 nm

Delay Range:
10 = 100 ps

Pass:
S = single
D = double

Fiber Type:
SS = SM
PP = PM Panda

Connector Type:
FC/PC, FC/APC
SC/PC, SC/APC or
NC = no connectors
Others specify

Configuration Notes:
1. Wavelength: 35 option (dual window 1310/1550nm) is available only for SM single-pass devices. PM or double-pass devices are single-window (1310 or 1550nm) only.
2. Double-pass only available with SM fiber

Dimensions (in inches):

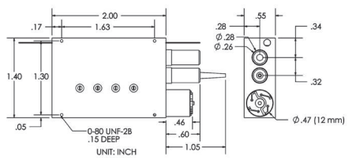

Figure 1. Mechanical dimensions

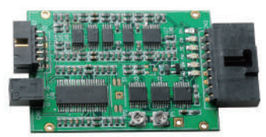

Driver board available

ACTIVE TIMING/ DELAY MODULES

Manual Variable Optical Delay Line - VariDelay™ I (VDL-001)

General Photonics' manual variable optical delay line provides precision optical path variation of more than 18 cm (600 ps). The compact, rugged design makes the device ideal for integration in network equipment, test instruments, and optical coherence tomography (OCT) systems for precision optical path length or timing alignment.

Specifications:

Operating Wavelength Range[1]	SM: 1260 to 1650 nm PM or double-pass: 1310 ± 50 or 1550 ± 50 nm
Optical Delay Range[2]	0 – 330 ps (single-pass model) 0 – 600 ps (single-pass model) 0 – 1200 ps (double-pass model)
Readout Scale Resolution	0.05 mm
Insertion Loss	1.0 dB nominal (single-pass) 1.5 dB nominal (double-pass)
Insertion Loss Variation	±0.3 dB over entire range for 330 ps model ±0.5 dB over entire range for 600 ps model ±0.7 dB over entire range for 1200 ps model
Return Loss	50 dB
Extinction Ratio	> 18 dB for PM model
Optical Power Handling	300 mW min.
Operating Temperature	0 to 40 °C
Storage Temperature	-40 to 60 °C
Fiber Type	SMF-28, or PM Panda fiber
Dimensions	330 ps model: 4.2" (L) × 2.1" (W) × 1.0" (H) 600 or 1200 ps models: 6.0" (L) × 2.1" (W) × 1.0" (H)

Notes:
Values in table are valid over a 1310 ± 50 or 1550 ± 50nm range for a device without connectors.
1. Other wavelengths, such as 1064 nm, also available.
2. The 1200 ps model is a double-pass device. Since input and output signals travel on the same pigtail, a circulator or PBS may be necessary to separate input and output signals for some applications.

Features:

- Space efficient
- Highest delay to length ratio
- Long delay: more than 600 ps
- Low insertion loss variation
- Rugged design

Applications:

- Optical Coherence Tomography (OCT) systems
- Passive time division multiplexing
- TDM bit alignment
- Fiber interferometers

Related Products:

- Motorized Delay Lines (MDL-002, MDL-003)
- Manual Delay Line (VDL-002)
- Components

Tech Info:

- Optical Coherence Tomography Technologies

FAQ:

- Delay Lines

Ordering Information:

VDL — 001 — □□ — □□ — □□ — □□

Wavelength:
13 = 1310 nm
15 = 1550 nm
35 = 1310 & 1550 nm

Delay Range:
33 = 330 ps
60 = 600 ps
12 = 1200 ps

Fiber Type:
SS = SM
PP = PM Panda

ConnectorType:
FC/PC, FC/APC
SC/PC, SC/APC or
NC = no connectors
Other specify

Configuration Notes:
1. For SM pigtails, the default configuration is 3mm jacketed. For PM pigtails, the default configuration is 900µm loose tube jacketed.
2. Wavelength: 35 option (dual window 1310/1550nm) is available only for SM single-pass devices (330 and 600 ps). PM or double-pass devices are single-window (1310 or 1550nm) only.
3. Double pass only available with SM fiber.

Manual Variable Optical Delay Line - VariDelay™ I (VDL-001)

Typical Performance Data:

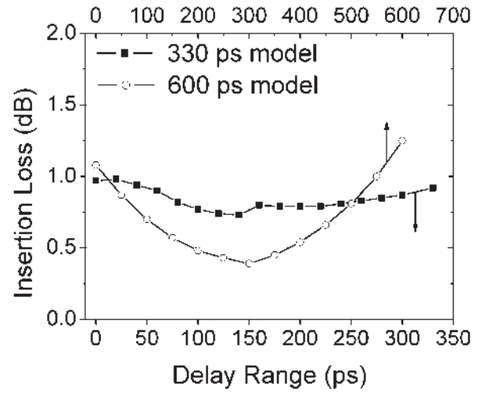

Figure 1. Insertion loss vs. optical delay.

Dimensions (in inches):

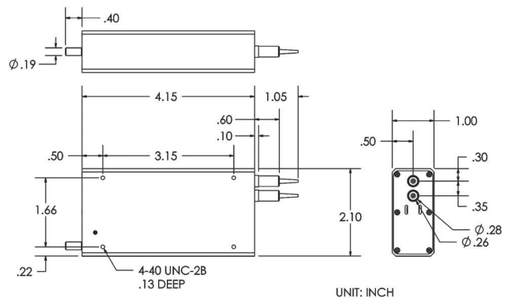

330 ps version

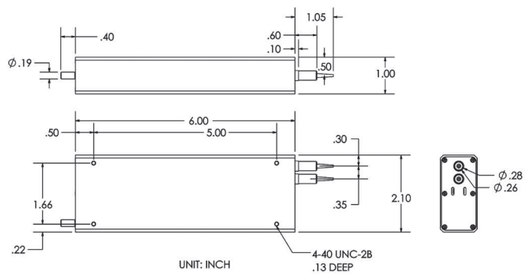

600 ps version

Miniature Manual Variable Optical Delay Line - VariDelay™ I (VDL-002)

The VDL-002 is a miniaturized variable optical delay line designed specifically for OEM applications. With a delay range of up to 250 ps, this device is a superior replacement for the variable RF phase shifters inadequately adapted from the RF/wireless field for fiber optic communications. It is especially useful in coherent detection systems for adjusting phase or delay differences between signals. The VDL-002 eliminates the VSWR problems of RF phase shifters for high frequency and broadband signals, especially at 40 and 100Gbps. A single device can be used for any data rate, simplifying inventory management. With a footprint of only 0.72" x 1.46" x 2.2" for a delay range of 100 ps, the device can be conveniently integrated into network modules, test instruments, and OCT equipment for precision optical path length control or timing alignment. An internal mirror can be installed to cause light to double pass the device, doubling the delay range. The unique design makes hermetically sealed packaging possible and enables Telcordia qualification when required. Finally, a locking mechanism is provided for locking the delay at a permanent position. The VDL-002 generally comes with single mode or PM fiber pigtails per customer requirement.

Specifications[1]:

Operating Wavelength	SM: 1260 to 1650 nm PM: 1310 or 1550 ± 50nm Other wavelengths may be available upon request
Optical Delay Range[2]	0 – 100 ps (3 cm) continuous for 100 ps model 0 – 250 ps (7.5 cm) continuous for 250 ps model Internal mirror option for doubling the range
Delay Stability	0.15 ps
Zero Point Delay Offset[3]	180 ps
Insertion Loss	1.0 dB nominal
Insertion Loss Variation	±0.3 dB over entire range
PDL	0.1 dB for single mode fiber
Return Loss	55 dB
Extinction Ratio	> 18 dB for PM model
Optical Damage Power Threshold	300 mW
Operating Temperature	-15 to 50 °C
Storage Temperature	-40 to 60 °C
Fiber Type	SMF-28 or PM Panda fiber
Position Locking	Included
Dimensions	2.20" (L) × 1.46" (W) × 0.72" (H) for 100 ps model 3.15" (L) × 1.46" (W) × 0.72" (H) for 250 ps model

Notes:
1. Specifications in table apply for a single-pass device without connectors, measured over 1310 ± 50 nm or 1550 ± 50 nm. The output pigtail can also be replaced with a Faraday mirror to create a double pass device with a total range of 200 or 500 ps, respectively. Some specifications will change for this case. Contact General Photonics for details
2. Double pass device has 200 ps or 500 ps delay range. Since input and output signals travel on the same pigtail, a circulator or PBS may be necessary to separate input and output signals for some applications.
3. Absolute delay at 0 ps setting measured to the edge of the enclosure (excluding caps, boots, and pigtails).

Features:

- Compact size
- High resolution
- Low insertion loss
- High stability
- Longevity

Applications:

- Coherent detection systems
- Optical time division multiplexing (OTDM)
- Optical coherence tomography (OCT)
- Optical interferometry
- Optical Fourier spectrum analysis
- Fiber sensors

Related Products:

- Motorized Delay Lines (MDL-002, MDL-003)
- Manual Delay Line (VDL-001)
- Components

Tech Info:

- Optical Coherence Tomography Technologies

FAQ:

- Delay Lines

Dimensions (in inches):

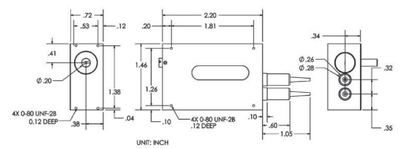

100 ps version

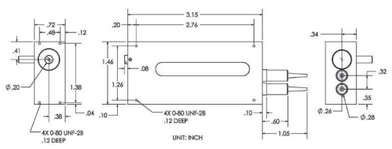

250 ps version

Ordering Information:

VDL — 002 — □□ – □□ – □ – □□ – □

Wavelength:
13 = 1310 nm
15 = 1550 nm
35 = 1310 & 1550 nm

Delay Range:
10 = 100 ps
25 = 250 ps

Pass:
S = single
D = double

Fiber Type:
SS = SM
PP = PM Panda.

Connector Type:
FC/PC, FC/APC
Others specify

Configuration Notes:
1. Wavelength: 35 option (dual window 1310/1550nm) is available only for SM single-pass devices. PM or double-pass devices are single-window (1310 or 1550nm) only.
2. Double pass only available with SM fiber.

Fiber Stretcher (FST-001)

The FST-001-B is a piezo-driven fiber stretcher with a long optical delay range of up to 3 mm. The device comes complete with a piezo driver packaged in a user-friendly small enclosure. Only +12 VDC is required to power the unit. One attractive feature is that the device is controlled by up to four independent PZTs, so that the user has the option to drive each PZT individually, for high resolution, or collectively, for large stroke. In addition, each PZT can be controlled either with an analog signal or a 12-bit TTL signal. During analog control, the driving circuit simply acts as a 4-channel voltage amplifier with 30V/V amplification. Alternatively, the output voltage can be controlled by a computer equipped with a digital I/O card, or by a microprocessor. The FST-001-B enables applications from sensing to medical imaging, interferometry, and spectrum analysis. At General Photonics, we stretch the fiber hard to make your work more relaxed.

Specifications[1]:

Optical Path Delay Range	> 3 mm (in air)
Phase Change Sensitivity	810 π/V at 1550nm, (analog input, using 4 channels)
Internal Voltage Amplification	30 V/V
Max. Voltage On PZT	140 volts
Resonance Frequency	2.2 ± 0.3 kHz
Insertion Loss	< 0.2 dB
Insertion Loss Variation	< 0.1 dB
Return Loss	> 65 dB
PDL	< 0.05 dB
Fiber Type	SMF-28 standard, others available by request
Wavelength Range[2]	1260 to 1620 nm
Maximum Optical Power	1000 mW min.
Analog Input	4 channels, 4.7 volts max. for each channel
Digital Input	20-pin digital connector to accept 12 bit TTL control signal.
Software	None
Operation Temperature	0 to 50 °C
Storage Temperature	-40 to 80 °C
Dimensions	170 (L) × 106 (W) × 38.6 (H) mm

Note:
1. Specifications in table are for standard configuration with SMF-28 fiber, without connectors, tested at 1550nm.

Features:

- Large Delay Range
- High Speed
- Low Insertion Loss
- Analog and Digital Control
- User Friendly

Applications:

- Sensors
- Interferometers
- Medical Imaging
- Spectrum Analysis
- OCT

Tech Info:

- Optical Coherence Tomography Technologies

Ordering Information:

FST — 001 — B — □□ – □□ – □□ – □□

Actuators:
04 = 4 PZT

Wavelength:
15 = 1550 nm
13 = 1310 nm

Fiber Type:
SM
PM

Connector Type:
FC/PC,
FC/APC
Others specify

Fiber Phase Shifter (FPS-001)

General Photonics' all fiber phase shifter/modulator provides phase shifts up to 15π at frequencies from DC to 20 kHz. The all fiber construction practically eliminates insertion loss and back reflection. This compact device is ideal for fiber laser systems, fiber resonators, and fiber interferometers for precision phase tuning or phase modulation.

Specifications:

Insertion Loss	< 0.1 dB
Return Loss	> 65 dB
Total Phase Shift (0 – 20 kHz)	> 8π
Half-wave Voltage (0 – 20 kHz)	< 20 V
Operating Wavelength	1260 to 1650 nm or 980 to 1310 nm standard
PDL	< 0.05 dB
Residual Amplitude Modulation	±0.01 dB
Operating Temperature	0 to 50 °C
Storage Temperature	-40 to 85 °C
Max. Applied Voltage	150 volts
Dimensions	Pigtailed: 1.38" (L) × 0.55" (W) × 0.55" (H) NoTail™: 2.90" (L) × 0.55" (W) × 0.55" (H)

Note:
Specifications in this table are for devices with SM fiber, without connectors. Information for devices with other types of fiber is available on request.

Dimensions (in inches):

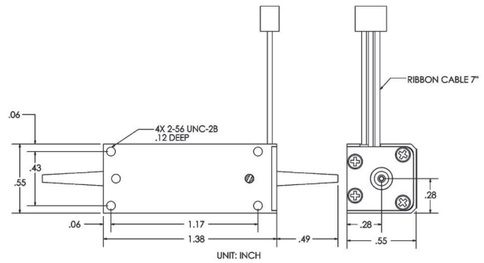

Ordering Information:

FPS — 001 — □□ – □□ – □□ – □□

Wavelength Range:
SM: 01 = 1260 - 1650 nm
02 = 980 - 1310 nm
PM: 15 = 1550 nm
13 = 1310 nm
10 = 1060 nm

Pigtail:
90 = 900 µm jacket
NT = NoTail™

Fiber Type:
SS = SM fiber
PP = PM fiber

Connector Type:
FC/PC, FC/APC
SC/PC, SC/APC or
NC = no connectors
Other specify

Features:

- Compact size
- Low insertion loss
- Low residual amplitude modulation
- Low PDL
- Low cost
- NoTail™ model available

Applications:

- Fiber interferometers
- Fiber laser systems
- Fiber sensor systems

Related Products

- Phase Shifters (FPS-002, FPS-003)

FAQ:

- Phase Shifters

Fiber Phase Shifter (FPS-002)

Coherent or interferometric sensor systems, such as distributed acoustic sensors (DAS), often require a low loss, low-cost phase shifter or modulator to obtain the desired sensing signals. General Photonics' 2nd generation all fiber phase shifter/modulator provides phase shifts up to 65π with a much lower half-wave voltage (~2 volts as compared with 10-20 volts for the 1st generation phase shifter) at frequencies from DC to 20 kHz. The all fiber construction results in low insertion loss and back reflection. In addition to fiber sensor systems, this compact device is ideal for fiber laser systems, fiber resonators, and fiber interferometers for precision phase tuning or phase modulation.

Specifications:

Wavelengths	1310/1550, 1060, or 780nm
Fiber Type	1310/1550nm: Corning ClearCurve ZBL or equiv. 1060nm: Corning HI1060 or equiv. 780nm: Corning HI780 or equiv.
Insertion Loss	<0.5 dB (at 1550nm, excluding connectors)
Return Loss	>58 dB without connectors >55 dB with APC connectors >50 dB with PC connectors)
Total Phase Shift @500Hz, Vpp=150V	>65π (at 1550nm)
Half Wave Voltage (Vπ) @500Hz	2.5-4.5V typical
Resonance Frequency	8-13kHz typical
Vπ @resonance frequency	0.1-0.5V typical
PDL	<0.05 dB
Residual Amplitude Modulation	±0.01 dB (at 1550nm)
Capacitance of Piezo	0.18μF
Maximum Applied Voltage	150V
Electrical Interface	Molex WM9131-ND or equivalent
Operation Temperature	0 to 50° C
Storage temperature	−40° to 85° C
Fiber Length (Total)	240 ±10 cm
Dimensions	35.0 (L) x 17.0 (W) x 10.0 (H) mm

Note:
Specifications in this table are for SM fiber. Information for devices with other types of fiber is available on request.

Features:

- All-fiber optical path
- Low half-wave voltage
- Large phase shift range
- Compact
- Low insertion loss
- Low residual amplitude modulation
- Low PDL
- Low cost

Applications:

- Fiber interferometers
- Fiber laser systems
- Fiber sensor systems

Related Products:

- Phase Shifters (FPS-001, FPS-003)

FAQ:

- Phase Shifters

Typical Performance Data:

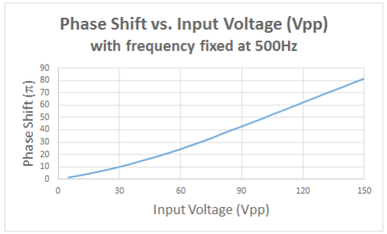

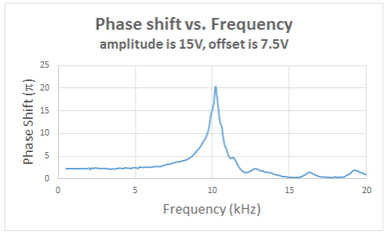

Dimensions (in mm):

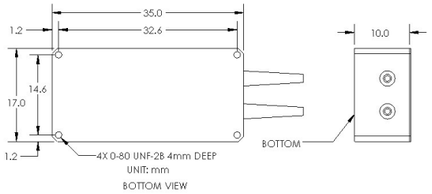

Ordering Information:

FPS — 002 — □□ — □□ — □

Wavelength:
35 = 1310/1550nm (SM only)
15 = 1550nm (PM)
13 = 1310nm (PM)
10 = 1060nm
78 = 780nm (SM only)

Fiber Type:
SS = SM fiber
PP = PM fiber

Connector Type:
FC/PC, FC/APC
SC/PC, SC/APC
NC = no connectors
Others specify

Fiber Phase Shifter (FPS-003)

The FPS-003 all fiber phase shifter/modulator combines a wide modulation bandwidth (up to 60 kHz) with low half-wave voltages to create a long-range device that can be driven by standard function generators. Like General Photonics' other phase shifters, it employs all fiber construction and has low insertion loss and back reflection. In addition to fiber sensor systems, this compact device is ideal for fiber laser systems, fiber resonators, and fiber interferometers for precision phase tuning or phase modulation.

Specifications:

Wavelengths	1310/1550, 1060, or 780nm
Fiber Type	1310/1550nm: Corning ClearCurve ZBL or equiv. 1060nm: 980-1550nm fiber with MFD 5μm at 980nm 780nm: Nufern 780HP or equiv.
Insertion Loss	<0.5 dB (at 1550nm, excluding connectors)
Return Loss	>55 dB (excluding connectors)
Total Phase Shift @500Hz, Vpp=150V	>55π (at 1550nm)
Half Wave Voltage (Vπ) @500Hz	1-3V typical
Resonance Frequency	36-39kHz typical
Vπ @resonance frequency	<150mV typical
PDL	<0.05 dB at 1550nm
Residual Amplitude Modulation	±0.01 dB (at 1550nm)
Capacitance of Piezo	5-12 nF
Maximum Applied Voltage	150V
Electrical Interface	Molex WM9131-ND or equivalent
Operation Temperature	10 to 50° C
Storage Temperature	−40° to 85° C
Fiber Length (Total)	500 ±10 cm
Dimensions	31.0 (L) x 31.0 (W) x 14.5 (H) mm

Note:
Specifications in this table are for SM fiber. Information for devices with other types of fiber is available on request.

Features:

- Wide frequency range
- Low half-wave voltage
- Large phase shift range
- Compact
- Low insertion loss
- Low residual amplitude modulation
- Low PDL

Applications:

- Fiber interferometers
- Fiber laser systems
- Fiber sensor systems

Related Products:

- Phase Shifters (FPS-001, FPS-002)

FAQ:

- Phase Shifters

Dimensions (in inches):

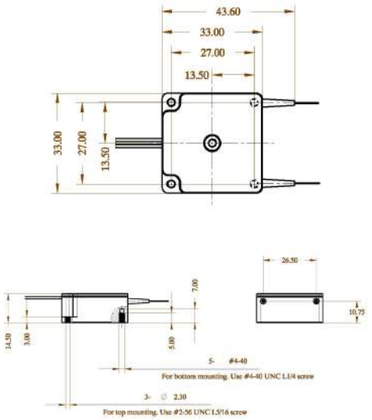

Typical Performance Data:

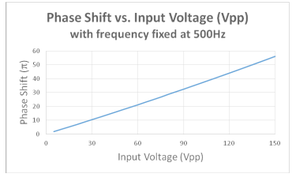

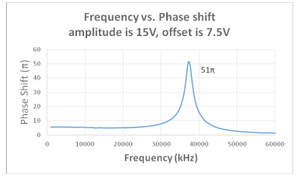

Note: Plots shown here are for FPS-003 with ClearCurve ZBL fiber, measured at 1550nm.

Ordering Information:

FPS — 003 — □□ — □□ — □

Wavelength:
35 = 1310/1550nm
10 = 1060nm
78 = 780nm

Fiber Type:
SS = SM fiber

Connector Type:
FC/PC, FC/APC
SC/PC, SC/APC
NC = no connectors
Others specify

Passive Timing/Delay Modules

Compact Time Delay Coil (TDC) 97
Fiber Gyro Coils (FC series) 98
Specialty Fiber Coils 100

Compact Time Delay Coil (TDC)

Winding a large fiber spool is easy, but making compact, low loss fiber coils requires attention, precision, and skill. Using specially designed computerized machinery and a proprietary manufacturing process, General Photonics can produce extremely low insertion loss fiber coils to fit your budget and space requirements. You no longer have to choose between large, bulky fiber spools and small, high loss coils. Our optical fiber coil fills a longstanding vacuum in the photonics market, where large time delay and small size are essential. Each coil is ruggedly packaged to withstand various environments in field applications.

Specifications:

Insertion Loss	< 0.3 dB/km typical, < 0.5 dB/km max. (above intrinsic loss)
Fiber Length	10 m to 4 km
Optical Delay	Nanoseconds to microseconds depending on fiber length and type
Operating Wavelength	1260 to 1650 nm standard, other specify
Fiber Type	SMF-28 standard, other specify
Operating Temperature	-40 to 85 °C
Storage Temperature	-40 to 85 °C
Dimensions	Enclosure: 6.00" (L) × 6.00" (W) × 1.59" (H)

Note:
Values are referenced without connectors.

Features:

- Compact for easy integration into modules
- Low insertion loss
- Customized delay length
- Rugged construction
- Variety of fiber types
- Wide spectral response range
- Plug and play for easy use

Applications:

- Optical buffer for optical networks
- Radar calibration and instrument calibration
- Laser spectroscopic measurement
- Time delay for opto-electronics oscillators
- Nonlinear fiber loop
- Optical network testing and analysis
- Optical packet switching, buffering, routing and input/output synchronization

Related Products:

- Fiber Gyro Coils (FC series)
- Specialty Coils

FAQ:

- Fiber Coils

Ordering Information:

TDC — □ — □ — □ — □

Fiber Length (m):
Example:
1000 = 1000m

Connector Type:
FC/PC, FC/APC
SC/PC, SC/APC or
NC = no connectors
Others specify

Fiber Type:
SM: Corning SMF-28
PM: Fujikura Panda
Others specify

E = with enclosure

Dimensions (in inches):

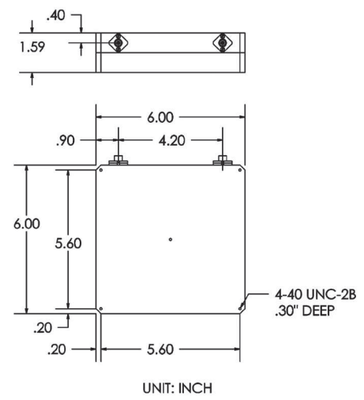

UNIT: INCH

Fiber Gyro Coils (FC series)

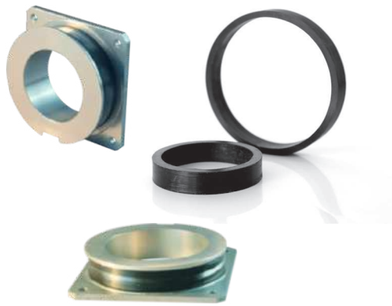

Through years of experience and hard work, General Photonics has perfected the art of coil winding for the fiber gyro industry. A suite of advanced polarization test instruments specially designed for testing the quality of fiber coils ensures the consistent production of high performance coils. General Photonics' PM coils can be wound with different winding patterns such as quadrupole, octupole, or other types to minimize the Shupe effect, which degrades the performance of a fiber gyro under temperature-varying conditions. In addition, special Shupe effect mitigation techniques are offered as a special service to customers with special requirements for superior coil performance in the most demanding temperature and vibration environments. Unlike other commercial coils on the market that come with only rudimentary specifications such as insertion loss and PER, which are insufficient to guarantee coil performance in a real world gyroscope, General Photonics offers the most comprehensive testing data on the market. Such data guarantees that the coils received are trouble free, which ultimately reduces troubleshooting, cost, and integration time. Comprehensive test data include polarization crosstalk vs. distance along the fiber at specified temperatures, with resolution of a few cm; PER, IL, etc. Our standard coils are frameless, held together with our specially formulated potting adhesives. However, they can be offered framed using General Photonics' proprietary techniques.

Specifications[1]:

Operating Wavelength[4]	840, 1060, 1310, or 1550 nm
Winding Induced IL	< 0.2 dB/km
PER[2]	> 24 dB, over full temperature range
PER variation over[2] (-40 °C to +80°C)	± 2 dB
Max polarization x- talk peak [2]	< −50 dB at 25 °C <−45 dB over the full temperature range
Number of polarization x-talk peaks above −55 dB[2]	<15 at 25 °C < 30 over the full temperature range
Average polarization x-talk [2]	< −68 dB at 25 °C < −65 dB over the full temperature range
Max bias error[3]	No Shupe mitigation: <2 degrees/hour typical peak-to-peak Level I Shupe mitigation: <1 degree/hour typical peak-to-peak Level II Shupe mitigation: < 0.5 degrees/hour typical peak-to-peak Level III Shupe mitigation: < 0.25 degrees/hour typical peak-to-peak
Fiber length[2]	10 m to 5 km
Fiber diameters[4]	135 µm, 165 µm, 250 µm
Coil ID	15 mm to 120 mm
Coil height	5 to 75 mm
Winding patterns	Quadrupole (Standard) Octupole or others (Special)
Operating Temperature	−40 C° to +80 C°
Storage Temperature	−-55 C° to +100 C°

Notes:
1. Specifications provided in the table above are for a sample coil with an ID of 80 mm and a length of 500 m. Actual specifications depend on many factors such as fiber type, fiber length, coil ID, winding pattern etc.
2. Typical values.
3. Shupe effect spec: defined as the maximum bias error caused by temperature transients of 1 degree per minute from -40 C° to 60 C°. (see Fig 2.a)
4. Specify if others.

Features:

- High Performance
- Fully Specified
- Low Polarization x-talk (PM)
- Low Temperature Sensitivity
- Low Vibration Sensitivity
- Highly Symmetric
- Available Frameless or Framed

Applications:

- Fiber Optic Gyroscope (FOG)
- Autonomous vehicles

Related Products:

- Time Delay Coils (TDC)
- Specialty Coils

Tech Info:

- A Novel Method for Determining and Improving the Quality of a Quadrupolar Fiber Gyro Coil under Temperature Variations
- Tomographic Inspection of Fiber Coils Using Optical Coherence Tomography

FAQ:

- Fiber Coils

Ordering Information:

FC – □ – □ – □ – □ – □ – □ – □ – □

Winding Type:
Q: Quadrupole
O: Octupole
S: Simple
Others specify

Coil ID:
in mm

Coil Height:
in mm

Coil Length:
in m

Fiber Diameter:
in µm

Wavelength:
15: 1550 nm
13: 1310 nm
10: 1060 nm
83: 830 nm
Others specify

Fiber Type:
SM
PM

Shupe Mitigation Level:
0 = No Shupe
A = Level 1
B = Level 2
C = Level 3

Fiber Gyro Coils (FC series)

Shupe Mitigation Options:

Level 1 (Part Number suffix "A"):
General Photonics will perform Shupe mitigation procedures based on an average optimization treatment.

Level 2 (Part Number suffix "B"):
General Photonics will perform additional Shupe mitigation treatment including more involved optimization procedures on each coil.

Level 3 (Part Number suffix "C"):
General Photonics will perform Shupe mitigation procedures based on individual optimization procedures specific to each coil including multiple iterations and multiple test procedures. General Photonics will supply details of Shupe errors versus time with step temperature changes. Shupe peak of less than 0.15°/H (or 0.3°/H peak-to-peak) at temperature steps of 1°C/min. are generally achieved. Before the delivery of production quantities of such high precision coils, a minimum of 3 trial coils should be ordered and manufactured, tested and the performance criteria would need to be agreed by both parties.

Typical Performance:

Low Polarization Crosstalk over Wide Temp Range

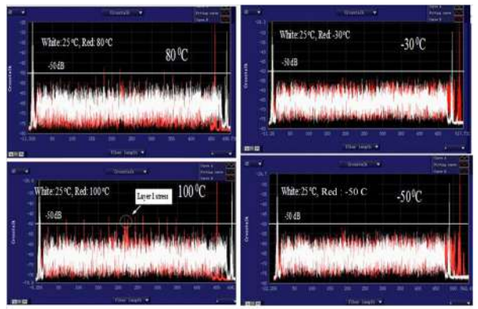

Fig. 1: Polarization crosstalk performance inside coil at -30, -50, 80, and 100°C vs. 25°C

PM Coil: Shupe Effect Mitigation

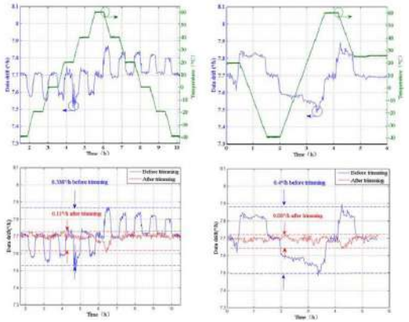

Fig. 2: Rotation rate error with a stairway temperature profile at a temperature c ramp rate of 1°C/ minute. Figures 2c and 2d illustrate the much lower rotation rate error after trimming.

PM Coil: PER Stability performance

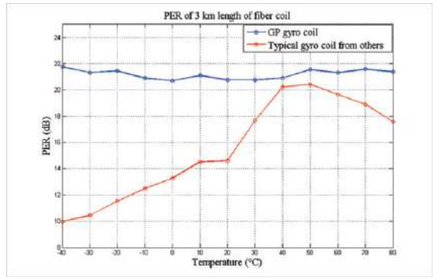

Fig. 3: PER vs. temperature of a 3 km coil from GP (blue) and another vendor (Red). PER variation over a 120°C temperature range: <2dB (GP) vs. >10 dB (others)

PM Coil: PER Repeatability performance

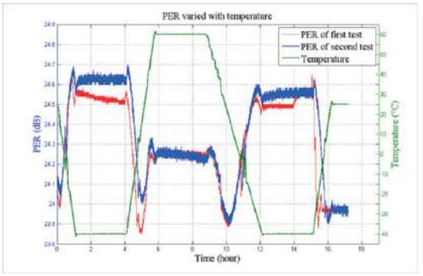

Fig. 4: Typical PER vs. temperature data (Red: 1st test, blue: 2nd test) of a 1.2km coil with PER>24dB and a PER variation of <1dB over a 120 °C temperature range

Specialty Fiber Coils

In addition to Fiber Optic Gyro (FOG) coils, General Photonics can wind specialty coils with key performance parameters optimized for the requirements of different applications. These include the following types of coils.

Microwave Photonics Coils

General Photonics' microwave delay coils have low temperature drift and can be made Doppler effect free, to satisfy the requirements of microwave photonics research and development. They can therefore play an important role in applications such as radar reflection time calibration,altimeter calibration, microwave phase noise measurements, and optoelectronic oscillators (OEO). The low insertion loss dispersive delay coil developed by General Photonics for optical phased array radar enables high speed modulation of the optical delay by modulating the laser wavelength. The coil is constructed by nesting several different low-loss fiber segments into a single coil structure using a special winding technique.

Specifications:

Fiber Length	<20 km
Doppler Effect Suppression	>95%
Dispersion Coupling Loss	<1 dB
Max. PMD (full temp. range)[1]	0.3 ps
Max. PDL (full temp. range)[1]	0.1 dB

Notes:
1. Typical. Values depend on configuration.

Typical Performance Data:

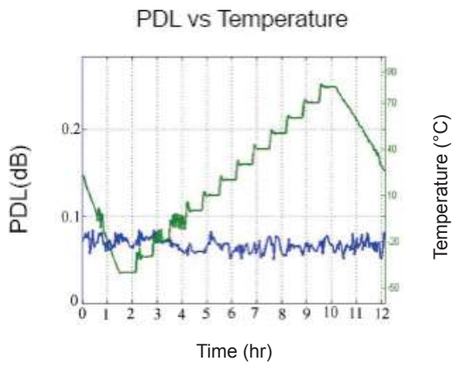

Figure 1. PDL (blue curve) is very stable over temperature variation (green curve)

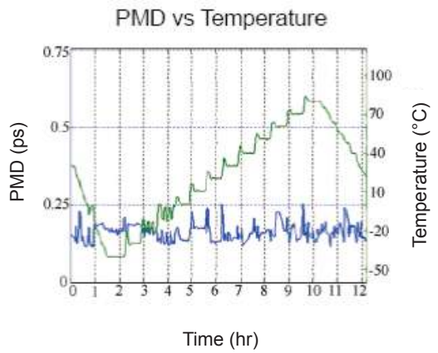

Figure 2. PMD (blue curve) is very stable over temperature variation (green curve)

Specialty Fiber Coils

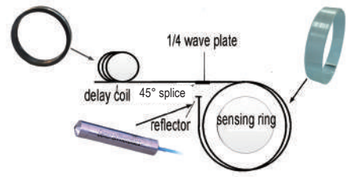

Fiber Optic Current Transformer Structural Diagram

Fiber Optic Current Sensor Coils

General Photonics' advanced coil production and measurement technologies enable the production of polarization maintaining fiber coils with extremely stable polarization extinction ratio (PER) over the entire temperature range and minimal stress-induced linear birefringence. These coils can significantly improve the ratio stability in fiber optic current transformers.

Specifications:

Fiber Length	<500 m
Average Polarization Crosstalk	<−68 dB
Max. Polarization Crosstalk	<−50 dB
PER Variation (full temp. range)	<3 dB
Accuracy (full temp. range)	<0.05%

Typical Performance Data:

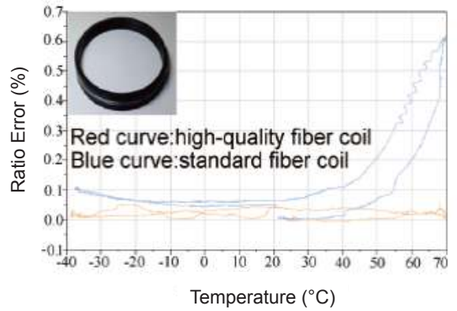

Figure 3. Ratio error vs. temperature for a temperature insensitive fiber coil (red) and a standard coil (blue). The ratio error is much lower for the temperature insensitive coil.

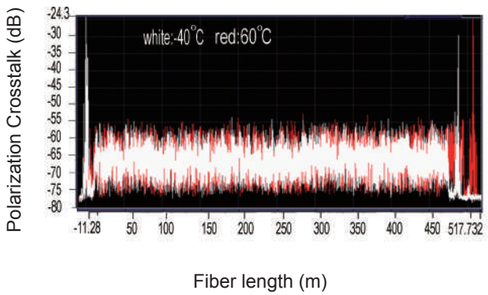

Figure 4. Polarization crosstalk vs. distance for a temperature insensitive coil. There is very little difference in the crosstalk at high temperatures (red curve: 60°C) and low temperatures (white curve: −40°C)

Specialty Fiber Coils

Fiber Hydrophone Coils

Fiber hydrophones require fiber coils designed to compensate for environmental effects, such as temperature variations and the earth's rotation, that can generate system noise. Fiber coil uniformity is also essential to the performance of the system. General Photonics can provide specialized coils, such as Doppler effect-free coils, cascaded fiber coil arrays, and extremely long coils with precise fiber lengths, to meet the requirements of particular applications.

Specifications:

Fiber Length Tolerance	<0.1%
Fiber Length Consistency (unit-to-unit variation)	<0.1%
Cascaded Array Coil	Up to 16 coils wound with a single fiber
Fiber Coil Diameter	Up to 1 m
Max. PMD (full temp. range)[1]	0.1 ps
Max. PDL (full temp. range)[1]	0.05 dB

Notes:
1. Typical. Values depend on configuration.

Related Products:

- Time Delay Coils (TDC)
- Fiber Gyro Coils (FC series)

FAQ:

- Fiber Coils

Detectors

Balanced Photodetector (BPD-002) 104
OEM Balanced Detector (BPD-003) 105
Polarization Diverse Balanced Photodetector (PBPD-001) 107
Polarization Diversity Detector (PDD-001) 108
Miniature Polarization Diversity Detector (PDD-003) 109
Fiber Pigtailed Free Space Interferometer (MZI-001) 110

Balanced Photodetector (BPD-002)

OCT and sensor systems require high performance balanced photodetectors to increase system signal to noise ratio. The BPD-002 is specially designed for use in research and development, with ease of use and high performance as the primary design goals. The device is fully enclosed in a compact, sturdy aluminum box with two optical input ports, a balanced RF output port, two 1-MHz monitor ports, and a power supply port. With a bandwidth up to 200 MHz, a trans-impedance gain larger than 30K and a saturation power larger than 130 µW, the BPD-002 is ideal for integration into laboratory or commercial OCT, fiber sensor, and high performance optical measurement systems.

Specifications:

Photodetector Type	InGaAs
Wavelength Range	1060nm, 1310nm, or 1550nm ±50nm
PD Responsivity	0.7 mA / mW @ 1310 nm
Transimpedance Gain (Total, including TIA and OP-AMP)	3×10^4 V / A
RF Bandwidth (3dB)	DC – 200, 100, 50, 10, or 5 MHz
CW Balanced Saturation Power	> 130 µW @ 1310 nm
PD Input Power Linear Range at Monitor Channels	0 to 1 mW @ 1310 nm
NEP (DC – 100MHz)	< 10 pW / $\sqrt{Hz}$
Common Mode Rejection Ratio	> 25 dB
RF Output Impedance	50 Ω
Electrical Connector	SMA
RF Output Voltage Range (at 50Ω)	±1.8 V
DC Offset RF Output	< ±3 mV
Monitor Output Impedance	200 Ω
Monitor Gain	10 V / mW (high impedance)
Monitor Bandwidth (3dB)	> 1000 Hz
Monitor Voltage	4 V max.
PD Damage Threshold Power	20 mW
Power Supply	±12 V
Operating Temperature	10 to 50 °C
Storage Temperature	-40 to 85 °C
Dimensions	3.82" (L) × 2.40" (W) × 0.75" (H)

Features:

- Ultra low noise
- Excellent CMRR
- High conversion gain
- Wide bandwidth
- Compact

Applications:

- Optical Coherence Tomography
- Fiber sensing interrogator
- Instrumentation
- R&D

Related Products:

- Balanced Detectors (BPD-003, PBPD-001)
- Polarization Diversity Detectors (PDD-001, PDD-003)

Tech Info:

- Optical Coherence Tomography Technologies

Ordering Information:

BPD — 002 — ☐ — ☐☐ — ☐

Bandwidth:
200 = 200 MHz
100 = 100 MHz
50 = 50 MHz
10 = 10 MHz
05 = 5 MHz

Wavelength:
10 = 1060nm
13 = 1310nm
15 = 1550nm

Connector Type:
FC/PC, FC/APC

Dimensions (in inches):

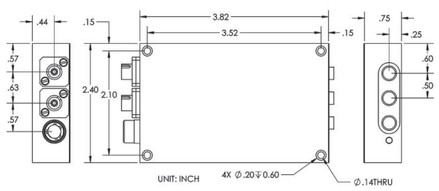

OEM Balanced Detector (BPD-003)

OCT and sensor systems require high performance balanced photodetectors to boost system signal to noise ratio. The BPD-003 is specially designed for OEM applications in such fields, engineered for low cost and small size as well as high performance. The device consists of an optical head and a post-amplification board with an SMA or SMB RF output. The optical head has two input fibers aligned with a pair of balanced photodetectors, followed by an integrated ultra low noise transimpedance amplifier (TIA) placed immediately after the photodetectors to amplify received signals with low noise and enhanced CMRR. The post-amplification circuit further conditions and amplifies the signal to a range of ±3.5 V maximum. With a bandwidth of up to 200 MHz and a high conversion gain, the BPD-003 is ideal for integration into OCT, fiber sensor and high performance optical measurement systems.

Specifications:

Photodetector	
Operating Wavelengths	1060, 1310, or 1550 ± 50nm
Photodetector Type	InGaAs
PD Responsivity[1]	> 0.8mA / mW at 1550nm > 0.7mA / mW at 1310nm > 0.5mA / mW at 1060nm
PDL	< 0.2 dB
Return Loss	> 45 dB
Maximum Input Power	10 mW
Pigtail Length	> 0.75m
Fiber Type	SMF - 28 for 1310 or 1550nm Hi1060 for 1060nm
RF Output	
RF Output Bandwidth (3dB)[2, 3]	DC to 200 MHz
Transimpedance Gain[3]	100×10^3 V/A (TIA + post amplifier)
Conversion Gain[4]	> 80×10^3 mV / mW at 1550nm > 70×10^3 mV / mW at 1310nm > 50×10^3 mV / mW at 1060nm
CW Balanced Saturation Power[5]	36 µW at 1550nm 42 µW at 1310nm 58 µW at 1060nm
Common Mode Rejection Ratio	> 35 dB (DC to 40MHz) > 15 dB (40 to 200MHz)
NEP (DC - 100MHz)	< 6 pW / $\sqrt{Hz}$
RF Output Impedance	50 Ω
RF Output Voltage (Linear Range)	±1.75 V at 50Ω load ±3.5 V at high impedance load
RF Output Connector	SMA or SMB
Power Supply Input Connector	6 - pin connector header with 0.1" pitch or 7 - pin SATA connector
Power Supply	±5 V / 200 mA
General	
Operating Temperature	10 to 50 °C
Storage Temperature	-40 to 85 °C
Dimensions	1.95" (L) × 0.85" (W) × 0.65" (H)

Notes:
Values are referenced without connectors.

1. Includes the coupling loss of fiber to photodiode.
2. Tolerance =20%.
3. Other bandwidths may be available.
4. Other gains are available.
5. For other transimpedance gains and wavelengths, CW Saturation Power is specified by (3.5V/Transimpedance gain)* Responsivity

OEM Balanced Detector (BPD-003)

Features:

- Ultra low noise
- Excellent CMRR
- High conversion gain
- Wide bandwidth
- Compact

Applications:

- Optical Coherence Tomography
- Fiber sensing interrogator
- Instrumentation
- R&D

Related Products:

- Balanced Detectors (BPD-002, PBPD-001)
- Polarization Diversity Detectors (PDD-001, PDD-003)

Tech Info:

- Optical Coherence Tomography Technologies

Dimensions (in inches):

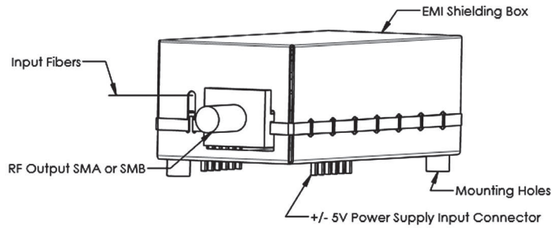

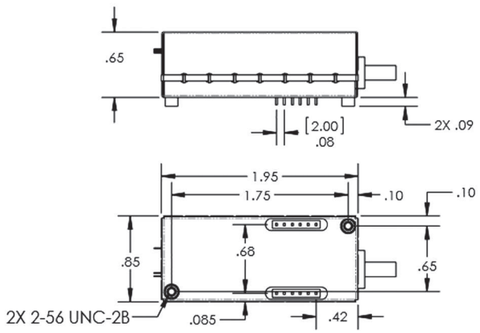

Ordering Information:

BPD — 003 — □□□ — □□ — □

Bandwidth:
200 = 200 MHz

Wavelength
10 = 1060nm
13 = 1310nm
15 = 1550nm

Connector Type:
FC/PC, FC/APC or
NC = no connectors
Others specify

Polarization Diverse Balanced Photodetector (PBPD-001)

OCT and sensor systems require high performance balanced photodetectors to increase system signal to noise ratio. Polarization sensitive OCT and similar applications require separate analysis of the two polarization components of a signal. The PBPD-001 is specially designed for use in such systems. The device is fully enclosed in a compact, sturdy aluminum box with two optical input ports, a balanced RF output port and two monitor ports for each polarization component, and a power supply port. With a bandwidth up to 200 MHz, a transimpedance gain larger than 30K and a saturation power larger than 130 µW, the PBPD-001 is ideal for integration into laboratory or commercial OCT, fiber sensor, and high performance optical measurement systems with polarization dependent detection requirements.

Specifications:

Operating Wavelength	1310 ± 50nm standard (1550 ± 50nm optional)
Polarization Crosstalk	< 25 dB (splitting element)
PDL (before polarization splitting)[1]	< 0.25 dB
Return Loss	> 50 dB
Input Power Damage Threshold	20 mW
Transimpedance Gain	3×10^4 V/A
Signal Conversion Gain	> 30 V/mW (interference signal)
RF Bandwidth	DC to 210 MHz
RF Output Impedance	50 Ω
RF Output Voltage Range	± 1.75 V @ 50Ω load ± 3.5 V @ high impedance load
RF Output DC Offset	< ±5 mV
CW Balanced Saturation Power (at input)	>150 µW
NEP	< 11 pW / $\sqrt{Hz}$
Overall Output Voltage Noise	< 5 mV RMS
Overall Common Mode Rejection Ratio	> 25 dB
Monitor Bandwidth	DC to 1MHz
Monitor Output Impedance	200 Ω
Monitor Conversion Gain	2 V/mW
Max. Monitor Voltage[2]	4 V
Power Supply	±12 V DC / 200 mA
Signal Output Connector	SMA
Input Optical Fiber	SMF - 28 standard (PMF optional)
Input Pigtail Length	> 0.75m
Operating Temperature	10 to 50 °C
Storage Temperature	-40 to 85 °C
Dimensions	100mm x 80mm x 27mm

Notes:
Specs in table apply for the standard configuration at 23 ± 5 °C.
1. At center wavelength.
2. Linear range.

Features:

- Low Noise
- Excellent CMRR
- High conversion gain
- Wide bandwidth
- Compact

Applications:

- Polarization sensitive OCT
- Fiber optic distributed sensing
- Polarization resolved sensing
- Instrumentation
- R&D

Related Products:

- Balanced Detectors (BPD-002, BPD-003)
- Polarization Diversity Detectors (PDD-001, PDD-003)

Tech Info:

- Optical Coherence Tomography Technologies

Ordering Information:

PBPD — 001 — □□□ — □□ — □

Bandwidth:
200 = 200 MHz

Wavelength:
13 = 1310nm
15 = 1550nm

Connector Type:
FC/PC, FC/APC or
NC = no connectors
Others specify

Polarization Diversity Detector (PDD-001)

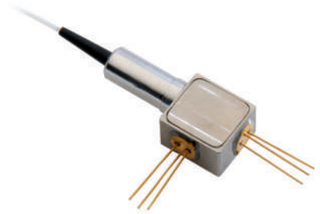

Simultaneously detecting the powers of two orthogonal polarization components is important for many sensor and measurement applications. A pigtailed polarization beam splitter coupled with two photodetectors can be used for such applications; however, this arrangement is bulky, troublesome to handle, and costly. By integrating polarization-splitting components with photodetectors, General Photonics created this compact device, which can be easily mounted onto a circuit board for customer applications. This Polarization Diversity Detector (PDD) features high detection sensitivity, high extinction ratio, high reliability, small size, and low cost. Once again, General Photonics leads the pack in providing solutions to customers' needs.

Specifications:

Detection Sensitivity	0.95 A/W at 1550 nm 0.90 A/W at 1310 nm	} for both channels
Operation Wavelengths	1310 nm, 1550 nm. Other: specify	
Wavelength Range	center wavelength ±75 nm	
Extinction Ratio	> 40 dB	
Return Loss	55 dB min	
Fiber Type	SM or PM (specify)	
Maximum Optical Power	20 mW	
Detector Rise / Fall Time	< 10 ns with 50 Ω load at 5 - volt bias	
Detector Capacitance	18 pf typical	
Detector Dark Current	< 0.20 nA at - 5 Volt bias at 23 °C < 20 nA at - 5 Volt bias at 70 °C	
Bias Voltage	15 volts max.	
Max. Reverse Current	5 mA	
Max. Forward Current	45 mA	
NEP	8.42E - 15 W /$\sqrt{Hz}$	
Detector Package	TO - 46	
Fiber Type	SM standard, PM specify, 900 µm jacket	
Operating Temperature	-20 to 70 °C	
Storage Temperature	-40 to 80 °C	
Dimensions	13 × 12 × 8 mm	

Note:
Customized detectors available. Contact General Photonics for details

Features:

- Low Cost
- High Extinction Ratio
- High Detection Sensitivity
- Easy to Use
- Compact

Applications:

- Sensor
- Performance Monitoring
- Polarization Analysis
- Instruments

Related Products:

- Balanced Detectors (BPD-002, BPD-003, PBPD-001)
- Polarization Diversity Detector (PDD-003)

Tech Info:

- Optical Coherence Tomography Technologies

Dimensions (in mm), Mounting, and PIN Information:

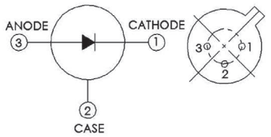

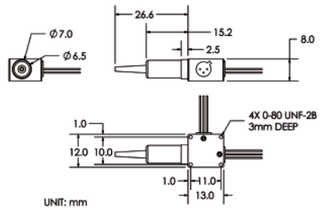

Ordering Information:

PDD — 001 — □□ — □□ — □□□

Wavelength:
13 = 1310 nm
15 = 1550nm

Fiber Type:
SM
PM

Connector Type:
FC/PC, FC/APC
LC/PC, LC/APC
SC/PC, SC/APC or
NC = No Connector

Miniature Polarization Diversity Detector (PDD-003)

Simultaneously detecting the powers of two orthogonal polarization components is important for many sensor and measurement systems, to either obtain polarization related information or minimize polarization sensitivity. By integrating polarization-splitting components with photodetectors, General Photonics created this compact device with a proprietary design, which can be easily mounted onto a circuit board for customer applications. With a size of only 6 mm (dia.) x 15 mm (length), the PDD-003 features high detection sensitivity, high extinction ratio, high reliability, small size, and low cost. At General Photonics, we provide innovative solutions to solve customers' polarization problems.

Specifications:

Operation Wavelengths	1310 ± 50nm or 1550 ± 50 nm.
Bandwidth	DC to 300 MHz
Photodiode Responsivity	> 0.8 mA / mW
Operating Input Power	0 to 1 mW
Capacitance at V_R = 5V	< 5 pF
Dark Current at V_R = 5V	< 10 nA
Overall Responsivity[1,2]	> 0.3 mA / mW
Detector Pinout (3 pins)	Anodes 1 and 2: Photocurrents of the two orthogonal polarization components Cathode: Common ground
Excess Loss[2]	< 0.8 dB
Return Loss[2]	> 40 dB
Polarization Extinction Ratio	> 20 dB
Imbalance[3]	< 10%
Max. Forward Current	5 mA
Max. Reverse Current	1 mA
Max. Reverse Voltage (V_R)	20 V
Max. Optical Power	2 mW
Fiber type	SMF - 28 with 900 µm loose tube
Termination	FC/PC, FC/APC, LC/PC, LC/APC, SC/PC, SC/APC
Pigtail Length	0.75 to 1.1m
Operating Temperature	-5 to 60° C
Storage temperature	-20 to 85° C
Operating Humidity	20 to 85%
Dimensions	Ø 6.0 mm × 14.9 mm (L)

Notes:
1. Overall responsivity includes photodiode responsivity with excess loss. Measured per channel using unpolarized input light.
2. Without optical fiber connector.
3. Imbalance = 100% * abs (I_1 - I_2) / [(I_1 + I_2) / 2], where I_1 and I_2 are output currents.

Features:

- Miniature size
- High extinction ratio
- High detection sensitivity
- Easy to use
- Low cost

Applications:

- Fiber optic sensor systems
- Performance monitoring
- Polarization analysis
- Instruments

Related Products:

- Balanced Detectors (BPD-002, BPD-003, PBPD-001)
- Polarization Diversity Detector (PDD-001)

Tech Info:

- Optical Coherence Tomography Technologies

Dimensions (in mm):

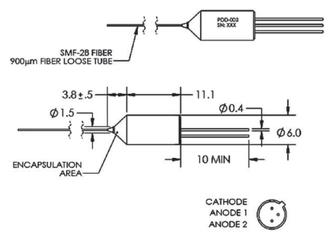

Ordering Information:

PDD — 003 — □□ — □□ — □□□

Wavelength:
13 = 1310 nm
15 = 1550 nm

Fiber Type:
SM

Connector Type:
FC/PC, FC/APC
LC/PC, LC/APC
SC/PC, SC/APC or
NC = No Connector

DETECTORS

Fiber Pigtailed Free Space Interferometer (MZI-001)

The MZI-001 is a fiber pigtailed compact Mach-Zehnder interferometer, based on free-space optics, for detecting changes in optical frequency. The device comes with two fast photodetectors for the balanced detection of the two complementary outputs of the interferometer. The free spectral range (FSR) or zero-cross spacing of the device is accurately defined to within 2%, a clear advantage over the all-fiber approach. In addition, the FSR can be selected from 10 GHz to as high as 100 GHz when ordering, making it flexible for system integration. Finally, the MZI-001's free-space optical design eliminates the polarization sensitivity commonly associated with all-fiber interferometers. The MZI-001 is ideal for applications in wavelength-swept light sources for determining their instantaneous frequencies, in OCT systems as a frequency clock for system triggering, in fiber sensors for detecting sensing signal spectral drift, and in coherent communication systems for detecting frequency drifts of the lasers.

Specifications:

Center Wavelengths[1]	1060, 1310, 1550 nm
Wavelength Range	±70 nm
FSR	10, 20, 30, 40, 50, 60, 70, 80, 90, 100 GHz, user selectable
FSR Tolerance	2%
Detector Responsivity	> 0.8 A/W
Overall Responsivity Per Channel	> 0.5 A/W
Detector Rise/Fall Time	0.3 ns with 50 Ω load
Detector Capacitance	0.7 pf
Return Loss	55 dB
Polarization Dependent Response	< 0.5 dB
Input Fiber	SMF-28 or Hi1060 fiber with 900 µm buffer
Optical Connectors	FC/APC or FC/PC, specify
Operating Temperature	-10 to 70 °C
Storage Temperature	-20 to 75 °C
Dimensions	2.11" (L) × 1.1" (W) × 0.37" (H)

Note:
1. Specifications in this table are given for 1550 nm operation. Performance at 1060 nm may be slightly different.

Features:

- Compact size
- Accurate free spectral range
- Temperature stable
- Polarization insensitive
- Fine optical frequency spacing
- Balanced photodetectors

Applications:

- Wavelength swept light source
- Optical Coherence Tomography (OCT)
- Fiber optic sensor
- Test & measurement
- Spectrum analysis
- Coherent detection systems

Tech Info:

- Optical Coherence Tomography Technologies

Dimensions (in inches and mm):

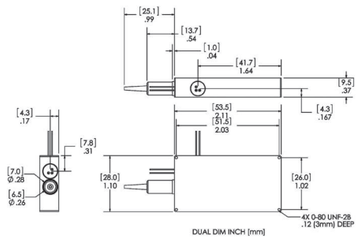

Ordering Information:

MZI — 001 — □□ — □□ — □

Wavelength:
10 = 1060 nm
13 = 1310 nm
15 = 1550 nm

FSR:
See options above

Connector Type:
FC/PC, FC/APC or
NC = no connectors

PASSIVE COMPONENTS

NoTail™ Components (Summary Sheet) 112
NoTail™ Drop-in Coupler (NTC) 113
Polarization Maintaining Coupler (PMC & NPMC) 114
Polarization Beam Combiner/Splitter (PB & NPB) 116
Faraday Rotator Mirror (FRM & NFRM) 117
In-line Polarizer (POL & NPOL) 119
In-line Isolator (ISO & NISO) 120
3-Port Fiber Optic Circulator (CIR & NCIR) 122

NoTail™ Components (Summary Sheet)

General Photonics' NoTail™ components offer the advantages of short optical path delay and of eliminating the polarization fluctuations that accompany fiber pigtail movement. In addition, many of them include magnets for temporary mounting on optical tables. They are ideal accessories for use with various instruments.

Features:

- No pigtails
- Solid construction
- Easy to use and handle
- Easy to store and reuse

Applications:

- Laboratory
- Benchtop
- Prototypes
- Polarization maintaining applications
- Instrumentation

Tech Info:

- Optical Coherence Tomography Technologies

Available Components:

NoTail™ Circulator

NoTail™ PM Coupler

NoTail™ PBC/PBS

NoTail™ Drop-in Coupler

NoTail™ Faraday Mirror

NoTail™ PM/SM Isolator

NoTail™ In-Line Polarizer

NoTail™ Drop-in Coupler (NTC)

These connectorized couplers are free of fiber pigtails and ready to be inserted in optical systems without the headaches of tinkering with fragile and messy fiber pigtails. Another important feature of these devices is the short optical path delay (~30 cm) between the input and the output, desirable in many systems where the optical path balance is important, such as interferometric systems, ultra-short pulse systems, and fiber laser systems. Additionally, these devices have four strong magnets mounted on the back for temporary but secure placement on standard optical tables.

Specifications:

Operating Center Wavelength	1310, 1550, or 1310/1550
Operating Bandwidth	±40 nm
Insertion Loss	See table below
Excess Loss	0.3 dB typical, 0.7 dB max.
Return Loss	FC/PC connectors: 50 dB, FC/APC connectors: 55 dB
PDL	0.1 dB typical
Thermal Stability	0.1 dB typical
Operating Temperature	0 to 70 °C
Storage Temperature	-40 to 85 °C
Fiber Type	SMF-28
Port Configuration	1 × 2 or 2 × 2
Dimensions	3.5" × 1.5" × 5/8" (L × W × H)

Note:
Values are referenced with connectors in table above.

Insertion Loss (IL) Table

Coupling Ratio	IL (Single Window)	IL (Dual Windows)
50/50	< 3.5/3.5	< 3.6/3.6
40/60	< 4.5/2.7	< 4.7/2.7
30/70	< 5.8/2.0	< 6.0/1.9
20/80	< 7.7/1.25	< 7.9/1.3
10/90	< 11.0/0.7	< 11.2/0.75
5/95	< 14.0/0.45	< 14.6/0.4
1/99	< 21.5/0.25	< 22.5/0.25

Note:
Values are referenced without connectors for IL table only.

Ordering Information:

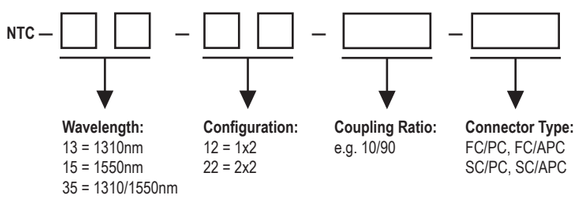

Features:

- Wide operating bandwidth
- Short optical path delay
- Compact and rugged design
- Easy to integrate into fiber optical systems
- Low excess loss
- High temperature stability

Applications:

- Power monitoring and sharing
- CATV
- Local area networks

Tech Info:

- Optical Coherence Tomography Technologies

Dimensions (in inches):

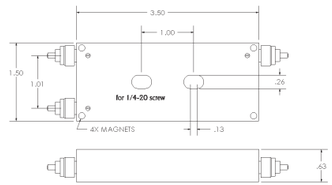

Polarization Maintaining Coupler (PMC & NPMC)

The polarization maintaining filter coupler can either split the light from an input PM fiber between 2 output PM fibers, or can combine light signals from 2 PM input fibers into a single PM output fiber. The device can be used to split high power linearly polarized light into multiple paths without perturbing the linear state of polarization (SOP). It can also be used as a power tap to monitor signal power in a PM fiber system without disturbing the linear SOP of the light propagating in the PM fiber. Applications include PM fiber interferometers, power sharing in polarization sensitive systems, and signal monitoring in PM fiber systems. The rugged stainless steel package is designed for high optical performance and stability. This compact device offers low excess insertion loss, low back reflection, and high extinction ratio. Split ratios from 1 to 50% are available.

Specifications:

Operating Center Wavelength	1550 nm, 1310 nm		1064 nm		
Operating Bandwidth	±40 nm		±20 nm		
Type	1 x 2	2 x 2	1 x 2	2 x 2	
Max. Excess Loss[1]	0.7 dB	1.0 dB	0.8 dB	1.2 dB	
Max. Uniformity	0.6 dB	0.8 dB	0.6 dB	0.8 dB	
Min. Extinction Ratio[2]	20 dB	18 dB	20 dB	18 dB	
Return Loss	50 dB		Split Ratio Tolerances:		
Split Ratio	1 ~ 50%		1 x 2	2 x 2	
Optical Power Handling	300 mW min.		99/1:	± 0.2%	± 0.2%
Operating Temperature	-5 to 70 °C		98/2:	± 0.4%	± 0.4%
Storage Temperature	-40 to 85 °C		95/5:	± 1%	± 1%
Fiber Type	PM fiber		90/10:	± 2%	± 2%
Dimensions	Pigtailed: Ø 5.5 × 35 mm		50/50:	± 7.5%[3]	± 10%
	NoTail: 3.5" (L) × 1.5" (W) × 5/8" (H)				

Notes:
Values in table are for filter couplers without connectors. Specs for fused fiber couplers may be different.

1. Excess loss for NoTail™ version is < 0.1 dB higher than for the corresponding pigtailed version, excluding connectors.
2. Extinction ratio can be higher for fast-axis blocked version.
3. ± 8% for 1064 nm version.

Features:

- Compact size
- Low insertion loss
- Low back reflection
- Rugged design

Applications:

- Power sharing in PM systems
- Power monitoring in PM systems
- PM fiber interferometers
- R&D laboratories

Tech Info:

- Optical Coherence Tomography Technologies

Polarization Maintaining Coupler (PMC & NPMC)

Dimensions:

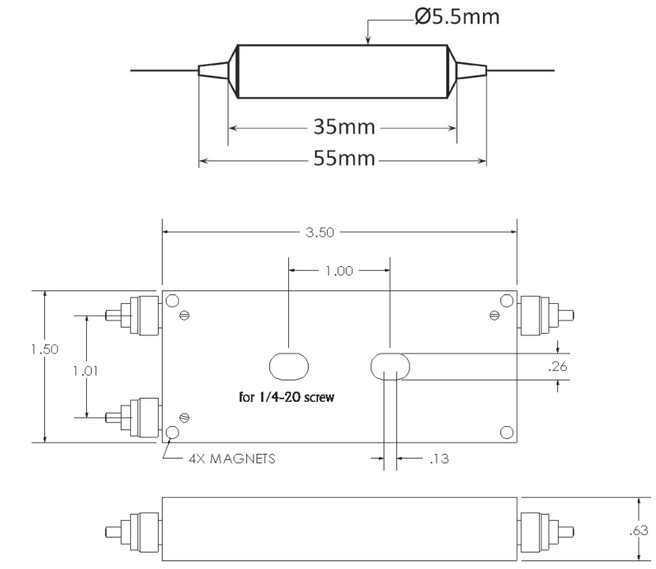

Ordering Information:

PMC — (Pigtailed) □□ – □ – □□ – □ – □□ – □

- **Wavelength:** 10 = 1064; 13 = 1310nm; 15 = 1550nm
- **Type:** T = Filter; C = Crystal; F = Fused Fiber
- **Configuration:** 12 = 1 x 2; 22 = 2 x 2
- **Coupling Ratio:** xx/yy, e.g. 10/90
- **Pigtail Type:** 25 = 250 µm*; 90 = 900 µm
- **Connector Type:** FC/PC, FC/APC; SC/PC,SC/APC; NC

Note:
* Connectors not recommended with bare fiber pigtails.

NPMC — (NoTail) □□ – □ – □□ – □ – □

- **Wavelength:** 10 = 1064; 13 = 1310nm; 15 = 1550nm
- **Type:** T = Filter; C = Crystal; F = Fused Fiber
- **Configuration:** 12 = 1 x 2; 22 = 2 x 2
- **Coupling Ratio:** xx/yy, e.g. 10/90
- **Connector Type:** FC/PC, FC/APC; SC/PC,SC/APC

Polarization Beam Combiner/Splitter (PB & NPB)

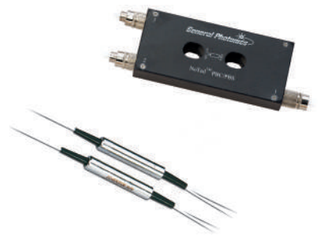

This device can be used either as a polarization beam combiner to combine light beams from two PM input fibers into a single output fiber, or as a polarization beamsplitter to split light from an input fiber into two output fibers of orthogonal polarization states. An important application of this device is polarization division multiplexing or demultiplexing in optical systems to increase their transmission capacity. In addition, as a pump combiner in optical amplifiers, the device efficiently combines the output from two pump lasers into a single fiber to increase the optical amplifier's saturation power and to reduce its polarization sensitivity. The wide operation bandwidth and high power handling capability make the device very attractive for next-generation amplifier systems. Finally, with a rugged stainless steel package designed for high optical performance and stability, this compact device offers low excess insertion loss, low back reflection, and high extinction ratio that equal or surpass others on the market.

Specifications:

Center Wavelength	1310, 1480, 1550 nm	1064 nm
Common Port Fiber Option	SMF-28 or PM Panda	HI 1060 or PM Panda
Operating Bandwidth	±40 nm	±20 nm
Insertion Loss[1]	0.4 dB typical 0.6 dB max.	0.6 dB typical 0.8 dB max.
Extinction Ratio (ER) (PBS Only)	22 dB	22 dB
Return Loss	50 dB	
Optical Power Handling[2]	500 mW	
Operating Temperature	-5 to 70 °C	
Storage Temperature	-40 to 85 °C	
Fiber type (Single Polarization Ports)	PM Panda Fiber	
Dimensions Pigtailed	Ø 5.5 × 35 mm	
Dimensions NoTail	3.5" (L) × 1.5" (W) × 5/8" (H)	

Notes:
Values are referenced without connectors.
1. Insertion loss for NoTail version is <0.1 dB higher than corresponding pigtailed device, excluding connectors.
2. Higher power handling available by special request.

Features:

- Compact size
- Low insertion loss
- High power handling
- Rugged design

Applications:

- Polarization division Mux/DeMux
- EDFA and Raman amplifiers
- Fiber Laser Systems
- Fiber Sensor Systems
- Instruments
- R&D Laboratories

Dimensions:

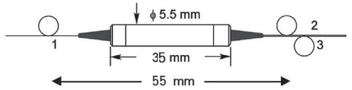

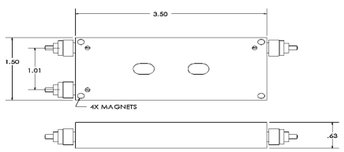

Ordering Information:

PB — (Pigtailed) — □□ — □□ — □□ — □

Wavelength:
10 = 1064
13 = 1310nm
15 = 1550nm

Configuration:
SM = Common port SM, split ports PM slow axis aligned
P1 = Common port PM 0˚, split ports PM slow axis aligned
P2 = Common port PM 45˚, split ports PM slow axis aligned

Pigtail Type:
25 = 250 µm*
90 = 900 µm

Connector Type:
FC/PC, FC/APC
SC/PC,SC/APC
NC

* Connectors not recommended with bare fiber pigtails.

NPB — (NoTail) — □□ — □□ — □

Wavelength:
10 = 1064
13 = 1310nm
15 = 1550nm

Configuration:
SM = Common port SM, split ports PM slow axis aligned
P1 = Common port PM 0˚, split ports PM slow axis aligned
P2 = Common port PM 45˚, split ports PM slow axis aligned

Connector Type:
FC/PC, FC/APC

Faraday Rotator Mirror (FRM & NFRM)

The Faraday rotator mirror is a fiber optic polarization rotation mirror designed for fiber optic networks and measurement applications. The state of polarization (SOP) of the reflected light is rotated 90 degrees from that of the input light. A unique property of Faraday rotator mirrors is that at any point along the fiber, the SOPs of the forward going and reflected light are always orthogonal to each other, regardless of the birefringence of the fiber. Therefore, when properly used, the device can help to eliminate polarization sensitivity in optical fiber systems. Applications include eliminating polarization-induced fluctuations in fiber interferometers, Brillouin amplifier systems, fiber laser systems, and fiber optic antenna remoting systems. The FRM's optical path is epoxy free and thus offers low insertion loss and high temperature stability. We also offer the NoTail™ version, which eliminates unwanted optical path delay and pigtail handling problems.

Specifications:

Operating Wavelength	1550 nm, 1310 nm	1064 nm
Operating Bandwidth	±50 nm	±5 nm
Insertion Loss	0.4 dB typical 0.6 dB max.	3.0 dB max.
Faraday Rotation Angle (single pass)	45 degrees	45 degrees
Rotation Angle Tolerance (Center Wavelength at 23 °C)	±2 degrees	±6 degrees
Rotation Angle Wavelength Dependence	-0.14 deg/nm (1550nm) -0.17 deg/nm (1310nm)	-0.26 deg/nm
Rotation Angle Temperature Dependence	-0.13 deg/°C (1550nm) -0.08 deg/°C (1310nm)	-0.14 deg/°C
PDL	0.1 dB	0.1 dB
PMD	0.05 ps	0.05 ps
Optical Power Handling	300 mW min.	150 mW
Operating Temperature	0 to 70 °C	-5 to 50 °C
Storage Temperature	-40 to 85 °C	-40 to 85 °C
Fiber Type	SMF-28	HI 1060 Fiber
Dimensions	Ø 3.8 x 22mm (pigtailed) Ø 9.5 × 50 mm (NoTail™)	Ø 3.8 x 22mm (pigtailed)

Note:
Values are referenced without connectors

Features:

- Compact size
- Low insertion loss
- High stability
- Rugged design
- NoTail™ model available

Applications:

- Polarization sensitivity elimination in:
- Fiber interferometers & sensors
- Fiber laser systems
- Brillouin amplifiers
- Fiber optic antenna remoting systems
- Fiber optic modules

Tech Info:

- Optical Coherence Tomography Technologies
- Faraday Rotator Mirror Application Note

Faraday Rotator Mirror (FRM & NFRM)

Typical Performance Data:

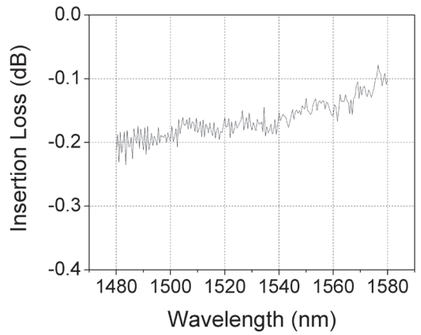

Figure 1. Insertion loss vs. wavelength

Dimensions:

NoTail:

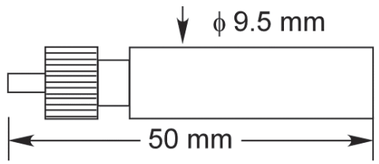

Pigtailed:

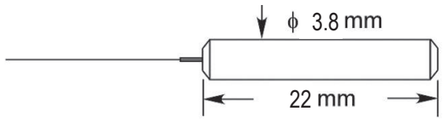

Ordering Information:

FRM – (Pigtailed) □□ – □□ – □□

- **Wavelength:** 10 = 1064; 13 = 1310nm; 15 = 1550nm
- **Pigtail Type:** 25 = 250 µm*; 90 = 900 µm
- **Connector Type:** FC/PC, FC/APC; SC/PC,SC/APC; NC

NFRM – (NoTail) □□ – □□

- **Wavelength:** 13 = 1310nm; 15 = 1550nm
- **Connector Type:** FC/PC, FC/APC

Note:
* Connectors not recommended with bare fiber pigtails.

In-line Polarizer (POL & NPOL)

This in-line polarizer is designed for fiber optic networks and measurement applications. Applications include polarization analysis, polarization monitoring and control, SNR monitoring, PMD monitoring, spectrum filtering and control, polarization extinction ratio improvement, fiber laser mode-locking, and polarization interferometry. When combined with a polarization controller, the polarizer can function as a variable optical attenuator to adjust the optical power in the fiber. It integrates a high-ER micro-polarizer in a rugged stainless steel package for high optical performance and stability. This compact device offers low insertion loss, low back reflection, and high extinction ratio. Both pigtailed and NoTail™ versions are available. The unique NoTail™ package has the advantage of eliminating polarization disturbances caused by fiber pigtails.

Specifications:

Operating Wavelength		1550, 1310 nm	1064 nm
Operating Bandwidth		±50 nm	±30 nm
Insertion Loss[1]		0.3 dB typical 0.5 dB max.	0.4 dB typical 0.6 dB max.
Return Loss		50 dB	50 dB
Extinction Ratio	SM Output	40 dB typical, 30 dB min.	30 dB typical, 28 dB min
	PM Output	30 dB typical, 28 dB min.	
Optical Power Handling		300 mW min.	
Operating Temperature		0 to 70 °C	
Storage Temperature		-40 to 85 °C	
Fiber Type		SM: SMF-28 or HI 1060	
		PM: PM Panda fiber	
Dimensions		Ø 5.5 × 35 mm (pigtailed) Ø 9.5 × 65 mm (NoTail™)	

Note:
Values are referenced without connectors.
1. Insertion loss for NoTail™ version can be up to 0.1 dB higher, excluding connector loss.

Features:

- Compact size
- Low insertion loss
- High extinction ratio
- Low back reflection
- Rugged design
- NoTail™ model available

Applications:

- Eliminating unwanted polarization state
- PMD monitoring
- Polarization interferometer

Dimensions:

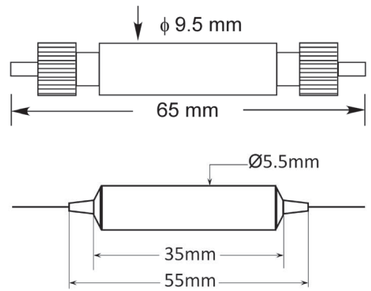

Ordering Information:

POL – (Pigtailed) □□ – □□ – □□ – □□

- **Wavelength:** 10 = 1064; 13 = 1310nm; 15 = 1550nm
- **Fiber Type:** SS = SM to SM; SP = SM to PM; PP = PM to PM
- **Pigtail Type:** 25 = 250 µm*; 90 = 900 µm
- **Connector Type:** FC/PC, FC/APC; SC/PC,SC/APC; NC

NPOL (NoTail) □□ – □□ – □□

- **Wavelength:** 13 = 1310nm; 15 = 1550nm
- **Fiber Type:** SS = SM to SM; SP = SM to PM; PP = PM to PM
- **Connector Type:** FC/PC, FC/APC

Note:
* Connectors not recommended with bare fiber pigtails.

In-line Isolator (ISO & NISO)

These isolators are the smallest in size but the highest in quality in the market. They are ruggedly built to function reliably in a wide variety of environments. Small size, low loss, and low back reflection combine to make these isolators ideal for integration in many fiber optic systems. We also offer the NoTail™ version to eliminate the problems that pigtails can cause. The short optical path (~ 7cm) of the NoTail™ isolator is desirable for ultra-short pulse and interferometric applications.

Specifications:

Operating Center Wavelength		1550 nm, 1310 nm		1064 nm	
Type		Single Stage	Double Stage	Single Stage	Double Stage
Operating Bandwidth		±20 nm	±20 nm	±5 nm	±5 nm
Peak Isolation		> 40 dB	> 52 dB	40 dB (SM)	55 dB (SM)
				38 dB (PM)	55 dB (PM)
Min. Isolation at 23°C		> 30 dB	> 45 dB	30 dB (SM)	45 dB (SM)
				35 dB (PM)	45 dB (PM)
Insertion Loss[1]	Typ	0.4 dB	0.5 dB	1.5 dB	2.4 dB
	Max	0.6 dB	0.7 dB	2.0 dB	3.4 dB
Return Loss (Input/Output)	SM	> 60/55 dB	> 60/55 dB	> 55/50 dB	> 55/50 dB
	PM	> 55/50 dB	> 55/50 dB		
PMD (SM)		< 0.2 ps	< 0.05 ps		
PDL (SM) at 23°C		< 0.05 dB	< 0.05 dB	0.15 dB	0.15 dB
Extinction Ratio (PM)		>20dB both axes open >25dB fast axis blocked	>20dB both axes open >25dB fast axis blocked	>20dB both axes open >23dB fast axis blocked	>20dB both axes open >23dB fast axis blocked
Optical Power Handling		300 mW		300 mW	
Operating Temperature		0 to 70 °C		-5 to 50 °C	
Storage Temperature		-40 to 85 °C		-40 to 85 °C	
Fiber Type		SM: SMF-28		SM: HI 1060	
		PM: PM Panda		PM: PM Panda	
Dimensions		Ø5.5 × 35 mm (pigtailed)		Ø5.5 × 35 mm (pigtailed)	
		Ø9.5 × 65 mm (NoTail™)		NA	

Notes:
Values are referenced without connectors.
1. Insertion loss for NoTail™ version can be up to 0.1 dB higher, excluding connector loss.

In-line Isolator (ISO & NISO)

Features:

- Polarization insensitive or polarization maintaining
- NoTail™ model available
- Low loss and low reflection
- Compact size
- Environmentally stable
- High quality

Applications:

- Fiber optic amplifier
- WDM systems
- Transmitters and fiber lasers
- R&D laboratories

Dimensions:

SM or PM isolator

Ordering Information:

ISO (Pigtailed) – □ – □□ – □ – □□ – □

- **Stages:** S = Single, D = Double
- **Wavelength:** 10 = 1064, 13 = 1310nm, 15 = 1550nm
- **Fiber Type:** SS = SM to SM, PP1 = PM, both axes open, PP2 = PM, fast axis blocked
- **Pigtail Type:** 25 = 250 µm*, 90 = 900 µm
- **Connector Type:** FC/PC, FC/APC, SC/PC,SC/APC, NC

Note:
* Connectors not recommended with bare fiber pigtails..

NISO (NoTail) – □ – □□ – □ – □

- **Stages:** S = Single, D = Double
- **Wavelength:** 13 = 1310nm, 15 = 1550nm
- **Fiber Type:** SS = SM to SM, PP1 = PM, both axes open, PP2 = PM, fast axis blocked
- **Connector Type:** FC/PC, FC/APC

3-Port Fiber Optic Circulator (CIR & NCIR)

General Photonics' fiber optic circulators are compact, high-performance light-wave components that separate signals traveling in opposite directions along fibers by transmitting signals from port 1 to port 2 and port 2 to port 3, while blocking signals traveling in the opposite directions. They offer excellent performance characteristics, including low insertion loss and high isolation. They are ideal components for add/drop filters, EDFAs, dispersion compensation, bi-directional communication and other applications.

Specifications[1]:

Center Wavelength	1310, 1550 nm		1064 nm	
Fiber Type	SM	PM[4]	SM	PM
Bandwidth	±20 nm	±30 nm	±5 nm	±5 nm
Insertion Loss[2]	0.6 dB typical 0.8 dB max.	0.7 dB typical 0.9 dB max.	1.8 dB typical 2.2 dB max.	1.8 dB typical 2.1 dB max.
Return Loss	50 dB	55 dB	50 dB	50 dB
PDL at 23°C	0.1 dB	N/A	0.2 dB	N/A
PMD	0.1 ps	N/A	0.1 ps	N/A
Extinction Ratio	N/A	22 dB min.	N/A	20 dB min.
Isolation (2 → 1 or 3 → 2, 23 °C)	50 dB typical 40 dB min.		25 dB typical 20 dB min.	30 dB typical 25 dB min
Cross Talk	50 dB		45 dB	50 dB
Optical Power Handling	300 mW			
Operating Temperature	0 to 70 °C		0 to 50 °C	
Storage Temperature	-40 to 85 °C			
Dimensions	Ø 5.5 x 50 mm (SM pigtailed, 1310 or 1550 nm) 34 x 8.4 x 8.4 mm (L x W x H) (SM 1064 nm) Ø 5.5 x 35 mm (PM pigtailed) 3.5" (L) x 1.5" (W) x 5/8" (H) (NoTail™)[3]			

Notes:
1. Values are referenced without connectors
2. Insertion loss for NoTail™ version can be 0.1 dB + connector loss higher.
3. 1064 nm SM version not available in NoTail configuration.
4. Standard configuration for PM circulators is fast axis blocked. Versions with both axes open may be available, but with different package size and specs.

Features:

- High quality and attractively priced
- Compact
- Exceptional environmental stability
- Low excess loss
- NoTail™ model available

Applications:

- Add-drop filter
- Digital, hybrid and AM-video system
- Dispersion compensator
- Fiber sensors
- Bi-directional communication

Tech Info:

- Optical Coherence Tomography Technologies

3-Port Fiber Optic Circulator (CIR & NCIR)

Dimensions:

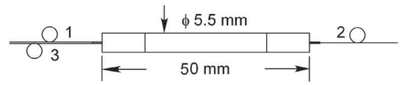

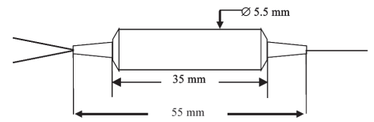

PM package

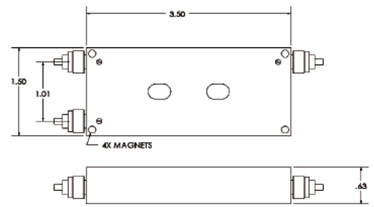

NoTail™ package

Ordering Information:

CIR (Pigtailed) – □□ – □□ – □□ – □

Wavelength
10 = 1064nm
13 = 1310nm
15 = 1550nm

Configuration
SM = SM in/out
P1 = PM w. both axes open
P2 = PM w. fast axis blocked

Pigtail Type
25 = 250 µm*
90 = 900 µm

Connector Type
FC/PC, FC/APC
SC/PC,SC/APC
NC

Note:
* Connectors not recommended with bare fiber pigtails.

NCIR (NoTail) – □□ – □□ – □

Wavelength
13 = 1310nm
15 = 1550nm

Configuration
SM = SM in/out
P2 = PM w. fast axis blocked

Connector Type
FC/PC, FC/APC

ACCESSORIES

Bare Fiber Adapter - PolaEZ™ (PEZ-001) 125

Rack Mount Kit (RCK-001) 126

Bare Fiber Adapter - PolaEZ™ (PEZ-001)

General Photonics' PolaEZ™ is a bare fiber adapter designed specifically for measurements of polarization related properties, including polarization extinction ratio (PER), polarization dependent loss (PDL), and polarization mode dispersion (PMD). The adapter exerts minimal stress on the optical fiber, and thus induces negligible birefringence and PDL. When used with PM fiber, extinction ratio of more than 50 dB can be achieved. The unique spring-loaded design makes insertion of optical fiber extremely easy. The adapter comes in a neatly designed black pouch with easy to understand instructions, a universal mating sleeve for connection to jumper cables, and a vial of clean-out wire for easy removal of fiber ends.

Specifications:

Fiber Type[1]	Single Mode
Connector Interface[1]	FC
Material (Adapter Body)	Aluminum, Stainless Steel
Ferrule	Zirconia
Bare Fiber Length Required	0.55"
Operating Temperature	-20 to 60 °C
Dimensions	1.9" (L) × 0.5" (W) × 0.69" (H)

Note:
1. Standard configuration. Connector heads for other types of fiber and connector interfaces are possible. Contact General Photonics for details.

Features:

- Negligible fiber stress
- > 50 dB PER possible
- Easy to use
- Interchangeable connector heads available

Applications:

- PER measurement
- PDL measurement
- PMD measurement

Related Products:

- Polarization Measurement System (PSGA-101A)
- ER Meter (ERM-202)
- Optical Component Analyzer (OCA-1000)

Ordering Information:

PEZ — 001 — □ — □ □

Fiber Size:
125 = 125μm cladding

Connector Type:
FC

Rack Mount Kit (RCK-001)

This rack mounting kit allows the user to mount most General Photonics instruments to a standard 19" rack. Two rubber feet attach to the bottom of each instrument via embedded screws. These feet also have threads to accept the mounting screws that secure the instrument to the shelf. A version with a faceplate is available for half-rack size instruments.

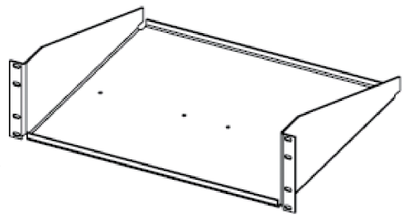

Specifications:

Dimensions	19" rack size, 15" depth
Instrument Compatibility	2U, 19" half-rack or 3/4 rack size GP Instruments, depending on version
Mounting Screws (Instrument to Shelf)	8-32 screws (2 per half-rack instrument or 4 per 3/4 rack instrument, supplied)
Mounting Screws (Shelf to Rack)	4 Phillips head screws (supplied)

Features:

- Secure
- Easy to Use
- Holds up to 2 instruments
- Compatible with all 2U size GP instruments

Applications:

- Test system assembly and shipping
- Earthquake proofing

Dimensions (in inches):

Note:
Drawings below represent RCK-001 model.

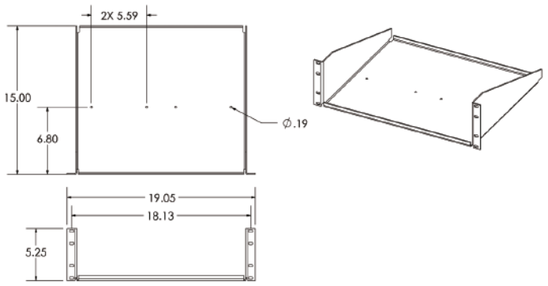

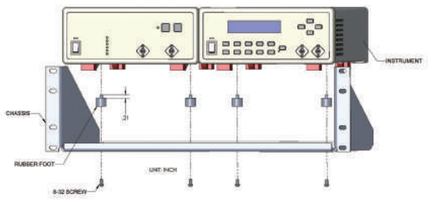

Top view of assembly schematic

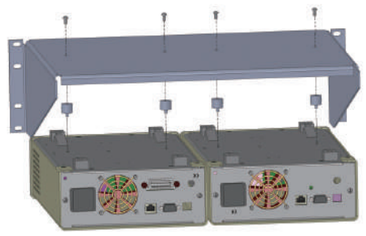

Bottom view of assembly schematic

Ordering Information:

RCK-001: shelf kit to fit 2 2U, half-rack instruments
RCK-001-1: shelf kit to fit 1 2U, half-rack instrument
RCK-FP1: faceplate for RCK-001-1
RCK-001-2: shelf kit to fit 1 2U, 3/4-rack instrument

APPLICATION GUIDE

White Papers

Journal Papers

Application Notes

White Papers

What is Polarization? 129
Polarization in Fiber Systems: Squeezing out More Bandwidth 131
Combat Polarization Impairments with Dynamic Polarization Controllers 136
Scrambling to Minimize Polarization Related Impairments 140
Polarization Related Tests for Coherent Detection Systems 143
Practical 4-Stage Optical PMD Compensator for
Mitigating 1st-and 2nd-Order PMD Impairments on 40-Gbit/s RZ-D(Q)PSK Signals 150
Polarization Crosstaik in PM Fiber 153
Distributed Polarization X-talk Measurement for the Production of Polarization-Maintaining Fiber Coils 156
Complete characterization of polarization-maintaining fibers using distributed polarization analysis 162

What is Polarization?

Polarization is a property that is common to all types of vector waves. In classical physics, light is modeled as a sinusoidal electromagnetic wave in which an oscillating electric field and an oscillating magnetic field propagate through space. Since the magnetic field is always perpendicular to the electric field, we usually sketch just the electric field when visualizing the optical wave's oscillations. Polarization is defined in terms of the pattern traced out in the transverse plane by the electric field vector as a function of time.

Light is called natural or unpolarized if its plane of polarization fluctuates randomly around the direction of light beam propagation, so that, on average, no direction is favored. For example, most naturally produced light (sunlight, firelight) is unpolarized. In any other case, the light beam can be considered to consist of partially polarized or fully polarized light.

The polarization of a light beam can be represented by its electric field vector. Its optical power is a scalar quantity that is proportional to the mean square of the electric field amplitude. Let z be the direction of propagation. Then, the polarization vector is in the x-y plane. By superposition of the x- and y-vector components at time t at any location, the polarization vector can be expressed:

$$\vec{E}(t) = \vec{E}_x(t) + \vec{E}_y(t)$$
$$= E_x \cos(\varpi t + \delta_x)\vec{e}_x + E_y \cos(\varpi t + \delta_y)\vec{e}_y$$

where E_x and E_y are the amplitudes of the x and y components of the electric field; e_x, e_y are the unit vectors of the x-y orthogonal reference system; ϖ is the angular frequency; and δ_x and δ_y are the phases of the electric field in the x and y directions, respectively. The phase difference is $\delta = \delta_x - \delta_y$.

Figure 1 shows electric field vectors in the x-y plane as a function of time. Figure 1(a) shows the two orthogonal electric field components with a relative phase difference of δ. In Figure 1(b) there is no phase difference between the two orthogonal components.

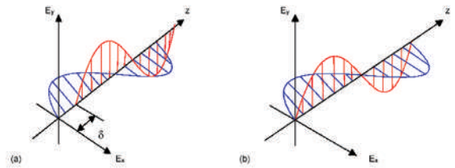

Fig. 1 Spatial representation of x- and y- electric field components over time. (a) with a phase difference, (b) no phase difference.

Polarized light may be classified into three groups by the values of δ, E_x, and E_y: linearly polarized, circularly polarized and elliptically polarized light. Linearly polarized light has no phase difference between the x and y electric field components (δ=0). Circularly polarized light has a fixed phase difference of 90 degrees, and the amplitudes of the two electric field components are the same (ie. δ = 90° and $E_x = E_y$). The polarization state is elliptical for all other values of δ, E_x, and E_y .

Poincaré Sphere and Stokes Vectors

The Poincaré sphere is used to describe the polarization and changes in polarization of a propagating electromagnetic wave. It provides a convenient way of representing polarized light, and of predicting how any given retarder will change the polarization form. Any given polarization state corresponds to a unique point on the sphere. The two poles of the sphere represent left- and right-hand circularly polarized light. Points on the equator indicate linear polarizations. All other points on the sphere represent elliptical polarization states. An arbitrarily chosen point H on the equator designates horizontal linear polarization, and the diametrically opposite point V designates vertical linear polarization.

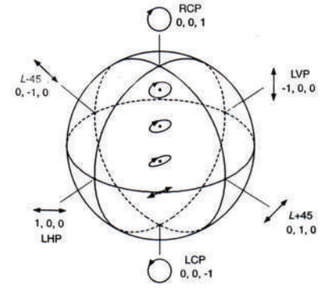

Fig. 2 Poincaré sphere representation of polarization states

The Stokes parameters have a simple physical interpretation related to Poincaré sphere representation. They also have a physical interpretation related to intensity measurement.

In a given Oxyz reference system (Oz being the direction of propagation of light), the Stokes vector can be expressed as:

$$S = \begin{bmatrix} S_0 \\ S_1 \\ S_2 \\ S_3 \end{bmatrix} = \begin{bmatrix} I_0 \\ I_x - I_y \\ I_{+45} - I_{-45} \\ I_L - I_R \end{bmatrix}$$

where I_0 is the total power of the light, I_x, I_y are the x- and y-linearly polarized light intensities, I_{+45}, I_{-45} are the 45° and -45° linearly polarized light intensities, and I_L, I_R are the left and right hand circularly polarized light intensities.

If we normalize $[S_1\ S_2\ S_3]$ by S_0, we will get the SOP $[s_1\ s_2\ s_3]$, which are the coordinates of one point on the Poincaré sphere.

The degree of polarization (DOP) is defined by:

$$DOP = \sqrt{s_1^2 + s_2^2 + s_3^2}$$

with a value between 0 and 1.

Whenever DOP=0, light is said to be unpolarized, and whenever

DOP=1, it is totally polarized. Intermediate cases correspond to partially polarized light.

DOP can also be expressed as:

$$DOP = \frac{I_{pol}}{I_{pol} + I_{unp}}$$

where I_{pol} , I_{unp} are the intensity of polarized light and unpolarized light, respectively.

What is Birefringence?

In a homogenous or isotropic medium, light propagates at the same speed regardless of polarization state. This speed, v, can be expressed as:

v = c/n

where c is the speed of light in a vacuum, and n is the index of refraction of the medium.

If the light is propagating in an anisotropic medium, the transmission speeds of light polarized along different directions are different. One may use two special orthogonal axes called principal axes to express the transmission properties of the medium.

Usually, this can be expressed through different indices of refraction, such as the ordinary index (n_o) and extraordinary index (n_e). The difference between n_o and n_e is called birefringence. Birefringence is also called double refraction.

Therefore, the index of refraction is a measure of how fast light transmits through a medium. If a medium is birefringent, plane-polarized light launched into one principal axis travels through the medium faster than plane-polarized light in the other principal axis. As a result, the two polarization components of a light signal projected along the two axes will experience a relative phase difference as they propagate through the material.

If an optical pulse is launched into a fiber made of a birefringent material with its polarization aligned with either of the fiber's principal axes, then the pulse transmits through the fiber and emerges in the same state of polarization in which it was launched. However, if we launch the pulse with randomly oriented polarization, then part of the pulse transmits along one of the principal axes, and part of the pulse transmits along the other principal axis. Because of the medium's birefringence, the two parts of the pulse travel at different speeds. Consequently, the pulse becomes broadened because the two parts exit the fiber at slightly different times, and the state of polarization changes.

What is PMD?

PMD stands for polarization mode dispersion. It occurs when different polarization components of light inside a fiber travel at slightly different speeds, as shown in Figure 3. PMD is caused directly by the birefringence of the optical fiber. The major causes of the birefringence are the asymmetry of the fiber-optic strand, where the fiber core is slightly oval or out-of-round, and mechanical stresses on the fiber. The asymmetry may be inherent in the fiber from the manufacturing process, or it may be a result of mechanical stress on the deployed fiber. The inherent asymmetries of the fiber are fairly constant over time, while mechanical stress due to movement or temperature change of the fiber can vary, resulting in a dynamic aspect to PMD. 1st order PMD is called differential group delay (DGD).

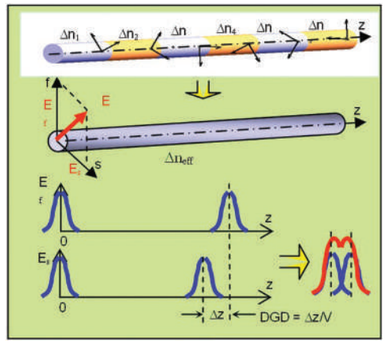

Fig. 3 A real fiber is like many retardation plates with different orientations and birefringences in series. It is equivalent to a single retardation plate having a slow and fast axis, and an effective birefringence. An optical pulse broadens because the two polarization components travel with different speeds.

Because of its dynamic properties, PMD does not have a single, fixed value for a given section of fiber. Rather, it is described in terms of average DGD, and a fiber has a distribution of DGD values over time. The probability of a DGD with a certain value at any particular time follows the Maxwellian distribution shown in Figure 4. As an approximation, the maximum instantaneous DGD is about 3.2 times the average DGD of a fiber.

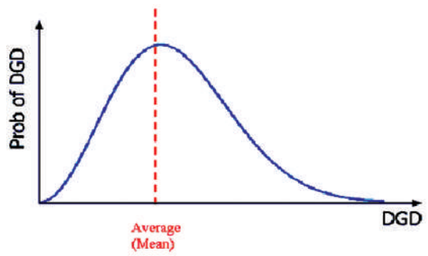

Fig. 4 Maxwellian distribution of DGDs.

Polarization in Fiber Systems: Squeezing out More Bandwidth

Steve Yao
General Photonics Corp.

To appease the demand for bandwidth, telecommunication operators are pushed to increase the per-channel data rate of wavelength division multiplexing (WDM) systems. Systems based on the 10 Gb/s channel rate are being deployed, and the deployment of 40 Gb/s systems is on the horizon.

As bit rates increase to meet expanding demand, systems have become increasingly sensitive to polarization-related impairments. These include polarization mode dispersion (PMD) in optical fibers, polarization-dependent loss (PDL) in passive optical components, polarization-dependent modulation (PDM) in electro-optic modulators, and polarization-dependent gain (PDG) in optical amplifiers.[1]

These impairments result from imperfections in the optical fibers. If the fibers were perfect, the state of polarization (SOP) of the signal would remain constant, and the polarization-related impairments could easily be eliminated. However, the SOP of light propagating in the standard communication fiber varies along the fiber because of the random birefringence induced by thermal stress, mechanical stress and irregularities of the fiber core. Generally, at the output end of the fiber, the light is elliptically polarized with varying degrees of ellipticity, and with the major elliptical axis at an arbitrary angle relative to some reference orientation. Worst of all, the induced birefringence changes with temperature, pressure, stress and other environmental variations, making polarization-related impairments unpredictable.

Because polarization-induced penalties are time dependent, mitigation of the polarization-related impairments must be dynamic and adaptive to random variations.

Dynamic polarization control

A dynamic polarization controller can convert any given polarization state to any desired polarization state. It is the single most important element of PMD compensation for overcoming these impairments. An ideal dynamic polarization controller should offer several important parameters as follows, in addition to low insertion loss and high return loss:

- High speed is essential for tracking fast polarization variations such as those caused by locomotives passing fibers laid along railway tracks or by ocean waves in undersea fiber trunks. In field measurements using a PMD transient recorder, fluctuations with a time scale of a few milliseconds have been observed. Therefore, the response time of the dynamic polarization controller for PMD mitigation must be less than 1 ms. In practice, a response time less than 100 μs is required.
- Activation loss measures the additional insertion loss caused in activating the device. It is defined as the difference of the maximum and minimum insertion losses of the device considering all possible activation conditions. This specification is particularly important because all the impairments compensation schemes for polarization-related impairments use feedback signals to activate the controller. The activation-induced loss or fluctuation causes errors in the feedback signal and directly degrades the performance of the compensation apparatus.

In addition, when an instrument for measuring the PDL of optical components includes a polarization controller, the activation-induced loss limits the resolution and accuracy of the measurement. Similarly, the controller's PDL also contributes to errors in a feedback system and complicates the design of compensation hardware and software.

- Wide operation bandwidth is important for dense WDM (DWDM) systems that cover a broad wavelength bandwidth. Wide-bandwidth polarization controllers function equally well for many wavelength channels, simplifying system design, reducing system cost and enabling the expansion of system bandwidth.
- Uninterruptibility is also critical for dynamic polarization controllers in optical networks because any polarization reset may cause unacceptable signal outage.

Commercial polarization controllers fall into three technology classifications: multiple wave plates with

Reprinted from the 2003 issue of The Photonics Handbook® **Laurin Publishing**

fixed retardations but variable orientation angles; a single wave plate with both variable retardation and orientation; and multiple wave plates with fixed orientation and variable retardation.

Controllers based on wave plates of fixed retardation are wavelength-sensitive. Those that rely on physical rotation are generally slow. Other than these fundamental limitations, all three approaches function reasonably well in principle. However, implementation of these approaches in practice determines the performance, cost and reliability of the devices.

A classic polarization controller consisting of three rotatable wave plates is illustrated in Figure 1a. In this configuration, a half-wave plate (HWP) is sandwiched between two quarter-wave plates (QWP) and the retardation plates are free to rotate around the optical beam with respect to each other. The first QWP converts any arbitrary input polarization into a linear polarization. The HWP then rotates the linear polarization to a desired angle so that the second QWP can translate the linear polarization to any desired polarization state. In this approach, the retardation of the plates is fixed, but the relative angles of the retardation plates are variable.

Commercial applications of this approach have produced respectable results. However, this technique does have drawbacks: Collimating, aligning and refocusing are time consuming and labor intensive. Also, the wave plates and microlenses are expensive and need antireflection coating or angle polishing to prevent backreflection. Insertion loss is high because the optical beam has to be coupled out of one fiber and refocused into another. Furthermore, the wave plates are inherently wavelength-sensitive (any fractional wave plate is always specified with respect to a particular wavelength), making the device sensitive to wavelength variations. Finally, electrical motors or other mechanical devices rotate the wave plates, limiting the controller speed.

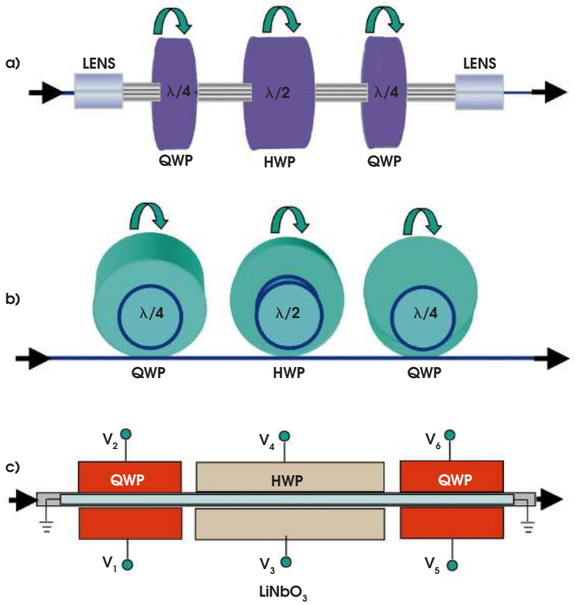

Figure 1. *Polarization controllers that use multiple wave plates with fixed retardation and variable orientation angles tend to be slow and wavelength-sensitive; (a) the free-space optics approach, (b) the fiber coil (mickey mouse ears) approach, and (c) the electro-optic waveguide approach.*

Unlimited options

An all-fiber controller based on this mechanism (Figure 1b) reduces the insertion loss and cost. In this device, three fiber coils replace the three free-space retardation plates. Coiling the fiber induces stress, producing birefringence inversely proportional to the square of the coils' diameters. Adjusting the diameters and number of turns can create any desired fiber wave plate.

Despite the reduced loss and cost, the device still suffers from wavelength sensitivity and low speed. In addition, because bending the fiber generally induces insertion loss, the fiber coils must remain large and the resulting device is generally bulky. Therefore, the use of these *mickey mouse ear* controllers is primarily limited to laboratories.

For network deployment, speed is essential and physically rotating the wave plates cannot meet the need. For this reason, $LiNbO_3$ based high-speed polarization controllers (Figure 1c) were developed. One such controller comprises three waveguide sections, two of which simulate a QWP, and one of which simulates an HWP. However, instead of rotating the wave plates, two voltages and the electro-optic effect determine the relative orientation (effective optical axis) of each. Proper voltage adjustments can achieve endless rotation of each wave plate. Examples of the control voltages for the three wave plates are illustrated below:

$$V_1 = V_a\sin\alpha - V_b\cos\alpha - V_c,$$
$$V_2 = V_a\sin\alpha + V_b\cos\alpha + V_c$$

$$V_3 = V_d\sin\beta - V_e\cos\beta - V_f,$$
$$V_4 = V_d\sin\beta + V_e\cos\beta + V_f$$

$$V_5 = V_g\sin\gamma - V_h\cos\gamma - V_i,$$
$$V_6 = V_g\sin\gamma + V_h\cos\gamma + V_i$$

where α, β, and γ are three endlessly adjustable parameters that determine the orientations of their

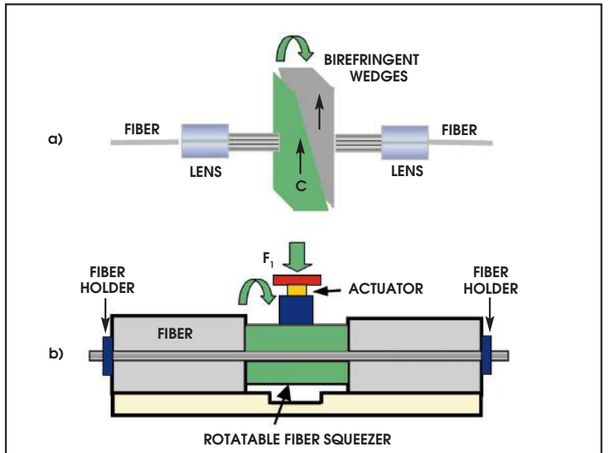

Figure 2. *Polarization control with a single wave plate with variable retardation and orientation is slow but wavelength-insensitive; (a) a free-space optics approach, (b) an all-fiber approach with rotatable fiber squeezer.*

corresponding wave plates, and V_a to V_i are nine predetermined voltage parameters.

Unfortunately, the price for this speed increase may not be acceptable for network applications. High insertion loss (~3 dB), high polarization-dependent loss (~0.2 dB), high activation loss (~0.15 dB) and high cost are the major disadvantages. The device also has at least nine parameters to optimize, making implementation complicated and costly.

In an alternative approach, a Babinet-Soleil compensator can convert any input polarization state into any desired output polarization state. The heart of such a device (Figure 2a) is a composite wave plate made from two birefringent crystal wedges. The thickness (and therefore the total retardation) of the wave plate varies by sliding the two wedges against one another. The orientation of the composite wave plate can also rotate around the optical beam.

Compared with the previous device (Figure 1a), this has the advantage of insensitivity to wavelength because precision retardation can be achieved for any wavelength. However, it suffers from high cost, high insertion loss and low speed.

To reduce the cost and insertion loss, an all-fiber polarization controller based on the Babinet-Soleil compensator principle was developed (Figure 3b) in 1996 with the trade name PolaRITE. The device comprises a fiber squeezer that rotates around the optical fiber. Applying a pressure to the fiber produces a linear birefringence, effectively creating a fiber wave plate whose retardation varies with the pressure. Simple squeeze-and-turn operations can generate any desired polarization state from any arbitrary input polarization.

In addition to low insertion loss and low cost, the device is small and wavelength insensitive, especially compared with the *mickey ear* controllers. This makes it useful for integration into WDM modules. However, similar to the controllers that rely on physical rotation, this device is too slow to be used for dynamic PMD compensation in fiber optic networks.

Polarization controllers also can be made with multiple free-space wave plates oriented 45° from each other (Figure 3a). The retardation of each wave plate varies with an applied voltage; however, the orientation angles are fixed. These variable retardation wave plates can be made with liquid crystals, electro-optical crystals or electro-optical ceramics. The disadvantage of the liquid crystal device is low speed and the electro-optical one generally requires high operation voltages. Such a polarization controller generally has high insertion loss, high cost and limited bandwidth due to the antireflection coatings and the microlenses.

All-fiber solutions

An all-fiber device based on the same operation principle (Figure 3b) would reduce the insertion loss and cost. The retardation of each wave plate varies with the pressure of each fiber squeezer. The challenge is making the device reliable, compact and cost-effective.

In PolaRITE II[2], a commercial dynamic polarization controller, piezoelectric actuators drive the fiber squeezers for high speed. Because it is an all-fiber device, it has no backreflection and has extremely low insertion loss and polarization-dependent loss. Its response time of 30 µs is fast enough to track the fastest polarization fluctuations in field-installed fiber links. With proper control procedures, endless (or reset-free) polarization control can be achieved without disruption.

With an activation-induced loss of less than 0.003 dB, it is also useful in high-precision PDL instrumentation and in feedback loops for compensating polarization-induced penalties. It is also independent of wavelength, working equally well for signals ranging from 1280 nm to 1650 nm.

System applications

A fiber-squeezer-based dynamic polarization controller (DPC) offers low insertion loss, low PDL, low activation loss, low backreflection, high speed and low cost. It is ideal for optical system applications to overcome the polarization-induced impairments, as shown in Figure 5a-e. The applications where DPC can play a significant role include:

• PMD compensation: A typical first-order PMD compensator (Figure 5a) comprises a dynamic polarization controller followed by a fixed or variable differential-group-delay (DGD) element.[3] The PMD along the link can be monitored through measuring the degree of polarization (DOP) by using an in-line polarimeter.[2] The DOP information is then fed back to control the DPC and the DGD value of the compensator. The typical response time of the monitor and DPC is less than 100 µs.

• Polarization optimization: Various optical components or modules in a transmission link, such as electro-optic (E-O) and electro-absorption (EA) modulators, optical interferometers and heterodyne optical receivers, are polarization sensitive. A dynamic polarization controller can be used in such a link to minimize the polarization sensitivity by optimizing the output power of the components or modules (Figure 5b). This scheme also can be used to reduce the effect of PDL in various passive components.

• Polarization-assisted crosstalk reduction: In order to increase the spectral efficiency of the DWDM systems, two polarization-related transmission techniques have been employed: polarization division multiplexing (PDM) where two channels have orthogonal polarizations at the same wavelength; and polarization interleaving where adjacent WDM channels have orthogonal polarizations.[4] For the polarization interleaving scheme shown in Figure 5c, a dynamic polarization controller followed by a polarizer is used to reduce polarization-induced crosstalk between the adjacent wavelength channels.

• Polarization scrambling: The fiber-squeezer-based controller can also work as a polarization scrambler to effectively randomize polarization states. With a built-in resonant enhanced circuit, the half-wave voltages of the device at scrambling frequencies are reduced to only a few volts. With properly selected driving parameters, the scrambler has successfully achieved a minimum polarization sensitivity of less than 0.05 dB and a degree of polarization less than one percent. The main applications of polarization scrambling include:

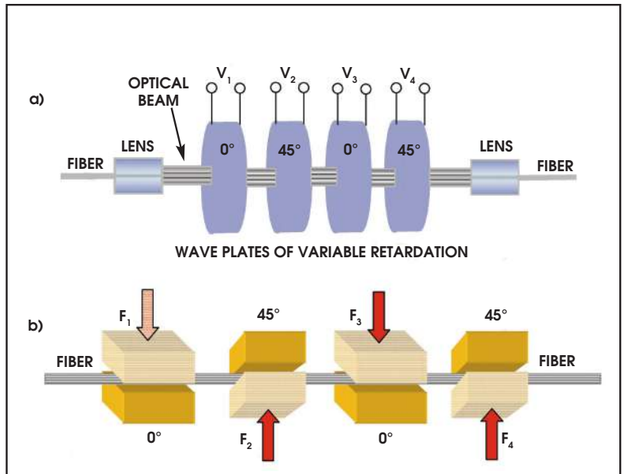

Figure 3. *Multiple wave plates with fixed orientation and variable retardation make dynamic polarization controllers that are fast and insensitive to wavelength; (a) the free-space optics approach has voltage, insertion-loss, cost and bandwidth limitations, (b) an all-fiber squeeze solution is fast, reliable and low cost.*

1. PDG mitigation: The performance degradation due to polarization-dependent gain (PDG) induced in optical amplifiers in transmission systems can be suppressed by scrambling the SOP. The PDG magnitude is proportional to the DOP. A low DOP can reduce polarization hole burning (PHB) and suppress PDG (Figure 5d).[5] DOP can be minimized by scrambling the SOP of the signal at frequencies that are higher than the inverse of the response time of the optical amplifiers (~milliseconds).

2. Polarization sensitivity elimination: The polarization scrambling can be used to eliminate an instrument's polarization sensitivity. Some optical instruments, such as diffraction-grating-based optical spectrum analyzers, are sensitive to the SOP of the input light. Scrambling the input polarization can remove the measurement uncertainties caused by polarization sensitivity.

3. Facilitating PMD compensation: Polarization scrambling also can be used in systems to facilitate and simplify PMD compensation.[6] For such an application, low residual phase modulation is essential. The fiber-squeezer-based polarization scrambler is especially suited for this application due to its lowest residual phase modulation.

• PDL characterization and compensation: Fast and accurate PDL characterization of fiber optic devices in a manufacturing environment is important.

Figure 4. *A fiber-squeezer-based dynamic polarization controller.*

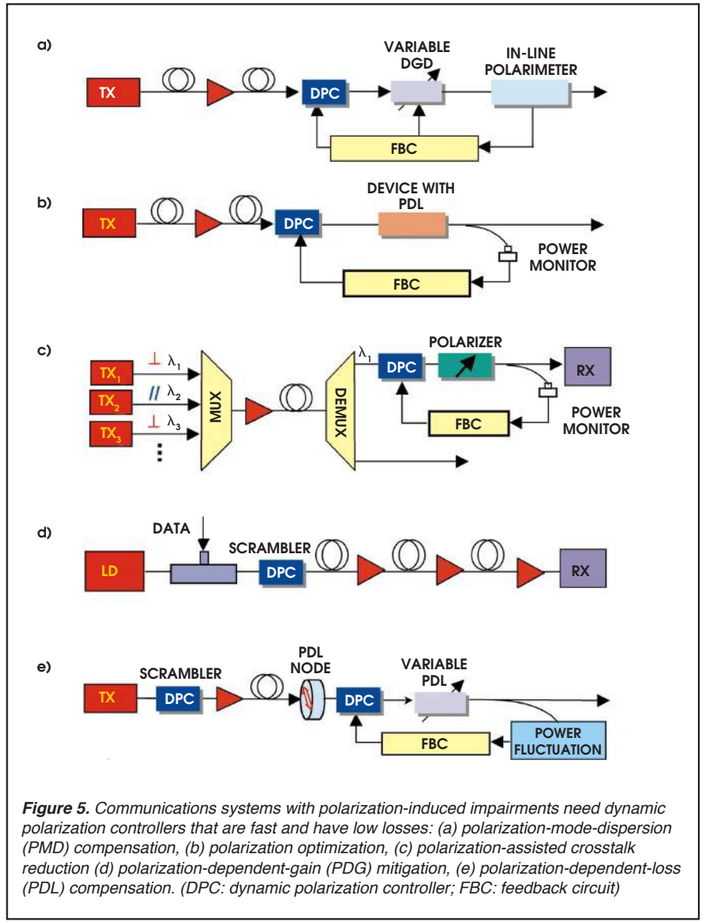

Figure 5. *Communications systems with polarization-induced impairments need dynamic polarization controllers that are fast and have low losses: (a) polarization-mode-dispersion (PMD) compensation, (b) polarization optimization, (c) polarization-assisted crosstalk reduction (d) polarization-dependent-gain (PDG) mitigation, (e) polarization-dependent-loss (PDL) compensation. (DPC: dynamic polarization controller; FBC: feedback circuit)*

Fiber-squeezer-based dynamic controllers are especially attractive for this application because their low activation loss and low PDL greatly improve the PDL measurement accuracy. At a system level, in order to monitor and compensate the PDL along the transmission link, a fast polarization scrambler should be placed after the transmitter to monitor PDL value from the power fluctuation induced by PDL of the components or optical modules (e.g., EDFAs). The feedback signal controls the DPC and variable PDL source to minimize the power fluctuation (Figure 5e).[7]

In summary, a dynamic polarization controller based on fiber-squeezer technology is a key unit to overcome the polarization-related impairments for the optical network systems and to characterize polarization for instrumentations. □

Acknowledgement

The author is grateful to the invaluable contributions by Lianshan Yan and James Shen of General Photonics Corp.

References

1. Chao Yeh et al (October 2000). Overcoming polarization impairment. *Fiberoptic Product News*.

2. Application notes on PolaRITE, polarimeter, and variable DGD, *General Photonics Corporation*, 2000-2001. www.generalphotonics.com.

3. H. Bulow, (1982). PMD mitigation techniques and their effectiveness in installed fiber, *Proc. OFC*, ThH1.

4. L.E. Nelson, T.N. Nielsen, and H. Kogenlnik, (2001). Observation of PMD-induced coherent crosstalk in polarization-multiplexed transmission. *IEEE Photonics Technol. Lett.*, vol.13.

5. E. Lichtman, (1995). Limitations imposed by polarization-dependent gain and loss on all-optical ultralong communication systems. *J. of Lightwave Technol.*, vol. 13.

6. H. Rosenfeldt et al (2001). Automatic PMD compensation at 40 Gbit/s and 80 Gbit/s using a 3-Dimensional DOP evaluation for feedback. *Proc. OFC*, paper PD27.

7. L.-S. Yan, Q. Yu, and A.E. Willner, (2001). Demonstration of in-line monitoring and dynamic broadband compensation of polarization dependent loss. *Proc. ECOC*.

Combat Polarization Impairments with Dynamic Polarization Controllers

Polarization related impairments have become the major obstacles to the increase of transmission rates in WDM systems. Such impairments include polarization mode dispersion (PMD) in optical fibers, polarization dependent loss (PDL) in passive optical components, polarization dependent modulation (PDM) in electro-optic modulators, and polarization dependent gain (PDG) in optical amplifiers. A dynamic polarization controller is identified as the single most important element in various schemes for overcoming these impairments.

The cause for these polarization impairments is the imperfection of the optical fibers. If the fibers were perfect, the state of polarization (SOP) of the light signal transmitting in the fiber would remain constant and the effects of PMD, PDL, PDM, and PDG could easily be eliminated. Unfortunately, the SOP of light propagating in a length of standard communication fiber varies along the fiber due to the random birefringence induced by the thermal stress, mechanical stress, and irregularities of the fiber core. Generally, at the output end of the fiber the light is elliptically polarized, with varying degrees of ellipticity, and with the major elliptical axis at an arbitrary angle relative to some reference orientation. Worst of all, the induced birefringence changes with temperature, pressure, stress and other environmental variations, making polarization related impairments time dependent.

Polarization Mode Dispersion (PMD)

PMD is often cited as the next critical hurdle for the high bit rate transmission systems (10Gb/s and higher) after chromatic dispersion and fiber nonlinearity impairments are successfully managed. As illustrated in Fig. 1, a fiber link can be considered as a concatenation of many, randomly oriented retardation plates. In the absence of PDL or PDG in the fiber link, these retardation plates are optically equivalent to a single retardation plate with an effective DGD and a pair of effective orthogonal principal axes (can either be linear or circular) for a given optical frequency. Upon entering the retardation plate, an optical pulse is decomposed into two polarization components along the two axes. Because the two components travel with different speeds in the retardation plate, they exit the plate with a relative time delay called Differential Group Delay (DGD). When DGD is comparable with the bit separation of a data stream, bit error rate may significantly increase.

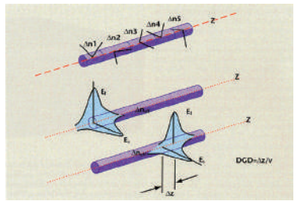

Fig. 1 A real fiber is like many retardation plates with different orientations and birefringences placed in serial. It is equivalent to a single retardation plate having a slow and fast axis and an equivalent birefringence. An optical pulse broadens because the two polarization components travel at different speeds.

The rms value of the DGD is often referred to as first order PMD. Similar to the famous random walk problem in which the rms distance of a drunken man to the origin is proportional to the square-root of the number of walking steps, PMD is proportional to the square-root of the number of cascaded retardation plates, or equivalently, to the square-root of the fiber length.

Contrary to the case of a true retardation plate, the DGD and the principal axes of the fiber link depend on the wavelength and fluctuate in time as a result of temperature variations and external constraints. Consequently, the corresponding pulse broadening is random, both as a function of wavelength at a given time and as a function of time at a given wavelength. As a rule of thumb, the maximum tolerable DGD value is 14% of the bit duration to ensure an outage probability of less than 5 minutes per year at a 3-dB power penalty. This translates to 14ps for a 10Gb/s system and 3.5ps for a 40Gb/s system. Unfortunately, for link distance greater than 300 km, 20% of the installed fiber plant is not suitable for 10Gb/s transmission and 75% is not suitable for 40Gb/s transmission at this outage tolerance level. Therefore, PMD compensation is required for these fiber links.

Unlike the effects of chromatic dispersion and fiber nonlinearity, which are deterministic and stable in time, the PMD-induced penalty can be totally absent at any given moment and adversely large enough several days later to cause an unacceptable bit-error-rate for no apparent reason. To ensure an acceptable outage probability for the fiber optic system, PMD compensation must be dynamic in nature and adaptive to the random time variations. Various schemes for mitigating the effect of PMD are illustrated in Fig. 2.

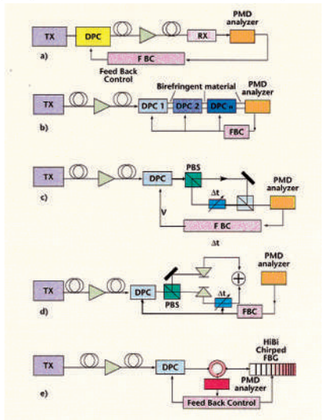

Fig. 2 Various PMD mitigation schemes: a) Principal state transmission method; b) Multiple retardation plates method; c) Optical delay line method; d) Electrical delay line method; e) Chirped HiBi fiber grating method. In all schemes, dynamic polarization controllers (DPC) having fast speed, low PDL, and low activation loss are required.

The schemes generally contain three key components: 1) the dynamic polarization controller (DPC), 2) the PMD analyzer, and 3) the feedback circuit. For some schemes, the dynamic variable delay line may also be required. The low insertion loss specification of the fiber squeezer based device becomes even more attractive for the schemes that require multiple polarization controllers capable of compensating higher order PMD effects. As will be discussed below, low PDL and low activation loss are also important parameters for the DPC to function properly in the feedback loops.

Polarization Dependent Loss (PDL)

The PDL of an optical component is defined as the difference between the maximum and the minimum insertion losses for all possible input SOPs. Optical components with PDL act as partial polarizers with two orthogonal axes (either linear or circular). A light signal experiences a maximum loss if its SOP is aligned with one axis and a minimum loss if aligned with the other axis.

Almost all fiber optic components have PDL and the causes may be different for different components. First of all, when light passes from an optical medium with an index of n1 to another medium with an index n2, reflection occurs. The reflection coefficients for the polarization states perpendicular and parallel to the plane of incidence are different if the angle of incidence is not normal (many fiber components have angled input and output surfaces for increased return loss.) Such a difference in reflection results in a difference in transmission loss or PDL. For example, an 8° angle polished connector (FC/APC or SC/APC) has a PDL of 0.022 dB. Fiber grating based devices may also exhibit PDL if the grating is not normal to the fiber longitudinal axis.

Second, for many optical components, such as isolators and circulators, birefringent crystals are often used. Because a birefringent crystal has two principal axes with different indexes of refraction, n_o and n_e, the Fresnel reflection coefficients of two polarization states perpendicular and parallel to the principal axes are different even at normal incidence, resulting in different transmission loss. The corresponding PDL is thus:

$$PDL=20^{*}\log|(n_e\text{-}1)(n_o+1)/(n_o\text{-}1)(n_e+1)|$$

Anti-reflection (AR) coatings can greatly reduce the reflection, however, they may not totally eliminate PDL because the optimal coating layer thickness is determined by the refractive index of the coated material: it is either optimized for n_o or n_e.

Diffraction grating based optical components or instruments generally have high PDL because the diffraction efficiencies for the two polarization states perpendicular and parallel to the plane of incidence are different.

Finally, any fiber component containing a dichroic material also has PDL. A dichroic material has two principal axes with different absorption or attenuation coefficients. The principal axes can either be linear (linear dichroism) or circular (circular dichroism). For example, the $LiNbO_3$ waveguide made with the proton exchange method exhibit strong linear dichroism and acts just like a polarizer.

In a fiber link which contains many optical components with different PDL values, the total PDL value depends on the SOPs of the light signal transmitted in the link and varies between a maximum and a minimum value. The maximum value is equal to the summation of the PDL values of all the components in the link. It is the difference between two insertion loss measurements of the link: the first one is when SOP of the light before each component is aligned with the minimum loss axis of the component and the second one is when SOP of the light before each component is aligned with the maximum loss axis.

The minimum PDL value corresponds to the case that the SOPs of a light signal before all the PDL components are arranged such that the PDLs cancel one another out. The net residual PDL is the minimum PDL of the link.

The presence of PDL in a fiber link also complicates PMD compensation. When PDL is present in the fiber link, the link is no longer equivalent to a single retardation plate. It instead is equivalent to two retardation plates with a partial polarizer sandwiched in between. Any PMD compensation scheme therefore must take the effect of the partial polarizer into account, which may increase the complexity of the compensation arrangement significantly.

Like the PMD penalty, the PDL effect in a fiber link containing multiple PDL components separated by sections of single mode fiber is also time dependent. At any moment, the states of polarization in different sections of the link may be oriented favorably to allow a low link loss such that the detected optical power at the receiver is high enough to achieve acceptable bit-error rate (or signal-to-noise ratio). However at a different moment, the link loss may be too high to achieve quality transmission due to the external thermal or mechanical stress on the fiber that causes the states of polarization in different fiber sections to re-arrange.

To combat the time-varying PDL problem, dynamic polarization controllers may be used at selected locations in the fiber link, as shown in Fig. 3. Each polarization controller assures that the light passing through the PDL component following the controller has the lowest loss.

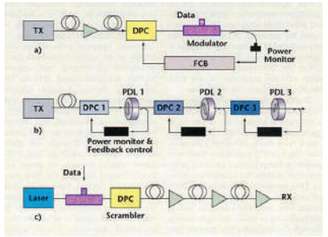

Fig. 3 Dynamic Polarization Controllers (DPC) for a) Polarization stabilization; b) PDL compensation; c) PDG mitigation.

Polarization Dependent Gain (PDG)

The gain of an optical amplifier for the stronger polarization component is less than that for the weaker component (because the stronger component saturates the gain more) and the gain difference is called polarization dependent gain (PDG). One cause for the PDG is that the cross sections of the stimulated emission for different polarization states are different. This polarization hole burning always gives more gain to the weaker polarization component and thus tends to cause the polarization state to change with time. In addition, when the input SOP changes, the signal gain may increase temporarily , then come down in a short period of time. Consequently, the polarization hole burning always encourages polarization fluctuations in a fiber laser system and thus causes mode-hopping and increases super-mode noise in a mode-locked laser.

An optical amplifier may at the same time exhibit PDL effect. For example, couplers and isolators are generally contained in an Er+ doped fiber amplifier (EDFA) and the presence of PDL in these components gives rise to the apparent PDL of the amplifier. Even in semiconductor optical amplifiers (SOA), the facets of the semiconductor chip are generally angle cleaved to prevent optical feedback into the amplifier. As discussed previously, these

angled interfaces exhibit large PDL, which directly contributes to PDL of the SOA.

In a fiber optic link with many optical amplifiers and many components with PDL, the effect of PDG can be significant at some moments and negligible at other times. When a large number of optical amplifiers are cascaded in a long haul fiber link, the performance degradation caused by PDG is significant even though each amplifier may have a very small PDG (~0.1 dB). The performance degradation becomes even worse when PDG is combined with the PMD and PDL of the fiber and other components in the link. Polarization scrambling at a frequency above amplifier's response rate (inverse of amplifier's upper energy level life time, ~ 500 Hz for EDFA) has proven to be effective in mitigating PDG impairment in long haul systems, as shown in Fig. 3. A factor of 2 increase in system Q factor was demonstrated in an 8100-km link containing 181 EDFAs with such a scheme.

Polarization Dependent Modulation (PDM)

In addition to PDL, external modulators, such as $LiNbO_3$ based electro-optical modulators and semiconductor electro-absorption modulators, also exhibit polarization dependent modulation in that the modulation depth of signals with different polarization states are different. As a result, the amplitude of the received data bits varies when the state of polarization of light before entering the modulator varies due to the fluctuation of temperature or other external constraints on the fiber, resulting in bit-error-rate fluctuation.

To assist polarization alignment, most Ti-indiffused $LiNbO_3$ modulators embed a polarizer at input or out of the waveguide and thus convert the PDM problem into a more easily identified PDL problem. The $LiNbO_3$ modulators made with proton exchange process act like a polarizer themselves without the embedded polarizer. Thus one method of eliminating PDM effects uses a fast response dynamic polarization controller placed in front of the modulator to assure that light passing through the modulator has minimal loss, as illustrated in Fig. 3.

"Dynamic" is the Magic Word for Polarization Control

Because polarization-induced penalties are time dependent, polarization-impairment mitigation must be dynamic and adaptive to random time variations. A dynamic polarization controller is the single most important element for overcoming these impairments.

Fast speed, low PDL, low insertion loss, and low activation loss are all critical parameters in evaluating a dynamic polarization controller. Activation loss measures the additional insertion loss caused by activation of the device and is defined as the difference between the maximum and minimum insertion losses of the device considering all possible activation conditions. This specification is particularly important because all polarization-impairment compensation schemes utilize a feedback signal to activate the polarization controller. The activation-induced loss causes errors in the feedback signal and directly degrades the performance of the compensation apparatus. In addition, when an instrument for measuring the PDL of optical components includes a polarization controller, the activation-induced loss limits the resolution and accuracy of the measurement. Similarly, a polarization controller's PDL also contributes to errors in a feedback system and complicates the design of compensation hardware and software.

Present dynamic polarization controllers on the market include free-space retardation plate based and Lithium Niobate waveguide based devices. The free-space devices contain multiple (sometimes three) retardation plates with different relative orientations. Applying a voltage to each retardation plate changes its retardation and hence the polarization of light passing through the plate. Because light has to exit the fiber, be collimated, pass through the plates and finally be focused back into the fiber when making such devices, the resulting labor costs, material costs, and insertion losses are high. The retardation plates may be made of liquid crystal or solid state electro-optical materials. Liquid crystal devices also suffer from low speed (10 to 100 ms), narrow operating temperature ranges, and high PDL.

Lithium Niobate based dynamic polarization controllers contain multiple sections of waveguide with different electrode (or crystal) orientations. Similar to the liquid crystal based devices, each waveguide functions as an electrically variable retardation plate. By applying different voltages to different waveguide sections, any polarization states can be generated. However, typical of lithium niobate waveguides, such a controller has high insertion loss (~ 4 dB), high polarization dependent loss (~0.2 dB), low return loss (45 dB), high cost, and narrow temperature range (0 to 60°C). In addition, the maximum power of the device is limited to 50 mW, making it impractical to use after optical amplifiers.

Advantages of Fiber Squeezer Polarization Controllers

Polarization controllers based on fiber squeezers have been investigated by researchers for over a decade. However, reliability concerns associated with fiber squeezing and high activation loss prevented such devices from becoming commercially feasible. In 1996, General Photonics Corporation in Chino, CA successfully introduced the first commercial fiber-squeezer based polarization controller (PolaRITE). Subsequently, the same company also introduced the first fiber squeezer-based polarization scrambler. Over the years, the company has perfected the art of fiber squeezing and developed several proprietary technologies.

Based on the prior experiences with fiber squeezers, General Photonics recently introduced the first multi-axis fiber-squeezer based dynamic polarization controller/ scrambler shown in Fig. 4. Similar to the bulk-wave plate and Lithium Niobate based polarization controllers, the fiber-squeezer controller contains multiple retardation plates with different orientation angles. Each retardation plate is created by squeezing a section of fiber with a PZT actuator and the retardation of the plate can be easily changed by varying the voltage applied to the PZT actuator. It can be shown that this device can convert any polarization state to any desired polarization state on the Poincare Sphere by controlling the voltages on different fiber sections.

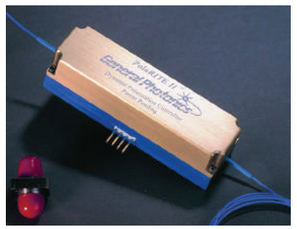

Fig. 4 Fiber squeezer dynamic polarization controllers have the advantages of no insertion loss, no backreflection, no wavelength dependence, extremely low PDL and activation loss, and high speed.

INSTRUMENTS
MODULES
PASSIVE COMPONENTS
ACCESSORIES
APPLICATION GUIDE
FAQS

Due to its all fiber nature, this device has practically no insertion loss, no back reflection, and no polarization dependent loss. In addition, it is has a response time of less than 35 µs, significantly faster than that of a liquid crystal based device. Such high speed operation is essential for tracking fast polarization variations which are caused either by passing locomotives as in fibers laid along railway tracks or by ocean waves as in the trans-oceanic fiber trunks.

Perhaps most impressively, General Photonics has succeeded in reducing activation-induced losses in its fiber squeezer controller to less than 0.003 dB. The low activation-induced loss makes these components ideal for use in high precision PDL instruments and in feedback loops for compensating for polarization induced penalties.

Another unique and attractive feature of General Photonics' device is that its performance is wavelength independent: the device functions equally well for signals ranging from 1280 nm to 1650 nm. This one-device-fit-all feature helps to simplify system design, lower implementation cost, and enables system's channel expandability.

Implementation of fiber squeezers is also cost effective. Half-wave voltage requirements of the fiber squeezer controllers have been reduced to less than 40 VDC. The low voltage requirements allow the use of readily available low cost electronics to drive and control the fiber squeezer controller. Reliability of the fiber squeezers has also proven to be very high. In testing, over 10 billion activation cycles at half wave voltages have been achieved without a single failure.

An additional application of the fiber squeezer controller is as a polarization scrambler to effectively randomize polarization states. With a built-in resonant enhanced circuit, the half wave voltages of the device at scrambling frequencies are reduced to only a few volts. Such low voltage requirement makes the driving electronics simple and low cost. With properly selected driving parameters, the scrambler has successfully achieved a polarization sensitivity of less than 0.05 dB and a degree of polarization less than 1%.

Applications

Due to its superior performance (low insertion loss, low PDL, low activation loss, low backreflection, high speed, and low cost), the fiber squeezer dynamic polarization controllers are ideal for PMD mitigation, PDL compensation, and PDG effect reduction, as illustrated in Figures 2 and 3.

Fig. 5 The polarization stabilizer has an input port, an output port, and two device ports for accepting the two ends of a polarization sensitive device, such as a $LiNbO_3$ modulator. The stabilizer automatically adjusts the SOP to the modulator and ensures a maximum light transmission. The heart of the stabilizer is a fiber squeezer polarization controller.

The fiber squeezer dynamic controllers can also be used for polarization stabilization, which is important for electro-optic and electro-absorption modulators, optical interferometers, and heterodyne optical receivers. We designed and buil a polarization stabilizer (Fig. 5) using the fiber squeezer-dynamic controller and have achieved output power stability to within 0.05 dB against all possible polarization variations.

The polarization scrambling feature of the fiber squeezer based device can also be used to eliminate instrument's polarization sensitivity. Some optical instruments, such as diffraction grating based optical spectrum analyzers, are sensitive to the state of polarization of the input light. Scrambling the input polarization is an effective way of removing the measurement uncertainties caused by the polarization sensitivity. The fiber-squeezer based dynamic polarization controller/scrambler is ideal for such an application because of its low scrambling voltages and multiple resonant scrambling peaks. The scrambler has successfully achieved a polarization sensitivity of less than 0.05 dB and a degree of polarization less than 1%.

Fast and accurate PDL characterization of fiber optic devices in a manufacturing environment is important. The dynamic polarization controller can be readily included in an instrument to automatically search for the maximum and minimum insertion loss of a device under test and calculate the corresponding PDL. Fiber-squeezer based dynamic controllers are especially attractive for this application because of their low activation loss and low PDL, which ultimately limit the PDL measurement accuracy. Our test indicates that a PDL measurement with a resolution of 0.01 dB can be readily achieved in a fraction of a second using a dynamic controller manufactured by General Photonics Corporation.

Conclusion

In conclusion, polarization related penalties, including PMD, PDL, PDG, and PDM, in fiber optic systems are all time-varying and unpredictable. Fast dynamic polarization controllers must be employed to mitigate the relevant impairments. Fiber-squeezer based polarization controllers are superior to other approaches in terms of insertion loss, back return loss, PDL, activation loss, and speed, and can efficiently squeeze out these polarization related problems.

Suggested Readings:

1) M. Chbat, "Managing polarization mode dispersion," Photonics Spectra, June 2000, pp. 100-104.

2) T. Ono and Y. Yano, "10 Gb/s PMD compensation field experiment over 452 km using principal state transmission method," Optics & Photonics News, p. 61, May 2000.

3) H. Buelow, "PMD mitigation techniques and their effectiveness in installed fiber," OFC'200 Proceedings, ThH1-1, p.110.

4) D.A. Watley et al, "Field evaluation of an optical PMD compensator using an installed 10 Gb/s system," OFC'2000 proceedings, ThB6-1, p.37.

5) Z. Pan et al, "Chirp-free tunable PMD compensation using Hi-Bi nonlinearly chirped FBGs in a dual-pass configuration," OFC'2000 Proceedings, ThH2-1, p113.

6) F. Bruyere, O. Audouin, V. Letellier, G. Bassier, and P. Marmier, "Demonstration of an optimal polarization scrambler for long-haul optical amplifier systems," IEEE Photonic Technology Letters, Vol. 6, pp. 1153-1155 (1994).

7) E. Lichtman, "Limitations imposed by polarization-dependent gain and loss on all-optical ultralong communication systems," J. of Lightwave Technol., Vol. 13, pp. 906-913 (1995)

Scrambling to Minimize Polarization Related Impairments

Steve Yao, Yongqiang Shi, and Jianwei Ma
General Photonics Corporation, Chino, CA 91710

Polarization Fundamentals

Polarization is a fundamental property of light. In classical physics, light is modeled as a sinusoidal electromagnetic wave in which an oscillating electric field and an oscillating magnetic field propagate through space. Polarization is defined in terms of the pattern traced out in the transverse plane by the electric field vector as a function of time.

For unpolarized light, the plane of polarization fluctuates randomly around the direction of light beam propagation. Therefore, on average, no direction is favored. The rate of the fluctuation is so fast that an "observer" or a detector cannot tell the state of polarization (SOP) at any instant in time. For example, natural light (sunlight, firelight, etc.) is unpolarized. In any other case, the light beam can be considered to consist of partially polarized or fully polarized light. Degree of Polarization (DOP) is used to describe how much of the total light intensity is polarized. For totally polarized light, the DOP is one. For completely unpolarized light, the DOP is zero. Most high performance lasers used in long-haul communication systems are polarized light sources.

The polarization of light beams is an important factor in high-speed optical communication network system design. As the bit rate increases, fiber optic communication systems become increasingly sensitive to polarization related impairments. Such impairments include polarization mode dispersion (PMD) in optical fibers, polarization dependent loss (PDL) in passive optical components, polarization dependent modulation (PDM) in electro-optic modulators, polarization dependent gain (PDG) in optical amplifiers, polarization dependent center wavelength (PDW) in WDM filters, polarization dependent response (PDR) in receivers, and polarization dependent sensitivity (PDS) in sensors and coherent communication systems.

Polarization scrambling can be used to mitigate many polarization related impairments. Light is called "scrambled" if the SOP of totally polarized light is made to vary randomly at a relatively low rate. At any instant of time, the SOP is well defined, and DOP is close to 1. However, on a time average, DOP is close to zero. Therefore, the DOP of scrambled light depends on the averaging time or the detection bandwidth of the observer.

Principles of Polarization Scrambling

A polarization scrambler actively changes the SOP using polarization modulation methods. Several polarization scramblers based on different technologies are available today, including $LiNbO_3$ based scramblers, resonant fiber coil based scramblers, and fiber squeezer based scramblers.

LiNbO3 scramblers use the electro-optic effect to modulate the state of polarization. For example, a $LiNbO_3$ phase modulator can be used as a scrambler when the input SOP is linearly polarized at 45 degrees with respect to the applied modulation electric field. Such a scrambler is high speed, but it suffers from high insertion loss, high PDL, high residual amplitude modulation (activation loss), high sensitivity to input polarization state, and high cost due to insertion of a waveguide in the fiber line. Multiple modulation sections with different electric

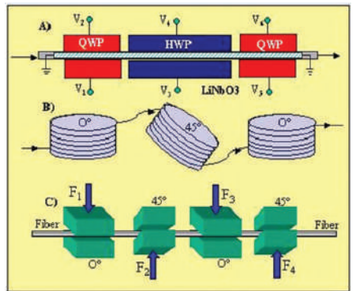

Fig. 1 Illustrations of different polarization scramblers. A) LiNbO3 based, B) Fiber resonant coil based, and C) fiber squeezer based.

field directions, as shown in Fig. 1A, may be used to make the device less polarization sensitive but at the expense of increased complexity and additional cost.

A resonant fiber coil based scrambler is constructed by winding fiber around an expandable piezo-electric cylinder. Applying an electric field to the cylinder causes it to expand, which in turn induces a birefringence in the fiber via the photoelastic effect. If the frequency of the electric field is in resonance with the piezo-electric cylinder, the induced birefringence will be large enough to cause sufficient polarization modulation with a relatively low applied voltage. In practice, multiple fiber cylinders with different orientations may be cascaded to make the scrambler less polarization sensitive, as shown in Fig. 1B. Compared with $LiNbO_3$ scramblers, the expanding fiber coil based scramblers have the advantages of low insertion loss, low PDL, and low cost. On the other hand, they suffer from large size, low scrambling speed, and large residual phase modulation resulting from the significant amount of fiber stretching when the fiber coil expands.

Squeezing fiber can induce large birefringence in the fiber via the photo-elastic effect, and can cause large polarization modulation if the input polarization is 45 degrees from the squeezing axis. A polarization insensitive scrambler can be constructed by cascading multiple fiber squeezers oriented 45 degrees from each other, as shown in Fig. 1C. The device can be operated either resonantly at higher scrambling frequencies or non-resonantly at lower scrambling frequencies. Compared with the LiNbO3 scrambler, this device has the benefit of low insertion loss, low PDL, and low cost. Compared with the fiber coil scrambler, it has the advantages of small size, low residual phase modulation, and scrambling flexibility. In addition, it has the advantages of low residual phase modulation and residual amplitude modulation (activation loss) over both the LiNbO3 and fiber coil scramblers. Low residual phase modulation is important for avoiding interference related noise in optical systems, and low residual amplitude modulation is critical for using the scrambler for PDL and DOP measurement of optical devices. Fig. 2A illustrates a fiber squeezer polarization scrambler board for OEM applications.

The performance of the scrambler is generally measured by the degree of polarization of the scrambled light over a certain period of time, and by the uniformity of the Poincaré sphere coverage of the SOP. In practice, the wavelength sensitivity and temperature sensitivity of the performance of the scrambler are also important for real world applications.

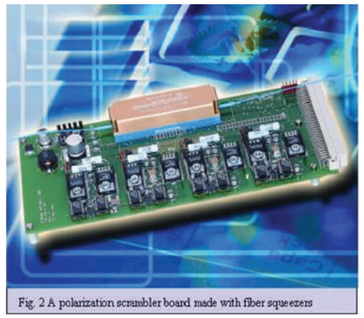
Fig. 2 A polarization scrambler board made with fiber squeezers

Fig. 3A shows the excellent scrambling uniformity on the Poincaré Sphere of the scrambler board in Fig. 2, while Fig. 3B shows its DOP as a function of detector bandwidth. The wavelength sensitivity is illustrated in Fig. 3B. As can be seen in Fig. 3C, a multi-stage fiber squeezer scrambler is much less sensitive to wavelength changes than other types of scramblers. Experimental results also indicate that the fiber squeezer scrambler is less sensitive to temperature change, as shown in Fig. 3D.

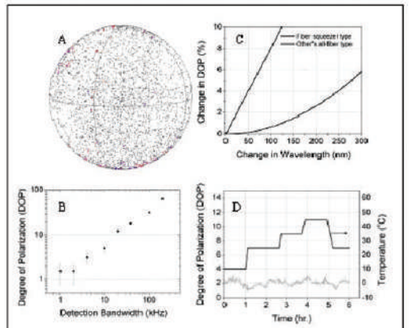

Fig. 3 Typical fiber squeeze r based scrambler performance data

Operation lifetime is always an important parameter to consider for system and industrial applications. Some users may question the lifetime of the fiber under stress in the fiber squeezers. Indeed, without proper treatment and protection, the fiber may break in a short period of time. General Photonics has spent a great deal of effort in finding fiber failure mechanisms under stress and corresponding methods for protection since 1996. With our proprietary and patented fiber protection methods, the fiber in our squeezer under maximum operation stress has an estimated mean time to failure (MTTF) of 2 billion years. Such a result is not surprising, considering that the stress in a PM fiber induced by the two stress rods is on the same order of magnitude as the stress applied to the fiber by the fiber squeezer. In our continued endurance test, the fiber squeezers have passed one trillion (10^{12}) activation cycles, and the number is expected to rise as the test continues.

There are a number of companies that manufacture different types of polarization scramblers, including a stand-alone desk-top instrument type made by ILX Lightwave (Model PSC 8420), a plug-in module type by EXFO (model IQS-5100B) as a part of a main-frame test instrument, and finally, board level scramblers designed for low cost system & OEM applications by General Photonics (model PCD-003/004). These scramblers have their own intended markets and their own advantages. What type is best suited for a particular user depends on the application, user preference, and budget.

Scramblers can also be classified by driving frequency. For fiber squeezer based scramblers, the driving frequencies of the different squeezers are different. To obtain the best results, they should not be harmonics or sub-harmonics of each other. The driving frequencies of some scramblers are factory-set and cannot be changed. Therefore, the scrambling rate for such scramblers is fixed. Such scramblers are generally designed for the highest possible scrambling rate by using the resonant nature of the piezo-electric transducers. In addition to such resonant-frequency scramblers, General Photonics has also designed a miniature scrambler for hand-held and field instruments. The scrambling rate of the miniature scrambler can be easily changed in steps from a few hertz to a few tens of kilohertz either by a push-button switch or via a computer command.

Polarization scramblers have numerous applications in optical communication networks, fiber sensor systems, and test and measurement systems. As shown in Fig. 4A, a polarization scrambler can be used at the transmitter side to minimize PDG or polarization hole burning of Erbium doped fiber amplifiers (EDFA) in ultra-long haul systems. For this application, the scrambling rate should be significantly faster than the inverse of the gain recovery time constant of the fiber amplifiers (on the order of 10 kHz).

Scramblers can also be used to assist in the monitoring of PMD in a WDM system, as illustrated in Fig. 4B. Generally speaking,

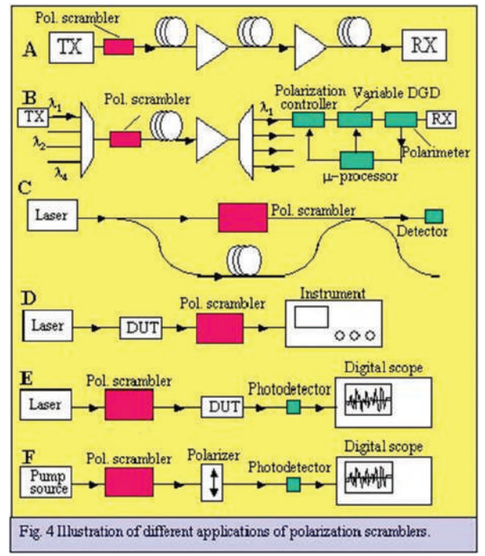

Fig. 4 Illustration of different applications of polarization scramblers.

PMD can be monitored by measuring the degree of polarization (DOP) of the optical data stream propagated through the fiber. Low DOP usually indicates a large PMD effect. However, such a measurement may be erroneous if the input SOP to the transmission fiber is substantially aligned with the principal state of polarization (PSP) of the fiber. In such a situation, the measured DOP is always large no matter how large the differential group delay (DGD) between the two principal states of polarization. A scrambler at the transmitter side can be used to effectively eliminate such an anomaly. Furthermore, it enables a polarimeter in the PMD compensator at the receiver side to identify the PSP, which in turn speeds up PMD compensation. Other optical network applications include signal to noise ratio monitoring of WDM channels with a polarizer placed after the scrambler.

Polarization scramblers can also be used to eliminate the polarization fading of a fiber sensor, as shown in Fig. 4C. In such a system, the envelope of the response curve is independent of the polarization fluctuation.

Placing a scrambler in front of a polarization- sensitive instrument, such as a diffraction grating based optical spectrum analyzer, can effectively eliminate its polarization dependence, as shown in Fig. 4D, if the scrambling rate is sufficiently faster than the detector speed in the instrument. In addition, as illustrated in Fig. 4E, polarization scramblers can be used to measure the PDL of a device under test (DUT) with the help of a digital scope. The resulting PDL of the device can be calculated as:

$$PDL = 10\log (Vmax/Vmin),$$

where Vmax and Vmin are the maximum and minimum signal displayed by the digital scope.

Raman amplifiers generally exhibit strong PDG if the pump laser is highly polarized. To minimize the PDG, a depolarized pump source must be used. The DOP of the pump source directly relates to the PDG of the amplifier, and therefore, must be carefully characterized. DOP can be measured using expensive polarimeter-based polarization analyzing instruments; however, such instruments are not accurate for low DOP (<5%) sources. Polarization scramblers, again, can be used to accurately measure the DOP with a digital scope, as illustrated in Fig. 4F. Assuming that the maximum and minimum voltages measured with the digital scope are Vmax and Vmin, respectively, the DOP of the light source can be calculated using the following formula:

$$DOP=(Vmax-Vmin)/(Vmax+Vmin)$$

In summary, a polarization scrambler is an important device for fiber optic communications, fiber sensors, and fiber optic test and measurement applications. With low insertion loss, low back reflection, low residual amplitude and phase modulation, low wavelength and temperature sensitivity, low cost, and small form factor, fiber squeezer based scrambler modules are especially well suited for OEM applications, where they can be readily integrated into various network equipment, fiber sensor systems, and test and measurement instruments.

Suggested Readings:

1. F. Heismann, S. Korotky, and J. Veselka, “Lithium Niobate integrated optics: selected contemporary devices and system applications”, Ch. 9, Optical Fiber Telecommunications, IIIB, edited by I. Kaminow and T. Koch, Academic Press, 1977

2. Steve Yao, “Have you hugged your fiber today?” Photonics Spectra, February 2001.

3. L. S. Yan, et al, “Differential Group Delay Monitoring used as feedforward information for polarization mode dispersion compensation,” Photonics Technology Letters, Vol. 14 (10) (2002)

4. H. Rosenfeldt, Ch. Knothe, R. Ulrich, E. Brinkenmeyer, “Automatic PMD compensation at 40 Gbits/s and 80 gbits/s using a 3 dimensional DOP evaluation for the feedback”, OFC 2001, Technical Digest Postconference Edition , March 2001.

INSTRUMENTS
MODULES
PASSIVE COMPONENTS
ACCESSORIES
APPLICATION GUIDE
FAQS

Polarization Related Tests for Coherent Detection Systems

INTRODUCTION

Coherent detection with polarization division multiplexing (PDM) has emerged as the key technology enabler for 40 Gbps and 100 Gbps networks because it significantly increases the spectral efficiency of each channel and allows each channel to transmit at a high bit rate with relatively small optical bandwidth. Consequently, 40 Gbps, 100 Gbps, or even 160 Gbps channels can be transmitted over existing 10 Gbps WDM infrastructures with 50 GHz channel spacing [1]. PDM doubles the spectral efficiency by combining two polarization channels of the same bit rate at the same wavelength [2-8]. Also, coherent detection allows multiple levels of phase and amplitude modulation at lower rates to be multiplexed on the same wavelength channel [9-16]. For example, PDM, together with quadrature-phase-shift-keying (QPSK) modulation, enables 40 Gbps transmission within the bandwidth of a 10 Gbps direct channel [13]. At such a small bandwidth, impairments due to polarization mode dispersion (PMD) and chromatic dispersion (CD) are greatly reduced and have less impact on the bit error rate (BER) of the transmission. In addition, because both the amplitude and phase information of the two orthogonal polarizations of a signal are preserved in a coherent detection system, PMD, PDL (polarization dependent loss) and CD compensations can be performed by digital signal processing (DSP) in the electrical domain to further extend system tolerance of the effects of PMD, PDL and CD.

A system deploying polarization multiplexing must be able to separate the two polarization channels at the receiving end. Such a task can be accomplished optically by controlling polarization with a feedback signal. Because both phase and amplitude information of both polarizations are maintained during coherent detection, the information can be obtained by digital signal processing (DSP). Digital polarization demultiplexing can significantly reduce cost and size, compared with optical demultiplexing.

POLARIZATION TEST REQUIREMENTS

Coherent detection systems generally perform the following polarization control functions:

- Polarization demultiplexing
- PMD compensation (PMDC)
- PDL compensation (PDLC)

These functions can be accomplished using high speed DSP circuits and algorithms in the transceivers. For transceiver developers, the evaluation of different DSP circuits and algorithms is critical. For the system integrators using the transceivers, it is important to compare the performance of transceivers from different vendors, including the three key polarization control functions. Finally, network operators using the systems developed by different system vendors can evaluate and compare the polarization performances from different vendors and optimize deployment decisions.

Polarization Demultiplexing Related Tests

For polarization demultiplexing, important testing parameters include:

- State of polarization (SOP) tracking speed
- SOP recovery time
- SOP orthogonality between the two polarization channels

SOP tracking speed is defined as the highest speed of SOP, measured in radians/second, at which a system can operate properly without losing track. It is a measure of how well the demultiplexing circuitry and algorithm track polarization variations of different patterns at different speeds.

SOP recovery time is defined as the time required for a system to recover from a loss of polarization track caused by an abrupt polarization change. It indicates how well the demultiplexing circuitry and algorithm respond to sudden SOP jumps.

Polarization orthogonality reflects the polarization channel crosstalk. In practice, it should be measured after two polarization channels are combined at the transmitter end and before they are separated at the receiving end. Ideally, the two polarization channels are perfectly orthogonal during transmission. However, imperfection in the polarization combiner can cause the two channels to be imperfectly orthogonal when they are combined. In addition, PMD, PDL, and nonlinearity may degrade the orthogonality of the two polarization channels and cause crosstalk. The degree of polarization (DOP) is an indication of polarization crosstalk. If there is no polarization crosstalk, the DOP is zero when the powers in the two polarization channels are equal. In the presence of crosstalk, the DOP is non-zero when the powers in the two polarization channels are equal.

PMD Related Tests

For PMD compensation, key performance indicators include SOP tracking speed, SOP recovery time, PMD tracking speed, PMD recovery time, and PMD tolerance range. Similar to their definitions in polarization demultiplexing, SOP tracking speed is defined as the highest polarization variation rate at which the PMD compensation (PMDC) hardware and algorithm can effectively reduce PMD related signal distortions, and SOP recovery time as the time required for a PMDC to recover from a loss of track caused by an abrupt polarization jump.

PMD tracking speed is defined as the highest PMD variation speed at which the PMD compensator is still effective in reducing PMD induced signal distortion. It is specified in picoseconds/second and defines how fast a PMDC can respond to PMD value changes.

PMD recovery time is defined as the time required for a PMDC to recover from a loss of track caused by an abrupt PMD value jump. It measures how well a PMDC responds to sudden changes in PMD.

PMD tolerance range is defined as the maximum PMD value in a transmission system with which data can be transmitted with a BER smaller than that required by system design. It is a measure of how well the PMDC works in mitigating PMD effects and extending the system’s PMD tolerance range.

PDL Related Tests

For PDL testing, the critical parameters are SOP tracking speed, SOP recovery time, PDL tracking speed, PDL recovery time, and PDL tolerance range. SOP tracking speed is defined

as the highest SOP variation speed at which the PDLC can still function effectively in reducing PDL related transmission errors. SOP recovery time is defined as the time required for a PDLC to recover from a loss of track caused by an abrupt polarization change. PDL tracking speed is defined as the highest rate of PDL change (in units of dB/s) at which a PDLC can effectively reduce PDL related errors. PDL recovery time is defined as the time required for a PDLC to recover from a loss of track caused by an abrupt PDL change. Finally, PDL tolerance range is the maximum PDL value in a transmission system with which data can be transmitted with an acceptable BER. It is a measure of how well a PDLC works in mitigating PDL effects and in extending the system's PDL tolerance range.

Table I (below) summarizes the tests required for each function of a coherent detection system.

Polarization Demux	PMDC	PDLC
SOP Tracking Speed	SOP Tracking Speed	SOP Tracking Speed
SOP Recovery Time	SOP Recovery Time	SOP Recovery Time
SOP Orthogonality	PMD Tracking Speed	PDL Tracking Speed
	PMD Recovery Time	PDL Recovery Time
	PMD Tolerance Range	PDL Tolerance Range

INSTRUMENTATION

Different instruments are required to perform the various tests listed in Table I.

SOP Tracking Speed and SOP Recovery Time Tests

SOP tracking speed and recovery time tests require a polarization controller with specific capabilities.

Fig. 1 shows a test setup including the General Photonics MPC-202:

Fig. 1 SOP tracking speed and recovery time tests in a coherent detection system. The General Photonics MPC-202 can be used for these tests.

The MPC-202 Multifunction Polarization Controller (Figure 2) has four functions that are uniquely suited to these tests.

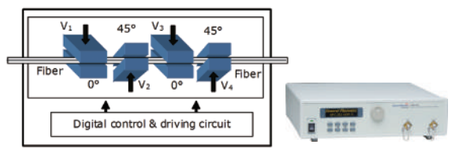

Fig. 2 Illustration of a multifunction polarization controller (MPC-202) constructed with multiple fiber squeezers.

1. Fast, Quasi-Uniform Rate Polarization Change

The new Tornado scrambling method covers the Poincaré sphere with a spiral SOP trace about a fixed or rotating axis. Unlike other scrambling methods, its polarization variation rate distribution is very narrow and concentrated at the high end of the distribution curve, a profile that greatly improves the reliability and repeatability of SOP tracking speed tests. The polarization variation rate can be up to 360 krad/s, much faster than the polarization variation found in real fiber (up to 280 krad/s).

This scrambling method is therefore uniquely suited to SOP tracking speed testing.

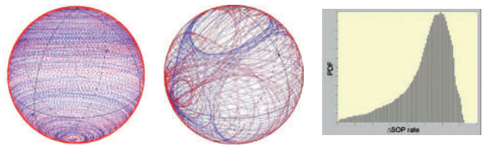

Fig. 3 a) Tornado SOP trace, fixed axis. b) Tornado SOP trace, rotating axis. c) Tornado scrambling SOP rate variation distribution.

2. Polarization Variation Emulation

SOP changes continuously in real fiber, as shown in Fig. 3d, with a variation rate that follows a Rayleigh distribution, as shown in Fig. 3e. The MPC-202 can generate this polarization variation pattern, with a mean rate of polarization variation that can be selected within a range of 0.01 to 2000 rad/s. This function can be used to model the effect of SOP variation in a real fiber system.

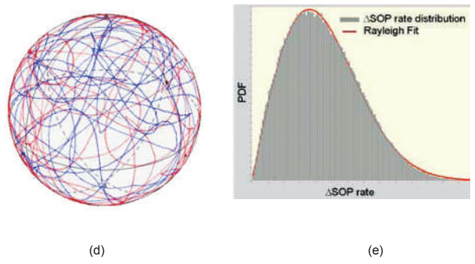

Fig. 3d) SOP trace generated by the Rayleigh scrambling function.
e) Rayleigh rate distribution

3. Abrupt, Random Polarization Change

The SOP changes between discrete points distributed uniformly across the Poincare Sphere, at a rate of change ranging from 0.01 to 20,000 points/s.

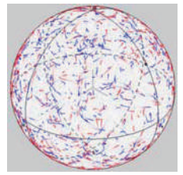

Fig. 3f) SOP points generated by the random scrambling function.

4. Generation of Polarization Variations with Waveforms

Polarization variations based on sine, triangle, and square waves of variable frequency and amplitude can be generated. Fig. 3g shows a square wave variation.

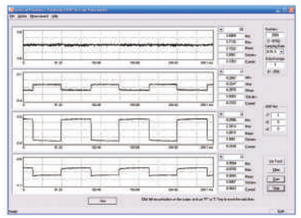

Fig. 3g) SOP traces (four Stokes parameters) generated by the square wave function, displayed on the POD-201's oscilloscope screen.

5. Triggered Random State Generation

The instrument can generate random polarization states on receipt of an external trigger signal, making it possible to test the response of the polarization tracking circuit/algorithm under test to a series of step polarization changes.

The MPC-202's square waveform function is a particularly useful tool for recovery time characterization because it generates an abrupt SOP transition of controllable magnitude at controllable intervals. The maximum slew rate for a square wave polarization modulation is 360 krad/s, more than sufficient to emulate the fastest polarization transitions in real fiber.

Figure 3h shows a circuit recovery time measurement using a square wave-induced change in SOP. The sharp rising edge causes the polarization tracking circuit to lose track before recovering.

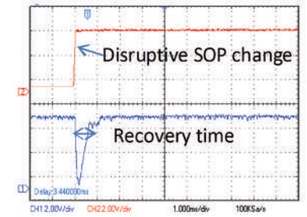

Fig. 3h) Tracking circuit recovery from disruptive SOP change (square wave transition).

Instruments that rely on mechanical motion, such as the Agilent model 11896A Polarization Controller, are bandwidth limited. For example, the Agilent unit can only generate variations up to three hertz, which may not be adequate for testing modern systems.

However, because the Agilent 11896A was the first mainstream polarization controller available, many engineers are familiar with and rely on its polarization scrambling characteristics. For compatibility with this early standard, the MPC-202 has an Agilent 11896A emulation function that replicates the scrambling function of the Agilent polarization controller.

Polarization Orthogonality Test

The SOPs of the two polarization channels should ideally be orthogonal in the transmission fiber from the time that they are combined (or multiplexed) by a polarization beam combiner (PBC) at the transmission side until they are separated (or demultiplexed) by a polarization beam splitter (PBS) at the receiving end. Imperfections in PBCs can cause non-orthogonality, and standard specifications, such as polarization extinction ratio (PER), do not always properly reflect the orthogonality performance of the PBC; special tests are therefore required.

Two General Photonics instruments can be used for testing the orthogonality of a PBC: the POD-201 in-line polarimeter and the PSGA-101A polarization measurement system (Figure 4).

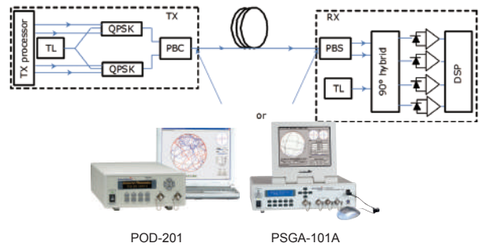

Fig. 4 SOP orthogonality test of two polarization multiplexed signals at the output of the polarization beam combiner (PBC) and at the input of the polarization beam splitter (PBS) in a polarization multiplexed coherent detection system. The POD-201 or the PSGA-101 can be used for the test.

During the test, the polarization channels are sequentially turned "off" and the SOP of the "on" channel is measured. The relative polarization angle between the two SOP points is obtained through the angle measurement function of the software. A relative angle of 90 degrees indicates perfect orthogonality, and the amount of deviation from 90 degrees of the actual angle is a measure of non-orthogonality.

Polarization orthogonality may also degrade during transmission due to the effects of PMD, PDL, or nonlinearity. Again, both the POD-201 and PSGA- 101 can be used to quantify the degradation by using the measurement method described above before the PBS at the receiver side.

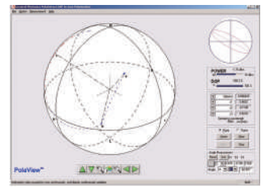

PolaView™ angle measurement function for testing SOP orthogonality.

PMD Tracking Speed and PMD Recovery Time Tests

For PMDC using DSPs in a coherent system, the circuit/ algorithm must track SOP variations and rapid PMD changes. In order to test a PMDC's PMD variation tracking speed and PMD recovery time, an instrument with fast PMD generation capability is required. The General Photonics PMDPro™ is recommended for these tests.

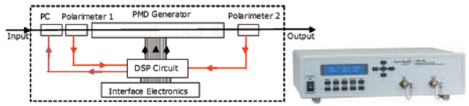

Fig. 5 Illustration of PMDPro™ polarization optimized PMD source. Its PMD generator can generate 1st and 2nd order PMD in less than 1 ms. The polarization controller (PC) is used to generate different SOP variations as in the MPC-202. In addition, the PC, together with the two polarimeters, is used to perform polarization optimization functions as well as polarization synthesis functions.

The PMDPro™ consists of a polarization controller, a front polarimeter, a PMD generator, and a rear polarimeter (Figure 5). The polarization controller can be used with the front polarimeter to automatically align and maintain the input SOP at 45° from the principal axis of the DGD element to obtain the worst-case first-order PMD effect. Alternatively, the controller can automatically adjust and maintain the input SOP using the feedback from the rear polarimeter to either minimize or maximize the output DOP for each PMD setting. Minimizing the output DOP enables testing of the worst-case total PMD effect, while maximizing the DOP turns the PMDPro™ into a PMD compensator, allowing the user to measure the PMD values of an active fiber link.

The PMDPro™ can also perform PMD emulation by generating statistical PMD distributions. Finally, the polarization controller and polarimeters can provide various polarization control functions, including variable rate polarization scrambling, polarization waveform generation, polarization trace generation and polarization stabilization at any SOP.

The PMD generator inside the PMDPro™ can deterministically generate both 1st and 2nd order PMD (SOPMD) values in a few milliseconds because the all digital design utilizes no mechanical rotators. Figure 6 shows available values of DGD and SOPMD.

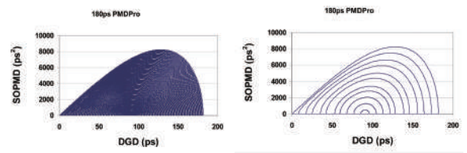

Fig. 6 The left plot is a comprehensive map of DGD vs. 2nd order PMD (SOPMD), showing the coverage of generated PMD values with dense (256) PMD traces. The right plot shows some typical PMD traces. PMD values can be varied quickly along those traces.

Different operation modes provide different PMD change patterns for the two different tests: For PMD recovery time testing, the discrete PMD generation mode allows the user to change PMD values discontinuously with user selected step sizes and dwell times. The abrupt PMD jump offered in this mode will cause loss of track in the PMDC and enable the user to measure the time required for the PMDC to regain track. For PMD tracking speed testing, the continuous PMD generation mode allows the user to vary PMD values along a trace like those shown in the second graph in Fig. 6. Operators can gradually increase the PMD variation speed until the PMDC can no longer follow.

PMD Tolerance Test

Coherent Detection systems use DSP to increase PMD tolerance. PMD tolerance tests measure the maximum PMD value that the system can tolerate. A typical test setup is shown in Fig. 7a.

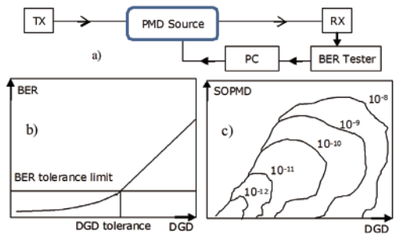

Fig. 7 a) PMD tolerance test setup using a PMDPro™ PMD source. The computer (PC) selects PMD settings and collects BER readings. b) A BER vs. DGD curve can be obtained, and the DGD tolerance for a given BER threshold can be deduced using the curve. c) Map of BER vs. DGD and SOPMD. Each contour represents a BER value, and the PMD tolerance can be obtained from the contour plot.

Test results can be used by network operators to compare systems made by different vendors and verify PMD related specifications promised by the vendors. They can also be used by system vendors to determine suitability of PMD algorithms, to tune algorithms, and for quality control screening of the transceivers. The key instrument in this setup is the PMD source used to generate precise 1st and 2nd order PMD values, as shown in Fig. 7a. The bit-error rate (BER) of the system, or another performance indicator parameter such as power penalty, is monitored as the 1st order PMD (DGD) values generated by the PMD source are increased until the BER reaches the limits of the system, as shown in Fig. 7b. The corresponding DGD is the 1st order PMD tolerance of the system. Both the 1st and 2nd order PMD (SOPMD) values can also be increased as the BER of the system is measured and plotted, as shown in Fig. 7c. The system outage probability can be calculated from the data obtained.

The effect of PMD on a system is highly dependent on the input SOP. To eliminate test uncertainties and increase test speed, the input SOP must be optimized and maintained against polarization fluctuations caused by external disturbances. For a single polarization system without multiplexing, the PMDPro™ has two modes of polarization optimization for PMD tolerance tests. One mode aligns the input SOP 45 degrees from the principal axes of the DGD generator to obtain the worst-case DGD effect. The second mode aligns the SOP by minimizing the output DOP to obtain the worst-case total PMD effect on the signal. Polarization optimization assures consistent and repeatable PMD tolerance test results.

In polarization multiplexed systems, where two orthogonal polarization channels are present simultaneously, the PMDPro™'s polarization optimization functions are not useful; however, the built-in polarization scrambling functions can be used to scan through all possible polarization states to assure that the worst-case polarization effects are properly characterized.

Polarization Dependent Loss (PDL) Tolerance Test

A coherent detection system generally includes hardware and algorithms to compensate for the effects of PDL (PDLC). System vendors and operators need to know how much PDL a transceiver can tolerate, and therefore must conduct tolerance range testing. A system vendor can use test results to optimize hardware and algorithms, and to perform quality checks. Network operators can use PDL tolerance range testing to qualify vendors and to perform quality inspection of incoming equipment to ensure the performance of their systems.

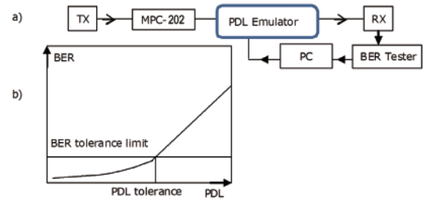

Fig. 8 a) PDL tolerance test setup. b) A typical BER vs. PDL curve

Fig. 8a shows a typical setup for measuring the PDL tolerance of a transceiver or system. A PDL emulator capable of generating any PDL value is essential for conducting a PDL tolerance range test. The PDL tolerance range can be determined from the BER vs. PDL graph, as shown in Fig. 8b. Because PDL effect on the signal is sensitive to SOP variation, an MPC-202 can be placed in front of the PDL emulator/source to generate the required SOP variations.

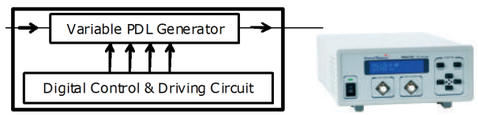

Fig. 9a) Construction and photo of PDLE-101.

General Photonics' PDL emulator, the PDLE-101, is designed for PDL related system tests, particularly PDL tolerance testing. The emulator can set any PDL value from 0 dB to 20 dB with a speed of less than 5 ms and a resolution of 0.1 dB. The PDL value can be set individually or can be scanned with a user defined range, waveform, and speed. In addition, random PDL variations can be generated to emulate PDL variations in a real system.

PDL Tracking Speed and Recovery Time Tests

PDL changes rapidly with time in real systems. It is therefore important to evaluate whether the PDL compensation can track the PDL changes. In order to test the PDL tracking speed of the PDL compensation, an instrument to generate fast PDL variations is essential. The PDLE-101's ability to generate PDL changes using different wave forms is uniquely suited to such an application. Fig. 9b shows such a PDL variation following a triangle wave modulation.

The PDLE-101 can also generate abrupt PDL jumps in the form of a square wave, as shown in Fig. 9c. The abrupt PDL jump can cause the PDLC to lose track of the PDL, enabling the measurement of the time required for the PDLC to regain track for PDL compensation.

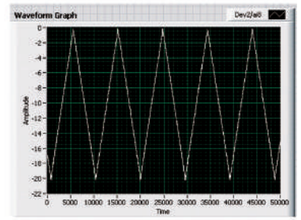

Fig. 9b) Triangle wave PDL variation

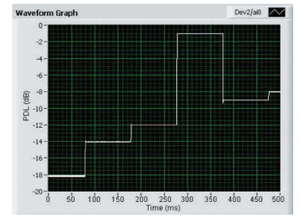

Fig. 9c) Random amplitude square wave PDL variation

Component Level PMD/PDL Measurements

The General Photonics PSGA-101A is recommended for characterization of PMD and PDL for component testing [17]. As shown in Fig. 10, the PSGA-101A consists of a tunable laser, a binary polarization state generator (PSG), a binary polarization state analyzer (PSA), and an internal computer.

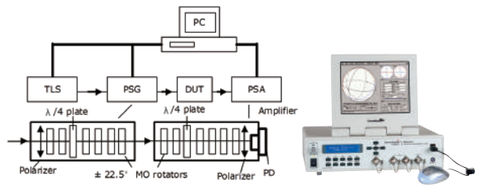

Fig. 10 Illustration of a PSGA-101A polarization analysis system based on a novel binary polarization analysis method which enables very high accuracy and repeatability.

The binary magneto-optic polarization rotator design of the PSGA provides measurement accuracy that can only be calibrated with NIST grade material standards. The values in the table below exceed those of any other instrumentation product on the market by an order of magnitude.

	DGD (1st Order PMD)	SOPMD (2nd Order PMD)	PDL
Accuracy	± 2.6 femtoseconds	± 1.39 ps²	± 0.06 dB
Resolution	1 femtosecond	0.005 ps²	0.01 dB
Repeatability	0.022 femtoseconds	0.28 ps²	0.034 dB

In-Circuit Link PMD Measurement

It is often desirable to be able to measure the PMD of a transmission link without interrupting signal transmission. The General Photonics PMDPro™ has an in-service PMD measurement function, which is accomplished by PMD compensation, as shown in Fig. 11. On the Tx side, a polarized broadband light source, centered on an ITU grid with a 3-dB bandwidth of 0.25 nm and obtained by passing an ASE source through a tunable filter, is fed into an idle channel at the multiplexer. On the Rx side, the test signal is dropped out from the demultiplexing port and passes through a PMDPro™. The instrument generates DGD values between 0 and 90 ps with an incremental step of 0.357 ps. The time required to run one step is less than 1 ms. At any DGD value, PMD compensation can be performed by feeding the DOP value to the DSP circuit for it to control the polarization controller to maximize the DOP. To measure the PMD of the light path, the DGD value generated by the compensator steps from zero to its maximum value, while PMD compensation is performed by maximizing the DOP for each step. When the test signal reaches its peak DOP value, as shown in Fig. 11b, the DGD value of the compensator at this point is equal to the PMD value of the light path.

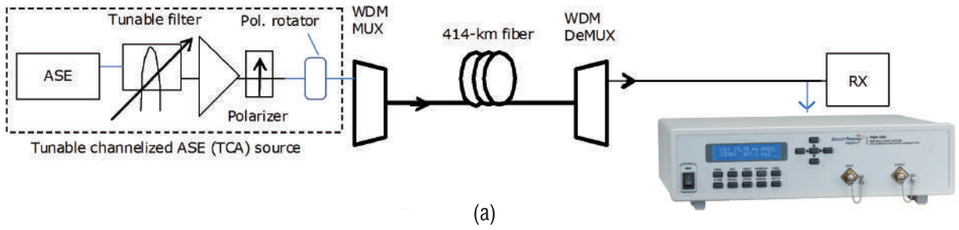

(a)

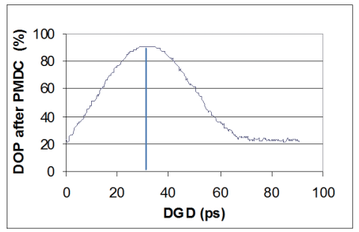

(b)

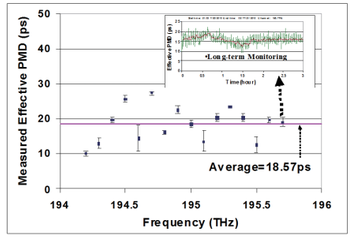

(c)

Fig. 11 In-service PMD measurement using a PMDPro™. a) System measurement setup. b) DOP vs. DGD curve. The DGD value corresponding to the DOP peak is the instantaneous effective PMD of the DWDM channel under test. c) Average PMD of the fiber link obtained by averaging instantaneous PMD of multiple DWDM channels measured at about the same time. Insert of c) shows the long term PMD monitoring result of a single channel.

General Photonics engineers demonstrated this in-service PMD characterization in a traffic carrying long haul network at a Verizon facility. The expected mean DGD of the route was calculated from the mean DGD values of the individual fiber sections using commercially available PMD measurement equipment before the long-haul system was installed and before traffic commenced. The calculated value was 19.77 ps. The length of the route is 414 kilometers with a ROADM at each end.

In the trial, the PMD values of 16 idle channels were measured. Figure 11c shows the measured DGD values of the 16 channels with error bars. The DGD value averaged over all 16 channels is 18.57 ps, which is very close to the expected mean DGD value of 19.77 ps. Considering the limited number of data points (channel numbers), the 6% difference between this result and the aforementioned “expected mean DGD” falls within the fundamental Gisin uncertainty [10].

The insert of Fig. 11c shows the results of a long-term PMD measurement of a single DWDM channel at 195.7 THz. Fairly stable PMD values for the channel were observed during the measurement period, taken around midnight. Note that the time average of single channel PMD for a much longer time can also yield the average PMD of the fiber link. The trial results show that the instrument is sufficiently accurate in PMD measurement, and that the measurement has no impact on the live traffic of other signal carrying channels.

We also successfully demonstrated the PMDPro™’s PMD measurement by PMD compensation function at Verizon’s 1500 km test bed using a 40Gbps signal itself as the signal source for the test with a DWDM channel for about 12 hours. The average PMD result obtained was very close to the expected value of the link. This result verified the usefulness of the PMDPro™ for the monitoring of the PMD of a fiber link over an in-use DWDM channel.

Summary

Coherent detection systems for 40Gbps and 100Gbps use digital signal processing for polarization demultiplexing, PMD compensation, and PDL mitigation. To quantify the performance of those functions, multiple tests are required. The first column of Table II (below) lists some polarization related tests of coherent detection systems. General Photonics provides an array of instruments, listed in the first row of Table II, to facilitate those tests. The applicability of each instrument to particular tests are checked in the table.

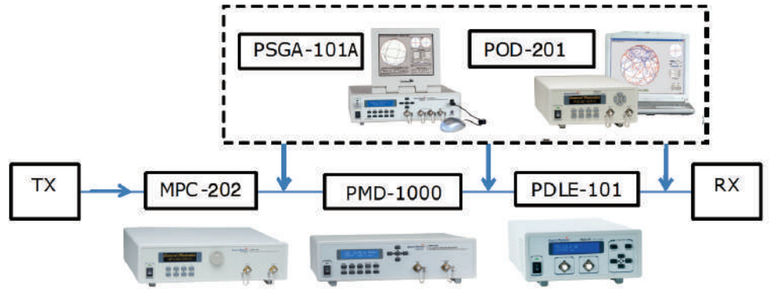

	Multifunction Polarization controller MPC-202	In-line polarimeter POD-201	PMD source PMD-1000	PDL source/ emulator PDLE-101	Polarization measurement system PSGA-101A
SOP tracking speed test	Yes	Yes	Yes		
SOP recovery time test	Yes	Yes	Yes		
SOP Orthogonality		Yes			Yes
SOP & DOP viewing and monitoring		Yes	Yes, but no graphic display		Yes
PMD tracking speed test			Yes		
PMD recovery time test			Yes		
PMD tolerance range test			Yes		
PDL tracking speed test				Yes	
PDL recovery time test				Yes	
PDL tolerance range test				Yes	
PMD/PDL measurement			Yes, in-service link		Yes

References

[1] T. J. Xia, et al, OFC’2008, paper NMC2
[2] S. Bhandare, et al, IEEE Photon. Technol. Lett., vol. 17, pp. 914-916, 2005
[3] D. Borne,S. Jansen, E. Gottwald, P. Krummrich, G. Khoe, and H. Waardt, OFC’2006, paper PDP34
[4] A. R. Chraplyvy, et al, IEEE Photon. Technol. Lett., vol. 8, pp. 1264-1266, 1996
[5] M. I Hayee, M. C. Cardakli, A. B. Sanhin, A. E. Willner, IEEE Photon. Technol. Lett., vol.13, pp.881-883, 2001
[6] X. Yao, L.-S. Yan, et al, Opt. Express, vol.15, pp.7407-7414, 2007
[7] Y. Han, G. Li, Electron. Lett., vol. 42, pp. 109-111, 2006
[8] R. Noe, S. Hinz, D. Sandel, F. Wust, J. Lightwave Technol., vol. 19, pp. 1469-1475, 2001
[9] T. Pfau, et al, OFC’2008, paper OTuM3
[10] C. Wree, D. Becker, D. Mohr, A. Joshi, OFC’2007, paper OMP6
[11] O. B. Pardo, OFC’2008, paper OTuM5
[12] Y. Cai, OFC’2008, paper OTuM1
[13] C. Laperle, et al., OFC’2007, paper PDP16
[14] G. Charlet, et al, OFC’2007, paper PDP17
[15] A. H. Gnauck, et al, OFC’2007, paper PDP19
[16] S. Chandrasekhar, X. Liu, OFC’2008, paper OThU7
[17] X. S. Yao, X. Chen, and T. Liu, “High accuracy polarization measurements using binary polarization rotators,” Optics Express, Vol. 18, No. 7, pp. 6667-6685, 2010

Practical 4-Stage Optical PMD Compensator for Mitigating 1st-and 2nd-Order PMD Impairments on 40-Gbit/s RZ-D(Q)PSK Signals

General Photonics Corp.

Abstract: A first practical 4-stage optical PMD compensator with ~1-ms response time is experimentally demonstrated for mitigating first- and second-order PMD impairments on 40-Gbit/s RZ-D(Q)PSK signals. BER and DOP degradations are significantly improved by this compensator and a power penalty of <0.5 dB is achieved at 10^{-9} BER in the presence of 25-ps DGD and 400-ps^2 SOPMD.

1. Introduction

As the data rate of optical channels increases to 40-Gbit/s and beyond, polarization mode dispersion (PMD) is considered to be a key limitation for deploying high-speed transmission systems. First-order PMD (i.e., differential group delay (DGD)) generally causes walk-off in time between the two orthogonal polarization states of the signal, resulting in spreading the pulse-width of the signal and thus increasing power penalty and service outage probability. Second-order PMD (SOPMD) results from the depolarization and frequency-dependent dispersion of a PMD vector and it has a statistical correlation to the increasing first-order PMD [1]. The PMD effects on the systems are inherently stochastic and change rapidly with time, making them difficult to mitigate.

Several prior approaches have been reported to combat the PMD effects for 40-Gbit/s deployment. The first is to select fiber routes with low PMD coefficients [2]. However, the PMD of a fiber route changes with time and environmental conditions and the interconnected routes may always have bad fiber sections with high PMD. The second approach is to utilize spectrally efficient modulation formats, such as differential quadrature phase-shift keying DQPSK. The PMD tolerance on the signal is greatly reduced, though never eliminated. Other electronic approaches include electronic dispersion compensator [3], forward error correction [4] and direct detection based digital equalizer [5]. The resulting PMD mitigation may be limited since directly detected signal lacks of phase/polarization information of the corresponding optical signal. Digital signal processing (DSP) is effective in mitigating PMD effect in a polarization multiplexed coherent detection system [6]; however, it may not be used in currently deployed 40-Gbit/s systems using single polarization D(Q)PSK schemes. Consequently, optical PMD compensation remains as an attractive option to effectively compensate for the total PMD [7-9]. It has been shown that multi-stage distributed PMD compensators are most effective in mitigating both the first- and higher- order PMD [10]; however, because of the complexity, single stage and one-and-half stage compensators are mostly developed [8]. PMD compensators (PMDC) of up to 3-stage were reported with limited results [10]. A laudable goal would be to develop efficient algorithm and hardware for adjusting all control parameters of a highly complex multi-stage compensator, and hence greatly reduce response time and improve compensator performance.

In this paper, we experimentally demonstrate a first practical 4-stage optical PMD compensator for mitigating both the first- and second-order PMD impairments on 40-Gbit/s RZ-D(Q)PSK signals. We show that the compensator can maintain the DOP of a 40-Gbit/s RZ-DQPSK signal above 98% with 25-ps DGD present and

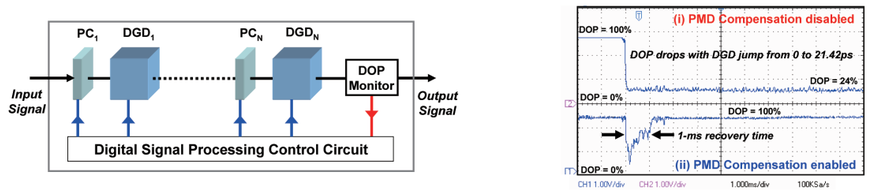

(a) (b)

Fig. 1. (a) Block diagram of a multi-stage DGD/SOPMD compensator (N=4), consisting of paired polarization controllers (PC) and DGD elements. (b) 1-ms recovery time of PMDC in the presence of the DGD jump from 0 to 21.42ps DGD. 2.5 V corresponds to a DOP of 100%.

94% with 25-ps DGD and 407.7-ps^2 SOPMD present, when the signal is continuously scrambled at a rate up to 500Hz before the signal going through the corresponding PMD emulator. We further show that the compensator can effectively reduce DGD/SOPMD induced power penalty of both 40-Gbit/s DQPSK and DPSK signals to less than 0.5 dB (at BER of 10^{-9}). Finally, with a response time of 1 ms, this modulation format-independent optical PMDC is capable of combating PMD impairments under fast PMD and polarization variations.

2. Concept and Device Response Time

The concept of our multi-stage optical PMD compensation technique is illustrated in Fig. 1(a). The compensator consists of 4 pairs of PCs and DGD elements, and is designed to compensate for an average PMD up to 20 ps (60 ps instantaneous DGD). The output signal is monitored by a high speed DOP meter placed at the end of this PMDC. The measured DOP, an indicator of PMD distortion on the signal, is continuously updated to the DSP control circuit to control each PC with an efficient reset-free algorithm to dynamically adjust the polarization alignment on each DGD element. All PCs are continuously adjusted to maximize the signal's DOP. Consequently, signal distortions induced by DGD and SOPMD can be rapidly and effectively mitigated.

Fig. 1(b) shows the measured recovery time of this PMDC in the presence of a DGD jump from 0 to 21.42 ps generated by a fast DGD/SOPMD source (General Photonics PMD-1000). The upper curve shows a corresponding DOP drop from 100% to less than 25% when the PMDC is disabled. In contrast, DOP quickly recovers to the original maximum value in about 1 ms when the PMDC is enabled. Although not shown here, the recovery time caused by an abrupt SOP change is also about 1 ms. Such a fast response time is sufficient to mitigate the fast changes of PMD effects caused by vibration or other fast disturbances in the fiber link.

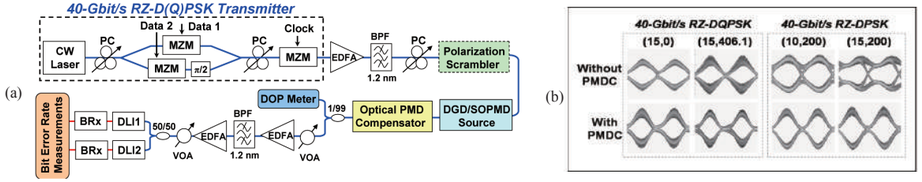

Fig. 2. (a) Experimental setup. (b) Eye diagrams of 40-Gbit/s RZ-DQPSK and RZ-DPSK signals with & without PMDC where (15,200) represents (15-ps DGD,200-ps^2 SOPMD).

3. System Experimental Results and Discussion

The system experimental setup is shown in Fig 2(a). The 40-Gbit/s RZ-D(Q)PSK signals are generated by a continuous-wave laser (1550.11 nm), externally modulated by a >40-GHz nested Mach-Zehnder modulator (MZM) and a RZ pulse carver, respectively. The signal is then boosted by an erbium-doped fiber amplifier (EDFA) and filtered by a 1.2-nm bandpass filter (BPF). A polarization controller (PC) is placed in front of a polarization scrambler (0.05~500 Hz scrambling rate) and a DGD/SOPMD source in order to generate different PMD effects. The signal, degraded by the DGD/SOPMD source, is sent through the 4-stage optical PMDC, with no prior PMD information required. Inside the compensator, about 1% of the output signal is tapped and sent to a DOP meter for measuring and monitoring, and 99% of the signal is sent to the bit error rate measurement set, including a variable optical attenuator (VOA), EDFAs, a BPF, a delay-line interferometer (DLI), and balanced receivers (BRx). Fig. 2(b) illustrates the captured eye diagrams of 40-Gbit/s RZ-D(Q)PSK signals without and with PMDC under different (DGD,SOPMD) combinations, respectively. The distorted signals are effectively improved by this PMDC.

A polarization scrambler with scrambling rates of 0.05~500 Hz is used to investigate the rapid compensation performance of this PMDC. Fig. 3(a) shows the long-term measurements of DOP, without and with PMDC, of a 40-Gbit/s RZ-DQPSK signal under 500 Hz scrambling and passing through a 25-ps DGD. Without PMD compensation, the signal's DOP fluctuates wildly between 15% and 100% under such high scrambling rate. On the other hand, the signal's DOP is stabilized with PMD compensation enabled. The average DOP values at a scrambling rate of 1~500 Hz are >98%. For another case with 25-ps DGD & 407.7-ps^2 SOPMD, the average DOP values at a scrambling rate of 1~500 Hz are >94%. Fig. 3(b) shows the measured DOP of 40-Gbit/s RZ-D(Q)PSK signals in the presence of different DGD values. As expected, the DOP value decreases with DGD increase. The DGD tolerance is different for 40-Gbit/s RZ-DQPSK and RZ-DPSK signals due to different spectral bandwidths. With PMDC, the DOP degradations are effectively compensated. Fig. 3(c) further shows the BER improvement in the presence of different DGD for 40-Gbit/s RZ-DQPSK and RZ-DPSK, respectively.

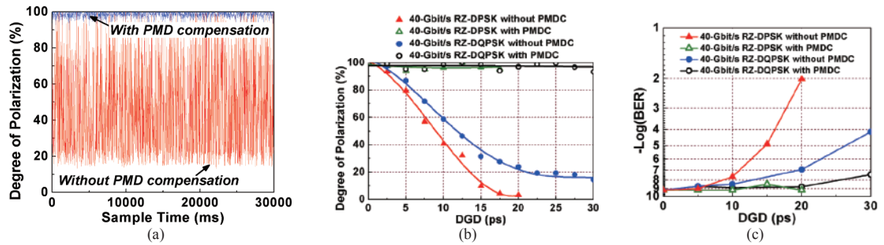

Fig. 3. (a) Long-term measurements (with and without PMDC) of DOP of a 40-Gbit/s RZ-DQPSK signal under 500-Hz scrambling and a 25-ps DGD. (b) and (c) DOP and BER degradations on 40-Gbit/s RZ-DPSK and RZ-DQPSK signals in the presence of different DGD values.

Fig. 4(a) illustrates the measured DOP variations of a 40-Gbit/s RZ-DQPSK signal in the presence of different DGD and SOPMD. The polarization scrambler is disabled in this case. Without PMDC, the measured DOP ranges from 100 to 3.3% in the presence of 0~40-ps DGD and 0~1200-ps^2 SOPMD. In contrast, the degraded DOP caused by various DGD and SOPMD is compensated and increases to >90% when the PMDC is enabled, showing the effective DOP improvement. Moreover, Fig. 5 shows the BER measurements of 40-Gbit/s RZ-DQPSK and RZ-DPSK signals in the presence of different DGD and SOPMD, respectively. For a 40-Gbit/s RZ-DQPSK signal, (20-ps DGD,400-ps^2 SOPMD) and (25-ps DGD,400-ps^2 SOPMD) cause >1-dB and >3-dB power penalty at a BER of 10^{-9}, respectively. With the PMDC, the measured power penalties of both cases are less than 0.5 dB. For a 40-Gbit/s RZ-DPSK signal, the tolerance becomes smaller as compared to 40-Gbit/s RZ-DQPSK. (10-ps DGD,200-ps^2 SOPMD) and (15-ps DGD,200-ps^2 SOPMD) induce >1.5-dB and >4-dB power penalty at a BER of 10^{-9}, respectively. Similarly, the measured power penalties for both cases are less than 0.5 dB with the PMDC.

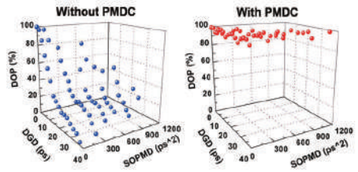

Fig. 4. Measured DOP (without PMDC and with PMDC) of a 40-Gbit/s RZ-DQPSK signal versus different DGD and SOPMD.

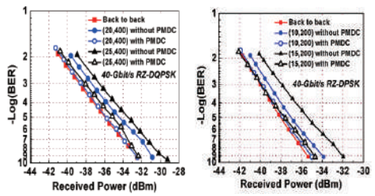

Fig. 5. BER measurements of 40-Gbit/s RZ-DQPSK and RZ-DPSK signals versus different DGD and SOPMD.

Acknowledgement

This work is supported by NSF-funded Center of Integrated Access Networks (CIAN) and General Photonics Corp. We thank Ernie Tan, Tao Yu, Lynn Lin for their contributions.

Reference

[1] H. H. Yaffe and D. L. Peterson, "Experimental determination of system outage probability due to first-order and second-order PMD," *J. Lightwave Technol.*, 24(11), 4155-4161 (2006).
[2] I. P. Kaminow and T. Li, *Optical Fiber Communication IVB*, Chapter 15, "Polarization Mode Dispersion", Elsevier (2002).
[3] H. Bulow, F. Buchali and A. Klekamp, "Electrical dispersion compensation," *J. Lightwave Technol.*, 26(1), 158-167 (2008).
[4] X. Liu, C. R. Gile, X. Wei, Y.-H. Kao, C. Xie, L. Moller, I. Kang and A. J. van Wijngaarden, "Experimental demonstration of broadband PMD mitigation through distributed fast polarization scrambling and FEC," *Proc. of ECOC'04*, paper WE2 (2004).
[5] R. A. Griffin, N. Swenson, D. Crivelli et al., "Combination of InP MZM transmitter and monolithic CMOS 8-state MLSE receiver for dispersion tolerant 10 Gb/s Transmission," *Proc. of OFC'08*, paper OThO2 (2008).
[6] H. Sun, K.-T. Wu, and K. Roberts, "Real-time measurements of a 40 Gb/s coherent system," *Opt. Express*, 16 (2), 873-879 (2008).
[7] H. Sunnerud, C. Xie, M. Karlsson, R. Samuelsson and P. A. Andrekson, "A comparison between different PMD compensation techniques," *J. Lightwave Technol.*, 20(3), 368-378 (2002).
[8] B. Heffner, T. Schmidt, R. Saunders, R. Hui, D. Richards and G. Nicholl, "43Gb/s adaptive polarization mode dispersion compensator field trial," *Proc. of OFC'07*, paper NTuA1 (2007).
[9] L.-S. Yan, X.. S. Yao, M. C. Hauer, and A. E. Willner, "Practical solutions to polarization-mode-dispersion emulation and compensation," *J. Lightwave Technol.*, 24 (11), 3992-4005 (2006).
[10] R. Noe, D. Sandel, M. Y.Dierolf et al., "Polarization mode dispersion compensation at 10, 20, and 40 Gb/s with various optical equalizers," *J. Lightwave Technol.*, 17 (9), 1602-1616 (1999).

Polarization Crosstaik in PM Fiber

Classification of polarization crosstalk by cause

Polarization crosstalk in a PM fiber arises from three principal causes. 1) Fiber axis misalignment at fiber connection interfaces, such as connectors or fusion splices, typically causes extremely localized, large-amplitude crosstalk. The amplitude depends on the misalignment angle. Examples are shown on the left side of Fig. 1. Fig. 1a shows crosstalk sources along a fiber, and Fig. 1b shows the resulting crosstalk measurement plot. 2) PM fiber imperfections, such as local birefringence variations, internal shape variations, or internal stress, cause polarization coupling that is generally small in amplitude and occurs gradually over a certain length of the PM fiber (see center section of Fig. 1). 3) External mechanical stresses on sections of the fiber, such as fiber bending, fiber crossing, fiber squeezing, or pressure on the fiber, can cause complicated composite crosstalk effects that can include polarization couplings that occur at sharp points in space, as well as some that occur gradually along a length of fiber, with varied amplitudes that depend on the stress orientations with respect to the slow axis and on the stress intensities, as shown in the right section of Fig. 1.

Classification of polarization crosstalk by measurement results

In general, the PXA-1000 distributed polarization crosstalk analyzer can accurately measure the strength of polarization crosstalk occurring at different locations along a fiber with a spatial resolution of a few centimeters. Although the causes of the crosstalk cannot always be identified from measurement results, educated guesses can be made based on the shape and strength of the measured crosstalk at each location. It is also feasible to classify the crosstalk based on the shapes of the measured curves, as discussed below.

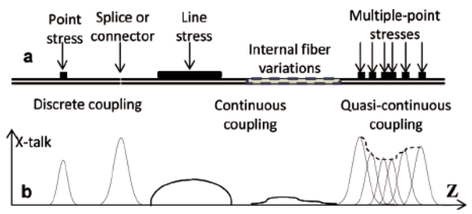

Fig. 1 Illustration of different types of polarization crosstalk. a) Different sources of polarization crosstalk. b) The resulting crosstalk peak profiles. Left: discrete polarization x-talk peaks induced by a point stress or a splice. Each such peak is a Gaussian curve with a shape determined by the coherence function of the light source. The spatial resolution is also determined by the width of the coherence function. Center: continuous polarization x-talk induced by a line stress and by internal fiber imperfections, respectively. Right: quasi-continuous x-talk induced by multiple densely packed stress points spaced on the order of or less than the resolution of the instrument.

1. X-talk caused by discrete polarization coupling points:

This category includes polarization coupling induced by a sharp stress, a splice point or multiple stress/splice points separated by distances much larger than the resolution of the measurement instrument, as shown on the left side of Fig. 1a. These types of discrete coupling result in sharp, distinct peaks in the x-talk measurement trace, with the width of the peak determined by the spatial resolution of the instrument, as shown in Fig. 1b. For this type of coupling, the peak x-talk value for each coupling point conveys useful information. The x-talk values listed in the table at the right of Fig. 2b result from such discrete coupling points.

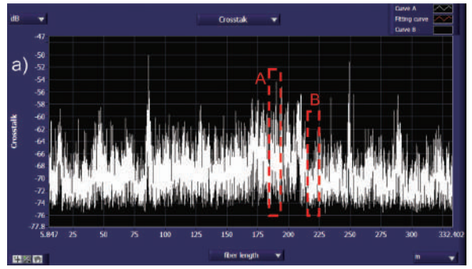

Fig. 2 a) X-talk measurement of a 340 meter long fiber coil. Two significant sections (labeled A and B) are marked. b) Closeup view of section A, showing both discrete and quasi-continuous coupling peaks. The table on the right of the screen lists the magnitudes of discrete x-talk peaks larger than -60 dB. Note that the shape and width of discrete x-talk peaks are determined by the coherence function of the light source.

2. X-talk caused by continuous polarization coupling:

This category includes polarization coupling that accumulates gradually over a section of fiber, induced by a line stress or by fiber internal imperfections, where the length of the affected section of fiber is comparable to or larger than the resolution of the measurement instrument, as shown in the center section of Fig. 1a. The crosstalk measurement result of such continuous coupling is a broad dome with a width and shape determined mainly by the length of the section of fiber under stress, as shown in Fig. 1b. In general, crosstalk caused by a section of imperfect fiber is very small in amplitude - on the order of -60 dB or lower. Because of this curve structure (low amplitude, wide peak), the peak x-talk value for crosstalk resulting from

continuous polarization coupling is not meaningful. However, the cumulative coupling occurring in a section of fiber can be obtained by defining the starting and ending positions of the continuous-coupling section of fiber using the PXA-1000 software's cursors, as shown in Fig. 3. In this example, the cumulative value is -61.32 dB.

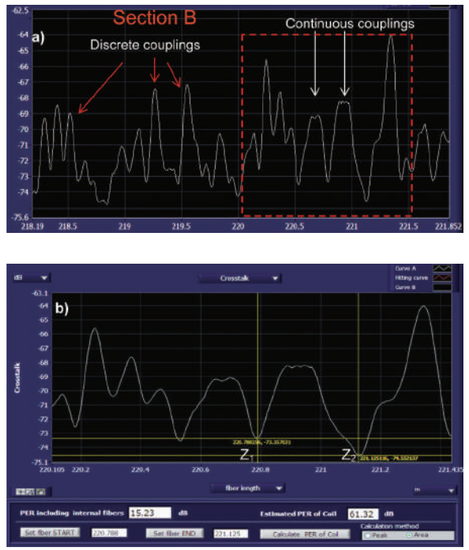

Fig. 3 a) Closeup view of section B of the x-talk measurement plot shown in Fig. 2a, in which two continuous or quasi-continuous x-talk peaks are identified. b) Cumulative x-talk value of a continuous/quasi-continuous coupling is obtained by setting the locations of cursors Z1 and Z2 and calculating the integrated PER of the corresponding fiber section. The resulting value, -61.32 dB, is shown at the bottom right of the screen.

3. X-talk caused by quasi-continuous coupling:

This category includes polarization coupling induced by multiple stress points spaced on the order of or less than the resolution of the measurement instrument, as shown in Fig. 1a. This type of polarization coupling appears in polarization crosstalk measurements as a broad composite peak with height variations, with a width and shape determined by the number of stress points, their relative positions, and their relative strengths, as shown in Fig. 1b. Quasi-continuous coupling cannot reliably be distinguished from continuous coupling. As in the case of continuous coupling, it is not meaningful to give a peak x-talk value for quasi-continuous coupling. However, the cumulative coupling occurring in a section of fiber can be obtained by defining the starting and ending positions of the continuous-coupling section of fiber using the PXA-1000 software's cursors, as shown in Fig. 4b.

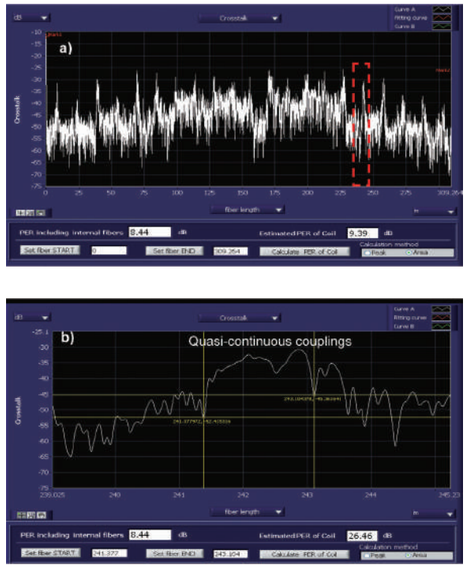

Fig. 4 a) X-talk measurement of a low quality PM fiber coil of length 309 meters. b) Closeup view of the boxed section in a), showing more detailed structure of quasi-continuous couplings. The cumulative x-talk of the region between the two cursors is -26.46 dB.

Capabilities and limitations of the PXA-1000

The PXA-1000 can take crosstalk measurements at spatial intervals of about 4-6 mm, much finer than the specified x-talk resolution of the instrument (on the order of 5 cm). The exact spacing between two adjacent data points is dependent on the birefringence of the fiber; it is defined as the ratio of the delay resolution of the variable delay line used in the PXA-1000 to the fiber birefringence. However, depending on the type of the polarization coupling, a given x-talk reading may not represent the true x-talk value at that point in space, as will be discussed below.

For X-talk induced by discrete polarization coupling points, the PXA-1000 is able to display the corresponding discrete x-talk peaks, to provide an accurate x-talk value for each x-talk peak, and to list in a table all peak values above a defined threshold, as shown in Fig. 2b. Note that each peak has a Gaussian shape corresponding to the coherence function of the light source used; however, only the peak value is meaningful and represents the x-talk value at the point in space at which the x-talk occurs. The other points on the Gaussian curve are due to the light source's coherence function and do not represent meaningful x-talk values for the corresponding points, as shown in Fig. 5. Note that the instrument's x-talk accuracy specification is based on measurement of the peak values of such discrete x-talk points.

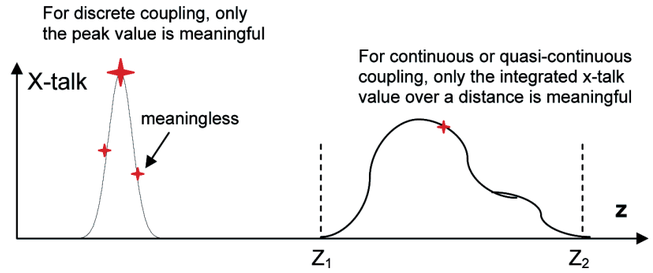

Fig. 5 Left: Illustration of a crosstalk peak caused by discrete coupling, with peak and off-peak values marked. The off-peak values are artifacts caused by the coherence function of the light source; they have no relation to real x-talk points on the fiber. Right: Illustration of a composite x-talk peak induced by continuous or quasi-continuous polarization coupling. A point on this curve does not correspond to a x-talk point on the fiber. In this case, only the integrated cross coupling between the points Z1 and Z2 is meaningful. Points Z1 and Z2 can be defined in the software interface.

For X-talk induced by the continuous or quasi-continuous coupling shown in Fig. 1, the x-talk value of any single point on the broad x-talk composite peak is not meaningful. The PXA-1000 is unable to give an accurate x-talk value for such a point, although the x-talk data file includes data points every 4-6 mm. For a x-talk composite peak caused by continuous or closely packed quasi-continuous coupling points, only the cumulative cross-talk value is meaningful, as shown in Fig. 3b and Fig. 4b. The PXA-1000's data display and analysis software, PolaXView, has a function that calculates the cumulative x-talk from point Z1 to point Z2, where Z1 and Z2 are defined by the locations of the cursors, as shown in Figs. 3b and 4b. In general, the distance between Z1 and Z2 should be much larger than the spatial resolution of the instrument in order to obtain an accurate result. In addition, the two points should also be chosen at valleys on the x-talk curve and the "Area" calculation method should be selected, as shown at the bottom right of Figs. 3b and 4b.

Note that the primary purpose of the PXA-1000 is to obtain accurate x-talk measurements of discrete x-talk peaks; the accuracy of a cumulative x-talk calculation is not guaranteed. However, the instrument records measurement data every 4-6 mm, and this data is available to users to optimize the calculation for specific cases where higher accuracy is required. Data is available to the user in two forms: the raw interferometer signal data as a function of the relative delay between the two arms of the interferometer ("Interferometer Only" data) and the x-talk data as displayed on the screen. The x-talk data is the raw interferometer data with the horizontal and vertical axes shifted according to internal position and x-talk references.

Distributed Polarization X-talk Measurement for the Production of Polarization-Maintaining Fiber Coils

Abstract: This note introduces the use of distributed polarization x-talk measurement for raw polarization maintaining fiber (PMF) quality inspection, PMF coil winding process monitoring, PMF coil adhesive curing and stress release monitoring, overall PMF coil quality inspection, and temperature induced stress determination. PMF birefringence temperature variation can also be precisely measured. The use of distributed polarization x-talk measurement at all of these stages of the process can greatly improve the performance of the finished PMF coils.

Keywords: fiber optical gyro; fiber coil winding; distributed polarization x-talk; on-line monitoring; polarization maintaining fiber (PMF); fiber winding defects, birefringence variation with temperature

1. Introduction

Fiber optic gyroscopes (FOGs) have many important applications in navigation systems and angular velocity sensors. The main component in an FOG is a fiber coil. The quality of the fiber and the coil winding directly affect the performance of the FOG.

Until recently, the evaluation of PM fiber for fiber coils consisted solely of measurements of insertion loss, extinction ratio, and other macroscopic performance characteristics. Distributed evaluation of the fiber was not possible. The use of multi-pole symmetric winding methods can improve transient characteristics of fiber coils [1]; however, such winding methods are difficult to implement because they require the correction of winding errors which can degrade the performance of the fiber coils. On-line winding monitoring methods include video monitoring [2], winding tension monitoring [3], and so on. Such methods are, at best, indirect indicators of the performance of the finished fiber coils; as they do not directly monitor performance during the winding process, they cannot always pinpoint the location of poorly wound sections. Traditional distributed analysis methods include the use of Brillouin Optical Time-Domain Reflectometry (B-OTDR) [4] to detect stress in the fiber coils [5, 6]. However, the spatial resolution and sensitivity of B-OTDR are low, as shown in Table 1, making it difficult to precisely pinpoint the location of stress points. In addition, thermal stress on fiber coils is difficult to test by traditional methods.

Distributed polarization crosstalk (x-talk) measurement has been found to be a powerful tool for evaluation and in-process monitoring of PMF coils for FOGs [7, 8, 9], since x-talk in the coils is a primary determinant of gyroscope performance [10]. General Photonics' distributed polarization x-talk analyzer (PXA-1000) obtains space-resolved stress information by analyzing stress-induced polarization cross-coupling along a length of polarization maintaining (PM) fiber [11]. It is based on a white light interferometer design, but eliminates many of the limitations of traditional white light interferometers. This technology is capable of high accuracy and spatial resolution [7, 14] and large dynamic range[12,13], and is also insensitive to optical power fluctuations [15]. In addition, it is capable of measuring fiber lengths on a scale needed for FOG coils. The PXA-1000 can therefore be used to implement raw PMF quality inspection, fiber winding process monitoring, monitoring of adhesive curing and stress release in PMF coils, overall PMF coil quality inspection, and temperature induced stress determination. The polarization x-talk in the PMF coils can be detected and controlled by such process monitoring.

Table 1 Performance of BOTDR vs. PXA-1000

	BOTDR	PXA-1000
Crosstalk sensitivity (dB)	-60	-95
Dynamic range (dB)	Max. 15	75
Spatial resolution (m)	1 - 22	0.05
Fiber measurement range (km)	1 - 80	0 - 2.6

2. Principles of polarization x-talk measurement

2.1 Polarization x-talk

Modal birefringence greater than 10^{-4} has been realized in PMF [16]. In undisturbed PMF, there is minimal x-talk between the orthogonal polarization modes, and the magnitude of the polarization x-talk remains below –80dB everywhere along the fiber [17]. However, in the presence of an external stress which induces x-talk, the fiber in the vicinity of the stress point can be modeled as a concatenation of three PMF sections [18, 19, 20]. As shown in Figure 1, the undisturbed PMF sections have the same beat length L_{bo}, and their birefringence axes are aligned. The stress on the middle section causes a rotation of angle θ of its birefringence axes relative to those of the other two PMF sections, and its beat length is also changed to a new value L_b. A fraction of the propagating optical power will therefore be transferred from one polarization mode to the other mode during the light's traversal of this section of fiber. This transfer is defined as polarization x-talk.

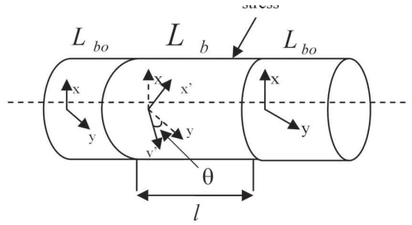

Figure 1 Model of the mechanism of polarization x-talk in PM fiber. The stress on the center section causes a relative rotation of the birefringence axes and hence the polarization x-talk.

Jones vector calculations can be used to determine the magnitude of x mode to y mode and y mode to x mode crosstalk [21].

$$h = h_{x\to y} = h_{y\to x} = \left|\sin\theta\cos\theta(1-\exp(-i2\pi l/L_b))\right|^2 = \sin^2(2\theta)\sin^2(\pi l/L_b) \qquad (1)$$

As shown in Eq. 1, x-talk magnitude is related to the length l, effective beat length L_b, and axis misalignment (relative to the unperturbed sections) θ of the perturbed section. During coil winding, factors such as excessive winding tension, adhesive-induced stress, or other winding defects can all result in crosstalk.

2.2 The PXA-1000

General Photonics' distributed polarization x-talk analyzer (PXA-1000) can pinpoint the locations of imperfections or areas of local stress on the fiber coil induced during the fiber winding process. Its 5 cm spatial resolution, -95 dB polarization x-talk sensitivity, and 2.6 km fiber measurement range make it uniquely suited to quality inspection and screening of PM fiber coils.

As shown in Figure 2, this distributed polarization x-talk analyzer is based on the structure of a "white light" interferometer. A broadband source (superluminescent diode, or SLD) couples a short-pulse wavetrain into one principal axis of a high birefringence PMF via a polarizer (point A in Figure 2a). At a polarization x-talk point caused by external stress, some light is coupled into a secondary low-power wavetrain in the orthogonal polarization (point B in Figure 2a). Because of the fiber birefringence, the wavetrains travel at different velocities. At the output of the fiber, their path difference is ΔnZ, where Δn is the birefringence index and Z is the fiber length between the x-talk point and the fiber end (point C in Figure 2a). A polarizer oriented at 45˚ to the principal axes, placed at the output of the fiber, projects both wavetrains onto the same state of polarization. The two wavetrains do not interfere if their path difference ΔZ is greater than the SLD's coherence length L_c, which is typically very short (about 10 µm). If the two wavetrains are sent into a scanned Michelson interferometer which can adjust the length of one optical path with a variable delay line (VDL), an interference signal occurs when the interferometer is balanced, but disappears when the path length imbalance is larger than the coherence length L_c. It reappears when the path length imbalance compensates for the path difference ΔZ between the two input wavetrains. Because, at this condition, interference occurs between the high-power primary wavetrain and the low-power secondary wavetrain, the interference signal intensity is equal to the power ratio between the two wavetrains. The x-talk point position can be calculated from $Z = \Delta Z / \Delta n$, and the x-talk intensity can be obtained from the interference signal strength [7].

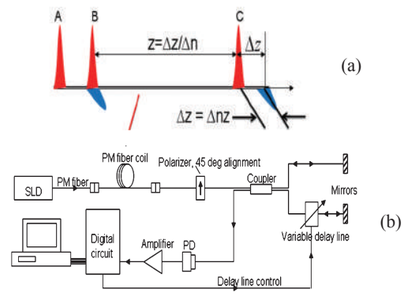

Figure 2 (a) Polarization crosstalk in a PM fiber. A single-polarization pulse is traveling in the fiber at point A. Crosstalk is induced by a stress at point B. The relative delay at output point C between the two pulses is ΔZ. The location Z of x-talk point B can be obtained from a measurement of relative delay ΔZ. (b) Structure of distributed polarization x-talk analyzer. A white light Michelson interferometer with a variable delay line is used to obtain the relative delay.

3 PMF coil evaluation via polarization x-talk testing

3.1 Polarization x-talk in a PM fiber coil

Stress on the PM fiber in a coil due to warping, pressure, tension, incorrect fiber position or other winding errors can cause high x-talk [16, 22, 23] at the stress location, which degrades the performance of the PMF [17, 24]. The magnitude and location of the x-talk caused by these winding errors can be measured with the system described above.

PMF coil polarization x-talk testing can be divided into several stages:

i. PM fiber QC: identify and eliminate intrinsic defects in the fiber used for fiber coils.
ii. On-line PMF winding monitoring: real-time detection of winding defects enables the winder to make corrections, control the winding tension, mark important winding positions, improve winding symmetry, reduce the coil defect rate, and generally improve coil quality.
iii. Adhesive curing and stress release monitoring.
iv. Overall PMF coil inspection.
v. Temperature induced stress measurement of the PMF coils provides understanding of the influence of the coil frame and adhesive on the performance of the coil.
vi. Measurement of the temperature variation of PMF birefringence by measuring polarization x-talk at different temperatures.

3.2 PM fiber QC

Figure 3 shows polarization x-talk measurement results for 1000 m of raw fiber. A high x-talk of -47 dB is observed at a location 381 m from the reference point. Detecting the position of defects in the fiber before winding allows the option of removing those sections of fiber.

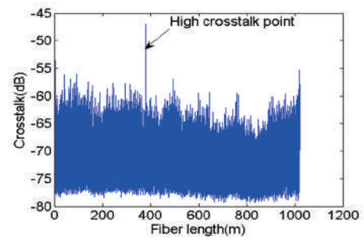

Figure 3 Polarization x-talk measurement of 1000 m of raw fiber. High x-talk (-47 dB) is observed at 381 m.

3.3 On-line PMF coil winding monitoring:

3.3.1 Real-time location of winding defects

Recently, fiber coils with the quadrupole symmetry winding method have come into common use for fiber gyro applications. In the quadrupole winding technique, the center of the fiber length to be wound is located, and the two halves of the fiber are wound onto holding spools (A and B). The coil winding begins at the midpoint of the fiber length, which is positioned at one side of the coil frame (side 1, in the picture below).

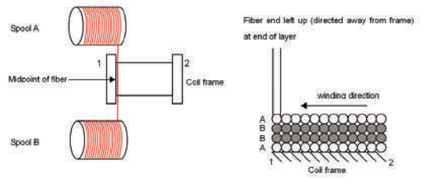

(a) (b)

Figure 4 Quadrupole coil winding method. a) Coil winding begins from the midpoint of the fiber, and one layer of fiber is wound onto the coil from side 1 to side 2 of the coil frame, using the fiber from spool A. b) Cross section of one quadrupole, which consists of 4 layers of fiber in an ABBA structure.

One quadrupole is composed of 4 layers of fiber. The first layer is formed by winding fiber from spool A onto the frame from side 1 to side 2, leaving the fiber at the end of the layer up so that it doesn't become buried by subsequent layers. The next two layers are formed by winding fiber from spool B onto the frame from side 1 to side 2, then back from side 2 to side 1, leaving the end up so that it remains accessible. Finally, fiber from spool A is wound from side 2 to side 1, completing the 4th layer in the sequence. This 4-layer sequence is repeated as many times as necessary until the full length of fiber is wound onto the coil frame. The lengths of fiber in each quadrupole from spool A and spool B must be matched.

During winding, any defect in the coil structure, such as fiber crossovers that can cause layers not to lie flat, can cause crosstalk. One common source of crosstalk is the handling of the fiber ends that are left up when the fiber source is changed from spool A to spool B or vice versa, for example, the segment of fiber from spool A between the end of layer 1 and the beginning of layer 4, or the segment of fiber from spool B between the end of layer 3 and the beginning of layer 6. On-line monitoring of the PMF winding process allows the immediate identification and location of winding defects.

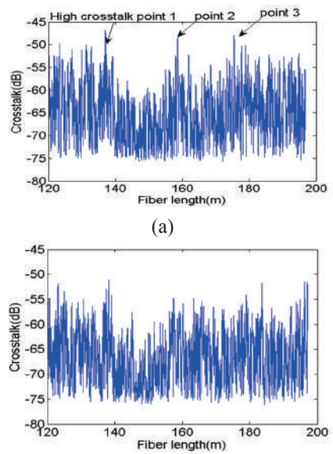

Figure 5 Polarization x-talk measurement results for layers 1-4 of a coil after initial winding (a) and after rewinding (b). Note that the high x-talk points observed during the initial winding are corrected by a more careful rewinding of the fiber.

Figure 5 shows the crosstalk measurements of layers 1-4 of a PM fiber coil after an initial winding attempt and then after a more careful rewinding. The measurement after the initial winding (Figure 5a) shows three high x-talk points at 136, 158 and 175m, with magnitudes -46, -47, and -48 dB, respectively, much higher than the average x-talk intensity in layers 1-4. When the four layers are rewound, the causes of the high crosstalk can be identified. In this case, the first high x-talk point occurs in the spool A fiber segment between layer 1 and layer 4, the second high x-talk point is due to a winding defect in the first layer, and the third high x-talk point occurs in the fiber segment between layer 3 and the next spool B layer. The on-line polarization x-talk testing identifies the errors in time for them to be remedied. When layers are rewound with better winding control, the most serious x-talk points can be eliminated. As shown in Figure 5(b), Table 2, and Table 3, polarization x-talk measurement results of layers 1-4 of the rewound coil show that the maximum x-talk is now -53 dB, the three previously observed high x-talk points have been eliminated, and the average x-talk of layers 1-4 is -66 dB, 2 dB lower than that of the coil after the initial winding.

Table 2 High x-talk points in layers 1-4 of the coil after initial winding.

	High x-talk point 1	High x-talk point 2	High x-talk point 3
position (m)	136.948	158.508	175.412
x-talk (dB)	-46.8799	-47.8237	-48.2796

Table 3 X-talk comparison of layers 1-4 after initial winding and after rewinding

	Initial winding	Rewinding
Average x-talk (dB)	-64.5541	-66.2945
Maximum x-talk (dB)	-46.8799	-53.3771
Position of maximum x-talk (m)	136.948	138.233

3.3.2 On-line control of winding tension

The distributed polarization x-talk analyzer can also be used to control the winding tension of a coil in real time by monitoring the magnitude of polarization x-talk in the fiber coil during winding. If the winding tension is very high, the polarization x-talk in the coil is correspondingly high. Comparing the x-talk intensity of the raw fiber and the fiber coils after winding indicates the amount of performance deterioration in the PMF due to winding, which can be used to determine the optimal range of winding tension.

As shown in Figure 6 and Table 4, the average x-talk intensity of fiber wound into two layers of a coil under high tension is -56 dB, 14 dB higher than that of the raw fiber, indicating significant deterioration of the fiber's polarization maintaining capability. The average x-talk intensity of the same fiber wound into two layers under a tension 4 times lower than that of the initial winding is -65 dB, 9 dB lower than the coil wound under high tension.

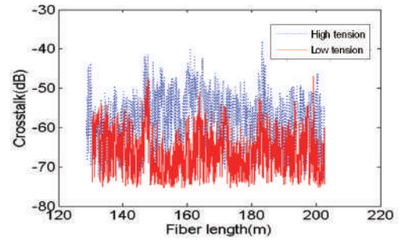

Figure 6 Polarization x-talk of layers 1-2 of a fiber coil wound at different tension levels. Solid line: low tension. Broken line: high tension

The coil winding tension must be maintained at a level high enough to maintain coil integrity, but low enough not to compromise the performance of the PMF.

Table 4 Polarization x-talk of fiber wound at different tension levels

	Average x-talk (dB)
High tension	-56.7677
Low tension	-65.6627
Raw fiber	-70.841

3.3.3 On-line testing for winding symmetry

The necessary winding symmetry can be achieved by using the counter on the winding machine or via polarization x-talk testing. As shown in Figure 7, the symmetry of the coiled fiber can be evaluated by marking the locations of selected points on the fiber by inducing temporary stress on the fiber at these points. When the first layer is finished, the position of the first layer end point (119.388m, in this example) can be obtained by polarization x-talk testing by temporarily stressing the fiber at that point. The fiber midpoint location in this case is 158.3m; therefore, the length of the fiber wound onto the frame from the A spool for the first quadrupole is 38.912m. Similarly, the length of the fiber wound onto the frame from the B spool for the first quadrupole is found to be 38.914m. The length difference is only 0.002m, indicating that the first quadrupole's symmetry is good. The PMF coils' symmetry can thus be assured by monitoring the position and length of every layer or quadrupole as it is formed using on-line testing of the polarization x-talk. Table 5 lists the positions and lengths of all quadrupoles in a 311 m fiber coil.

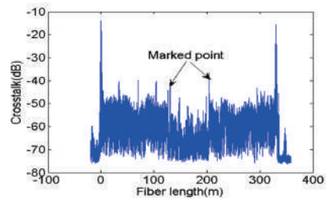

Figure 7 Identification of the locations of selected points on the fiber by inducing temporary stress on the fiber at these points.

Table 5 Positions and fiber lengths of quadrupoles in a 311 m fiber coil

	spool	Position (m)	length (m)
1st quadrupole	A	119.388	38.912
	B	197.214	38.914
2nd quadrupole	A	80.894	38.494
	B	235.572	38.358
3rd quadrupole	A	42.69	38.204
	B	273.688	38.106
4th quadrupole	A	3.1	39.59
	B	313.2	39.512
		A total length	155.2
		B total length	154.89

3.4 Monitoring PMF coil adhesive curing and stress release.

FOG performance, in terms of vibration-induced bias, is significantly influenced by the adhesive used. Both adhesive application and curing techniques can influence the polarization x-talk in the PMF coils. Polarization x-talk testing can therefore be used to analyze physical characteristics of different adhesives as well as techniques for adhesive curing and stress release, in order to optimize the adhesive process.

As shown in Figure 8 and Table 6, after adhesive curing and stress release, a coil's average polarization x-talk decreases relative to its level immediately after adhesive application (by about 6dB in this example). It is therefore important to monitor the process of adhesive curing and stress release. If adhesive curing and stress release of the PMF coils are poorly done, the PMF coils' polarization-maintaining performance can be seriously degraded.

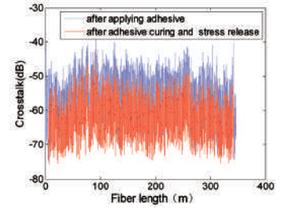

Figure 8 Polarization x-talk measurements of a PM coil after adhesive application and after adhesive curing and stress release. After adhesive curing and stress release (solid red line), the coil's average polarization x-talk decreases by 6dB relative to its level immediately after adhesive application (dashed blue line).

Table 6 Polarization x-talk of PMF coil after adhesive application and after adhesive curing and stress release

	After adhesive application	After adhesive curing and stress release
Average x-talk (dB)	-55.7442	-61.5071
Maximum x-talk (dB)	-37.6478	-43.0919
Position of maximum x-talk (m)	91.4709	91.8827

3.5 Overall PMF coil inspection

The overall polarization x-talk profile of a 311m PMF coil is shown in Figure 9 and Table 7. The average x-talk in this coil, which was optimized by on-line coil monitoring, raw PMF testing and other previously described techniques, is -68 dB, 2 dB higher than that of raw PMF (-70 dB); therefore, this coil's winding quality can be taken to be relatively good. However, high x-talk (-46dB) is still observed at 57m at a layer transition where the source spool is changed. In many cases, high x-talk points can be reduced or eliminated by improving the winding technique.

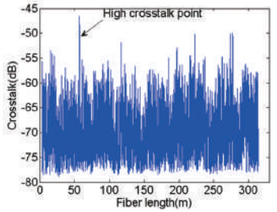

Figure 9 Polarization x-talk profile of a 311 m PMF coil. The overall polarization x-talk is relatively low for this coil; however, some high x-talk points can still be observed.

Table 7 Polarization x-talk in a 311 m coil

Average x-talk (dB)	-68.7424
Maximum x-talk (dB)	-46.6234
Position of maximum x-talk (m)	56.98

3.6 Measurement of temperature induced stress in PMF coils

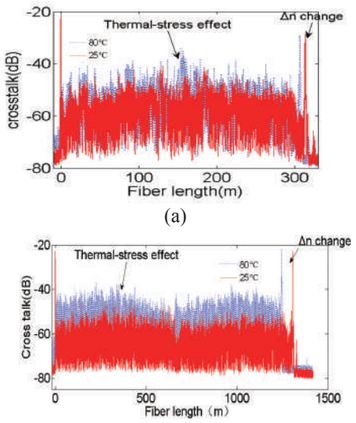

Figure 10 Changes in polarization x-talk of 315 m and 1300 m PMF coils due to thermal-stress effects. (a) 315 m coil (b) 1300 m coil.

Solid red lines: measured at 25°C; Dashed blue lines: measured at 80°C. Temperature induced birefringence changes can also be obtained from the location difference of the high x-talk points from the fiber connection points at the far right.

The polarization-maintaining performance of a PM fiber coil deteriorates after heating, because the PMF, frame, and adhesive have different physical characteristics. A 315m PMF coil with a frame but no adhesive and a 1300m PMF coil with adhesive but no frame were heated from room temperature (25 °C) to 80 °C to observe changes in polarization x-talk caused by thermal-stress.

As shown in Figure 10 and Table 8, the average x-talk rises by 4 dB in the 315m coil and by 9 dB in the 1300m coil after heating. The average x-talk intensity of the 1300m coil increases by a greater amount because of the stress on the fiber caused by the temperature expansion coefficient of the adhesive. As shown in Figure 10 (a), the x-talk intensity of the 315m coil increases sharply at the midpoint of the fiber due to stress from the frame. The midpoint of the 1300m coil shows much lower thermal stress than that of the 315m coil because the 1300m coil has no frame. Evaluating changes in polarization x-talk of PMF coils caused by thermal stress effects at different temperatures can aid in the selection of adhesive and frame material for optimum performance of the completed FOG.

Table 8 Polarization x-talk of 315 m and 1300 m fiber coils at different temperatures

	315m 25°C	1300m 25°C	315m 80°C	1300m 80°C
Average x-talk (dB)	-57.258	-62.840	-53.898	-53.889
Maximum x-talk (dB)	-40.626	-45.843	-34.215	-36.925
Position of maximum x-talk (m)	130.620	142	153.880	224.165

3.7 Measurement of temperature variation of PM fiber birefringence

As shown in Figure 10, the temperature induced birefringence change can also be obtained from the change in location Z of the high x-talk points corresponding to the fiber connection points at the far right of the measurement plot. Δn for the PM fiber can be calculated at different temperatures using the simple formula

$$\Delta n_1 Z_1 = \Delta n_2 Z_2 \qquad (2)$$

Table 9 lists a 330m PMF coil's birefringence Δn at different temperatures.

The birefringence temperature variation coefficient 5.3E-7 can be obtained from the slope of the fitted line of the Δn vs. temperature plot, as shown in Figure 11. Test results for PMF coils produced by different manufacturers are listed in Table 10. The average birefringence temperature variation coefficient is 5.6E-7 (°C^{-1}).

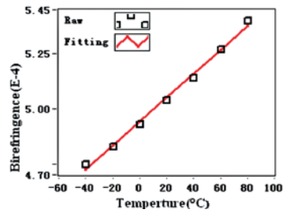

Figure 11 Linear fit to a plot of Δn vs. temperature for a PM fiber coil. The birefringence temperature variation coefficient 5.3E-7 can be obtained from the slope of the fitted line.

Table 9 Δn of a 330m PMF coil at different temperatures

Temperature (°C)	-40	-20	0	20	40	60	80
Δn(E-4)	4.75	4.83	4.93	5.04	5.14	5.27	5.40

Table 10 Birefringence temperature variation of PMF coils from different manufacturers

	Coil 1	Coil 2	Coil 3	Coil 4	*Coil 5	*Coil 6	Average
birefringence variation with temperature (°C^{-1})	5.5e-7	5.6e-7	6.0e-7	5.8e-7	5.3e-7	5.4e-7	5.6e-7

* Denotes a different manufacturer

Summary

Distributed polarization x-talk measurement has been demonstrated to be an effective method for improving the quality of PMF coils at various stages in the coil production process, including raw PMF quality inspection, in-process coil winding monitoring, overall PMF coil inspection, and temperature induced stress testing. Test results can be used to identify coil imperfections as they occur, reduce the defect rate, monitor adhesive curing and stress release, and improve general coil quality. Distributed polarization x-talk measurement also enables precise measurement of PM fiber birefringence variation with temperature.

References

[1] Frigo N J. Compensation of Linear Source of Non-reciprocity in Sagnac Interferometers[J]. SPIE, 1983,412: 268–270.

[2] Andre Sharon, Stephen Lin. Development of an automated fiber optic winding machine for gyroscope production[J]. Robotics and Computer Integrated Manufacturing, 2001,17: 223–231.

[3] Meng Zhao Kui, Zhang Chun Xi, Yang Yuan Hong. Analysis of stress in winding fiber—optic ring[J]. Journal of Beijing University of Aeronautics and Astronautic, 2005,31(3):307–310.

[4] ANDO Electric CO LTD. AQ 8603 optical fiber strain analyzer instruction manual[M]. Japan: Ando Electric Co. Ltd, 2002.

[5] ZHU Hui,CEN Song-yuan, WANG Dong-yun ,et al. Measurement and analysis about the strain of fiber optical loop[J]. OPTICALIN STRUMENTS,2004,26 (4):3–6.

[6] YANG Yuan-hong, YI Xiao-su, MENG Zhao-kui. Experimental Study on Strain Distribution in Fiber Coil Used in Fiber Optics Gyroscope[J].PIEZOELECTRICS &ACOUSTOOPICS,2005,27(2):98–101.

[7] P.Martin, G.Le Boudec, H.C Lefèvre. Test apparatuses of distributed polarization coup1ing in fiber gyro coils using white light interfereometry Fiber Optic Gyros[J].15th Anniversary Conference SPIE, 19911585:173–179.

[8] H.C. Lefèvre, Comments about fiber-optic gyroscopes, SPIE Proceedings, Vol. 838, 86–97,

[9] DING ZhenYang, Steve YAO, LIU TieGen, et al. Improving the Quality of Polarization-Maintaining Fiber Coils Using Distributed Polarization Crosstalk Testing[J]. Journal of Optoelectrnics Laser, 2010,21(3):430–434.

[10] H.C. Lefèvre, J.P. Bettini, S. Vatoux and M. Papuchon, Progress in optical fiber gyroscopes using integrated optics, proceedings of AGARD/NATO, CPP-383, pages 9N1–13, (1985)

[11] H. Takada, J. Noda, K. Okamoto, "Measurement of spatial distribution of mode coupling in birefringent polarization-maintaining fiber with new detection scheme", Optics Letters, 11, 680–682, (1986)

[12] TSUBOKAWA M., HIGASHI T., SASAKI Y., Measurement of mode couplings and extinction ratios in polarization-maintaining fibers, Journal of Lightwave Technology 7(1), 1989, pp. 45–50.

[13] RAO Y.-J., JACKSON D.A., Recent progress in fiber optic low-coherence interferometry, Measurement Science and Technology 7(7), 1996, pp. 981–999.

[14] TAKADA K., NODA J., OKAMOTO K., Measurement of spatial distribution of mode coupling in birefringent polarization-maintaining fiber with new detection scheme, Optics Letters 11(10), 1986, pp. 680–682.

[15] KEMMLER M.W., BUESCHELBERGER H.J., White light interferometry for testing FOG components, Proceedings of SPIE 1585, 1992, pp. 357–364.

[16] OKAMOTO K., SASAKI Y., SHIBATA N., Mode coupling effects in stress-applied single polarization fibers, IEEE Journal of Quantum Electronics 18(11), 1982, pp. 1890–1898.
Fig. 9. Enhancement of contrast ratio with rotation of analyzer at two different points. 90 T. XU et al.

[17] NODA J., OKAMOTO K., SASAKI Y., Polarization-maintaining fibers and their applications, Journal of Lightwave Technology 4(8), 1986, pp. 1071–1089; TSUBOKAWA M., HIGASHI T., NEGISHI Y., Mode coupling due to external forces distributed along a polarization-maintaining fiber: an evaluation, Applied Optics 27(1), 1988, pp. 166–173.

[18] Makoto Tsubokaw, Tsunehito Higashi, Ybkiyasu Negish. Mode coupling due to external forces distributed along a Polarization-maintaining fiber: an evaluation [J].Applied Optics, 1988, 27(1):166–173.

[19] Jian Zhang,Handerek,V.A.,Cokgor I.,et al. Distributed sensing of Polarization mode coupling in high birefringence optical fibers using intense arbitrarily polarized coherent light[J]. Journal of Lightwave Techoology,1997,15(5) :794– 802.

[20] T.H.Chua, Chin-Lin Chen. Fiber polarimetric stress sensors-Applied Optics-1989,28 (15):3158–3165.

[21] Tianhua Xu, Feng Tang, Wencai Jing, et al. Distributed measurement of mode coupling in birefringent fibers with random polarization modes[J]. Optica Applicata 2009,39,(1):77–90

[22] SEARS F.M., Polarization-maintenance limits in polarization-maintaining fibers and measurements, Journal of Lightwave Technology 8(5), 1990, pp. 684–690.

[23] SAKAI J., KIMURA T., Birefringence and polarization characteristics of single-mode optical fibers under elastic deformations, IEEE Journal of Quantum Electronics 17(6), 1981, pp. 1041–1051.

[24] RONGFENG GUAN, FULONG ZHU, ZHIYIN GAN, DEXIU HUANG, SHENG LIU, Stress birefringence analysis of polarization maintaining optical fibers, Optical Fiber Technology 11(3), 2005, pp. 240–254.

Complete characterization of polarization-maintaining fibers using distributed polarization analysis

Zhihong Li[1,2], X. Steve Yao[1,3], Xiaojun Chen[3], Hongxin Chen[3] and Zhuo Meng[1,2]

[1] Polarization Research Center, College of Precision Instrument & Opto-electronics Engineering and Key Laboratory of Opto-electronics Information and Technical Science, Ministry of Education, Tianjin University, Tianjin 300072, China
[2] Suzhou Opto-ring Co. Ltd, Suzhou 215123, China
[3] General Photonics Corporation, 5228 Edison Ave, Chino, CA 91710, USA

Abstract

We present methods and processes of using a ghost-peak-free distributed polarization crosstalk analyzer (DPXA) to accurately obtain all polarization related parameters of polarization-maintaining (PM) fibers. We show that by first inducing a series of equidistant periodic polarization crosstalk peaks along a PM fiber and then measuring the positions and the widths of these peaks using the analyzer, all birefringence-related parameters of the PM fiber, including group birefringence, group birefringence variation along the fiber, group birefringence dispersion, and group birefringence temperature coefficient, can be accurately obtained. We further show that the DPXA has the ability to identify and eliminate polarization crosstalk contributions of connectors or splices in the measurement system and therefore can be used to obtain high accuracy measurement of the polarization extinction ratio (PER) of PM fibers. Finally, we propose a set of parameters based on the distributed polarization analysis to quantitatively evaluate the quality of PM fibers. We believe that the methods and processes described in this paper can be widely applied in the industry for the complete characterization of PM optical fibers.

Index Terms—Polarization-maintaining fiber, ghost-peak-free, equidistant periodic polarization crosstalk, group birefringence, group birefringence dispersion.

I. Introduction

POLARIZATION-MAINTAINING optical fibers, which use a high internal birefringence that greatly exceeds perturbing birefringence effects to maintain a linear polarization along the fiber, are important to fiber optic communications and fiber optic sensors, particularly fiber optic gyroscopes. The polarization maintaining ability of a PM fiber is generally characterized by its polarization extinction ratio (PER) or h-parameter (PER per unit length), while the fundamental parameter governing the performance of a PM fiber is actually its group birefringence. Therefore, it is important for manufacturers and users of PM fibers to know not only the PER of a fiber, but also its group birefringence and all other group birefringence related parameters, including the variation in group birefringence with wavelength (group birefringence dispersion [1,2]), with temperature (group birefringence thermal coefficient [3,4]), and along the fiber (group birefringence uniformity [5]).

The PER or h-parameter of a PM fiber can be measured with a polarization cross talk method specified in standards TIA-544-193 and TIA-544-192 [6,7], where the 3-dB spectral width of the light source is required to be greater than 10 nm (or the corresponding coherence length should be much less than the differential group delay of the PM fiber under test), to avoid measurement fluctuations caused by coherent addition of the two orthogonal polarization components inside the fiber. However, such a measurement system is cumbersome to set up, and its measurement accuracy is affected by the birefringence of the lenses and connectors, as well as by misalignment of the polarization of the light input to the PM fiber. Commercially available PER meters can be used to directly measure the PER of a PM fiber; however, their measurement accuracies are still limited by 1) the polarization misalignment of light at the input end of the PM fiber under test (FUT); and 2) the polarization misalignments of the light source and its fiber pigtail; making the measurement of high PER fibers cumbersome and decreasing the repeatability of the measured results.

One or two of the four group birefringence related parameters, as well as PER, can be measured with different implementations of white light interferometry [3,8-11], spectral interferometry [12-14], the wavelength sweeping technique [15], the transient Brillouin grating technique [16,17], Brillouin optical correlation-domain reflectometry [18], and the optical heterodyne detection technique [19]. All of these methods are complicated to set up and require in-depth knowledge and experience to implement. Consequently, their practical use in the industry is limited.

Optical frequency-domain reflectometry (OFDR) to measure the local birefringence and PER of a short PM fiber taper has been reported [20]; however, its ability to characterize a long length of PM fiber with a large number of cross talk points is yet to be proved.

We reported previously the use of a distributed polarization crosstalk analyzer (DPXA) to accurately measure the thermal coefficient [4] and dispersion [21] of PM fibers' birefringence. In this paper, we demonstrate methods and processes to simplify the measurements and improve measurement accuracy, and to expand the measurement capabilities of the DPXA to include all polarization related parameters, including PER (or h-parameter), group birefringence, group birefringence uniformity, group birefringence dispersion, and group birefringence thermal coefficient. In particular, we introduce a simple fixture to induce a series of polarization crosstalk peaks of equal spacing to assist in the measurements. To enable such methods and processes, we devise a mechanism inside the DPXA (General Photonics PXA-1000) to specifically eliminate the ghost interference peaks caused by zero- and 2nd-order interferences of light from polarization crosstalk points [22], and therefore make it possible to obtain the true locations and strengths of a large number of polarization crosstalk points along the PM fiber without ambiguity. As will be shown below, the combination of the fixture and ghost-peak elimination simplifies the measurement process and reduces many potential measurement errors; it therefore assures accurate measurement results even by minimally trained personnel. Furthermore, we show that the DPXA can readily be used to identify polarization crosstalk induced by the connectors and splices in the measurement setup, and therefore eliminate their contributions to the total PER of a PM fiber under test (FUT), resulting in more accurate measurement results without the need for careful polarization alignment of light at the input and output ends of the PM fiber under test (FUT). Finally, we propose a set of measurement parameters obtained by a DPXA to quantify the performance of a PM fiber, with test examples of different PM fibers. We believe that the methods and processes described in this paper can be widely applied in the industry for the complete characterization of PM fibers, especially considering that the ghost-peak-free DPXA is becoming commercially available with the efforts of some of the authors [23].

II. Basic configuration of DPXA

Fig. 1 illustrates a basic configuration for a distributed polarization crosstalk analyzer (DPXA)[4, 21]. A polarized superluminescent diode source (SLED) at 1310 nm with a very short coherence length (~25μm, corresponding to a 3-dB Gaussian linewidth of 30 nm) is coupled into the slow axis of a PM fiber under test (FUT) (point A of inset in Fig.1). Assume at point B, some polarization crosstalk is induced by an external disturbance, causing some light to be coupled into the fast axis of the PM fiber with a coupling coefficient parameter $h = I_1/I_2$, where I_1 and I_2 are the light intensities in the fast and slow axes of the PM fiber, respectively. Because the polarized light aligned to the fast axis travels faster than that aligned to the slow axis, at the output of the fiber, the faster light component will be ahead of the slow component by $\triangle Z = \triangle nZ$, where $\triangle Z$ is an optical path length difference, $\triangle n$ is a group birefringence of the PM fiber and Z is the fiber length between the point where the crosstalk occurs (B) and the output end (point C). A polarizer oriented at 45° to the slow axis of the PM FUT was placed at the end of the fiber. Polarization components from both slow and fast axes were projected onto the same direction - the linear polarizer axis - so as to produce an interference pattern between the two components in a scanning Michelson interferometer. When the relative optical path length is scanned, an interference peak appears when the two polarization components overlap in space but disappears when they are separated by more than the coherence length of the light source (i.e. SLED). The group birefringence $\triangle n$ of the PM FUT between positions B and C can then be calculated as follows:

$$\triangle n = \triangle Z/Z \qquad (1)$$

It is evident from Eq. (1) that the accuracy of $\triangle n$ depends on the measurement accuracies of both $\triangle Z$ and Z.

Note that the illustration in Fig. 1 assumes only one polarization crosstalk point along the fiber. If there are multiple polarization crosstalk points, second order interference peaks will occur. That is, the light in the fast axis resulting from the coupling at a crosstalk point will couple back to the slow axis at subsequent crosstalk points further down the fiber. As shown in Fig. 2a, consider a situation where there are three coupling points X_1, X_2, and X_3 along the PM fiber, and the light input to the PM fiber is polarized along the slow axis of the PM fiber, with no fast axis component. At each coupling point, light is coupled not only from the polarization mode along the slow axis to the polarization mode along the fast axis, but also from the polarization mode along the fast axis to the polarization mode along the slow axis. As a result of this coupling, the resulting wave packet series output by the PM fiber include wave packets caused by multiple couplings. As shown in Fig. 2b, four wave packets, including zero order coupling S_0 (no coupling) and second order couplings S_{12}, S_{23} and S_{13} emerging at the output are aligned to the slow axis of the PM fiber, and three main wave packets f_1, f_2 and f_3 emerging at the output are aligned to the fast axis of the PM fiber, where they are generated by coupling from the slow axis to the fast axis (first order coupling) at points X_1, X_2 and X_3, respectively.

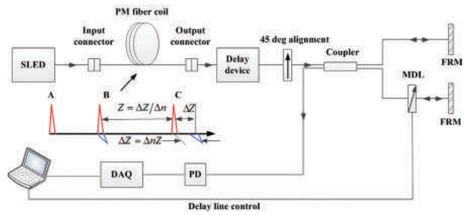

Fig.1. Illustration of a ghost-peak-free distributed polarization crosstalk analyzer using a scanning white light Michelson interferometer. The inset shows the delay relation between the original and crosstalk components. Light with a short coherence length travelling in the fiber is polarized along its slow axis at input point A. Crosstalk is induced by a stress at point B where a small portion of light is coupled into the fiber's fast axis. A relative delay at the output point C between the two polarization components is △Z. The location Z of crosstalk point B can be obtained from a measurement of △Z. FRM, MDL, PD, and DAQ are Faraday rotator mirror, Motorized Delay Line, photodetector, and data acquisition card, respectively.

After passing through the 45 degree oriented polarizer, the wave packets aligned to the slow and fast axes were projected onto the same direction - the linear polarizer axis, as shown in Fig. 2c. When this mixed light is input to the interferometer, a series of interference peaks can be observed as the delay in one arm of the interferometer is changed. In the simple white light interferometers described in [10,11,24], these second order couplings cause ghost crosstalk peaks which result in ambiguity. As shown in Fig. 1, we use a differential group delay (Delay Device) inside a DPXA to remove all the ghost crosstalk peaks resulting from the second order couplings [22], making it possible to accurately identify and measure large numbers of polarization crosstalk points along a PM fiber without ambiguity. In particular, as illustrated in Fig. 2d, the Delay Device adds an additional delay L between polarization components in the slow and fast axes. This delay L in vacuum should be longer than $\triangle Z$, where the additional delay L is added to the light polarized along the slow axis of the PM fiber. Thus, the two wave packet sequences from the fast-axis and slow-axis are separated in time (or space) after the light passes through the analyzer. If we preset the same delay offset between the fixed and moving arms in the interferometer and restrict the range of the variable delay line in the moving arm, the undesired zero order (S_0 with S_0, S_{ij} with S_{ij}, and f_i with f_i) and the second order (S_0 with S_{ij},

and f_i with f_j) interference signals (ghost interference peaks) will not be generated as the delay line scans. Only the desired first order interference signals (S_0 with f_i) and the much weaker third order interference signals (f_i with S_{nm}) will be present. Note that the third order peaks are negligible (less than -75 dB) if the first order coupling f_i is less than -25 dB. More detailed description of such a ghost-peak-free DPXA can be found in [22].

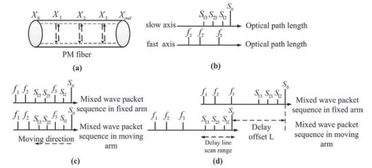

Fig.2. a) Illustration of polarization coupling at locations X_1, X_2, and X_3 along the PM fiber; b) the wave packet sequences polarized along the slow (denoted by S) and fast (denoted by f) axes at the output of the PM fiber; c) Wave pockets in the two interferometer arms after light passing through the 45° oriented analyzer, where the wave packets aligned to the slow and fast axes are mixed together. When this mixed light is input to the interferometer in Fig. 1, a series of interference peaks, including multiple ghost peaks, will be observed as the delay in one arm of the interferometer is changed; d) Wave pockets in the two interferometer arms after the Delay Device in Fig.1 is inserted between the PM fiber's output and the 45 degree polarizer's input. This differential delay adds an additional delay between the slow axis and the fast axis of the PM fiber. Only the first order interference peaks between S_0 and f_i and the third order interference peaks between f_i and S_{ij} can be generated.

III. Measurement fixture, methods and results

A. Measurement Fixture

To facilitate easy and accurate measurements of group birefringence related parameters, we designed a spool-like fixture to induce periodically spaced polarization crosstalk peaks along a PM fiber under test (FUT), as shown in Fig. 3a. In our experiment, we simply use a standard fiber spool from the fiber manufacturer and affix a piece of thin metal rod with a diameter of 2 mm across its width. A single layer of FUT of length 280 m is wound on the spool with a 10-gram winding tension, and each turn of the fiber is placed adjacent to the previous turn, as shown in Fig. 3b. It takes us about four hours to wind such a spool using a simple spool winding machine, and the time can be reduced to less than an hour with more practice and process optimization. Re-spooling fiber is a common practice in the industry for fiber manufacturers and fiber spooling/winding machines are commercially available, for example, from Showmark LLC.

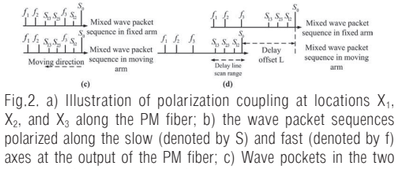

Fig.3 (a) Illustration of a length of PM fiber wound on a fiber spool with a thin metal rod to induce periodic transversal stresses on the PM fiber at the locations where the fiber crosses the rod. (b) Detailed view of the fiber when fiber is transitioning from one turn to the next. (c) Detailed view of the fiber when it crosses the metal rod.

As will be shown next, the accuracy of the length of each fiber turn on the spool is critical to the measurement accuracies of the birefringence parameters of the PM fiber to be measured. As shown in Fig. 3, the length l of each fiber turn is the circumference l_c of the spool plus the additional length δ_{l1} caused by transitioning each turn of fiber to the next (Fig. 3b) and the additional length δ_{l2} caused by the presence of the metal rod (Fig. 3c):

$$\begin{aligned} l &= l_c + \delta_{l1} + \delta_{l2} \\ &= \pi d_c + d_c \cdot \left(\sqrt{d_c \cdot d_1} / (d_c - d_1) - \arccos\left((d_c - d_1)/(d_c + d_1) \right)/2 \right) \\ &+ 2 \cdot d_c \cdot \left(\sqrt{d_c \cdot d_2} / (d_c - d_2) - \arccos\left((d_c - d_2)/(d_c + d_2) \right)/2 \right) \end{aligned} \quad (2)$$

The length l can be precisely determined when the diameters of the spool (d_c), the fiber (d_1), and the metal rod (d_2) are known. In practice, one may use l_c to approximate l. For our experiment with $d_c = 0.17$ m, $d_1 = 1.65 \times 10^{-4}$ m and $d_2 = 2 \times 10^{-3}$ m, the relative length error $(\delta_{l1}+\delta_{l2}) / l_c$ for the approximation is about 0.1%. The relative length error can be reduced to less than 0.015% with a metal rod of diameter $d_2 = 5 \times 10^{-4}$ m. Note that the measurement accuracy of the circumference l_c is about 0.006% when a Vernier caliper is used for measuring the diameter of the spool. In comparison, the fiber length measurement accuracy in [4] is limited by the accuracy of an OTDR (optical time domain reflectometer) or a ruler, to on the order of 1%.

As expected, "point-like" stresses are automatically applied to the fiber at the points where the fiber crosses the metal rod (Fig. 3c) to produce multiple periodic polarization crosstalk points, with a periodicity precisely defined by Eq. (2). These periodic crosstalk peaks act like embedded ruler marks on the fiber, which automatically yields precise length information essential for group birefringence related measurements, as required by Eq. (1). Note that if the ghost peaks caused by second order coupling are not eliminated, there would be many false peaks between the true periodic peaks, making it difficult to identify the positions of the true peaks.

In practice, such a spool-like fixture can be machined with a precise predetermined diameter (or circumference) and with a thin slot or bump across its width to induce periodic polarization crosstalk points, making the embedded ruler more accurate. It is important to point out that the reasons for making such a fixture are 1) to precisely define the lengths between crosstalk peaks, because the accuracy of group birefringence measurement is proportional to the accuracy of such lengths, as shown in Eq. (1), and 2) to create a distribution of crosstalk peaks to reflect the local group birefringences along the fiber. Note that the spatial resolution of the local group birefringence is determined by the circumference of the fixture, on the order of the 0.5 m in our experiment. It can be easily improved by reducing the diameter of the fixture, considering that the spatial resolution of the DPXA is around 6 cm (assuming the group birefringence of the PM fiber is (5×10^{-4}), although the 0.5 m resolution is sufficient for most PM fiber characterization.

B. Group birefringence and group birefringence uniformity measurements

Fig. 4a is the measured polarization crosstalk curve of a PM PANDA fiber with a core diameter of 6 μm, a cladding diameter of 80 μm, and a buffer diameter of 165 μm, as a function of the interferometer delay △Z, showing the polarization crosstalk points

induced by the line-pressure from the metal rod on the fiber. The peaks at the far left and right correspond to polarization crosstalk induced at the output and input connectors, respectively, due to slight misalignment of the light coupling into the fiber axis. Fig. 4b shows the detailed view of the equidistant periodic crosstalk peaks caused by transversal pressure induced whenever the fiber crosses the metal rod. As one can see, these measured crosstalk amplitudes vary from peak to peak because of the angle variation between the direction of transversal pressure and the fiber's principal axes during the winding of the fiber onto the spooling wheel; however, such an amplitude variation does not affect the periodicity measurement, which is important to the group birefringence measurement. One can readily obtain the spacing between any two stress crosstalk points by simply multiplying the circumference of the spool by the number of stress-induced crosstalk peaks between the two points. In addition, one can precisely obtain the relative delay △Z with the encoder of the motorized delay line.

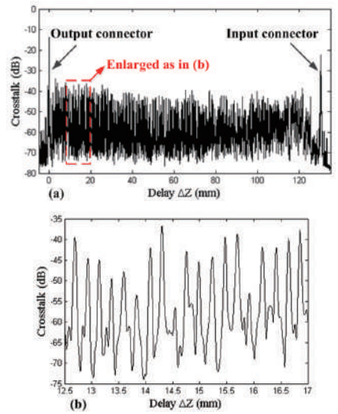

Fig.4 (a) Polarization crosstalk curve of 280 meter PM fiber wound on a spool as a function of the interferometer delay △Z inside the DPXA. The peaks at the far right and left correspond to the crosstalk induced at the input and output connectors, respectively, from slight axis misalignment between the light polarization and the PM fiber axis; (b) the equidistant periodic crosstalk peaks are induced by the pressure of the metal rod on the PM fiber.

When Eq. (1) is used to obtain $\triangle n$, the total relative error $\delta_{\triangle n} / \triangle_n$ can be expressed as [4]:

$$\delta_{\Delta n} / \Delta n = \sqrt{(\delta_{\Delta Z}/\Delta Z)^2 + (\delta_Z / Z)^2} = \sqrt{(\delta_{\Delta Z}/\Delta n)^2 + (\delta_Z)^2} \Big/ Z \quad (3)$$

where $\delta_{\triangle n}$ is the group birefringence inaccuracy, $\delta_{\triangle z}$ is the reading error of the delay △Z of the variable delay line inside the DPXA, and δ_z is the measurement error of length Z. Note that in the previous reports [4, 21], the absolute length of the FUT must be accurately measured in order to obtain an accurate group birefringence $\triangle n$ according to Eq. (3). Any length measurement error will proportionally contribute to the accuracy of $\triangle n$. In contrast, here we can use the relative length defined by the circumference of the fiber spool to eliminate the need for absolute length measurement and its associated error, and Eq. (1) can be rewritten as:

$$\triangle n = (\delta z / N l) \quad (4)$$

where l is the fiber length corresponding to the period of the crosstalk peaks defined in Eq. (2), N is an integer to represent the number of periods we choose in the calculation, and δz is the corresponding delay in the interferometer for the N periods. The error sources for $\triangle n$ are from both the relative location inaccuracy $\delta_{\triangle z}$ between the polarization crosstalk peaks measured with the variable delay line inside the DPXA and the error in the measurement of l. Note that the delay line generally has an error independent of the traveling distance; we therefore choose to use multiple periodicities (N>>1) in the experiment to reduce the effect of delay line error $\delta_{\triangle z}$, similar to the case of measuring the thickness of a stack of paper in order to accurately determine the thickness of a single sheet of paper. We found in our experiment that when N≥5, the measurement uncertainty is sufficiently small. The average $\triangle n$ obtained is $\triangle n = 4.65 \times 10^{-4}$ when N=5.

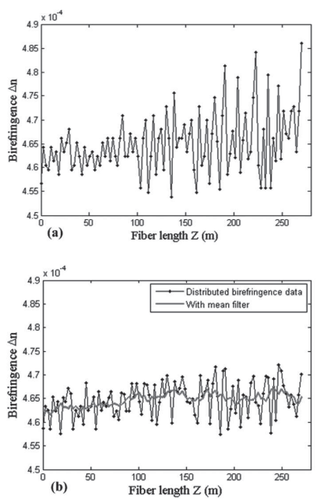

Fig.5 (a) Measured group birefringence as a function of distance along the 280 meter fiber with N=5, without applying dispersion compensation, where the fiber length between any neighboring crosstalk peaks is defined by Eq. 2 (0.535 m in the experiment) of the fiber spool. The measurement uncertainty is shown to increase with the distance. (b) Measured group birefringence as in a);, but with dispersion compensation. The measurement uncertainty at large distances is significantly reduced. The 6-point windowed sweeping average of the group birefringence as a function of distance is shown by the red line. In both a) and b), the zero position is placed at the FUT's output connector.

Fig. 5a shows the variation of $\triangle n$ as a function of distance Z along the fiber for the case of N=5, where Z is obtained by dividing △Z by the average $\triangle n$ obtained in Fig. 4, as defined in Eq. (1). The large data fluctuations at large distances are caused by dispersion induced peak broadening caused by group birefringence dispersion [21], which will be discussed in Section III C, because the broadening increases the uncertainty of $\delta_{\triangle z}$ in Eq. (4). Dispersion compensation procedures described in

[21] can be used to further improve the measurement accuracy by multiplying the distributed crosstalk curve with a dispersion compensation function when the group birefringence dispersion of the FUT is measured, as described in Section III C. Fig. 5b is the measured group birefringence as a function of distance along the fiber, showing that the measurement uncertainties are greatly reduced when the dispersion compensation procedure in [21] is applied. It is also evident that the mean $\triangle n$ slightly varies along the fiber length for the FUT.

Note that the tension applied to the fiber when winding the fiber on the spool is not critical to the measurement accuracy. In a separate experiment, we found no noticeable differences in measured birefringence using the same method when three different tension settings (5, 10, and 15 grams) of the fiber winding machine were used to wind the spool.

C. Group birefringence dispersion measurement

As discussed in [21], the envelope of a measured crosstalk peak (i.e. the interference peak) is influenced by the SLED's spectral distribution and by the group birefringence dispersion $\triangle D$ of the PM fiber. In fact, the envelope width increases quadratically with the distance Z due to the effect of the group birefringence dispersion. The relationship between envelope broadening W and group birefringence dispersion $\triangle D$ can be expressed as [21]:

$$W/W_0 = (1 + (\alpha \triangle D)^2 Z^2)^{1/2} \qquad (5)$$

where

$$\alpha = 2\pi c(\triangle \lambda/\lambda_0)^2 \qquad (6)$$

In the equations above, c is the speed of light in vacuum, $\triangle \lambda$ is the 3-dB spectral width of the light source with a Gaussian line shape, and λ_0 is the center wavelength of the light source used for the measurement, respectively. W_0 is the $1/e$ width of the interference envelope when the dispersion $\triangle D$ or Z equals zero. As shown in [21], one may simply measure the widths of any two polarization crosstalk peaks with a known spacing Z between them to obtain the dispersion $\triangle D$ using Eq. (5). However, in order to increase measurement accuracy of $\triangle D$, the widths of crosstalk envelopes at multiple locations along the PM FUT are measured, and $\triangle D$ is then obtained by curve-fitting to Eq. (5).

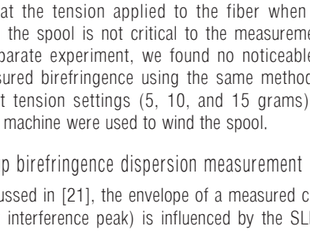

Fig.6. Envelope widths of crosstalk peaks induced by stress at various locations along the fiber. The envelope widths of polarization cross talk peaks broaden as fiber length increases due to group birefringence dispersion. Curve-fitting determines the group birefringence dispersion of the FUT to be $\triangle D = 0.0079$ ps/(km · nm).

Fig. 6 shows the widths of the crosstalk peaks as a function of their locations along the fiber. The distance is measured from the first induced crosstalk peak and evaluated every 20 peaks (N=20 or 10.7 m). Unlike in [21], in which the locations of crosstalk peaks were calculated using Eq. (1), which requires the total fiber length Z to be measured precisely, for this case, only the relative locations are required, and they can be precisely obtained by multiplying the circumference of the fixture by the number of peaks, minimizing the error contribution of fiber distance in dispersion measurement. One may argue that the group birefringence dispersion may also be obtained using Eq. (5) by measuring the widths of the crosstalk peaks caused by the output and input connectors; however, the error of the fiber distance measurement also contributes to the dispersion measurement. In addition, such a two-point measurement is sensitive to measurement uncertainties of the widths. The method presented here can effectively avoid such error sources. As can be seen from Fig. 6, the widths of cross-talk peak start to show significant broadening at a distance larger than 100 m. The group birefringence dispersion $\triangle D$ of the PM fiber is accurately obtained by a least-square fitting to Eq. (5) to be $\triangle D = 0.0079$ ps/(km · nm).

Note that a dispersion compensation function can be obtained once the $\triangle D$ of the fiber is determined, as described in [21]. This dispersion compensation function can be used to remove the broadening of the crosstalk peaks, and hence, to reduce the measurement uncertainties of the group birefringence along the fiber, as described in Section III B.

D. Group birefringence thermal coefficient measurement

As discussed in [4], the PM fiber is expected to be sensitive to temperature because of anisotropic strain which is caused by differential thermal expansion at different regions in the fiber cladding, and which varies linearly with temperature in the vicinity of room temperature. The group birefringence $\triangle n$ can be written as [4]:

$$\triangle n = \gamma (T_0 - T) \qquad (7)$$

where T is the temperature of the FUT, T_0 is the softening temperature of silica glass with dopants in the stress-inducing region of the cladding, and γ is the thermal coefficient of group birefringence of the PM fiber to be measured.

As in [4], we place the fiber spool of Fig. 3a into a temperature chamber, with two fiber pigtails outside of the chamber. Fig. 7a shows two typical polarization crosstalk curves of a PM FUT as a function of relative delay for two different temperatures: 80°C and 40°C. Clearly, the positions of all polarization crosstalk peaks are shifted with the temperature, as predicted in Eq. (7). In our previous report [4], we obtain the thermal coefficient of group birefringence by measuring the position of the crosstalk peak induced by the input connector as a function of temperature. However, as described in [4], there are two major error sources that affect the measurement accuracy: 1) fiber length measurement error, and 2) the fiber length outside the temperature chamber. In order to make accurate measurements, the fiber inside the chamber must be sufficiently long and the fiber pigtails must be kept sufficiently short.

In this section, we show that both the error sources can be effectively minimized for the following reasons: 1) because the periodic polarization crosstalk peaks induced by the measurement fixture act as ruler marks along the fiber, the fiber length measurement between any two peaks can be easily obtained with a high precision, and 2) we only measure the relative position variation with temperature between any two periodic crosstalk peaks on the fiber section inside the chamber, and therefore eliminate the error contribution of fiber sections outside of the chamber. In this experiment, we choose to measure the spacing $\triangle Z$ between the 1st and 50th peaks, and to measure the group birefringence $\triangle n$ as a function of temperature. As shown in Fig. 7b, the peak positions of the 48th, 49th, and 50th peaks shift to the left as temperature increases, reducing the spacing $\triangle Z$. The fact that the spacing $\triangle Z$ decreases with temperature indicates that $\triangle n$ has a negative thermal coefficient. As mentioned previously, the thermal coefficient of the group birefringence γ can be obtained by linear-fitting of $\triangle n$ to Eq. (7) using the least square fitting method at each different temperature. Note that in order to reduce the effect of dispersion, we choose the crosstalk peaks close to the output end of the fiber under test, although dispersion compensation as described in Section III B and 3.3 may also be used to reduce peak broadening and improve measurement accuracies for measuring peaks closer to the input connector (N>>50).

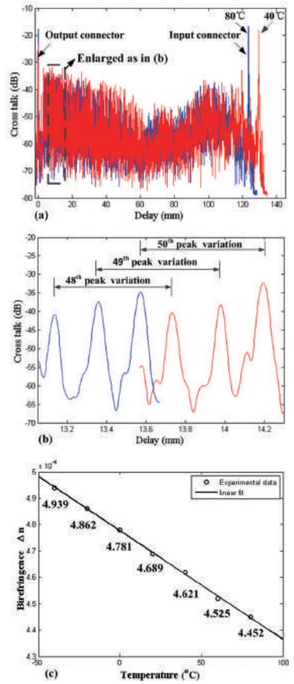

Fig. 7 (a) polarization cross talk curves of a PM fiber as a function of the relative delay at 80°C (blue) and 40°C (red); (b) The expanded view of the positions of the 48st, 49th, and 50th peaks at 80°C (blue) and 40°C (red); (c) $\triangle n$ obtained at seven different temperatures by measuring the spacing between the 1st and the 50th crosstalk peaks at different temperatures using Eq. (4).

In our experiment we measured $\triangle n$ for one PM fiber at seven different temperatures (i.e. -40°C, -20°C, 0°C, 20°C, 40°C, 60°C, 80°C) and the results are plotted in Fig. 7c. Linear-fitting $\triangle n$ to Eq. (7) yields a group birefringence thermal coefficient γ of 4.123×10^{-7}.

E. PER measurement

As mentioned in the introduction, traditional methods of PM fiber characterization described in [6,7], or methods that use a PER meter for measuring the PER of a PM fiber, are susceptible to 1) polarization misalignment at the input end of the fiber under test (FUT), and 2) polarization misalignment between the light source and its fiber pigtail if a pigtailed light source is used. Using a DPXA, one can readily identify the crosstalk contributions from the polarization misalignments at the two fiber ends, as well as at the interface between the pigtail and the light source, and eliminate their contributions to the total PER, because the corresponding polarization crosstalk peaks measured with a DPXA are spatially separated. Note that for the PER measurement described in this section, we do not induce the periodic polarization crosstalk peaks as in the previous sections.

Fig. 8 shows the measured polarization crosstalk curves of a PM fiber jumper with FC/PC connectors and a spool of PM fiber of length 250 meters directly from a PM fiber vendor, fusion spliced with two FC/PC connectors. When a FUT is connected to the DPXA, the polarization misalignment at the connection points induces significant crosstalk peaks. An auto-search program can be implemented in the DPXA software to automatically identify those peaks, because the polarization crosstalk signatures of the fibers inside the DPXA are known, as shown in Fig. 8. In addition, the polarization crosstalk peak resulting from the light source and its pigtail is located outside the region defined by the two connectors, and thus is not included for PER calculation. By definition, the PER of the fiber can be calculated as:

$$PER = 10\log(P_s/P_f) \qquad (8)$$

where P_f is the total power coupled to the fast axis from the slow axis and can be obtained by integrating all polarization crosstalk peaks between the two connectors, and P_s is the total power remaining in the slow axis $P_s = P - P_f$, where P is the total received power at the fiber output.

We implement an algorithm in the DPXA software to automatically calculate the PER while excluding the contributions of the two end connectors from the crosstalk measurement curve, as shown in Fig. 8a. One may also use the DPXA software to calculate the total PER contribution between any two points along the fiber, and therefore to further exclude the contributions from the two fusion splicing points, as shown in Fig. 8b. Table 2 compares multiple PER measurement results of a 13 meter fiber jumper and a 250 meter PM fiber coil obtained with a commercial PER meter and a DPXA. It is evident that the PER value obtained by the PER meter is several dB smaller than that obtained with a DPXA, due to the contributions of crosstalk from the polarization misalignment at the input connector. In addition, as anticipated, the measurement repeatability of a DPXA is much better that that of a PER meter. Therefore, it is much easier to use a DPXA to obtain more accurate PER measurements than to use a PER meter.

Note that we used a SLED source with a spectral width around 30 nm when using a PER meter for the PER measurement, in accordance with the requirement of test standard TIA-544-193 [7] to avoid measurement fluctuations caused by coherent effects resulting from the use of a narrow line-width laser [25].

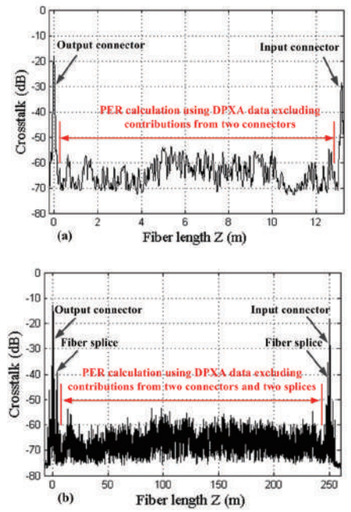

Fig.8 (a) Polarization crosstalk curves of a 13 m jumper with two FC/PC connectors and (b) a 250 m PM fiber coil spliced with two FC/PC connectors. PER measurement with a commercial PER meter always includes the contributions of the input connector and two splices, while the DPXA has the ability to identify and eliminate polarization crosstalk contributions of all connectors and splices in the measurement system. Note that fiber length in the horizontal axis is obtained by dividing the fiber delay line distance △Z by the average group birefringence obtained using the procedure described in Section III B.

Table 2. Comparison of PER measurements of a 13 m PM fiber jumper and a 250 m PM fiber coil obtained with a commercial PER meter and a DPXA

Measurement #	PER of Fiber jumper		PER of Fiber coil	
	ERM(dB)	DPXA (dB)	ERM(dB)	DPXA (dB)
1	22.5	34.81	25.7	30.82
2	24.9	34.27	21.8	30.81
3	23.3	35.06	25.4	30.31
4	26.8	34.64	22.5	30.90
5	25.8	35.14	23.8	31.09
Uncertainty (Max-Min)(dB)	4.3	0.87	3.9	0.78

F. PM fiber quality evaluation

Until now, the only parameter available to a user to characterize the polarization performance of a PM fiber from a vendor has been PER or h-parameter, which may not be able to reflect the true polarization performance of the fiber, especially considering that PER measurement using conventional methods may have significant fluctuations, as discussed previously. Here, we propose to use a set of parameters obtained from a single DPXA scan to fully and unambiguously describe the fiber's polarization performance.

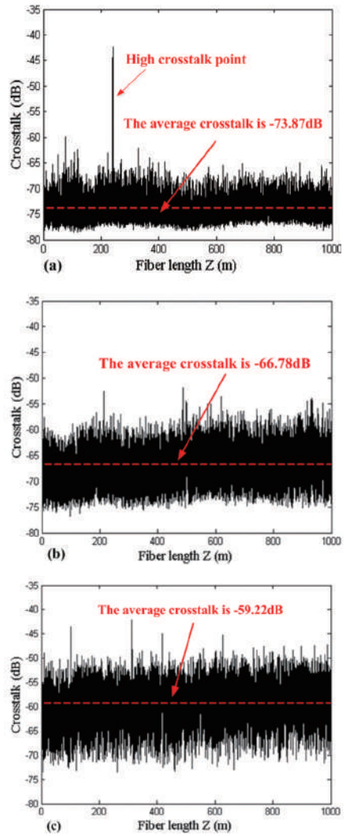

Fig.9 Polarization cross talk curves of three different PM fibers. a) a PANDA PM fiber at 1310 nm with a buffer diameter of 250 μm. A defect point is seen at around 220 m; b) a PANDA fiber at 1310 nm of the same core/cladding diameters as in a), but with a reduced buffer diameter of 169 μm; c) a third PANDA PM fiber at 1310 nm with similar cladding diameters as in a), but with an even more reduced buffer diameter of 136 μm. Two major defect points with crosstalk more than 45 dB are seen.

Fig. 9 shows DPXA scans of three different PM fibers measured directly while still on the fiber spool from the vendor. We propose to use four parameters to characterize the quality of a PM fiber with respect to its polarization related performance: 1) the average polarization crosstalk, 2) the maximum crosstalk, 3) the number of crosstalk peaks above a certain threshold defined by the manufacturer or the user, and 4) PER. The average crosstalk is the major contributor to the value of PER and is closely related to h-parameter (PER per unit fiber length). The maximum crosstalk is an indication of whether the PM fiber is degraded or damaged during manufacturing, packing or shipping of the PM fiber, although a single or a few high crosstalk peaks contribute insignificantly to the total PER of a long fiber. For some applications, such as fiber gyro coils, the high crosstalk sections must be removed to assure high quality fiber coil production. A large number of high crosstalk peaks present in the fiber may indicate problems in the fiber drawing or packaging processes. It also makes it impractical to sort out only good fiber sections for demanding applications.

Table 3. lists these four parameters for three different fibers under test, obtained from Fig. 9. Fiber I is a commercial PANDA fiber at 1310 nm with a beat length of 2.57 mm, a core diameter of 6 μm, a cladding diameter of 125 μm, and a buffer diameter of 250 μm. Fiber II is a different PANDA fiber at 1310 nm with the same core diameter as Fiber I, but with a different beat length (2.13 mm), a cladding diameter of 80 μm, and a buffer diameter of 169 μm. Finally, Fiber III is a third type of PM fiber at 1310 nm with a beat length of 2.6 mm, a core diameter of 6.4 μm, a cladding diameter of 80 μm, and a buffer diameter of 136 μm. It is evident from Fig. 9a that Fiber I has the lowest average crosstalk, resulting in the highest PER of 28.78 dB; however, it has a defect point about 220 m from the output connector, with a high crosstalk peak of -42.36 dB, probably caused by mishandling when winding the fiber to the spool. Such a defect cannot be identified with a simple PER measurement. We find in experiments that such a defect may be permanent, i.e. the fiber cannot recover even when the corresponding stress is released. Conversely, Fiber III has the highest average crosstalk of -59.22 dB, corresponding to a low PER of 16.25 dB. It also has a large number of high crosstalk peaks above -55 dB, probably because the thin buffer layer (136 μm) cannot effectively protect the fiber from external stresses. Therefore, all four parameters collectively give a full picture of the quality or performance of the PM fiber under test.

Table 3. Four parameters to fully characterize the quality of three different PM fibers

	Average crosstalk (dB)	Maximum crosstalk (dB)	Number of crosstalk peaks above -55 (dB)	PER (dB)
Fiber I	-73.87	-42.36	1	28.8
Fiber II	-66.78	-51.88	23	23.6
Fiber III	-59.22	-42.15	1711	16.5

IV. Conclusions

In summary, we demonstrate methods and processes for using a ghost-peak-free DPXA to fully characterize all polarization related parameters of a polarization-maintaining fiber, including group birefringence, group birefringence variation along the fiber, group birefringence dispersion, group birefringence temperature coefficient, and PER. In particular, we devise a fixture to induce periodic polarization crosstalk peaks with equal spacing and measure the locations and widths of the peaks to obtain all group birefringence related parameters. The periodicity defined by the circumference of the fixture can be used as a built-in ruler to avoid the need for measuring the fiber length, whose measurement error causes a significant error for the group birefringence measurement. In addition, we show that a DPXA is capable of identifying crosstalk caused by the polarization misalignments at the fiber input and output ends, as well as at the fiber pigtail of the light source, and to eliminate their contributions to the PER of the fiber, enabling easier and more accurate PER measurements. Finally, we propose a set of parameters obtained from the DPXA measurement of a PM fiber that fully quantify the fiber's polarization related performance. We believe that the methods and processes described in this paper can be readily applied in the industry to completely characterize PM fibers with ease and with high repeatability.

V. Acknowledgments

This work was supported by the National Basic Research Program of China (973 Program) under grant 2010CB327806, National Instrumentation Program under grant 2013YQ03015, the International Science & Technology Cooperation Program of China under grant 2009DFB10080 and 2010DFB13180, China Postdoctoral Science Foundation under grant 20100470782, the Medical Instruments and New Medicine Program of Suzhou under grant No. ZXY2012026, the Foundation Research Project of Jiangsu Province under grant No. BK20130373 and No. BK20130374, and the Internal Development Funding of General Photonics Corporation.

REFERENCE

[1] M. Tsubokawa, N. Shibata, T. Higashi, and S. Seikai, "Loss of longitudinal coherence as a result of the birefringence effect," J.Opt. Soc. Am. A4, 1895-1901 (1987).

[2] T. Xu, W. Jing, H. Zhang, K. Liu, D. Jia, and Y. Zhang, "Influence of birefringence dispersion on a distributed stress sensor using birefringengct optical fiber," Optical Fiber Technology, 15, pp. 83-89 (2009).

[3] K. Mochizuki, Y. Namihira, and Y. Ejiri, "Birefringence variation with temperature in elliptically cladded single-mode fibers," Appl. Opt. 21, 4223-4228 (1982).

[4] Z. Ding, Z.Meng, X. S. Yao, X. Chen, T. Liu, and M. Qin," Accurate method for measuring the thermal coefficient of group birefringence of polarization-maintaining fibers," Opt.Lett.36, 2173-2175 (2011).

[5] H. Zhang, G. Wen, Y. Ren, D. Jia, T. Liu, and Y. Zhang, "Measurement of beat length in polarization-maintaining fibers with external forces method," Optical Fiber Technology 18, pp. 136-139 (2012).

[6] H-Parameter test method for polarization-Maintaining Optical Fiber, TIA-455-192.

[7] Polarization crosstalk method for polarization-Maintaining Optical Fiber and Components, TIA-455-193.

[8] D. A. Flavin, R. McBride, and J. D. C. Jones," Dispersion of birefringence and differential group delay in polarization-maintaining fiber," Opt. Lett.27, 1010-1012 (2002).

[9] P. L.Francois, M. Monerie, C.Vassallo, Y. Durteste, and F.alard, "Three ways to implement interfacial techniques: application to measurements of chromatic dispersion, birefringence, and nonlinear susceptibilities," J.Lihgtwave Technol.7,500-513 (1989).

[10] F. Tang, X. Wang, Y. Zhang, and W. Jing, "Distributed measurement of birefringence dispersion in polarization-maintaining fibers," Opt. Lett., Vol. 31 (23), pp. 3411-3413 (2006).

[11] F. Tang, X. Wang, Y. Zhang, and W. Jing, "Characterization of birefringence dispersion in polarization-maintaining fibers by use of white light interferometry," Applied Optics, Vol. 46 (19), pp. 4073-4080 (2007).

[12] M. G. Shlyagin, A. V. Khomenko, and D. Tentori, "Birefringence dispersion measurement in optical fibers by wavelength scanning," Opt.Lett. 20, 869-871 (1995).

[13] P. Hlubina and T.Martynkien," Dispersion of group and phase modal birefringence in elliptical-core fiber measured by white-light spectral interferometry," Opt.Express 11, 2793-2798 (2003).

[14] X. Chen, T. Liu, H. Zhang, W. Lu, L. Huang, L. Cheng, Y. Zhang, "Spectral-domain measurement of beat length in polarization-maintaining fibers, Optical Fiber Technology Vol. 18, pp. 527-531 (2012).

[15] Z.-L. Duan, L.-Y. Ren, Y.-N. Zhang, H.-Y. Wang, B.-L. Yao,and W. Zha,. "Theoretical and experimental study of polarization characteristics of polarization maintaining fiber based on wavelength-sweeping modulation," Microwave and Opt. Technol. Lett. 52, 1466-1469 (2010).

[16] Yongkang Dong, Liang Chen, and Xiaoyi Bao, "Truly distributed birefringence measurement of polarization -maintaining fibers based on transient Brillouin grating," Opt. Lett.35,193-195 (2010).

[17] Yongkang Dong, Hongying Zhang, Zhiwei Lu, Liang Chen, and Xiaoyi Bao. "Long-Range and High-Spatial -Resolution Distributed Birefringence Measurement of a Polarization-Maintaining Fiber Based on Brillouin Dynamic Grating," J. Lightwave Technol. 31, 2981-2986 (2013).

[18] Y. Mizuno, Z. He, and K. Hotate, "Polarization beat length distribution measurement in single-mode optical fibers with Brillouin optical correlation-domain reflectometry," Applied Physics Express 2, 046502 (2009).

[19] M. Trubokawa, T. Higashi, and Y. Sasaki, "Measurement of mode couplings and extinction ratios in polarization-maintaining fibers," J. Lightwave Technol. 7, 45-50 (1989).

[20] X. Wang, G. Niedermayer, Ganbin Lin, P. Liu, B. Wang, Liang Chen, and Xiaoyi Bao. "Polarization-maintaining property of tapered polarization-maintaining fibers," Appl. Opt., 52, 1550-1554 (2013).

[21] Zhihong Li, Zhuo Meng, Xiaojun Chen, Tiegen Liu, and X. Steve Yao, "Method for improving the resolution and accuracy against birefringence dispersion in distributed polarization cross-talk measurements," Opt.Lett.37,2775-2777 (2012).

[22] Xiaojun Chen and X. Steve Yao, "Measuring distributed polarization crosstalk in polarization maintaining fiber and optical birefringence material," US Patent number 8,599,385 (2013).

[23] www.generalphotonics.com.

[24] P. Martin, G. Le Boudec, and H.C. Lefevre, "Test apparatus of distributed polarization coupling in fiber gyro coils using white light interferometry," Proc. SPIE 1585, 173-179 (1991).

[25] Andrew R.Grant, Paul F.Wysocki, Douglas P.Holcomb, "Polarization effects in polarization-independent and polarization maintaining fiber amplifiers". IEEE/LEOS Summer Topical Meeting (2006).

Journal Papers

In-service light path PMD (polarization mode dispersion) monitoring by PMD compensation 172

High accuracy polarization measurements using binary polarization rotators 185

Highly Repeatable All Solid-State Polarization State Generator 204

Self-calibrating Binary Polarization Analyzer 207

A novel scheme for achieving quasi-uniform rate polarization scrambling at 752 krad/s 210

Automatic Maximum-Minimum Search Method for Accurate PDL and DOP Characterization 219

Real-Time Optical Spectrum Analysis of a Light Source Using a Polarimeter 226

Programmable optical delay generator with uniform output and double-delay capability 236

Distributed Transverse Stress Measurement Along an Optic Fiber Using Polarimetric OFDR 242

A Novel Method for Determining and Improving the Quality of a Quadrupolar Fiber Gyro Coil under Temperature Variations 246

Method for Improving the Resolution and Accuracy against Birefringence Dispersion in Distributed Polarization Cross-Talk Measurements 256

Accurate Method for Measuring the Thermal Coefficient of Group Birefringence of Polarization-Maintaining Fibers 259

Tomographic Inspection of Fiber Coils Using Optical Coherence Tomography 262

In-service light path PMD (polarization mode dispersion) monitoring by PMD compensation

X. Steve Yao,[1,2,*] Xiaojun Chen,[2] T. J. Xia,[3] Glenn Wellbrock,[3] David Chen,[3] Daniel Peterson,[3] Paul Zhang,[2] Ansel Belisle,[2] Lei Dong[2] and Tao Yu[2]

[1]*Optical Polarization Research Center, College of Precision Instrument and Opto-electronics engineering, Tianjin University, Tianjin 300072, China*
[2]*General Photonics Corporation, 5228 Edison Ave., Chino, California 91710, USA*
[3]*Verizon Communications, 2400 N. Glenville Dr., Richardson, Texas 75082, USA*
**syao@generalphotonics.com*

Abstract: We describe a novel method of measuring PMD (polarization mode dispersion) of an in-service DWDM system by PMD compensation. We successfully demonstrate the method in a 1500-km ultra-long haul DWDM test bed. We further verify the feasibility of the method for in-service light path PMD monitoring in a field trial in a revenue-generating route in Verizon Network, and obtain an accurate PMD value without impacting live network traffic. The discrepancy between the measured and expected PMD values is less than 6% for all cases tested.

© 2010 Optical Society of America

OCIS codes: (060.4510) Optical communications; (230.2035) Dispersion compensation devices; (060.2300) Fiber measurement.

References and links

1. T. J. Xia, G. Wellbrock, W. Lee, G. Lyons, P. Hofmann, T. Fisk, B. Basch, W. Kluge, J. Gatewood, P. J. Winzer, G. Raybon, T. Kissel, T. Carenza, A. H. Gnauck, A. Adamiecki, D. A. Fishman, N. M. Denkin, C. R. Doerr, M. Duelk T. Kawanishi K. Higuma Y. Painchaud, and C. Paquet, "Transmission of 107-Gb/s DQPSK over Verizon 504-km Commerical LambdaXtreme Transport System,"OFC'2008, paper NMC2.
2. S. H. Kogelnik, and R. Jopson, "Polarization-mode dispersion", in Optical Fiber Telecommunications, IVB, Edited by I. Kaminow and T. Li, Academic Press, ISBN 0–12–395173–9.
3. C. D. Poole, and J. A. Nagel, "Polarization effects in Lightwave systems, in Optical Fiber Communications IIIA, I. P. Kaminnow and T. L. Koch, eds., Academic Press, CA. pp. 114-161.
4. H. Bulow, "System outage probability due to first- and second-order PMD," IEEE Photon. Technol. Lett. **10**(5), 696–698 (1998).
5. R. Jopson, L. Nelson, G. Pendock, and A. Gnauck, "Polarization-mode dispersion impairment in return-to-zero and nonreturn-to-zero systems," Proc. Optical Fiber Communication Conference, OFC'99, paper WE3 (1999).
6. C. D. Poole, J. H. Winters, and J. A. Nagel, "Dynamical equation for polarization dispersion," Opt. Lett. **16**(6), 372–374 (1991).
7. H. Bulow, W. Baumert, H. Schmuck, F. Mohr, T. Schulz, F. Kuppers, and W. Weiershausen, "Measurement of the maximum speed of PMD fluctuation in installed field fiber," Proc. OFC '99, Technical Digest, W: 83–85 (1999)].
8. J. Cameron, L. Chen, X. Bao, and J. Stears, "Time evolution of polarization mode dispersion in optical fibers," IEEE Photon. Technol. Lett. **10**(9), 1265–1267 (1998).
9. D. Waddy, P. Lu, L. Chen, and X. Bao, "The measurement of fast state of polarization changes in aerial fiber," Proc.OFC '01, paper ThA3 (2001).
10. G. J. Foschini, and C. D. Poole, "Statistical theory of polarization dispersion in single mode fibers," J. Lightwave Technol. **9**(11), 1439–1456 (1991).
11. F. Curti, B. Daino, D. De Marchis, and F. Matera, "Statistical treatment of the evolution of the principle state of polarization in single mode fibers," J. Lightwave Technol. **8**(8), 1162–1166 (1990).
12. M. Karlsson, J. Brentel, and P. Andrekson, "Long term measurement of PMD and polarization drift in installed fibers," J. Lightwave Technol. **18**(7), 941–951 (2000).
13. C. Poole, and R. Wagner, "Phenomenological approach to polarization dispersion in long single-mode fibers," Electron. Lett. **22**(19), 1029–1030 (1986).
14. N. Gison, and J. Pellaux, "Polarization mode dispersion: Time versus frequency domains," Opt. Commun. **89**(2-4), 316–323 (1992).
15. B. Heffner, "Automated measurement of polarization mode dispersion using Jones matrix eignenanalysis," IEEE Photon. Technol. Lett. **4**(9), 1066–1069 (1992).
16. X. S. Yao, X. Chen, and T. Liu, "High accuracy polarization measurements using binary polarization rotators," Opt. Express **18**(7), 6667–6685 (2010).
17. L. Nelson, R. Jopson, and H. Kogelnik, "Muller matrix method for determining polarization-mode dispersion vectors," Proc. European Conference on Optical Communications," ECOC'99, Vol. 2, p. 10 (1999).
18. C. Poole, and D. Favin, "Polarization-mode dispersion measurements based on transmission spectra through a polarizer," J. Lightwave Technol. **12**(6), 917–929 (1994).
19. K. Mochizuki, Y. Namihira, and H. Wakabayashi, "Polarization mode dispersion measurement in long single mode fibers," Electron. Lett. **17**(4), 153–154 (1981).
20. L. Thevenaz, J. Pellaux, N. Gisin, and J. von der Weid, "Birefringence measurement in fibers without polarizer," J. Lightwave Technol. **7**(8), 1207–1212 (1989).
21. D. Bebbington, J. Ellison, R. Schuh, X. Shan, A. Siddiqui, and S. Walker, "Fully polarimetric optical time-domain reflectometer with 1-m spatial resolution," Proc. Optical Fiber Communication Conference, OFC'97, Technical Digest, pp. 185–186 (1997).
22. H. Sunnerud, B. Olsson, and P. Andrekson, "Technique for characterization of polarization mode dispersion accumulation along optical fibers," Electron. Lett. **34**(4), 397–398 (1998).
23. N. Gisin, B. Gisin, J. von der Weid, and R. Passy, "How accurately can one measure a statistical quantity like polarization-mode dispersion?" IEEE Photon. Technol. Lett. **8**, 1671–1673 (1996).
24. J. Cameron, L. Chen, X. Bao, and J. Stears, "Proc. European Conference on Optical Communication, ECOC'99, Vol. 1, p. 308 (1999).
25. David.Chen, private communications.
26. L. Yan, C. Yeh, G. Yang, L. Lin, Z. Chen, Y. Shi, A. Willner, and X. Steve Yao, "Programmable Group-Delay Module Using Binary Polarization Switching," J. Lightwave Technol. **21**(7), 1676–1684 (2003).
27. N. Kikuchi, "Analysis of signal degree of polarization degradation used as control signal for optical polarization mode dispersion compensation," J. Lightwave Technol. **19**(4), 480–486 (2001).
28. M. Karlsson, C. Xie, H. Sunnerud, and P. Andrekson, "Higher-order polarization mode dispersion compensator with three degrees of freedom," Proc. Optical Fiber Communication Conference, OFC'01, Paper MO1 (2001).
29. S. Lanne, W. Idler, J.-P. Thiery, and J.-P. Hamaide, "Demonstration of adaptive PMD compensation at 40Gb/s," Proc. Optical Fiber Communication Conference, OFC'01, Paper TuP3 (2001).
30. J. Nagel, M. Chbat, L. Garrett, J. Soigne, N. Weaver, B. Desthieux, H. Bulow, A. McCormick, and R. Derosier, "Long-term PMD mitigation at 10Gb/s and time dynamics over high-PMD installed fiber, Proc. European Conference on Optical Communication, ECOC'2000, Vol. 2, p. 31(2000).

1. Introduction

As the bit rate of fiber optic communication systems increases from 10 Gbps to 40Gbps, 100 Gbps [1], and beyond, polarization mode dispersion (PMD) has more and more impact on signal transmission [2–5]. PMD generally causes two principle polarization components of a light signal to travel at different speeds and hence spreads the bit-width of the signal. Consequently, it causes the increase of bit-error rate (BER) and service outage.

Unlike system impairments caused by chromatic dispersion (CD), nonlinearity, or noise, the signal distortion caused by PMD is random in nature and changes with time. At any instant, it depends on not only the PMD value of the signal channel, but also the state of polarization (SOP) of the signal itself. For signal channel of a given PMD value, the signal distortion is maximum when the input SOP is either circular or linear with a 45-degree orientation from the principle state of polarization (PSP) of the signal channel [5,6]. On the other hand, the PMD has little effect on the signal when the input SOP is aligned or counter-aligned with PSP of the signal channel, assuming first order PMD is dominant. Although both are time varying, in general, SOP changes much faster than PMD value of the signal channel [2,7]. The rapid varying SOP is mainly due to external disturbances on the fiber, such as vibration, wind, and temperature changes [8,9].

On the other hand, the PMD value of a signal channel changes randomly when the temperature or mechanical stress on the fiber cable changes, with a probability following Maxwellian Distribution [2,10,11]. For a fiber link with multiple WDM signal channels, the instant PMD values of different signal channels (or wavelengths) may differ, however, they all follow the same Maxwellian Distribution with the same average PMD value if monitored for a sufficiently long period of time, generally tens of hours. Similarly, at a same instant of time, the PMD values of different WDM channels or wavelengths also follow the same Maxwellian Distribution with the same average PMD value. Therefore, one may obtain the

average PMD of a fiber link either by averaging PMD values of a signal channel over time, or by averaging PMD values of different DWDM channels at about the same time [12–14].

Generally, the average PMD value reflects the mechanical stress condition of the fiber link itself, and it also changes when the mechanical stress redistributes along the fiber cable due to the changes in environmental conditions along the fiber route, such as snow, rain, flood, mud slide, or earthquakes. Therefore, the average PMD value of a fiber link obtained in prior times may not valid at present and future times. It needs to be monitored to ensure the healthy operation of all the WDM channels of the fiber link, because a WDM channel worked well before may not anymore due to increased PMD. In addition, the signal entering a receiver may come from different routes due to ROADM dynamic reconfiguration and hence experiences different PMD. Such PMD monitoring is useful for diagnosing channel problems and identifying its cause among several possibilities, including CD, PMD or signal to noise ratio degradations. Special measures must be taken to mitigate the PMD effect if identified.

Several methods [2] can be used to accurately measure the PMD of a fiber link, including Jones Matrix method [15,16], Muller Matrix method [16,17], fixed polarizer method [18], white light interferometer method [19,20], and polarization sensitive OTDR method [21,22]. The first three methods require precise polarization control of light signal inputting to the fiber and fast analysis of the received signal before light signal's SOP changes caused by the external mechanical or temperature disturbances, and therefore not practical for field applications. In addition, the first four methods all require a large wavelength range of tens of nanometers [2,23,24] and not suitable for in-service WDM networks with a typical channel spacing of 50GHz, although they can generally be used to measure the PMD of installed dark fibers themselves without multiplexers, demultiplexers, add-drops multiplexers, and ROADMs. The polarization sensitive OTDR has the advantage of identifying distance resolved PMD of a fiber link, however, its application is limited because its measurement range of about 20 km is much less than a typical fiber span of 80 km. Therefore, no practical method exists for the PMD monitoring of an in-service WDM system.

In this paper, we describe and demonstrate a novel method for measuring PMD in an in-service fiber network by PMD compensation. The basic concept was first suggested by D. Chen [25] and implemented by General Photonics. Using filtered and polarized ASE source with a bandwidth of 0.3 nm as the input light, we successfully demonstrate the method in Verizon's 1500-km ultra-long haul DWDM test bed over 10 DWDM channels. We further verify the feasibility of the method using an in-service 40Gbps signal itself in the test bed. Finally, we demonstrate the effectiveness of the method in a field trial with a revenue-generating route in Verizon Network. The trial is performed on a single fiber in a selected long-haul fiber route with 23 revenue-generating DWDM channels. No impact of the in-service PMD measurement to the live traffic in the neighboring channels is observed by the network operation center (NOC). The relative error between the measured and expected PMD values is less than 6% for all the cases tested. We anticipate that this method is effective in monitoring PMD in a fiber link having an average PMD larger than 5 ps.

The method has the following advantages: 1) It accurately measures the cascaded PMD of all passive and active components and mixed fiber sections in the fiber route, including EDFAs, multiplexers, demultiplexers, ROADMs, optical fibers. 2) It can obtain the instantaneous effective PMD of each DWDM channel, without requiring a large bandwidth. Even an in-service 40Gbps signal itself can be used as the light source for the measurement. The PMD obtained reflects the effective PMD for the particular modulation format used. 3) It can be used to obtain the average PMD of the whole fiber link by long term monitoring a single DWDM channel. 4) Finally, with proper under and over compensation adjustment, we can see the real time BER impact on a specific channel with any bit rate and modulation format.

In-service light path PMD (polarization mode dispersion) monitoring by PMD compensation

2. Concept and system description

The basic concept of PMD measurement by PMD compensation is illustrated in Fig. 1, where an optical signal passes through a fiber link with a certain amount of PMD (labeled as PMD_f herein). At the receiving end, a PMD compensator, consisting of a polarization controller, a variable PMD generator, and a PMD effect monitor, is used to compensate the signal distortion caused by PMD_f. The PMD effect monitor is used to provide the feedback signal to the polarization controller to adjust the polarization of the input signal as to minimize the PMD effect. When properly adjusted, signal's slow polarization component is aligned with the fast axis of the PMD generator, while its fast component is aligned with the slow axis. At the output end of the compensator, the two relatively delayed polarization components are brought closer together. When performing PMD compensation, the compensator will vary the PMD generator and look for a PMD value, PMD_b, which can best compensate the signal distortion caused by PMD_f. Assuming the resolution of the internal PMD generator is sufficiently high, the PMD value for the best PMD compensation, PMD_b, must be the PMD value of the fiber link, PMD_f. Such a compensator is sometimes called PMD nulling compensator [2].

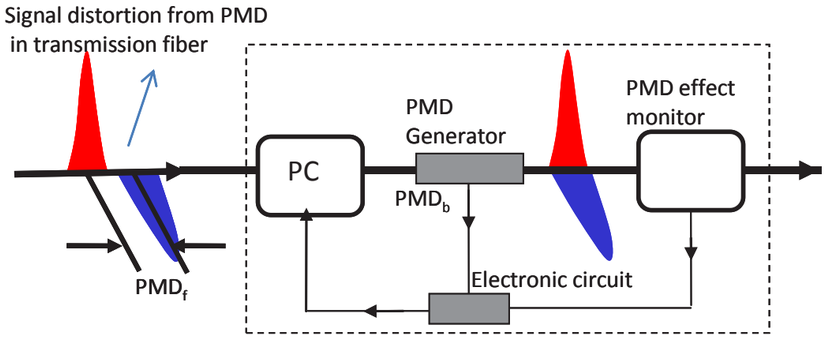

Fig. 1. The concept illustration of PMD monitoring by PMD compensation. PMD_f is the PMD value of the fiber link and PMD_b is the PMD setting of the compensator for best compensation.

Figure 2 shows the system diagram of our implementation of the PMD compensator (a function in General Photonics PMD-1000). Our variable PMD generator is made of 9 pieces of birefringence crystals, with a magneto-optic polarization rotator sandwiched between two adjacent crystals [26], as shown in the insert of Fig. 2. The lengths of the crystals are decreasing successively by a factor of two. Different PMD values can be generated when the solid state polarization rotators rotate signal's polarization between the crystals. The PMD generator in our system can generate 256 precise DGD values with a resolution of 0.35 ps and a range of 90 ps.

We use degree of polarization (DOP) of the signal as the PMD effect monitor and use an in-line polarimeter to obtain the DOP [27]. A polarimeter (Polarimeter 1) before the PMD generator was used to measure the DOP before PMD compensation and a second polarimeter (polarimeter 2) after the PMD generator was used to provide the feedback DOP signal to the digital signal processing (DSP) circuit. The DSP circuit changes the PMD setting step by step and controls the polarization controller to maximize the DOP received by polarimeter 2 for each PMD setting. A plot of DOP vs. PMD shown in the insert of Fig. 2 can be obtained and the PMD setting corresponding to the maximum DOP value is the PMD of the fiber link at the measured wavelength. It is important to note that the comparison between the two DOP values reveals the effectiveness of PMD compensation and can be used for data analysis, as will be discussed below. Note that with the PMD compensator of Fig. 2, one may vary both 1st and

2nd order PMD during the optimization process of PMD compensation. However, because a large number of 1st and 2nd order PMD values to scan through, the time for finding the optimized PMD is much too long to be practical. Therefore we choose to only vary 1st order PMD (DGD) during the PMD optimization process, even though the PMD in the DWDM channel have both 1st and 2nd order PMD components. The obtained optimized PMD (DGD) value actually contains the contribution of both the PMD components from the fiber because the PMD nulling compensator can also mitigate some higher order PMD [28–30], although only 1st order PMD (DGD) is used in compensation. We therefore call it the effective PMD and anticipate that the average PMD obtained using this method through either wavelength average or time average is sufficiently close to the real PMD of the fiber link. In our PMD compensator of Fig. 2, the time for obtaining the optimized PMD value among 256 DGD choices is about 2 seconds.

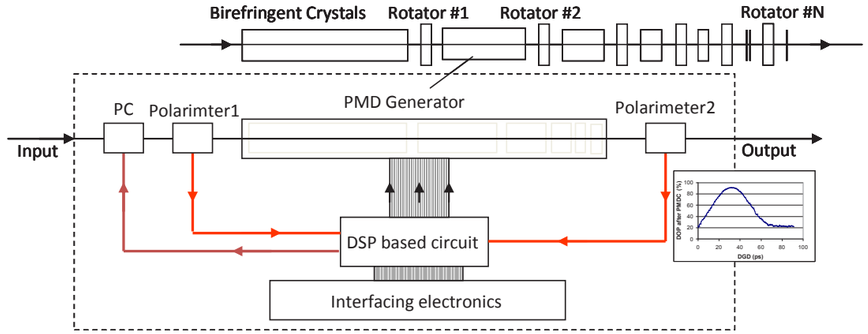

Fig. 2. Illustration of PMD compensator construction. PC: polarization controller. The PMD generator is made of 9 birefringence crystals, sandwiched with 8 MO polarization rotators. The PMD deterministically generator can generate 256 precise DGD values with a resolution of 0.35 ps and a range of 90 ps. The insert at right shows a typical DOP vs. DGD curve obtained by performing PMD compensation at each DGD setting.

In operation, The DOP measured by Polarimeter 1 in the compensator, DOP_1, is an indication whether the SOP of the signal is aligned with PSP of the transmission fiber or not. A value of DOP_1 close to 100% indicate that the input signal's SOP is nearly aligned with fiber's PSP and very little PMD distortion is caused by PMD in the fiber. As a result, the DOP after the compensator measured by Polarimeter 2, DOP_2, is always close to 100% with and without the compensation action. Consequently, the obtained PMD value for the best compensation is less accurate and the corresponding data points can be removed in post data processing.

On the other hand, a small (less than 90%) value of DOP_1 indicates a sufficiently large PMD induced signal distortion and the PMD compensation action is effectively in restoring the signal and bringing the DOP_2 back to its maximum. The PMD values obtained for the best compensation for these data points are therefore accurate and can be kept in the data processing.

As expected, this PMD measurement method is less accurate if the PMD in the transmission system is sufficiently small and the corresponding DOP is always larger than 90%, regardless of the polarization launching condition. On the other hand, one usually does not care about small PMD values in the system because their impact on signal transmission is negligible. Therefore this method is very practical for the deployed Long-Haul and Ultra-Long-Haul systems.

In-service light path PMD (polarization mode dispersion) monitoring by PMD compensation

INSTRUMENTS
MODULES
PASSIVE COMPONENTS
ACCESSORIES
APPLICATION GUIDE
FAQS

3. Laboratory experiments with a channelized ASE source

PMD only impacts signals with a sufficient large bandwidth. For a 40 Gbps signal, the typical bandwidth is around 0.2 to 0.3 nm. To evaluate the feasibility of PMD measurement by PMD compensation for DWDM systems, we first made a tunable channelized ASE (TCA) source to emulate a 40 Gbps signal, as shown in Fig. 3. The TCA source (General Photonics TCA-1000) consists of an ASE source, a tunable band-pass filter with a 3-dB bandwidth of 0.3 nm, an Er + doped fiber amplifier (EDFA), a polarizer, and a binary polarization rotator with +/– 22.5 degree rotations. The tunable filter can be precisely tuned to WDM ITU grid to simulate WDM channels.

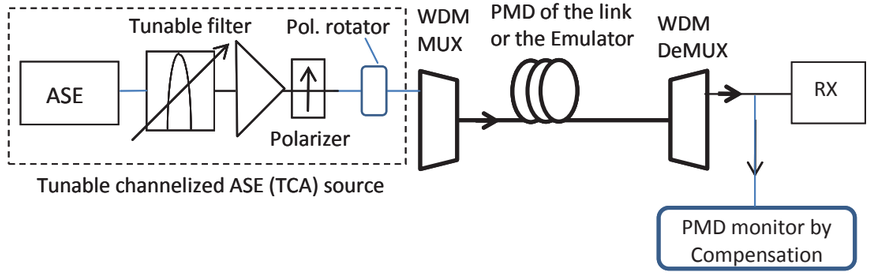

Fig. 3. System configuration for in-service PMD measurement by PMD compensation with a compensator shown in Fig. 2. The tunable channelized ASE (TCA) source with a 3-dB bandwidth around 0.3 nm can be precisely tuned to WDM ITU grid and is used to emulate 40Gbps WDM channels.

As illustrated in Fig. 3, the light signal from the TCA source first goes through a PMD emulator before entering the PMD compensator. The SOP of the light input to the emulator is uncertain and changes with time with respect to fiber's PSP, causing varied PMD distortion on the light signal, which can be measured by its DOP (DOP_1). In operation, the polarization rotator is used to switch the polarization by 45 degrees periodically with a periodicity more than twice longer than the time required for the compensator to obtain best PMD value for compensation (about 2s), and it is not necessary to be synchronized with the PMD compensator. If the input SOP to the transmission fiber is close to the fiber's PSP, as indicated by a DOP_1 close to 100%, a 45 degree rotation will cause it to be at the worst launching condition for PMD distortion, indicated by a DOP_1 of a small value. Therefore, the periodical 45 degree polarization rotations assure that a sufficient large number of PMD data points obtained are valid, corresponding to the case of sufficiently small DOP_1 values. As describe previously, we will remove the invalid data points with DOP_1 close to 100% in post data processing.

Figure 4a shows a typical curve of compensator's output DOP (DOP_2) vs. compensator's DGD. The compensator has an automatic search algorithm for obtaining the PMD value based on maximizing DOP. The average time for taking each curve is about 2 seconds. We use a piece of PM fiber as the PMD emulator. It is evidence that the DGD value corresponding to the peak DOP is 17.9 ps, the same as that measured with a high precision polarization analysis system [16]. We made 10 tests at different times at each wavelength to obtain the repeatability of our method, and the result is shown in Fig. 4b. The corresponding standard deviation is less than 0.6 ps.

We also made measurements with PMD emulators of different PMD values and found that this method is sufficiently accurate in measuring PMD in a fiber link having an average PMD larger than 5 ps.

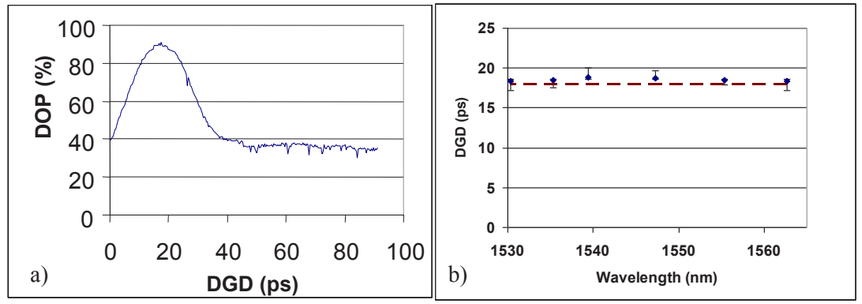

Fig. 4. a) A typical DOP vs. DGD curve of PMD compensation at different DGD values. The DGD value at the peak DOP location is the effective PMD of the DUT (device under test) or SUT (system under test). In this case, the PMD of DUT is 17.9 ps. b) The PMD of DUT measured at different wavelength channels. The standard deviation of measurement is 0.6 ps.

4. Experimental results with Verizon 1500 km ultra-long haul test bed

In order to further confirm its feasibility for field applications, we tested our PMD monitoring method with Verizon 1500-km ultra-long haul test bed in Richardson, Texas, as shown in Fig. 5. The system has a residue PMD on the order of 5 ps. We inserted two PMD emulators of different average values, one at a time, in the system at a location around 700 km from the transmitter side, as shown in Fig. 5. Each PMD emulator is made with multiple sections of PM fibers of different lengths fusion-spliced together with randomly relative orientations. The instantaneous PMD value of each emulator at each wavelength channel is expected to change with time due to temperature variations and the changing rate is on the order of several ps per minutes in an air-conditioned laboratory environment. We measured PMD of both the emulators using a highly accurate PMD analyzer, PSGA-101 from General Photonics [16], and the results are shown in Figs. 6a and 6b. The first emulator, purchased from EXFO, has an average PMD of 11.2 ps, and the second PMD emulator, made by General Photonics, has an average PMD value of 21.6 ps. Considering the residue PMD value around 5 ps in the system, the expected PMD values for the two cases are 12.3 ps and 22.2 ps respectively, following

$$PMD = \sqrt{PMD_1^2 + PMD_2^2} \qquad (1),$$

where PMD_1 and PMD_2 are the emulator PMD and system residual PMD respectively.

We performed three different types of test to cross check the measurement results. The first is to measure the PMD values of the system over 10 DWDM channels in a short period of time, using a TCA source described in Fig. 3. The average PMD across the 10 channels over 27 nm wavelength range is a good estimation of the average PMD of the link. Table 1 lists detailed experimental conditions of each channel, where TCA Output is the center wavelength and bandwidth of each TCA channel input to the system and Verizon System Output is the corresponding center wavelength and bandwidth measured at the output end of the system. One may notice that although the bandwidth of the input signal (TCA output) is about 0.3 nm, the final output bandwidth is around only 0.2 nm, narrowed by the ROADMs in the system by about 30%. Our PMD monitoring system actually compensates the PMD of a signal of 0.2 nm bandwidth, although the signal inputting at the transmitter end has a bandwidth of 0.3 nm.

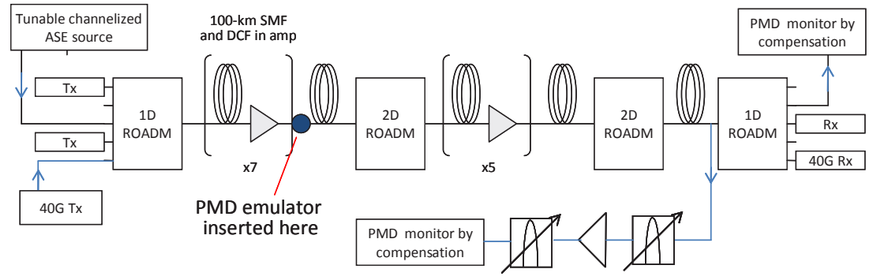

Fig. 5. Demonstration setup at Verizon's 1500 km ultra-long haul test bed in Richardson, Texas. Top portion: Using a TCA source to measure PMD in the system. Bottom portion: using an in-service 40Gbps signal to measure the PMD in the system.

Table 1. Experimental conditions of the 10 DWDM channels

Channel #	Freq. (THz)	WL(nm)	TCA Output		Verizon System Output	
			Center WL (nm)	3dB BW (nm)	Center WL (nm)	3dB BW (nm)
6	195.85	1530.725	1530.717	0.325	1530.751	0.22
10	195.65	1532.290	1532.33	0.317	1532.373	0.22
16	195.35	1534.640	1534.676	0.317	1534.719	0.217
26	194.85	1538.580	1538.547	0.306	1538.594	0.208
35	194.4	1542.140	1542.143	0.292	1542.151	0.209
11	194.35	1542.540	1542.517	0.293	1542.56	0.212
45	193.45	1549.720	1549.669	0.284	1549.71	0.205
50	193.2	1551.721	1551.721	0.281	1551.712	0.021
55	192.95	1553.730	1553.743	0.28	1553.75	0.225
65	192.45	1557.770	1557.817	0.282	1557.819	0.231

Figure 6c and Fig. 6d show the experimental results of the PMD measurements of the 10 DWDM channels. The average PMD values over the wavelength channels are 12.6 ps, and 23.4 ps for the cases of inserting 11.2 ps, and 21.6 ps PMD emulators respectively. The PMD values obtained by the average of 10 DWDM channels are sufficient close to those expected values of 12.3 and 22.2 ps respectively. The corresponding errors are 2.4% and 5.4% respectively.

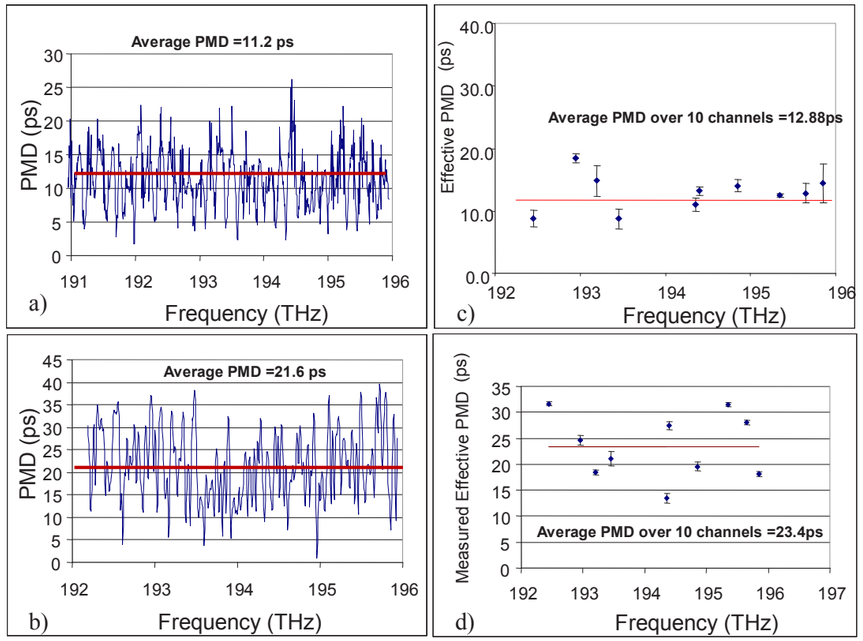

Fig. 6. Experimental results of in-service link PMD measurement by PMD compensation. a) and b): PMD measurement of two emulators using a highly accurate PMD analyzer. c) and d): Instantaneous PMD (dots with error bars) and average PMD (line) obtained by PMD compensation method. The average PMD values obtained for the two different cases are close to those expected based on off-line measurement using a high precision PMD analyzer, considering that the PMD in the system include the contributions from the PMD emulator and the residue PMD of the system itself.

The second test is to monitor the PMD of a single WDM channel (#50) over a long period of time (over 12 hours) using the channelized ASE source, and obtain the average PMD of the system. We inserted a PMD emulator with an average PMD of 11.3 ps. The total expected PMD in the system is about 12.3 ps, considering the residue PMD in the system. In the measurement, the polarization input to the fiber link was periodically rotated 45 degrees every 30 seconds to make sure sufficient data points are acceptable, as described previously. Figure 7a is the processed PMD data points of a DWDM channel, as a function of time, in which bad data points corresponding to bad SOP launching condition (indicated by high DOP_1 values of larger than 90%) were removed. Figure 7b shows the average PMD of the DWDM channel as the sample points increase with time. The average PMD gradually stabilizes with time toward the expected value of 12.3 ps of the fiber link. Longer time may be required for the measured average PMD to have an even better agreement with the expected value. The probability density of the measured PMD values is shown in Fig. 7c and its distribution resembles that of a Maxwellian, with an average value of 12.6 ps, sufficiently close to fiber link's expected value of 12.3 ps. In the measurement, the polarization rotator in the TCA source is not synchronized with the PMD compensator in order to simulate the real field test situation.

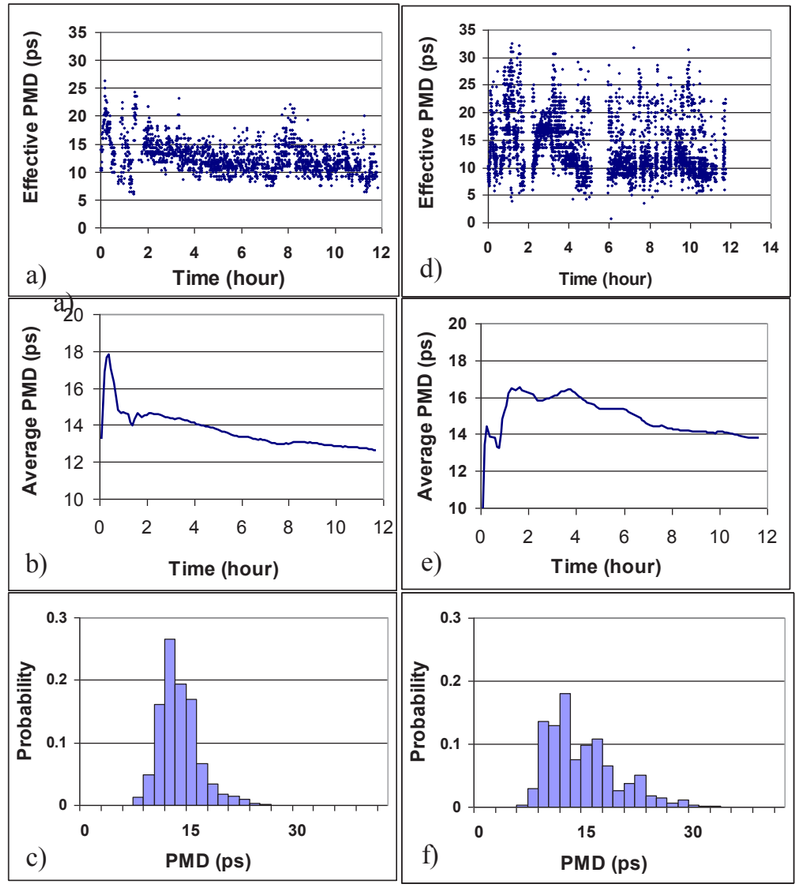

Fig. 7. (a)-(c): experimental results of long term PMD monitoring using TCA source. (d)-(f): experimental results of long term monitoring using 40Gbps signal itself. (a) & (d): instant PMD vs. time; (b) & (e): average PMD vs. time; (c) & (f) probability density function of PMD of all PMD values in (a) and (d) respectively. Note that in the test of using TCA source, there are much more valid data points available because of the periodic 45 degree polarization rotation capability of the TCA source.

Finally, we use a 40Gbps signal with advanced DPSK modulation format itself to perform long term monitoring of the PMD in a system. The test setup is shown in the lower half of Fig. 5 and the results are shown in Figs. 7d-7f. Here we use a different DWDM channel to perform PMD measurement from that using a TCA source shown in Figs. 7a-7c. Because we have no freedom of rotating the input SOP, much fewer data points are valid. As discussed previously, all data points with a DOP_1 above 90% were removed during data processing and the processed data are shown in Fig. 7d. The data discontinuities in Fig. 7d are the results of removed invalid data points with DOP_1 larger than 90%. As shown in Fig. 7e, the average PMD stabilizes with time, as the data points increase, towards the expected value of 12.3 ps. The probability density as a function of PMD is shown in Fig. 7f and the resulting average PMD is 13.7 ps. Because much fewer data points are valid for a certain period of time than in the case of Figs. 7a-7c, much longer monitoring time is required for getting more accurate

result than for the case of using TCA source. Unfortunately, we were only allocated 12 hours for the test. Nevertheless, the obtained 13.7 ps is already sufficiently close to the expected value of 12.3 ps. Note that because measurements using TCA source and 40Gbps signal are performed with different DWDM channels at different times, their instantaneous PMD values are expected to be different, as shown in Figs. 7a and 7d. The results of PMD long-term monitoring at Veriizon 1500km test bed is summarized in Table 2 below. In the table, the test on channel #35 using TCA is also included.

Table 2. Summary of demonstration at Verizon 1500-km test bed

	PMD by time average	PMD by channel average	Expected PMD
TCA to empty channel #35 (13 hours)	12.9ps	12.9ps	12.3ps
TCA to empty channel #50 (12 hours)	12.6ps		
40G signal in channel 193.1 THz (12 hours)	13.7ps		

5. Experimental results of field trial

To further test the feasibility of the method for a field technician to measure and identify the PMD of an installed link, we performed the in-service PMD measurement field trial in a long-haul route in an operational network. The expected mean DGD of the route is 19.77 ps, calculated from the mean DGD values of the individual fiber sections, each measured using commercially available PMD measurement equipment before the long-haul system was installed. The length of the route is 414 km with a ROADM at each end, as illustrated in Fig. 8. There are four in-line optical amplifiers in the route. Add/drop ports are accessible in both ROADMs. In this trial a TCA signal shown in Fig. 3 is injected at Node A and is dropped at Node B to be used for PMD measurement. There are 23 traffic-carrying channels along the route, most having a data rate of 10 Gb/s. 16 idle DWDM channels, from 194.20 to 195.70 THz with a channel spacing of 100 GHz, are used for this trial. Another key objective of the trial is to confirm that our in-service PMD measurement is safe to the live traffic. To this end, the performance of all the working channels is monitored by the NOC during the trial. To ensure that the test signal passes through the route, the idle channels are maintained open temporarily by the NOC during the trial. When the test signal is injected into an idle port, the DWDM system adjusts its optical gain in each amplifier to accommodate the added signal.

We performed two different tests of PMD monitoring: one is to measure the PMD of the route over the 16 WDM channels sequentially in a short period of time (around 15 minutes per channel, including the setup time for each channel) and the other one is to perform long term monitoring for about 3 hours. For the short term PMD test, at least 20 valid data points were taken for each channel and the polarization from TCA source was periodically rotated by 45 degrees every 90 seconds to avoid invalid data points. The average value and its standard deviation of each channel are shown in Fig. 9a. The average PMD over all 16 wavelength channels is 18.57 ps, sufficiently close to the expected value of 19.77 ps. The corresponding error is 6%. The average of more wavelength channels should give even better accuracy. It should be noted that the possible impact of the in-service measurement on the live traffic was monitored very closely with NOC. The measurements triggered no minor or major alarms,

thereby demonstrating that in-service PMD measurement methods may safely be applied to traffic-carrying networks.

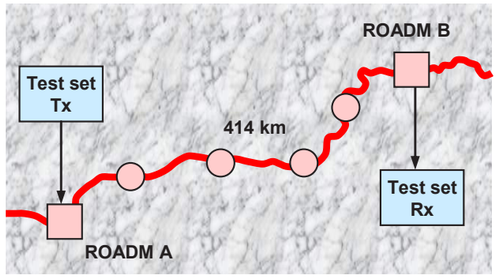

Fig. 8. Field fiber route for the PMD measurement trial.

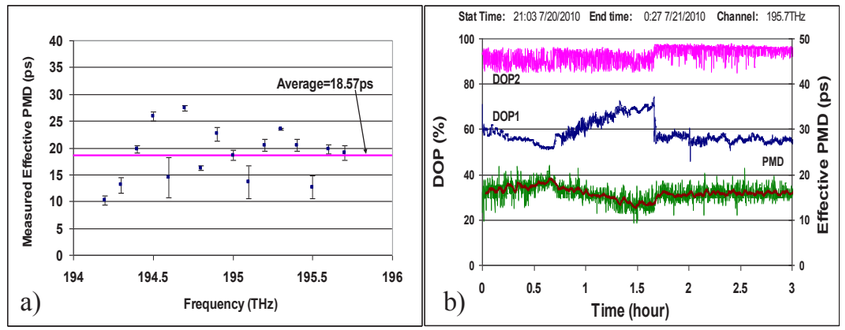

Fig. 9. Field trial results. a) PMD measured over 16 DWDM empty channels. b) PMD monitoring over time of a single channel. DOP1 is the DOP measured before PMD compensator and DOP2 is the DOP after PMD compensator. The PMD in a real system is much more stable than that in a test bed.

We used a DWDM channel at 195.7 THz for long term monitoring experiment and the results are shown in Fig. 9b. Compared with the test at 1500-km test bed, the PMD value is much more stable with time for the selected DWDM channel, especially after 11:00 PM at night. It is likely because the fiber is buried underground. In order to obtain the statistical average PMD of the fiber route, much longer monitoring time (on the order of 10 days) may be required.

6. Conclusion

In summary, we describe a novel method of using PMD compensation to obtain the PMD value of a fiber DWDM channel of an in-service multiple mixed fiber optic network. The method is simple, fast and does not require a tunable or wide bandwidth light source. There is absolutely no impact to the live long-haul and ultra-long-haul traffic to service provider. Only 2 seconds are required to make a measurement. Either a channelized ASE source with a bandwidth around 0.2 nm or a 40Gbps signal itself of any modulation format can be used as the signal source to the PMD monitoring. We successfully demonstrated the method in Verizon's 1500-km ultra-long haul test bed in Richardson, Texas and in a field trial in a 414-km revenue-generating fiber route using both channel (wavelength) averaging and time averaging methods. The differences between our measured average PMD values and expected PMD values are less than 6% for the cases tested. We anticipate that the method is accurate for a link with an average PMD of 5 ps or more.

This method can be used 1) for accurately measuring the cascaded PMD of all active and passive components and mixed fiber sections in a fiber route, including EDFAs, multiplexers, demultiplexers, ROADMs, optical fibers; 2) for obtaining the instantaneous effective PMD of each DWDM channel, without requiring a large bandwidth scanning and without interrupting in-service 40G or 100Gbps traffic. The PMD obtained reflects the effective PMD for the particular modulation format used and can be used to determine whether PMD compensation is required for the channel; 3) for obtaining the average PMD of the whole fiber link by long term monitoring a single DWDM channel and gaining knowledge about the PMD degradation of a fiber route. 4) We can also use under or over compensation to reflect the impact on the BER for a specific channel with any type of modulation.

Acknowledgements

We thank Shoa-kai Liu for his great support and Lynn Lin, Hemin Zhang, Zhanfeng Wang, and Jianwei Ma of General Photonics for their design and engineering contributions to the equipment used in this work.

High accuracy polarization measurements using binary polarization rotators

X. Steve Yao[1, 2]*, Xiaojun Chen[2], and Tiegen Liu[1]

[1]*Optical Polarization Research Center and Key Laboratory of Opto-electronics Information and technical Science of China Ministry of Education, College of Precision Instrument and Opto-electronics engineering,Tianjin University, Tianjin, 300072, China*

[2]*General Photonics Corporation, 5228 Edison Av., Chino, CA 91710, USA*

**syao@generalphotonics.com*

Abstract: We report a novel system for the accurate measurement of all polarization related parameters, including polarization mode dispersion and polarization dependent loss, using binary magneto-optic polarization rotators. By taking advantage of the binary nature of the rotators, we achieved unprecedented DGD, SOPMD, and PDL accuracies of 2.6 fs, 1.39ps^2, and 0.06 dB respectively; repeatabilities of 0.022 fs, 0.28 ps^2, and 0.034dB respectively; and resolutions of 1 fs, 0.005 ps^2 and 0.01dB respectively, from 1480 to 1620 nm.

©2010 Optical Society of America

OCIS codes: (120.5410) Polarimetry; (080.2730) Matrix methods in paraxial optics; (060.2300) Fiber measurements; (260.5430) Polarization; Polarization mode dispersion; Polarization dependent loss.

References and links

1. X. S. Yao, "Controlling polarization related impairments," Lightwave Magazine, October 31, 2000.
2. H. Kogelnik, R. Jopson, and L. Nelson, "Polarization-Mode Dispersion," in *Optical Fiber telecommunications, Vol. IV-B, Systems and Impairments*, I. P. Kaminow and L. Tingye ed., (Elsevier Science (USA)
3. E. Lichtman, "Limitations imposed by polarization-dependent gain and loss on all-optical ultralong communication systems," J. Lightwave Technol. **13**(5), 906–913 (1995).
4. X. S. Yao, L.-S. Yan, B. Zhang, A. E. Willner, and J. Jiang, "All-optic scheme for automatic polarization division demultiplexing," Opt. Express **15**(12), 7407–7414 (2007).
5. E. Ip, A. P. Lau, D. J. Barros, J. M. Kahn, "Coherent detection in optical fiber systems," Opt. Express **16**(2), 753–791 (2008).
6. H. Sun, K. T. Wu, and K. Roberts, "Real-time measurements of a 40 Gb/s coherent system," Opt. Express **16**(2), 873–879 (2008).
7. R. A. Chipman, and Ch. Polarimetry, 22 in Handbook of Optics, vol. II, 2nd Ed. M. Bass ed., McGraw-Hill, New York, 1995.
8. D. H. Goldstein, "Mueller matrix dual-rotating retarder polarimeter," Appl. Opt. **31**(31), 6676–6683 (1992).
9. P. A. Williams, "Rotating-wave-plate stokes polarimeter for differential group delay measurements of polarization-mode dispersion," Appl. Opt. **38**(31), 6508–6515 (1999).
10. E. Dijkstra, H. Meekes, and M. Kremers, "The high-accuracy universal polarimeter," J. Phys. **24**(10), 1861–1868 (1991).
11. P. A. Williams, A. H. Rose, and C. M. Wang, "Rotating-polarizer polarimeter for accurate retardance measurement," Appl. Opt. **36**(25), 6466–6472 (1997).
12. A. De Martino, Y. K. Kim, E. Garcia-Caurel, B. Laude, and B. Drévillon, "Optimized Mueller polarimeter with liquid crystals," Opt. Lett. **28**(8), 616–618 (2003).
13. B. Wang, J. List, and R. Rockwell, "Stokes polarimeter using two photoelastic modulators," in Polarization Measurement, Analysis, and Applications V, D. H. Goldstein and D. B. Chenault, eds., Proc. SPIE 4819, 1–8 (2002).
14. R. M. A. Azzam, "Arrangement of four photodetectors for measuring the state of polarization of light," Opt. Lett. **10**(7), 309–311 (1985).
15. R. M. Craig, S. L. Gilbert, and P. D. Hale, "High-resolution, nonmechanical approach to polarization-dependent transmission measurements," J. Lightwave Technol. **16**(7), 1285–1294 (1998).
16. A. Zadok, N. Simon, and A. Eyal, "The dependence of the output stokes parameters on the state of an arbitrarily located polarization controller in PMD mitigation schemes," J. Lightwave Technol. **22**(6), 1533–1538 (2004).
17. M. Petersson, H. Sunnerud, M. Karlsson, and B. E. Olsson, "Performance monitoring in optical networks using stokes parameters," IEEE Photon. Technol. Lett. **16**(2), 686–688 (2004).
18. W. Xiang, and A. M. Weiner, Digest of the LEOS Summer Topical Meetings, "Fast multi-wavelength polarimeter for polarization mode dispersion compensation systems," WB2.4/67–173.

#123233 - $15.00 USD Received 25 Jan 2010; accepted 21 Feb 2010; published 16 Mar 2010
(C) 2010 OSA

19. X. S. Yao, L. Yan, and Y. Shi, "Highly repeatable all-solid-state polarization-state generator," Opt. Lett. **30**(11), 1324–1326 (2005).
20. X. S. Yao, X. Chen, and L. Yan, "Self-calibrating binary polarization analyzer," Opt. Lett. **31**(13), 1948–1950 (2006).
21. B. L. Heffner, "Automated measurement of polarization mode dispersion using Jones matrix eigenanalysis," IEEE Photon. Technol. Lett. **4**(9), 1066–1069 (1992).
22. B. L. Heffner, "Deterministic, Analytically Complete Measurement of Polarization-Dependent Transmission Through Optical Devices," IEEE Photon. Technol. Lett. **4**(5), 451–454 (1992).
23. R. M. Craig, S. L. Gilbert, and P. D. Hale, "High-resolution, nonmechanical approach to polarization-dependent transmission measurements," J. Lightwave Technol. **16**(7), 1285–1294 (1998).
24. H. Dong, P. Shum, M. Yan, J. Q. Zhou, G. X. Ning, Y. D. Gong, and C. Q. Wu, "Generalized Mueller matrix method for polarization mode dispersion measurement in a system with polarization-dependent loss or gain," Opt. Express **14**(12), 5067–5072 (2006).
25. P.A Williams, S.M. Etzel, J. D. Kofler and C.M Wang, "Standard Reference Material 2538 for Polarization-mode dispersion (Non-mode coupled)," NIST special publication 260–145.
26. S. M. Etzel, A. H. Rose, and C. M. Wang, "Dispersion of the temperature dependence of the retardance in $SiO_{(2)}$ and MgF(2)," Appl. Opt. **39**(31), 5796–5800 (2000).
27. J. P. Gordon, and H. Kogelnik, "PMD fundamentals: polarization mode dispersion in optical fibers," Proc. Natl. Acad. Sci. U.S.A. **97**(9), 4541–4550 (2000).
28. X. Y. Kalisky, p.168 in *The Physics and Engineering of Solid State Lasers*, (SPIE Press, Bellingham, Washington, 2005).
29. M. Born, and E. Wolf, p38-p54, in *Principles of Optics*, 7th ed. University Press, Cambridge, UK, 1999.
30. *BK7 Glass data sheet,* http://www.us.schott.com/advanced_optics/us/abbe_datasheets/datasheet_n-bk7.pdf?highlighted_text=BK7
31. Y. Shi, L. Yan, and X. S. Yao, "Automatic maximum-minimum search method for accurate PDL and DOP characterization," J. Lightwave Technol. **24**(11), 4006–4012 (2006).
32. E. Collett, Chapter 9 in Polarized Light in Fiber Optics (The PolaWave Group Lincroft, New Jersey, USA, 2003).
33. N. G. Walker, and G. R. Walker, "Polarization control for coherent communications," J. Lightwave Technol. **8**(3), 438–458 (1990).
34. Data sheet of Agilent N7788B/N7788BD optical component analyzer *http://www.home.agilent.com/agilent/redirector.jspx?action=ref&cname=AGILENT_EDITORIAL&ckey=1203309*.
35. Date sheet of Thorlabs PMD/PDL Analysis System PMD5000, *http://www.thorlabs.us/NewGroupPage9.cfm?ObjectGroup_ID=1592*.
36. B. L. Heffner, "Attosecond-resolution measurement of polarization mode dispersion in short sections of optical fiber," Opt. Lett. **18**(24), 2102–2104 (1993).
37. D. Derickson, Chap 6 in *Fiber Optic Test and Measurement* (Prentice-Hall, Upper Saddle River, New Jersey, 1998).
38. R. M. Craig, "Interlaboratory comparison of polarizationcrosstalk measurement methods in terminated high birefringence optical fiber," in *Optical Fiber Communication Conference (OFC)*, Vol. 2 of 1998 OSA Technical Digest Series (Optical Society of America, 1998), pp. 180–181.
39. D. Penninckx, and N. Beck, "Definition, meaning, and measurement of the polarization extinction ratio of fiber-based devices," Appl. Opt. **44**(36), 7773–7779 (2005).
40. S. C. Rashleigh, "Measurement of fiber birefringence by wavelength scanning: effect of dispersion," Opt. Lett. **8**(6), 336–338 (1983).
41. T. Ritari, H. Ludvigsen, M. Wegmuller, M. Legré, N. Gisin, J. Folkenberg, and M. Nielsen, "Experimental study of polarization properties of highly birefringent photonic crystal fibers," Opt. Express **12**(24), 5931–5939 (2004).
42. Corning panda PM specialty fibers, PI936, *http://www.corning.com/WorkArea/downloadasset.aspx?id=18341*

1. Introduction

As the bit rate of fiber optic communication systems increases from 10 Gbps to 40Gbps, 100Gbps, and beyond, polarization related issues have more and more of an impact on system performance [1]. Polarization related impairments such as polarization mode dispersion (PMD) [2] and polarization dependent loss (PDL) [3] degrade system performance and cause service outages. On the other hand, signals with orthogonal states of polarization can be multiplexed and demultiplexed to double the transmission rate and enable high bit-rate transmission while using smaller bandwidth [4]. Finally, coherent detection, which is critical to 40Gbps and 100Gbps systems, relies on precise polarization management [5, 6]. Consequently, the need for rapid, precise measurement of all polarization related parameters of components and systems is becoming correspondingly acute.

Until recently, optical polarization related measurements have relied on analog technologies [7], including rotating retarders [8,9], rotating polarizers [10,11], liquid crystal cells [12], phase modulators [13], and four-detector methods [14]. Such analog technologies

#123233 - $15.00 USD Received 25 Jan 2010; accepted 21 Feb 2010; published 16 Mar 2010
(C) 2010 OSA

suffer from inherently low repeatability and require complicated compensation techniques in order to achieve high accuracy measurements. Polarization analysis based on binary ferroelectric liquid crystals was reported recently [15–18] and was shown to have certain advantages over its analog counterparts. However, its accuracy and repeatability are yet to be proved.

In a previous publication [19], we reported the development of a binary polarization state generator (PSG) capable of generating five or six particular polarization states on the Poincaré Sphere with a repeatability of better than 0.1° using binary magneto-optic (MO) polarization rotators. We subsequently reported [20] a highly accurate self-calibrating polarization state analyzer (PSA) using the same binary polarization rotators. We pointed out in [19, 20] that a PSG-PSA pair can be used to accurately measure an optical component's polarization dependent loss (PDL), polarization mode dispersion (PMD), retardation, and birefringence. In this paper, we describe in detail the setup and theory for the use of a binary PSG and PSA for component characterization, and then present experimental data to show the accuracy and repeatability of the technique. In order to determine the accuracy of our binary measurement system, we designed and fabricated several PMD and PDL artifacts with precisely known PMD and PDL values to verify our measurement results. We then performed multiple PMD and PDL measurements to determine the resolution, accuracy, and repeatability of the binary approach. With PMD, SOPMD and PDL accuracies of 2.6 fs, 1.39 ps^2, and 0.06dB, respectively; repeatabilities of 0.022 fs, 0.28 ps^2, and 0.034 dB, respectively; and resolutions of 1 fs, 0.005 ps^2 and 0.01dB, respectively, the binary technique has wide potential for applications in fiber characterization, optical component measurements, and optical component manufacturing. Finally, we describe the use of our binary measurement system for additional applications, including the measurement of polarization extinction ratio and PM fiber beat length.

2. System description

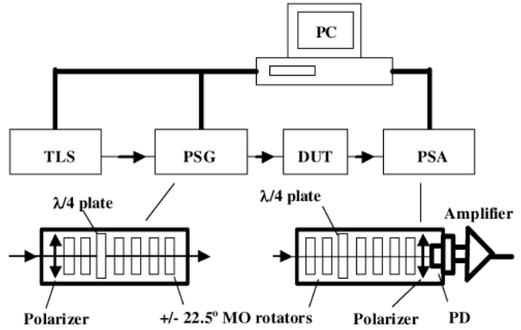

Fig. 1. The construction of a binary polarization measurement system comprised of a PSG and a PSA made with binary magneto-optic polarization rotators, a tunable laser, and a computer.

As shown in Fig. 1, the binary polarization measurement system consists of a tunable laser (TLS), a binary MO PSG, a binary MO PSA, and a control computer (PC). The device under test (DUT) is placed between the PSG and PSA. The PSG and PSA each contain 6 binary MO polarization rotators, a polarizer, and a quarter wave plate. The PSA also contains a photodetector (PD) and a signal amplification circuit. As described in [19] and [20], our MO rotators have the following attractive binary properties: when a positive magnetic field above a saturation level is applied, the rotator rotates the SOP by a precise angle θ. When a negative magnetic field beyond the saturation level is applied, the rotator rotates the SOP by precisely –θ. For the purposes of the PSG and PSA, θ is designed to be around 22.5°. Therefore, when two rotators rotate the SOP in the same direction, the net rotation is +45° or –45°. Conversely,

#123233 - $15.00 USD Received 25 Jan 2010; accepted 21 Feb 2010; published 16 Mar 2010
(C) 2010 OSA

if the two rotators rotate the SOP in opposite directions, the net SOP rotation is zero. With the rotation directions of each rotator controlled by the PC, the PSG can generate 6 particular polarization states and the PSA can accurately measure the state of polarization (SOP) and the degree of polarization (DOP) of light entering it by analyzing voltages generated in the photodetector using Mueller Matrix analysis. As described in [20], the binary PSA can also be self-calibrated to remove inaccuracies caused by imperfections in components and workmanship, yielding extremely high measurement accuracies.

Both Jones and Mueller matrix analysis methods can be used to obtain the complete set of polarization related information of a DUT, including PMD (birefringence), PSP (orientation angle of birefringence), PDL (diattentuation), and PDL orientation angle. Other methods, such as the wavelength scanning method, can be used to obtain PMD information only. The system shown in Fig. 1 can be used to implement all of the measurement methods described above, but in this paper, we will concentrate on its use with the Jones and Mueller matrix methods to measure and calculate the complete polarization information of a DUT. We will then validate our measurement system by using it to measure specially made PMD and PDL artifacts and compare the measurement results with the theoretical values of the artifacts. Finally, we will describe the use of this system for other applications, including the measurements of the polarization extinction ratio (PER) of a polarization maintaining (PM) fiber, the stress in a PM connector, and the beat length of a PM fiber.

3. Theoretical background

3.1 Jones Matrix eigenanalysis method (JME)

Obtaining the Jones Transfer Matrix: Generally, the polarization transfer matrix of an optical device under test (DUT) can be described by a 2x2 complex Jones transfer matrix **Γ**, and the input and output polarization states are related by [21]

$$\begin{bmatrix} J_x^{PSA} \\ J_y^{PSA} \end{bmatrix} = c^* \begin{bmatrix} \Gamma_{00} & \Gamma_{01} \\ \Gamma_{10} & 1 \end{bmatrix} \begin{bmatrix} J_x^{PSG} \\ J_y^{PSG} \end{bmatrix}, \quad (1)$$

where J^{PSG} is the normalized Jones vector of the light output generated by the PSG, J^{PSA} is the normalized Jones vector of the light measured by the PSA, and c* is a complex constant related to the absolute amplitude and absolute phase of the light wave. Note that the ratio of $\frac{J_x^{PSA}}{J_y^{PSA}}$ is

$$\frac{J_x^{PSA}}{J_y^{PSA}} = \frac{\Gamma_{00}^J J_x^{PSG} + \Gamma_{01}^J J_y^{PSG}}{\Gamma_{10}^J J_x^{PSG} + J_y^{PSG}} \quad (2)$$

and is independent of the constant c*. If three sets of vectors $\mathbf{J}^{PSG}$ and $\mathbf{J}^{PSA}$ are generated and measured, we can obtain the following equations:

$$\begin{aligned} J_{0,x}^{PSG} J_{0,y}^{PSA} \Gamma_{00}^J + J_{0,y}^{PSG} J_{0,y}^{PSA} \Gamma_{01}^J - J_{0,x}^{PSG} J_{0,x}^{PSA} \Gamma_{10}^J &= J_{0,y}^{PSG} J_{0,x}^{PSA} \\ J_{1,x}^{PSG} J_{1,y}^{PSA} \Gamma_{00}^J + J_{1,y}^{PSG} J_{1,y}^{PSA} \Gamma_{01}^J - J_{1,x}^{PSG} J_{1,x}^{PSA} \Gamma_{10}^J &= J_{1,y}^{PSG} J_{1,x}^{PSA} \\ J_{2,x}^{PSG} J_{2,y}^{PSA} \Gamma_{00}^J + J_{2,y}^{PSG} J_{2,y}^{PSA} \Gamma_{01}^J - J_{2,x}^{PSG} J_{2,x}^{PSA} \Gamma_{10}^J &= J_{2,y}^{PSG} J_{2,x}^{PSA} \end{aligned} \quad (3)$$

Let $k_{i,0} = J_{i,x}^{PSG} J_{i,y}^{PSA}$, $k_{i,1} = J_{i,y}^{PSG} J_{i,y}^{PSA}$, $k_{i,2} = -J_{i,x}^{PSG} J_{i,x}^{PSA}$, and $k_{i,3} = J_{i,y}^{PSG} J_{i,x}^{PSA}$ (i=0,1,2), then Eq. (3) can be simplified to

#123233 - $15.00 USD
Received 25 Jan 2010; accepted 21 Feb 2010; published 16 Mar 2010
(C) 2010 OSA

$$\begin{aligned} k_{00}\Gamma_{00}^J + k_{01}\Gamma_{01}^J + k_{02}\Gamma_{10}^J &= k_{03} \\ k_{10}\Gamma_{00}^J + k_{11}\Gamma_{01}^J + k_{12}\Gamma_{10}^J &= k_{13} \\ k_{20}\Gamma_{00}^J + k_{21}\Gamma_{01}^J + k_{22}\Gamma_{10}^J &= k_{23} \end{aligned}, \quad (4)$$

and the Jones transfer matrix **Γ** of the DUT can be easily calculated using

$$\Gamma_{00} = \frac{\begin{vmatrix} k_{03} & k_{01} & k_{02} \\ k_{13} & k_{11} & k_{12} \\ k_{23} & k_{21} & k_{22} \end{vmatrix}}{\begin{vmatrix} k_{00} & k_{01} & k_{02} \\ k_{10} & k_{11} & k_{12} \\ k_{20} & k_{21} & k_{22} \end{vmatrix}}, \quad \Gamma_{01} = \frac{\begin{vmatrix} k_{00} & k_{03} & k_{02} \\ k_{10} & k_{13} & k_{12} \\ k_{20} & k_{23} & k_{22} \end{vmatrix}}{\begin{vmatrix} k_{00} & k_{01} & k_{02} \\ k_{10} & k_{11} & k_{12} \\ k_{20} & k_{21} & k_{22} \end{vmatrix}}, \quad \Gamma_{10} = \frac{\begin{vmatrix} k_{00} & k_{01} & k_{03} \\ k_{10} & k_{11} & k_{13} \\ k_{20} & k_{21} & k_{23} \end{vmatrix}}{\begin{vmatrix} k_{00} & k_{01} & k_{02} \\ k_{10} & k_{11} & k_{12} \\ k_{20} & k_{21} & k_{22} \end{vmatrix}} \quad (5)$$

It is important to note that in Eqs. (3) to (5), the three polarization states generated by the PSG are not specified in our analysis. Any three non-degenerate SOPs generated by the PSG can be used to obtain the 2x2 complex Jones transfer matrix **Γ.** The lack of restrictions on the SOPs used eliminates the accuracy requirement for the PSG and makes our system less susceptible to variations caused by the wavelength and temperature dependences of the PSG. By comparison, other Jones Matrix analysis implementations [21] require precise polarization state generation at specific points on the Poincaré Sphere (0, 45, and 90 degrees), rendering the measurement system more susceptible to imperfections in the PSG.

Obtaining PDL: For a given optical frequency, the PDL of a DUT can be calculated as [22, 23]:

$$PDL = 10 * \log\left|\frac{r_1}{r_2}\right|, \quad (6)$$

where $r_{1,2} = \frac{m_{11}+m_{22}}{2} \pm \sqrt{(\frac{m_{11}+m_{22}}{2})^2 - m_{11}m_{22} + m_{12}m_{21}}$ are the eigenvalues of the matrix M $=(\mathbf{\Gamma}^{-1})^* \bullet \mathbf{\Gamma} = \begin{bmatrix} m_{11} & m_{12} \\ m_{21} & m_{22} \end{bmatrix}$, $\mathbf{\Gamma}^{-1}$ is the transpose of Jones transfer matrix **Γ,** and the star * indicates the complex conjugate.

Obtaining PMD [21]: For two adjacent optical frequencies, define a matrix:

$$T(\Delta\omega) = \Gamma(\omega_2)\Gamma(\omega_1)^{-1} \quad (7)$$

The complex eigenvectors ρ_s and ρ_f of matrix T(Δω) are the fast and slow principal states of polarization of the DUT, and the differential group delay (**DGD**) τ(ω) can be calculated from

$$\tau(\omega) = |\tau_s - \tau_f| = \left|\frac{Arg(\rho_s/\rho_f)}{\omega_1 - \omega_2}\right|, \quad (8)$$

where

$$\omega = \frac{\omega_1 + \omega_2}{2} \quad (9)$$

and $Arg(\rho_s/\rho_f)$ stands for the phase angle of ρ_s/ρ_f. The wavelength dependent PMD vector $\vec{W}$ can be defined as

#123233 - $15.00 USD
Received 25 Jan 2010; accepted 21 Feb 2010; published 16 Mar 2010
(C) 2010 OSA

$$\vec{W}(\omega) = \tau(\omega)\vec{q}(\omega) \tag{10}$$

where $\vec{q}(\omega)$ is the unit vector of the fast principal state of polarization. The second-order PMD, defined as the frequency derivative of the PMD vector $\vec{W}$, can be calculated as

$$SOPMD = \frac{d\vec{W}(\omega)}{d\omega} = \frac{d\tau(\omega)}{d\omega}\vec{q}(\omega) + \tau(\omega)\frac{d\vec{q}(\omega)}{d\omega} \tag{11}$$

3.2 Mueller matrix measurement method (MMM)

Obtaining the Mueller matrix: Let the Stokes vector of the ith output of the PSG be

$$S_i^{PSG} = \begin{pmatrix} S_{0i}^{PSG} \\ S_{1i}^{PSG} \\ S_{2i}^{PSG} \\ S_{3i}^{PSG} \end{pmatrix}, \tag{12}$$

The corresponding Stokes vectors measured by the PSA after the light passes through the DUT are related to Mueller Matrix M by:

$$S_i^{PSA} = \begin{pmatrix} S_{0i}^{PSA} \\ S_{1i}^{PSA} \\ S_{2i}^{PSA} \\ S_{3i}^{PSA} \end{pmatrix} = \begin{pmatrix} m_{00} & m_{01} & m_{02} & m_{03} \\ m_{10} & m_{11} & m_{12} & m_{13} \\ m_{20} & m_{21} & m_{22} & m_{23} \\ m_{30} & m_{31} & m_{32} & m_{33} \end{pmatrix} \begin{pmatrix} S_{0i}^{PSG} \\ S_{1i}^{PSG} \\ S_{2i}^{PSG} \\ S_{3i}^{PSG} \end{pmatrix} \tag{13}$$

At least 4 non-degenerate SOPs must be generated by the PSG and analyzed by the PSA to completely determine Mueller Matrix M by solving Eq. (13). In such a case, i = 0, 1, 2, 3 in Eqs. (12) and (13). However, for higher accuracies, we require that as many as 6 non-degenerate SOPs be generated by the PSG and analyzed by the PSA, so that i = 0, 1, 2…5. Define a new matrix $\mathbf{S}^{PSA}$ as

$$\begin{aligned} \mathbf{S}^{PSA} &= \begin{pmatrix} S_{00}^{PSA} & S_{01}^{PSA} & S_{02}^{PSA} & S_{03}^{PSA} & S_{04}^{PSA} & S_{05}^{PSA} \\ S_{10}^{PSA} & S_{11}^{PSA} & S_{12}^{PSA} & S_{13}^{PSA} & S_{14}^{PSA} & S_{15}^{PSA} \\ S_{20}^{PSA} & S_{21}^{PSA} & S_{22}^{PSA} & S_{23}^{PSA} & S_{24}^{PSA} & S_{25}^{PSA} \\ S_{30}^{PSA} & S_{31}^{PSA} & S_{32}^{PSA} & S_{33}^{PSA} & S_{34}^{PSA} & S_{35}^{PSA} \end{pmatrix} \\ &= \begin{pmatrix} m_{00} & m_{01} & m_{02} & m_{03} \\ m_{10} & m_{11} & m_{12} & m_{13} \\ m_{20} & m_{21} & m_{22} & m_{23} \\ m_{30} & m_{31} & m_{32} & m_{33} \end{pmatrix} \begin{pmatrix} S_{00}^{PSG} & S_{01}^{PSG} & S_{02}^{PSG} & S_{03}^{PSG} & S_{04}^{PSG} & S_{05}^{PSG} \\ S_{10}^{PSG} & S_{11}^{PSG} & S_{12}^{PSG} & S_{13}^{PSG} & S_{14}^{PSG} & S_{15}^{PSG} \\ S_{20}^{PSG} & S_{21}^{PSG} & S_{22}^{PSG} & S_{23}^{PSG} & S_{24}^{PSG} & S_{25}^{PSG} \\ S_{30}^{PSG} & S_{31}^{PSG} & S_{32}^{PSG} & S_{33}^{PSG} & S_{34}^{PSG} & S_{35}^{PSG} \end{pmatrix} \\ &= \mathrm{M} \bullet \mathrm{S}^{PSG} \end{aligned} \tag{14}$$

Consequently, the Mueller matrix of the DUT can be obtained from

$$\mathrm{M} = \mathrm{S}^{\mathrm{PSA}} \bullet (\mathrm{S}^{\mathrm{PSG}})^{T} \bullet [\mathrm{S}^{\mathrm{PSG}} \bullet (\mathrm{S}^{\mathrm{PSG}})^{T}]^{-1} \tag{15}$$

where $(\mathbf{S}^{\mathrm{PSG}})^{\mathrm{T}}$ is the transpose of matrix $\mathbf{S}^{\mathrm{PSG}}$.

Obtaining PDL: For a given optical frequency, the PDL of a DUT can be obtained [23] from

#123233 - $15.00 USD Received 25 Jan 2010; accepted 21 Feb 2010; published 16 Mar 2010
(C) 2010 OSA

$$PDL = -10\times\log(\frac{P_{Min}}{P_{Max}}) = -10\times\log\frac{m_{00} - \sqrt{m_{01}^2 + m_{02}^2 + m_{03}^2}}{m_{00} + \sqrt{m_{01}^2 + m_{02}^2 + m_{03}^2}} \tag{16}$$

Obtaining PMD: For two adjacent optical frequencies, define a matrix

$$M_{\Delta}(\overline{\omega}) = M(\omega_2)M^{-1}(\omega_1) \tag{17}$$

The complex PMD vector $\vec{W} = \vec{\Omega} + i\vec{\Lambda}$ can be found from the matrix $\mathbf{M}_{\Delta}$ [24], where $\vec{\Omega}$ and $\vec{\Lambda}$ are the real and complex components of $\vec{W}$, respectively. The expression for $\vec{W}$ is rather complicated, so we will obtain the result numerically. The DGD and PSP vectors can be calculated using

$$DGD = \mathrm{Re}(\sqrt{\vec{W} \bullet \vec{W}}) \tag{18}$$

$$q(\omega)_{\pm} = \frac{\pm\vec{\Omega} + \vec{\Omega}\otimes\vec{\Lambda}}{\vec{\Omega}\bullet\vec{\Lambda}} \tag{19}$$

where q_{+} and q_{-} are the unit vectors of the slow and fast PSP, respectively. The symbol "$\otimes$" in Eq. (19) stands for cross product, and "$\bullet$" stands for inner product. As with the case using the JME method, the second order PMD can be calculated numerically using Eq. (11), but with q replaced by q_{-}.

4. PMD and PDL artifacts

To validate the accuracy of our binary polarization measurement technique, PMD and PDL artifacts with precise PMD and PDL values were required. We fabricated such PMD and PDL standards, shown in Fig. 2, with PMD and PDL values defined by quantities that are precisely known, as described below.

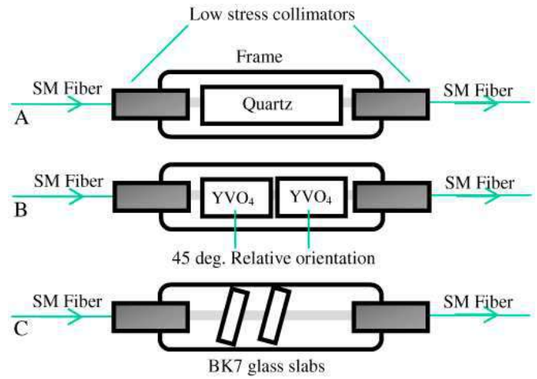

Fig. 2. Schematic design of DGD, SOPMD, and PDL artifacts. (A) Precision wavelength independent DGD artifact. (B) Wavelength independent combined DGD and SOPMD artifact. The birefringence axes of two YVO_4 crystals are oriented 45° from each other. (C) Wavelength independent PDL artifact. Fused silica, BK7 or other types of glass can be used to make the artifact.

4.1 DGD artifacts

1st order PMD (DGD) artifacts were constructed using quartz crystals of precise lengths, whose DGD values can be obtained by:

#123233 - $15.00 USD Received 25 Jan 2010; accepted 21 Feb 2010; published 16 Mar 2010
(C) 2010 OSA

$$DGD = \Delta n_g L / c \tag{20}$$

where L is the length of the quartz crystal, c is the speed of light in vacuum, and Δn_g is the group birefringence defined as:

$$\Delta n_g = \Delta n - \lambda \frac{d\Delta n}{d\lambda} \tag{21}$$

In Eq. (21), Δn is the phase birefringence and λ is the wavelength in vacuum.

Quartz is the most well-known birefringent crystal, with birefringences at different wavelengths precisely known to an accuracy of about 0.25% [25]. In addition, quartz crystals have excellent temperature stability with respect to both dimension and birefringence, with an extremely low temperature coefficient of 1.232x10^{-4}/°C [9, 26] for total retardation. Furthermore, the processes for cutting and polishing quartz crystals are mature, and the dimensional tolerance is better than 10μm. Finally, quartz crystals are environmentally stable and their physical properties are generally not affected by aging. We enclosed a quartz crystal of 20mm length in a 27 x 6 x 6 (mm) stainless steel package, pigtailed using a pair of low-stress fiber collimators, as shown in Fig. 2(A). The collimators are soldered to the stainless steel package using a standard process for making telecom grade fiber optic components with high environmental and long-term stabilities. The use of low-stress fiber collimators is necessary to minimize stress-induced birefringence and its effect on the overall DGD accuracy. As a result, the overall DGD accuracy at 1550nm is better than 2.03 fs within a temperature range of 23±5 °C at all times, as shown in Table 1. This DGD artifact can therefore be used as a "golden" calibration standard for calibrating different PMD measurement instruments.

Table 1. Summary of sources of DGD uncertainty in a quartz DGD artifact*

Uncertainty Source	Uncertainty	Artifact DGD Uncertainty
Δn_g	0.000026 [25]	$\sigma_{\Delta ng}$=1.7fs
Length of quartz crystal	±10μm	σ_L=0.3fs
Temperature of crystal	±5°C	σ_T=0.4fs
Pigtail birefringence	±1fs	$\sigma_{Pigtail}$=1.0fs
Total uncertainty $\sigma_{DGD} = \sqrt{\sigma_{\Delta n_g}^2 + \sigma_L^2 + \sigma_T^2 + \sigma_{Pigtail}^2}$ =2.03fs		

* The artifact is made with a 20mm long quartz crystal with a DGD value of 627.7fs at 1550nm

4.2 SOPMD artifacts

Wavelength independent second order PMD (SOPMD) artifacts were constructed by cascading two birefringent YVO_4 crystals with their birefringent axes oriented 45 degrees from each other, as shown in Fig. 2(B). The SOPMD can be calculated as [27]:

$$SOPMD = \tau_1 \tau_1 \sin(2\theta) \tag{22a}$$

The corresponding DGD is

$$DGD = \sqrt{\tau_1^2 + \tau_1^2 + 2\tau_1 \tau_2 \cos(2\theta)} \tag{22b}$$

where θ is the relative orientation angle between the two crystal sections. Like quartz, YVO_4 is a commonly used birefringent crystal with precisely known birefringences at different wavelengths. However, with a birefringence about 23 times larger than that of a quartz crystal, it is a better choice for making compact SOPMD artifacts with practical SOPMD values. YVO_4 also has reasonable temperature stability with respect to both dimensions and

#123233 - $15.00 USD Received 25 Jan 2010; accepted 21 Feb 2010; published 16 Mar 2010
(C) 2010 OSA

birefringence, with a fairly low thermal optic coefficient (<1x10^{-5}/°C) [28]. Like quartz crystals, YVO_4 crystal elements can be made with a dimensional tolerance better than 10μm and are environmentally stable, with their physical properties unaffected by aging. We used the same packaging materials and process used for the DGD artifacts to assemble and pigtail SOPMD artifacts of different SOPMD values. The relative orientation angle can be readily controlled to within ±1 degree. The resulting accuracy is 0.86 ps^2 for an artifact made by cascading two 16mm YVO_4 crystals (see Table 2); its anticipated DGD and SOPMD values are 16.15ps and 130.2 ps^2, respectively.

Table 2. Summary of sources of uncertainty in a YVO_4 SOPMD artifact*

Uncertainty Source	Uncertainty	Artifact SOPMD Uncertainty
DGD of Crystal 1	0.04ps	σ_{DGD1}=0.46ps^2
DGD of Crystal 2	0.04ps	σ_{DGD2}=0.46ps^2
Temperature (±5°C)	5x10^{-5} /°C	σ_T=0.04ps^2
Pigtail birefringence	0.002ps	$\sigma_{Pigtail}$=0.032ps^2
Relative orientation angle	±1degree	$\sigma_{Orientation}$=0.32ps^2
Total uncertainty $= \sqrt{\sigma_{\Delta DGD1}^2 + \sigma_{\Delta DGD2}^2 + \sigma_T^2 + \sigma_{Pigtail}^2 + \sigma_{Orientation}^2}$ =0.73ps^2		

*The artifact is constructed with two 16mm YVO_4 crystals cascaded with a 45 degree orientation with respect to each other. The anticipated DGD and SOPMD values are 16.15ps and 130.2ps^2, respectively

4.3 PDL artifacts

We also designed and fabricated PDL artifacts using BK7 glass slabs oriented at different angles with respect to the direction of incident light, as shown in Fig. 2(C). Because the transmittances of the p- and s-components are different and are wavelength independent, the transmitted light will have a wavelength independent polarization dependent loss (diattenuation). The transmittance of the p- and s- polarization components at an interface of an optical slab can be readily calculated using Fresnel equations [29]:

$$T_p = \frac{\sin 2\theta_i \sin 2\theta_t}{\sin^2(\theta_i + \theta_t)\cos^2(\theta_i - \theta_t)} \tag{23}$$

$$T_s = \frac{\sin 2\theta_i \sin 2\theta_t}{\sin^2(\theta_i + \theta_t)}, \tag{24}$$

where θ_i and θ_t are the incidence and refraction angles, and are related by Snell's Law: $\sin(\theta_i)/\sin(\theta_t)=n_i/n_t$. The corresponding PDL can be calculated using

$$PDL = \left|10\log(\frac{T_p}{T_s})\right| = -10\log\left[\cos^2(\theta_i - \theta_t)\right] \tag{25}$$

Because each slab has front and rear surfaces, the PDL value of a PDL artifact containing a single slab of BK7 is the summation of the PDL values from both surfaces. Similarly, the PDL value of a PDL artifact made with multiple slabs is the summation of the PDL values of all slabs used in the artifact. We chose BK7 glass [30] for its temperature stability, dimensional stability, and ease of fabrication. In order to minimize the interference of light reflected from the front and rear surfaces, the rear surface is polished at a 0.5° tilt angle with respect to the front surface. Table 3 summarizes the PDL uncertainties caused by different factors. Clearly, the largest uncertainty factor is the incidence angle to the slab.

#123233 - $15.00 USD Received 25 Jan 2010; accepted 21 Feb 2010; published 16 Mar 2010
(C) 2010 OSA

Table 3. Summary of uncertainty sources in a PDL artifact

Uncertainty Source	Uncertainty	Artifact PDL Uncertainty	
		0.4-dB artifact *	2-dB artifact*
Incidence angle tolerance	0.5°	0.013dB	0.050dB
Tolerance of angle between front and rear surfaces	0.1°	0.002dB	0.014dB
Tolerance of index of BK7 slab	<0.001	0.0012dB	0.004dB
Temperature [30]	±5°C ($\Delta n=\pm 1.2\times10^{-5}$)	$<1.6\times10^{-5}$	0.00005dB
Total uncertainty:		**0.013dB**	**0.052dB**

The nominal incidence angles are 33.92° and 62.93°, respectively, for the 0.4-dB and 2-dB artifacts.

As shown in Table 3, the largest contributions to the total uncertainty are caused by the tolerances of the incidence angle and the angle between the slab's two surfaces. These are fixed once the fiber collimators are soldered to the case, as shown in Fig. 2. To counter their effect, we calibrated the artifacts' PDL values using the maximum and minimum search method [31]. Specifically, we searched for the maximum and minimum output powers from an artifact while varying the input polarization. The power difference in dB is the PDL value of the artifact. The calibration results are 0.387±0.005dB for a nominally 0.4-dB artifact and 1.959±0.010dB for a nominally 2-dB artifact. For the calibration, we used a highly stable laser source (Agilent 81640A), a high quality polarization controller with extremely low activation loss (General Photonics Model PCS-4X with activation loss less than 0.005 dB) and a polarization insensitive power meter built with an integrated optical sphere (ILX Lightwave FPM-8210). Once calibrated, the PDL variation due to temperature variation is negligible, as shown in Table 3.

5. Experimental results

5.1 PMD measurement resolution

To characterize the resolution of our measurement system, we measured the PMD value of a piece of single mode fiber. We placed a 2-cm section of the bare fiber in a fiber squeezer (General Photonics' fiber squeezer polarization controller, PLC-003) to induce a small amount of birefringence or PMD in the fiber via the photo-elastic effect, and then measured the PMD value of the fiber as the pressure on the fiber was increased. As shown in Fig. 3(A), as the pressure on the fiber section increases, the SOP traces out a circle on the Poincaré Sphere [32, 33]. A complete circle corresponds to a 2π retardation caused by pressure induced birefringence or, at a wavelength of 1550nm, a DGD of 5.2 fs. Therefore, the pressure induced DGD value can be approximated by counting the SOP revolutions as the pressure on the fiber section is increased using the fiber squeezer. Figure 3(B) shows the DGD as a function of wavelength, measured with the binary system described in Fig. 1 using the Jones Matrix method for two cases: one with no applied pressure and the other with an applied pressure corresponding to a SOP rotation angle of 2π. It is evident that our system can easily distinguish PMD value changes as small as 1 fs. The measured DGD of 0.82fs with no applied pressure is the combination of the DGD of the fiber itself and the noise floor of the measurement system. It can therefore be concluded that the DGD measurement resolution of our measurement system is better than 1 fs. The same resolution is also obtained when the Mueller Matrix method is used. Figure 3(C) shows the pressure induced DGD as a function of SOP rotation angle. The dashed line is the DGD obtained from the SOP rotation angle, while the black dots represent the DGD obtained with our measurement system. The measured DGD shows good agreement with that obtained by SOP angle counting. Again, a measurement resolution of less than 1 fs is clearly demonstrated.

#123233 - $15.00 USD
Received 25 Jan 2010; accepted 21 Feb 2010; published 16 Mar 2010
(C) 2010 OSA

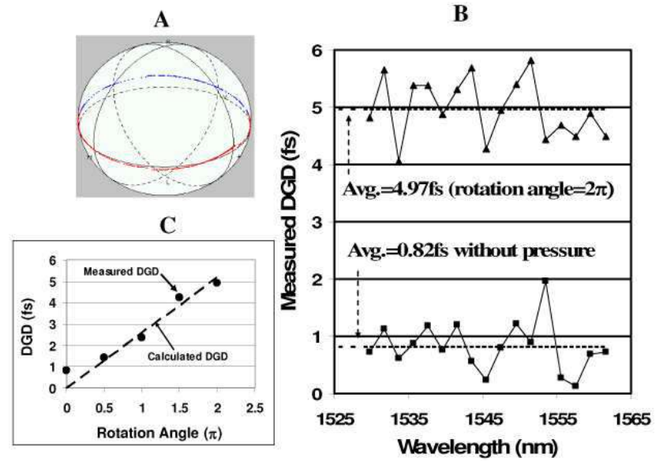

Fig. 3. (A) SOP evolution as the pressure on the fiber is increased. (B) Experimental results illustrating the PMD measurement resolution of the measurement system using binary MO polarization rotators. (C) Pressure induced DGD as a function of SOP evolution angles at 1550 nm. Black dots: DGD obtained with binary measurement system. Dashed line: DGD obtained by SOP angle counting. A PMD measurement resolution of 1 fs is clearly demonstrated in both B and C. In addition, the measurement accuracy is also confirmed by the rotation angle of the SOP: the 5.2 fs DGD corresponds to a total SOP rotation angle of 2π at 1550 nm.

5.2 DGD and SOPMD measurements

We constructed a DGD artifact using a 20 mm long quartz crystal and measured its DGD value using the binary system described in Fig. 1. The DGD value calculated from Eqs. (20) and (21) and birefringence data at 1550 nm from [25] is 627.7fs±2.03 fs (see Table 1). The measured DGD values, averaged over the c-band, using the Jones matrix eigenanalysis (JME) and Mueller matrix measurement (MMM) methods are 627.0 fs and 628.1 fs, respectively. The measured DGD as a function of wavelength is shown in Fig. 4. The wavelength variations of the measured DGD are ± 2.75fs and ±2.93fs, respectively, obtained with the JME and MMM methods. As shown in Fig. 4, our measurement system can resolve SOPMD values as small as 0.001 ps^2. However, since the largest measured SOPMD value is 0.004 ps^2 for a DGD artifact with a theoretical SOPMD value of zero ps^2, we can conservatively conclude that our measurement system has a SOPMD resolution of 0.005 ps^2. This high resolution reflects the excellent repeatability of our binary PSG and the resolution of our binary PSA used in the system.

#123233 - $15.00 USD
Received 25 Jan 2010; accepted 21 Feb 2010; published 16 Mar 2010
(C) 2010 OSA

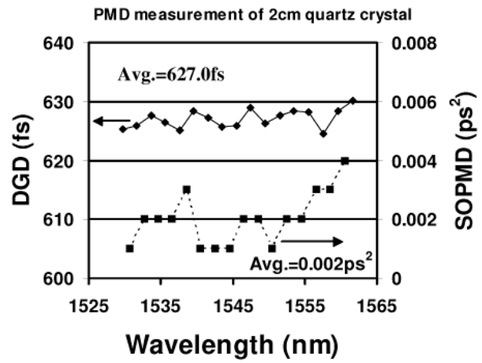

Fig. 4. 1st and 2nd order PMD of a 2-cm quartz crystal DGD artifact (calculated DGD=627.7fs), measured with Jones Matrix Eigenanalysis method using 2 nm wavelength step. Similar results are obtained with MMM method.

We constructed another PMD artifact by cascading two YVO_4 crystals of 16mm length with a 45 degree relative orientation angle, as described in Section 4.2. The DGD values of the two crystals, measured with the binary measurement system described in Fig. 1, are 11.410 ps and 11.416 ps, respectively. The expected DGD and SOPMD values of the PMD artifact are 16.14 ps and 130.2 ps^2, calculated from Eq. (22). As shown in Fig. 5, using the same measurement system, the measured DGD and SOPMD are 16.06 ps and 127.5 ps^2, respectively, using Jones matrix analysis, and 16.07 ps and 130.2 ps^2, respectively, using the Mueller Matrix Method. The corresponding DGD and SOPMD deviations of the measurement from the theoretical DGD and SOPMD values of the artifacts are 0.08 ps and 2.7 ps^2 using the Jones Matrix and 0.07 ps and <0.01 ps^2 using the Mueller Matrix Method. Clearly, the Mueller Matrix Method has a smaller PMD measurement deviation than the Jones Matrix Method for the PMD range tested. In addition, as can be seen in Section 5.4, the Mueller Matrix Method also has better measurement repeatability than the Jones Matrix Method.

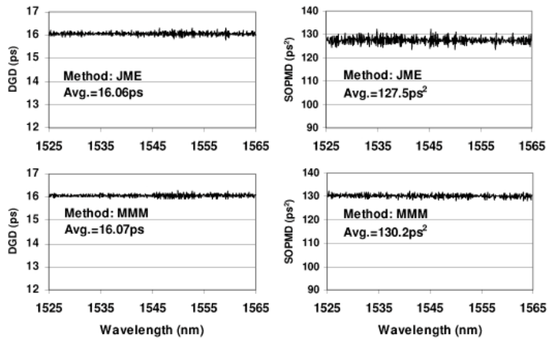

Fig. 5. DGD and SOPMD measurement results for a PMD artifact made from two 16 mm long YVO_4 crystals with a relative orientation angle of 45 degrees. (A) and (B) DGD values vs. wavelength obtained using JME and MMM methods, respectively. (C) and (D) SOPMD values vs. wavelength obtained using JME and MMM methods, respectively.

#123233 - $15.00 USD
Received 25 Jan 2010; accepted 21 Feb 2010; published 16 Mar 2010
(C) 2010 OSA

5.3 PDL measurement

We also constructed two PDL artifacts using the method described in Section 4.3. The calibrated PDL values are 1.959±0.01 dB and 0.387±0.005 dB, respectively, as shown in Section 4.3. Their PDL wavelength dependences, measured using our binary system, are shown in Fig. 6. The average measured PDL values of the two artifacts are 1.964 dB and 0.375 dB, respectively, using the Mueller matrix method, and 2.01dB and 0.416dB, respectively, using the Jones matrix method. As can be seen in Fig. 6, the values measured using the two methods are slightly different, and those measured with the Mueller matrix method show less wavelength variation. As shown in the next section, the Mueller matrix method also has better measurement repeatability. This is because the Mueller matrix method relies on power measurement, while the JME method is based on SOP measurement. As a result, the Mueller matrix method generally has better accuracy and repeatability (as shown in the next section) than the JME method for low PDL measurement because power measurement generally has better accuracy and repeatability than SOP measurement.

As can be seen from Fig. 6, the fluctuations in the measured PDL vs. wavelength values are about ±0.03dB for the Jones matrix method and ±0.005dB for the Mueller matrix method. Theoretically, the artifact's PDL should be wavelength independent. The observed fluctuation is mainly due to system noise and the wavelength dependence of the fiber pigtail's PDL vector, because the total PDL is the vector summation of the PDL of the artifact and its fiber pigtails. Based on these results, the worst-case PDL measurement resolution should be better than 0.01dB for the Mueller matrix method and 0.06dB for the Jones matrix method.

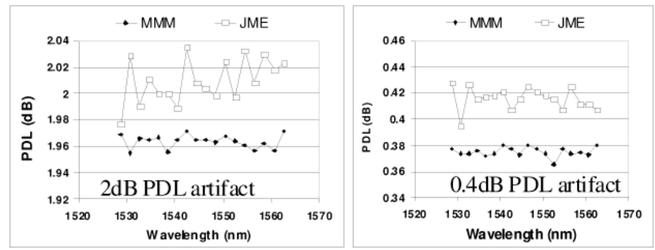

Fig. 6. Measured PDL as a function of wavelength using the JME and MMM methods. (A) PDL vs. wavelength of a "2dB" artifact, and (B) PDL vs. wavelength of a "0.4 dB" artifact. PDL obtained using MMM method has much less wavelength variation than that obtained using JME method.

5.4 Repeatability measurements and Accuracy determination

In order to determine the repeatability of our measurement system, we measured the PMD and PDL artifacts multiple times. The results are listed in Table 4. The Mueller Matrix Method data are shown to have better repeatability and accuracy than the corresponding Jones Matrix Method data; therefore, we will use Mueller Matrix results to determine the accuracy and repeatability of our measurement system. It is evident that our binary measurement system has a remarkable DGD repeatability of 0.022 fs for a 627.7 fs DGD artifact, a SOPMD repeatability of 0.28 ps^2 for a 130.2 ps^2 SOPMD artifact, a PDL repeatability of 0.041dB for a 2-dB PDL artifact, and a PDL repeatability of 0.034dB for a 0.4-dB PDL artifact, measured using the Mueller Matrix Method. Note that the DGD repeatability of our binary system is more than 100 times better than those of commercially available systems on the market [34, 35]. No published repeatability data for SOPMD measurement were found for either research or commercial measurement systems.

B. L. Heffner reported a DGD repeatability of about 0.05 fs for the measurement of an 11.423 fs quartz slab, where the measured DGD was averaged over a 1304 nm to 1540 nm range [36]. However, such a large wavelength range is difficult to obtain for practical use. By

#123233 - $15.00 USD
Received 25 Jan 2010; accepted 21 Feb 2010; published 16 Mar 2010
(C) 2010 OSA

contrast, our DGD repeatability of 0.022 fs for a 627.7 fs artifact was obtained by averaging data only from 1528nm to 1563nm, a wavelength range well within the tuning range of a commercially available tunable laser.

Note that the total PDL vector of a device under test is the vector summation of the PDL vectors of all components in the measurement setup, including connectors, fiber pigtails, and the DUT itself. The positions of the fiber pigtails determine the relative orientation of the PDL vectors involved, and hence affect the total PDL values. During measurement, we arranged the fiber pigtails of the PDL artifacts in different positions to account for PDL variation caused by the residual PDL values of the fiber pigtails and connectors. The measurement results therefore include these residual PDL contributions.

As discussed in Section 4, the 2-cm quartz DGD artifact has a "standard" DGD value of 627.7±2.03 fs (see Table 1). The worst deviations between the measured and standard DGD values are –0.70 fs and 0.41 fs, measured using JME and MMM, respectively. These deviations are well within the uncertainty range of the DGD artifact. Therefore, the absolute DGD measurement accuracies are determined to be better than |2.03fs|+|–0.68fs|+|0.39fs|=3.1fs for the JME method, and |2.03fs|+|0.41fs|+|0.19fs|=2.6fs for the MMM method, where 0.39 fs and 0.19 fs are the DGD measurement repeatabilities of our system when JME and MMM analysis methods, respectively, are used, as shown in Table 4. Note that the largest contribution to the inaccuracy is not from our measurement system itself, but from the artifact's DGD value uncertainty (2.03 fs). A much higher measurement accuracy might be claimed if an artifact with a much tighter DGD value tolerance were available. Nevertheless, it is also important to point out that the DGD measurement accuracy of our measurement system is more than 10 times better than those of commercial PMD measurement systems on the market [34].

In order to verify the measurement uniformity of our measurement method, we measured the same DGD artifact using three identical measurement systems built according to the design shown in Fig. 1, using three different PSG-PSA pairs and three different tunable lasers. The measured DGD values are 628.1 fs, 627.7 fs and 629.0 fs. The spread is well within the artifact's DGD range of 627.7 ±2.03fs.

The SOPMD artifact has a "standard" SOPMD value of 130.3±0.73 ps^2 (see Table 2). The worst measured result deviates by –2.01ps^2 and 0.38 ps^2 from the standard value when JME and MMM analysis methods, respectively, are used. Consequently, the worst-case absolute accuracy for SOPMD measurement using our system can be estimated to be |0.73 ps^2|+|–2.01 ps^2|+|1.35 ps^2|=4.18ps^2 using the JME method, and |0.73 ps^2|+|0.38 ps^2|+|0.28 ps^2|=1.39ps^2 using the MMM method, where 1.35 ps^2 and 0.28 ps^2 are the corresponding measurement repeatabilities of the two methods, as shown in Table 4. To the best of the authors' knowledge, this SOPMD measurement accuracy of 1.39 ps^2 represents the highest reported SOPMD accuracy to date.

Accuracy estimations similar to those described above for DGD and SOPMD yield a PDL measurement accuracy better than 0.223dB (JME) and 0.074dB (MMM) for the 2-dB PDL artifact, and 0.17dB (JME) and 0.06dB (MMM) for the 0.4-dB artifact.

As previously pointed out, our system generally has better accuracy and repeatability using the MMM method; therefore, we will use MMM analysis method results to determine the performance of our measurement system. We therefore conclude that our binary measurement system has DGD, SOPMD, and PDL accuracies of 2.6 fs, 1.39 ps^2, and 0.06 dB, respectively.

#123233 - $15.00 USD
Received 25 Jan 2010; accepted 21 Feb 2010; published 16 Mar 2010
(C) 2010 OSA

Table 4. Statistical results of 50 measurements

	Artifacts	Average	Maximum	Minimum	Max.–Min.
2-cm quartz DGD artifact (JME)	Average DGD in the wavelength range of 1530nm~1560nm with a λ step size of 2nm	627.02fs	627.033fs	627.000fs	0.033fs
	@1550nm with a λ step size of 2nm	627.757fs	627.955fs	627.567fs	0.388fs
2cm quartz DGD artifact (MMM)	Average DGD in the wavelength range of 1530nm~1560nm with a λ step size of 2nm	628.111fs	628.108fs	628.107fs	0.022fs
	@1550nm with a λ step size of 2nm	627.663fs	627.700s	627.511fs	0.189fs
SOPMD artifact (JME)	Average SOPMD in the range of 1550nm ~1552nm with a λ step size of 0.1nm	128.43 ps^2	129.64 ps^2	128.29 ps^2	1.35 ps^2
	SOPMD @ 1550nm with a λ step size of 0.1nm	129.31 ps^2	132.01 ps^2	126.70 ps^2	5.31 ps^2
SOPMD artifact (MMM)	Average SOPMD in the wavelength range of 1550nm~1552nm with a λ step size of 0.1nm	130.07ps^2	130.20 ps^2	129.92 ps^2	0.28 ps^2
	SOPMD @ 1550nm with a λ step size of 0.1nm	129.95 ps^2	131.40 ps^2	128.27 ps^2	3.13 ps^2
2-dB PDL artifact (JME)	Measured at 1550nm with different fiber pigtail positions	1.963	2.04dB	1.91dB	0.13dB
2-dB PDL artifact (MMM)	Measured at 1550nm with different fiber pigtail positions	1.965dB	1.982dB	1.941dB	0.041dB
0.4-dB PDL artifact (JME)	Measured at 1550nm with different fiber pigtail positions	0.389	0.437dB	0.326dB	0.11dB
0.4-dB PDL artifact (MMM)	Measured at 1550nm with different fiber pigtail positions	0.377dB	0.395dB	0.361dB	0.034 dB

5.5 PM fiber PER [37–39] and connector stress measurements

To minimize polarization dependent effects, it is often desirable to maintain a constant state of polarization as light propagates through an optical system. With regard to such systems, polarization extinction ratio (PER), or polarization crosstalk, is a measure of the degree to which the light is confined in the principal polarization mode. It is defined as the ratio of the power in the principal polarization mode to the power in the orthogonal polarization mode after propagation through the system, expressed in dB.

Polarization maintaining (PM) optical fibers have an optical (slow) axis defined by a strong linear birefringence. If light input to an ideal PM fiber is polarized along the fiber's optical axis, the state of polarization (SOP) will be maintained during propagation through the fiber. However, if the input light's SOP is misaligned, or the light is not fully polarized, the polarization component in the slow axis will propagate at a different speed from the polarization component aligned to the fast axis. Therefore, there will be a relative phase difference between the two polarization components. The resulting SOP at the exit of the fiber will change when the relative phase changes. For the case of a linearly polarized light beam

#123233 - $15.00 USD
Received 25 Jan 2010; accepted 21 Feb 2010; published 16 Mar 2010
(C) 2010 OSA

launched into a PM fiber with a misalignment angle of θ from the fiber's slow axis, as shown in Fig. 7, the extinction ratio due to the misalignment can be calculated as

$$PER = -10\log(\tan^2\theta) \tag{26}$$

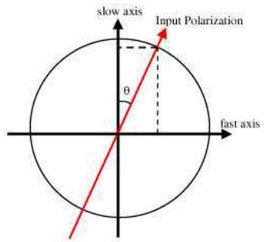

Fig. 7. A representation of linearly polarized light misaligned by an angle θ from the slow axis of a PM fiber

The PSA in the measurement system shown in Fig. 1 can be used to precisely measure the PER. If the slow axis of a PM fiber is aligned to the reference plane of the PSA at the PSA entrance, the normalized SOP can be calculated as

$$\begin{pmatrix} \cos 2\theta \\ \sin 2\theta\cos\delta \\ \sin 2\theta\sin\delta \end{pmatrix} \tag{27}$$

where θ and δ are the misalignment angle and the phase difference between the slow and fast axes, respectively. Variations in the input wavelength or in the fiber length due to temperature changes or mechanical stress will cause a variation in the relative phase δ, which in turn will cause the SOP to rotate about axis (1,0,0) on the Poincaré sphere when the relative phase δ is changed.

If the slow axis is misaligned to the PSA's reference plane by an angle 2ψ, the measured normalized polarization state can be expressed as:

$$\begin{pmatrix} \cos 2\psi\cos 2\theta - \sin 2\psi\sin 2\theta\cos\delta \\ \sin 2\psi\cos 2\theta + \cos 2\psi\sin 2\theta\cos\delta \\ \sin 2\theta\sin\delta \end{pmatrix} \tag{28}$$

It can be shown that the output SOP rotates about the slow axis (cos2ψ, sin2ψ, 0) to trace out a circle as δ increases or decreases, as illustrated in Fig. 8. Note that changes in wavelength, fiber length, or temperature will cause δ to change. The radius of the circle can be calculated to be R=sin2θ, and the PER can be calculated as

$$PER = -10\log\left(\frac{\sin^2\theta}{\cos^2\theta}\right) = -10\log\left(\frac{1-\cos 2\theta}{1+\cos 2\theta}\right) = -10\log\left(\frac{1-\sqrt{1-R^2}}{1+\sqrt{1-R^2}}\right) \tag{29}$$

#123233 - $15.00 USD
Received 25 Jan 2010; accepted 21 Feb 2010; published 16 Mar 2010
(C) 2010 OSA

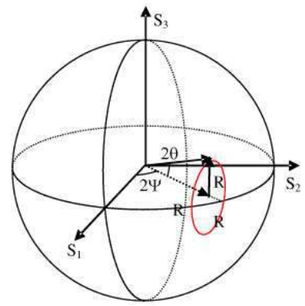

Fig. 8. Poincaré Sphere illustration of polarization state rotation of output light from a PM fiber due to wavelength variation or to thermal or mechanical stress

Essentially, the PER measured by our system, defined in Eq. (29), indicates the degree of linear polarization of light inside the PM fiber, or how well the input linear polarization is aligned with the slow (or fast) axis of the PM fiber. For a perfect polarization alignment, R approaches 0 (the circle collapses to a point), and the corresponding PER approaches infinity. At the other extreme, if the light power is equally split between the fast and slow axes, R approaches 1 (the SOP traces a great circle on the circumference of the Poincaré Sphere) and the corresponding PER approaches 0.

In our measurement system, because light output from the PM fiber is directly coupled into the PSA via free space, there is no alteration of the SOP before the light is analyzed. Consequently, the rotation axis of the circle is in the plane of the Poincaré sphere's equator and the angle Ψ is the angle between the slow axis and the reference plane of the PSA, as shown in Fig. 8. The PSA adapter has a reference key slot to accept a keyed PM fiber connector. Because the key slot is perpendicular to the PSA's reference plane, the angle between the slow axis of the PM fiber and the connector key is therefore 90-Ψ degrees. For example, Ψ=90° (the circle rotates around S_2 in Fig. 8) means that the slow axis of the PM fiber is vertical and aligned to the alignment key direction, and Ψ=0° indicates that the slow axis of the PM fiber is horizontal and perpendicular to the alignment key direction.

In practical measurement, the center of the circle generally deviates from the plane of the equator. This deviation is caused by stress induced birefringence and/or other polarization altering effects caused by the connector. The effect is equivalent to that of a PM fiber followed by a waveplate. Generally speaking, a greater deviation from the equator indicates a higher stress level. Such a measurement capability is very useful for PM fiber connectorization, because it can reveal information about whether an epoxy or a curing process used for the connectorization induces enough stress on the fiber to cause degradation of the polarization extinction ratio. The final degraded PER can be measured with a standard PER meter made with a rotating linear polarizer [37].

Figure 9 shows PER measurement results for two PM fibers with FC/PC connectors. The effect of stress is clearly shown in one of the PM connectors. In Fig. 9(A), the SOP evolution circle is centered on the equator, indicating negligible stress on the output fiber tip caused by connectorization. Consequently, the difference in PER values measured with our system and with a rotating polarizer is negligible. By contrast, in Fig. 9(B), the center of the SOP evolution circle is displaced from the equator, indicating a relatively large stress on the fiber. The stress induced birefringence of the output fiber tip can therefore be expected to degrade the output polarization extinction ratio. Indeed, the PER of the light after the output fiber connector is reduced to 31.1 dB measured with a rotating polarizer, although the PER of the light inside the fiber is as high as 39.6 dB measured with our measurement system.

In conclusion, by observing the size and position of the SOP evolution circle on the Poincaré Sphere, one can readily distinguish the PER degradation of a PM fiber caused by input SOP misalignment (size of the circle) from that caused by connectorization induced

#123233 - $15.00 USD
Received 25 Jan 2010; accepted 21 Feb 2010; published 16 Mar 2010
(C) 2010 OSA

stress (deviation of the circle from the equator). Such a capability is a useful tool for determining the quality of PM fiber connectorization by identifying stress induced birefringence.

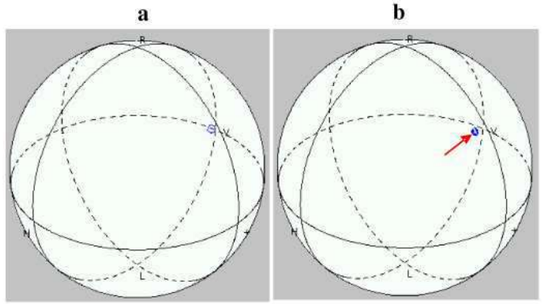

Fig. 9. PER measurement results: (A) PER measurement result with low stress on output FC/PC connector. (B) PER measurement result with relatively high stress on output FC/PC connector. The corresponding PER of light in the PM fiber is 39.6 dB; however, the PER of the output light is reduced to 31.1 dB due to stress induced birefringence. The deviation of the SOP evolution circle from the equator can be used to indicate stress induced birefringence at the exit end of the PM fiber.

5.6 PM fiber beat length estimation and results

Beat length is important because it measures how well a fiber maintains polarization. It is a measure of how fast the two orthogonal modes become decoupled and thus cease to exchange energy. Fibers with short beat lengths preserve polarization more strongly than those with long beat lengths.

Beat length L_B is defined by the ratio of the wavelength of the transmitted light λ to the fiber's phase birefringence Δn [40, 41],

$$L_B = \frac{\lambda}{\Delta n} \tag{30}$$

The beat length of PM fiber can be estimated by measuring its differential group delay (DGD) [40, 41]. The DGD measured by our measurement system is related to the group birefringence Δn_g by

$$DGD = \Delta n_g L / c \tag{31}$$

and the group birefringence is related to the phase birefringence by

$$\Delta n_g = \Delta n - \lambda \frac{d\Delta n}{d\lambda}. \tag{32}$$

The beat length can be calculated from the measured DGD by

$$L_B = \frac{\lambda}{\frac{DGD * c}{L} + \lambda \frac{d\Delta n}{d\lambda}} \tag{33}$$

If the chromatic dispersion equation of a fiber is

$$n^2 = 1 + \frac{B_1\lambda^2}{\lambda^2 - C_1} + \frac{B_2\lambda^2}{\lambda^2 - C_2} + \frac{B_3\lambda^2}{\lambda^2 - C_3}, \tag{34}$$

#123233 - $15.00 USD
Received 25 Jan 2010; accepted 21 Feb 2010; published 16 Mar 2010
(C) 2010 OSA

the beat length can be calculated from

$$L_B = \frac{\lambda * y}{\frac{DGD * c}{L}} \tag{35}$$

where

$$y = 1 - \frac{1}{n}\left[n^2 - 1 - \left(\frac{B_1\lambda^4}{(\lambda^2 - C_1)^2} + \frac{B_2\lambda^4}{(\lambda^2 - C_2)^2} + \frac{B_3\lambda^4}{(\lambda^2 - C_3)^2}\right)\right] \tag{36}$$

We measured the beat length of a 1.16m Panda PM fiber and obtained a DGD of 1.578ps. The corresponding beat length from Eq. (36) is 3.86mm, consistent with the manufacturer's specified value of 3~5mm [42].

For a PM fiber with $DGD_{\lambda 2} \approx DGD_{\lambda 1}$, the beat length at λ_2 can be estimated by using the beat length measurement result at λ_1:

$$L_{B\lambda_2} = \frac{\lambda_2}{\lambda_1} L_{B\lambda_1} \tag{37}$$

For example, if we measure the DGD and beat length L_{B1550} of a PM fiber at 1550 nm, its beat length L_{B1310} at 1310 nm is simply $L_{B1310}=(1310/1550)L_{B1550}=0.845L_{B1550}$.

6 Summary

In summary, we describe a novel polarization measurement system consisting of a binary MO polarization state generator (PSG), a binary MO polarization state analyzer, a tunable laser, and a personal computer. Because of its binary nature, the system can be easily calibrated against imperfections in the optical components used in the system, caused by wavelength and environmental variations. Consequently, we have achieved the unprecedented PMD measurement sensitivity or resolution of 1 fs, PMD measurement accuracy of 2.6 fs, PMD measurement repeatability of 0.022 fs, SOPMD resolution of 0.005 ps^2, SOPMD accuracy of 1.39 ps^2, SOPMD repeatability of 0.28 ps^2, PDL resolution of 0.01 dB, PDL accuracy of 0.06 dB, and PDL repeatability of 0.034 dB. We also describe and demonstrate some other interesting applications of the system, including PER measurement, PM fiber connector stress analysis, and PM fiber beat length measurement. This extremely accurate polarization measurement system will find a wide range of applications in optical component characterization, optical fiber link characterization, PM fiber connectorization, and PM fiber characterization.

Acknowledgements

We thank Lynn Lin, Heming Zhang, and Qing Wan of General Photonics Corporation for mechanical, electronics and software designs used in this paper. We also thank Susan Wey for the proof-reading of the manuscript. This work was supported by a research funding of General Photonics Corporation.

#123233 - $15.00 USD
Received 25 Jan 2010; accepted 21 Feb 2010; published 16 Mar 2010
(C) 2010 OSA

Highly Repeatable All Solid-State Polarization State Generator

X. Steve Yao

Optical Polarization Research Center, Tianjin University, Tianjin, China, and General Photonics Corporation, 5228 Edison Avenue, Chino, California 91710

Lianshan Yan and Yongqiang Shi

General Photonics Corporation, 5228 Edison Avenue, Chino, California 91710

Received December 14, 2004

We report an all solid-state polarization-state generator that uses magneto-optic polarization rotators. The device can generate either five or six distinctive polarization states uniformly across a Poincaré sphere with repeatability better than 0.1°. It is ideal for polarization analysis, swept-wavelength measurement, and monitoring of polarization-related parameters and signal-to-noise ratios of optical networks. © 2005 Optical Society of America

OCIS codes: 120.5410, 080.2730, 060.2300, 260.5430.

Generating at least four distinctive polarization states across a Poincaré sphere with high repeatability, such as at 0°, ±45°, and 90° and right-hand circular (RHC) and left-hand circular (LHC), is important for analyzing polarization properties of light-wave components or systems by use of the Mueller matrix method.[1,2] The information obtained from such analyses can be used to measure other parameters, such as birefringence, polarization mode dispersion, polarization-dependent loss, degree of polarization, signal-to-noise (SNR), and state of polarization (SOP).[3–6] Such a polarization-state generator (PSG) can be constructed from rotating quarter-wave (λ/4) and half-wave plates.[1] However, owing to its mechanical nature, such a device generally has the disadvantages of slowness, short lifetime, low repeatability, and high cost. A PSG that uses ferroelectric liquid crystals has been reported[4,7]; however, its temperature stability and reliability are concerns for production and field deployment in telecommunication systems. We report what is to our knowledge the first PSG that uses magneto-optic (MO) crystals. For a given wavelength, the device can generate highly repeatable polarization states at 0°, ±45°, and 90° and LHC and RHC across a Poincaré sphere. The measured repeatability is better than 0.1° on the Poincaré sphere. Other advantages of the device are its predictable wavelength and temperature dependence, with typical tolerances of −0.067°/nm and 0.1°/C, respectively. The fiber-to-fiber insertion loss of the device is less than 0.9 dB, and its return loss is better than 55 dB. The same device can also be used as a Mueller matrix polarization analyzer.

As shown in Fig. 1, the five-state PSG consists of an optional polarizer, two pairs (four pieces) of MO rotators, and a λ/4 plate. The polarizer is placed at the input end of the device, and the λ/4 plate is sandwiched between the first and the second pairs of MO rotators. The optional polarizer is used for aligning the input SOP with respect to the optical axis (*c* axis) of the λ/4 plate. The polarizer can be aligned with, orthogonal to, or 45° from the *c* axis of the λ/4 plate or at other predetermined angles.

Our MO rotator has the following attractive properties: When a positive magnetic field is applied above a saturation field, the rotator rotates the SOP by a precise angle near 22.5°. When a negative magnetic field is applied beyond saturation, the rotator rotates the SOP by a precise angle near −22.5°. Therefore, when both rotators in each pair rotate in the same direction, the net rotation is +45° or −45°. If the two rotators rotate in opposite directions, however, the net SOP rotation is zero. Assuming that the polarizer is aligned with the *c* axis of the λ/4 plate, the following SOPs can be generated (referenced with respect to the polarizer direction):

(1) A linear SOP at 0° when the rotators in both pairs rotate in opposite directions.
(2) A linear SOP at +45° when the rotators in the first pair rotate in opposite directions but the rotators in the second pair both rotate +22.5°.
(3) A linear SOP at −45°, when the rotators in the first pair rotate in opposite directions but the rotators in the second pair both rotate −22.5°.
(4) RHC, when the rotators in the first pair both rotate 22.5°.
(5) LHC, when the rotators in the first pair both rotate −22.5°.

Note that there are 16 SOP combinations of 4 bits; however, only five states are distinctive and the rest are degenerate. For applications for which only linear

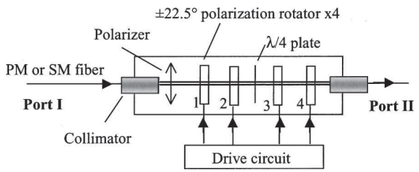

Fig. 1. Schematic of a five-state PSG. For a six-state PSG, two more MO rotators (5 and 6) are added after rotator 4.

0146-9592/05/111324-3/$15.00 © 2005 Optical Society of America

Table 1. Six Typical Combinations of MO Switches and Generated Output Polarization States[a]

Rotator						
R1	R2	R3	R4	R5	R6	SOP
+	−	+	−	+	−	0° linear
+	−	+	−	+	+	45°
+	−	+	−	−	−	−45°
+	−	+	+	+	+	90°
+	+	+	+	+	+	RHC
−	−	−	−	−	−	LHC

[a] + and −, −22.5° and −22.5°, respectively.

SOPs are required, the λ/4 plate can be removed. The device can then generate four linear SOPs, oriented at 0, ±45°, and 90°.

For Mueller matrix calculations, only four distinctive SOPs are required. However, some applications may require six distinctive SOPs for better calibration accuracy. To generate six such polarization states we added another MO rotator pair to the device (after the second pair) to produce additional +45° and −45° rotations. Note that this 6-bit device (with six binary MO switches) can theoretically generate 64 states; however, only six states are nondegenerate. Table 1 lists six typical combinations of this 6-bit device to generate six distinctive SOPs [0° linear, +45° linear, −45° linear, ±90° linear (degenerate), RHC, and LHC]. In the table, R1 stands for rotator 1 and + and − stand for +22.5° and −22.5°, respectively.

We fabricated multiple five- and six-state PSGs and measured their performance with the experimental setup shown in Fig. 2. Using an Agilent 8509C polarization analyzer, we carefully measured the SOPs generated on the Poincaré sphere that corresponded to each activation combination, and the results are shown in Figs. 3(a) and 3(b) for five- and six-state devices, respectively. Points A–E in Fig. 3(a) clearly show five distinctive SOPs generated by the five-state PSG; A is ~LHC, C is ~RHC, D is ~0° linear, B is ~−45° linear, and E is ~45° linear. During the measurement we used the polarization controller in Fig. 2 to align the SOPs with the major axes of the Poincaré sphere. The traces connecting the points show the transient SOP paths when the SOPs are switched from one SOP to another.

Similarly, points A–F in Fig. 3(b) are six distinctive SOPs generated by the six-state PSG. Assuming that a PSG is made with ideal components, many of the bit combinations will produce the same SOP, resulting in so-called degeneracy. However, in practice, because of imperfections of the components used, these supposed degeneracy states are slightly off center and produce a cluster of SOPs in the vicinity of the targeted SOP. This is why we see multiple traces of similar orientation, but with some deviation, passing through each targeted SOP. When we use the device we simply select six bit combinations to generate six consistent SOPs. For example, the bit combinations that correspond to the six SOPs shown in Fig. 3(b) are (010001), (001101), (011101), (011100), (011111), and (111011).

We also measured the wavelength dependence of the devices, and the result is shown in Fig. 4. The vertical axis corresponds to the solid angle between two SOPs separated by ~90° on the Poincaré sphere (~45° of physical rotation). As shown in Fig. 4, a measured solid angle has a linear dependence on wavelength, with a slope of −0.134°/nm. Therefore the physical rotation angle dependence is ~−0.067°/nm. We also found that the wavelength dependence is different for different polarization states.

Note that, for Mueller matrix polarization analysis, the inaccuracies of generated polarization states with respect to the targeted polarization states (0°, +45°, −45°, 90°, RHC, and LHC), such as that caused by wavelength dependence, can be calibrated out in calculations.

SOP repeatability is in fact a more important specification for Mueller matrix analysis because it generally involves taking a reference measurement and device-under-test measurements. The repeatability of the generated SOPs between the reference

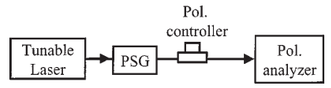

Fig. 2. Measurement setup for characterization of PSGs: Pol., polarization.

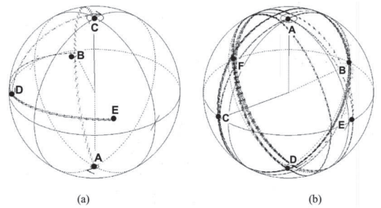

Fig. 3. Poincaré sphere illustration of SOPs generated by the PSG measured with an Agilent 8509C polarization analyzer. SOPs generated by (a) a five-state PSG (b) a six-state PSG.

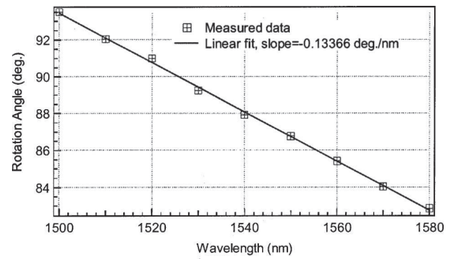

Fig. 4. Wavelength dependence of the polarization rotation angle of the six-state PSG measured on a Poincaré sphere. The physical rotation angle is one-half that measured on the sphere.

measurement and the device-under-test measurements directly affects the accuracy of the resultant Mueller matrix analysis.

Figure 5(a) shows the measured SOP repeatability between polarization states A and B on a Poincaré sphere with 100 samples. As can be seen, the two states (two end points in the figure) are exactly repeatable, with no observable differences. It is interesting to note that the switching traces from A to B and from B to A are highly repeatable as well. However, they are not exactly the same and are interwoven. This trace nonreciprocal property does not affect the performance of the device in any way; however, its cause is still under investigation.

We also evaluated the SOP repeatability of all six states in Fig. 3(b) by repeatedly switching among the states 100 times and measuring the corresponding Stokes parameters of each state. The excellent repeatability of the Stokes parameters of a polarization state is shown in Fig. 5(b). All other five states show the same high repeatability. The solid angles between the states were also calculated for each corresponding sample point, and a typical result is shown in Fig. 5(c), illustrating a high repeatability. The measured solid angle repeatability is better than 0.1°, limited by the accuracy of the measurement system.

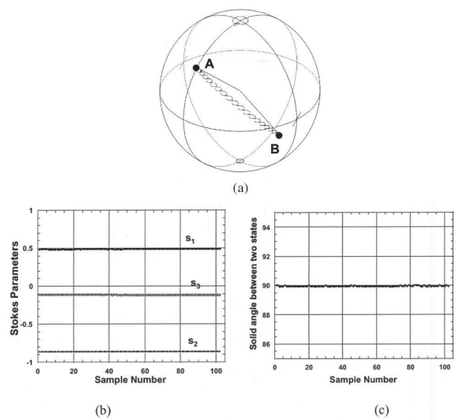

Fig. 5. Repeatability measurement of a six-state PSG [100 samples were taken for each of (a)–(c)]. (a) Poincaré sphere illustration of the repeatability when the device was switched between two polarization states. (b) Stokes parameters illustration of repeatability as a function of sample points. (c) Solid angle illustration of repeatability as a function of sample points. All the measurements show the excellent repeatability of the generated SOPs.

The device may find many applications ranging from polarization analysis to monitoring of network performance, material birefringence, and measurement of polarization mode dispersion, swept-wavelength measurement, medical imaging (e.g., polarization-resolved coherent topology measurement[8–10]), and fiber sensor systems. In particular, the PSG described in Fig. 1 can be used as a polarization analyzer if it is used in reverse order, that is, to input an optical signal from port II into Fig. 1 and detect the signal from port I. Thus two identical devices can be used (i.e., one as a PSG and the other as polarization-state analyzer) to measure or monitor the corresponding properties or perturbation of optical medium. Notably, owing to its high speed and high repeatability, if a spectrum-disperse device, such as a grating or a wavelength-division demultiplexer, is connected to port I, the device can simultaneously analyze multiple wavelength channels in parallel to characterize or monitor various parameters, such as state and degree of polarization as well as polarization mode dispersion and polarization-dependent loss of devices under test.

We thank Lynn Lin for the mechanical design and Jane Chen for assembly of the device. X. S. Yao's e-mail address is syao@generalphotonics.com.

References

1. R. A. Chipman, in *Handbook of Optics*, 2nd ed., M. Bass, ed. (McGraw-Hill, New York, 1995), Vol. II, Chap. 22.
2. D. H. Goldstein and R. A. Chipman, J. Opt. Soc. Am. A **1**, 693 (1990).
3. A. E. Willner, S. M. R. Motaghian Nezam, L.-S. Yan, Z. Pan, and M. C. Hauer, J. Lightwave Technol. **22**, 106 (2004).
4. R. M. Craig, S. L. Gilbert, and P. D. Hale, J. Lightwave Technol. **16**, 1285 (1998).
5. A. Zadok, N. Simon, and A. Eyal, J. Lightwave Technol. **22**, 1533 (2004).
6. M. Petersson, H. Sunnerud, M. Karlsson, and B. E. Olsson, IEEE Photonics Technol. Lett. **16**, 686 (2004).
7. W. Xiang and A. M. Weiner, in *Digest of the LEOS Summer Topical Meetings* (Institute of Electrical and Electronics Engineers, Piscataway, N.J., 2003), p. WB2.4/67.
8. B. H. Park, M. C. Pierce, B. Cense, and J. F. de Boer, Opt. Lett. **29**, 2512 (2004).
9. W. Urbanczyk, Opt. Acta **33**, 53 (1986).
10. A. M. Baldwin, J. R. Chung, J. S. Baba, C. H. Spiegelman, M. S. Amoss, and G. L. Cote, in *Proceedings of the 25th Annual International Conference of the IEEE* (Institute of Electrical and Electronics Engineers, Piscataway, N.J., 2003), Vol. 2, p. 1027.

Self-calibrating Binary Polarization Analyzer

X. Steve Yao

Optical Polarization Research Center, Tianjin University, Tianjin, China, and General Photonics Corporation, 5228 Edison Avenue, Chino, California 91710

Xiaojun Chen and Lianshan Yan

General Photonics Corporation, 5228 Edison Avenue, Chino, California 91710

Received February 13, 2006; accepted April 7, 2006; posted April 24, 2006 (Doc. ID 68011)

We report a self-calibrating polarization analyzer fabricated with binary magneto-optic polarization rotators. The device automatically overcomes wavelength and temperature dependent inaccuracies and has impressive state of polarization and degree of polarization accuracies of 0.3° and ±0.5%, respectively, from 1460 to 1580 nm. © 2006 Optical Society of America

OCIS codes: 120.5410, 080.2730, 060.2300, 260.5430.

Accurate optical polarization analysis for various applications has been an active topic of research for the past 30 years.[1–7] In a previous publication,[8] we reported a magneto-optic (MO) polarization-state generator (PSG) for generating 5 or 6 distinctive polarization-states across the Poincaré sphere with a high repeatability of better than 0.1°. We pointed out in Refs. 8 and 9 that the same device can also function as a polarization-state analyzer (PSA). In this Letter, we describe in detail the operation of such a polarization analyzer and show that it is highly accurate due to the binary high repeatability of the MO crystals. To overcome the wavelength and temperature dependences of the optical components used inside the device, we developed a self-calibrating methodology to automatically extract the effects of wavelength and temperature variations on measurement accuracy. With the device, we achieved a remarkable degree of polarization (DOP) accuracy of ±0.5%, a state of polarization (SOP) accuracy of better than 1.3%, and angular accuracy and resolution of 0.3° and 0.02°, respectively, from 1460 to 1580 nm. This binary MO PSA has the attractive features of low cost, compact size, high repeatability, no moving parts, no wavelength and temperature dependence, and no need for calibration. The device is ideal for low-cost and high-accuracy polarization analysis, system signal-to-noise ratio monitoring,[9] and accurate measurements of polarization mode dispersion, polarization-dependent loss,[3] birefringence, and material properties of thin films[5,10] when paired with a PSG as described in Ref. 8.

The binary MO PSA is composed of nine or seven functional components: a quarter-wave plate (QWP), two MO rotators before the QWP, four or two MO rotators after the QWP, a polarizer P, and a photodetector, as shown in Fig. 1.

Our MO rotators have the following attractive binary properties[8]: a highly repeatable SOP rotation angle around 22.5° or −22.5° can be obtained with each rotator by applying either a positive or negative magnetic field above a saturation field. Therefore, when two rotators rotate in the same direction, the net rotation is +45° or −45°. On the other hand, if the two rotators rotate in the opposite direction, the net SOP rotation is zero.

The output power of the PSA can be calculated by multiplying the Mueller matrices of all components in Fig. 1:

$$\begin{aligned} I_{\text{out}}(\alpha,\beta) = 0.5 \times \{S_0 + [&\cos 2\alpha \cos 2(\beta - \theta_p) \\ &- \sin 2\alpha \sin 2(\beta - \theta_p)\cos\Gamma]\, S_1 \\ &- [\sin 2\alpha \cos 2(\beta - \theta_p) + \cos 2\alpha \sin 2(\beta \\ &- \theta_p)\cos\Gamma]\, S_2 - [\sin 2(\beta - \theta_p)\sin\Gamma] S_3\}, \end{aligned} \tag{1}$$

where θ_p is the relative orientation angle between the QWP and the polarizer, $\Gamma(\lambda)$ is the retardation of the QWP, (S_0, S_1, S_2, S_3) are the Stokes parameters of the input SOP, α is the net rotation angle of the two MO rotators before the QWP, and β is the net rotation angle of the MO rotators after the QWP. α, β can be expressed as

$$\alpha = \sum_{n=1}^{2} -(-1)^{bn}\theta, \quad \beta = \sum_{n=3}^{6} -(-1)^{bn}\theta, \tag{2}$$

where

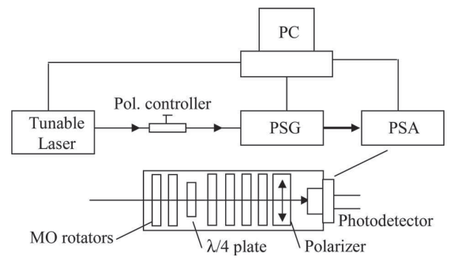

Fig. 1. Schematic of a binary MO PSA and experiment setup. Light exits a PSG and enters a PSA in free space. A high-accuracy reference PSA is put in the place of the PSA under test for comparison.

0146-9592/06/131948-3/$15.00 © 2006 Optical Society of America

Table 1. α, β and Logic States of a 6-bit PSA

I_i	α	β	DLS	I_i	α	β	DLS
I_1	-2θ	-4θ	1	I_9	2θ	0	1
I_2	0	-4θ	2	I_{10}	-2θ	2θ	6
I_3	2θ	-4θ	3	I_{11}	0	2θ	6
I_4	-2θ	-2θ	4	I_{12}	2θ	2θ	6
I_5	0	-2θ	4	I_{13}	-2θ	4θ	1
I_6	2θ	-2θ	4	I_{14}	0	4θ	2
I_7	-2θ	0	3	I_{15}	2θ	4θ	3
I_8	0	0	5				

$$\theta = 22.5 + \Delta\theta_0 + k(\lambda - \lambda_0) \tag{3}$$

is the rotation angle of each MO rotator when a magnetic field above saturation is applied, and b_n is 1 or 0 to represent the binary operation of each MO rotator (θ or $-\theta$ rotation, respectively). In deriving Eqs. (2) and (3), we have assumed that all MO rotators are identical (with the same $\Delta\theta_0$, k, and λ_0) and that each rotator has the same rotation angle in both directions. It should be pointed out that $\Delta\theta_0$, k, and λ_0 are functions of temperature in general.

Because each MO rotator is binary with two rotation angles, I_{out} has 64 possible values for each input SOP for a device with a total of 6 MO rotators and 16 possible values for a device with 4 MO rotators in general. Assuming that the rotators are identical and the rotation angles in both directions are the same, one can readily conclude by inspecting Fig. 1 or Eq. (2) that α only has three possible values $(0, 2\theta, -2\theta)$ and that β has only five possible values $(0, 2\theta, 4\theta, -2\theta, -4\theta)$ for devices with 6 MO rotators (4 rotators after the QWP). Therefore, I_{out} in Eq. (1) has only $3 \times 5 = 15$ different values, as shown in Table 1. The rest are degenerate. Similarly, β has three possible values $(0, 2\theta, -2\theta)$ for devices with a total of 4 MO rotators (2 after the QWP) and I_{out} has $3 \times 3 = 9$ different values.

Further degeneracy occurs when the MO rotators, the QWP, and the polarizers are perfect, i.e., $\theta = 22.5°$, $\Gamma = \pi/2$, and $\theta_p = 90°$. In this case, I_{out} has only 6 different values for a device with 6 rotators and 5 different values for a device with 4 rotators. Therefore, out of the 15 logic states in Table 1, there are only 6 nondegenerate states for a perfect 6-bit PSA. Even in a nonperfect situation, these 6 states are more distinctive from one another than the rest, which are nearly degenerate. We call these 6 states distinctive logic states (DLSs). Similarly, there are only 5 DLSs for a 4-bit PSA.

Assuming that all the parameters in Eq. (1), namely, θ_p, Γ, $\Delta\theta_0$, k, and λ_0, are known, the output of PSA for the ith logic state can be rewritten as

$$I_i = (M_{i0}\ M_{i1}\ M_{i2}\ M_{i4})(S_0 S_1 S_2 S_3)^T \ (i = 1, 2, \ldots 2^N), \tag{4}$$

where N is the total number of rotators and M_{i0}, M_{i1}, M_{i2}, and M_{i3} can be obtained from Eq. (1) for all MO rotation combinations. For calculating four Stokes parameters of the input light, at least four different equations are required. Therefore, by measuring four output powers (I_a, I_b, I_c, I_d) of four nondegenerate logic states, one obtains

$$\begin{pmatrix} I_a \\ I_b \\ I_c \\ I_d \end{pmatrix} = \begin{pmatrix} 0.5 & M_{a1} & M_{a2} & M_{a3} \\ 0.5 & M_{b1} & M_{b2} & M_{b3} \\ 0.5 & M_{c1} & M_{c2} & M_{c3} \\ 0.5 & M_{d1} & M_{d2} & M_{d3} \end{pmatrix} \begin{pmatrix} S_0 \\ S_1 \\ S_2 \\ S_3 \end{pmatrix} = \mathbf{M} \begin{pmatrix} S_0 \\ S_1 \\ S_2 \\ S_3 \end{pmatrix}. \tag{5}$$

The four Stokes parameters can therefore be obtained by the reverse transform of Eq. (5), and the corresponding DOP can be calculated using

$$\text{DOP} = \sqrt{S_1^2 + S_2^2 + S_3^2}/S_0.$$

The four powers can be selected from the 15 nondegenerate logic states listed in Table 1. For calculation accuracies, the four equations chosen should be as distinctive as possible and therefore should be chosen from the powers of the 6 distinctive logic states defined previously.

The Mueller matrix method described above requires the parameters of all the components inside a PSA to be known at all wavelengths and all temperatures. However, it is extremely time consuming to measure the wavelength and temperature dependences of all the components. Even if the wavelength and temperature dependences are known, it is often difficult to know the exact wavelength and temperature during measurements. To overcome these difficulties, we describe below a self-calibrating methodology to automatically extract the effects of wavelength and temperature variations on measurement accuracy. One may rewrite Eq. (1) as

$$I_i = f[S_0, S_1, S_2, S_3, \alpha_i, \beta_i, \Delta\Gamma(\lambda),\ \theta_p], \tag{6}$$

where $i = 1, 2, \ldots 2^N$, N is the total amount of rotators in the PSA, and I_i is the output power of PSA for the ith logic states. In practice, we have 15 nondegenerate equations available for the calculation of a 6-bit PSA and 9 for a 4-bit PSA. Rotation angles α and β, Stokes parameters (S_0, S_1, S_2, S_3) of input light, $\Delta\Gamma(\lambda)$ of the QWP, and θ_p of the polarizer can be calculated simultaneously by numerically solving Eq. (6), without the need of knowing wavelength and temperature. This is the basic concept of self-calibration. A method of solving Eq. (6) is basically to numerically search for the optimized values of S_0, S_1, S_2, S_3, $\Delta\theta_0(\lambda, T)$, $\Delta\Gamma(\lambda, T)$, $k(T)$, and θ_p to make $\Sigma_j (f_j - I_j)^2$ minimum. Note that one should not use only the distinctive states for the calculation because the slight nondegeneracy of the other states actually contains the information on the deviation caused by wavelength and temperature dependences. Using this method, one can obtain not only the Stokes parameters of the input light but also all the component parameters. In fact, the component parameters obtained at different wavelength and temperature can then be used in Mueller matrix method.

We evaluated the performance of multiple PSAs with the experimental setup in Fig. 1. A PSG as described in Ref. 8 was used to generate 6 distinctive

SOPs at different wavelengths and a PSA under test obtains the corresponding Stokes parameters. The results are then compared with those obtained with a commercial high-performance reference PSA, which replaces our PSA in Fig. 1.

The top row and bottom left part of Fig. 2 show some typical measurement results of an input SOP using the self-calibration method, and the bottom right part shows the obtained wavelength dependences of the rotation angle deviation (from 22.5°) of the MO rotators and the retardation Γ of the QWP. The polarizer angle θ_p obtained is 90.38°. Note that θ, Γ, and θ_p are the averages of six measurements using six distinctive input SOPs (LVP, LHP, L−45, L+45, RCP, and LCP). Curve fitting in Fig. 2(d) yields all the parameters in Eq. (3) for the MO rotators: $k = -0.035$/nm and $\Delta\theta_0 = -1.359°$. (λ_0 is set at 1550 nm.) In the bottom right part a small relative alignment error between the PSA and the reference PSA was removed.

The relative SOP error can be obtained by comparing the results with those of the commercial reference PSA using $\sigma = [(S_1' - S_1)^2 + (S_2' - S_2)^2 + (S_3' - S_3)^2]^{1/2}$, where S_i' are the Stokes parameters measured using the reference PSA. The DOP accuracies can be obtained by comparing the measurement results with unity because a high extinction ratio

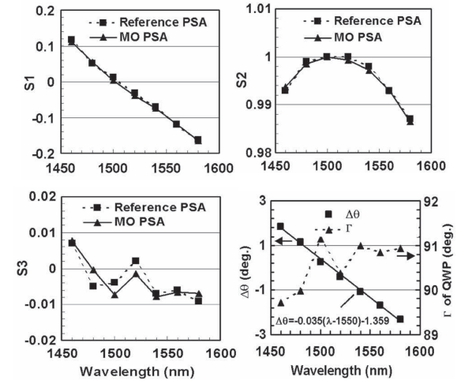

Fig. 2. Experimental results of measured Stokes parameters as a function of wavelength compared with a reference PSA (top left and right, bottom left). The input SOP generated by the PSG is nominally at 45°, linear with a certain wavelength dependence. Bottom right, wavelength dependence of the MO rotators and the QWP inside the PSA, obtained simultaneously using the self-calibration method.

Table 2. Comparison with a Reference PSA (1500–1580 nm)

Method	Self-cal.	Mueller
Max. SOP error	1.3%	1.5%
Max. DOP error	±0.35%	±0.65%
DOP standard deviation	0.28%	0.4%

Table 3. Accuracy Measurements with a Polarizer (1460–1580 nm)

	6-bit		4-bit
Method	Self-cal.	Mueller	Self-cal.
Angle resolution	0.02°	>0.02°	0.02°
Max. angle error	0.30°	0.27°	0.34°
Standard deviation (SDTV) of angle	0.12°	0.09°	0.12°
Max. DOP error	±0.5%	±0.75%	±1.0%
DOP average	0.999	0.999	1.003
DOP STDV	0.37%	0.46%	0.58%

(>50 dB) polarizer was placed at the input of the PSG to ensure the DOP of the input light 100%. With both the self-calibration and the Mueller matrix methods (after the component parameters are obtained using the self-calibration method), we characterized multiple 6-bit PSA units at different wavelengths from 1460 to 1580 nm. As shown in Table 2 and Fig. 2, the measurement accuracy remains the same despite the strong wavelength dependences of MO rotation angle θ and QWP retardation Γ.

Note that the measurement errors presented in Table 2 actually include the contributions of PSG fluctuation and the inaccuracy of the reference PSA. To remove these additional uncertainties, we used a polarizer on a precision rotation stage to replace the PSG. Because the input SOP to the PSA is set by the polarizer and is known, the absolute PSA accuracy can be evaluated. As shown in Table 3, the 6-bit PSA has an angular resolution and accuracy of 0.02° and 0.3°, respectively. The DOP accuracy is better than ±0.5% using the self-calibration method. As can be seen, the 6-bit PSA is more accurate than a 4-bit PSA. We took 50 to 100 measurements per SOP state and found that the device has a remarkable repeatability of SOP and DOP of less than 0.3%.

X. S. Yao's e-mail address is syao@generalphotonics.com.

References

1. R. A. Chipman, in *Handbook of Optics*, Vol. II, 2nd ed., M. Bass, ed. (McGraw-Hill, 1995), Chap. 22.
2. D. H. Goldstein and R. A. Chipman, J. Opt. Soc. Am. A **7**, 693 (1990).
3. P. A. Williams, Appl. Opt. **38**, 6508 (1999).
4. R. Azzam, Opt. Lett. **1**, 181 (1977).
5. E. Compain, S. Poirier, and B. Drevillon, Appl. Opt., **38**, 3490 (1999).
6. A. De Martino, Y. K. Kim, E. Garcia-Caurel, B. Laude, and B. Drevillon, Opt. Lett. **28**, 616 (2003).
7. S. X. Wang and A. Weiner, Opt. Lett. **29**, 923 (2004).
8. X. S. Yao, L. S. Yan, and Y. Q. Shi, Opt. Lett. **30**, 1324 (2005).
9. L. S. Yan, X. S. Yao, C. Yu, Y. Wang, L. Lin, Z. Chen, and A. E. Willner, IEEE Photon. Technol. Lett. **18**, 643 (2006).
10. D. Goldstein, in *Polarized Light*, 2nd ed. (Marcel Dekker, 2003), Chap. 22.

A novel scheme for achieving quasi-uniform rate polarization scrambling at 752 krad/s

Leon Yao,[1,*] Hao Huang,[1] James Chen,[2] Ernie Tan,[2] and Alan Willner[1]

[1]*Department of Electrical Engineering, University of Southern California, Los Angeles, California 90089, USA*
[2]*General Photonics Corporation, Chino CA 91710, USA*
[*]*leonxyao@gmail.com*

Abstract: We propose and demonstrate a novel scheme for obtaining quasi-uniform rate polarization scrambling at up to 752 krad/s in fiber optic systems by using cascaded multiple fiber squeezers with each one placed in a certain orientation. Additionally, this polarization scrambler is compatible with both single-polarization and polarization-multiplexing systems. We also show that scrambled SOP with this scheme uniformly covers the whole Poincare Sphere and that the scrambling rates are mostly concentrated towards the high end of the rate distribution histogram. Such a scrambling scheme is advantageous for the deterministic characterization of performances for modern fiber optic transceivers, especially those deploying coherent detection techniques, against rapid polarization variations.

©2012 Optical Society of America

OCIS codes: (060.0060) Fiber optics and optical communications; (060.2340) Fiber optics components; (060.1660) Coherent communications.

References and links

1. M. G. Taylor, "Coherent detection method using DSP for demodulation of signal and subsequent equalization of propagation impairments," IEEE Photon. Technol. Lett. **16**(2), 674–676 (2004).
2. F. Derr, "Coherent optical QPSK intradyne system: concept and digital receiver realization," J. Lightwave Technol. **10**(9), 1290–1296 (1992).
3. E. Ip, A. P. Lau, D. J. Barros, and J. M. Kahn, "Coherent detection in optical fiber systems," Opt. Express **16**(2), 753–791 (2008).
4. J. Zyskind, R. Barry, G. Pendock, M. Cahill, and J. Ranka, "High-capacity, ultra-long haul networks," Ch. 5, in *Optical Fiber Telecommunication IVB, Systems and Impairments*, eds. I. Kaminow and T. Li (Academic Press, San Diego, 2002).
5. H. Kogelnik, R. Jopson, and L. Nelson, "Polarization mode-dispersion," in *Optical Fiber Telecommunication IVB, Systems and Impairments*, eds. I. Kaminow and T. Li, (Academic Press, San Diego, 2002) chap. 15.
6. P. M. Krummrich and K. Kotten, "Extremely fast (microsecond scale) polarization changes in high speed long hail WDM transmission systems," in Proc. OFC 2004, paper FI3.
7. D. L. Peterson, P. J. Leo, and K. B. Rochford, "Field measurements of state of polarization and PMD from a tier-1 carrier," Proc. OFC 2004, paper FI1.
8. M. Boroditsky, M. Brodsky, N. J. Frigo, P. Magill, and H. Rosenfeldt, "Polarization dynamics in installed fiber optic systems," Proc. LEOS 2005, paper TuCC1.
9. P. J. Leo, G. R. Gray, G. J. Simer, and K. B. Rochford, "State of polarization changes: classification and measurement," J. Lightwave Technol. **21**(10), 2189–2193 (2003).
10. P. M. Krummrich, E.-D. Schmidt, W. Weiershausen, and A. Mattheus, "Field trial on statistics of fast polarization changes in long haul WDM transmission systems," in Proc. OFC 2005, paper OThT6.
11. L. Yan, Q. Yu, and A. E. Willner, "Uniformly distributed states of polarization on the Poincare Sphere using an improved polarization scrambling scheme," Opt. Commun. **249**(1-3), 43–50 (2005).
12. Y. K. Lize, R. Gomma, R. Kashyap, L. Palmer, and A. E. Willner, "Fast all-fiber polarization scrambling using re-entrant Lefevre controller," Opt. Commun. **279**(1), 50–52 (2007).
13. B. Koch, R. Noé, V. Mirvoda, and D. Sandel, "100-krad/s endless polarisation tracking with miniaturised module card," Electron. Lett. **47**(14), 813–814 (2011).
14. http://www.novoptel.de/Scrambling/EPS1000_flyer.pdf
15. A. Hidayat, B. Koch, H. Zhang, V. Mirvoda, M. Lichtinger, D. Sandel, and R. Noé, "High-speed endless optical polarization stabilization using calibrated waveplates and field-programmable gate array-based digital controller," Opt. Express **16**(23), 18984–18991 (2008).
16. S. Yao, "Polarization in fiber systems: squeezing out more bandwidth," in *The Photonics Handbook* (Laurin Publishing, Pittsfield, MA 2004).
17. R. Noe, H. Heidrich, and D. Hoffmann, "Endless polarization control systems for coherent optics," J. Lightwave Technol. **6**(7), 1199–1208 (1988).
18. W. H. J. Aarts and G. Khoe, "New endless polarization control method using three fiber squeezers," J. Lightwave Technol. **7**(7), 1033–1043 (1989).
19. E. Collett, *Polarized Light in Fiber Optics* (PolaWave Group, Lincroft, New Jersey, 2003).
20. A. M. Smith, "Single-mode fibre pressure sensitivity," Electron. Lett. **16**(20), 773–774 (1980).
21. M. Martinelli, P. Martelli, and S. M. Pietralunga, "Polarization stabilization in optical communications Systems," J. Lightwave Technol. **24**(11), 4172–4183 (2006).
22. http://www.generalphotonics.com/pdf/FAQPolariteII.pdf

1. Introduction

As the appetite for bandwidth continues to sky rocket, polarization multiplex and coherent detection [1–3] are being used for increasing the transmission speed to reach 100 Gbit/s and beyond. As a result, polarization issues, i.e., time-varying polarization mode dispersion (PMD), polarization dependent loss (PDL), and state of polarization (SOP) become increasingly critical for an optical fiber communication system [4, 5]. Therefore, performance tests of a system against these polarization-related parameters are extremely important for assuring the healthy operation of high speed fiber optic communication systems. As such, a polarization scrambling device for changing SOP at an adjustable rate to reach all possible SOP is required to test the performance of the systems against rapid SOP variations. It has been reported that SOP changing rate in a real fiber optic system can be as high as 280 krad/s [6]. Therefore for testing the performance of coherent detection systems, a polarization scrambling scheme must be able to generate SOP changes faster than this rate. On the other hand, for the deterministic test of the polarization response of coherent receivers, a uniform rate polarization scrambling is desired, because non-uniform rate polarization scrambling introduces large test uncertainty and less test repeatability.

Present adjustable-rate polarization scramblers are generally made with different types of polarization controllers and are programmed so that SOP traces uniformly cover the whole Poincare Sphere. Some polarization scramblers are made with a SOP changing rate following Rayleigh Distribution [7], mainly for emulating SOP variations in a real fiber optic transmission system for statistical system testing [8–10]. Other scramblers are made to change SOP as fast and randomly as possible for mitigating polarization related transmission impairments, with unspecified scrambling rate distributions [11, 12]. Some literatures suggested that polarization scramblers using $LiNbO_3$ based rotating wave plate approach can simultaneously satisfy both the uniform rate and high scrambling speed requirements, up to 10 Mrad/s [13, 14], however no detailed discussion on rate distribution was reported. In addition, it is preferable to find an alternative technology to $LiNbO_3$ waveguide [15] for fast scrambling applications to avoid the disadvantages of high cost, high insertion loss, high PDL associated with $LiNbO_3$ approach.

In this paper, we propose and demonstrate a novel scheme to uniformly scramble polarization at a quasi-uniform rate using multiple variable phase retarders, such as fiber squeezers [16–19], with low cost, low insertion loss, and low PDL. To overcome the speed limitation of the fiber squeezers, we additionally propose and demonstrate an approach to effectively multiply the scrambling rate by cascading multiple fiber squeezers in series. Finally, by combining the quasi-uniform rate scheme with the rate multiplication method, we achieve polarization scrambling at an adjustable quasi-uniform rate of up to 752 krad/s. The method is polarization insensitive, wavelength insensitive, and scalable to even higher scrambling rates by adding more squeezers. Such a polarization scrambling scheme is attractive for testing the performance of coherent detection systems and coherent receivers against rapid polarization variations.

2. Concept and principle of operation

2.1 Device construction

Polarization scrambling is generally realized by programming a polarization controller with a certain control algorithm such that the output SOP changes with time and distributed

uniformly over the whole Poincare Sphere. Although high-cost $LiNbO_3$ waveguide based polarization controller [15] has the advantage of high speed, in this paper, we concentrate on using low-cost fiber squeezers [16–19] to realize polarization scrambling with adequate speed and uniform rate for testing the performance of coherent receivers.

The propose polarization scrambler and the experimental demonstration setup is shown in Fig. 1, where multiple fiber squeezers are cascaded in series. Each squeezer is driven by an amplified electrical control signal. The first three fiber squeezers are oriented 45 degrees from one another, and the last three fiber squeezers have the same orientation as the third squeezer for overcoming the speed limitation of the fiber squeezers, as will be explained below.

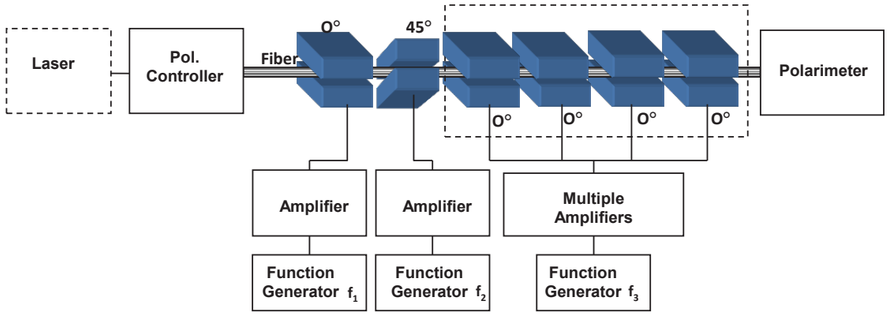

Fig. 1. Fiber squeezer arrangement and experiment setup for demonstrating different scrambling approaches. The first three fiber squeezers are oriented 45 degrees from one another and the last three are oriented the same as the third squeezer. The polarization controller in front of the fiber squeezers is for adjusting the input SOP into the fiber squeezers, and the polarimeter is for observing SOP changes on a Poincare Sphere.

2.2 Simulation program

In order to quickly verify the feasibility of new polarization scrambling ideas and learn how different parameters affect scrambling, it is necessary to simulate how SOP varies when a specific scrambling scheme is applied to the fiber squeezers in Fig. 1. We developed a Labview based simulation program to calculate SOP variations caused by N fiber squeezers of different orientations when they are driven by N electrical signals of different waveform, frequencies, and amplitude, and display SOP traces on Poincare Sphere. In addition, the program can calculate the SOP variation rate and plot the rate distribution histogram. Moreover, the time or point averaged DOP can also be obtained with the program to reflect SOP coverage uniformity of a particular scrambling scheme [11].

In the simulation program, the i^{th} fiber squeezer wave plate is represented by a Mueller Matrix [19]:

$$M_i = \begin{pmatrix} 1 & 0 & 0 & 0 \\ 0 & \cos 4\theta_i \sin^2\phi_i/2 + \cos^2\phi_i/2 & \sin 4\theta_i \sin^2\phi_i/2 & 0 \\ 0 & \sin 4\theta_i \sin^2\phi_i/2 & -\cos 4\theta_i \sin^2\phi_i/2 + \cos^2\phi_i/2 & -\cos 2\theta_i \sin\phi_i \\ 0 & 0 & \cos 2\theta_i \sin\phi_i & \cos\phi_i \end{pmatrix} \quad (1)$$

where θ_i is the orientation angle and ϕ_i is the retardation of the fiber squeezer. The Stokes vector S_i of the output SOP from the i^{th} fiber squeezer is obtained by multiplying its Muller matrix M_i with the previous Stokes vector S_{i-1}:

$$S_i = M_i S_{i-1} \quad (2)$$

The SOP variation rate is obtained by first calculating the angle between two consecutive points $\vec{S}_m$ and $\vec{S}_n$ on the SOP trace using:

$$\cos\theta_{mn} = \vec{S}_m \bullet \vec{S}_n / |S_m||S_n|, \quad (3)$$

where $\vec{S}_m \bullet \vec{S}_n$ is the dot product of the two SOP vectors; and dividing the angle by the time interval between the two points. The rate distribution can be obtained by calculating all the rates between two adjacent SOP points and displaying them on a histogram.

Finally, the averaged DOP of the scrambled polarization can be calculated using

$$< DOP >= \sqrt{< S_1 >^2 + < S_2 >^2 + < S_3 >^2} / S_o \quad (4)$$

where < > denotes for either time or point average. With this simulation program, we can easily analyze scrambling schemes with different combinations of driving frequencies and determine which scheme has the required SOP coverage uniformity and scrambling rate distribution.

2.3 SOP changes induced by fiber squeezers

The retardation of each fiber squeezer is varied linearly by applying a driving voltage to the piezo-electric actuator on the fiber squeezer [20]. As the retardation is varied from 0 to 2π, the output SOP from the fiber squeezer traces out a complete circle on the Poincare Sphere [17–19]. The radius of the circle depends on the angle between the input SOP with respect to birefringence axis of the variable phase plate, i.e., 45 degree angle results in the largest circle on the Sphere while a small or large angle produces small SOP changes and hence small radius, as shown in Fig. 2. In addition, for a given retardation variation of the fiber squeezer, the SOP variation rate is proportional to the radius of curvature of the SOP trace. The largest radius of curvature produces the largest rate of SOP variation for a given retardation variation.

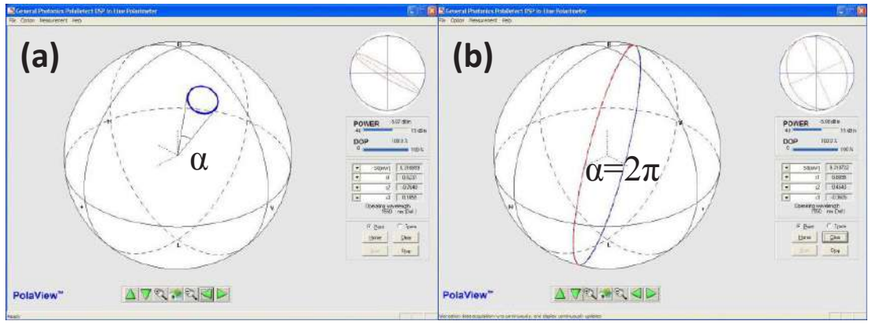

Fig. 2. (a) When SOP traces out a small circle on Poincare Sphere, the SOP variation angle α is small (a small fraction of 2π) and so is the SOP changing rate; (b) when SOP trace out a great circle on Poincare Sphere, corresponding to the case that input SOP to the wave plate is 45 degree from its birefringence axis, the angular change per circle reaches its largest value of 2π. The corresponding SOP changing rate is also maximized. In general, for a given retardation variation, the smaller the radius of curvature of the SOP trace, the smaller the rate of SOP variation.

Two circular traces generated by two adjacent fiber squeezers with a relative orientation of 45 degrees are orthogonal from each other. It can be shown that at least three fiber squeezers are required to generate SOPs to cover the whole Poincare Sphere from any input SOP [17–19]. To program the fiber squeezers for effective polarization scrambling, four parameters on the driving signals can be selected: waveform, frequency, amplitude, and phase. The most

important considerations of a polarization scrambling scheme include: 1) SOP coverage uniformity, 2) maximum scrambling rate, and 3) scrambling rate distribution.

3. Experimental results

SOP coverage uniformity describes how uniform SOPs are distributed on Poincare Sphere after a certain time, and is generally characterized by observing SOP distribution on Poincare Sphere and average DOP over time or over SOP points [6]. The point-averaged degree of polarization (DOP) is a good indicator for uniform SOP coverage, i.e., the smaller the averaged DOP, the better the SOP uniformity is. In particular, if the scrambled SOP can reach the entire sphere with equal probability, the averaged DOP will be zero.

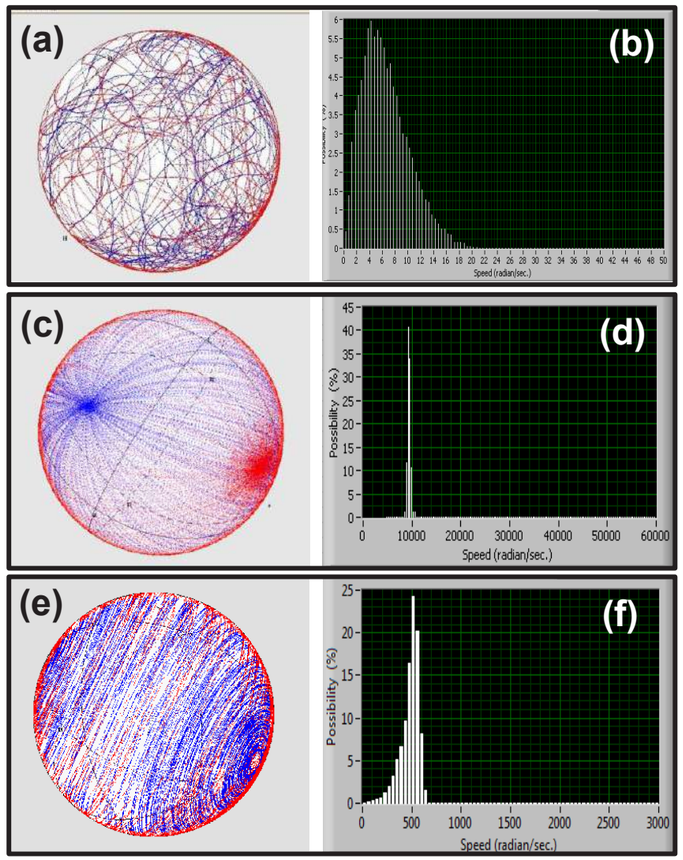

Fig. 3. (a) Illustration of random SOP variation of a conventional scrambling scheme; (b) The corresponding SOP variation rate histogram following Rayleigh distribution; (c) Measured SOP trace of the uniform rate scrambling approach, where the trace evolves like a circle spinning around a diametric axis; (d) Polarization scrambling rate histogram showing a single scrambling rate; (e) Measured SOP trace of the quasi-uniform rate scrambling approach. SOP rotates around Poincare Sphere at a high speed to form a circle, which moves back and forth along the rotation axis of the circles to cover the whole sphere. (f) Polarization scrambling rate histogram showing a quasi-uniform scrambling rate.

INSTRUMENTS
MODULES
PASSIVE COMPONENTS
ACCESSORIES
APPLICATION GUIDE
FAQS

3.1 Conventional polarization scrambling

Conventional polarization scramblers make the SOP trace move randomly on Poincare Sphere with time and covers the whole sphere uniformly, as shown in Fig. 3(a). However, because of the randomly varying trace, the corresponding radius of curvature of the SOP trace also changes randomly, resulting in a wide spread of SOP variation rates, as shown in Fig. 3(b). As mentioned previously, such a wide rate distribution is not desirable for testing the polarization response of a system due to the lack of repeatability.

3.2 Uniform rate scrambling

One simple method to achieve uniform rate polarization scrambling is only using the first two fiber squeezers in Fig. 1. The input SOP has to be aligned to 45 degrees from the first fiber squeezer. Both the first and the second squeezers are modulated by a triangle wave with an amplitude of $2V_\pi$ (2π phase retardation). However, the frequency of the driving signal on the first squeezer (f_1) is much higher than that on the second (f_2). In this way, the first squeezer causes the SOP go around the Poincare Sphere in a great circle at a high speed, while the second squeezer rotates the great circle in one of its diametric axis, as shown in Fig. 3(c), to cover the whole sphere completely and uniformly (a video showing the SOP evolution during the scrambling can be seen at http://www.youtube.com/watch?v=SIdA2en4-lc). In the experiment, the two driving frequencies are f_1 = 180 Hz and f_2 = 1.1459 Hz. The scrambling rate using this approach is uniform, as shown in Fig. 3(d), because SOP always moves around the great circles of equal radius. The small rate spread is cause by limited sampling point in the polarimeter. The measured 10000- point averaged DOP is about 6.8%, indicating a uniform SOP coverage over entire Poincare Sphere is achieved. The non-zero DOP is obtained here due to the high sensitivity to the input polarization as it is difficult to align the input SOP at perfect 45 degrees from the first fiber squeezer. Even low DOP is expected to be achieved with a better alignment of the input SOP. The experimental results in Fig. 3(c) and Fig. 3(d) also agree with the simulation results by using our Labview program under the same driving conditions.

Although the uniform rate polarization scrambling can be achieved, this method requires that the SOP of the input optical signal has to maintain 45 degree with the first fiber squeezer. However, the SOP in a real fiber system is not stationary and varies with time. Therefore, in order to keep the SOP input to the first fiber squeezer at 45 degrees, a polarization stabilizer must be used. As we know that a polarization stabilizer generally uses a polarizer or polarization beam splitter to derive a feedback signal for polarization stabilization [15, 17, 18, 21]) and therefore only one polarization state is supported. This not only adds cost, but also causes problems with polarization multiplexed signals in most coherent systems.

3.3 Quasi-uniform rate scrambling

In order to overcome the problems described above, we propose a new method of polarization scrambling with a nearly uniform rate. The new scheme requires at least three variable phase retarders oriented 45 degrees from one another, as shown in Fig. 1. The first two squeezers are driven by two triangle waves of different frequencies but with the same amplitude of $2V\pi$. The 3rd squeezer, oriented 45 degrees from the 2nd one, is driven by a triangle wave of the same amplitude, but a much higher frequency than these of first two squeezers. The frequency relationships of the driving signals on the three squeezers are: $f_3 >> f_2 >> f_1$ (or $f_3 >> f_1 >> f_2$).

One may visualize that the first two squeezers cause SOP to vary along certain paths on Poincare Sphere in the absence of the 3rd squeezer. With the 3rd squeezer driving at much higher rate, each SOP point generated by the first two squeezers becomes the starting point for a complete SOP circle. All the circles have the same rotation axis, but different diameters. The circle moves back and forth along circle's axis as the SOP changes by the action of the first two squeezers, and eventually covers the whole Poincare Sphere.

Figure 3(e) shows the experimental result of SOP coverage using the quasi-uniform rate scrambling (a video showing the SOP evolution during the scrambling can be seen at

http://www.youtube.com/watch?v=aiO0wVgyKzY). The evolution of the SOP trace with time agrees with our reasoning and simulation described above. The three driving signals are all triangle waves with 60 volts amplitude for inducing 2π phase retardation, with frequencies of f_1 = 0.1 Hz, f_2 = 1.414 Hz, and f_3 = 34.6 Hz respectively. We purposely choose low driving frequencies here is for the easy observation of SOP evolution on Poincare Sphere. The measured DOP (10000 point average) is only about 3.2%, indicating uniform SOP coverage over the entire sphere. Finally, as shown in Fig. 3(f), the scrambling rate concentrates heavily at the highest end of the rate distribution histogram with a narrow spread. It is important to note that for this proposed scheme, the SOP coverage and scrambling rate distribution of this scheme are not sensitive to the input polarization variations, and therefore no stabilizer is required for implementing the scheme in real systems. Most importantly, the scheme works equally well for signals of both single polarization and polarization-multiplexed signals. Although the scrambling rate in this scheme is not ideally uniform as the scheme in Fig. 3(d), we anticipate it is sufficient for the high speed polarization-related testing of coherent systems with high repeatability.

3.4 Rate multiplication method for overcoming fiber squeezer speed limitations

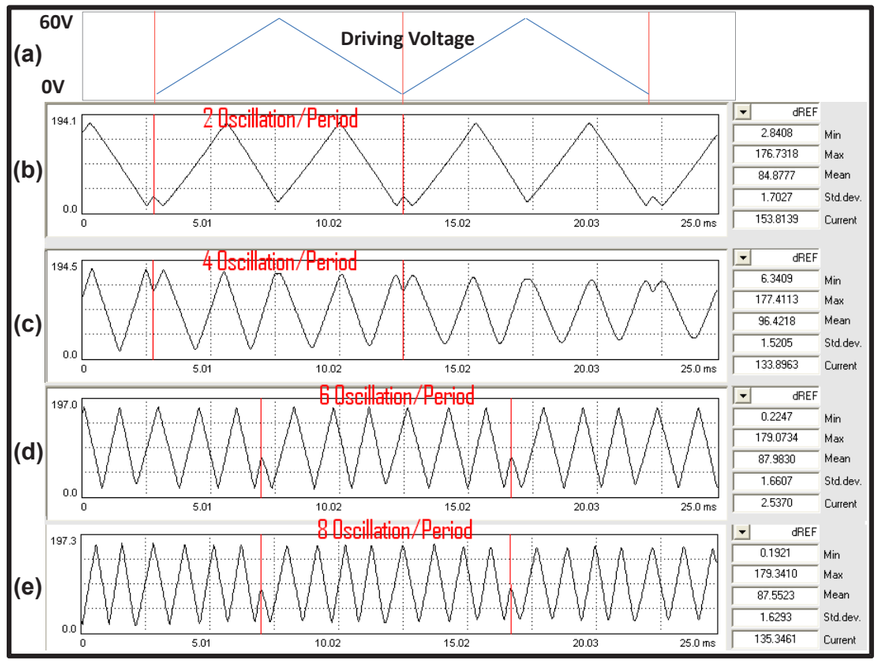

Fig. 4. Experimental results showing that SOP variation rate adds up with multiple fiber squeezers oriented in the same directions. In the experiment, the triangle wave with a frequency of 101.9 Hz and an amplitude of 60 volts drives the SOP to rotate a full circle on Poincare Sphere (phase retardation of 2π). (a) Driving signal with a triangle waveform. (b), (c), (d) and (e) correspond to the SOP variation as a function of time for simultaneously using 1, 2, 3, and 4 fiber squeezers respectively.

Fiber squeezers generally have a speed limit around 30π krad/s. Such a speed is not sufficient to achieve 100π krad/s scrambling required for testing the performance of coherent receivers. Therefore it is important to find a way to extend the speed limit of the fiber squeezers.

It can be shown mathematically that when N squeezers are placed in succession with the same relative angle, the phase retardations add up. If all the fiber squeezers are driven by a same triangle signal with the same frequency, the phase variation rate will be increased by a factor of N. Consequently, if this composite fiber squeezer is used as the 3rd squeezer in the quasi-uniform rate scrambling scheme in Fig. 1, the total scrambling rate will also be increased by a factor of N. Note that this method can be applied to any scrambling device using multiple wave plates.

Figure 4 shows the experimental results demonstrating the rate additive effect. In the experiment, the last four fiber squeezers in Fig. 1 are used and the amplitude of the triangle wave is adjusted to induce a full circle on the Poincare Sphere with each squeezer. The manual polarization controller is adjusted so that SOP traces out a great circle on Poincare Sphere. A polarimeter (POD-101D) is used to record SOP variation in the oscilloscope mode when 1, 2, 3, and 4 squeezers are driven with the same signal and the results are shown in Fig. 4. Note that the vertical axis is dREF, representing the relative angle between a moving SOP point and a reference SOP point on the SOP circle calcultated using Eq. (3), with a maximum angle of 180 degrees (π). Therefore, when SOP rotates a complete circle of 2π, dREF moves from 0 to a maximum value of π, and comes back to 0. As shown in Fig. 4(a), in a period of triangle wave for inducing a maximum retardation of 2π, we see two periods of dREF variation, with a single squeezer. One corresponds to voltage ramping up, and the other voltage ramping down. It is evident from Fig. 4 that when N squeezers are used, 2N dREF oscillations per triangle wave period are present. The additive effect is immediately evident because with increased number of fiber squeezers in each succeeding curves, the number of dREF period increase per 9.8 ms triangle wave period, indicating that the increase of SOP changing rate is proportional to the number of fiber squeezers N. We also observe the rate additive effect on Poincare Sphere: N fiber squeezers induce N circles per period of the driving signal. Note that we chose a low frequency in this experiment in order to demonstrate the concept more clearly because of the limited response time of the polarimeter.

3.5 Achieving 752 krads/s quasi-uniform rate polarization scrambling

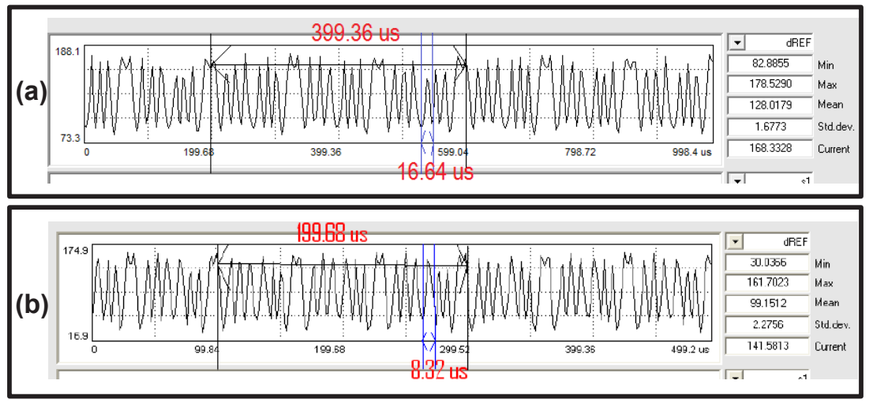

Fig. 5. Experiment data (a) for demonstrating quasi-uniform rate scrambling at 120π krad/s (376 krad/s). With an SOP angle change of 2π in 16.64 us, corresponding to a SOP variation rate of 120π krads/s (2π/16.64 us). (b) Experimental data demonstrating scrambling rate at 240π krad/s (752 krad/s).

As mentioned previously, fiber coherent optic communication systems require polarization scrambling with a uniform rate of at least 280 krad/s for testing performances with a good repeatability. Because of the incompatibility with the polarization multiplexing system, the uniform rate scheme using a polarization stabilizer cannot be used. Here, we describe combining the quasi-uniform rate scrambling scheme with the rate-additive multiple squeezer

approach to satisfy the requirements for nearly uniform rate and high-speed scrambling up to 752 krad/s.

In the experiment, six fiber squeezers are arranged as in Fig. 1. The last four squeezers are oriented in the same direction and are driven by the same triangle wave with the amplitude of 60 volts. Because of the rate additive effect, the total phase changing rate is quadrupled and readily to achieve a total rate of 120π krads/s, assuming each squeezer can operate at 30π krad/s. Figure 5(a) shows the measured SOP variation curve using a polarimeter (General Photonics POD-101D), when the frequency and amplitude of the driving triangle signal are set at 7.5 kHz and 60 volts, respectively. As in Fig. 4, dREF is recorded as a function of time. Clearly, a SOP variation rate of 120π krads/s, i.e., 376 krad/s, is achieved. It is noted that the data curve is not as clean as those in Fig. 4, caused by the limited bandwidth of polarimeter's electronics circuit. When taking the data, the first two fiber squeezers are disabled in order not to affect the rate measurement in Fig. 5. When the first two fiber squeezers are enabled, the SOP points immediately fill out the whole Poincare Sphere, and it is difficult to see the SOP evolution as shown in Fig. 3(e). In experiments, we also tried using 15 kHz triangle wave to drive the squeezers and achieved a SOP variation rate of 240π krad/s (752 krad/s), as shown in Fig. 5(b). Although the recorded curves are even more distorted due to the limitations of polarimeter's speed and the electrical amplifier for driving the squeezers, it shows the potential of achieving even higher scrambling speed for the proposed scheme.

Note that that a scrambling rate of 376 krad/s is sufficient to meet the requirements of system tests in general, since the maximum polarization variation rate in a real system is about 280 krad/s [6]. Considering that each PZT actuator in our fiber squeezers has a capacitance of 0.18 uF, the minimum total power consumption is about 20 watts for the scrambler operating at 376 krad/s, and ~40 Watts at 752 krad/s. In practice, 50% more power may be required to account for power consumption overhead by electronic circuit itself. For longtime reliability, we recommend to add more fiber squeezers for scrambling rate higher than 376 krad/s. This will help to lower the driving current or voltage on each PZT actuator and ensure longtime reliability. In addition, one may operate the fiber squeezers at resonant frequencies [22], which can significantly lower the power consumption, while increasing the scrambling rate, although this may compromise the scrambling rate adjustability by the users. Finally, it should be pointed out that fiber squeezer technology for polarization control and scrambling has proven to be commercially reliable with more than 10 years production history. We anticipate similar reliability for scrambling operation at 376 krad/s, especially when we double the number of parallel fiber squeezers in Fig. 1 and thus halve the driving voltage on each fiber squeezer, which allows us to operate each fiber squeezer at a modest driving condition of 30 volts at 7.5 kHz.

4. Conclusion

We propose and demonstrate a new scheme for quasi-uniform rate polarization scrambling for deterministic system performance tests that accommodate both single polarization and polarization multiplexed systems. A scheme to overcome the speed limitations of fiber squeezers is also demonstrated by using rate additive effect of multiple fiber squeezers. By combining both the quasi-uniform rate scrambling scheme and the cascaded multiple fiber squeezer approach, we achieve a 240π krad/s (752 krad/s) quasi-uniform rate polarization scrambler. The proposed scheme is scalable to even higher scrambling rates by adding more fiber squeezers. Furthermore, the schemes described in this paper still work if the fiber squeezers used are replaced with different types of variable phase retarders.

Acknowledgments

We thank General Photonics Corp. for providing special fiber squeezers arranged according to our specifications and Steve Yao for enlightening technical discussions, suggestions, and proof-reading of this paper.

4006 JOURNAL OF LIGHTWAVE TECHNOLOGY, VOL. 24, NO. 11, NOVEMBER 2006

Automatic Maximum-Minimum Search Method for Accurate PDL and DOP Characterization

Yongqiang Shi, *Member, IEEE*, *Member, OSA*, Lianshan Yan, *Senior Member, IEEE*, *Member, OSA*, and X. Steve Yao, *Member, IEEE*, *Member, OSA*

***Abstract*—A fully automatic deterministic maximum–minimum search method for fast accurate polarization-dependent loss (PDL) and degree of polarization (DOP) characterization is described. It is shown theoretically, based on a three-dimensional (3-D) surface model, that the method can unambiguously determine PDL and DOP values. Because it measures PDL and DOP values according to their definitions and without the need for scanning over a large number of polarization states or engaging in extensive intermediate calculations, this method provides the attractive features of high speed, wide measurement range, wavelength insensitivity, and calibration-free operation. The new PDL/DOP characterization method was experimentally demonstrated in a prototype instrument using an in-line polarization controller with ultralow activation loss and PDL.**

***Index Terms*—Degree of polarization (DOP), polarization, polarization-dependent loss (PDL), maximum–minimum search.**

I. Introduction

POLARIZATION-DEPENDENT loss (PDL) and its effects on long-haul fiber-optic networks have been studied extensively. Theoretical and experimental investigations showed that PDL could couple with network polarization mode dispersion (PMD) to degrade data quality and PMD compensator performance [1]–[5]. To ensure network quality of service, the PDL of each component should be minimized, and the cumulative PDL of the network must be managed within a desired limit. Therefore, accurate PDL measurements are required for almost all optical components, submodules, and modules as part of the specified standard parameters [6]. Once the optical-component PDL values are known, the network global PDL due to multiple PDL concatenation can be statistically estimated from individual component PDL data [7].

The PDL of an optical component is the maximum optical power transmittance change over all polarization states and is defined as PDL $= 10\log(T_{\max}/T_{\min})$ in terms of decibels. For large-scale production environments, automatic PDL measurement is required because manual measurement at a single wavelength can take several minutes or longer. Several approaches have been developed to measure PDL automatically by using either random or defined input polarization states, namely 1) the pseudorandom or deterministic polarization scanning method [8], [9], 2) Jones-matrix method [10], 3) Mueller-matrix method [11]–[13], and 4) Mueller–Stokes method [14], [15]. The polarization-scanning and Mueller-matrix approaches have been adopted as two standard measurement methods [8], [16]. Both the random-scanning and matrix methods have their own advantages and limitations, such as measurement speed, accuracy, optical bandwidth, and calibration requirements. In general, most commercial PDL measurement instruments using the random-scanning, Jones-matrix, or Mueller-matrix methods yield accurate PDL measurement values that are typically between 0.05 and 15 dB. At PDL extremes, particularly the high-PDL end, either the measurement accuracy deteriorates significantly or a much longer scanning time is required. The main reason for the accuracy deterioration at the high- and low-PDL extremes is that all of these methods do not truly measure the maximum and minimum transmittances used for PDL calculation. The scanning method uses a polarization generator or scrambler to generate either a deterministic or a pseudorandom subset of all possible states of polarization (SOPs) at the input light source; PDL is then calculated from the maximum and minimum power values obtained from the subset. Depending on the Poincaré sphere coverage and the PDL range, the scanned results may not be the exact maximum and minimum transmission of the component. On the other hand, the Jones-matrix, Mueller-matrix, and Mueller–Stokes methods all measure the optical transmission at a set of fixed SOPs that do not generally coincide with the maximum and minimum transmissions. The PDL is calculated from the matrix elements that were obtained from the optical intensity measurements. Small measurement errors or circuit noise can affect the results significantly. An additional drawback is that most of such deterministic fixed SOP measurements require system or wavelength calibrations.

Another polarization-related parameter is the degree of polarization (DOP). The DOP can be useful in monitoring network PMD and optical signal-to-noise ratio for network health evaluation [17]–[19]. Depolarized light sources with low-DOP values are critical to Raman amplifiers [20], [21] and fiber-sensor systems [22]; therefore, accurate DOP characterization is important for such applications. DOP measurements are typically performed using polarization-scrambling methods or polarimeters [23], which employ the same principle as the polarization-scanning and Mueller-matrix methods for PDL characterization.

In this paper, we describe a maximum–minimum (max–min) search method for deterministic PDL and DOP measurements. The concept of the method may sound obvious from the PDL

Manuscript received April 11, 2006; revised July 20, 2006.

Y. Shi was with the General Photonics Corporation, Chino, CA 91710 USA. He is now with Boeing Satellite Systems, Los Angeles, CA 90009-2919 USA (e-mail: yongqiang.shi@boeing.com).

L. Yan and X. S. Yao are with the General Photonics Corporation, Chino, CA 91710 USA (e-mail: lsyan@generalphotonics.com).

Color versions of Figs. 5–8 are available online at http://ieeexplore.ieee.org.

Digital Object Identifier 10.1109/JLT.2006.883121

0733-8724/$20.00 © 2006 IEEE

definition; however, to our knowledge, no detailed theoretical and experimental works were performed to validate its feasibility for automatic and unambiguous determination of PDL. Based on a simple three-dimensional (3-D)-surface contour model in Stokes space, we show theoretically that the true maximum and minimum transmittances of a device can be uniquely determined because no local maximums or minimums exist and therefore validate the approach. We implement the max–min search method by employing an active feedback polarization control algorithm using a fiber squeezer polarization controller (PC) to systematically and rapidly search for the maximum and minimum transmittances without the need to measure all possible SOPs. The direct measurement of maximum and minimum power transmittances assures calibration-free highly accurate high-speed measurement over a larger PDL or DOP range. In the succeeding sections, we will present the theoretical background of the proposed approach, the measurement implementation, and experimental results from a prototype measurement system.

II. Polarization Dependent Transmittance in Stokes Space

When a partially polarized monochromatic optical beam propagates through a nondepolarizing optical system, the transmission characteristics of the optical system can be modeled as a single partial polarizer [24]. Although PMD may depolarize light in general, for monochromatic light sources commonly used for measurements, such a depolarization can be neglected. Using a Stokes-vector representation and Mueller-matrix treatment, the optical intensity transmission can be expressed as a function of the input SOP, i.e.,

$$T = m_{11} + P(m_{12}s_1 + m_{13}s_2 + m_{14}s_3) \tag{1}$$

where m_{1i} represents the first-row Mueller-matrix elements, P is the DOP of the light source, and s_i represents the normalized Stokes parameters of the totally polarized light component of the light source. If we define vectors $\mathbf{s} = \{s_1, s_2, s_3\}$ and $\mathbf{m} = \{m_{12}, m_{13}, m_{14}\}$ in the Stokes subspace (S1, S2, S3), the optical transmittance can be expressed as a function of a single variable θ, which is the angle between vectors $\mathbf{s}$ and $\mathbf{m}$, i.e.,

$$\begin{aligned} T &= m_{11} + P(\mathbf{m}\cdot\mathbf{s}) \\ &= m_{11} + P|\mathbf{m}|\cos\theta. \end{aligned} \tag{2}$$

In Stokes space, the transmittance of the optical system can be described by a 3-D surface formed by the revolution of the limaçon of Pascal [25] about the m-axis. This result is similar to that obtained from a depolarization optical system treatment [26]. Because the optical transmittance T is always positive, i.e., $0 \le P|\mathbf{m}| \le m_{11}$, (2) represents a family of ordinary limaçons with a circle ($|\mathbf{m}| = 0$) and a cardioid ($|\mathbf{m}| = m_{11}$ and $P = 1$) at the two extremes, as shown in Fig. 1, in a plane containing $\mathbf{m}$. Based on the properties of the ordinary limaçon, the polarization-dependent transmission depends only on the angle θ between the $\mathbf{m}$ and $\mathbf{s}$ vectors. The maximum and minimum transmissions are obtained when θ becomes 0 and π, respectively, i.e.,

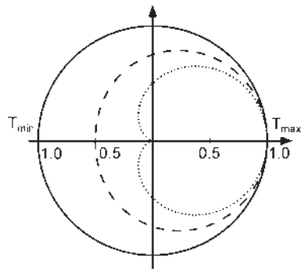

Fig. 1. Cross-sectional view of the limaçon of revolution with PDL = 0 (solid line), PDL = 3 dB (broken line), and an ideal polarizer (dotted line). The horizontal axis is along the vector $\mathbf{m}$ direction, and the vertical axis is set for a $\theta = 90^\circ$ reference. The maximum transmittance is normalized to unity.

$$\begin{pmatrix} T_{\max} \\ T_{\min} \end{pmatrix} = \begin{pmatrix} m_{11} + P|\mathbf{m}| \\ m_{11} - P|\mathbf{m}| \end{pmatrix}. \tag{3}$$

Obviously, the two polarization states that correspond to the maximum and minimum transmittances in (3) are orthogonal. The vectors that describe these two states are antiparallel in Stokes space, and the points that represent the two SOPs on the Poincaré sphere are symmetric about the origin. Equation (2) also tells us that the optical transmission changes monotonically from maximum to minimum and vice versa. The rotational symmetry of the limaçon of revolution allows us to reach either the maximum or minimum transmittances along any arbitrary path on the 3-D surface that links the two points.

Equations (2) and (3) form the basis of our automatic max–min search method for PDL and DOP measurements. In this method, the input SOP is systematically adjusted to make $\mathbf{s}$ parallel and antiparallel to $\mathbf{m}$ so that the maximum and minimum transmittances of the optical system are obtained. The monotonic relationship in (2) ensures that the maximum and minimum transmittances are unique. There are no local minima or maxima on the transmission surface along any paths between $T_{\max}$ and $T_{\min}$.

Equation (3) has two equations with three variables, and the DOP and PDL are coupled. Therefore, a light source of known DOP or a component of known PDL is required for PDL or DOP measurement, respectively. A totally polarized light source ($P = 100\%$) is convenient for PDL measurement. In this case, $T_{\max}$ and $T_{\min}$ from (3) can be used to calculate the PDL according to the definition.

For DOP measurement, a linear polarizer placed between the PC and the photodetecctor is an excellent optical element with known PDL. Assuming that an ideal PC and a linear polarizer aligned in the x-direction are used so that $|\mathbf{m}| = |m_{12}| = m_{11}$, DOP measurement also reduces to the search for and measurement of the maximum and minimum transmittances, i.e.,

$$P = \frac{T_{\max} - T_{\min}}{T_{\max} + T_{\min}} \times 100\%. \tag{4}$$

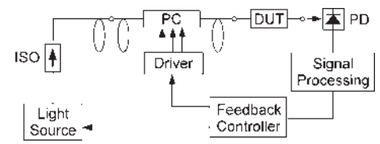

Fig. 2. Block diagram of the automatic max–min transmittance search implementation (PC, fiber-squeezer-based PC; DUT, device under test; PD, photodetector; ISO, optical isolator).

Therefore, both PDL and DOP characterizations can share the same max–min search algorithm, and both functions can be integrated in a single measurement system.

III. Automatic MAX–MIN Search Method Implementation

The proposed PDL and DOP measurement system is shown in Fig. 2, where the light source is a totally polarized highly stable laser or a light source to be characterized for the PDL and DOP measurements, respectively. For DOP measurements, the device under test (DUT) will be replaced with a high extinction ratio (ER) linear polarizer. Because both PDL and DOP measurements require active searching for the maximum and minimum transmittances, a fast low-PDL low-activation-loss PC plays a key role in the measurement system. In our system, a high-performance fiber-squeezer-based PC was selected for the application [27].

The PC is a cascaded three-stage variable-waveplate PC with the optic axes of the three plates fixed at 0°, 45°, and 0° orientations, respectively, as shown in Fig. 3. The variable-waveplate effect is achieved by applying radial stress to the optical fiber with a piezoelectric actuator. The phase retardation of each plate is linearly proportional to the voltage applied to the piezoelectric actuator. At the ith waveplate, the phase retardation can be expressed as

$$\varphi_i = \pi \frac{V}{V_{\pi,i}} + \varphi_{0,i} \tag{5}$$

where $V_{\pi,i}$ and $\varphi_{0,i}$ are the half-wave voltage and initial phase bias retardation, respectively. Neglecting insertion loss and PDL, the Mueller matrix of the PC can be written in (6), shown at the bottom of the page. As each φ_i varies between 0 and 2π, any arbitrary output SOP can be obtained from any input SOP [28], [29]. Complete Poincaré-sphere coverage ensures that the search results are the true maximum and minimum transmittances.

The simplest automatic max–min search operation can be achieved using a dc control voltage actuation algorithm. Starting from an arbitrary SOP, the controller takes an initial optical

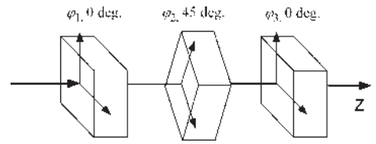

Fig. 3. Schematic diagram of the three-stage fiber-squeezer-based variable-waveplate PC.

intensity measurement and steps the dc voltage applied to one waveplate of the PC while holding the voltages at the other waveplates constant. A new photodetector output is obtained and then compared with the previous value. Based on the comparison results of the dc output intensities, the controller determines the voltage-step direction and voltage-step amplitude. This search process repeats for each waveplate until the optical power change is within the limit of the noise floor or the resolution of the detector circuit. When the maximum or minimum intensity is reached, the controller records the signal-level value and starts to search for the other extreme. To overcome the limited dynamic range of the circuit and improve the accuracy in high-PDL or highly polarized light DOP measurements, the minimum transmittance search can be combined with an automatic-gain-control approach that effectively expands the dynamic range of the measurement system. By comparison, in a fast random-scan algorithm [30], it is very difficult to implement the automatic gain control.

A different signal processing approach is to combine a small sinusoidal ac modulation with the dc control voltage to the PC waveplates. From (2), the output spectrum distribution changes as the angle between $\mathbf{m}$ and $\mathbf{s}$ changes. At the maximum and minimum intensity levels, the ratio of the second harmonic to the fundamental frequency of the sinusoidal modulation signal is maximized. A sensitive lock-in amplifier or digital signal processing circuit can be implemented to accurately determine the maximum and minimum transmittances using this algorithm. Since narrow-band filters can be implemented for noise rejection, the ac signal processing method is typically more accurate than the dc voltage-step method but requires additional implementation hardware.

Once the maximum or minimum transmittance is obtained, we can use the orthogonality property described in Section II to speed up the searching process for the other transmission extreme. Mathematically, the jump from the current SOP to the orthogonal state is achieved by reversing the signs of the 3×3 sub-Mueller-matrix elements m_{ij}, where $i, j \ge 2$. The desired result is to reach the orthogonal SOP state with the least number of steps; ideally, it can be done in a single step. However, with a fiber-squeezer-based PC, reversing the signs of all 3×3 sub-Mueller-matrix elements requires a polarimeter

$$M(\varphi_3, \varphi_2, \varphi_1) = \begin{pmatrix} 1 & 0 & 0 & 0 \\ 0 & \cos\varphi_2 & -\sin\varphi_2\sin\varphi_1 & \sin\varphi_2\cos\varphi_1 \\ 0 & -\sin\varphi_3\sin\varphi_2 & \cos\varphi_3\cos\varphi_1 - \sin\varphi_3\cos\varphi_2\sin\varphi_1 & \cos\varphi_3\sin\varphi_1 + \sin\varphi_3\cos\varphi_2\cos\varphi_1 \\ 0 & -\cos\varphi_3\sin\varphi_2 & -\sin\varphi_3\cos\varphi_1 - \cos\varphi_3\cos\varphi_2\sin\varphi_1 & -\sin\varphi_3\sin\varphi_1 + \cos\varphi_3\cos\varphi_2\cos\varphi_1 \end{pmatrix} \tag{6}$$

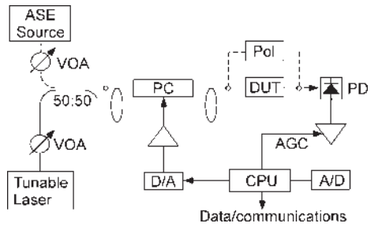

Fig. 4. Prototype automatic max–min search PDL/DOP measurement setup (VOA, variable optical attenuator; Pol, polarizer; A/D, analog-to-digital converter; D/A, digital-to-analog converter).

measurement of the current SOP and current phase retardation of each waveplate. For a simple measurement system with fiber-squeezer-based PC implementation, we can set the initial step to be as large as π-phase retardation at any waveplate of the PC. For example, a half-wave or π-phase change, i.e., a V_π voltage step on the last actuator, can effectively invert the s_2 and s_3 components in Stokes space.

IV. Experimental Results

To verify the proposed max–min search approach and performance, we implemented the prototype measurement setup shown in Fig. 4. A microprocessor is used for system control and signal processing in the prototype setup. A personal computer with a LabVIEW data acquisition program was used to acquire measurement results and to control the wavelength sweep. A polarized (ER $>$ 40 dB) tunable laser with a wavelength range of 1520–1620 nm was used as the light source for PDL characterization, and an unpolarized amplified spontaneous emission (ASE) source was combined with the tunable laser to create a test light source for DOP measurement. A fiber-squeezer-based PC with half-wave voltages of $\sim$25 V was selected for the prototype system. The activation loss and built-in PDL of the PC were $<$ 0.01 dB when the PC was actuated sequentially. The typical phase-retardation range is 0–5π for each waveplate. The photoreceiver circuit consisted of an InGaAs detector and an adjustable-gain transimpedance amplifier. Because our experiment was designed only to verify the concept, no attempt was made to correct the polarization-dependent responsivity (PDR) of the photodetector.

In our prototype setup, the dc voltage actuation algorithm discussed in Section III was used for its easy implementation and system control. Experiment results showed that the search-state switching using orthogonal SOP property resulted in much faster convergence when the search mode changed from maximum to minimum and vice versa. A dc voltage step of V_π is applied to one of the PC stages during the changeover.

We selected three different test devices to cover a large PDL range. A fiber connectorized/angle-polished connector (FC/APC)–air interface was used at the low-PDL extreme, while an in-line fiber polarizer represented the high-PDL extreme. The third component was a regular 2 $\times$ 2 10-dB fused-fiber coupler. The PDL of each component was measured repetitively over a period of more than 30 min, and the measurement results were recorded by a personal computer. As shown in Fig. 5(a) and (b), the max–min search method performs consistently at both very low and very high PDL extremes, which are still challenges to most of the commercial PDL meters. Note that in Fig. 5(a), the measured PDL of the FC/APC–air interface is a vector sum of connector PDL and photodetector PDR. Nevertheless, the measurement stability at very low PDL was clearly demonstrated.

For comparison purposes, we also measured the PDL on the 10-dB port of a 2 $\times$ 2 fused-fiber coupler using both our prototype setup and the Jones-matrix eigen-analysis (JEA) method on a commercial instrument. As shown in Fig. 6, despite a small difference in average PDL values between the two methods (partially due to the detector PDR in our prototype setup), the max–min search approach resulted in a much tighter distribution than the measurement on commercial instrument. The standard deviations of the measured PDL using the max–min search and JEA methods were 0.002 and 0.009 dB, respectively. The increase in PDL near measurement number 2000 was attributed to fiber movement coupled with detector nonzero PDR.

The measurement repeatability over time and wavelength was investigated by conducting PDL measurements over two weeks at wavelengths ranging from 1520 to 1620 nm in 2-nm steps. A 2 $\times$ 2 directional coupler was used as the DUT sample. The coupler and fiber jumpers were taped to the surface of an optical table to minimize data fluctuations due to photodetector PDR. Except for a few wavelengths near 1590 nm, the prototype system demonstrated a repeatability of 0.02 dB for all wavelengths over the test period, as shown in Fig. 7.

The DOP measurement was carried out by replacing the DUT in the setup with a linear polarizer shown in Fig. 4. The ASE source was switched on and combined through a 3-dB 2 $\times$ 2 fused coupler with the output of the tunable laser set at 1550 nm. The optical power of each path could be adjusted independently using two variable optical attenuators. The DOP of the mixed beam was adjustable from $\sim$3% to 100%. The 3% residual DOP of the ASE source is mainly due to the PDL of the 3-dB fused coupler. Using this light source, we measured DOP values using both the max–min search method and an Agilent 8509 C lightwave polarization analyzer. The measured DOP values matched very well, as shown in Fig. 8.

V. Discussion

The experimental results from the prototype PDL/DOP measurement setup demonstrate that the automatic max–min search method is a promising approach for accurate high-speed PDL/DOP characterization. Based on the experimental results, the max–min search approach offers many unique advantages. It effectively reduces a two-dimensional pseudorandom or deterministic scanning search over the entire Poincaré sphere to a deterministic quasi one-dimensional line search with unique search results. Therefore, an active and efficient search-and-measure algorithm can be implemented for fast PDL and DOP measurements. Like the all-states scanning approach, the max–min search method does not require optical power or wavelength-calibration matrices. Furthermore, the automatic max–min search method can overcome the wavelength

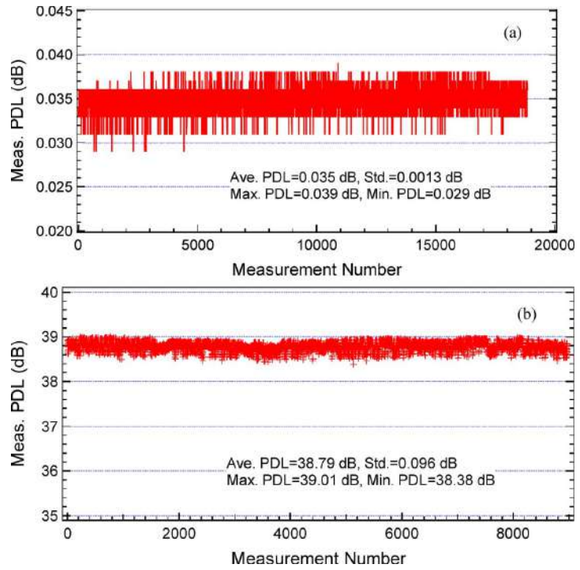

Fig. 5. PDL measurement data and statistics for (a) an FC/APC–air interface and (b) an in-line fiber polarizer at 1550 nm.

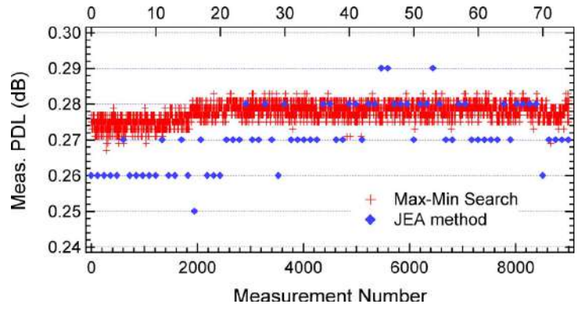

Fig. 6. PDL repeatability measurement on the 10-dB port of a 2 $\times$ 2 coupler using the prototype max–min search setup. JEA repeatability measurement was performed on a commercial instrument (with the measurement numbers on the top axis) using the same coupler ports.

dependence of polarization scramblers that operate in the resonant mode. Therefore, its operation wavelength range is very wide and is limited only by the light source, fiber bandwidth, and detector response. This approach also offers a large measurement dynamic range for both PDL and DOP. PDL in the range of more than 30 dB can be measured accurately, as demonstrated in our experiment.

The measurement speed depends on the response time of the PC and data processing electronics. In our prototype PDL/DOP measurement setup, we obtained 9000 data points in a 30-min interval, with a speed of 5 measurements/s. In this system, we found that the measurement speed was mainly limited by electronics. The intrinsic rise/fall time of the PC is in the order of 35 μs for each voltage step. With properly designed electronics, 10 ms will be sufficient for PC actions. The measurement speed can be further increased if an ultrahigh speed PC such as those made of $LiNbO_3$ [31] is employed in the system. Therefore, the max–min search approach offers significant measurement-speed advantages over the random-scanning method.

The measurement-speed advantage can also be attributed to the calibration-free feature of the max–min search method. The self-referencing nature of this approach makes the measurement insensitive to common sources of uncertainty, such as source-laser output-power wavelength dependence, source-laser output-SOP drift due to fiber movement, photodetector wavelength-dependent response, and amplifier gain.

The accuracy of the max–min search measurement system depends on system noise, circuit architecture, measurement

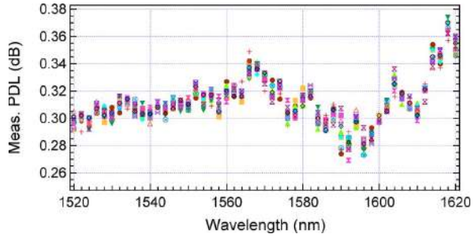

Fig. 7. Long-term automatic max–min search PDL measurement repeatability over C- and L-band wavelengths measured for a 2×2 fused coupler.

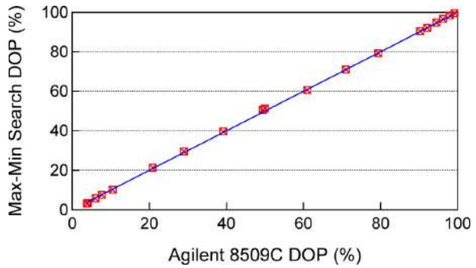

Fig. 8. DOP measurement correlation between the prototype automatic max–min search method and Agilent 8509 C. The straight line represents 100% correlation.

control, and the PDL of the optical components used in the measurement system. Limitations due to the optical system can be analyzed in analogy to the all-state scanning method because they share the same optical implementation configuration. The PDL from the PC and the following components will add to the DUT's PDL value vectorally and increase measurement uncertainty. Therefore, all optical components must have negligible PDL when compared with the DUT. DOP measurement accuracy also depends on the system PDL, e.g., a small amount of system PDL can directly affect the DOP measurement accuracy, particularly at the low-DOP end, as follows:

$$\Delta\text{DOP}(\%) = 11.5 \times \text{PDL [in decibels]}. \tag{7}$$

The system PDL includes contributions from the PC, the fiber segments to and from the DUT, the fiber connectors, and the photodetector. The selection of PC provided us with a very low PDL PC that is ideal for high-accuracy PDL/DOP measurement applications. Once the photodetector PDR is minimized, the accuracy of the max–min search method can reach < 0.02 dB. In addition, the optical source for PDL measurement must be very stable over the measurement time interval.

The noise effect on the measurement accuracy is often manifested at low- and high-PDL/DOP values. Circuit noise can result in the inversion of the maximum/minimum optical transmittance at low PDL and DOP that gives negative PDL and DOP. At the high-PDL end, the circuit noise limits the maximum PDL value. The PDL measurement accuracy also becomes input light level dependent. In our prototype measurement setup, signal average and automatic gain control were implemented to reduce the noise effect.

VI. Summary

We showed theoretically that the polarization-dependent transmittance of monochromatic light passing through an optical component or system can be described by a limaçon of revolution in Stokes space (S1, S2, S3). There is only one unique maximum and one unique minimum on an ordinary limaçon contour. The optical transmission changes monotonically between the minimum and maximum values. Therefore, a simple line search of the maximum and minimum transmission powers can determine the PDL and DOP values without ambiguity.

Using a PC with ultralow activation loss and PDL, we successfully implemented the max–min search method to accurately characterize component PDL and light-source DOP. We demonstrated that the method has the advantages of high measurement speed, high accuracy, large measurement dynamic range, wavelength insensitivity, and calibration-free operation.

Acknowledgment

The authors would like to thank A. Yang, L. Lin, J. Chen, and Dr. C. Yeh for their help in constructing the prototype PDL/DOP meter.

References

[1] F. Bruyere and O. Audouin, "Penalty in long-haul optical amplified system due to polarization dependent loss and gain," *IEEE Photon. Technol. Lett.*, vol. 6, no. 5, pp. 654–656, May 1994.

[2] E. Lichtman, "Limitations imposed by polarization dependent gain and loss on all-optical ultralong communication systems," *J. Lightw. Technol.*, vol. 13, no. 5, pp. 906–913, May 1995.

[3] N. Gisin and B. Huttner, "Combined effects of polarization mode dispersion and polarization dependent losses in optical fibers," *Opt. Commun.*, vol. 142, no. 1–3, pp. 119–125, Oct. 1997.

[4] L. Yan, Q. Yu, Y. Xie, and A. Willner, "Experimental demonstration of the system performance degradation due to combined effect of polarization-dependent loss with polarization mode dispersion," *IEEE Photon. Technol. Lett.*, vol. 14, no. 2, pp. 224–226, Feb. 2002.

[5] N. Kim, D. Lee, H. Yoon, J. Park, and N. Park, "Limitation of PMD compensation due to polarization-dependent loss in high-speed optical transmission links," *IEEE Photon. Technol. Lett.*, vol. 14, no. 1, pp. 104–106, Jan. 2002.

[6] Telcordia, *Generic Requirements for Passive Optical Components*, 2001. GR-1209-CORE, issue 3.

[7] A. El Amari, N. Gisin, B. Perny, H. Zbinden, and C. W. Zimmer, "Statistical prediction and experimental verification of concatenations of fiber optic components with polarization dependent loss," *J. Lightw. Technol.*, vol. 16, no. 3, pp. 332–339, Mar. 1998.

[8] TIA/EIA-455-157, *Measurement of Polarization Dependent Loss (PDL) of Single-Mode Fiber Optic Components (ANSI/TIA-455-157)*. Arlington, VA: Telecommun. Ind. Assoc., May 1995.

[9] C. Hentschel and D. Derickson, "Insertion loss measurements," in *Fiber Optic Test and Measurement*, D. Derickson, Ed. Upper Saddle River, NJ: Prentice-Hall, 1998, ch. 9.

[10] B. Heffner, "Deterministic, analytically complete measurement of polarization-dependent transmission through optical devices," *IEEE Photon. Technol. Lett.*, vol. 4, no. 5, pp. 451–454, May 1992.

[11] B. Nyman, D. Favin, and G. Wolter, "Automated system for measuring polarization dependent loss," in *Proc. Opt. Fiber Commun. Conf., Tech. Dig.*, San Jose, CA, pp. 230–231.

[12] D. Favin, B. Nyman, and G. Wolter, "System and Method for Measuring Polarization Dependent Loss," US Patent 5371597, Dec. 6, 1994.

[13] C. Hentschel and S. Schmidt, *PDL Measurements Using the HP 8169 a Polarization Controller*. Palo Alto, CA: Agilent Technologies, 2002.

[14] R. Craig, S. Gilbert, and P. Hale, "High accuracy, nonmechanical approach to polarization dependent transmission measurements," *J. Lightw. Technol.*, vol. 16, no. 7, pp. 1285–1294, Jul. 1998.

[15] R. Craig, "Accurate spectral characterization of polarization-dependent loss," *J. Lightw. Technol.*, vol. 21, no. 2, pp. 432–437, Feb. 2003.

[16] TIA/EIA-455-198, *Measurement of Polarization Dependence of Insertion Loss of Single-Mode Fiberoptic Components by a Mueller Matrix Method (TIA 455-198)*. Arlington, VA: Telecommun. Ind. Assoc., Dec. 2002.

[17] S. M. R. M Nezam, L. Yan, J. E. McGeehan, Y. Shi, A. E. Willner, and S. Yao, "Enhancing the dynamic range and DGD monitoring windows in DOP-based DGD monitors using symmetric and asymmetric partial optical filtering," *J. Lightw. Technol.*, vol. 22, no. 4, pp. 1094–1102, Apr. 2004.

[18] L.-S. Yan, X. S. Yao, Y. Shi, and A. E. Willner, "Simultaneous monitoring of both optical signal-to-noise-ratio and polarization-mode-dispersion using polarization scrambling and polarization-beam-splitting," *J. Lightw. Technol.*, vol. 23, no. 10, pp. 3290–3294, Oct. 2005.

[19] L.-S. Yan, X. Yao, C. Yu, Y. Wang, L. Lin, Z. Chen, and A. E. Willner, "High-speed and highly repeatable polarization-state analyzer for 40-Gb/s system performance monitoring," *IEEE Photon. Technol. Lett.*, vol. 18, no. 4, pp. 643–645, Feb. 2006.

[20] X. Zhou, P. Magill, and M. Birk, "Model for polarization-dependent gain due to pump depletion in a WDM system with forward-pumped Raman amplification," *J. Lightw. Technol.*, vol. 23, no. 3, pp. 1056–1062, Mar. 2005.

[21] S. Namiki and Y. Emori, "Ultrabroad-band Raman amplifiers pumped and gain-equalized by wavelength-division-multiplexed high-power laser diodes," *IEEE J. Sel. Topics Quantum Electron.*, vol. 7, no. 1, pp. 3–16, Jan. 2001.

[22] B. Szafraniec and G. Sanders, "Theory of polarization evolution in interferometric fiber-optic depolarized gyros," *J. Lightw. Technol.*, vol. 17, no. 4, pp. 579–590, Apr. 1999.

[23] X. Yao, "Accurate DOP characterization with less effort," in *Fiberopt. Prod. News*. New York: Reed Elsevier, Dec. 2003.

[24] R. M. A. Azzam and M. Bashara, *Ellipsometry and Polarized Light*. Amsterdam, The Netherlands: North-Holland, 1987, ch. 1–2.

[25] W. H. Beyer, *CRC Standard Mathematical Tables*, 28th ed. Boca Raton, FL: CRC, 1987, pp. 220–221.

[26] B. DeBoo, J. Sasian, and R. Chipman, "Degree of polarization surfaces and maps for analysis of depolarization," *Opt. Express*, vol. 12, no. 20, pp. 4941–4958, Oct. 2004.

[27] PolaRite II polarization controller, General Photonics Corp. [Online]. Available: http://www.generalphotonics.com/PolariteIImanual.htm

[28] E. Collett, *Polarized Light in Fiber Optics*. Lincroft, NJ: PolaWave Group, 2003, ch. 9, pp. 219–225, Sec. 11.

[29] L.-S. Yan, Q. Yu, and A. E. Willner, "Uniformly distributed states of polarization on the Poincare sphere using an improved polarization scrambling scheme," *Opt. Commun.*, vol. 249, no. 1–3, pp. 43–50, May 2005.

[30] J. Kim and B. W. Lee, "A new high speed measurement method of polarization dependent loss," in *Proc. NFOEC*, Baltimore, MD, Jul. 2001.

[31] F. Heismann, "Analysis of a reset-free polarization controller for fast automatic polarization stabilization in fiber-optic transmission systems," *J. Lightw. Technol.*, vol. 12, no. 4, pp. 690–699, Apr. 1994.

Yongqiang Shi (M'03) received the B.S. degree from Suzhou University, Suzhou, China, in 1982, the M.S. degree in physics from Hangzhou University (now Zhejiang University), Hangzhou, China, in 1984, and the Ph.D. degree in electrical engineering from the University of Southern California, Los Angeles, in 1992.

He is currently with Boeing Satellite Systems, Los Angeles, where he conducts optical communication research and engineering. Prior to joining Boeing Satellite Systems, he was the Chief Scientist with General Photonics, where he was in charge of daily research and development activities including polarization control, polarization-mode-dispersion emulation, and compensation components and instruments. From 1999 to 2001, he was a member of the Technical Staff with Lucent Technologies, where he conducted 40-Gb/s electrooptic modulator research and development. He was also a Staff Scientist with the TACAN Corporation, where he was in charge of integrated nonlinear optical device research and development programs. His research interests include integrated optics, optical components, nonlinear optics and optical materials, high-speed modulator design and packaging, polarization control optics, RF photonics, and optical information processing.

Dr. Shi is a member of the Optical Society of America.

Lianshan Yan (S'99–M'05–SM'06) received the B.E. degree in optical engineering from Zhejiang University, Hangzhou, China, in 1994 and the Ph.D. degree in electrical engineering from the University of Southern California (USC), Los Angeles, in 2005.

From 1994 to 1999, he was with North China Research Institute of Electro-optics, where he worked on solid-state lasers. In September 1999, he joined the Optical Communications Laboratory, USC. He is currently a Senior Scientist and the Manager of engineering with General Photonics Corporation, Chino, CA, concentrating on polarization, timing, and spectrum control. He is the author and a coauthor of more than 100 papers in prestigious journals and conference proceedings. He is the holder of four U.S. patents and about ten pending ones. His research interests include enabling technologies for long-haul wavelength-division-multiplexing systems and polarization effects in fiber transmission.

Dr. Yan was a recipient of the IEEE Lasers and Electro-Optic Society (LEOS) Graduate Fellowship in 2002. He serves as a frequent referee for ten journals. He is a Senior Member of the IEEE LEOS and a member of the Optical Society of America and the Sigma Xi society.

X. Steve Yao (M'97) received the M.S. and Ph.D. degrees in electrical engineering/electrophysics from the University of Southern California, Los Angeles, in 1989 and in 1992, respectively.

From 1985 to 1987, he was an Optical Engineer with ADC Fiber Optics (a division of ADC Telecommunications), where he developed the first generation of fiber-optic wavelength-division-multiplexing devices. From 1990 to 2000, he was with the Jet Propulsion Laboratory, NASA, Pasadena, CA, where he worked on research and development of microwave photonic devices and systems and invented the optoelectronic oscillator that generates the world's cleanest 10–80-GHz signals. He was responsible for the design and demonstration of the X-band fiber-optic antenna remoting system for NASA's Deep Space Network. He is currently the Chief Technology Officer with General Photonics Corporation, Chino, CA, which is a company that provides the most complete product selections for polarization and timing control for the telecommunications and sensor industry. He is the author of more than 40 referred journal publications and a book chapter in *RF Photonic Technology in Optical Fiber Links* (Cambridge Univ. Press, 2002), which details his breakthrough research in an optoelectronic oscillator for generating 10-GHz and higher frequency signals. He has given invited speeches in numerous major photonics-related conferences and holds more than 30 issued U.S. patents and 15 pending applications.

Dr. Yao is a recipient of 29 innovation awards from NASA. Two products based on his inventions have won the Photonics Circle of Excellence Awards in 2000 and 2001, respectively. The awards are given to the top 25 most innovative products around the world each year. He also served as a member of the Technical Committee of the Optical Fiber Communications conferences and was an organization committee member for the Microwave Photonics Conference in 2000.

Real-Time Optical Spectrum Analysis of a Light Source Using a Polarimeter

X. Steve Yao[1,2], Bo Zhang[2,3], Xiaojun Chen[2], and Alan E. Willner[3]

[1]*Polarization Research Center and Key Laboratory of Opto-electronics Information and Technical Science (Ministry of Education), Tianjin University, Tianjin 300072, China*
[2]*General Photonics, 5228 Edison Ave. Chino, CA 91710 USA, Email: syao@generalphotonics.com*
[3]*Department of Electrical Engineering – Systems, University of Southern California, Los Angeles, CA 90089-2565, USA, Email: boz@usc.edu*

Abstract: Optical spectrum analysis and polarization analysis are not generally related by conventional wisdom. In this paper, we show that the spectrum of a light beam can be obtained using a polarimeter, with a resolution and a speed that cannot be achieved with traditional spectrum analysis methods. We experimentally demonstrate a novel polarimeter-based optical spectrum analyzer (P-OSA) and show that the high-speed and high-resolution nature of the device enables rapid measurement of the spectrum of swept laser sources at a repetition rate of more than 100 kHz. We show the generation of a unique 3-D plot of the spectral shape of a light source as its center wavelength is swept.

©2008 Optical Society of America

OCIS codes: (260.5430) Polarization; (070.4790) Spectrum Analysis

References and links

1. B. J. Pernick, D. Yustein, and C. Bartolotta, "An Optical Spectrum Analyzer for Power Spectral Density Measurements," Appl. Opt. **8**, 65-73 (1969)
2. T. K. Gaylord and M. G. Moharam, "Analysis and applications of optical diffraction by gratings," in Proceedings of the IEEE, **73**, 894-937 (1985)
3. M. Takeda, H. Ina, and S. Kobayashi, "Fourier-transform method of fringe-pattern analysis for computer-based topography and interferometry," J. Opt. Soc. Am. **72**, 156-160 (1982)
4. D. Derickson, *Fiber optic test and measurement*, (Prentice Hall, 1998.), Chap. **3-6**, pp. 12.
5. D. M. Baney, B. Szafraniec, and A. Motamedi, "Coherent Optical Spectrum Analyzer," IEEE Photon. Technol. Lett. **14**, 355-357 (2002).
6. http://generalphotonics.com/POD-101D.htm
7. C. R. S. Fludger, T. Duthel, D. van den Borne, C. Schulien, E. Schmidt, T. Wuth, J. Geyer, E. De Man, G. Khoe, and H. de Waardt, "Coherent Equalization and POLMUX-RZ-DQPSK for Robust 100-GE Transmission," J. Lightwave Technol. **26**, 64-72 (2008)
8. M. Born and E. Wolf, *Principles of Optics: Electromagnetic Theory of Propagation, Interference and Diffraction of Light* (7th ed.), (Cambridge University Press, 1999).
9. http://www.lambdaquest.com/products.htm
10. D. Huang, E. A. Swanson, C. P. Lin, J. S. Schuman, W. G. Stinson, W. Chang, M. R. Hee, T. Flotte, K. Gregory, C. A. Puliafito, and J. G. Fujimoto, "Optical coherence tomography," Science **254**, 1178-1181(1991).
11. R. Huber, M. Wojtkowski, and J. G. Fujimoto, "Fourier Domain Mode Locking (FDML): A new laser operating regime and applications for optical coherence tomography," Opt. Express **14**, 3225-3237 (2006).
12. S. Tammela, H. Ludvigsen, T. Kajava, M. Kaivola, "Time-resolved frequency chirp measurement using a silicon-wafer etalon," IEEE Photon. Technol. Lett. **9**, 475-477 (1997)

1. Introduction

Traditional optical spectrum analyzers (OSAs) are usually realized using one of the following three methods: 1) a spatially dispersive element, such as a diffractive grating, 2) a tunable narrow-band filter, such as a Fabry-Perot (F-P) resonator or a tunable fiber Bragg grating, and 3) path-length-difference varying interferometer (Michelson or Mach-Zehnder) followed by FFT analysis [1-3]. However, design tradeoffs exist among the resolution, the spectral range, and the measurement speed [4], and therefore it is difficult to achieve all three parameters simultaneously. For example, the spectral resolution and the measurement range (free

#100540 - $15.00 USD Received 25 Aug 2008; revised 2 Oct 2008; accepted 6 Oct 2008; published 20 Oct 2008
(C) 2008 OSA

spectral range) of an F-P filter based OSA are inversely proportional to each other. In order to achieve fine resolution, the spectral range tends to be sacrificed. Improved resolution and dynamic range are possible with coherent analysis techniques, yet it requires an advanced swept local oscillator with polarization control [5]. Furthermore, for fast swept tunable lasers with a scanning range of > 160 nm and a sweeping rate of tens of kHz, it is desirable to measure the changing wavelength as a function of time. Unfortunately, none of the method described above can simultaneously meet the speed, resolution, and range requirements for characterizing such a swept tunable laser. For example a diffraction grating based spectrum analyzer with a CCD can be sufficiently fast, however, its resolution or range is not sufficient due to limitations imposed by the size of the CCD and the appearance of higher diffraction orders from the grating when the spectrum range is too large or when the grating period is too small.

In this paper, we propose and demonstrate a novel polarimeter-enabled optical spectrum analyzer (P-OSA). Our method is based on analyzing both the state of polarization (SOP) as well as the degree of polarization (DOP) information of the light source after it passes through a variable differential group delay (DGD) module. Thanks to the high-speed polarimeter [5], our proposed P-OSA can readily achieve a measurement speed on the order of MHz, and is therefore capable of measuring the center wavelength of a fast scanning laser as a function of time. The measurement speed is limited only by the bandwidth of the photo-detectors, the RF amplifiers, and digital processing electronics, and can be up to tens of GHz in principle [7].

Another unique and attractive feature of the P-OSA is that it can determine the direction of the frequency change, a capability unobtainable with most of the conventional spectrum analysis methods. Consequently, the P-OSA is capable of having arbitrarily high frequency resolution, yet, with arbitrarily large spectral range, provided that the measurement speed is sufficiently fast compared with the rate of the SOP change caused by the spectral change of the light source and that the signal-to-noise ratio in P-OSA's detection circuit is sufficiently high for accurate SOP measurement. Such a feature opens a wide door for many spectral related measurements not imaginable with conventional spectrum analysis methods.

Finally, the P-OSA can measure the spectral shape (power vs. frequency) of a swept-wavelength light source. With this unique capability, we report the generation of a 3-D plot of the spectral shape of a modulated light signal as a function of center wavelength of a wavelength-scanned light source. This capability enables detailed spectral characterization of a fast swept-wavelength source that cannot be obtained with other conventional methods.

2. Swept-frequency (wavelength) measurement

2.1 Concept

The basic concept of the P-OSA for measuring the instantaneous wavelength of a swept laser source is shown in Fig. 1(a), where the input light source first enters a fixed differential group delay (DGD) element (e.g. a birefringent crystal) before being analyzed by a high-speed polarimeter. It is known that when a tunable light source passes through a DGD element, its SOP will trace a circle on the Poincare sphere when the wavelength of the light source is tuned [4, 8], as shown in Fig. 1(b). The rate of the SOP change as a function of frequency is determined by the value of the DGD element. Therefore, one can obtain the DGD value from the SOP trace on the Poincare Sphere.

If we choose a precisely known DGD element, by using the reverse effect, the frequency of the light source can be determined from the SOP trace on the Poincare sphere. Let τ be the DGD value of the DGD element, the complex amplitude of the electrical field of the light after the DGD element can be expressed as,

$$\vec{E} = (E_x e^{i2\pi f\tau}\hat{e}_x + E_y\hat{e}_y)e^{i\phi_o} \quad (1)$$

#100540 - $15.00 USD Received 25 Aug 2008; revised 2 Oct 2008; accepted 6 Oct 2008; published 20 Oct 2008
(C) 2008 OSA

where E_x and E_y are the amplitudes of the electrical field along the x and y directions of the chosen coordinate system, $\hat{e}_x$ and $\hat{e}_y$ are the unit vectors along the x and y directions, and ϕ_o is the common phase term.

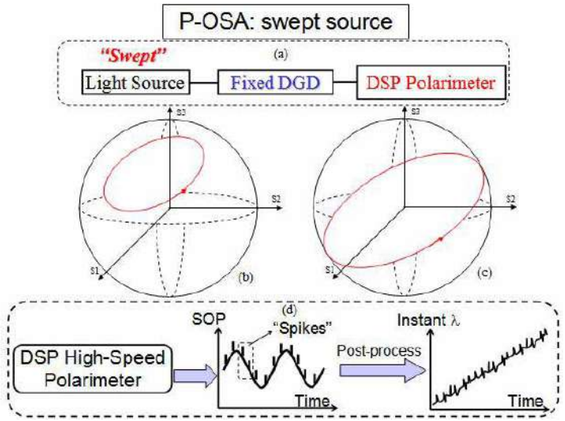

Fig. 1. Concept of the proposed real-time polarimeter-based optical spectrum analyzer used for a swept-wavelength source.

If $E_x = E_y$, the SOP will trace a largest circle on the Poincare sphere, as shown in Fig. 1(c), resulting in the highest frequency measurement resolution or sensitivity. When considering two specific frequency values, f_1 and f_2, during a wavelength sweep , the angular difference, denoted as Δθ, between the two polarization states of these two different frequencies is simply the phase difference in Eq. (1), which can be expressed as,

$$\Delta\theta = 2\pi(f_1 - f_2)\tau \tag{2}$$

For a known differential delay τ, the frequency difference can be calculated from the SOP angular difference on Poincare Sphere as,

$$f_1 - f_2 = \frac{1}{2\pi}\frac{\Delta\theta}{\tau} \tag{3}$$

Figure 1(d) shows the working principle of the swept-wavelength operation mode. The high-speed polarimeter collects the time-resolved SOP traces, which carries the detailed polarization evolution information. Based on the known DGD value, one can translate the SOP traces into the instantaneous wavelength evolution by calculating the polarization rotation angle on the Poincare sphere using Eq. (3).

2.2 Spectral range and resolution

For conventional OSAs, such as those based on F-P interferometer, free spectral range (FSR) is defined as the spacing between the periodic passbands. The FSR usually determines the spectral measurement range of the analyzer. One of the major tradeoffs for the conventional OSAs is that the FSR is always inversely proportional to the spectral resolution. This means that the high spectral resolution will always result in limited measurement range.

For our proposed P-OSA, if we consider that the SOP resolution is 0.36 degree, we can have 360/0.36 = 1000 points resolved in a full circle (one-cycle) on the Poincare Sphere. From

#100540 - $15.00 USD Received 25 Aug 2008; revised 2 Oct 2008; accepted 6 Oct 2008; published 20 Oct 2008
(C) 2008 OSA

Eq. (3), we can see that for a given τ, the resolution for measuring the center frequency and the one-cycle measurement range of the polarimeter based spectrum analyzer are,

$$\text{Frequency Resolution:} \quad \delta f = \Delta f / 1000 = 10^{-3}/\tau \tag{4}$$

$$\text{One-Cycle measurement range:} \quad \Delta f = 1/\tau \tag{5}$$

As an example, for a DGD value of 1000 ps, the frequency resolution will be 1 MHz, and the one-cycle measurement range will be 1 GHz. The tradeoff between the resolution and the range still exists if we consider only one-cycle on the Poincare sphere.

However, since the SOP circle will be able to repeat itself on the sphere if the frequency variation range Δf is larger than $1/\tau$, we can utilize the valuable information of the direction of the SOP evolution. By combining Eq. (5) with the SOP direction information, we obtain the following equation as the total measurement range by the multiplication of the SOP cycle number,

$$\text{Total measurement range:} \quad \Delta f = N \times 1/\tau \tag{6}$$

where N can be any arbitrarily large integer number.

This results in the unique feature of arbitrarily large spectral range, without any compromise to the spectral resolution. Since only the value of the fixed DGD element determines the spectral resolution, one can simply improve the resolution by introducing arbitrarily large DGD element without sacrificing the measurement range. The proposed P-OSA is thus not limited by the traditional tradeoff between the spectral range and frequency resolution.

2.3 Experimental setup and results

As shown in Fig. 2, we choose two representatives as the swept input source. The first one is a spectral spliced ASE source using a high speed Fabry-Perot tunable filter [9] (up to 40 KHz sweeping speed). The second swept source is the HP 8164A tunable laser source (TLS) with a sweep step size of 0.05 nm and a dwell time of 0.1 second. A 5.7-ps birefringent crystal is applied as a fixed DGD element, with input adjusted by a polarization controller for equal power splitting between two eigen polarization states. The output port of the DGD element is directed to the General Photonics' high-speed DSP in-line polarimeter (POD-101D) for real-time Poincare sphere display and SOP trace recording at a sampling rate near ~1 MHz [6].

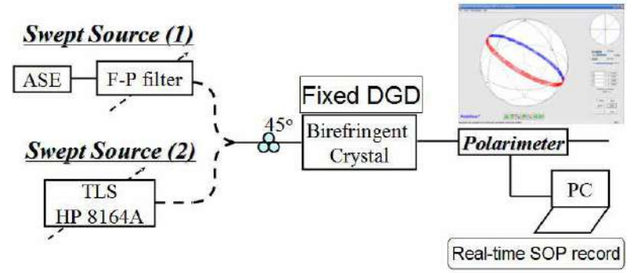

Fig. 2. P-OSA experimental setup for analyzing two types of swept sources. Note that only one source is connected at a time. The SOP of the input light is adjusted to 45 degrees with respect to the birefringent axis of the DGD.

Figures 3 and 4 show the results of the swept-wavelength input using a high speed F-P filter based spectral-slicing source. A high power EDFA with output of ~15 dBm is used as the ASE source. The sweeping wavelength range of the high-speed tunable filter is properly

#100540 - $15.00 USD Received 25 Aug 2008; revised 2 Oct 2008; accepted 6 Oct 2008; published 20 Oct 2008
(C) 2008 OSA

adjusted using a function generator, with frequency, amplitude and offset matched to the EDFA gain bandwidth. Figure 3(a) shows the modulation of one (S1) of the recorded Stokes parameters from the polarimeter when the tunable filter is swept at 1-KHz rate. The amplitude and the offset from the sinusoidal function generator are set to be 10V and 3.5V, respectively. By utilizing the directional SOP evolution, we obtain the accumulated polarization rotation angle, as shown in the right Y axis of Fig. 3(b). Note that the multiple full circle of the SOP modulation can be correctly interpreted to the accumulated rotation angle. From Eq. (3), we further derive the swept wavelength as a function of time (in the left Y axis of Fig. 3(b)) from the accumulated polarization angle. The starting wavelength is determined using a spectrum analyzer. In practice, we can utilize a tunable DGD element and obtain the reference wavelength using the method described in section 3.1. We can see that the swept wavelength curve resembles well with the sinusoidal sweeping function and the time period is determined by the swept frequency of 1-KHz.

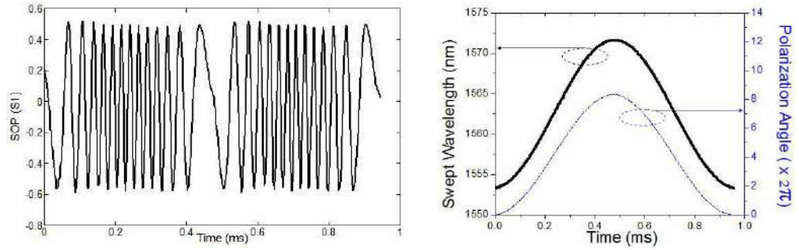

Fig. 3. 1-KHz tuning F-P filter (a): SOP (S1) trace. (b): swept wavelength. Note that the starting wavelength is obtained from a commercial spectrum analyzer, although the P-OSA can also determine the absolute starting wavelength directly, as described in the next section.

Figure 4(a) shows one of the recorded Stokes parameters from DSP polarimeter when the tunable filter is swept at a higher rate of 10-KHz. The amplitude and the offset of the function generator are 5V and 4.5V, respectively. Figure 4(b) shows the derived swept wavelength as a function of time. A period of 100 μs proves the swept frequency of 10-KHz. Due to the limited sampling rate of the DSP polarimeter, the recovered SOP trace can not be as smooth as that of the 1-KHz case. Improved results are expected if the sampling rate of the polarimeter is increased. The reduced SOP modulation cycle and thus the reduced swept wavelength range is due to the smaller amplitude swing applied to the F-P filter.

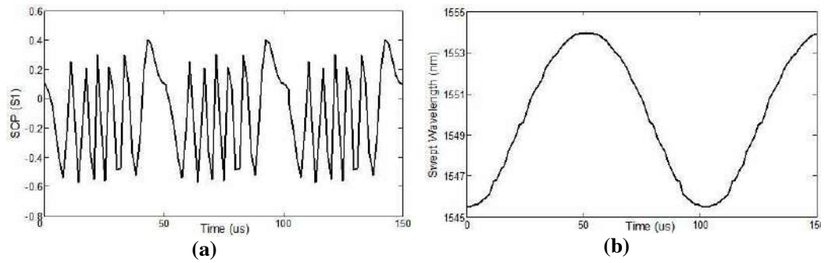

Fig. 4. 10-KHz tuning F-P filter (a). SOP (S1) trace. (b). swept wavelength. Note that the starting wavelength is obtained with a commercial spectrum analyzer, although the P-OSA can also determine the absolute starting wavelength directly, as described in the next section.

#100540 - $15.00 USD Received 25 Aug 2008; revised 2 Oct 2008; accepted 6 Oct 2008; published 20 Oct 2008
(C) 2008 OSA

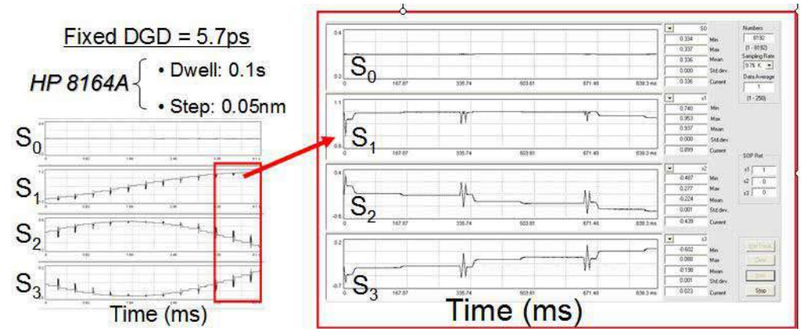

Fig. 5. POD-101D oscilloscope mode. SOP evolutions are recorded when the input is swept at a speed of 0.1 sec.

Figures 5 and 6 show the results of the swept-wavelength input using HP 8164A. Figure 5 shows the screen shots of the oscilloscope mode of the POD-101D, where the SOP traces (S_0, S_1, S_2, S_3) are recorded. Remarkably, the SOPs not only describe the sinusoidal behaviour when the input HP 8164A light source is 0.05 nm step swept, but also the "spiky" details when the wavelength is stepped from one value to the next.

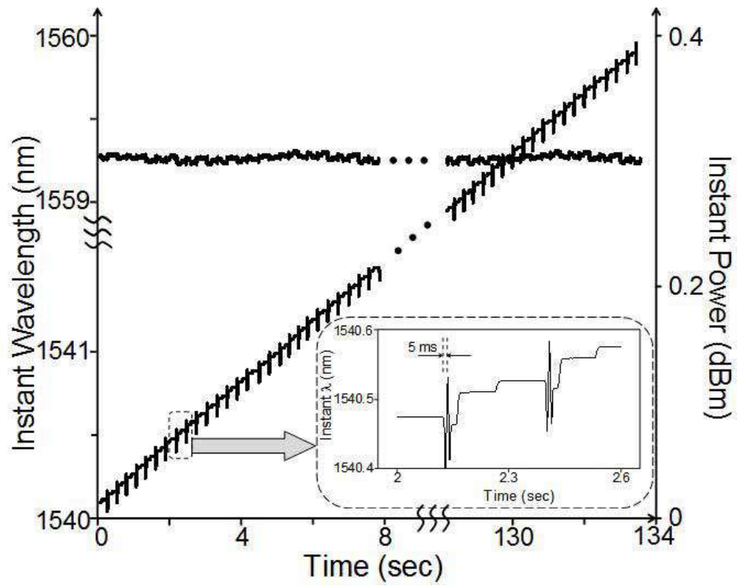

Fig. 6. Instantaneous wavelength and power as the input light source is swept at a speed of 0.1 sec. The starting wavelength is from the setting of the commercial tunable laser. Note that the transient dynamics of the swept laser source can be clearly revealed, as shown in the inset.

Based on the sampled SOP traces, we post-process the recorded SOP data by calculating the accumulated polarization rotation angle, taking into account the direction of the rotation. The polarization rotation angle can be further translated into the time-resolved swept

#100540 - $15.00 USD Received 25 Aug 2008; revised 2 Oct 2008; accepted 6 Oct 2008; published 20 Oct 2008
(C) 2008 OSA

frequency, as shown in Fig. 6, where the instantaneous wavelength is obtained from 1540 to 1560 nm using the periodic nature of the SOP traces in Fig. 5. The starting wavelength is the setting of the tunable laser and its value is not obtained from the analysis, although the P-OSA is capable of determining the absolute wavelength as described in the next section. Note that the range can be further increased by recording more SOP evolution circles. A zoom in of the curve in Fig. 6 proves that a relatively low speed (0.1 second) swept source actually has a fast transition time on the order of millisecond. This reveals that when the light source is stepped from one wavelength to the next, it experiences a fast initialization stage in which the wavelength is oscillating. It then quickly jumps to the desired value within several tens of milliseconds. However, most of the time is then used for wavelength locking and stabilization. From Fig. 5 and Fig. 6, we can see that P-OSA exhibits the powerful capability of capturing the transient dynamics of a swept source. This capability greatly surpasses those of the conventional OSAs. The instantaneous power evolution is also measured from the time-resolved S_0 trace.

The direction of the SOP traces has another interesting usage for determining the direction of the wavelength change. As can be seen from the inset of Fig. 6, the fast oscillation (on the order of millisecond) occurred during wavelength transitioning can be resolved in terms of the direction of the instantaneous frequency changing, which can be well correlated to the SOP evolutions shown in Fig. 5. This unique feature is also unobtainable with traditional OSAs, and can find interesting applications in the field of swept spectral analysis.

3. Spectral shape analysis

3.1 Concept

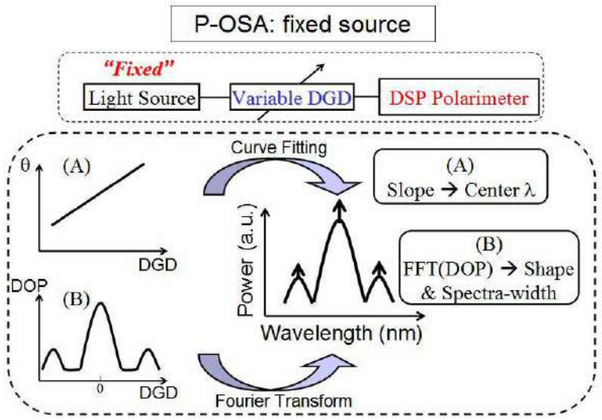

Fig. 7. Concept and principle of the proposed real-time polarimeter-based optical spectrum analyzer used for spectral shape analysis. Curve fitting of (A) determines the center frequency while Fourier transform of (B) yields the spectral shape and width. The spectral resolution is inversely proportional to the range of the variable DGD.

Figure 7 shows the concept and principle of the proposed P-OSA used for analyzing the spectrum of a fixed wavelength source. In this spectrum analysis mode, a variable DGD element is applied and the spectrum of the light source is analyzed by post-processing the recorded SOP and DOP information from the polarimeter as the DGD is tuned. For a fixed wavelength input source, the polarization rotation angle is a linear function of the DGD (τ) value. By curve fitting the measurement data using Eq. (7), one can readily obtain the center frequency of the light source.

#100540 - $15.00 USD Received 25 Aug 2008; revised 2 Oct 2008; accepted 6 Oct 2008; published 20 Oct 2008
(C) 2008 OSA

$$\theta = \theta_o + 2\pi f \tau \tag{7}$$

In order to determine the spectral shape and width of the input source, we utilize the DOP information of the light as the DGD value is varied from zero to well beyond the coherence length of the source. Since the DOP is well correlated with the self-correlation function of the light source [8], which in turn relates to the power spectrum by the Fourier transform, we obtain the following expression of the power spectrum for the case of equal power splitting between two principle polarization states of the DGD element.

$$P(\omega) = S_o \int_{-\infty}^{\infty} DOP(\tau) e^{i\omega\tau} d\tau \tag{8}$$

where S_0 is the total received power and ω is the relative angular frequency. From Eq. (7) and (8), one can conclude that for a fixed wavelength input, the spectrum of the source can be obtained accurately by measuring both the SOP and the DOP as a function of DGD, as shown in Fig. 7.

3.2 Experimental setup and results

The experimental setup for the spectrum analysis of a fixed wavelength source is shown in Fig. 8. In order to verify the capability of the proposed P-OSA, we generate two interesting spectral features by modulating a narrowband tunable laser using two different on-off-keying (OOK) modulation formats (non-return-to-zero (NRZ) and return-to-zero (RZ)) at 40-Gbit/s. The variable DGD module consists of a 2x2 polarization beam splitter (PBS) for splitting the input light into two orthogonal polarization states (port 1 → port 2 and 3) and combining them again at the output (port 2 and 3 → port 4). One motorized delay line (MDL), with a tuning range of 560 ps, is inserted in one of the arms. Both arms are path length matched when the MDL is set at its origin. Two Faraday rotating mirror (FRM) are placed at the end of both arms for ensuring polarization orthogonality and stability of the light in the two arms when they recombine at the PBS. The output port of the PBS is directed to the DSP in-line Polarimeter [6]. A polarization controller is placed at the input of the polarimetric interferometer to ensure equal power splitting of the two arms when they recombine at the PBS, and thus the largest SOP circle (shown in the inset) on the Poincare sphere, resulting in the highest frequency resolution.

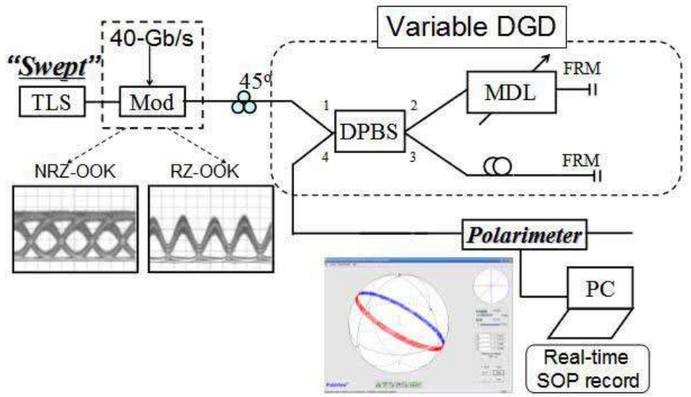

Fig. 8. Experimental setup for spectrum analysis of fixed wavelength source.

#100540 - $15.00 USD Received 25 Aug 2008; revised 2 Oct 2008; accepted 6 Oct 2008; published 20 Oct 2008
(C) 2008 OSA

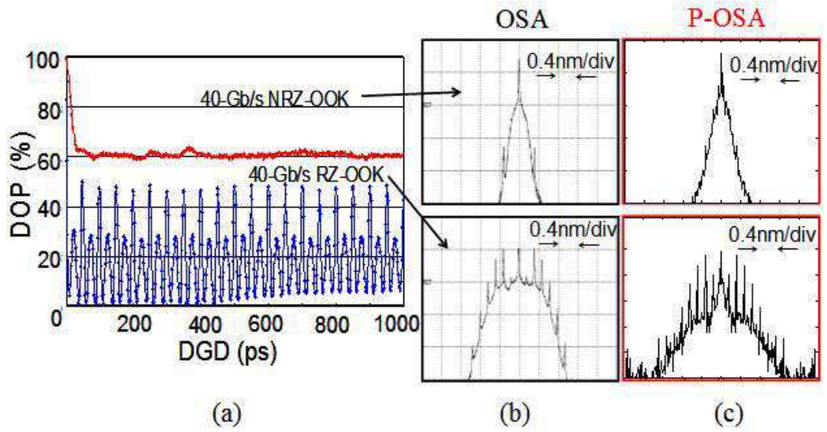

Fig. 9. (a). Experimental results of DOP values when the DGD is changed from 0 to 1000 ps for both 40-Gb/s NRZ-OOK and RZ-OOK signals. (b). The measured OSA spectra. (c). The derived P-OSA spectra for comparison.

Figure 9 shows the experimental results of the spectra analysis operation of the P-OSA. DOP of both the 40-Gb/s NRZ-OOK and RZ-OOK are recorded as the MDL values are increased from 0 to 500 ps. This corresponds to 1000 ps DGD tuning range due to the double pass configuration of the experimental setup. We can see from the DOP vs. DGD curve that the NRZ-OOK curve remains almost constant around 60% when the DGD is beyond 25 ps, while the RZ-OOK curve exhibits periodic DOP natures due to the fact that it has pronounced 40-GHz tones and some residual 20-GHz tones. By using conventional OSAs, Fig. 9(b) shows the measured spectra of both NRZ-OOK and RZ-OOK, which exhibits dominant 40-GHz spaced tones and much wider spectrum width. Based on Eqs. (7) and (8), we obtain the spectra for the two different formats by processing the rotation angle for center frequency as well as the DOP curve for spectral shape and width. Fig. 9(c) shows the derived spectra using our P-OSA method. For the same horizontal and vertical scales, we can see that the P-OSA provides very similar spectra width and shapes, with a much better spectral resolution due to the 1000-ps DGD tuning range, which corresponds to a line-width resolution of less than 1 GHz.

3.3 Spectral shape measurement of swept-wavelength source

The spectral shape and the width of a swept-wavelength source at each wavelength is an important parameter, since it contains the coherence length information of such sources for optical coherence tomography (OCT) applications [10]. However, they cannot be directly measured with conventional OSAs [11]. In this section, we demonstrate that the P-OSA can directly measure the spectral shape of a fast swept-wavelength source, in addition to the measurement of the spectral shape (power vs. frequency) of a fixed wavelength source, as described in section 3.2. With such a capability, we report, for the first time to the best of our knowledge, a unique 3-D plot of the spectral shape of a wavelength-swept light source with feature-rich spectrum as a function of its center wavelength.

Figure 10 shows the unprecedented 3-D display of our proposed P-OSA with an added dimension of the swept wavelength or time. For the swept-frequency input, every time the DGD module is tuned to a specific value, the SOP and DOP information are recorded when the wavelength of the source is swept a full cycle. By tuning the DGD element gradually from minimum to maximum value, we obtain the whole set of SOP and DOP as two dimensional matrices with respect to both swept wavelength values as well as tuned DGD points. By

#100540 - $15.00 USD Received 25 Aug 2008; revised 2 Oct 2008; accepted 6 Oct 2008; published 20 Oct 2008
(C) 2008 OSA

rearranging the two dimensional matrices, one can display each spectrum at every swept wavelength using Eqs. (7) and (8). For Fig. 10, during each wavelength scan ranging from 1540 to 1560 nm, we generate alternative 40-Gb/s NRZ-OOK or 40-Gb/s RZ-OOK modulation formats so as to obtain feature-rich yet contrasting spectra. The RZ-OOK spectrum shows a better distinguishable and equally spaced carrier tones, as well as a much wider spectrum. This capability enables detailed spectral characterization of a fast swept-wavelength source that cannot be obtained with any conventional methods.

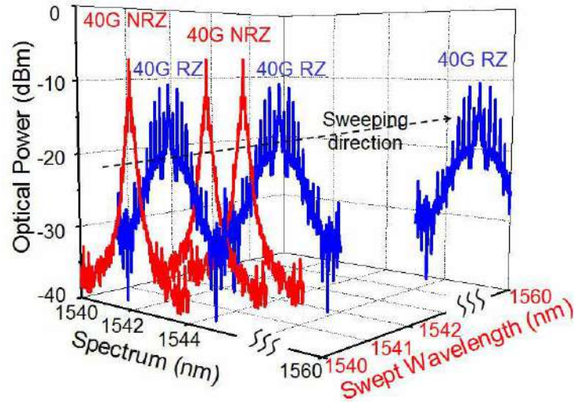

Fig. 10. A 3-D plot using the proposed P-OSA. Swept wavelength is the added dimension compared to the conventional OSAs. Note that the absolute wavelengths are directly obtained with P-OSA via curving fitting.

4. Conclusion

In summary, we have proposed and experimentally demonstrated a novel polarimeter-based optical spectrum analyzer, which utilizes both the state of polarization as well as the degree of polarization information of the light source after it passes through a variable DGD element. The speed, measurement range and the frequency resolution of the proposed P-OSA greatly surpass those of the conventional OSAs. The high speed capability is enabled by the fast sampling polarimeter and is thus ideal for measuring the spectrum of fast sweeping laser sources. This will find broad application in swept-source OCT imaging [11], as well as in the measurement of time-resolved frequency chirping [12]. The large measurement range and high resolution capability are realized by utilizing the unique information of the directional SOP evolution. This will be very useful for measuring the spectra drift of ultra-narrow line width lasers. Finally, we have also demonstrated a unique 3-D plot which displays the spectral shape of a swept-wavelength light source at each instantaneous wavelength.

#100540 - $15.00 USD Received 25 Aug 2008; revised 2 Oct 2008; accepted 6 Oct 2008; published 20 Oct 2008
(C) 2008 OSA

Vol. 6, No. 1 / January 2007 / JOURNAL OF OPTICAL NETWORKING 13

Programmable optical delay generator with uniform output and double-delay capability

L.-S. Yan, L. Lin, A. Belisle, S. Wey, and X. Steve Yao

General Photonics Corporation, 5228 Edison Avenue, Chino, California 91710, USA
lsyan@generalphotonics.com

Received June 28, 2006; revised October 23, 2006; accepted October 31, 2006; published December 13, 2006 (Doc. ID 72385)

We demonstrate a programmable optical delay generation scheme incorporating both single- and double-pass configurations. The generator uses fiber coils with binary lengths separated by microelectro mechanical systems (MEMS)-based optical switches and can provide a delay range of up to 80 and 160 μs for single- and double-pass configurations, respectively, with corresponding resolutions of ~39 and 78 ns. The response time of the delay generation is <1 ms with an output power variation of <0.3 dB as the delay varies. The described approach can be applied to packet-switching optical networks, microwave photonic networks, and measurement systems. © 2006 Optical Society of America

OCIS codes: 060.2360, 060.4250.

1. Introduction

Programmable time-delay lines with ranges from nanoseconds to milliseconds are key elements in various applications, such as optical networking functions (buffering, dispersion management, slowing light, encoder–decoders, etc.), rf systems (radar, wireless communication, rf link emulation, cell site characterization, and calibration, etc.), as well as measurement systems (laser linewidth, phase noise, etc.) [1–10]. Various configurations have been proposed and demonstrated to generate tunable time delays, including fiber coils [11,12], fiber Bragg gratings [8–13], integrated waveguide techniques [14,15], fiber loops [2], microelectro mechanical systems (MEMS)-switch-based configurations [16–18], and other methods [19,20]. Most of the generated delays (except fiber-coil-based ones) are limited to a range of picoseconds to nanoseconds. On the other hand, the fiber-coil-based time-delay approach is an old concept and has been demonstrated using either the square-root cascaded delay line configuration (SRODEL) [11] or the binary delay line configuration (BIFODEL) [12]. The BIFODEL architecture is the optimum choice for implementation of delay-compressive delay lines [7].

In this paper, we demonstrate a BIFODEL-architecture-based programmable optical delay generation scheme incorporating both single- and double-pass configurations. The generator uses fiber coils with binary lengths separated by MEMs-based optical switches and can provide a delay range of up to 80 and 160 μs for single- and double-pass configurations with corresponding resolutions of ~39 and 78 ns. The response time of the delay generation is <1 ms with an output power variation of <0.3 dB as the delay varies. The double-path configuration has the advantages of polarization-independent (i.e., polarization maintaining with single-mode fiber) and saving fiber coils for less space (size) requirements. Furthermore, we also discuss the applications of such approach into packet-switching optical networks, microwave photonic networks, and measurement systems.

2. Concept and Setup

The ODG setup is shown in Fig. 1. Twelve MEMS-based 2×2 optical switches are cascaded and controlled by a microprocessor. For each optical switch (except the last one), one output is directly connected to the input of the following switch, while the other output is connected through an optical fiber delay coil manufactured from standard

1536-5379/06/010013-6/$15.00 © 2006 Optical Society of America

Vol. 6, No. 1 / January 2007 / JOURNAL OF OPTICAL NETWORKING 14

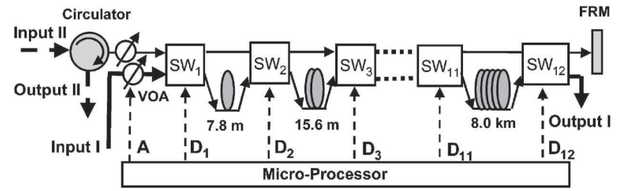

Fig. 1. Configuration of the programmable delay generator (ODG), single-pass (input I and output I) and double-pass (input II and output II); SW_i, MEMs-based optical switches; FRM, Faraday rotator mirror; VOA, Variable optical attenuator.

single-mode fiber (SMF). The lengths of the fiber coils are designed in a binary order from ~7.8 m (corresponding to ~39 ns delay) to ~8.0 km; thus, the total generated optical delay T_{total} is given by

$$T_{\text{total}} = \Delta T \sum_{n=1}^{N} [1 - (-1)^{d_n}] 2^{n-2}, \tag{1}$$

where ΔT is the delay of the minimum length coil (7.8 m), N is the total number of switches, and $d_n(=0,1)$ is the binary value of the nth switch condition, which determines whether or not the fiber coil following the nth optical switch is incorporated into the optical path.

To enhance the delay generation capability without complicated hardware modification, we simply incorporate an optical circulator and a Faraday rotator mirror (FRM) into the setup to create a double-pass configuration. This approach can significantly reduce the required package space of the delay line without adding another switch and a much longer delay coil (two times longer of the most significant coil). The result is two possible modes of operation: (i) For single-pass delay generation, light enters from one input port of the first switch and passes through all of the other switches and/or fiber coils, then exits from one output port of the last switch. (ii) Alternatively, light can be input from the first port of the circulator, which connects to the other input port of the first switch, then go through the other 11 switches and/or coils. After output from the last optical switch, the light is reflected at the FRM, passes back through the same optical path, and finally exits from the third port of the circulator. This configuration doubles the generated optical delay using the corresponding logic control.

Using the single- and double-pass configurations described above, delay ranges of up to 80 (corresponding to ~16 km SMF) and 160 μs are achieved. Note that the FRM in the setup provides the additional advantage of eliminating polarization-dependent effects along the optical path. The state of polarization (SOP) is maintained for the input and output light without the use of PM fiber; therefore, the delay generator can provide a low-cost solution for applications that require stable polarization. In addition, variable optical attenuators (VOA) are used to dynamically tune the insertion loss at different delay states, allowing the output power to remain relatively constant during delay switching.

3. Experimental Results

Insertion loss is one of the key parameters for programmable delay lines. Its variation with changes in delay is of particular interest. Figure 2 illustrates the insertion loss variation of the delay generator with delay and wavelength change. Figures 2(a) and 2(b) show the loss variation with delay change at 1550 nm for the single-pass case. Before the output power balancing using the VOA, the output power changes a lot at different delays. The typical loss ranges from ~3.4 to 8.5 dB including both the fiber coils and switches [Fig. 2(a)]. In our design, the VOA is automatically controlled by the microprocessor, using a look-up table to balance the output power at different logic states (delays). Therefore, the loss variation is limited to <0.3 dB over all delay states [Fig. 2(b)]. This feature ensures a stable performance for the applications that are sensitive to optical-signal-to-noise ratio (OSNR). Figure 2(c) shows the insertion loss profile of our delay generator over different wavelengths at a single switching condi-

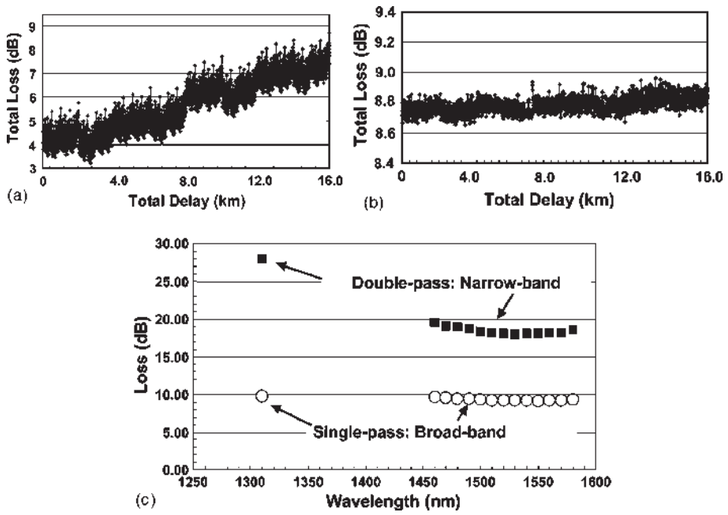

Fig. 2. (a), (b) Insertion loss variation at different delay settings (2048 logic states for the single-pass configuration at 1550 nm): (a) without automatic power balancing (b) using the VOA to automatically control the overall loss, thus the total variation <0.3 dB. (c) Insertion loss variations of the ODG at different wavelengths (single pass at 40 μs and double pass at 80 μs).

tion (40 and 80 μs delay for single- and double-pass. At 1550 nm, the typical insertion losses for single and double passes are ~9.1 and 18.5 dB with the VOA's automatic balancing. Since the optical switches are broadband devices (>400 nm), the insertion loss variation in the single-pass configuration is mainly due to the fiber coil itself (the range of wavelengths measured is limited by the experimental setup). However, there are two narrowband devices in the double-pass configuration: the optical circulator and the FRM; thus, the insertion loss of the double-pass configuration is much higher than twice that of the single-pass configuration at 1310 nm. The insertion loss of the single- and double-pass configurations at 1310 nm are ~10.0 and 28.4 dB, respectively. Note that the loss variation at different wavelengths is not necessary to be corrected using VOA due to the extremely high loss at certain wavelengths.

As mentioned, incorporating the FRM into the double-path configuration has another advantage, i.e., reducing the polarization-dependent effects, which is a desirable feature for some field applications (e.g., airborne systems). This is shown in Fig. 3(a), where the output polarization state keeps stable on the Poincaré sphere even under strong polarization perturbation on the delay line. Moreover, a fast response time is also required for dynamic applications. The delay generation speed of

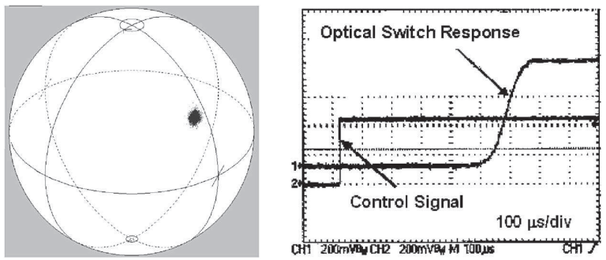

Fig. 3. (a) Polarization stability of the double-path configuration with external polarization perturbation; (b) measurement result of the response time for the ODG: <1 ms (~700 μs).

the ODG was characterized by measuring the transient traces from one delay to another, as shown in Fig. 3(b). The control signal is the electronic signal from the microprocessor, while the optical switch response is measured using a fast photodetector. If all 12 switches respond simultaneously (in parallel), the total response time is <700 μs, suitable for most applications.

4. Applications

As mentioned in Section 1, the programmable optical delay generator can generate a series of digitized delay values for various applications, while it cannot provide continuous tuning for some special applications. In addition, the resolution of the ODG is limited by the "ability to manufacture" the minimum optical fiber length for fusion splicing (typically several tens of centimeters, with corresponding delays of hundreds of picoseconds), which may also be inadequate in some application. The demonstrated ODG can find its applications in the following areas:

(i) Optical networking functions: Due to the dynamic nature of optical packet-switching networks, programmable optical delay lines are essential for applications [1–4] such as optical buffering, temporal encoding to decoding, or even the management of optical dispersive effects. Buffers with tunable size are desirable to handle different packet sizes or variable bit rate (VBR) for optical networks (Fig. 4). Compared with previous looplike configurations, the ODG approach has the advantages of easier control and higher resolution. In addition, network carriers or equipment manufactures may use the ODG as an environmental emulator to evaluate the performance of the equipment or the system tolerance assuming data traffic from different nodes.

(ii) Microwave photonic networks: Optical delay lines have many applications for microwave photonic networks, such as phased-array antenna systems, optical wireless networks, signal processing (transversal filters), wireless (radar) ranging and calibration, and so on. Fixed delay arrays are used for some applications, while programmable delay lines are valuable to calibration procedures of wireless (cell) stations. An illustration of such an application is shown in Fig. 5. The wireless signal is separated into two paths: one is transmitted normally through the air and received by a wireless receiver, while another path is first converted into an optical signal using electro-optic modulator, and then transmitted through the programmable ODG. After ODG, the signal is converted back to the rf signal through optical-to-electronic conversion. The two rf signals will be combined and analyzed; therefore the ranging, noise, and related information of the wireless signal can be retrieved.

(iii) Measurement systems: Fiber delay lines are also very useful for some measurement systems, especially the linewidth of a laser source, phase noise, and so on. Figure 6 shows a typical diagram of a delayed self-heterodyne method to measure the linewidth of a laser source. It is an interferometric technique that incorporates a certain length of fiber delay coil in one arm. The superimposed beams from two arms are detected through a photodetector and thus analyzed using a spectrum analyzer. If the time delay is larger than the coherence length of the laser (normally at least five times longer is recommended for measurements), the phases of two beams are essen-

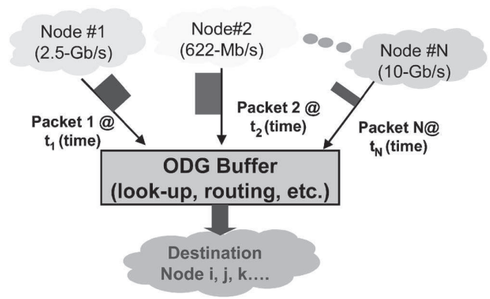

Fig. 4. Using ODG as a tunable optical buffer for a dynamic packet-switching network.

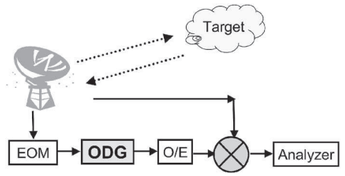

Fig. 5. Illustration of a rf ranging or calibration system utilizing the ODG platform. EOM, electro-optic modulator.

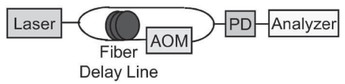

Fig. 6. Diagram of a delayed self-heterodyne measurement of a laser linewidth.

tially uncorrelated. Therefore the final output spectrum is a simple self-convolution of the spectrum of the laser itself, from which the linewidth can be readily obtained. As examples, a tunable laser with 50 kHz linewidth has a coherence length ~1.9 km, while the coherence length of a regular distributed feedback (DFB) laser with 50 MHz linewidth is approximately 190 m. Due to the variety of current available laser sources (Tunable, DFB, feedback positive, etc.), and the corresponding linewidth ranges from tens of kilohertz to gigahertz, a tunable (or programmable) optical delay generator certainly will facilitate such measurements.

5. Conclusions

The single- and double-path configurations of the above-demonstrated optical delay generator provide programmable optical delays with uniform output power, which is desirable for most of the applications. Advantages also include fast response time, large number of control bits, and high resolution. The potential delay range up to 0.25 ms with the same package size is under design and evaluation using the similar approach. When incorporating delay lines with more precise tuning resolutions [21], a widely and fully tunable delay generation is possible for various applications.

References

1. Y.-K. Yeo, J. Yu, and G.-K. Chang, "A dynamically reconfigurable folded-path time delay buffer for optical packet switching," IEEE Photon. Technol. Lett. **16**, 2559–2561 (2004).
2. R. Langenhorst, M. Eiselt, W. Pieper, G. Grosskopf, R. Ludwig, L. Kuller, E. Dietrich, and H. G. Weber, "Fiber loop optical buffer," J. Lightwave Technol. **14**, 324–335 (1996).
3. T. J. Eom, S. J. Kim, T.-Y. Kim, C.-S. Park, U.-C. Paek, and B. H. Lee, "Realization of true-time-delay using cascaded long-period fiber gratings: theory and applications to the optical pulse multiplication and temporal encoder/decoder," J. Lightwave Technol. **23**, 597–608 (2005).
4. R. Geldenhuys, Z. Wang, N. Chi, I. Tafur Monroy, A. M. J. Koonen, H. J. S. Dorren, F. W. Leuschner, G. D. Khoe, and S. Yu, "Multiple recirculations through crosspoint switch fabric for recirculating optical buffering," Electron. Lett. **41**, (2005).
5. J. Mora, B. Ortega, A. Di'ez, M. V. Andrés, J. Capmany, J. L. Cruz, and D. Pastor, "Highly tunable optically switched time delay line for transversal filtering," Electron. Lett. **39**, 1799–1800 (2003).
6. T. Duthel, S. L. Jansen, M. Otto, P. M. Krummrich, and C. G. Schaffer, "Tunable all-fiber delay line filter for residual dispersion compensation in 40-Gbit/s systems," Electron. Lett. **40**, 1291–1292 (2004).
7. A. P. Goutzoulis and D. K. Davies, "Hardware compressive 2-D fiber optic delay line architecture for time steering of phased array antennas," Appl. Opt. **29**, 5353–5359 (1990).
8. J. L. Corral, J. Marti, S. Regidor, J. M. Foster, R. Laming, and M. J. Cole, "Continuously variable true time-delay optical feeder for phased-array antenna employing chirped fiber grating," IEEE Trans. Microwave Theory Tech. **45**, 1531–1536 (1997).
9. H. Tsuchida, "Simple technique for improving the resolution of the delayed self-heterodyne method," Opt. Lett. **15**, 640–642 (1990).
10. O. Raz, R. Rotman, and M. Tur, "Wavelength-controlled photonic true time delay for wide-band applications," IEEE Photon. Technol. Lett. **17**, 1076–1078 (2005).
11. R. A. Soref, "Programmable time-delay devices," Appl. Opt. **23**, 3736–3737 (1984).
12. A. P. Goutzoulis, D. K. Davies, and J. M. Zomp, "Prototype binary fiber optic delay line," Opt. Eng. (Bellingham) **28**, 1193–1202 (1989).

13. V. Italia, M. Pisco, S. Campopiano, A. Cusano, and A. Cutolo, "Chirped fiber Bragg gratings for electrically tunable time delay lines," IEEE J. Sel. Top. Quantum Electron. **11**, 408–416 (2005).
14. B. Vidal, J. L. Corral, and J. Marti, "Optical delay line employing an arrayed waveguide grating in fold-back configuration," IEEE Microw. Wirel. Compon. Lett. **13**, 238–240 (2003).
15. B. Howley, Y. Chen, X. Wang, Q. Zhou, Z. Shi, Y. Jiang, and R. T. Chen, "2-bit reconfigurable true time delay lines using 2×2 polymer waveguide switches," IEEE Photon. Technol. Lett. **17**, 1944–1946 (2005).
16. J. D. Shin, Y. M. Yoon, B. M. Jung, and B.-G. Kim, "A 4-bit optical true time-delay for 10-GHz phased array antennas using optical MEMS switches and fiber-optical delay lines," in *The 17th Annual Meeting of the IEEE Laser and Electro-Optics Society (LEOS)* (2004), Vol. 1, pp. 274–275.
17. J. D. Shin, B.-S. Lee, and B.-G. Kim, "Optical true time-delay feeder for X-band phased array antennas composed of 2×2 optical MEMS switches and fiber delay lines," IEEE Photon. Technol. Lett. **16**, 1364–1366 (2004).
18. V. Kaman, X. Zheng, R. J. Helkey, C. Pusarla, and J. E. Bowers, "A 32-element 8-bit photonic true-time-delay system based on a 288×288 3-D MEMS optical switch," IEEE Photon. Technol. Lett. **15**, 849–851 (2003).
19. P. Maak, I. Frigyes, L. Jakab, I. Habermayer, M. Gyukics, and P. Richter, "Realization of true-time delay lines based on acoustooptics," J. Lightwave Technol. **20**, 730–739 (2002).
20. O. Raz, R. Rotman, Y. Danziger, and M. Tur, "Implementation of photonic true time delay using high-order-mode dispersion compensating fibers," IEEE Photon. Technol. Lett. **16**, 1367–1369 (2004).
21. Data sheet of miniature motorized optical variable delay line MDL-002, Web site http://www.generalphotonics.com/MiniMDL.htm.

Letter Vol. 41, No. 12 / June 15 2016 / Optics Letters 2819

Optics Letters

Distributed Transverse Stress Measurement Along an Optic Fiber Using Polarimetric OFDR

CHANGJIANG WEI,[1] HONGXIN CHEN,[2] XIAOJUN CHEN,[2] DAVID CHEN,[3] ZHIHONG LI,[4] AND X. STEVE YAO[1,2,*]

[1]Photonics Information Innovation Center (PIIC), Hebei University, Baoding, China
[2]General Photonics Corporation, 5228 Edison Ave., Chino, California 91710, USA
[3]Verizon Communications, 2400 N. Glenville Dr., Richardson, Texas 75082, USA
[4]Suzhou Optoring, Jiansu Province, China
*Corresponding author: steveyao888@yahoo.com

Received 4 April 2016; revised 29 May 2016; accepted 30 May 2016; posted 31 May 2016 (Doc. ID 262457); published 15 June 2016

We report a novel polarimetric optical frequency domain reflectometer (P-OFDR) that can simultaneously measure both space-resolved transverse stresses and light back-reflections along an optic fiber with sub-mm spatial resolution. By inducing transversal stresses and optical back-reflections at multiple points along a length of optic fiber, we demonstrate that our system can unambiguously distinguish the stresses from the back-reflections of a fiber with a fiber length longer than 800 m, a spatial resolution of 0.5 mm, a maximum stress level of up to 200 kpsi (1379 Mpa), a minimum stress of about 10 kpsi (69 Mpa), and a stress measurement uncertainty of 10%. We show that our P-OFDR can clearly identify the locations and magnitudes of the stresses inside a fiber coil induced during a fiber winding process. The P-OFDR can be used for fiber health monitoring for critical fiber links, fiber gyro coil characterization, and other distributed fiber sensing applications. © 2016 Optical Society of America

OCIS codes: (060.2270) Fiber characterization; (060.2370) Fiber optics sensors; (120.4640) Optical instruments; (260.5430) Polarization.

http://dx.doi.org/10.1364/OL.41.002819

Connectivity is arguably one of the most important aspects of our society today. Fiber optic telecommunication systems make up the backbone of such connectivity, and its reliability is becoming increasingly more important. Therefore, health monitoring for the fiber infrastructure networks for applications, such as stock exchanges, financial institutions, and military installations, are becoming increasingly critical. An ideal fiber health monitoring system is required not only to be able to detect a broken fiber, but also to detect and locate the section of an unhealthy fiber, such as a fiber section with tight bending or with high internal stresses, before it breaks, to allow the service providers to proactively prevent unexpected service failures.

Distributed stress sensing is another area of active research with many important applications [1–4], one of which is to measure the stresses along the fiber in a fiber gyro coil, the most critical component whose quality directly affects the accuracy of the gyro [5,6]. One of the most common coil defects is the stress induced during the coil winding process. In a fiber coil made with polarization maintaining (PM) fiber, the winding stresses at different locations can introduce polarization crosstalks at these locations along the fiber, which can be detected by a distributed polarization crosstalk analyzer [7]. However, a fiber coil made with non-polarization maintaining single-mode (SM) fiber is commonly used for the depolarized fiber optic gyro [8]. In such SM fiber coils, the microbending can induce large stress on the fiber, especially at crossover locations where the fiber transitions from one layer to another. We speculate that such bending, together with the action of potting adhesive, can introduce large polarization dependent loss (PDL) and polarization mode dispersion (PMD) in the fiber coil, which may degrade the performance of the SM fiber coils.

Current commercially available optical time-domain reflectometer (OTDR) can monitor, detect, and locate a section of broken fiber or a fiber section with significant fiber losses caused by severe fiber bending [9]. However, in such situations, the network failure has already occurred and the damage is already done. Although a Brillouin OTDR is able to detect potential optical cable fault due to excessive strain, such a technique may give fault alarms because it cannot distinguish the temperature effect from that of the strain [10,11]. Polarization sensitive OTDRs were reported for measuring the distributed polarization mode dispersion (PMD) in telecommunication fiber links [12,13]. However, the spatial resolution of the proposed method were not sufficient for detecting the extremely high stress-induced birefringence for the applications intended in this Letter, limited by the pulse width and the speed of the electronics. In 2004, Froggatt *et al.* used a technique of cross-correlating a current measured optical frequency domain reflectometry (OFDR) signal with a reference OFDR trace to obtain the space-resolved strain changes along the optical fiber [14]. However, such a method also suffers from the deficiency that it cannot distinguish the strain from the temperature. In addition, no absolute strain or stress information can be obtained because such a measurement is only relative to the reference. The polarimeteric OFDRs reported in [15–18] are capable of detecting distributed PMD and different birefringences along the fiber; however, they required the fiber under test (FUT) to be stable to avoid polarization fluctuation during the measurement, which is not practical for field applications. Therefore, there is a need for a fiber stress and bend monitoring system to unambiguously detect and locate unhealthy fiber sections with excessive stress caused by tight bends or transverse pressure so as to prevent unexpected failures or breakage in fiber optic networks. Similarly, there is also a need to use a length of fiber to measure the space-resolved stresses with absolute values (not relative) along the fiber for distributed sensing applications.

In this Letter, we report a novel polarimetric optical frequency domain reflectometer (P-OFDR) for space-resolved transverse stress or bend measurements along an optic fiber, which does not require the FUT to be physically stable. The method is based on measuring the local birefringence induced by transverse stress via the photoelastic effect in the fiber. By inducing stresses via fiber bending at multiple points along the optical fiber, we demonstrate that our system can simultaneously obtain both the distributed stress and the reflection curves as a function of distance along the fiber, unambiguously distinguishing the stresses from the optical back-reflections. Our preliminary experiments show that our prototype system has a spatial resolution of 0.5 mm, a measurable distance of over 800 m, a maximum stress level of up to 200 kpsi (1 kpsi = 6.9 MPa), a minimum stress (or sensitivity) of about 10 kpsi, and a stress measurement uncertainty around 10%. Note that unlike the cross-correlation method in [14], in our system, the temperature does not affect the stress or birefringence measurement, unless the temperature change induces a real stress on the fiber via other effects, such as the thermal expansion of a bobbin beneath the fiber or the thermal crimping of adhesives around the fiber. Therefore, our reported technique can also be implemented for the distributed fiber sensing applications for detecting the value of stress along the fiber, although it cannot differentiate whether the stress is applied or thermally induced. As an example for the distributed sensing applications, we show that our prototype can clearly identify transversal stress points in a fiber coil induced during the winding process when the fiber transitioning from one layer to the other. The reported method is not sensitive to the state of polarization (SOP) variations from fiber cable movement so that potentially it is well suitable for the field fiber network health monitoring and fiber sensing applications.

In the sections below, we describe the hardware configuration and the theory behind our P-OFDR for measuring the space-resolved transverse stress along an optical fiber with the advantages of single-end operation, high spatial resolution, high stress range, and insensitivity to temperature and SOP variations in comparison to other measurement techniques [10–15]. Figure 1 shows the setup for our P-OFDR measurement system, where a tunable laser with a linewidth around 100 kHz is continuously tuned up to 4 nm around 1550 nm. A small fraction of light ~5% from coupler 1 is split and then sent to a Faraday rotation mirror (FRM) based Michelson interferometer with a relative time delay of 10 μs for generating clock signals at each "zero-crossing" position of the optical interference fringe signals. The generated real-time clock signals were then used for the P-OFDR raw data sampling. The light was then further split by a 90/10 coupler (coupler 3), in which 10% of the light was used as a local oscillator light to coherently probe Rayleigh back scattering (RBS) light, and 90% of the light was then sent to the fiber under test (FUT) via a circulator. The SOP before entering and after exiting the FUT is randomly varied by an all-fiber polarization controller to uniformly cover the Poincaré sphere. The Rayleigh backscattered light from different locations of the fiber is brought to interfere with the portion of light directly from the tunable laser via a polarization diversity interferometer (the dotted-line box in Fig. 1). The interference signals of the two polarization components are analyzed after detection by PD2 and PD3, and the local birefringence information is then calculated. The transverse stress related to the birefringence is then obtained using the signal analysis procedures described below.

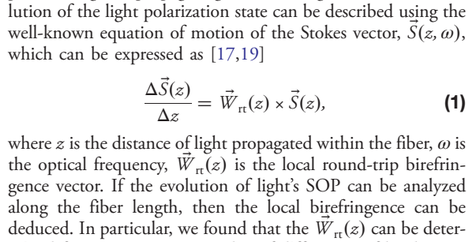

Fig. 1. Experimental setup of distributed transversal stress measurement using a P-OFDR. PBS, polarization beam splitter; PD 1–3, photo detectors. Note that the pigtails of couplers 1 and 3 are of polarization maintaining (PM) to avoid polarization fluctuations when light interferes. PBS 1 and 2 are free-space polarization beam splitters; BS 1 and 2 are free-space polarization insensitive beam splitters. The PM fiber inputting to PBS2 is oriented such that the power is equally split by PBS2.

The optical fibers with non-perfect circular symmetry or with bend, twist, or other transverse stress often exhibit local birefringence. Under assumption of no polarization-dependent loss (PDL), the light passing through a section of optical fiber with birefringence will experience a variation of SOP. When a polarized light is propagating in a birefringence fiber, the evolution of the light polarization state can be described using the well-known equation of motion of the Stokes vector, $\vec{S}(z,\omega)$, which can be expressed as [17,19]

$$\frac{\Delta\vec{S}(z)}{\Delta z} = \vec{W}_{\pi}(z) \times \vec{S}(z), \tag{1}$$

where z is the distance of light propagated within the fiber, ω is the optical frequency, $\vec{W}_{\pi}(z)$ is the local round-trip birefringence vector. If the evolution of light's SOP can be analyzed along the fiber length, then the local birefringence can be deduced. In particular, we found that the $\vec{W}_{\pi}(z)$ can be determined from a mean-square value of differences of local transmission between two closely spaced fiber sections, similar to [13] in which the local birefringence was obtained by analyzing the SOP evolution between two closely spaced frequencies of light. Assuming the local birefringence $W(z) = W_{\pi}(z)/2$ and following the same procedure as in [13], except substituting the changes in optical frequency ω in [13] with Δz, we obtain

$$W(z) = \frac{1}{2\Delta z} \cdot \sqrt{15\langle \Delta T^2(z)\rangle_{1/O\text{-}SOP}}, \tag{2}$$

0146-9592/16/122819-04 Journal © 2016 Optical Society of America

where $\Delta T(z) = T(z + \Delta z/2) - T(z - \Delta z/2)$ is the normalized light power difference between two positions at $z + \Delta z/2$ and $z - \Delta z/2$, and $T(z) = P_i(z)/[P_2(z) + P_3(z)]$ is the normalized light power at the location z, where $P_i(z)$ is the light power of one polarization component from PBS1 at z measured with one of the detectors PD_i $(i = 2, 3)$. In Eq. (2), $\langle \Delta T^2(z) \rangle_{I/O\text{-}SOP}$ stands for averaging over random input and output SOP variations. The fiber transverse stress as a function of the distance can be extracted from measured distributed fiber birefringence [20,21].

A key aspect of our P-OFDR approach is that the back-reflected light from the FUT at the two neighboring locations is subsequently detected, and their SOPs are analyzed for many random and uniformly distributed input and output SOPs that are uncorrelated with respect to each other. It is worthy to note that because the input SOPs incident into and the output SOP exited from FUT are random and without specific requirement, the system is independent of the SOP variations from fiber cable movement and, therefore, is well suited for field applications, where the SOP along the fiber is constantly changing [13].

An example of the measured reflection trace for an FUT length up to 860 m is shown in Fig. 2, where the OFDR back-reflection curve was extracted from the sum of two squared light intensities measured by two detectors (PD2 and PD3), and its reflectivity was calibrated by an internal reference reflector (not shown in Fig. 1).

To demonstrate the measurement principle described in the sections above, we made an experimental test by using bending-induced transverse stresses along a FUT made with a bending insensitive SM fiber (Corning ClearCurve ZB) where eight bending loops at eight different FUT locations were designed. The bending radius is different at different positions, and they are typically between 5 to 15 mm. In addition to the eight bends, there are also six FC/APC connectors and a fiber splice. The results are illustrated in Fig. 3. In our experiment, the polarization controller randomly adjusted its launched SOP, and the receiver analyzed the received signal corresponding to 200 different polarization controller settings randomly distributed on the Poincaré sphere. The tunable laser is scanned in a range of 4 nm with a scanning speed of 10 nm/s. The results, as shown in the upper and lower plots of Fig. 3, were acquired simultaneously by the same data sampling of the raw data, but with different signal processing algorithms, where the reflection trace in the upper plot was computed by the sum of the squared measured results from two photodetectors (PD2 and PD3 in Fig. 1), and the fiber birefringence trace $W(z)$ was extracted using Eq. (2) with an average of over 200 inputs and analyzed

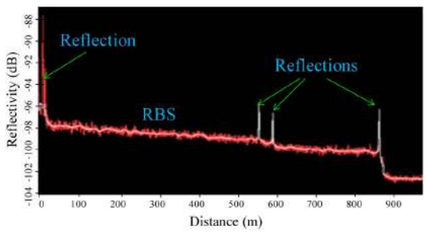

Fig. 2. Measured OFDR reflection trace with back-reflections for a FUT with a length up to 860 m.

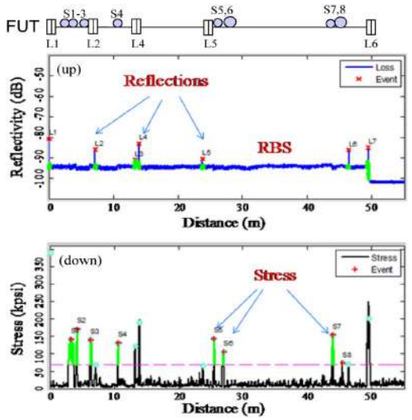

Fig. 3. P-OFDR signal from a length of fiber with six connectors and one splice for introducing reflections and eight fiber loops with different diameters for inducing different amount of stresses. Upper curve, measured reflections L1–7; lower curve, measured fiber-bending-induced stress S1–8.

SOPs. The displayed stress value was obtained by a calibration procedure with a calibration weight. The measurement and computation take about 5 min to complete.

As we can see, in the reflection trace (the upper plot of Fig. 3), there are seven light back-reflections associated with six connectors (L1, 2, and 4–7) and a fiber splice (L3). Of particular interest is the stress measurement as shown on the lower plot of Fig. 3 with features associated with fiber bendings, connectors, and splice. With the cross-reference of reflection trace, eight fiber-bending-induced stresses features S1–8 that can be unambiguously distinguished from those of light back-reflections. It is worth noting that the induced transverse stress is higher for smaller bend radii than for larger bend radii, consistent with the bending-induced birefringence calculations [20]. All eight bending-induced fiber birefringence events are seen cleanly with a signal-to-noise ratio over 2. The spatial resolution of our system for the stress measurement is of 0.5 mm, determined by the wavelength scanning range of the laser. The measurement uncertainty from multiple measurements is ~10% when 200 randomly distributed SOPs were used, and it can be reduced by averaging more SOPs, but with longer measurement time. The relative stress levels of all eight fiber loops are consistent with [20].

As an example for distributed stress sensing, we use our P-OFDR to identify stress locations and magnitudes along the optical fiber inside a fiber coil, as mentioned in the introduction. The information obtained can be used for improving the winding process and minimizing such stresses for making better fiber coils, such as a crossover free coil. To demonstrate its capabilities, our prototype system is used to measure a fiber coil with a diameter of 80 mm and clearly identifies periodic stress peaks, as shown in Fig. 4. The periodicity of 23 peaks is the same as the length of each layer of the coil, which is consistent with the expectation that stresses are induced at fiber crossover

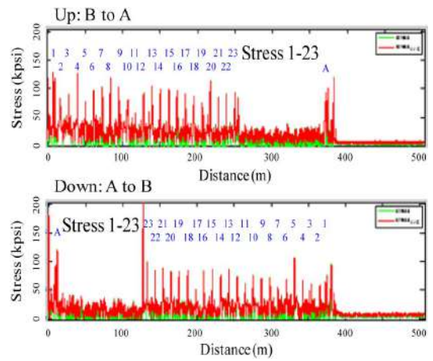

Fig. 4. Distributed stress measurement of a 250 m fiber coil connected with a loose fiber about 130 m in length. Upper, light enters the fiber from the coil side B; Lower, light enters the fiber from the spool side A. The fiber used is the bend insensitive fiber Corning ClearCurve ZBL single-mode optical fiber, and the tension for winding the coil is about 10 g.

points when the fiber transitioning from one layer to the other during the winding process. There are 23 peaks in total, corresponding to the 23 layers of fiber in the fiber coil. To further prove that the periodic peaks are, indeed, from the coil winding, we spliced a length of fiber around 130 m loosely wound on a large spool of about 50 cm onto the coil and perform the distributed stress tests from both ends of the combined fibers A and B, with the A side being the large spool and the B side being the fiber coil. Indeed, we only observed the periodic stress peaks in the fiber coil, not in the loosely wound fiber spool, no matter which direction we launched the light. This preliminary test result of transversal stresses on the fiber coil indicate that our P-OFDR is sufficiently sensitive to detect such a small winding induced stresses and is promising for the production process control to improve the fiber coil quality. All measurements are conducted at room temperature.

In conclusion, we demonstrated a novel polarimetric OFDR system that can measure space-resolved transversal stresses along an optic fiber from a single-end of an optic fiber or fiber cable, independent of the temperature of the FUT. By inducing transversal stresses and reflections at multiple points along an optic fiber, we demonstrated that our P-OFDR prototype system can simultaneously obtain both the distributed stress and reflection curves as a function of distance from the same acquisition, unambiguously distinguishing the stresses from any light back-reflections, including the Rayleigh backscattering and Fresnel back-reflection. Our P-OFDR system can measure fiber transversal stress or bend for over 800 m with a spatial resolution of 0.5 mm, a maximum stress of up to 200 kpsi (1379 Mpa), a minimum stress of 10 kpsi (69 Mpa), and a measurement uncertainty of 10%. The latter two can be reduced with lower noise electronics and more SOP averages. Stress larger than 200 kpsi can be achieved by increasing the wavelength scanning range and, hence, enhancing the spatial resolution. We expect the measurement range can be increased to over 20 km with a tunable laser with a linewidth less than 5 kHz with appropriate frequency turning linearity [22]. We further demonstrate that our system is sufficiently sensitive to identify stress points in a fiber coil induced during the winding process when the fiber transitioning from one layer to the other, and can be used for fiber gyro coil inspection applications. Finally, our P-OFDR system is robust against SOP variations caused by fiber cable movement and is well suited for the field measurement of stresses in the fiber and, therefore, is ideal for the fiber infrastructure health monitoring and for distributed fiber optical sensing applications. Note that unlike the reports in [16–18], we aim at detecting the high birefringence induced by large stresses, which may cause the premature failures of optical fibers, especially the bending insensitive fibers with negligible bending losses. Portion of this Letter were presented at OFC2016 [23].

Funding. Comprehensive Capability Enhancement Program of Regional Universities in Central Western China; Advanced Talents Program of Hebei Educational Committee (GCC20144020); International Science and Technology Cooperation Program of China (2010DFB13180, 2014DFA12930); Foundation Research Project of Jiangsu Province (BK20130373, BK20130374); Internal Development Funding of General Photonics Corporation.

Acknowledgment. We thank the fruitful discussions with Dr. Zhenyang Ding of Tianjin University.

REFERENCES

1. B. Soller, D. Gifford, M. Wolfe, and M. Froggatt, Opt. Express **13**, 666 (2005).
2. D. P. Zhou, Z. Qin, W. Li, L. Chen, and X. Bao, Opt. Express **20**, 13138 (2012).
3. X. Bao and L. Chen, Sensors **12**, 8601 (2012).
4. Z. Ding, X. S. Yao, T. Liu, Y. Du, K. Liu, Q. Han, Z. Meng, and H. Chen, Opt. Express **20**, 28319 (2012).
5. Z. Li, Z. Meng, L. Wang, T. Liu, and X. S. Yao, IEEE Photon. Technol. Lett. **27**, 549 (2015).
6. Z. Li, Z. Meng, T. Liu, and X. S. Yao, Opt. Express **21**, 2521 (2013).
7. Z. Li, X. S. Yao, X. Chen, H. Chen, Z. Meng, and T. Liu, J. Lightwave Technol. **33**, 372 (2015).
8. B. Szafraniec and G. A. Sanders, J. Lightwave Technol. **17**, 579 (1999).
9. H. Chen and M. LeBlanc, IEEE Photon. Technol. Lett. **16**, 2198 (2004).
10. Y. G. Lu, X. P. Zhang, Y. M. Dong, F. Wang, and Y. H. Liu, J. Phys. Conf. Ser. **48**, 1387 (2006).
11. Y. Dong, L. Chen, and X. Bao, Opt. Lett. **36**, 277 (2011).
12. A. Galtarossa, D. Grosso, and L. Schenato, IEEE Photon. Technol. Lett. **20**, 1944 (2008).
13. N. Cyr, H. Chen, and G. Schinn, J. Lightwave Technol. **27**, 4164 (2009)
14. M. Froggatt, B. Soller, D. Gifford, and M. Wolfe, in *Optical Fiber Communication Conference (OFC)* (Optical Society of America, 2004), paper PDP17.
15. X. Fan, Y. Koshikiya, and F. Ito, Opt. Lett. **35**, 25 (2010)
16. L. Palmieri, A. Galtarossa, and T. Geisler, Opt. Lett. **35**, 2481 (2010)
17. L. Palmieri, Opt. Fiber Technol. **19**, 720 (2013).
18. A. Galtarossa, D. Grosso, and L. Palmieri, IEEE Photon. Technol. Lett. **21**, 1713 (2009).
19. P. Wai and C. R. Menyuk, J. Lightwave Technol. **14**, 148 (1996).
20. R. Ulrich, S. C. Rashleigh, and W. Eickhoff, Opt. Lett. **5**, 273 (1980).
21. A. Galtarossa, L. Palmieri, A. Pizzinat, M. Schiano, and T. Tambosso, J. Lightwave Technol. **18**, 1389 (2000).
22. Z. Ding, X. S. Yao, T. Liu, Y. Du, K. Liu, J. Jiang, Z. Meng, and H. Chen, Opt. Express **21**, 3826 (2013).
23. D. Z. Chen, X. S. Yao, C. Wei, H. Chen, X. Chen, and Z. Li, in *Optical Fiber Communication Conference (OFC)* (Optical Society of America, 2016), paper W2A.29.

A Novel Method for Determining and Improving the Quality of a Quadrupolar Fiber Gyro Coil under Temperature Variations

Zhihong Li,[1,2] Zhuo Meng,[1,2] Tiegen Liu,[1] and X. Steve Yao[1,*]

[1]*Polarization Research Center, College of Precision Instrument & Opto-electronics Engineering and Key Laboratory of Opto-electronics Information and Technical Science, Ministry of Education, Tianjin University, Tianjin 300072, China*

[2]*Suzhou Opto-ring Co. Ltd., Suzhou 215123, China*

[*]*steveyao888@yahoo.com*

Abstract: We introduce a parameter called pointing error thermal sensitivity (PETS) for quantitatively determining the quality of a quadrupolar (QAD) fiber coil under radial temperature variations. We show both analytically and experimentally that the pointing error of a fiber gyro incorporating the fiber coil is linearly proportional to the final radial thermal gradient on the coil, with PETS as the proportional constant. We further show that PETS is linearly proportional to another parameter called effective asymmetric length of the coil. By thermally inducing different radial thermal gradients on the fiber coil and measuring the corresponding pointing errors in a gyroscopic measurement setup, we can confidently determine the PETS of the fiber coil and its associated effective asymmetric length caused by imperfections in coil winding. Consequently, we are able to precisely trim the coil to achieve best thermal performance.

©2013 Optical Society of America

OCIS codes: (060.0060) Fiber optics and optical communications; (060.2430) Fibers, single-mode; (060.2800) Gyroscopes.

References and links

1. V. Vali and R. W. Shorthill, "Fiber ring interferometer," Appl. Opt. **15**(5), 1099–1100 (1976).
2. H. C. Lefevre, "Fundamental of interferometeric fiber optic gyroscope," in Fiber Optic Gyros: 20 Anniversary Conf., Proc. SPIE **2837**, 46–60 (1996).
3. G. A. Sanders, B. Szafraniec, R. Y. Liu, M. S. Bielas, and L. Strandjord, "Fiber-optic gyro development for a broad range of applications," Proc. SPIE, Fiber Optic and Laser Sensors XIII **2510**, 2–11(1995).
4. G. A. Sanders, B. Szafraniec, R. Y. Liu, C. L. Laskoskie, L. K. Strandjord, and G. Weed, "Fiber optic gyros for space, marine, and aviation applications," in Fiber Optic Gyros: 20 Anniversary Conf., Proc. SPIE **2837**, 61–71 (1996).
5. M. Chomát, "Efficient suppression of thermally induced nonreciprocity in fiber-optic Sagnac interferometers with novel double-layer winding," Appl. Opt. **32**(13), 2289–2291 (1993).
6. R. Dyott, "Reduction of the Shupe effect in fibre optic gyros; the random-wound coil," Electron. Lett. **32**(23), 2177–2178 (1996).
7. R. P. Goettsche and R. A. Bergh, "Trimming of fiber optic winding and method of achieving same," U.S.Patent:5528715, 6–18 (1996).
8. F. Mohr, "Thermooptically induced bias drift in fiber optical Sagnac interferometers," J. Lightwave Technol. **14**(1), 27–41 (1996).
9. D. M. Shupe, "Thermally induced nonreciprocity in the fiber-optic interferometer," Appl. Opt. **19**(5), 654–655 (1980).
10. W. Feng, X. Wang, and W. Wang, "Effect of turns' difference in each layer on temperature performance of fiber optic gyroscopoe," Journal of Chinese Inertial Technology **19**, 487–493 (2011).
11. C. Mao, Z. Gong, X. Mou, and G. Yang, "Finite difference method for temperature field in fiber optical gyroscope," Piezoelectrics and Acoustooptics **25**, 98–101 (2003).
12. M. Li, T. Liu, Y. Zhou, J. Jiang, L. Hou, J. Wang, and X. S. Yao, "A 3-D model for analyzing thermal transient effects in fiber gyro coils," Proc. SPIE, Advanced Sensor Systems and Applications III, 6830–6834 (2007).
13. C. M. Lofts, P. B. Ruffin, M. D. Parker, and C. C. Sung, "Investigation of the effects of temporal thermal gradients in fiber optic gyroscope sensing coils," Opt. Eng. **34**(10), 2856–2863 (1995).
14. J. Sawyer, P. B. Ruffin, and C. Sung, "Investigation of the effects of temporal thermal gradients in fiber optic gyroscope sensing coils, part II," Opt. Eng. **36**(1), 29–34 (1997).

A Novel Method for Determining and Improving the Quality of a Quadrupolar Fiber Gyro Coil under Temperature Variations

1. Introduction

It has been more than 35 years since fiber-optic gyroscope (FOG) was first proposed by V. Vali and R. Shorthill [1]. Nowadays, FOGs are in mass production and are widely used in various military and civilian applications [2–4], such as in aircrafts, vessels, and land vehicles for precision rotation rate and angle detection. A key component in a FOG is a fiber coil, which must be wound painstakingly with special geometries [5–8], such as quadrupolar winding pattern, to reduce a nonreciprocal effect caused by thermal variations known as Shupe effect [9]. Despite a large amount of FOGs have been produced for various applications, the making of good fiber coils still remains a work of art, with large variations in performance for coils made with even the same process. Test standards are available for testing the performance of a whole fiber gyro in operation, including combined contributions from the light source, Y-coupler, passive components, fiber coil, mechanical structure and enclosure, and electronics. However, to the best of authors' knowledge, no published test standards or comprehensive methods are available for testing a fiber coil's performance under temperature variations alone, although some attempts were made to measure coils asymmetry with inconclusive results [10]. Such a test is important for ensuring that good quality fiber coils can be mass produced with good uniformity and efficiency. In order to determine the quality of a coil alone, meaningful test parameters and associated test methods must be defined and developed. Such a parameter can relate to winding imperfections for engineers to find out the root causes of the problem coils, and implement corrective measures or process improvements.

In this paper, we introduce a parameter called pointing error thermal sensitivity (PETS) for quantifying the performance of a quadrupolar fiber coil subject to a time-dependent radial temperature gradient. We show that the pointing error (asymptotic angular error) of a gyro system incorporating the quadrupolar fiber coil is linearly proportional to the final temperature gradient between the inner and outer coil surfaces in the radial direction, with PETS as the proportional constant. We further show that PETS is linearly proportional to a parameter called effective asymmetric length of the fiber coil, caused by imperfections in fiber winding. In addition, by thermally inducing different time-varying radial temperature gradients on the fiber coil (as will be shown in inset b of Fig. 3) and measuring the corresponding pointing errors in a gyroscopic measurement setup, we can confidently determine the PETS of the fiber coil and its associated effective asymmetric length. Such parameters can be directly used to trim the fiber coil [7, 11] for better temperature performance, feedback to coil production for improving winding process, or simply be used to quantitatively determine the quality of fiber gyro coils. Finally, we trim multiple coils according to the obtained asymmetric lengths to achieve best thermal performance, and experimentally verify the usefulness and correctness of the PETS definition and the asymmetry length relations.

It should point out that our experiments indicate that the PETS measurement results are robust against environment temperature variations and sensitive only to coil's asymmetry, and therefore is a practical parameter for characterizing the thermal performance of fiber coils, determining the coil asymmetry length, and guiding the coil trimming.

2. Pointing error caused by time-dependent radial thermal gradient

In this section, we first derive an expression for the angular error of a gyro system incorporating an imperfectly wound fiber coil with a certain length asymmetry. We then introduce and define PETS to describe the performance of the coil against temperature variations, and another parameter called effective asymmetric length to reflect the accumulative winding imperfections.

With the origin of the coordinate located at the fiber coil midpoint $s = L/2$ (L is the total fiber length), the nonreciprocal phase shift $\Delta\varphi_e$ induced by the Shupe effect in the single-mode fiber can be expressed as [12–14]:

$$\Delta\varphi_e(t)=\frac{2\tau}{L}\beta_0\frac{\partial n}{\partial T}\left[\int_0^{L/2}\frac{\partial T(s,t)}{\partial t}sds-\int_0^{L/2}\frac{\partial T(s',t)}{\partial t}s'ds'\right] \quad (1)$$

where τ is the transit time of light through the fiber coil, $\beta_0=2\pi/\lambda_0$ is the wave number, n is the effective refractive index, $\partial n/\partial T$ is its temperature coefficient, $\partial T(s,t)/\partial t$ is the temperature variation along the fiber, and s and s' are distances along the fiber coil. They are both positive, but are measured in opposite directions, with s increasing in the clockwise (CW) direction and s' in the counter clockwise (CCW) direction.

Accordingly, the rotation rate error induced by a thermal transient is:

$$\Omega_e(t)=\frac{4\gamma}{L}\left[\int_0^{L/2}\frac{\partial T(s,t)}{\partial t}sds-\int_0^{L/2}\frac{\partial T(s',t)}{\partial t}s'ds'\right] \quad (2)$$

where γ is a parameter relating to the thermal coefficient of the fiber and the diameter D of the coil and is defined as:

$$\gamma=\frac{n}{2D}\frac{\partial n}{\partial T} \quad (3)$$

By integrating the rate error $\Omega_e(t)$ over time, the pointing error (asymptotic angular error) ψ_e induced by the temperature variation is obtained as:

$$\psi_e(t')=\int_0^{t'}\Omega_e(t)dt=\frac{4\gamma}{L}\left[\int_0^{L/2}\Delta T(s,t')sds-\int_0^{L/2}\Delta T(s',t')s'ds'\right] \quad (4)$$

where $\Delta T(s,t)=T(s,t)-T(s,0)$.

For a quadrupole-wound coil with 8 layers of fiber shown in Fig. 1(a), we use full lines labeled *A* to denote fiber layers winding in the CCW direction and broken lines labeled *B* to denote the fiber layers winding in the CW direction [7]. As shown in Fig. 1(b), we use A_i and B_i to number the fiber layers in CCW and CW directions respectively. The corresponding quadrupolar winding pattern can therefore be described as ABBA-ABBA. In Table 1.we designate fiber layer numbers and list the height and length of each fiber layer.

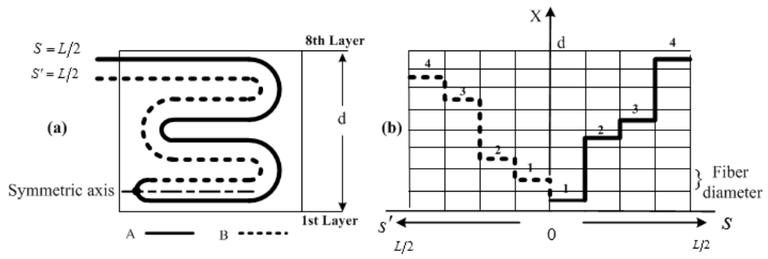

Fig. 1. Illustration of a quadrupole-wound fiber coil, where *A* and *B* are used to denote fiber layers wound in CCW (solid line) and CW (broken line) directions respectively, and *d* is the fiber coil thickness. (a) The relative positions of CCW and CW layers. (b) The numbering of each fiber layer in CCW and CW directions, where the height of each grid cell indicates the diameter of the fiber and the lines represent the position of fiber's center line in the vertical axis.

We examine the case in which the temperature variation is only along the radial direction of the coil, and is independent of the axial position and azimuth angle. Therefore, the temperature on each fiber layer is constant and Eq. (4) can be simplified to the following expression, assuming that the fiber coil is symmetrically wound around coil midpoint, as illustrated in Fig. 2(a):

$$\psi_{e0}(t)=\frac{4\gamma}{L}\sum_{i=1}^{4}\left[\Delta T(A_i,t)-\Delta T(B_i,t)\right]\cdot\int_{(i-1)L/8}^{iL/8}s\cdot ds \quad (5)$$

Table 1. Height and Length of Each Fiber Layer

Winging pattern	A	B	B	A	A	B	B	A
Global layer number	1	2	3	4	5	6	7	8
CCW layer number	1			2	3			4
CCW layer length (m)	0~*L*/8			*L*/8~L/4	*L*/4~3*L*/8			3*L*/8~*L*/2
CCW layer height (m)	*d*/16			7*d*/16	9*d*/16			15*d*/16
CW layer number		1	2			3	4	
CW layer length (m)		0~*L*/8	*L*/8~*L*/4			*L*/4~3*L*/8	3*L*/8~*L*/2	
CW layer height (m)		3*d*/16	5*d*/16			11*d*/16	13*d*/16	

However, if the coil is not wound perfectly symmetric, the position of the midpoint where two counter propagating light waves meet will change. As shown in Fig. 2(b), if the CCW wound fiber (denoted by A) is shortened by *l*, the midpoint for the counter-propagating light waves to meet will move to the longer fiber side (denoted by B) by *l*/2. In practice, even if the fiber lengths for CCW and CW fiber sections are the same, the optical path lengths may be different due to refractive index variations along the fiber caused by imperfection of the fiber and different stresses on the fiber. Therefore, we introduce a quantity called effective asymmetric length l_{eff} to denote the shortened optical path length of CCW fiber section, which will result in a shift of coil midpoint by $l_{eff}/2$ fiber length to the CW section. Consequently, the pointing error resulting from such an imperfect coil can be expressed as:

$$\psi_e(t)=\frac{4\gamma}{L}\left\{\sum_{i=1}^{4}\left[\Delta T(A_i,t)-\Delta T(B_i,t)\right]\cdot\int_{(i-1)\frac{L}{8}+\frac{l_{eff}}{2}}^{i\frac{L}{8}}s\cdot ds+\sum_{i=1}^{3}\left[\Delta T(A_i,t)-\Delta T(B_{i+1},t)\right]\cdot\int_{i\frac{L}{8}-\frac{l_{eff}}{2}}^{i\frac{L}{8}+\frac{l_{eff}}{2}}s\cdot ds\right\} \quad (6)$$

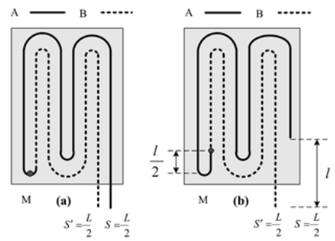

Fig. 2. Illustration of asymmetrical fiber wounding. (a) CCW (denoted by A) and CW (denoted by B) wound fiber sections have the same length. (b) CWW section is short by a length of *l*, resulting in a shift of *l*/2 of the coil midpoint to the CW side.

The total accumulated angular error ψ_e (pointing error), which reflects the performance of the fiber coil under a temperature variation, can be determined at thermal equilibrium ($t\to\infty$) when the thermally induced nonreciprocity in the fiber coil diminishes. Note that the temperature change $\Delta T(x)$ on each layer can be described as follows:

$$\Delta T\,(A_i) = \Delta T_{inner} + \delta T\,\frac{x_i}{d}, \left(x_i = d\,/16, 7d/16, 9d/16, 15d\,/16\right) \tag{7a}$$

$$\Delta T\,(B_i) = \Delta T_{inner} + \delta T\,\frac{x_i}{d}, \left(x_i = 3d/16, 5d/16, 11d/16, 13d/16\right) \tag{7b}$$

where $\delta T = \Delta T_{outer} - \Delta T_{inner}$, $\Delta T_{outer} = TC_1 - T_{room}$, $\Delta T_{inner} = TC_2 - T_{room}$, T_{room} is the room temperature, and d is the coil width.

Substitution of (7) in (5) and (6) yields:

$$\psi_{e0} = \gamma \frac{L}{8^2}\delta T \tag{8a}$$

$$\psi_e = \gamma\left(\frac{L}{8^2} - \frac{7}{8} l_{eff}\right)\delta T \tag{8b}$$

where ψ_{e0} and ψ_e are the pointing errors for coils without and with winding induced length asymmetry l_{eff}.

It can be shown that for a fiber coil with N layers, the pointing errors caused by a radial temperature variation can be expressed as:

$$\psi_{e0} = \gamma \frac{L}{N^2}\delta T \tag{9a}$$

$$\psi_e = \gamma_T\,\delta T = \psi_{e0} - \frac{N-1}{N}(\gamma \delta T) l_{eff} \tag{9b}$$

$$\gamma_T = \gamma\left(\frac{L}{N^2} - \frac{N-1}{N} l_{eff}\right) = \gamma \cdot l_{all} \tag{9c}$$

where $l_{all} = L/N^2 - (N-1)/N \cdot l_{eff}$ is the overall asymmetric length of the coil to be discussed shortly.

γ_T is an important parameter and is named as the pointing error thermal sensitivity (PETS) of the coil. It is directly proportional to coil's asymmetric length, and as will be shown next, it can be obtained experimentally by changing δT while measuring the pointing error ψ_e.

Although a similar equation to Eq. (9a) for a perfect symmetric quadruple-winding coil was obtained previously [8], it cannot used to evaluate imperfect fiber coils. As will be shown next, Eq. (9b) obtained in this paper is the most important equation for characterizing the symmetry property of a quadruple-winding fiber coil.

It is interesting to notice from Eq. (9c) that for a perfect geometrically symmetric coil ($l_{eff} = 0$), the thermally induced pointing error is non-zero and decreases quadratically with N. The pointing error can be reduced to zero if an asymmetry $l_{eff} = L/\left[N\left(N-1\right)\right]$ is purposely introduced. Such an asymmetry is understandable, considering that the "A" portion fiber has two layers at the inner and outer most surfaces, as shown in Fig. 1 and Fig. 5(a), and they are impacted more by the temperature changes than the "B" layers beneath them. Consequently "A" portion should be shortened to match the temperature effect on the "B" portion by $L/\left[N\left(N-1\right)\right]$. In other words, $L/\left[N\left(N-1\right)\right]$ is the intrinsic asymmetric length relating to quardruplar winding pattern and can be compensated by trimming "A" portion fiber by the equal amount. For a fiber coil with 8 and 24 layers, the required trimming lengths are 1.78% and 0.18% of the coil length, respectively. Therefore, we introduced an overall coil asymmetric length l_{all} in Eq. (9c) to take into account of both intrinsic and winding asymmetries.

3. Experimental result and discussions

Three frameless SM fiber coils with conductive potting adhesives are used in this study and all of them were wound with the quadrupolar winding scheme. The coils are approximately 1.25cm in height with an inner diameter of 5.3cm. The total length of fiber on each coil is 240m, producing 24 fiber layers. Each fiber coil is placed in an open-loop gyroscopic setup shown in Fig. 3 to form a complete fiber gyro and to be evaluated for its thermal performance. As shown in insets a) and b), a temperature gradient is applied to a coil in the radial direction such that the fiber in each layer experiences the same temperature. The temperatures both at coil's inner and outer surfaces were monitored with two separate thermocouples. In the experiments, we always keep the lengths of fiber pigtails constant at 2 meters each.

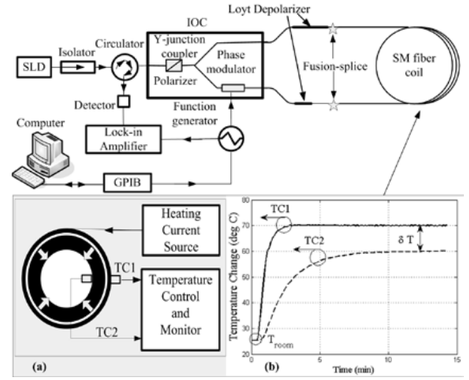

Fig. 3. Gyroscopic setup for measuring thermal induced error signals. Inset a) shows a ribbon heater with a width and a length equal to the width and the perimeter of the coil is wrapped around coil to apply a radial temperature gradient. TC1 and TC2 are the temperatures measured at the outer and inner surfaces of the fiber coil. Inset b) shows TC1 and TC2 as a function of time when a radial temperature excitation is applied, and are stabilized at 70.2°C and 54.3°C respectively, resulting a temperature gradient $\delta T = TC1 - TC2 = 15.9$ °C

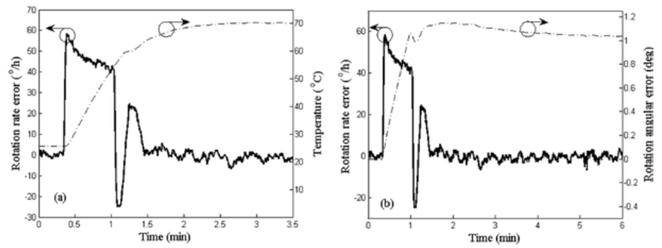

Fig. 4. (a) Measured rotation rate error (solid line) of a gyro system in Fig. 3 when the fiber coil's outer layer is subject to a temperature change TC1 (dotted line). (b) Angular error of the gyro system steadily approaches asymptotic value (pointing error), despite the fast fluctuation of the corresponding rate error (solid line).

A varying temperature gradient on the fiber coil will cause a nonreciprocal phase shift, which will result in rotation rate and pointing errors for a gyro system incorporating the fiber coil. Figure 4(a) shows the rotation rate error of a gyro system in Fig. 3 as a function of time when a temperature gradient shown in the insets of Fig. 3 is applied to the fiber coil. By integrating the rate error $\Omega_e(t)$ over time, the angular error can be obtained, as shown in Fig. 4(b). It should be pointed out that the angular error signal steadily approaches an asymptotic value ψ_e around 1.04 degrees (pointing error), despite large fluctuations of the measured rate error.

3.1 Experimental verification of Eq. (9)

Equation (9b) shows that the pointing error is linearly proportional to the effective asymmetry length l_{eff} of the coil and can be experimentally verified by fixing δT while changing l_{eff} by trimming the length of "A" side (e.g. CCW side) of the coil. In Eq. (9b), the effective asymmetry length l_{eff} can be expressed as:

$$l_{eff} = l_{eff\,0} + l \tag{10a}$$

where $l_{eff\,0}$ is the initial effective asymmetry length before trimming the coil and l is the trimming length. Substitution of Eq. (10a) in Eq. (9b) yields:

$$\psi_e = \psi'_{e0} - \frac{N-1}{N}(\gamma\delta T)\cdot l \tag{10b}$$

where the pointing error before coil trimming ($l = 0$) is

$$\psi'_{e0} = \psi_{e0} - \frac{N-1}{N}(\gamma\delta T)\cdot l_{eff\,0} \tag{10c}$$

When trimming a coil, we unwrap some turns from the coil outer layer ("A" side or CCW side), as shown in Fig. 5(a) and cut a length of fiber equal to the unwrapped portion to keep the fiber pigtail length constant. The trimming length l is defined positive when cutting fiber from the outer layer ("A" side) of a coil.

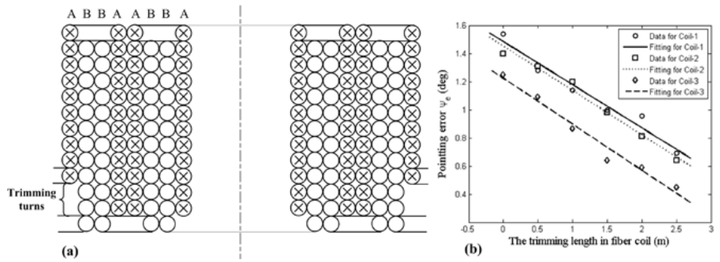

Fig. 5. (a) Illustration of coil trimming with two fiber turns unwrapped from the outer layer of the coil. (b) Measured pointing error ψ_e of fiber coil as a function of the trimming lengths l when a temperature excitation profile from room temperature to 70°C is applied to the outer layer of the coil.

We trimmed and tested three fiber coils of the same diameter and made with the same fiber. The measured pointing error ψ_e of the gyro system incorporating the coils as the function of the trimming length l is shown in Fig. 5(b). The same temperature profile shown in Fig. 3 was applied to each coil's outer layer and each coil is trimmed at six trimming lengths (l = 0m, 0.5m, 1m, 1.5m, 2m, 2.5m). It is evident that the pointing error is linearly proportional to the trimming lengths l and hence to the effective asymmetry length l_{eff}, agrees well with Eq. (9b). Because the three coils have the same diameters and are made with the same fibers, γ in Eq. (9) are expected to be the same according to Eq. (3). In addition, the temperature gradients applied to the three coils are also the same so that that the slope $(N-1)/N\cdot\gamma\delta T$ in Eq. (9b) of the three coils are also expected to the same. Indeed, the experimental results in Fig. 5(b) agree well with the prediction of Eq. (9b). It is important to point out that by curve fitting to Eq. (9b) one can obtain $\gamma\delta T$ and consequently γ because δT can be obtained independently in the experiment.

Table 2. Measurement Results of $\gamma\delta T$ and ψ'_{e0} of Three Fiber Coils

	Coil-1	Coil-2	Coil-3
Measured δT	15.86	15.43	15.3
$(N-1)/N\cdot\gamma\delta T$	0.311	0.315	0.321
γ	0.0188	0.0196	0.0201
ψ'_{e0} (Deg)	1.483	1.451	1.223

Table 2. shows the slope $\gamma\delta T$ and the intercept ψ'_{e0} of each fiber coil. The slopes are slightly different due to the slightly fluctuation of δT among three coils, possibly caused by non-identical winding and potting of the coils. The average γ obtained for this coil type is 0.0195 $/(^{\circ}C\cdot m)$ (for each coil type γ can be determined by performing the trimming procedure described above). The different intercepts ψ'_{e0} of the three curves in Fig. 5(b) and in Table 2 indicate that the three coils have different initial effective asymmetric lengths $l_{eff\,0}$, according to Eq. (10c).

3.2 Determination of coil's pointing error thermal sensitivity and asymmetric length

After verifying Eq. (9) experimentally, we now can confidently use it to determine the pointing error thermal sensitivity (PETS) γ_T of a fiber coil and its effective asymmetric length l_{eff} by measuring ψ_e at different δT.

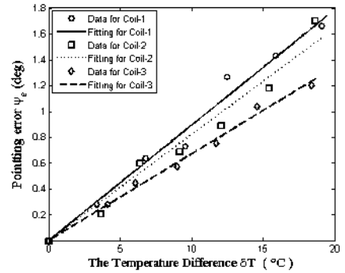

Fig. 6. The pointing error taken before coil trimming. The lines indicate the best linear fit through the data points.

Using the setup in Fig. 3, we applied six different temperature excitation profiles to the outer layer of each coil (TC_2 = 30°C, 40°C, 50°C, 60°C, 70°C, 80°C). The corresponding temperature differences δT for the three coils are shown in Table 3. Figure 6 shows the measured ψ_e as a function of δT of the three coils without trimming. The pointing error

increases linearly with δT , agreeing well with Eq. (9b). By curve-fitting ψ_e to Eq. (9b), we obtain PETS γ_T of three coils and the results are shown in Table 3.

Table 3. Outer Surface Temperature, Final Temperature Gradient, and γ_T of Three Coils Under Test

Outer surface temperature (°C)		30	40	50	60	70	80	γ_T (deg / °C)
δT (°C)	Coil-1	4.11	6.80	9.55	12.49	15.86	19.06	0.086
	Coil-2	3.68	6.40	9.15	12.09	15.43	18.65	0.083
	Coil-3	3.37	6.11	8.99	11.72	15.3	18.38	0.067

From Eq. (9c), we obtain the overall asymmetry lengths l_{all} of the three coils as 4.3 m, 4.1 m, and 3.33 m respectively, where $\gamma = 0.0195$ is used in the calculation. The corresponding effective asymmetric lengths $l_{eff\,0}$ of the coils from winding imperfections can be found as:

$$l_{eff\,0} = L/\left[N\,(N-1)\right] - N \cdot l_{all}/(N-1) \qquad (11)$$

Substitution of L = 240m and N = 24 in Eq. (11), we obtain the initial effective asymmetry lengths of the three coils as –4.16m, –3.98m and –3.12m, respectively. The minors sign indicates that the length of "A" portion fiber is longer than that of "B" portion fiber in the coils.

We further measured the pointing error as a function of final temperature gradient of the three coils with different trimming lengths, with the result of coil-2 shown in Fig. 7(a). Clearly, pointing error is almost insensitive to variations in thermal gradient with a trimming length about 4.5 m, corresponding to a near zero overall asymmetric length. Pointing error starts to increase in the negative direction with the thermal gradient when the coil is over trimmed with a trimming length of 5 m. These results are consistent with the prediction of Eqs. (9b) and (9c). Evidently, PETS is an excellent parameter to quantify the thermal performance of fiber coils: a larger PETS corresponds to a larger overall asymmetric length. The smaller the PETS of a coil, the smaller the thermal induced pointing error of the gyro incorporating the coil.

Figure 7(b) shows PETS obtained by curve fitting in Fig. 7(a) as a function of trimming length. The solid line is the plot of Eq. (9c) using experimental parameters (L = 240m, N = 24 and $\gamma = 0.0195\ /(^{\circ}C \cdot m)$), and it agrees with the experimental data reasonably well.

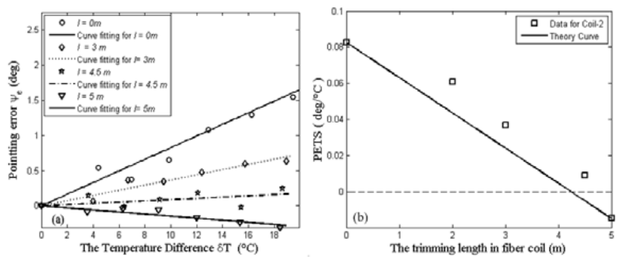

Fig. 7. (a) Pointing error of Coil-2 with different trimming lengths on the "A" portion fiber. The slope of each curve is the PETS of the coil. (b) PETS of Coil-2 as a function of trimming length l and the corresponding theoretical curve of Eq. (9c) for L = 240m, N = 24 and $\gamma = 0.0195$

4. Summary

In summary, we have proposed and demonstrated a practical approach to quantitatively determine the performance of a fiber gyro coil subject to thermal variations. We show both theoretically and experimentally that the pointing error of a fiber gyro is linearly proportional to its fiber coil's radial thermal gradient, and define the proportional constant as the pointing error thermal sensitivity (PETS) to quantify the thermal performance of fiber coils. In addition, we introduce a parameter called overall asymmetric length of the coil and show that it includes two contributions: one is intrinsic to the coil winding pattern and the other from imperfections made during coil winding. We further show both analytically and experimentally that the asymmetric length is linearly proportional to PETS and can be obtained once PETS is measured by measuring the pointing error as a function of radial thermal gradient. Finally, we prove experimentally that the thermal sensitivity of a fiber coil can be reduced to near zero by trimming the fiber coil by the amount equaling the overall asymmetric length obtained.

Our experiments indicate that the proposed PETS measurement is robust against environment temperature variations and sensitive only to coil's asymmetry, and therefore is a practical parameter for determining the thermal performance of fiber coils, determining the coil asymmetry length, and guiding the coil trimming. More experiments are under the way to quantitatively determine the influence, if any, of environmental temperature on PETS measurements.

Acknowledgments

This work was supported by the National Basic Research Program of China (973 Program) under grant 2010CB327806, International Science & Technology Cooperation Program of China under Grants No. 2009DFB10080 and No. 2010DFB13180, China Postdoctoral Science Foundation under Grant No. 20100470782.

July 15, 2012 / Vol. 37, No. 14 / OPTICS LETTERS 2775

Method for Improving the Resolution and Accuracy against Birefringence Dispersion in Distributed Polarization Cross-Talk Measurements

Zhihong Li,[1,3] Zhuo Meng,[1,3,*] Xiaojun Chen,[2] Tiegen Liu,[1] and X. Steve Yao[1,2]

[1]*Polarization Research Center, College of Precision Instrument & Opto-electronics Engineering and Key Laboratory of Opto-electronics Information and Technical Ministry of Education, Tianjin University, Tianjin 300072, China*

[2]*General Photonics Corporation, 5228 Edison Avenue, Chino, California 91710, USA*

[3]*Suzhou Optoring Technology Co. Ltd., Suzhou 215123, China*

**Corresponding author: tjictom@gmail.com*

Received April 2, 2012; revised May 13, 2012; accepted May 14, 2012; posted May 15, 2012 (Doc. ID 165977); published June 29, 2012

We present a novel method for improving the spatial resolution and amplitude accuracy of distributed polarization cross-talk measurements in a polarization maintaining (PM) fiber against its birefringence dispersion. We show that the broadening of measured polarization cross-talk peaks caused by birefringence dispersion can be restored by simply multiplying the measurement data with a compensation function. The birefringence dispersion variable in the function can be obtained by finding the widths of measured cross-talk envelopes at known distances along the fiber. We demonstrate that this method can effectively improve spatial resolution and amplitude accuracy of the space-resolved polarization cross-talk measurements of long PM fibers. © 2012 Optical Society of America

OCIS codes: 060.2310, 060.2300, 060.2370, 060.2420, 060.2800.

Space-resolved polarization cross-talk measurements along a polarization maintaining (PM) fiber have multiple important applications, including distributed stress sensing [1], fiber gyro coil inspection [2], PM fiber birefringence and beat length measurement [3], polarization cross-talk location identification in a PM fiber interferometer system, and PM fiber quality inspection [4]. Scanning Michelson white light interferometers can be used to obtain such distributed polarization cross-talk measurements [3,5]. Unfortunately, as the length of the fiber under test (FUT) increases, the measured cross-talk peaks will be broadened due to birefringence dispersion [6], resulting in reduced spatial resolution and degraded cross-talk amplitude measurement accuracies [7–9] for PM fibers with a length exceeding a few hundred meters.

Birefringence dispersion of PM fibers can be obtained using several different methods, including those of white-light spectral interferometry [10], wavelength scanning [11,12], and dispersive Fourier transform spectroscopy [13]. However, few attempts have been made to reduce the degrading effect of birefringence dispersion on the spatial resolution and amplitude accuracy of measured cross-talk peaks along the PM fiber.

In this Letter, we report a novel method to mathematically compensate the birefringence dispersion in polarization cross-talk measurements of a PM fiber to improve the spatial resolution and measurement accuracy. We first derive a compensation function to prove that the effect of birefringence dispersion on polarization cross-talk measurements can be compensated mathematically. We next use a white light interferometer based distributed polarization cross-talk analyzer (General Photonics PXA-1000) to obtain the initial space-resolved polarization cross-talk peaks along the PM fiber and then get the birefringence dispersion by measuring the widths of the cross-talk peaks as a function of their location along the fiber to complete the dispersion compensation function. Finally, we numerically multiply the compensation function with the original measured cross-talk data to eliminate the dispersion induced broadening of the cross-talk peaks. Our experiment with a PM fiber coil of 1.05 km length demonstrates that the method is effective in improving the spatial resolution and cross-talk amplitude measurement accuracy and can be readilyincorporated in the analysis software. This method is especially useful for obtaining accurate polarization cross-talk measurements of PM fiber coils with lengths of longer than a few hundred meters.

Figure 1 illustrates the basic configuration of a distributed polarization crosstalk analyzer [3]. A polarized super luminescent diode source (SLED) at 1310 nm with a short coherence length about 32.5 μm is coupled into the slow axis of a PM fiber (point A of inset in Fig. 1). Assume at point B, a polarization cross talk is induced by an external disturbance and some light is coupled into

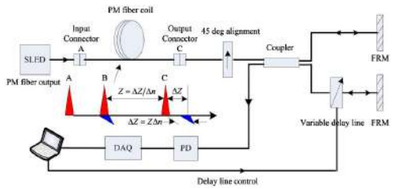

Fig. 1. (Color online) Illustration of a distributed polarization cross-talk analyzer based on a scanning white light Michelson interferometer. The inset shows the delay relation between the original and the cross talk components. Light with a short coherence length travelling in the fiber is polarized along its slow axis at input point A. Crosstalk is induced by a stress at point B where a small portion of light is coupled into fiber's fast axis. The relative delay at output point C between the two polarization components is ΔZ. The location $Z$of cross-talk point B can be obtained from a measurement of ΔZ. FRM, PD, and DAQ are Faraday rotation mirror, photodetector, and data acquisition card, respectively.

0146-9592/12/142775-03$15.00/0 © 2012 Optical Society of America

2776 OPTICS LETTERS / Vol. 37, No. 14 / July 15, 2012

the fast axis of the PM fiber with a coupling coefficient parameter $h = I_1/I_2$, where I_1 and I_2 are the powers in the fast and slow axes of the PM fiber, respectively. Because light polarized along the fast axis travels faster than that along the slow axis, at the output of the fiber, the faster component will be ahead of the slow component by ΔnZ, where Δn is the group birefringence of the PM fiber and Z is the fiber length between the cross-talk point and the fiber end (point C in Fig. 1). A polarizer oriented at 45 deg to the slow axis placed at the output of the fiber projects both polarization components onto the same direction to cause interference between the two components in a scanning Michelson interferometer. When the relative optical path length is scanned, an interference peak appears when the polarization components overlap in space and disappears when they are separated more than the coherence length of the light source. The location where the cross-talk occurs can be calculated from $Z = \Delta Z/\Delta n$ and cross-talk amplitude h can be obtained from the interference signal amplitude.

The envelope of a measured cross-talk peak (the interference peak) is influenced by the SLED's spectral distribution and the birefringence dispersion ΔD of the PM fiber [6–8]. Assume that the SLED has a Gaussian spectral shape; the cross-talk envelope (the degree of coherence) γ can be derived as the function of birefringence dispersion ΔD and the distance Z of cross-talk point measured from the output [6–8]:

$$|\gamma(Z,\Delta D)| = \frac{\sqrt{h-h^2}}{(1+\rho^2)^{1/4}} \exp\left\{-\left[\frac{2\delta d}{(1+\rho^2)^{1/2}W_0}\right]^2\right\}, \quad (1)$$

where

$$\delta d = (\Delta nZ - d), \quad (2)$$

$$\rho = 2\pi c(\Delta\lambda/\lambda_0)^2\Delta DZ = \alpha\Delta DZ, \quad (3)$$

$$\Delta D = d\tau/d\lambda = -[\omega^2/2\pi c](d^2\Delta\beta/d\omega^2)_0. \quad (4)$$

In the equations above, d is the path length imbalance of the scanned Michelson interferometer, ρ is the accumulated birefringence dispersion along the fiber, α is a parameter accounting for the contribution of the light source's characteristics to the total dispersion effect, c is the speed of light in free space, $\Delta\lambda$ and λ_0 are the spectral width and center wavelength of the light source, $\Delta\beta$ is the propagation constant difference of two polarization eigenmodes, and W_0 is the $1/e$ width of the interference envelope when the dispersion ρ is zero. This width is also the coherence length of the light source. From Eq. (2), one can see that δd can be adjusted by varying the path length difference d of the delay line in the interferometer. The interference signal appears when the path length imbalance d compensates for optical path length difference ΔnZ between two polarization modes.

Inspecting Eqs. (1)–(4), we can learn that both the magnitude and the shape of the measured cross-talk envelope are functions of ΔD and Z. The degrading effects of birefringence dispersion ΔD on a cross-talk measurement are the reduction of the cross-talk envelope's amplitude and the broadening of its shape as Z increases.

Fercher *et al.* described a complicated Fourier domain numerical dispersion compensation technique for removing dispersion in optical coherence tomography signals [14]. Here we find that the effects of birefringence dispersion can be directly removed by multiplying the cross-talk measurement data with a dispersion compensation function $K(\rho)$:

$$K(\rho) = \sqrt[4]{1+\rho^2}\exp\left\{-\left[\frac{2\delta d\rho}{(1+\rho^2)^{1/2}W_0}\right]^2\right\}. \quad (5)$$

As can be seen, the original cross-talk envelope can be completely restored by simply multiplying Eq. (5) with Eq. (1):

$$\gamma(Z,\Delta D)\cdot K(\rho) = \sqrt{h-h^2}\exp\left[-\left(\frac{2\delta d}{W_0}\right)^2\right]. \quad (6)$$

In order to complete the compensation function, the birefringence dispersion ΔD or ρ must be obtained first. From Eq. (1), one yields the relation between envelop broadening and birefringence dispersion as

$$W/W_0 = (1+\rho^2)^{1/2} = (1+(\alpha\Delta D)^2Z^2)^{1/2}. \quad (7)$$

Therefore, in principle, the birefringence dispersion ΔD can be readily calculated by measuring the widths of cross-talk envelops at input ($Z = L$) and output ($Z = 0$) ends of the PM fiber. In practice, in order to increase the accuracy of ΔD, widths of cross-talk envelops

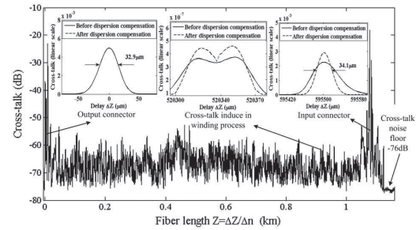

Fig. 2. Polarization cross-talk curve of a PM fiber coil. The insets show the zoom-in view of both the amplitude and width of cross-talk envelopes at output and input connectors, as well as in the middle region of the fiber, where two irresolvable peaks before dispersion compensation (solid line) can be clearly resolved after dispersion compensation (dotted line). The 9/125 μm PANDA fiber under test has a birefringence of $\Delta n = 6.1\times10^{-4}$ and the cross-talk measurement curve has dispersion-free spatial resolution of 5.4 cm. Note that our system has a noise floor of −76 dB, so that the noise has negligible effect on the measurements of cross-talk peaks larger than −66 dB.

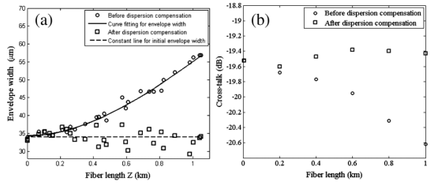

Fig. 3. (a) Envelope widths of cross-talk peaks induced by stress at various locations along the fiber; (b) measured cross-talk amplitude of the input connector with six different fiber lengths (5 m, 205 m, 405 m, 605 m, 805 m, and 1005 m). The cross-talk of the input connector is fixed; however, five segments of fibers with a length of 200 m each are sequentially spliced to the pigtail of the input connector for increased dispersion. The amplitude of polarization cross-talk decreases with the fiber length Z due to birefringence dispersion ΔD and is restored after performing the compensation.

at multiple locations along the PM fiber are measured, and ΔD is obtained by curve-fitting to Eq. (7).

Figure 2 is a measured polarization cross-talk curve of a PANDA PM fiber coil, showing the effects of birefringence dispersion on the measured cross-talk peaks and how the compensation removes those effects. The peaks at far left and far right correspond to cross-talks induced at output and input connectors from slight fiber axis misalignment. The small peaks in between are the cross-talks induced by stresses during the fiber winding process. The solid line on the right inset shows that birefringence dispersion broadens the envelop and diminishes the amplitude of the cross-talk peak occurring at input connector. The dotted line shows that both the envelope and the amplitude of the cross-talk peak are restored after dispersion compensation is performed.

In particular, the envelope width of the peak at the input connector is 34.1 μm after dispersion compensation, which is very close to 32.4 μm of the left peak induced by the output connector with zero dispersion ($Z = 0$).

Figure 3 shows the measured cross-talk peaks (both the width and amplitude of the cross-talk envelope) as a function of distance Z. In experiment, we measured multiple polarization cross-talks at different locations along the PM fiber. Clearly the width increases quadratically with distance Z due to the effect of birefringence dispersion, in agreement with Eq. (7). Such a width broadening starts to degrade the spatial resolution of polarization cross-talk measurements for a distance larger than 200 m.

The birefringence dispersion ΔD of the PM fiber is then accurately obtained by the least-squares fitting the data to Eq. (7) to be 0.0014 ps/(km nm). Substituting the fitting obtained values of $\alpha\Delta D$ into Eq. (5), we complete the dispersion compensation function. Finally, we numerically multiply the function with the original measured cross-talk data to cancel the dependence of polarization cross-talk on birefringence dispersion ΔD. The squares in Fig. 3(a) show that the width broadenings of the cross-talk peaks are removed after dispersion compensation is performed. Figure 3(b) shows the dependence of polarization cross-talk amplitude on the birefringence dispersion before and after dispersion compensation. It is evident that the cross-talk amplitude reduction caused by the dispersion is also removed by the dispersion compensation. Therefore, the compensation technique can effectively improve the spatial resolution and accuracy of cross-talk amplitude measurements using a white-light interferometer based polarization cross-talk analyzers. The fluctuations of data in Fig. 3 may be caused by the slight nonuniformity of birefringence dispersion along the fiber and some measurement errors.

In conclusion, we propose and demonstrate a novel method for compensating the degrading effects of birefringence dispersion on polarization cross-talk measurements by multiplying the original cross-talk data with a compensation function. The compensation function can be obtained by simply measuring the width of cross-talk envelops at known distances. We experimentally verify that the method is effective in improving the spatial resolution and amplitude accuracy of polarization cross-talk measurements of long PM fibers.

This work was supported by the National Basic Research Program of China (973 Program) under grant 2010CB327806, the International Science & Technology Cooperation Program of China under grants 2009DFB10080 and 2010DFB13180, and the China Postdoctoral Science Foundation under grant 20100470782.

References

1. T. Saida and K. Hotate, IEEE Photon. Technol. Lett. **9**, 484 (1997).
2. P. Martin, G. Le Boudec, and H. C. Lefevre, Proc. SPIE **1585**, 173 (1991).
3. Z. Ding, Z. Meng, X. S. Yao, X. Chen, T. Liu, and M. Qin, Opt. Lett. **36**, 2173 (2011).
4. Z. Ding, X. S. Yao, T. Liu, and G. Li, J. Optoelectron. Laser **21**, 430 (2010).
5. K. Takada, J. Noda, and K. Okamoto, Opt. Lett. **11**, 680 (1986).
6. N. Shibata, M. Tsubokawa, T. Nakashima, and S. Seikai, J. Opt. Soc. Am. A **4**, 494 (1987).
7. N. Shibata, A. Nakazono, and Y. Inoue, J. Lightwave Technol. **23**, 1244 (2005).
8. F. Tang, X. Wang, Y. Zhang, and W. Jing, Opt. Lett. **31**, 3411 (2006).
9. F. Tang, X. Wang, Y. Zhang, and W. Jing, Appl. Opt. **46**, 4073 (2007).
10. M. Shlyagin, A. Khomenko, and D. Tentori, Opt. Lett. **20**, 869 (1995).
11. P. Hlubina and T. Martynkien, Opt. Express **11**, 2793 (2003).
12. P. L. Francois, M. Monerie, C. Vassallo, Y. Durteste, and F. Alard, J. Lightwave Technol. **7**, 500 (1989).
13. D. A. Flavin, R. McBride, and J. D. C. Jones, Opt. Lett. **27**, 1010 (2002).
14. A. F. Fercher, C. K. Hitzenberger, M. Sticker, R. Zawadzki, B. Karamata, and T. Lasser, Opt. Express **9**, 610 (2001).

Accurate Method for Measuring the Thermal Coefficient of Group Birefringence of Polarization-Maintaining Fibers

Zhenyang Ding,[1] Zhuo Meng,[1,*] X. Steve Yao,[1,2] Xiaojun Chen,[2] Tiegen Liu,[1] and Mingliang Qin[3]

[1]*Polarization Research Center, College of Precision Instrument & Opto-electronics Engineering and Key Laboratory of Opto-electronics Information and Technical Science (Tianjin University), Ministry of Education, Tianjin University, Tianjin 300072, China*

[2]*General Photonics Corporation, 5228 Edison Avenue, Chino, California 91710, USA*

[3]*Suzhou Guanghuan Co. Limited, Suzhou 215123, China*

**Corresponding author: tjictom@gmail.com*

Received March 16, 2011; revised April 19, 2011; accepted April 22, 2011; posted May 4, 2011 (Doc. ID 144281); published June 1, 2011

We present a method to accurately measure the group birefringence variation with temperature in high-birefringence polarization-maintaining (PM) fibers using a distributed polarization analyzer. By analyzing polarization cross-talk peaks purposely induced at both ends of a PM fiber, the temperature coefficient of group birefringence can be accurately obtained. We confirm the theoretical prediction that the group birefringence of PANDA and TIGER PM fibers decrease linearly with temperature from −40 °C to 80 °C, and find that the temperature coefficients are -5.93×10^{-7} °C^{-1} and -5.29×10^{-7} °C^{-1} for two types of PANDA fibers, and -5.36×10^{-7} °C^{-1} for a TIGER fiber. © 2011 Optical Society of America

OCIS codes: 060.2420, 260.1440, 260.2030, 060.2300, 120.3180, 060.2370.

The stress-induced birefringence, such as that in PANDA and TIGER polarization-maintaining (PM) fibers, is expected to be temperature dependent because it is caused by anisotropic strain resulting from the differential thermal expansion of different regions in the fiber cladding, and to vary linearly with temperature in the vicinity of room temperature [1]. The thermal coefficient of the group birefringence is an important parameter for the application of PM fibers in different temperatures; however, few measurement results [1,2] are found in literature. The only plausible data were published by Flavin *et al.* [2], who measured the temperature dependence of the differential group delay of a PM fiber and obtained a linear temperature coefficient of -1.733 fs/°C · m (or -5.2×10^{-7} °C^{-1}) from 625 to 1075 nm.

The thermal coefficient of the group birefringence can be obtained by the accurate measurements of the group birefringence or beat length at different temperatures. Therefore, a good measurement setup must not only be able to measure the birefringence, but also allow the fiber under test to be placed in a temperature chamber without introducing significant measurement errors. The common methods for the beat length measurements of PM fibers include those of white-light spectral interferometry [1,3], wavelength scanning [4,5], and dispersive Fourier transform spectroscopy [2,6]. However, experimental setups for these methods are complicated and it is difficult to put the fiber under test into a temperature chamber without introducing large errors.

In this Letter, we report a new method of measuring the temperature variation of group birefringence of PM fibers using a distributed polarization cross-talk analyzer (General Photonics PXA-1000) and present the measurement results of three different PM fibers from three different manufacturers (PANDA-I, PANDA-II, and a TIGER PM fiber). The equipment can measure PM fibers with lengths up to 1.3 km and therefore allows a spool of PM fiber under test to be placed inside a temperature chamber with negligible error introduced. By linear-fitting data to the theoretical formula using the least squares method, we confirm that the group birefringence in PM fibers of stress-induced birefringence, such as PANDA and TIGER fibers, decreases linearly with temperature. We show analytically that the major measurement error is inversely proportional to the fiber length and the method has an accuracy of less than 1.5% when fiber length is longer than 40 m. We find with high confidence that the temperature coefficients of group birefringence are -5.93×10^{-7} °C^{-1}, -5.29×10^{-7} °C^{-1}, and -5.36×10^{-7} °C^{-1} for PANDA-I, PANDA-II, and the TIGER fiber, respectively.

PANDA and TIGER PM fibers belong to stress-induced birefringent fibers and their birefringence Δn_b can be expressed by [1,7]

$$\Delta n_b = \gamma(T_0 - T), \tag{1}$$

where T is the temperature of the fiber under test, T_0 is the softening temperature of the silica glass with dopants in the stress-inducing region of the cladding, and γ is the thermal coefficient of birefringence of the PM fiber, the parameter to be measured in this paper.

The basic construction of a distributed polarization cross-talk analyzer [8] is shown in Fig. 1. A polarized super luminescent diode source (SLED in this Letter) with an extremely short coherence length (about 25 μm) is coupled into a PM fiber with its polarization aligned with the slow axis of the fiber. Assume at point B, a polarization cross talk is induced by an external disturbance and some light is coupled into the fast axis of the PM fiber, as shown in the insert of Fig. 1. Because light polarized along the fast axis travels faster than that along the slow axis, at the output of the fiber, the faster component will be ahead of the slow component by

0146-9592/11/112173-03$15.00/0 © 2011 Optical Society of America

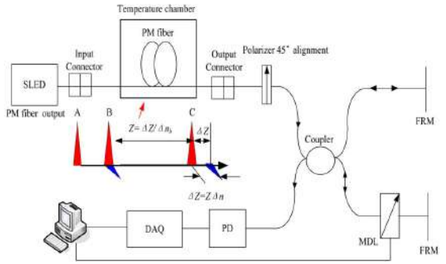

Fig. 1. (Color online) Simplified illustration of a distributed polarization cross-talk analyzer designed to obtain space-resolved polarization coupling along a length of PM fiber. The insert shows the delay relation between the original and the cross talk components. The PM fiber under test is placed inside a temperature chamber to expose it to different temperatures. Slight fiber axis misalignments at input and output connectors are induced to cause large polarization cross talks. MDL, FRM, PD, and DAQ are motorized delay line, Faraday rotation mirror, photodetector, and data acquisition card, respectively.

$$\Delta Z = Z\Delta n_b, \tag{2}$$

where Δn_b is the group birefringence of the PM fiber and Z is the length between the point where the cross talk occurs (B) and the output end (point C). The polarization components in the slow and fast axes are brought to interfere in the Michelson interferometer after going through a polarizer oriented 45° from the slow axis to produce interference peaks as a function of the relative delay. The coherence length of the light source (~25 μm with the SLED used) defines the spatial resolution of the polarization cross-talk measurement and is sufficiently high for the accurate measurement of cross talk locations.

Figure 2(a) shows typical polarization cross-talk curves of a PM fiber coil (PANDA-I) of 350.3 m at three different temperatures (40 °C, 0 °C, and −40 °C), as a function of relative delay. Because the distance Z between the two connectors (fiber length) can be measured by a ruler or an optical time-domain reflectometer (OTDR) and the relative delay ΔZ between the two high cross-talk points caused by input and output connectors

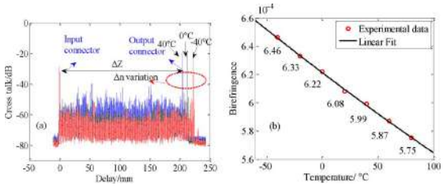

Fig. 2. (Color online) (a) Polarization cross-talk curves of a PM fiber as a function of the relative delay at 40°C, 0°C, and −40 °C. The peaks at the far left and right correspond to the cross talk induced at the input and output connectors, respectively, by slight axis misalignment. The rest of the peaks are induced by the stress of the fiber in various locations, which are not the concern of this paper. (b) Measured Δn_b at seven different temperatures.

on the far left and far right can be obtained precisely with the encoder of the motorized delay line, Δn_b can be obtained using Eq. (2). Clearly, the position of the peak corresponding to the output connector changes with temperature, as expected from Eq. (2). The fact that ΔZ decreases as the temperature increases indicates that Δn_b has a negative thermal coefficient. As mentioned previously, the thermal coefficient of the group birefringence γ can be obtained by linear-fitting Δn_b to Eq. (1) using the least squares method at different temperatures.

We measure Δn_b of the PANDA-I coil at seven different temperature points (−40°C, −20°C, 0°C, 20°C, 40°C, 60°C, and 80 °C) using the polarization cross talk analysis method and the results are plotted in Fig. 2(b). As will be discussed later, we chose such a long fiber length (350.3 m) to minimize multiple measurement errors. Linear-fitting Δn_b to Eq. (1) obtains a thermal coefficient γ of -5.86×10^{-7} °C^{-1}. To obtain the repeatability of the measurement, we take three different measurements and the results are shown in Table 1.

To further verify the feasibility of this method, we measure Δn_b of other two PM fiber coils of the same length at the seven temperature points. One of them is also a PANDA PM fiber (PANDA-II), but is from a different manufacturer than PANDA-I. The other is a TIGER fiber. The measurement results are summarized in Table 1. The average thermal coefficients γ of the three types of PM fibers are -5.93×10^{-7} °C^{-1} (PANDA-I), -5.29×10^{-7} °C^{-1} (PANDA-II), and -5.36×10^{-7} °C^{-1} (TIGER).

Several error sources may contribute to the final measurement error of Δn_b, including the measurement errors δ_z of fiber length Z and $\delta_{\Delta z}$ of relative delay ΔZ in Eq. (2). Consequently, the total relative error $\delta_{\Delta z}/\Delta n_b$ can be obtained by the error transfer formula

$$\delta_{\Delta n_b}/\Delta n_b = \sqrt{(\delta_{\Delta Z}/\Delta Z)^2 + (\delta_Z/Z)^2} = \sqrt{(\delta_{\Delta Z}/\Delta n_b)^2 + (\delta_Z)^2}/Z. \tag{3}$$

It is important to notice that the relative error is largely inversely proportional to the total fiber length under test. In order to reduce the measurement error, the fiber length inside the temperature chamber should be sufficiently long. Table 2 lists all potential measurement errors contributing to the overall measurement accuracy. It is interesting to notice that the dominant error sources are the fiber pigtail length outside of the temperature chamber and the fiber length measurement tolerance. In general, if a fiber length can be accurately measured, a total fiber length larger than 40 m should be sufficient for accurate thermal coefficient γ measurement with an accuracy of less than 1.5%, assuming total fiber pigtail

Table 1. Measurement Results of the Thermal Coefficient γ of Three Different PM Fibers

Fiber Type	PANDA-I	PANDA-II	TIGER
1	-5.86×10^{-7}	-5.25×10^{-7}	-5.33×10^{-7}
2	-5.96×10^{-7}	-5.25×10^{-7}	-5.43×10^{-7}
3	-5.96×10^{-7}	-5.36×10^{-7}	-5.32×10^{-7}
Average γ	-5.93×10^{-7}	-5.29×10^{-7}	-5.36×10^{-7}

Table 2. Description and Estimation of Measurement Errors[a]

Error Source	Error Description	Error Magnitude	Relative Error ($\Delta n_b \sim 5 \times 10^{-4}$)
$\delta_{\Delta z}$	$\delta_{\Delta z1}$: delay accuracy of the motorized delay line	$\delta_{\Delta z1} = 1\mu$m	2×10^{-3}/Z
	$\delta_{\Delta z2}$: position error of the input connector's cross-talk peak, about 1/2 of the peak width W_0 (coherent length of the light source).	$\delta_{\Delta z2} = 12.5\,\mu$m	2.5×10^{-2}/Z
	$\delta_{\Delta z3}$: position error of the output connector's cross-talk peak broadened by birefringent dispersion [9], about 1/2 of the broadened peak width $W = [1 + 2\pi cZ(\Delta\lambda/\lambda)^2\Delta D]^{1/2}W_0$.	$\delta_{\Delta z3} = 1/2W = (156.25 + 2.78Z)^{1/2}$	$(6.25 + 0.11Z)^{1/2} \times 10^{-2}/Z$
	$\delta_{\Delta z4}$: total length Z_{pigtail} of two fiber pigtails of the fiber spool outside of the temperature chamber that will introduce an error in ΔZ measurement at different temperatures: $\Delta Z = Zn_b(T) + Z_{\text{pigtail}}[\Delta n(T_R) - \Delta n_b(T)]$, where T_R is the room temperature	$\delta_{\Delta z1} = Z_{\text{pigtail}}[\Delta n_b(T_R) - \Delta n_b(T)]$	$0.1 \times Z_{\text{pigtail}}/Z$, assuming $\Delta T = 100$ °C
δ_z	δ_{z1}: error in fiber length measurement by a ruler or OTDR	$\delta_{z1} = 1\%Z$ by ruler $\delta_{z1} = 1.5$ m by OTDR	1% by ruler $1.5/Z$ by OTDR
	δ_{z2}: fiber length Z variation due to thermal expansion at different temperatures: however, a constant fiber length is assumed in Eq. (1)	$\delta_{z2} = 10^{-6}Z \times \Delta T$	10^{-4}, assuming $\Delta T = 100$ °C

[a]Note that in Table 2, Z is measured in meters, ΔD [~0.018 ps/(km.nm)] is the coefficient of birefringence chromatic dispersion, and λ_0 and $\Delta\lambda$ are the center wavelength and the FWHM of the power spectrum of the light source (30 nm), respectively. In the error estimation of the position of a cross-talk peak, a readily achievable number of half of the peak width is used, although more accurate determination can be achieved with advanced data analysis [10].

length outside the temperature chamber is less than 4 m. In the measurements of Table 1, we choose a fiber length of 350 m to ensure measurement accuracy. Since there is no "golden standard" fiber available with an accurately known thermal coefficient of birefringence, the relative error's inverse proportionality to the fiber length is difficult to be verified experimentally. Nevertheless, the analytical results in Table 2 serve as a good guidance to performing the actual measurements.

In summary, we propose and demonstrate a novel method of using a distributed polarization cross-talk analyzer to measure the thermal coefficient of the group birefringence in high-birefringence polarization-maintaining fibers. The method is nondestructive, easy to implement, highly sensitive, and highly accurate. Finally, we quantitatively analyze potential error sources of the measurement method and find that the measurement error decreases linearly with the fiber length. The method has an overall accuracy of less than 1.5%.

This work was supported by the National Basic Research Program of China (973 Program) under grant 2010CB327806 and the International Science & Technology Cooperation Program of China under grants 2009DFB10080 and 2010DFB13180.

References

1. K. Mochizuki, Y. Namihira, and Y. Ejiri, Appl. Opt. **21**, 4223 (1982).
2. D. A. Flavin, R. McBride, and J. D. C. Jones, Opt. Lett. **27**, 1010 (2002).
3. P. Hlubina and D. Ciprian, Opt. Express **15**, 17019 (2007).
4. K. Kikuchi and T. Okoshi, Opt. Lett. **8**, 122 (1983).
5. Z.-L. Duan, L.-Y. Ren, Y.-N. Zhang, H.-Y. Wang, B.-L. Yao, and W. Zha, Microw. Opt. Technol. Lett. **52**, 1466 (2010).
6. P.-L. Francois, M. Monerie, C. Vassallo, Y. Durteste, and F. R. Alard, J. Lightwave Technol. **7**, 500 (1989).
7. K.-H. Tsai, K.-S. Kim, and T. F. Morse, J. Lightwave Technol. **9**, 7 (1991).
8. P. Martin, G. Le Boudec, and H. C. Lefèvre, Proc. SPIE **1585**, 173 (1992).
9. F. Tang, X. Wang, Y. Zhang, and W. Jing, Opt. Lett. **31**, 3411 (2006).
10. H. Y. Choi, G. Mudhana, K. S. Park, U.-C. Paek, and B. H. Lee, Opt. Express **18**, 141 (2010).

IEEE PHOTONICS TECHNOLOGY LETTERS, VOL. 27, NO. 5, MARCH 1, 2015 549

Tomographic Inspection of Fiber Coils Using Optical Coherence Tomography

Zhihong Li, Zhuo Meng, Longzhi Wang, Tiegen Liu, and Steve X. Yao

***Abstract*— We report the first study of using optical coherence tomography (OCT) to inspect the winding quality of fiber optical gyro coils. We use a swept-source OCT system to scan a quadrupole-wind fiber coil for obtaining its two-dimensional and three-dimensional (3D) tomographic images. The defects beneath the surface of the fiber coil, which otherwise are invisible by video inspection, can be clearly identified with such tomographic images. The winding quality of each layer can also be independently visualized with the reconstructed 3D images from different angles or in different sections. We believe that the proposed method will be useful to ensuring the quality production of each and every fiber gyro coil.**

***Index Terms*— Optical coherence tomography, fiber-optic gyroscope (FOG), quadrupole gyros coil.**

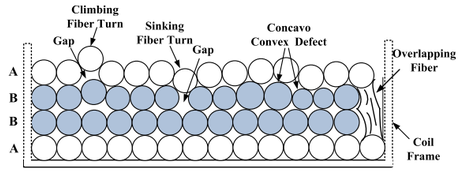

Fig. 1. Illustration of different winding defects in a quadrupole wound fiber coil, where fiber from two different supply spools labeled A and B are wound alternatively on the coil spool with the pattern ABBA, ABBA, and etc., starting from the center between spools A and B.

I. Introduction

A FIBER coil is a key component in a fiber optic gyroscope (FOG) for the precision detection of rotation rate and angle based on the Sagnac effect [1]. The fiber coil must be wound carefully with special geometries [2]–[5], such as quadrupole winding pattern, to reduce a nonreciprocal effect caused by thermal variations known as Shupe effect [6]. The winding quality of the fiber coil directly affects the performance of the FOG. Despite a large amount of FOGs have been produced for various applications, the making of quality fiber coils consistently is still a challenge, with large variations in performance for coils made with even the same process, mainly due to the inability of effective quality inspection [7].

In a perfect fiber coil, each fiber turn lays right next to the adjacent turn, as shown with the bottom two layers in Fig. 1. In addition, each fiber layer is perfectly flat with no bumps and humps. However, the following winding errors illustrate in Fig.1 are commonly found in fiber coils [8], [9]: (1) Fiber climbing, that a fiber turn climbs above its current layer, caused by pressure from its neighboring fiber turns. (2) Fiber sinking, that a fiber sinks down from its current layer, caused by inconsistent fiber winding tension. (3) Fiber gapping, that two or more fiber turns settle incorrectly from its proper positions. (4) Concavo-convex defect of the fiber layer, mainly caused by the irregularity of the fiber diameter. (5) Fiber overlapping, which often occurs at both ends of the coil when the fiber turn transitions from a lower layer to an upper layer during winding process.

These defects are more or less present in a final fiber coil product and compromise the performance of a resulting FOG, such as the bias stability and the rate or angular errors caused by thermal variation and mechanical vibrations. Therefore it is important to evaluate the quality of fiber coils, during the winding process and in the finished product, to ensure high quality production.

Video inspection with CCD cameras is commonly used to monitor the winding of a fiber coil, however it only provides surface images and is difficult to identify the defects and pinpoint the location of poor wound sections beneath surface of the fiber coil.

Manuscript received November 15, 2014; revised December 11, 2014; accepted December 17, 2014. Date of publication December 19, 2014; date of current version February 11, 2015. This work was supported in part by the Medical Instruments and New Medicine Program of Suzhou under Grant ZXY2012026, in part by the International Science and Technology Cooperation Program of China under Grant 2009DFB10080 and Grant 2010DFB13180, in part by the National Instrumentation Program under Grant 2013YQ03015, in part by the National Basic Research Program (973 Program) of China under Grant 2010CB327806, in part by the China Post-Doctoral Science Foundation under Grant 20100470782, in part by the Foundation Research Project of Jiangsu Province under Grant BK20130374 and Grant BK20130373. *(Corresponding author: Zhuo Meng.)*

Z. Li is with the Key Laboratory of Optoelectronics Information Technology Polarization Research Center, College of Precision Instrument and Optoelectronics Engineering, Ministry of Education, Tianjin University, Tianjin 300072, China, and also with Suzhou Opto-ring Company Ltd., Suzhou 215123, China (e-mail: zhihong.li2007@163.com).

Z. Meng is with the Key Laboratory of Optoelectronics Information Technology Polarization Research Center, College of Precision Instrument and Optoelectronics Engineering, Ministry of Education, Tianjin University, Tianjin 300072, China (e-mail: tjictom@126.com).

L. Wang is with the College of Precision Instrument and Opto-Electronics Engineering, Tianjin University, Tianjin 300072, China, and also with the College of Automobile and Transportation, Tianjin University of Technology and Education, Tianjin 300222, China (e-mail: longzhi_wang@sina.com).

T. Liu is with the College of Precision Instrument and Opto-Electronics Engineering, Tianjin University, Tianjin 300072, China, and also with the Key Laboratory of Opto-Electronics Information Technical Science, Ministry of Education, Tianjin University, Tianjin 300072, China (e-mail: tgliu@tju.edu.cn).

S. X. Yao is with the College of Precision Instrument and Opto-Electronics Engineering, Tianjin University, Tianjin 300072, China, the Key Laboratory of Opto-Electronics Information Technical Science, Tianjin University, Ministry of Education, Tianjin 300072, China, and also with General Photonics Corporation, Chino, CA 91710 USA (e-mail: steveyao888@yahoo.com).

Color versions of one or more of the figures in this letter are available online at http://ieeexplore.ieee.org.

Digital Object Identifier 10.1109/LPT.2014.2384837

1041-1135 © 2014 IEEE. Personal use is permitted, but republication/redistribution requires IEEE permission.
See http://www.ieee.org/publications_standards/publications/rights/index.html for more information.

550 IEEE PHOTONICS TECHNOLOGY LETTERS, VOL. 27, NO. 5, MARCH 1, 2015

Optical coherence tomography (OCT) is a relatively new imaging technique for detecting the internal microstructures of a sample and obtaining its tomographic images with high spatial resolution. It is most widely used for medical applications, such as those in ophthalmology [10], [11], cardiovascular disease diagnosis [12], dentistry [13], dermatology [14], endoscopy [15], blood glucose monitoring [16], and diagnosis of bronchus [17] and macular problems [18]. Recently, OCT has also been applied to industrial applications to exploit its advantages of being noninvasive, high speed, and 3-dimensional [19]–[22].

We believe OCT is particularly suited for the quality inspection of fiber coils, because its inherent advantages can be well utilized to characterize fiber coils. First, a fiber coil is generally made by layers of optical fibers with diameters ranging from 100 to 250 microns. Such a layered structure is most easily analyzed with tomographic images obtained by OCT. Each fiber layer under coil's surface can be clearly viewed and each fiber in each layer can be inspected individually. Other tomographic imaging techniques, such as X-ray computerized tomography (CT), may not have sufficient spatial resolution. Second, a fiber coil may also contain adhesives surrounding each turn of optical fiber, with an index refraction and a scattering coefficient different from those of the fiber. OCT images therefore can clearly identify the interfaces between the fiber turns and the adhesive, and detect any winding defects. Finally, all tomographic images can be reconstructed into a three dimensional (3D) images to be viewed at different angles and different sections of viewer's choice, making the visual inspection more user friendly.

In this letter, we report what we believe the first experimental study of using OCT to qualitatively evaluate the quality of fiber optical gyroscope coils. We show how to obtain different OCT images of a fiber coil in experiments and demonstrate the ability of using OCT images to visualize the conditions of fibers in different layers for identifying winding anomalies. We then discuss how to implement the OCT inspection technique for fiber coil production and quality insurance. Finally, we discuss the limitations of current OCT system and area for improvement. We believe that OCT inspection can be a useful tool for the production of quality fiber coils.

II. Principle

Fig. 2 shows the experimental setup for obtaining OCT images of a fiber coil. We use a commercial swept source OCT (SSOCT) system from Thorlabs with performance parameters shown in Table I to perform the experiments. A 3D reconstruction software was developed for the OCT system to allow the user to visualize data with different viewing angles and perspectives, with the flexibility of selecting proper experimental parameters, such as the lateral scanning range, the step width and the data sets to be accessed off-line for further image processing and data analysis. In the experiment, we selected a lateral scanning range of 8 mm and a step size of 25μm. As shown in Fig. 2a, the center axis of the fiber coil is affixed to the spindle of a lathe or a fiber winding machine, rotating slowly for a complete rotation at constant rate of 1 rpm, while the OCT probe beam is scanned back and forth rapidly along the X axis at a high speed about 100mm/s. Such a slow rotation rate, combined with the high scanning speed, assures that 1) the whole coil surface can be scanned when the coil completes a 360-degree rotation, 2) each cross section view of the coil is in the XZ plane with a negligible tilting angle of 0.12 degrees, as shown in Fig. 2, and 3) the resolution of the resulting OCT image is not compromised.

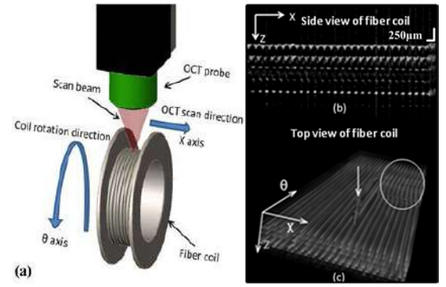

Fig. 2. (a) Illustration of OCT image acquisition of a fiber coil. The fiber coil is affixed on a spindle of a lathe or a winding machine, and is rotated along its center axis at a fixed speed. The probe of the OCT system is above the fiber coil. X axis is the OCT scan direction and θ axis is the rotating direction of the fiber coil. (b) The 2D tomographic image of the coil along the X axis. (c) The reconstructed 3D OCT image of a four-layer fiber coil without adhesive.

TABLE I
Performance Parameters of the Swept Source OCT, Assuming an Index of Refraction of 1.5 in Fiber

Wave-length, μm	1325
Spectral bandwidth, nm	100
Axial Resolution (Air/Fiber), μm	12/8
Transverse Resolution (Air), μm	25
Axial scans rate, KHz	16
Maximum transverse scan rate, mm/s	100
Max. lateral scanning range, mm	10
Maximum image depth (Air/Fiber), mm	3/2

Fig. 2b shows a typical 2D tomographic image obtained by the setup and Fig. 2c shows the reconstructed 3D OCT image when the fiber coil makes one complete rotation (360 degrees). By using the setup and process described above, the circular fiber coil can be viewed as a rectangular volumetric image after 3D reconstruction is performed, making it more convenient for the viewer to identify fiber winding defects inside the fiber coil. In Figs. 2b and 2c, the dark areas are locations of optical fibers because of their weak scatting while the white areas are the interfaces of the fiber and air. In Fig. 2c, a fiber climbing defect marked with a white arrow and the non-uniform fiber turns marked with a white circle are clearly identified.

III. Experimental Results and Discussion

Defects invisible to video inspection can be clearly seen by OCT tomographic images. For example, the non-uniform

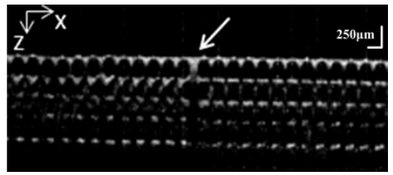

Fig. 3. OCT tomographic image taken during the winding process of a 4-layer fiber coil with potting adhesive, where the low scattering fiber appears dark while the adhesive appears grey or white due to large scattering.

adhesive potting often occurs in a fiber coil, which may affect the thermal performance of the resulting FOG. Fig. 3 shows an OCT image of a 4-layer fiber coil with 200 μm coating fiber. At the location pointed with a white arrow, a defect of excessive adhesive can be clearly identified, because the fiber and the adhesive have different scattering coefficients and contrast sharply in OCT images. On the other hand, such a defect is not visible in a CCD image because the surfaces of both the fiber and the adhesive appear the same and no information below the surface is available.

In Fig. 3, the interfaces between the fiber and the adhesive appear to be white and can be easily visualize due to strong light scattering, while the body of the fiber appears dark in the absence of light scattering. We can also see that the adhesive region with strong scattering (pointed with a white arrow) diminishes the light beneath it and casts a shadow. Such a "shadowing" effect generally prevents the formation of clear OCT images of morphological features in the shadow. This disadvantage can be eliminated by the OCT derivative image which enhanced the morphological features beneath the shadow [23]. On the other hand, as the axial scanning depth increased, the images become less clear due to the strong attenuation of light in the adhesive with less light reaching lower layers. An image enhancement algorithm may be used for improving the image quality in the deep regions [24].

Using the 3D reconstruction software, we obtained the 3D image of the coil with 6 layers. Figs. 4a to 4f show different views of the obtained 3D image. In the figures, the dark areas represent the location of fiber due to its low scattering, while the white areas represent the locations of potting adhesives because of the relative large scattering. In Figs. 4a and 4b, the six layers of fibers are clearly recognized. We believe that the imperfect fiber placements (the lumps and humps) in the upper layers may actually introduce phase distortion and affect the image of fiber arrangements in the lower layers. Therefore some of the apparent winding quality degradation in the lower layers may come from such image distortions introduced from upper layers, which can be compensated in software. Nevertheless, winding defects, such as the concavo-convex defect or fiber overlapping defect in layer 3, can be still clearly identified with the top and side views, as shown in Figs. 4d and 4f marked with red circles. For comparison, the fiber in Fig. 4e are mostly parallel, but is bent in Fig. 4f, probably caused by the squeezing action from other fiber

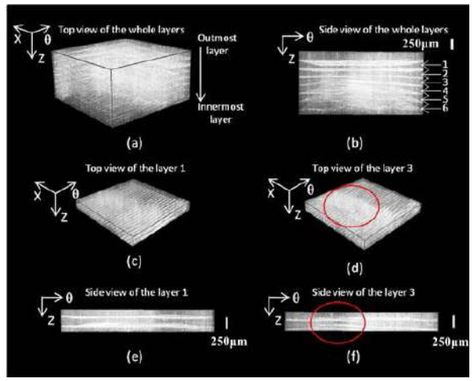

Fig. 4. 3D OCT images of a six-layer fiber coil. (a) volumetric view of a section with all six layers; (b) side view of (a); (c) top view of the top layer with parallel fiber lines; (d) top view of the 3rd layer with defective curved fiber lines; (e) and (f) are the side views of the (c) and (d), respectively.

layers or the irregularity of the fiber diameter. Therefore, by viewing the OCT image from different angles, in different layers, or at different cross sections, one can conveniently identify different winding defects in the fiber coil.

We anticipate this OCT inspection method can be applied to both online (while the coil is being wound on the winding machine) and offline (after the winding is completed) inspections of fiber coils. During fiber winding, the non-uniform pressure or force from the top layers may distort the fiber arrangement in the layers below. With OCT online inspection, not only one can see the winding condition of the top layer, but also whether and how winding a new fiber layer affects the layers below, a capability not attainable with video online inspection. If defects are found, the operator can unwind and rewind the related layers. For this application, imaging 2 to 4 fiber layers is generally sufficient. Our current OCT system has an effective imaging depth about 3 mm in air (2 mm in fiber with an index of refraction of 1.5), limited mainly by the coherence length of the swept-wavelength source and the focusing optics of the probe. Therefore it can obtain images of up to 8 layers of fibers with a coating diameter of 0.25 mm and 12 layers of fibers with a coating diameter of 0.165 mm.

For offline inspection, a quality inspector can evaluate all fiber layers using an OCT system in Fig. 2. Fiber coils with a total number of layers from 8 to 32 are common in practice and the imaging depth up to 5.4 and 8 mm in air may be required for fibers with coating diameters of 0.165 and 0.25 mm, respectively. However, our current OCT system only has an imaging depth of 3 mm in air. One may improve the depth range of an OCT system by 1) increasing the laser coherence length, 2) increasing the Rayleigh range of the probe beam with a proper optic design, and 3) implementing an image enhancement algorithm in the software for lower layers [24]. We are developing software to remove the image distortion in lower layers caused by upper layer winding imperfections.

IV. Conclusion

In conclusion, we propose and demonstrate a novel approach to inspect the quality of fiber coils in both online and offline applications by using OCT. Winding defects in both the top and inner layers can be really identified with the tomographic OCT images. With the aid of a 3D reconstruction software, a fiber coil can be viewed from different angles, at different sections, or in different layers of viewer's choice, making it very convenient to identify, record, and show to others any defects in the coil. We anticipate that the proposed OCT fiber coil inspection method has the potential to become a very useful tool to improve the production quality of the fiber gyroscope coils.

References

[1] V. Vali and R. W. Shorthill, "Fiber ring interferometer," *Appl. Opt.*, vol. 15, no. 5, pp. 1099–1100, 1976.
[2] M. Chomát, "Efficient suppression of thermally induced nonreciprocity in fiber-optic Sagnac interferometers with novel double-layer winding," *Appl. Opt.*, vol. 32, no. 13, pp. 2289–2291, 1993.
[3] R. B. Dyott, "Reduction of the Shupe effect in fibre optic gyros; the random-wound coil," *Electron. Lett.*, vol. 32, no. 23, pp. 2177–2178, Nov. 1996.
[4] R. P. Goettsche and R. A. Bergh, "Trimming of fiber optic winding and method of achieving same," U.S. Patent 5 528 715, Jun. 18, 1996, pp. 6–18.
[5] F. Mohr, "Thermooptically induced bias drift in fiber optical Sagnac interferometers," *J. Lightw. Technol.*, vol. 14, no. 1, pp. 27–41, Jan. 1996.
[6] D. M. Shupe, "Thermally induced nonreciprocity in the fiber-optic interferometer," *Appl. Opt.*, vol. 19, no. 5, pp. 654–655, 1980.
[7] Z. Li, Z. Meng, T. Liu, and X. S. Yao, "A novel method for determining and improving the quality of a quadrupolar fiber gyro coil under temperature variations," *Opt. Exp.*, vol. 21, no. 2, pp. 2521–2530, 2013.
[8] T. De Fazio, K. L. Belsley, R. H. Smith, G. B. Shank, Jr., and W. H. Culver, "Development issues for automating quadrupole-pattern optical-fiber coil-winding for fiber-optic gyro manufacture," in *Proc. IEEE Int. Conf. Robot. Autom.*, May 1994, pp. 202–207.
[9] M. Ivancevic, "Quadrupole-wound fiber optic sensing coil and method of manufacture thereof," U.S. Patent 4 856 900, Aug. 15, 1989.
[10] D. Huang *et al.*, "Optical coherence tomography," *Science*, vol. 254, no. 5035, pp. 1178–1181, 1991.
[11] W. J. Choi *et al.*, "Phase-sensitive swept-source optical coherence tomography imaging of the human retina with a vertical cavity surface-emitting laser light source," *Opt. Lett.*, vol. 38, no. 3, pp. 338–340, 2013.
[12] G. J. Ughi, T. Adriaenssens, W. Desmet, and J. D'hooge, "Fully automatic three-dimensional visualization of intravascular optical coherence tomography images: Methods and feasibility *in vivo*," *Biomed. Opt. Exp.*, vol. 3, no. 12, pp. 3291–3303, 2012.
[13] Z. Meng *et al.*, "Measurement of the refractive index of human teeth by optical coherence tomography," *J. Biomed. Opt.*, vol. 14, no. 3, p. 034010, 2009.
[14] C. Blatter *et al.*, "*In situ* structural and microangiographic assessment of human skin lesions with high-speed OCT," *Biomed. Opt. Exp.*, vol. 3, no. 10, pp. 2636–2646, 2012.
[15] Y. Pan, H. Xie, and G. K. Fedder, "Endoscopic optical coherence tomography based on a microelectromechanical mirror," *Opt. Lett.*, vol. 26, no. 24, pp. 1966–1968, 2001.
[16] Y. Su, Z. Meng, L. Wang, H. Yu, and T. Liu, "Effect of temperature on noninvasive blood glucose monitoring *in vivo* using optical coherence tomography," *Chin. Opt. Lett.*, vol. 12, no. 11, p. 111701, 2014.
[17] S. Lam *et al.*, "*In vivo* optical coherence tomography imaging of preinvasive bronchial lesions," *Clin. Cancer Res.*, vol. 14, pp. 2006–2011, Apr. 2008.
[18] S. Wolf and U. Wolf-Schnurrbusch, "Spectral-domain optical coherence tomography use in macular diseases: A review," *Ophthalmologica*, vol. 224, no. 6, pp. 333–340, 2010.
[19] R. Su, M. Kirillin, P. Ekberg, A. Roos, E. Sergeeva, and L. Mattsson, "Optical coherence tomography for quality assessment of embedded microchannels in alumina ceramic," *Opt. Exp.*, vol. 20, no. 4, pp. 4603–4618, 2012.
[20] K. Fujiwara and O. Matoba, "High-speed cross-sectional imaging of valuable documents using common-path swept-source optical coherence tomography," *Appl. Opt.*, vol. 50, no. 34, pp. H165–H170, 2011.
[21] D. Stifter, "Beyond biomedicine: A review of alternative applications and developments for optical coherence tomography," *Appl. Phys. B*, vol. 88, no. 3, pp. 337–357, 2007.
[22] P. Targowski and M. Iwanicka, "Optical coherence tomography: Its role in the non-invasive structural examination and conservation of cultural heritage objects—A review," *Appl. Phys. A*, vol. 106, no. 2, pp. 265–277, 2012.
[23] L. Z. Wang, "OCT based studies of skin features and their applications in the non-invasive blood glucose test," Ph.D. dissertation, College Precision Instrum. Opto-Electron. Eng., Tianjin Univ., Tianjin, China, 2013, pp. 41–46.
[24] L. Z. Wang *et al.*, "An optical coherence tomography attenuation compensation algorithm based on adaptive multi-scale retinex," *Chin. J. Lasers*, vol. 40, no. 12, pp. 1204001-1–1204001-6, 2013.

Application Notes

Polarization Optimized PMD Source Applications 267
PolaRITE™ Polarization Controllers 272
PolaRITE™ II/III Polarization Controllers/Scramblers 275
Faraday Rotator Mirror 278
Application Note for PDL Measurement 279
Accurate DOP Characterization with Less Effort 282
Optical Coherence Tomography Technologies 285

Polarization Optimized PMD Source Applications

PMD mitigation in 40Gb/s systems

As the bit rate of fiber optic communication systems increases from 10 Gbps to 40Gbps, 100 Gbps, and beyond, polarization mode dispersion (PMD) has more and more impact on system performance. PMD generally causes the two principal polarization components of a light signal to travel at different speeds and hence spreads the bit-width of the signal, as shown in Figure 1A. Consequently, it causes an increase in bit-error rate (BER) and service outage probability. Unlike other system impairments, such as chromatic dispersion (CD), the PMD effect on the system is random in nature and changes rapidly with time, making it difficult to mitigate.

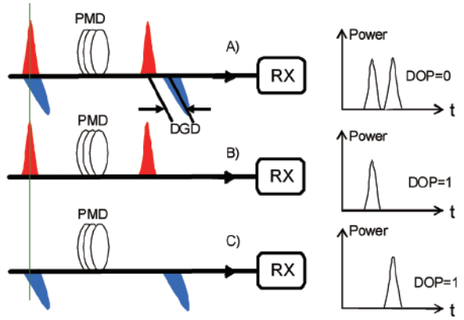

Figure 1 Illustrations of the PMD effect on an optical signal. A) The SOP of the input signal is aligned 45 degrees from the PSP of the fiber link, causing the worst-case signal distortion. In this case, if the DGD is larger than the width of one bit, then the DOP=0 because the two orthogonal polarization components have the same power, with no phase relationship. B) and C) The SOP of the input signal is aligned with the slow or fast PSP axis, respectively. In these cases, no signal distortion occurs except the slight late or early arrival, respectively, of the pulse. The DOP of the signal remains at 1. In all 3 cases, the PMD of the link remains the same, but the effect on the signal is different due to the different input polarization states.

Several methods with varying success rates exist to mitigate PMD effects for 40G deployment. The first is to select fiber routes with low PMD coefficients. Such a method requires extensive survey of all available fiber routes to identify and cherry-pick those with sufficiently low PMD. However, such an approach has three potential drawbacks: First, the PMD of a fiber route changes with time as the environmental conditions around the fiber change, including land movements caused by earthquake, flood, or mud-slides. A route that is good today may become bad in the future. Second, interconnected fiber routes may always have bad fiber sections with high PMD, rendering the selection of low PMD fiber routes throughout the system impractical. Finally, the supply of fiber routes with low PMD values will eventually be exhausted as 40G deployments increase.

The second method is to use bandwidth efficient modulation formats, such as DPSK or DQPSK. Such modulation formats reduce the effective bandwidth of a 40Gb/s channel to that of a 20Gb/s or even a 10Gb/s channel. Consequently, the impact of PMD on the signal is greatly reduced, though never eliminated.

The third approach is electronic PMD compensation, in which forward error correction (FEC) or other algorithms are used to reduce the PMD effect on the signal after the optical signal is converted into an electrical signal. However, because the electrical signal does not contain the phase information of the corresponding optical signal, the resulting PMD effect reduction is limited.

Optical PMD compensation is another attractive approach. An optical PMD compensator generally contains one or more polarization controllers, a PMD generation device, a PMD monitoring device, and a microprocessor based circuit, as shown in Figure 2. The circuit receives an error signal from the PMD monitoring device and instructs the PMD generation device to adjust the PMD values and the polarization controller to adjust the polarization state input to the PMD generation device to minimize the error signal from the PMD monitoring device. The PMD is compensated when the PMD generated by the PMD generating device is the same in value as that of the fiber link, but with its slow axis aligned with the fast axis of the fiber link.

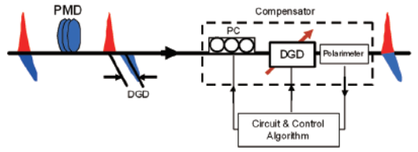

Figure 2 Optical PMD compensation. The DOP measured by the polarimeter is used as PMD effect indicator.

The final approach is polarization multiplexed coherent detection. Because the detected electrical signals in this approach contain all of the amplitude, phase, and polarization information of the corresponding optical signal, any optical signal impairments, including PMD, can be compensated by digital signal processing. In addition, because of the quadrupled spectrum efficiency resulting from QPSK modulation and polarization multiplexing, the effective optical signal bandwidth of a 40G channel is about the same as that of a 10G TDM channel. Consequently, the PMD effect on such a narrow band signal is also greatly reduced even without PMD compensation. Although transceivers incorporating polarization multiplexed coherent detection may still not be cost-effective compared with other approaches for 40Gb/s transmission, they are most attractive for 100Gb/s and higher speed transmissions.

Instruments required for PMD related tests

PMD source for PMD tolerance test

No matter which approach is taken, it is desirable to have an instrument capable of testing the performance of different methods in mitigating PMD effects. This test is called a PMD tolerance test. The general setup is shown in Figure 3A. The key instrument in this setup is the PMD source, which can generate precise 1st and higher order PMD values. The bit-error rate (BER) of the system, or another such performance indicator, is measured as the 1st order PMD (DGD) values generated by the PMD source are gradually increased until the BER reaches

the limit set for the system, as shown in Figure 3B. The corresponding DGD is the 1st order PMD tolerance of the system. Both the 1st and 2nd order PMD (SOPMD) values can also be increased as the BER of the system is measured and plotted, as shown in Figure 3C. The system outage probability can be calculated from the data obtained.

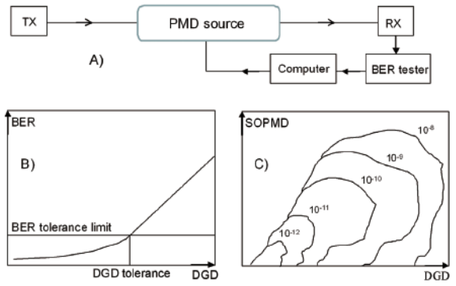

Figure 3 A) PMD tolerance test setup using a PMD source. The computer selects PMD settings and collects BER readings. B) BER vs. DGD curve. The DGD tolerance of the system for a given BER threshold can be deduced using the curve. C) Map of BER vs. DGD and SOPMD. Each contour represents a BER value. The PMD tolerance can be obtained from the contour plot.

PMD tolerance test results can be used by network operators to compare systems made by different vendors and to verify the PMD related specifications promised by the vendors. They can also be used by system vendors to 1) determine which PMD mitigation approach is most suitable to adopt, 2) to fine tune the PMD mitigation related parameters in the transceivers during system development, and 3) to perform output quality control of the final system, including transceivers, for the PMD related specifications.

Importance of polarization optimization:

The PMD effect on a system is highly polarization dependent. When the input state of polarization (SOP) is aligned or counter-aligned with the principal state of polarization (PSP) of the fiber link or the PMD source, the PMD has no effect on the signal, and therefore no effect on system performance, as shown in Figure 1. By contrast, when the input SOP is aligned 45 degrees from the PSP of the fiber link or PMD source, the PMD has its maximum effect on the transmitted optical signal, and hence its worst-case effect on system performance. The effect of PMD on data can be characterized by the degree of polarization (DOP) of the optical signal, because PMD causes depolarization of the optical signal, as shown in Figure 1. The smaller the DOP, the larger the PMD effect. In general, the DOP of the signal passing through a medium with nonzero 1st order PMD can be expressed as:

$$DOP(\tau) = \sqrt{4(\gamma^2 - \gamma)[1 - R^2(\tau)/R^2(0)] + 1} \qquad (1)$$

where τ is the DGD value of the medium, γ is the power distribution ratio of the two polarization components with respect to the principal state of polarization (PSP) of the DGD element (γ = ½ when the powers of the two polarization components are equal or when the input SOP to the medium is oriented 45 degrees from its PSP) and $R(\tau)$ is the self correlation function of the optical signal, which decreases as τ increases. Clearly, the DOP reaches a minimum value of $R(\tau)/R(0)$ when γ = ½ or when the input SOP is 45 degrees from the PSP of the DGD medium. At this SOP, the PMD has its worst effect on the quality of the signal. Conversely, when γ = 1 or when the input SOP is aligned with the PSP, the DOP always remains at its maximum value of 1, regardless of the DGD value.

When higher order PMD is present, the PSP is different for different wavelength components of the signal and Eq. (1) may no longer hold. Nevertheless, there always exists an input SOP for which the DOP of the signal at the output end is at a minimum and therefore, for which the PMD has the most severe impact on the quality of the signal. There also exists an input SOP at which the PMD has the least effect on the quality of the signal.

Coherent detection systems:

Most coherent detection systems use polarization multiplexed signals. Since both polarization components are present, the DOP of the signal is not a reliable indicator of the severity of the PMD effect. Therefore, to ensure that the worst-case PMD effect is achieved, polarization scrambling must be used before the PMD generator.

PMD source for PMD compensator evaluation

A PMD source is also necessary to evaluate the performance of a PMD compensator, whether optical or electrical, as shown in Figure 4. First, one can evaluate the system improvement margin at different PMD settings. Second, by gradually increasing the PMD values while measuring the BER of the fiber link, one can evaluate the PMD compensation range of the compensator. 3) Third, by changing the PMD value rapidly, one can determine the speed of the compensator response to quick PMD variations in the link. Finally, by changing the SOP rapidly at different PMD settings, one can determine the response time of the compensator to the change in SOP at each PMD setting. Therefore, a PMD source with fast PMD change and fast polarization control capabilities is attractive for PMD compensator evaluation.

Figure 4 PMD source for PMD compensator evaluation. For electrical compensation, the compensator may be inside the receiver (RX). The plots shown in Figure 3 can be generated here with PMD compensation at different PMD settings of the PMD source.

PMD analyzer or monitor for link PMD determination

The PMD values of fiber routes generally must be measured before link deployment. This requires PMD analyzers. In general, a PMD analyzer requires a large-bandwidth light source, whether it is tunable laser-based or broadband source-based. As mentioned previously, the PMD of fiber routes may change with time, due to changes in environmental conditions. For a ROADM network, after the fibers are lit, the wavelength channel for each transceiver pair is determined and is confined within a 50GHz bandwidth. Therefore, PMD analyzers requiring broadband light sources cannot be used to characterize such a system. In addition, it is undesirable to disconnect the transceivers and insert a PMD analyzer in the link, because this would cause a severe service interruption. It is therefore attractive to be able to determine the PMD value of a live link while both the transmitter and receiver are operational. This capability is important for the diagnosis of fiber routes with performance issues.

Drawbacks of PMD sources currently on the market

Currently available PMD sources, such as those from NewRidge, are rather rudimentary. They are capable of generating both 1st and 2nd order PMD, but the input SOP to the PMD source is not controlled and therefore changes with external disturbances on the input fiber. Consequently, the effect of the PMD on the signal is unpredictable and changes randomly, because the PMD effect on the signal is strongly dependent on the input SOP, as shown in Figure 1. In order to obtain predictable test results, it may be necessary to scramble the input SOP to obtain a PMD effect on the signal that is averaged over a large numbers of input SOPs. However, such a process not only significantly slows down each test point, but also adds the cost of a polarization scrambler to the test setup.

Other drawbacks of present PMD sources include a slow PMD change speed and low PMD value repeatability. One PMD source on the market uses multiple birefringent crystals aligned linearly. Each crystal can be rotated by an electrical motor. Different PMD values are generated by rotating different crystals at different angles. Consequently, the speed and repeatability of PMD generation are limited by the speed and angular accuracy of the electrical motors and their associated control circuits.

Desirable features for a PMD source

High repeatability and high speed of generation of 1st and higher order PMD values are desirable in a PMD source because they enable fast, repeatable PMD tolerance tests and PMD compensator evaluation.

Automatic optimization of input SOP is also highly advantageous. As described previously, PMD tolerance tests can be made much simpler if the input SOP to the PMD elements inside a PMD source can be controlled and optimized such that each PMD value has the most severe possible impact on the quality of the optical signal, regardless of polarization changes caused by disturbances to the fiber link. Specifically, the input SOP can be automatically maintained at an alignment of 45 degrees from the PSP of the PMD source, or the output DOP can be automatically maintained at a minimum value by actively controlling the input SOP.

PMD compensation is also an extremely attractive function. First, system vendors and network operators need to know how much system performance can be improved by adding PMD compensation in order to decide whether to deploy PMD compensators on a link with performance issues. Second, if PMD compensation significantly improves the system performance, it can be determined that PMD is the major cause of performance degradation; otherwise, other impairments should be considered. Therefore, a PMD source with PMD compensation capability can be used for the diagnosis of system problems. Finally, optimized PMD compensation can help to determine the PMD values of the fiber link, because the PMD value used for optimal PMD compensation is close to the real PMD value of the fiber link. Such a feature is attractive for frequent PMD monitoring of a live fiber link, a task that cannot be accomplished with PMD analyzers currently on the market.

The polarization optimized PMD source

General Photonics' polarization optimized PMD source meets all of the requirements described above. This advanced PMD source is constructed with a polarization controller (PC), a polarimeter at the input end, a PMD generator, a second polarimeter at the output end, and a digital signal processor (DSP) based electronic circuit, as shown in Figure 5. The two polarimeters are used to provide feedback signals to the DSP circuit for full polarization optimization. The circuit receives the polarization measurements from the two polarimeters, processes them, then sends commands to control the PMD generator and the polarization controller. The circuit can use the SOP information from the input polarimeter as the feedback to control the PC and generate any SOP the user prefers. In particular, it can automatically align the SOP to 45 degrees from the PSP of the PMD generator. This polarization state causes the PMD generator to have the worst-case 1st order PMD (DGD) effect on the optical signal at any DGD setting, and is therefore the preferred SOP for DGD tolerance tests for transceivers and fiber systems. Alternatively, the circuit can use the DOP information from the output polarimeter as the feedback to control the PC. The input SOP that minimizes the output DOP causes the PMD generator to have the worst-case total PMD effect on the optical signal, and is therefore the optimal polarization state for total PMD tolerance tests of transceivers and fiber systems. Finally, the optimized input SOP obtained by maximizing the DOP from the second polarimeter enables PMD compensation.

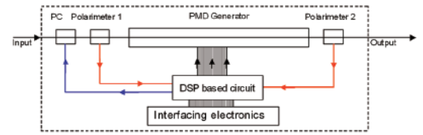

Figure 5 System diagram of polarization optimized PMD source. The DSP based circuit is used to 1) process information from the polarimeters and control instructions from users, 2) instruct the PMD generator to select desired PMD values, 3) control the PC to optimize the input SOP for various functions.

The PMD generator used in the PMD source is based on General Photonics' patent pending ternary polarization rotation technology. The generator is constructed using a series of birefrigent crystals, with a ternary polarization rotator sandwiched between each pair of adjacent crystal segments, as shown in Figure 6. The crystals are arranged in descending order, with lengths decreasing sequentially by a factor of 2. Each rotator is capable of rotating the state of polarization (SOP) by +45, 0, or -45 degrees.

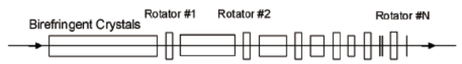

Figure 6 The construction of a PMD generator made with birefringent crystals and ternary polarization rotators which can rotate SOP in 3 ways.

When the rotator between two adjacent crystals rotates the SOP +45˚, the optical axes of the two crystals are aligned to produce the maximum combined DGD. When the rotator between two

adjacent crystals rotates the SOP -45˚, the optical axes of the two crystals are counter-aligned to produce the minimum combined DGD. When the rotator between two adjacent crystals rotates the SOP 0˚ (no rotation), the optical axes of the two crystals are aligned 45˚ from each other, producing higher order PMD. This higher order PMD generation capability is not available in previous DGD generator designs in which the polarization rotators can only generate ± 45˚ polarization rotations. The 0 degree polarization rotation is essential for the generation of higher order PMD.

The total number of PMD values that can be generated with N+1 sections of birefringent material and N rotator pairs is 3^N. For N=8, the total number of PMD states is 6561. The total number of DGD-only (1st order PMD) states is 2^N. For N=8, the total number of DGD-only states is 256.

Unlike the analog crystal rotators used in PMD sources from other vendors, which suffer from slow speed and low repeatability, the digital ternary operation method of this PMD source makes PMD value generation fast and highly repeatable.

In addition to the digital ternary rotators described above, General Photonics' PMD source uses a quasi-continuous rotator to achieve independent DGD and SOPMD control, allowing it to uniformly cover the PMD space, as shown in Figure 7. Note that the SOPMD values generated using this method are wavelength independent, so there are no FSR issues.

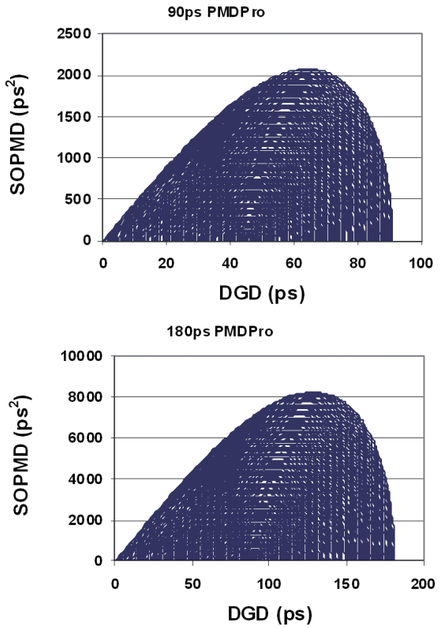

Figure 7 DGD and wavelength independent SOPMD range
A) 90 ps PMDPro™
B) 180 ps PMDPro™

Summary: Advantages and applications of the polarization optimized PMD source

The polarization optimized PMD source, constructed with digital ternary polarization rotators, offers the following attractive features for PMD related testing:

1) High precision, high repeatability PMD generation, resulting from the highly repeatable rotation angles of each ternary rotator. In its discrete digital control mode, the PMD source can generate a total of 6561 different PMD states, of which 256 are DGD-only, 1024 have DGD and wavelength independent SOPMD, and the rest are wavelength dependent PMD. In its quasi-continuous operation mode, it can generate states with independently controllable DGD and wavelength independent SOPMD values. Users can select individual PMD states or scan sequences of PMD states at user defined time intervals.

2) High PMD generation speed (minimum time interval around 1 ms), resulting from the high speed switching of the ternary polarization rotators. This high speed operation can speed up PMD tolerance tests and can be used to test the response time of a PMD compensator against sudden PMD changes.

3) Automatic optimization of input polarization for worst-case 1st order and 2nd order PMD tolerance tests, regardless of rapid polarization changes before the input to the PMD source. The polarization optimization eliminates test uncertainties and significantly reduces the time required to complete tests. It is, therefore, ideal for PMD tolerance tests for transceiver production lines, as shown in Figure 3.

4) Integrated polarization scrambler for PMD tolerance tests of coherent detection systems: Since coherent detection systems use polarization multiplexed signals, automatic polarization optimization cannot be used. Therefore, the input polarization must be scrambled to ensure that the worst-case PMD effect is achieved. The integrated polarization controller has a built-in scrambling function for this purpose.

5) PMD compensation using either an automatically optimized PMD value or a user selected PMD value. The PMD compensation is accomplished by maximizing the DOP detected by the polarimeter at the output port. Both PMD and DOP values will be shown on the front panel LCD display. By stepping the PMD values up and down and looking at the maximized DOP values, the user can directly see how the PMD value chosen affects PMD compensation. When optimized PMD mode is selected, the instrument will go through all PMD states and search for the maximum DOP. The PMD state with the maximum DOP is selected as the optimized PMD for PMD compensation.

6) PMD value determination of an in-service fiber link. The optimized PMD compensation mode can be used to determine the PMD in the link, as shown in Figure 8, because the optimized PMD value for compensation should be close to the PMD value of the fiber link. Therefore, the PMD value of a fiber link can be determined by simply inserting a polarization optimized PMD source in the light path and enabling the PMD compensation function. The optimized PMD value identified by the instrument is then the PMD value of the link. It may also be necessary to characterize the PMD of a particular channel route in an in-service ROADM network to determine its feasibility for 40G operation before installing 40G transmitters and receivers. In such a situation, an ASE source can be placed at the transmitter end

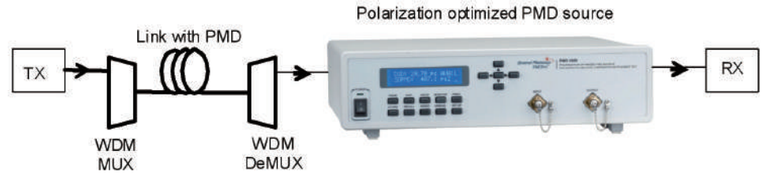

Figure 8 Polarization optimized PMD source in an in-service WDM link for the determination of its PMD and diagnosis of performance issues.

and a polarization optimized PMD source at the receiver end to perform PMD compensation. The optimized PMD value identified by the PMD source is then the PMD value of the fiber route. With this information, it is possible to decide whether the route is suitable for 40G transmission and whether a PMD compensator is required. An EDFA may be used before the PMD source to boost the signal level.

7) System impairment diagnosis. It can be difficult to identify the cause of performance problems in a fiber link. Signal degradation can be caused by PMD, chromatic-dispersion (CD), signal-to-noise ratio (SNR) issues, or other problems. Performing PMD compensation can help determine whether the problem is principally due to PMD: If PMD compensation substantially solves the transmission problem, it can be deduced that PMD is the principal cause of the problem. If not, it may be possible to rule out PMD. With such a diagnosis, it is possible to decide whether PMD compensation is required for the fiber link.

8) PMD emulation. The PMD generator can generate statistical PMD distributions to emulate PMD variations in fiber systems.

9) Polarization control functions. Using its built-in polarization controller and polarimeters, this instrument can perform all polarization control functions, including deterministic SOP generation, polarization scrambling, and polarization trace generation. It can therefore be used as a general purpose polarization synthesizer/controller for all polarization control needs.

Polarization optimization is used in the following three functions.

a. DGD tolerance test: Optimize input SOP using the SOP information from the first polarimeter as feedback to obtain the worst-case signal degradation caused by DGD.

b. PMD tolerance test: Optimize input SOP to minimize the DOP detected by the second polarimeter to obtain the worst-case signal degradation caused by both DGD and SOPMD.

c. PMD compensation: Optimize input SOP by maximizing DOP detected by the second polarimeter to minimize signal degradation caused by DGD and SOPMD.

PolaRITE™ Polarization Controllers

In fiber optic communication and sensing systems, many devices, such as interferometers and electro-optic modulators, are polarization sensitive. In order for these polarization sensitive devices to function properly, the polarization state of the input light must be precisely aligned with a particular axis of these devices. Unfortunately, the polarization state of light propagating in a length of standard circular fiber varies along the fiber due to the random birefringence induced by thermal stress, mechanical stress, and irregularities in the fiber core. Generally, at the output end of the fiber, the light is elliptically polarized, with varying degrees of ellipticity, and with the major elliptical axis at an arbitrary angle relative to some reference orientation. To properly connect such a strand of standard fiber to a polarization sensitive device, one must first convert the arbitrarily polarized light from the standard fiber to linearly polarized light and align it with the correct axis of the device.

One method to accomplish such a task is to use a combination of several bulk phase retarders, as shown in Fig. 1. Because the bulk phase retarders only function properly with collimated light, the light from the fiber must first be collimated using a microlens. The collimated beam will then pass through the phase retarders and then be refocused using a second lens to couple the light to the fiber pigtail of the polarization sensitive device, or directly to the device. These phase retarders are free to rotate independently to generate the desired linear polarization. Unfortunately, such a device is inherently high cost and high loss. First, the collimation, alignment, and refocusing process is time consuming, resulting in high labor costs. Second, the phase retarders are expensive, resulting in high material costs. In addition, the phase retarders and microlenses have to be anti-reflection coated or angle polished to prevent back reflection, creating extra manufacturing costs. Finally, because the light has to be coupled out of the fiber and then refocused into a fiber, the insertion loss is high. Additionally, the phase retarders are wavelength sensitive, making the device sensitive to wavelength variations in the input light.

Fig. 1

"Fiber coil" polarization controllers[1] which use a combination of all fiber phase retarders are also available for polarization control in fiber optic systems. In such a device, the half wave and quarter wave phase retarders are actually made of optical fiber coils. Coiling the fiber induces stress on the fiber, and therefore produces birefringence in the fiber coil via the photoelastic effect. The amount of birefringence is inversely proportional to the radius squared of the coil. By adjusting the radius of the coil and the number of turns in the coil, any desired fiber wave plate can be created. Because the phase retarders are made of fiber, it is not necessary to bring the light out of the fiber; therefore, the time consuming process of collimation, alignment, and refocusing is eliminated. In addition, because fiber phase retarders are much less expensive than bulk phase retarders, material costs are also greatly reduced. However, the "fiber coil" polarization controller is far from perfect. First, it is bulky. Current commercial polarization controllers of this kind have a height of 6 cm and a length of 30 cm. It is therefore difficult to use such devices in situations where size is of importance, such as in commercial optical receivers and transmitters. Second, because the fiber's diameter and material properties vary from batch to batch and from vendor to vendor, the birefringence of the fiber coils varies from fiber to fiber and has to be adjusted accordingly. However, such a precise adjustment is difficult to accomplish in this device because the radius of the fiber coils is difficult to change once created. Finally, the device is wavelength sensitive, again due to the difficulty of changing the radius of the fiber coil.

General Photonics Corporation's patented PolaRITE™ Polarization Controller is designed specifically for converting input light of an arbitrary polarization to output light of any desired polarization. Compared with a polarization controller made of bulk phase retarders, it has the advantages of no intrinsic loss, no intrinsic back reflection, simple construction, and low cost, due to its all fiber construction. Compared with a "fiber coil" all fiber polarization controller, it enjoys an edge in compactness, insensitivity to wavelength variations, insensitivity to fiber variations, and insensitivity to vibrations. In addition, the PolaRITE™ only has two knobs to control, compared with three knobs in the "fiber coil" controller, resulting in easier operation and reduced adjustment time for the device.

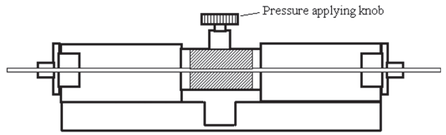

Fig. 2

As illustrated in Fig. 2, the device consists of a strand of single mode fiber, a rotatable fiber squeezer (center), and two fiber-holding blocks (left and right). The center portion of the fiber strand is sandwiched in the fiber squeezer. Turning the knob on the fiber squeezer clockwise will apply a pressure to the fiber center portion and produce a linear birefringence in this portion of fiber. According to previous studies[2,3] the amount of birefringence δ per unit length is proportional to the applied pressure and is given by the equation:

$$\delta \sim 6\times10^{-5}\frac{F}{\lambda d}\quad \mathbf{rad\ m^{-1}} \qquad (1)$$

where F is the applied force in Newtons, d is the fiber diameter in meters, and λ is the wavelength of light in μm.

With applied pressure, the fiber center portion acts as a birefringent wave plate with its slow axis in the direction of applied pressure, as shown in Fig. 3a. The retardation between slow axis and fast axis can be varied between 0 and 2π by changing the applied pressure.

When the rotatable fiber squeezer is rotated while pressure is applied, the fiber center portion is also rotated, altering the incident polarization angle of the light with respect to the slow axis of the fiber center portion. On the other hand, the rotation will also cause the segments of fiber at the left and right sides of the fiber squeezer to twist in the opposite senses. This twist-induced optical activity will rotate the incident polarization by an angle of $\Theta'=\eta\Theta$ in the direction of twist, where Θ is the physical rotation angle, shown in Fig. 3b, and η is a coefficient of twist-induced optical activity. For single mode fibers, η is on the order of 0.08[4-6]. Consequently, for a physical rotation of Θ degrees, the net change of the incident angle between the slow axis of the fiber center portion and the input polarization is $(1-\eta)\Theta$ degrees.

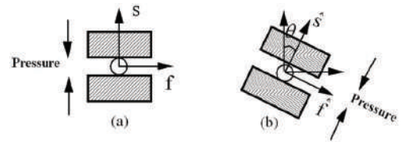

Fig. 3

Preferably, one may rotate the fiber squeezer without causing the left segment and the right segment to twist, by first releasing the pressure on the fiber squeezer, then rotating the squeezer, and finally applying pressure to the fiber squeezer again. In this way, for a physical rotation of Θ degrees, the net change of the incident angle between the slow axis of the fiber center portion and the input polarization is also Θ degrees. This rotate-without-twist procedure is recommended for coarse adjustment of polarization. When the output polarization is close to the desired state, the rotate-with-twist procedure can be used to fine tune the output polarization.

By applying pressure to the fiber center portion, the rotatable fiber squeezer causes the fiber center portion to act as a wave plate of variable retardation and rotatable birefringent axes, or as a Babinet-Soleil compensator [7]. If one chooses the slow and fast axes of the squeezed fiber center portion as a coordinate system, as shown in Fig. 3, the Jones matrix describing the birefringence of the squeezed fiber center portion can be written as:

$$\begin{bmatrix} e^{-i\frac{\Gamma}{2}} & 0 \\ 0 & e^{i\frac{\Gamma}{2}} \end{bmatrix} \qquad (2)$$

where $\Gamma \equiv 2\pi\Delta n l/\lambda = \delta l$ is the phase retardation of the squeezed fiber center portion. In this expression, l is the length of the squeezed fiber center portion and Δn is the index difference between slow axis and fast axis. In the same coordinate system, the Jones vector of the arbitrary input polarization is:

$$\vec{E}_{in} = \begin{bmatrix} E_s \\ E_f e^{i\phi} \end{bmatrix} = E\begin{bmatrix} \cos\alpha \\ \sin\alpha e^{i\phi} \end{bmatrix} \qquad (3)$$

where E_s is the amplitude of the light field projected on the slow axis, E_f is the amplitude projected on the fast axis, ø is the phase retardation between the two components, $E \equiv \sqrt{E_f^2 + E_s^2}$, and $\alpha \equiv \tan^{-1}(E_f/E_s)$

After the squeezed fiber center portion, the output light field can be written as:

$$\vec{E}_{out} = E\begin{bmatrix} e^{-i\frac{\Gamma}{2}} & 0 \\ 0 & e^{i\frac{\Gamma}{2}} \end{bmatrix}\begin{bmatrix} \cos\alpha \\ \sin\alpha e^{i\phi} \end{bmatrix} = Ee^{-i\Gamma/2}\cos\alpha\begin{bmatrix} 1 \\ \chi \end{bmatrix} \qquad (4)$$

where $\chi = \tan\alpha e^{i(\varphi+\Gamma)}$. Because α can be varied from 0 to π/2 by rotating the fiber squeezer, and Γ can be changed from 0 to 2π by changing the pressure on the fiber center portion, χ can take any value on the complex plane Re(χ) vs. Im(χ). Because each point in the complex plane is associated with a polarization state[8], the rotatable fiber squeezer is capable of generating any output polarization from an arbitrary input polarization.

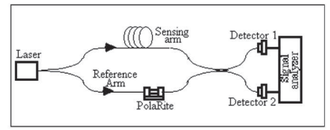

Fig. 4 Using a PolaRITE to maximize the detection sensitivity of a sensor system based on a Mach-Zehnder interferometer. Here the polarization state of the reference arm is adjusted so that the maximum interferometric visibility is detected by the signal analyzer.

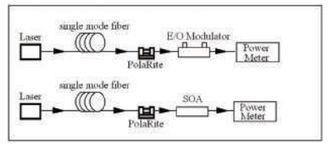

Fig. 5 Using a PolaRITE to adjust the state of the polarization so that it is aligned with the operating axis of the modulator or semiconductor optical amplifier (SOA). When the polarization is adjusted correctly, the maximum optical power is received by the power meter.

Referring to Fig. 4 and Fig. 5, the following procedures are recommended for the adjustment of the PolaRITE™ polarization controller:

1) Apply a pressure to the center portion of the fiber strand by tightening the knob on the rotatable fiber squeezer while monitoring the interferometric visibility, in the case of Fig. 4, or the output power, in the case of Fig. 5. If applying a pressure causes a significant increase in monitored interferometric visibility or optical power, then keep on going until the monitored visibility or optical power starts to decrease.

2) Rotate the rotatable fiber squeezer while maintaining the pressure to fine tune the output polarization. Adjust the pressure and orientation of the rotatable fiber squeezer iteratively until a maximum monitored visibility or optical power is obtained. This is the indication that the desired polarization is achieved.

3) If applying a pressure causes little change in monitored visibility or optical power, or causes the visibility or optical power to decrease, then release the pressure and rotate the center portion to a new position. Repeat step 1 and 2 if turning the knob causes a significant increase in monitored visibility or optical power.

Polarization Maintaining Fiber Adapter

Polarization maintaining (PM) fibers are widely used in fiber optic sensors and other applications where a particular, stable polarization is required. Because many polarization sensitive devices are pigtailed with polarization maintaining fibers, a device for connecting PM fibers is of great importance.

A PM fiber is a strongly birefringent fiber with predetermined slow and fast axes. If the polarization of input light is linear and aligned with one of the axes, it will remain unchanged after propagating in the fiber. However, if the input polarization is not linear, or is linear but not aligned with the axis, the polarization will go through periodic changes along the fiber, and the output from the fiber will be elliptically polarized, with the ellipticity and orientation determined by the fiber length.

Connecting two PM fibers is a difficult task, which involves precise alignment of fiber axes while maintaining low connection loss. Fusion splicers exist for splicing PM fibers. However, they are very expensive, and not practical for field installations. Connectors have been introduced previously for connecting PM fibers. In such connectors, fibers have to be precisely aligned with an orientation key of the connector. Consequently, assembly of such PM connectors requires large capital investment and is time consuming. In addition, connectors from different manufacturers may have different orientation key positions, making it difficult to connect fibers connectorized by different vendors. Finally, because all connectorizations have to be done by the connector manufacturer, devices have to be sent back and forth between the device manufacturers and the connector manufacturers, resulting in long delay times and increased damage rates.

The PolaRITE™ described above can be used to connect two strands of PM fibers. The linear polarization from the input PM fiber can be rotated to align with the slow (or fast) axis of the receiving PM fiber by properly adjusting the pressure and the orientation of the rotatable fiber squeezer. However, because the PolaRITE™ has non-polarization maintaining pigtails, disturbances to the pigtails will cause the polarization to change and destroy the polarization alignment.

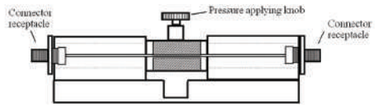

Fig. 6

General Photonics Corporation's solution to this problem is to eliminate the non-PM fiber pigtails of the PolaRITE™. As shown in Fig. 6, the patented PolaRITE™ PM Fiber Adapter has both ends connectorized with receptacles to receive standard FC/PC, FC/APC, SC, angled SC, ST, angled ST connectors, or any type of connectors of the user's choice. By doing so, the standard fiber used to construct the device is completely contained in an enclosure, isolated from external disturbances. In addition, the pressure of the fiber squeezer can be pre-adjusted so that the pressure-induced retardation is half wave for a specified wavelength. The PM fibers to be connected only need to be connectorized with corresponding standard connectors, without special attention to the orientation of the retardation axes of the PM fiber. To use the PolaRITE™ PM fiber adapter, simply fasten the two connectors onto the receptacles at each end of the PolaRITE™ PM fiber adapter and rotate the center portion of the adapter until the desired polarization is received by the receiving fiber, as shown in Fig. 7.

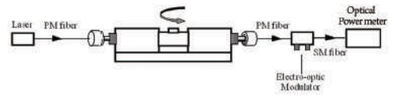

Fig. 7

The PolaRITE™ PM fiber adapter can also be used as a variable attenuator if it is connected to a polarizer, a piece of polarizing fiber, or a device with a strong polarization dependent transmission (such as a $LiNbO_3$ waveguide made by proton exchange process), as shown in Fig. 8. Variable attenuation is obtained by simply rotating the fiber squeezer at the center.

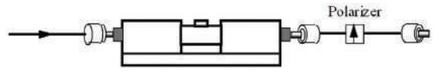

Fig. 8

REFERENCES

1. H. C. Lefevre, "Single-mode Fiber Fractional Wave Devices and Polarization Controllers," Electronics Letters, Vol. 16, No. 20, pp. 778-780, 1980).

2. A. M. Smith, "Single-mode fiber pressure sensitivity," Electronics Letters, Vol. 16, No 20, pp 773-774 (1980).

3. J. Sakai and T. Kimura, "Birefringence and Polarization Characteristics of Single-Mode Optical Fibers under Elastic Deformations," IEEE Journal of Quantum Electronics, Vol. QE-17, No. 6, pp 1041-1051 (1981).

4. R. Ulrich and A. Simon, "Polarization optics of twisted single-mode fibers," Applied Optics, Vol. 18, No. 13, pp 2241-2251 (1979).

5. A. Smith, "Birefringence induced by bends and twists in single-mode optical fiber," Applied Optics, Vol. 19, No. 15, pp 2060-2611 (1980).

6. M. Monerie and L. Jeunhomme, "Polarization mode coupling in long single-mode fibers," Optical and Quantum Electronics, Vol. 12, pp 449-461 (1980).

7. M. Born and E. Wolf, Principles of Optics, New York: Pergamon Press, Sixth edition, 1980, pp. 693-694.

8. A. Yariv and P. Yeh, Optical Waves in Crystals, New York: John Wiley & Sons, 1984, pp. 61-62.

PolaRITE™ II/III Polarization Controllers/Scramblers

Principle of Operation

The PolaRITE™ II/III Polarization Controller consists of multiple fiber squeezers oriented 45˚ from each other. Models PCS-3X and MPC-3X contain 3 squeezers, while PCS-4X and MPC-4X contain 4. Each fiber squeezer is driven by an applied voltage signal. Squeezing the optical fiber produces a linear birefringence in the fiber, and thus alters the state of polarization of a light signal passing through it. General Photonics uses proprietary technologies to treat the fiber that significantly increase fiber reliability under stress. In our tests, over 10 billion activation cycles at half wave voltages have been achieved without a single failure.

Any arbitrary polarization state of monochromatic light can be represented by a single point on the Poincaré Sphere, as shown in Fig. 1. In principle, increasing the voltage (increasing the squeezing pressure) of one fiber squeezer (X1 or X3) effectively causes the polarization state to rotate clockwise about the OQ axis, while decreasing the voltage causes the point to rotate counter-clockwise. On the other hand, increasing the voltage in a second fiber squeezer (X2) oriented 45˚ from the first one causes the polarization state to rotate clockwise about an axis (OH) orthogonal to the first one, while decreasing the voltage rotates the polarization counterclockwise. It is conceivable that one may generate any polarization state from any arbitrary input polarization state by using a minimum of two such fiber squeezers, as long as the input principal state is not parallel to an axis of either the first or second fiber squeezer.

Unique Features

Due to its all-fiber nature, the PolaRITE™ II/III has practically no insertion loss, no back reflection, and no polarization dependent loss. In addition, it has a response time of less than 35μs, significantly faster than that of a liquid crystal based device. This high-speed operation is essential for tracking fast polarization variations like those caused by passing locomotives, as in fibers laid along railway tracks, or by ocean waves, as in trans-oceanic fiber trunks.

Perhaps most impressively, General Photonics has succeeded in reducing activation-induced losses in its fiber squeezer controller to less than 0.002 dB. The low activation-induced loss makes these components ideal for applications in high precision PDL measurement instruments, and in feedback loops for compensating for polarization induced penalties. For the standard product, the activation loss is specified to be less than 0.01 dB, which is sufficient for most applications. General Photonics can also provide units with lower activation loss at a premium.

Another unique and attractive feature of General Photonics' device is that its performance is wavelength independent: the device functions equally well for optical signals ranging from 1260 nm to 1650 nm. This one-device-fits-all feature helps to simplify system design, lower implementation cost, and enable system channel expandability.

The implementation of fiber squeezers is also cost effective. Half-wave voltage requirements of the fiber squeezer controllers have been reduced to less than 30 VDC at 1550 nm. The low voltage requirements allow the use of readily available low cost electronics to drive and control the fiber squeezer controller. The half-wave voltage $V_\pi(\lambda)$ at a wavelength λ other than 1550 nm can be easily calculated by:

$$V_\pi(\lambda) = V_\pi(1550nm) \times \lambda / 1550 \qquad (1)$$

where $V_\pi(1550nm)$ is the half-wave voltage at 1550 nm. For example, the half-wave voltage at 1310 nm is 85% of the half-wave voltage at 1550 nm.

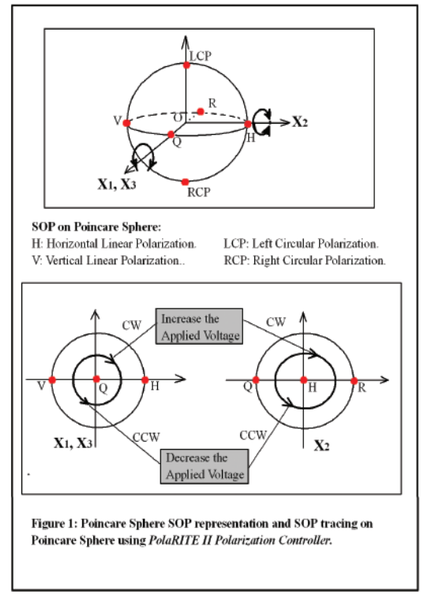

Figure 1: Poincare Sphere SOP representation and SOP tracing on Poincare Sphere using *PolaRITE II Polarization Controller.*

Operation Procedures

The PolaRITE™ II/III has four modes of operation: simple polarization control, reset free polarization control, slow polarization scrambling, and fast polarization scrambling.

There are eight electrical connection pins. The pin assignments are shown in Figure 2(a)-(d). There are slight differences between different device models and applications. Please be advised that only positive voltages (0 ~ 150 volts) should be applied to these pins.

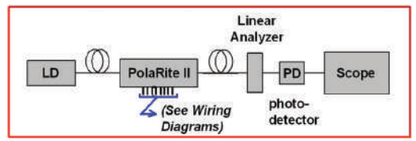

Fig. 2 A simple set-up for monitoring PolaRITE II/III polarization control and scrambling. Wiring diagrams are illustrated in Figures 2(a) to 2(d) for different types of PolaRITE II/III.

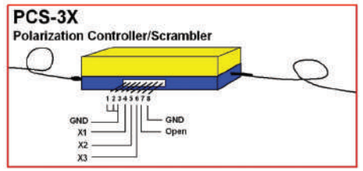

Fig. 2(a) Wiring diagram of PCS-3X and MPC-3X as polarization controller and/or scrambler. Pin 8 and pins 1-3 are connected internally.

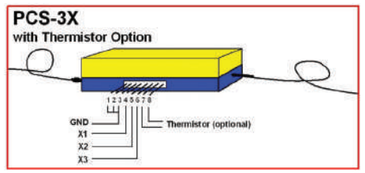

Fig. 2(b) Wiring diagram for PCS-3X and MPC-3X with thermistor option.

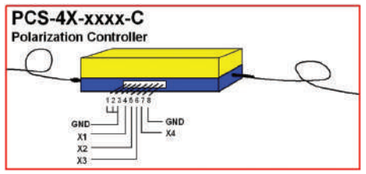

Fig. 2(c) Wiring diagram of PCS-4X-XXXX-C and MPC-4X model for polarization control applications. Pin 8 and pins 1-3 are connected internally.

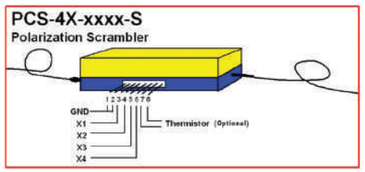

Fig. 2(d) Wiring diagram of PCS-4X-XXXX-S model for polarization scrambling.

A. Instructions for Simple Polarization Control

In this operation mode, three or four DC voltages are required to activate the actuators. Please be advised that the following procedures are for reference only. Other control procedures can also be implemented.

Step 1: Applied voltages on channels X1, X2 and X3 can range from 0 to 150 volts.

Step 2: To measure the half-wave voltage of channel 1 (i.e. X1 V_{π} (DC)): one can obtain the DC half-wave voltage by monitoring the optical power at the photodetector in the setup shown in Figure 2. As the applied voltage between pin 4 and GND increases, the output optical power (photodetector photocurrent or voltage) will vary periodically. The voltage change corresponding to one period will be twice the DC half-wave voltage of X1.

Step 3: Half-wave voltages for channels 2 and 3 (X2 and X3) can be determined by following the same procedures described in Step 2, with the voltages applied between (pin 5 & GND → X2) and (pin 6 & GND → X3).

Factory measured DC half-wave voltages for all actuators are provided on the device data sheet for customer reference.

B. Reset Free Polarization Control

Follow the procedures specified in the references below (see footnotes (a)-(c)) for reset free operation. In general, a 4-squeezer (model PCS-4X or MPC-4X) polarization controller is preferred for convenient reset-free operation, although a 3-squeezer (model PCS-3X or MPC-3X) polarization controller can also be used to fix the output polarization against input polarization fluctuations.

C. Slow Polarization Scrambling (0 ~ 20 kHz)

Slow polarization scrambling is preferred for PDL measurement, because most precision power meters have slow response times. PolaRITE II/III half-wave voltages (DC) are typically about 30 volts for each actuator. A voltage of 2X half-wave voltage is required to fully trace one closed circle on the Poincaré Sphere. At slow scrambling frequencies (typically below 20 kHz), the half-wave voltages at different frequencies do not differ significantly from the half-wave voltage at DC. If the driving voltages are sinusoidal, the required peak-to-peak voltages and frequencies should be satisfied by the following conditions (Golden Rules):

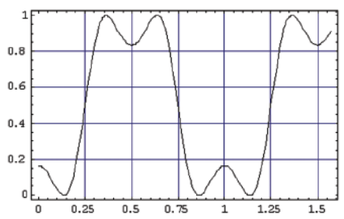

Fig. 3 The optical transmission waveform detected from scope under the condition V_{pp}= 1.53 V_{π}

$$V_{pp1}=1.53\ V_{\pi 1} \quad (2)$$

$$V_{pp2}= 1.53\ V_{\pi 2} \quad (3)$$

$$f_1 \neq nf_2 \text{ and } f_1 \neq 2nf_2/(2m+1) \quad (4)$$

n, m = 1, 2, 3,…

where Vpp1 and Vpp2 are the peak-to-peak amplitudes of the sinusoidal voltage signals applied to X1 and X2, respectively. With the amplitude defined in Eq. 2, the detected waveform from the power meter in Fig. 2 is illustrated in Fig. 3. Please note that the scrambling result will be degraded if Eq. 2 and Eq. 3 are not satisfied.

1 a) N. G. Walker and G. R. Walker, "Endless polarization control using four fiber squeezers," Electron Letters, Vol. 23, No. 6, pp. 290-292 (1987).
b) R. Noe, "Endless polarization control in coherent optical communications," Electron Letters, Vol. 22, No. 15, pp.772-773 (1986).
c) R. Noe, H. Heidrich, and D. Hoffmann, "Endless polarization control for coherent optics," Journal of Lightwave Technology, Vol. 6, No. 7, pp. 1199-1207 (1988).

When the input optical signal polarization is unknown or changes with time, another driving voltage is applied to the third actuator at a different frequency to eliminate the input polarization dependence. The amplitude of the driving voltage should be adjusted to have the same relationship to $V_{\pi 3}$ as in Eq. 2-3. The third stage is important when the input polarization is aligned along the squeezing axis of the first actuator.

D. Fast Polarization Scrambling

Note: PolaRITE III is not recommended for fast scrambling applications.

Fast polarization scrambling is required to eliminate the polarization dependent gain (PDG) of EDFAs. PolaRITE™ II has several low driving voltage scrambling frequencies (~ 60 kHz, 100 kHz, and 130 kHz - consult the data sheet for the exact peak scrambling frequencies) at which the half wave voltages are reduced significantly to only a few volts (The exact peak scrambling frequencies and the corresponding half-wave voltages are provided in the data sheet of each unit.).

Fig. 4 The small signal frequency response for a typical fiber squeezer.

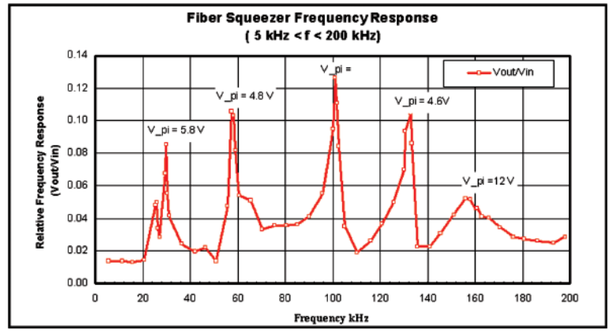

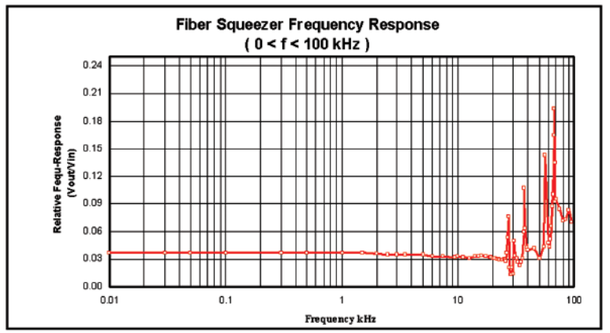

Fig. 4 shows the small-signal frequency response of a typical fiber squeezer. It is evident that at the peak frequencies, the device is much more efficient than at other frequencies, resulting from their much lower half-wave voltages. Therefore, scrambling at these peak frequencies is most energy efficient and cost effective. Again, at least two sinusoidal signals satisfying Eq. 2-4 should be applied to two adjacent actuators. The driving voltage signals can be generated directly from a function generator. Again, the scrambling result will degrade if Eq. 2-3 are not satisfied. Applying the third driving voltage to the X3 actuator at a different frequency will eliminate the input polarization dependence.

Faraday Rotator Mirror

Introduction

General Photonics' Faraday Rotator Mirror (FRM) is a fiber optic polarization rotation mirror designed for fiber optic networks and measurement applications. The state of polarization (SOP) of the reflected light is rotated 90° from that of input light. One unique property of the FRM is that at any point along the fiber, the SOPs of the forward and backward optical wave are always orthogonal to each other, regardless of the birefringence of the fiber. Our epoxy free optical path Faraday Rotator Mirror offers low insertion loss, low PDL, and high temperature stability. The NoTail™ version is also available to eliminate the headaches of pigtail handling and unwanted optical path delay. This device is ideal for polarization control in fiber laser systems, fiber sensors, and fiber interferometers, as well as for polarization sensitivity elimination in bulk diffraction grating systems.

This application note is intended to offer guidance on the principle, construction, dimensions, performance, and applications of the device. For additional information, please contact General Photonics Corporation at (909) 590-5473.

Principle and Construction

The Faraday Rotator Mirror is a Faraday Effect device in which a non-reciprocal rotation of a polarization state occurs as it passes through a special optical medium under a magnetic field. Our FRM consists of a fiber collimator, Faraday rotator, and mirror, as shown in Figure 1.

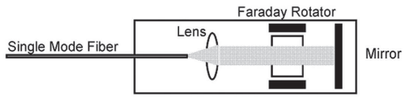

Fig. 1 Internal construction of Faraday Rotator Mirror

In single mode fiber systems, random birefringence due to stress or unevenness in the fiber core makes the SOP of an optical beam fluctuate along the fiber line. Installed at the end of an optical fiber, the Faraday Rotator Mirror is designed to rotate an input signal's SOP by 45°. When the signal is reflected back, it passes the Faraday rotator again. Since the Faraday Effect is non-reciprocal, the resultant SOP is rotated by 90° with respect to the original signal. The FRM thus functions as a phase conjugate mirror and cancels out all linear birefringent effects in this round trip.

Dimensions

The compact cylindrical package of this Faraday Rotator Mirror is easy for users to integrate into test and measurement systems, networks, fiber sensors, fiber interferometers, and fiber laser systems. The dimensions of the Faraday Rotator Mirror are illustrated in Figure 2.

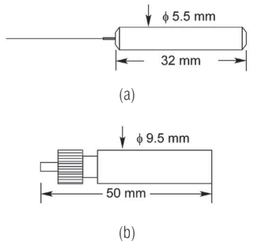

Fig. 2 Mechanical dimensions of the Faraday Rotator Mirror.
(a) Standard pigtailed package; (b) NoTail™ package

Applications

The Faraday Rotator Mirror has a wide range of applications in bulk grating systems, Erbium doped fiber amplifiers, tunable fiber lasers, fiber interferometers, and fiber sensors. Figure 3 shows some typical applications.

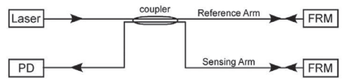

Fig. 3(a) Interferometric fiber sensor using Faraday Rotator Mirror

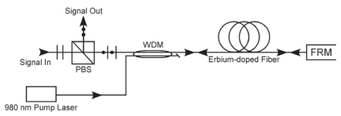

Fig. 3(b) Fiber amplifier using Faraday Rotator Mirror where signal can double pass the Erbium doped fiber to increase the efficiency.

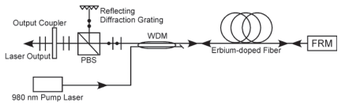

Fig. 3(c) Tunable Fiber laser using Faraday Rotator Mirror. Narrow linewidth and high power laser output can be achieved by changing the reflecting diffraction grating mirror setting.

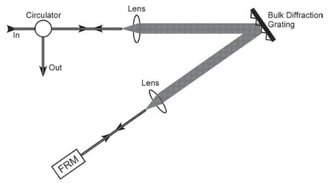

Fig. 3(d) PDL elimination in bulk diffraction grating systems using a Faraday Rotator Mirror.

Application Note for PDL Measurement

Introduction:

Polarization-dependent-loss (PDL) measurement is extremely sensitive to unwanted variations in the measurement system, including light source instability, connector back reflections, and even the layout of the test fiber cables. Large measurement inaccuracies or fluctuations may occur if the test setup is not properly arranged, even if a high accuracy measurement instrument is used. This application note describes precautions for accurate PDL measurements in general and ways to minimize measurement inaccuracies using General Photonics' PDL multimeter (PDL-201).

PDL is defined as:

$$\text{PDL} = 10 \text{ Log } \frac{P_{max}}{P_{min}} \qquad (1)$$

where P_{max} and P_{min} are the maximum and minimum output optical power passings, respectively, through a device under test (DUT) when the input light is scanned over all possible polarization states, as shown in Fig. 1.

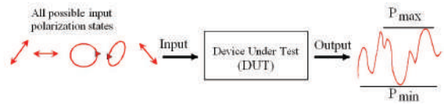

Figure 1 Illustration of PDL definition

Several possible errors or uncertainties may be introduced during measurements, including:

1. Error caused by light source fluctuation

As indicated in Eq. (1), if the power from the light source fluctuates with time, the measured P_{max} and P_{min} also fluctuate, resulting in measurement inaccuracies. Therefore, a light source used for PDL measurement must be highly stable.

Even if the light source itself is highly stable, small back reflections from various positions in the measurement system may feed back to the laser, disturbing its operation and causing output instabilities. Therefore, it is highly recommended that an isolator be used at the input of the PDL measurement instrument to minimize back reflections, even though the laser source may already have an isolator at its output. In addition, all of the connectors between the light source and the PDL meter must be APC type to minimize connector back reflection.

2. Error caused by double reflections

There may be small reflections from some components used in the measurement setup, including the connectors and the DUT itself. As shown in Fig. 2, reflected light from a component may be reflected again by another component. The double-reflected light travels in the same direction as the main input light and can therefore interfere with it. The total output optical power is thus:

$$P = P_{in} + P_{dr} + 2\sqrt{P_{in}P_{dr}\hat{e}_{in}\cdot\hat{e}_{dr}}\cos\phi \qquad (2)$$

where P_{in} and P_{dr} are the powers of the main and double reflected light beams, $\hat{e}_{in}$ and $\hat{e}_{dr}$ are the unit complex vectors of the states of polarization (SOP) of the main and double reflected light beams, and ϕ is the relative phase between them.

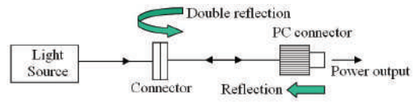

Figure 2 Illustration of double reflection

Because the relative phase and the SOPs of both the double-reflected light and the main light beam change when the fiber is disturbed, their interference causes the total output power to fluctuate. The magnitude of the relative fluctuation, in dB, from Eq. (2) is:

$$\Delta = 10\log[2\sqrt{P_{in}P_{dr}}/(P_{in}+P_{dr})] \approx 10\log(2\sqrt{P_{dr}/P_{in}} \qquad (3)$$

Although the double-reflected light is very weak, its contribution cannot be ignored because it interferes with a strong light signal (the input). For example, if a light beam is first reflected by an open PC connector with the typical 4% reflectivity, and is then reflected again by a mated PC connector with a reflectivity of 0.01% (a return loss of 40 dB), the detected power fluctuation can be as large as 0.017 dB. This power fluctuation will cause a PDL measurement fluctuation of 0.017 dB. Such a value cannot be ignored when measuring DUTs with similar PDL values. If an APC connector with a return loss of 60 dB is used instead of the mated PC connector in the previous example, the PDL fluctuation is reduced to 0.0017 dB, which can be ignored in most cases.

To minimize the contributions from double reflections, APC type connectors with low reflections should be used, if possible. Alternatively, a light source with a short coherence length (shorter than the optical path difference between the double reflected light and the main light beam) can also be used. This way, the interference described in Eq. (2) cannot take place; therefore, the resultant interference fluctuations described in Eq. (3) do not occur.

3. Error from connector and cable contributions

In addition to the DUT, the fiber cables and/or connectors used in the PDL measurement also have small PDL values. For example, optical cable itself may have a PDL value on the order of 0.01 dB, and this value may increase when it is bent with a small radius of curvature. Connectorized fiber jumpers may also have a small amount of PDL, on the order of 0.01-0.02 dB. Poorly connectorized jumpers can have even higher PDL values, probably caused by excess stress on the fiber during connectorization. Angle polished connectors (APC) generally have high PDL, especially when not mated with another APC connector. Therefore, it is possible that a connectorized fiber jumper used in the measurement can contribute a PDL error of 0.02 dB or higher to the PDL measurement of a DUT.

4. Variation caused by PDL vector summation

PDL can be viewed as a vector in a 3D space, because P_{max} and P_{min} in Eq.(1) correspond to two orthogonal states of polarization of the input light, which can be represented on a Poincaré

Sphere. Therefore, when two or more components in the measurement setup have non-zero PDL values, the total PDL is the vector summation of the PDL values of all of the components. For example, for the setup shown in Fig. 3, the total measured value of PDL is the vector summation of the PDLs of fiber connectors A, B, C, D, and the DUT (assuming for simplicity 's sake that the fiber cables have zero PDL):

$$PDL_T\hat{e}_T = PDL_a\hat{e}_a + PDL_b\hat{e}_b + PDL_c\hat{e}_c + PDL_d\hat{e}_d + PDL_{DUT}\hat{e}_{DUT} \quad (4)$$

where PDL_T and $\hat{e}_T$ are the value and complex unit vector of the total PDL; PDL_a, PDL_b, PDL_c, PDL_d, and PDL_{DUT} are the PDL values; and $\hat{e}_a$, $\hat{e}_b$, $\hat{e}_c$, $\hat{e}_d$, and $\hat{e}_{DUT}$ are the complex PDL unit vectors of connectors A, B, C, D, and the DUT, respectively. Fig. 4 shows graphically how the PDL vectors add up. The maximum PDL results if the PDL vectors of all of the components are parallel:

$$PDL_{T\max} = PDL_a + PDL_b + PDL_c + PDL_d + PDL_{DUT} \quad (5)$$

The minimum PDL results if the PDL vectors of all connectors are aligned, but are counter-parallel with the PDL vector of the DUT, assuming that the DUT's PDL value is larger than the sum of the connector PDL values:

$$PDL_{T\min} = PDL_{DUT} - (PDL_a + PDL_b + PDL_c + PDL_d) \quad (6)$$

The direction of each component's PDL vector relates to the orientation of the component and to the stress induced birefringence of the fiber cable. When the fiber between two components is disturbed, the relative directions of the PDL vectors are also changed, resulting in measurement variations. The maximum PDL value variation is therefore:

$$\Delta PDL_T = PDL_{T\max} - PDL_{T\min} = 2(PDL_a + PDL_b + PDL_c + PDL_d) \quad (7)$$

If the PDL value of the DUT is much larger than those of the connectors, the relative measurement error is small. A large relative error will result if the DUT has a PDL value similar to those of the connectors. Therefore, for accurate characterization of DUTs with small PDL values (such as fused couplers), the PDL values of any connectors and cables connecting to the DUT must be extremely small. The limiting factor for measurement accuracy is often not the accuracy of the instrument itself, but the residual PDL of the connectors and cables connecting to the DUT.

Table I: Typical PDL values of common optical components:

Component	Typical PDL value
1 meter single mode fiber	<0.02 dB
10 km single mode fiber	<0.05 dB
PC type connector	0.005 ~ 0.02 dB
APC type connector	0.02 ~ 0.06 dB
50% fused coupler, single window	0.1 ~ 0.2 dB
50% fused coupler, dual window	0.15 ~ 0.3 dB
90/10 fused coupler, through path	0.02 dB
90/10 fused coupler, -10 dB path	0.1 dB
Isolator	0.05 ~ 0.3 dB
3-port circulator	0.1 ~ 0.2 dB
DWDM	0.05 ~ 0.15 dB
Polarizer	30 ~ 50 dB

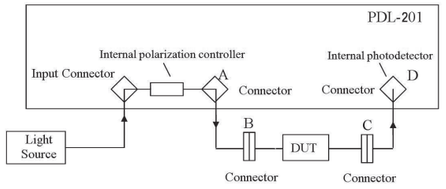

Figure 3 PDL measurement setup using the PDL-201 with 4 connectors: A, B, C, and D

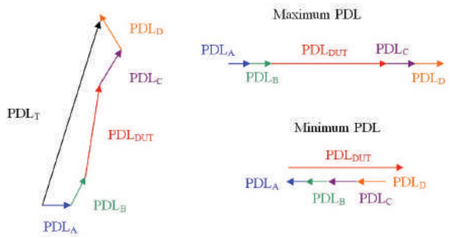

Figure 4 Illustration of the vector summation of PDL contributions from all connectors and DUT. The measured PDL fluctuates between a maximum value and a minimum value, depending on the relative orientations of each PDL vector.

Summary of good practices for minimizing PDL measurement errors

Keeping in mind the sources of PDL measurement errors described above, here is a summary of good practices for PDL measurement, using General Photonics' PDL-201 multimeter as an example. A typical measurement setup is shown in Fig. 5.

1. The light source used for PDL measurement must be highly stabilized, with a short-term stability similar to the intended PDL measurement accuracy. For example, if a PDL accuracy of 0.02 dB is to be achieved, the laser source's short-term power stability must be better than 0.02 dB.

2. An isolator at the input of the PDL-201 is recommended for minimizing the amount of back-reflected light from the downstream connectors and DUT that goes back into the light source. General Photonics' NoTail isolator, which has no fiber pigtails, is preferred.

3. Only APC connectors should be used between the light source and the PDL-201 input, in order to minimize back reflection to the light source, and consequently to minimize back-reflection induced instability of the light source. The NoTail isolator described in step 2 should therefore be APC connectorized.

4. The polarization of the light source should be relatively stable. Lasers with fast polarization fluctuation will cause measurement fluctuations.

5. The wavelength of the light source should be relatively stable, because fast wavelength fluctuation of the light source will cause fast polarization fluctuation due to the birefringence of the fiber cable connecting the laser and the instrument.

6. Fiber jumpers with low PDL should be used for connecting to the DUT.

7. To minimize the error contribution from double reflection, APC connectors should be used for inputting light into the instrument and to the DUT. The PDL-201 has APC bulkhead connectors (input connector and connector A in Figs. 5 and 6) mounted on the front panel for this purpose. For accurate measurement of low-PDL DUTs (less than 0.1 dB), index matching gel can be used at connectors B and C to reduce back reflection and residual PDL.

8. To minimize connector PDL contributions, a PC type connector should be used to send the output light from the DUT into the instrument (connector D in Figs. 5 and 6). Light from the PC connector will be directly incident onto a free space photodetector inside the instrument. If an APC connector were used here, a PDL error contribution of 0.03 ~ 0.04 dB would result.

9. There should be no sharp bending or tight coiling of the fiber cable between connectors A and D, because bending can introduce non-negligible PDL in the fiber cable.

10. For pre-connectorization measurement of pigtailed components on the production floor, the setup shown in Fig. 6 should be used. In this setup, a fiber pigtail with an APC connector at one end is connected to bulkhead connector A. The other end is left free for fusion splicing. The operator may fusion splice the free pigtail to that of the DUT input, and use a removable PC type bare fiber adapter at the DUT output to connect to bulk-connector D. Index matching gel may be used with APC connector A to minimize its PDL contribution.

Note: Connector A in Figs. 5 and 6 will also contribute a slight background PDL. Therefore, for pre-connectorization measurement of pigtailed components (especially low-PDL components), it can be replaced with a fiber pigtail which can be fusion spliced to the DUT input (Fig. 7). Please contact General Photonics for desired configuration before ordering.

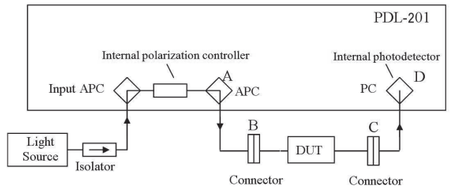

Figure 5 Typical setup for measurement of a connectorized DUT with the PDL-201.

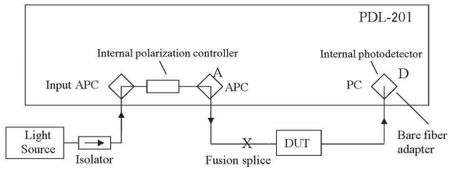

Figure 6 Production floor setup to measure an unconnectorized, pigtailed DUT using fusion splice to a free pigtail and bare fiber adapter to connect to the PDL-201.

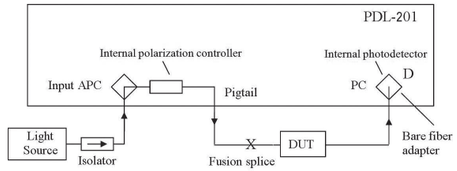

Figure 7 Production floor setup to measure an unconnectorized, pigtailed DUT using only fusion splice and bare fiber adapter to connect to the PDL-201.

Accurate DOP Characterization with Less Effort

Steve Yao
General Photonics Corporation

Degree of Polarization (DOP) is an important property of light sources. It directly relates to the accuracy of optical component characterization, the sensitivity of sensor systems, and the quality of optical signals in optical communication systems. Therefore, the accurate and fast characterization of DOP is increasingly important. This article first reviews the fundamentals of DOP and summarizes the DOP properties of various light sources. It then describes different methods of DOP measurement, and compares their pros and cons. Finally, it describes some unique applications that an accurate DOP meter can offer for light source production, system monitoring, and quality assurance.

DOP describes how much of the total light power is polarized. Mathematically, it is defined as the power of the total polarized portion of a light beam divided by the total optical power (sum of the total polarized portion and the total unpolarized portion):

$$DOP = \frac{P_{polarized}}{P_{total}} = \frac{P_{polarized}}{P_{polarized} + P_{unpolarized}} \qquad (1)$$

The DOP of totally polarized light is unity, while the DOP of completely unpolarized light is zero.

Classification of Light Sources:

The DOP of different light sources ranges from 0 to 1. High DOP sources include DFB lasers and external cavity lasers. They are generally incorporated in laser transmitters in telecommunication systems, and are used as light sources in interferometers.

At the other end of the spectrum, amplified spontaneous emission (ASE) sources, light emitting diodes (LED), and super-luminescence light emitting diodes (SLED) represent sources with low DOP. Such low DOP sources are important to minimize polarization sensitivity in sensor applications. For example, SLED and ASE sources are ideal for the fiber gyro, a rotation sensor for measuring the rate and degree of rotation of an object. Low DOP sources are also attractive for accurate characterization of optical components, because they can remove PDL effects in the measurement system, including the polarization sensitivity of photodetectors. Therefore, accurate characterization of the DOP of these light sources is extremely important for both optical component manufacturers and users.

Optical amplifiers are critical devices in fiber optic communication and sensing systems. One of the important parameters of the amplifiers is low polarization sensitivity. Unfortunately, both Er^{3+} doped amplifiers and Raman amplifiers have polarization dependent gain (PDG). In particular, the PDG of Raman amplifiers can be much stronger than that of Er^{3+} amplifiers.

Raman amplifiers are based on stimulated Raman scattering of optical signals by optical phonons excited by a pump laser in an optical fiber. A weak optical signal is amplified by stimulating the excited phonons to release energy into the signal. This process is called stimulated Raman scattering. PDG is particularly strong for Raman amplifiers because in stimulated Raman scattering, an incident photon can only stimulate a phonon contributed by a pump photon of the same polarization. Raman gain is the strongest when the polarization of the signal is aligned with that of the pump, but is negligible if the polarization of the signal is orthogonal to that of the pump.

One effective method to minimize the PDG or polarization sensitivity of a Raman amplifier is to pump it with depolarized laser sources. A depolarizer may be used to convert a polarized pump laser into a depolarized source with DOP close to zero, as shown in Fig. 1. Such a depolarizer can be made with birefringent crystals, PM fibers, or other methods. Alternatively, a polarization beam combiner can be used to obtain a nearly unpolarized light beam by combining two laser sources of similar frequency but orthogonal polarization, as illustrated in Fig. 1.

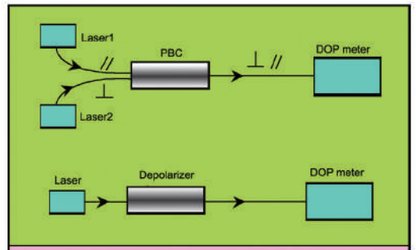

Fig.1. Monitoring DOP of depolarized pump sources for Raman amplifiers. Upper: Depolarization by polarization combining. Bottom: Depolarization with a depolarizer.

Because the DOP of pump sources directly relates to the polarization sensitivity of the amplifier, accurate characterization of their DOP is of paramount importance for Raman amplifier manufacturers. For example, the DOP of the combined pump source critically depends on the power balance between the two orthogonally polarized pump lasers, so a fast, inexpensive DOP meter is desirable for the live adjustment of the pump lasers on the manufacturing floor.

DOP Measurement Methods

Polarimeter method

DOP may be measured with a traditional polarimeter, an instrument that fully characterizes the polarization properties of light sources, using the four Stokes parameters S_0, S_1, S_2, and S_3. Fig. 2 illustrates two polarimeter configurations. The first is based on a rotating waveplate and a polarizer, while the second is based on separating the incoming light beam into four beams so that each beam is analyzed with an analyzer of a different orientation.

Fundamentally, the Stokes parameters fully define the polarization characteristics from power measurements only:

$$S_0 = P_0 \ (polarized + unpolarized) \qquad (2a)$$

$$S_1 = P_x - P_y \qquad (2b)$$

$$S_2 = P_{45} - P_{-45} \qquad (2c)$$

$$S_3 = P_L - P_R \qquad (2d)$$

where P_0 is the total power, and P_x , P_y , P_{+45}, P_{-45}, P_R, P_L are the powers along the x-axis, y-axis, +45° axis, -45° axis, right hand circular axis, and left hand circular axis, respectively.

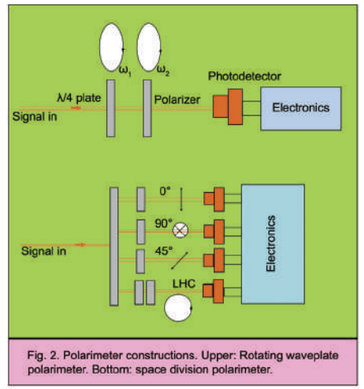

Fig. 2. Polarimeter constructions. Upper: Rotating waveplate polarimeter. Bottom: space division polarimeter.

The DOP of the light beam is related to the Stokes parameters by the following formula:

$$DOP = \sqrt{S_1^2 + S_2^2 + S_3^2} \Big/ S_o \qquad (3)$$

For completely unpolarized light, all SOP states exist, so that $P_x = P_y = P_{45} = P_{-45} = P_L = P_R$. Consequently, S1, S2, and S3 are all theoretically zero. However, in reality, uncertainties due to detector noise, digital noise, signal power fluctuation, rotating optics' repeatability, gain balances between analyzing channels, imperfections of the optical elements inside the polarimeter, and wavelength dependence of the elements all cause measurement errors for each Stokes parameter. From Eq. 2, the DOP is just the root-mean–square of the last three Stokes parameters, normalized by the total optical power S_0. Therefore, errors in Stokes parameters add up to signify the error in DOP measurement. As a rule of thumb, the polarimeter is less accurate in measuring low DOP light sources. Other disadvantages of the polarimeter method include high cost, wavelength sensitivity, cumbersome calibration requirements, and complexity of operation.

Polarization scrambling method

Another commonly used method is the scrambling method, in which a polarization scrambler is placed in front of a polarizer and a photodetector, as illustrated in Fig. 3.

Ideally, at some points during the scrambling cycle, the polarized portion of the signal will either be aligned or orthogonal to the polarizer's passing axis. When aligned, all of the polarized portion passes through the polarizer, corresponding to a maximum power level at the photodetector. When orthogonal, the polarized portion is blocked by the polarizer, assuming that the extinction ratio of the polarizer is sufficiently high, corresponding to a minimum power level at the photodetector. Therefore, the difference P_{max}-P_{min} equals $P_{polarized}$ in Eq. (1).

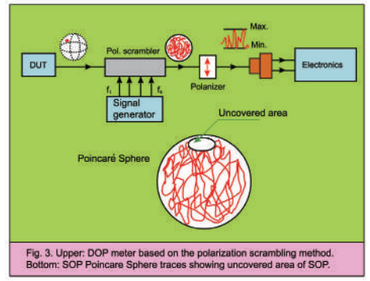

Fig. 3. Upper: DOP meter based on the polarization scrambling method. Bottom: SOP Poincare Sphere traces showing uncovered area of SOP.

The unpolarized portion, on the other hand, is not affected by the scrambler. Its contribution to the total detected power is constant, but reduced by half by the polarizer. Because the contribution of the polarized portion is zero at P_{min}, $P_{min} = P_{unpolarized}/2$. The DOP from Eq. (1) then can be calculated as:

$$DOP = (P_{max} - P_{min})/(P_{max} + P_{min}) \qquad (4)$$

Therefore, the DOP of the signal can be easily determined by measuring the maximum and minimum power levels at the detector while scrambling the incoming signal.

However, in order for the method to be practical, the scrambler must first be sufficiently fast to cover the whole Poincaré Sphere in a short period of time. Second, the scrambler itself must have negligible activation loss (the maximum insertion loss variation during scrambling). Finally, the detection electronics must be fast and accurate enough to correctly detect the maximum and minimum power levels.

Scramblers with activation loss less than 0.01 dB are available off the shelf from General Photonics. The 0.01 dB activation loss contributes to a negligible DOP error of 0.12%. Electronics can also be made to satisfy the speed and accuracy requirements. However, no matter how fast and uniform the scrambler is, the Poincaré Sphere cannot be completely covered in a finite time. There will always be uncovered areas (as shown in the bottom portion of Fig. 3), which contribute to the DOP measurement uncertainty. The faster the measurement requirements, the larger the uncertainty. Such uncertainty makes the scrambling method less accurate, especially for measuring light sources with high DOP. However, for low DOP values, the requirements for coverage of the Poincaré Sphere are less stringent, and therefore the scrambling method is more accurate and faster than the polarimeter. In addition, compared with the polarimeter method, it has the advantage of wavelength insensitivity, calibration free operation, high power capability, simplicity, and low cost.

Maximum/minimum search method

To remove the measurement uncertainty in the polarization scrambling method, General Photonics invented and implemented a deterministic maximum and minimum search method. As illustrated in Fig. 4, a feedback circuit is used to direct the polarization controller to adjust for the maximum and minimum power levels in the detector. Instead of trying to hit the right polarization states by luck, as in the scrambling method, the maximum/minimum search method assures that the instrument unmistakably finds P_{max} and P_{min}, and then uses them in the final DOP calculation in Eq. 4.

Because only two points on the Poincaré Sphere are required, and can be found deterministically and precisely, measurement speed

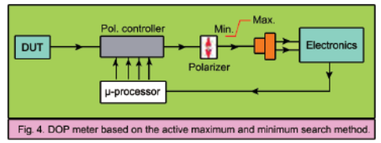

Fig. 4. DOP meter based on the active maximum and minimum search method.

and accuracy are guaranteed for both low and high DOP sources. Consequently, such an approach overcomes the shortcomings of both the polarimeter method (less accurate for low DOP values) and the polarization scrambling method (less accurate for high DOP values). Fig. 5 is a photo of General Photoncs' DOP meter.

Fig. 5. Photo of a max/min search method based DOP meter by General Photonics.

The maximum/minimum search method is essentially a closed loop polarization scrambling method. It eliminates the inaccuracies, but inherits all the advantages of, the scrambling method, including wavelength insensitivity, calibration free operation, high power capability, easy operation, simple construction, and low cost. In addition, it also enjoys the edge of high measurement speed (less than 0.2 seconds).

High-power handling approaches

The optical powers of different light sources vary dramatically, ranging from microwatts for LEDs to watts for pump lasers. However, typical DOP meters have a dynamic range on the order of 30 dB. Users may specify their intended power range, e.g., from –30dBm to 0 dBm, or from –10 dBm to 20 dBm. For high power light sources, such as Raman pump lasers with powers up to 500 mW, fixed attenuators may be used. To preserve the DOP accuracy, these attenuators must have low PDL, because PDL generally repolarizes the light source. As a good estimation, the DOP error introduced by a PDL source when measuring an unpolarized source is

$$DOP\,(\%) = 12 \cdot PDL\,(dB) \qquad (5)$$

For example, the DOP error introduced by an attenuator with a PDL of 0.1 dB is 1.2%.

Other applications

In addition to being able to simply determine the DOP value, an accurate and fast DOP meter is also important on the manufacturing floor for tuning the DOP values of light sources. For example, by monitoring DOP in real time while adjusting the power balance of the two pump lasers in Fig. 1, an extremely low DOP value for the Raman pump can be achieved. Polarimeters are generally too expensive to be used in production stations, too complicated to operate for less sophisticated production personnel, and not accurate enough for so demanding an application. By contrast, due to its low cost, simplicity to operate, and high accuracy, the DOP meter based on the max/min. search by General Photonics is ideal for such applications.

Besides measuring the DOP of light sources, a high-speed DOP meter can also be used in optical networks to monitor PMD or optical signal to noise ratio (OSNR), as illustrated in Fig. 6. Because PMD in an optical system degrades the DOP of the optical signal, monitoring the DOP directly reveals the influence of PMD on optical signals.

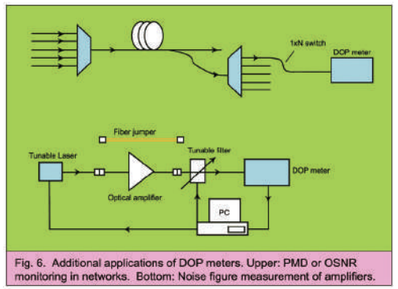

Fig. 6. Additional applications of DOP meters. Upper: PMD or OSNR monitoring in networks. Bottom: Noise figure measurement of amplifiers.

In the absence of PMD influence, OSNR can also be obtained from DOP measurement by (assuming signal is totally polarized and noise is totally unpolarized):

$$OSNR = 10 \text{ Log } [(P_{max} - P_{min})/(2P_{min})] = 10 \text{ Log } [DOP/(1-DOP)] \qquad (6)$$

An accurate DOP meter can also be used to measure the noise figure of an amplifier, as shown in Fig. 6. One may first measure the OSNR of the signal source without the amplifier ($OSNR_0$) by inserting a jumper in the place of the amplifier, and then measure the OSNR of the signal after the amplifier ($OSNR_{amplifier}$). The noise figure of the amplifier is simply the difference between the two OSNR measurements, in dB. In practice, noise figure is generally given within a 0.1 nm bandwidth; therefore, the effects of the bandwidth and shape of the filter need to be taken into account in determining the final OSNR value. With the aid of a computer, the wavelength dependence and power dependence of the noise figure can also be determined.

In summary, the DOP meter is an important instrument for accurate characterization of the DOP values of different light sources for communication, manufacturing, testing and sensing applications. The newly developed DOP meter based on the maximum and minimum power search method has the advantages of low cost, simple operation, high speed, and low wavelength sensitivity, and does not need calibration. It offers high accuracy for both high and low DOP values with less cost, less effort, and less measurement time.

The author would like to thank Drs. Y. Shi and J. Ma for helpful suggestions.

Optical Coherence Tomography Technologies

Optical coherence tomography (OCT) is an optical imaging technique which can provide high resolution, cross-sectional tomographic (or 3-dimensional) imaging of the internal microstructure of materials and biological systems by measuring backscattered or backreflected light. The resolution of the OCT image is 1 to 15 µm, about 100 times better than conventional ultrasound, and therefore has profound implications for the diagnosis of internal problems in biological tissues (such as human bodies) as well as inorganic samples. It has become increasingly popular for medical applications such as noninvasive opthalmological imaging and endoscopic gastrointestinal tract imaging. It also has applications in other fields that require rapid, nondestructive imaging.

Two types of OCT technologies are available today: frequency domain OCT (FD-OCT) and time domain OCT (TD-OCT). TD-OCT is based on low coherence interferometry, with the depth resolution of the system determined by the coherence length of the light source. The basic setup resembles a Michelson interferometer, as shown in Fig. 1. Light from a broadband optical source is divided to illuminate both the sample and reference arms of the interferometer. The reflected light from both arms is recombined and sent to a detector. An interference pattern is created only when the path lengths in the two arms are matched to within the coherence length of the light source. Scanning the length of the reference arm over the range of interest using a fast delay line thus yields a one-dimensional reflectivity vs. depth profile of the sample. Adding x-y scanning optics in the sample arm enables the combination of depth scans from multiple points to create 2 or 3-dimensional images.

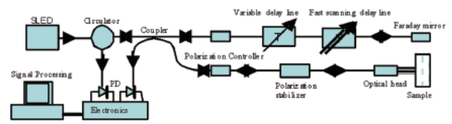

Fig. 1 Time Domain Optical Coherence Tomography (TD-OCT)

FD-OCT can be further divided into scanning laser-based FD-OCT and spectrometer-based FD-OCT, as shown in Fig. 2 and Fig. 3, respectively. Like TD-OCT, they are constructed with a Michelson interferometer, but they do not require a fast scanning delay line. For a scanning laser based FD-OCT, a fast scanning laser is used to replace the broadband source. The Fourier transform of the detected interferometric signal gives the reflectivity vs. depth information of the sample to be imaged. One problem associated with scanning laser FD-OCT is the high cost of the tunable laser. General Photonics has developed a new wide range, low ripple, high power wavelength swept laser for just this application.

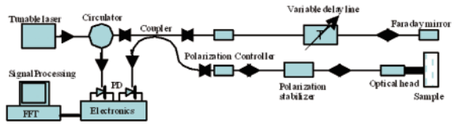

Fig. 2 Scanning Laser Based Frequency Domain OCT (FD-OCT)

Spectrometer based FD-OCT uses a broadband source as the input and a high speed spectrometer to receive and analyze the returned interferometric signal. The Fourier transform of the spectral information reveals the reflectivity vs. depth information. The drawback of this method is the small size of the achievable depth range, which is limited by the spectral resolution of the spectrometer.

Figures 1, 2, and 3 also show the key optical components used to construct an OCT system. Two primary issues for an OCT system are polarization control and optical delay balance. In order to produce a good interferometric signal, the state of polarization (SOP) of the two interfering arms should be aligned; therefore, polarization controllers must be used. For some applications, dynamic polarization control is required for tracking real time polarization changes. For a polarization sensitive OCT (PS-OCT) system, more sophisticated polarization control and analysis devices are required, such as a polarization switch or polarization state generator. General Photonics is proud to offer a complete array of polarization control and analysis solutions, ranging from manual polarization controllers to high speed dynamic polarization controllers and high speed polarimeters.

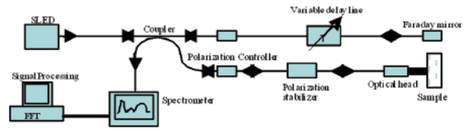

Fig. 3 Spectrometer based Frequency Domain Optical Coherence Tomography (FD-OCT)

Another factor necessary to achieve good interferometric signals in both TD-OCT and FD-OCT systems is the optical path length balance of the two interfering arms. General Photonics' manual variable delay lines (VDL) are perfect for this application. With a delay variation range up to 40 cm, these delay lines can quickly compensate for large delay imbalances between the two interfering arms.

A depth "zooming" function is desirable for some applications, such as opthalmological imaging of the front and back of an eye. General Photonics' motorized delay line (MDL-002) is ideal for such an application. With sub-micron resolution and a total delay of up to 40 cm, the MDL-002 enables the OCT system to "zoom" to any desired position.

The most important component for TD-OCT is a fast scanning delay line with a range of 3 to 5 mm and a speed of up to a few kHz. General Photonics provides fiber stretchers (FST) with varying speeds and delay ranges for this application

General Photonics also provides other components for OCT applications, such as wideband couplers, polarization maintaining couplers, circulators, and Faraday mirrors. Our bench-top SLED source is convenient for OCT related research. We are the one-stop shop for almost all optical components for OCT applications. Please contact us if you do not see the products you need in the catalog. We will be happy to listen to your requirements and modify or customize our products to meet your needs

FAQS

Dynamic Polarization Controllers.....287
Polarization Scramblers.....291
Depolarizers.....294
Polarization Stabilizers.....295
ER Measurement.....296
Polarimeters.....298
Phase Shifters.....300
Delay Lines (MDL/VDL, ODG).....301
Fiber Coils.....303
Other products.....304

Dynamic Polarization Controllers

Optics

Q. What is the operation wavelength range (or bandwidth) of the PolaRITE™ II/III?

A. General Photonics' standard PolaRITE™ II/III devices are designed for wavelengths from 1260nm-1650nm. Typical communication wavelengths are all covered in this wavelength range. The typical device performance data for PolaRITE™ II/III are specified at 1550 nm. Performance data at 1310 nm can be provided upon customer request.

An ultra-broadband version that covers 970-1650 nm is also available. (Note: Data sheets for operation wavelengths other than 1550 nm or 1310 nm may not be available.)

Q. Can I operate the PolaRITE™ II/III at 980 nm, 1060 nm, 1310 nm or 530 nm wavelengths?

A. Yes. PolaRITE™ II/III devices can be manufactured with either user-provided fiber or General Photonics' in-house fiber for use at wavelengths other than the conventional 1550 nm, such as 1310 nm, 1060 nm, 980 nm, or 530 nm for single mode propagation. Operation wavelength should be specified when ordering. Please note that General Photonics' standard fibers cover either the 1260-1650nm or 980-1310nm ranges. Polarization controllers made with nonstandard fibers may have different performance characteristics and may carry different warranty terms from standard units.

Q. What is the insertion loss of the PolaRITE™ II/III?

A. PolaRITE™ II/III devices are manufactured with continuous optical fiber. The total insertion loss (IL) consists of intrinsic fiber loss along with loss from mechanical effects. Typically IL for PolaRITE™ II/III devices is on the order of ~ 0.05 dB at 1550 nm.

Q. What is the activation loss of the PolaRITE™ II/III?

A. Activation loss is defined as the change in device insertion loss due to operation of the device. In the case of PolaRITE™ II/III devices, the activation loss is a function of the external drive voltages, and results from the loss of optical power in the fiber core during the activation of the PZTs. Micro-bending can be the major contributor to this loss. The activation loss data listed on the device data sheet is the device insertion loss change under full DC voltage (i.e. 150 volts) loading. General Photonics PolaRITE™ II and III are designed for extremely low activation loss, typically under 0.01 dB. Devices with activation loss less than 0.005 dB can also be provided by special request.

Q. Why is low activation loss preferred in most applications?

A. Some important applications of polarization controller devices include polarization dependent loss (PDL) measurement and polarization scrambling. In a PDL measurement, the activation loss of the polarization controller will add measurement uncertainty to the results. For example, if the activation loss is 0.2 dB, the PDL measurement uncertainty will be at least 0.2 dB higher. For the scrambler application, the activation loss adds an amplitude noise term to the optical light signal. This noise can interfere with optical signals or degrade signal detection in demanding applications. Therefore, low activation loss is preferred for polarization controllers.

Q. What is the PDL of the PolaRITE™ II/III?

A. PDL is defined as the difference between maximum and minimum optical power transmission over all input states of polarization (SOP), expressed in dB. Typically, the PDL of the PolaRITE™ II/III is ~ 0.01 dB.

Q. What is the PMD of the PolaRITE™ II/III?

A. Our measurements indicate the following PMD results for the PolaRITE™ II: PMD max < 60 fs (PCS-3X); PMD max < 80 fs (PCS-4X). The maximum PMD occurs near the maximum driving voltage (~ 4 to 5 V_{π}). For polarization scrambler applications, the drive voltage will be about 1.5 times V_{π}. At this drive voltage, the PMD will be limited to less than 40 fs (PCS-3X) or 50 fs (PCS-4X). PMD for the PolaRITE™ III is about the same as for the PolaRITE™ II. These results are summarized in the following table.

PolaRITE™ II/III	Controller	Scrambler
PCS/MPC-3X	PMD < 60 fs	PMD < 40 fs
PCS/MPC-4X	PMD < 80 fs	PMD < 50 fs

Q. What is the operation principle of PolaRITE™ polarization controllers? What are the differences between the PolaRITE™, PolaRITE™ II, and PolaRITE™ III?

A. All PolaRITE™ polarization controllers have the same operation principle. They are all constructed based on fiber squeezing technology, and all are capable of transforming any input SOP to any arbitrary output SOP. The differences between them are mainly in form factor and control methods. PolaRITE™ manual polarization controllers require external rotation (moving) control. They come in a variety of sizes and connector combinations, and are usually

used in static or quasi-static polarization control. PolaRITE™ II comes in 3-axis and 4-axis versions, and is actuated electrically with no external moving parts. In practical use, the electronic control interface of the PolaRITE™ II allows its use in automatic and high-speed applications. PolaRITE™ III is very similar to PolaRITE™ II. The main difference is that PolaRITE™ III is specifically designed for system integration, with a small form factor and high temperature stability.

Q. What is the $V_{\pi, DC}$ and $V_{\pi, AC}$ of the PolaRITE™ II?

A. Both $V_{\pi, DC}$ and $V_{\pi, AC}$ are defined as the voltage change required to offset the relative phase of the two eigen-polarization states by π. $V_{\pi, DC}$ refers to slow, quasi-DC voltage change, while $V_{\pi, AC}$ refers to the voltage change at AC frequency f required for a π phase change. A typical $V_{\pi, DC}$ value for the PolaRITE™ II is approximately 30V. It remains nearly constant from DC to ~20 KHz. Because $V_{\pi, DC}$ and $V_{\pi, AC}$ are equal at low frequencies, we usually do not specify them separately, except at resonance frequencies.

Q. What is the resonant frequency and resonant V_{π} of the PolaRITE™ II?

A. The electric actuator and its mechanical enclosure can enhance actuation of the PolaRITE™ II device at some characteristic frequencies. These characteristic frequencies (typically near 60 kHz, 100 kHz, 130 kHz and 160 kHz) are called resonant or resonance frequencies of the PolaRITE™ II. The profile of the resonance frequencies depends on the actuator and mechanical boundary conditions of the package. At these frequencies, the half wave voltage V_{π} is significantly reduced from its DC value. A typical V_{π} at a resonance frequency is ~ 2-10V, which is much smaller than the ~ 30V $V_{\pi,DC}$.

Q. What is the major difference between a Polarization Controller and Scrambler?

A. PolaRITE™ II can perform two major functions: static or quasi-static polarization control and polarization scrambling. Different characteristics are important for these two applications. For scramblers, the device is optimized for low activation loss (< 0.01 dB) and low resonant V_{π}, For polarization controller applications, speed and bandwidth are optimized.

Q. How do PolaRITE™ II/III devices function as polarization controllers?

A. A PolaRITE™ II/III device can be modeled as three (for PCS/MPC-3X) or four (for PCS/MPC-4X) cascaded variable wave plates. The optical axes of the first and the third waveplates are aligned in the same direction, and the second and the fourth waveplates have optical axis orientations offset by 45 degrees with respect to the first and the third waveplates. In theory, a three variable waveplate combination is enough to convert any input SOP to any output SOP, even if the input SOP is an eigenstate of the first waveplate. Therefore, the PolaRITE™ II/III can function as an electrically actuated polarization controller. One can adjust the DC voltages applied to the connection pins of a PolaRITE™ II/III to obtain the desired SOP. On the Poincaré Sphere surface, two waveplates oriented 45 degrees from each other generate orthogonal SOP traces. This orthogonality makes a polarization state control algorithm much easier than approaches using other mechanisms.

Q. How should the PolaRITE™ II be driven to function as a polarization scrambler?

A. For minimum degree of polarization (DOP), two conditions are suggested for using PolaRITE™ II in scrambling operations.

1. Amplitude conditions:
   $V_{pp1} = 1.53\ V_{\pi 1}$ and $V_{pp2} = 1.53\ V_{\pi 2}$

2. Frequency conditions:
   $\omega 1 \neq \omega 2$ and $(2m+1)\ \omega 1 \neq 2n\ \omega 2$ (n, m = 1, 2, 3...)

Q. What is the major difference between PCS/MPC-3X and PCS/MPC-4X?

A. The major difference between these models is the numbers of actuators: PCS/MPC-3X has three actuators, and PCS/MPC-4X has four actuators. For endless polarization control, people prefer to use PCS/MPC-4X.

Q. What is the response time of PolaRITE™ II/III?

A. When driven by a low amplitude square wave, the optical responses for both rise time and fall time (or switch-on time) are approximately 30 µs.

Q. How fast can you switch from one SOP to another SOP using PolaRITE™ II/III?

A. The switching speed depends on the number of steps used by the controlling algorithm and the actuators to reach the desired SOP. The fastest switching speed, ~ 30 µs, occurs when only one step is involved. Generally speaking, the SOP switching speed will be proportional to the number of steps, ~ N x 30 µs (N=1,2,3…m). At the end of the operation, there might be a small settling time while the final SOP stabilizes. In other words, the SOP switching speed depends on the algorithm for the operation.

Q. Can SOP Stokes values be maintained when the driving voltage is switched from ON to OFF? How repeatable is it?

A. We tested the SOP drift issue using the PCS-3X with driving voltages V1=V2=V3=70V (DC) as a constant loading condition. Based on two uncorrelated measurements, one with driving voltage off; the other with driving voltage on (i.e. V1=V2=V3=70 V), with the fiber taped tightly to an optical table, the drift rate (measured as the difference in the transmission optical power) over 12 hours' monitoring was approximately 0.01 dB/hr. (The difference is for the purpose of background random drift deduction.)

Q. Is there any hysteresis in your actuator?

A. Yes. A non-symmetric displacement occurs as a forward and reverse voltage is applied to the actuator. You can observe a hysteresis curve in optical transmission on an oscilloscope when an oscillating voltage is applied to the actuator. This hysteresis becomes more and more pronounced as the amplitude of the sweep voltage increases.

Q. Can I eliminate this hysteresis?

A. Yes. You can develop a non-symmetric compensation drive voltage source such that the forward applied voltage is smaller than the reverse voltage, resulting in a reverse voltage trace identical to the forward trace.

Q. How can I use PolaRITE™ II as a polarization stabilizer?

A. An SOP stabilization system requires three elements: an SOP generator, an SOP monitor, and a control circuit. The PolaRITE™ II/III functions as the SOP generator in this system. General Photonics' PolaDetect™ polarimeter or similar devices can be used to monitor SOP. Based on the driving conditions and the signal from the SOP monitor, a control circuit can be designed for open loop or closed loop SOP stabilization. General Photonics' polarization stabilizer (POS-20X) incorporates all three elements to form such a system.

Q. Can PolaRITE™ II/III generate all SOPs over the entire Poincaré Sphere?

A. Yes, PolaRITE™ II/III devices can generate SOPs over the entire Poincaré Sphere.

Q. What happens if the input SOP is an eigenstate of your first actuator?

A. If the input SOP is an eigenstate of the first actuator, that is, linearly polarized light with electric field vector either parallel or perpendicular to the actuation direction, the first actuator will only modulate the phase front of the light beam. It will not change the SOP. Therefore, a control voltage must be applied to the third actuator to fix this singularity problem.

Q. How can I remove the gold-colored fiber coating before splicing the fiber?

A. A cigarette lighter can be used to burn off the fiber coating. Flame exposure time should be minimized to avoid fiber damage. The fiber should then be wiped with alcohol to remove the residue.

Q. What is the highest optical power that the PolaRITE™ II/III can handle?

A. The optical power handling capability is the same as that of the optical fiber used in PolaRITE™ II/III construction (typically SMF-28). Based on manufacturer data, optical power up to 1,000 mW CW at 1550 nm can be launched into this device. Basically, the optical power output of most fiber-coupled devices should be safe for the PolaRITE™ II/III.

Q. (a). Can the PolaRITE™ II/III perform endless polarization control? (b). Is there any information on how to operate the PC in endless mode? (c). What is the response time when my PolaRITE™ II/III device is operating in endless mode?

A. (a). Both the PCS/MPC-3X and PCS/MPC-4X can provide endless polarization control, but the control algorithms for the four axis versions are less complicated than for the three axis versions.

(b). Please refer to the following references regarding endless polarization control:

(1). N. G. Walker and G.R. Walker, "Endless Polarization Control using four fiber squeezers," Electron Letters, vol.23, No. 6, pp.290-292 (1987).

(2). R. Noe, "Endless polarization control in coherent optical communications," Electron Letters, vol. 22, No. 15, pp.772-773 (1986).

(3). R. Noe, H. Heidrich, and D. Hoffmann, "Endless polarization control for coherent optics," Journal of Lightwave Technology, Vol.6, No. 7, pp.1199-1207 (1988).

(c). The response time depends on how you write the algorithms.

Q. Will your electro-mechanical actuator damage optical fiber?

A. NO. We all know that polarization maintaining fibers are very reliable. In PolaRITE™ II/III, the maximum mechanical stress applied to the optical fiber due to actuation is slightly smaller than or about the same as that in a typical polarization maintaining fiber. In addition, General Photonics Corporation has implemented manufacturing processes and used specially selected materials to safeguard device durability. Therefore, fiber damage is not a concern in PolaRITE™ II/III devices. Under the most extreme activation conditions, the fiber's lifetime (MTTF) is estimated to be over one billion years, based on extensive in-house stress experiments and commonly used fiber stress analysis modeling.

Q. What is the lifetime of PolaRITE™ II/III?

A. The lifetime of the device is limited by the lifetime of the piezo-electric actuators used, which is mainly affected by humidity. With hermetical sealing, the lifetime (MTTF) would be about 40 years. If there is a requirement, General Photonics could develop a hermetically sealed version of the PolaRITE III.

Q. What current is required to drive the PolaRITE™ II/III?

A. The piezo can be considered a pure capacitive load with a capacitance of 0.18μF. Therefore, the total current has the following dependence on drive voltage and frequency:

I (t) = C dV/dt

where C is the capacitance. For a sinusoidal drive signal

$V = V_0 * \sin(2\pi f t + \varphi)$,

$dV/dt = 2\pi V_0 f * \cos(2\pi f t + \varphi)$,

The peak current is then $2\pi V_0 f$.

For a linear ramp, I = C * ΔV/Δt.

For example, the current required to drive a piezo with a capacitance of 0.18μF from 0 to 20V in 100μs is I = 0.18μF * 20V/100μs = 36 mA.

Q. How is the performance of the PolaRITE™ II/III affected by temperature?

A. The recommended operating temperature range of both devices is -25 to 80°C (outer case temperature). The resonance frequencies of the device may change with temperature, which may affect resonant scrambling performance, but non-resonance half-wave voltages should be relatively uniform within the specified temperature range.

Electronics

Q. What drivers are available for the PolaRITE II/III polarization controllers?

A. The PolaRITE III polarization controller is available either with (PCD-M02) or without (MPC-3X/4X) an integrated driver board.

The PCD-M02 has an on-board DC/DC converter, so it does not require an external high-voltage power supply. It can accept either a 0-5V analog control signal or a digital TTL control signal. A mini version (PSM-003) with integrated driver is also available for OEM applications.

Q. What are the frequency limits for the PCD-M02?

A. The operation bandwidth of the PCD-M02 depends on the required output voltage level.

For the PCD-M02 with I_{max} = 60 mA and C = 0.18μF, $V_{pp} \cdot f_{max} \approx 100$ V•kHz. This determines the single-channel maximum output voltage and frequency conditions. For I_{RMS} = 20 mA, $V_{pp} \cdot f_{cont} \approx 50$ V•kHz. This determines the maximum output voltage and frequency conditions when all output channels are used simultaneously with the same driving signal.

If the voltage-frequency product exceeds the guidelines set out here, waveform distortion can result.

For full range (V_{pp}=150V) operation, one can achieve 4~5 π retardation on each actuator section, but the operation frequency is limited to 0~333 Hz for the PCD-M02 (using all channels).

In most cases, however, during continuous operation of the PCD-M02 for polarization scrambler applications, only 1.53π retardation is required for each actuator. The corresponding driving voltage is on the order of V_{pp}= ~50V. In this situation, the operation frequency range can be extended to 0-1kHz .

The PCD-M02 is not recommended for driving at resonant frequencies. Because most resonant frequencies are distributed between 50 kHz and 200 kHz, and the driving voltage at resonant frequencies is typically <10V, a function generator can be an alternative driver if users desire operation at these resonant peaks.

Q. What is the upper limit on input frequency for your PolaRITE™ II/III drivers such that the output waveform remains undistorted?

A. Strictly speaking, the upper limit of the non-deformed frequency depends on the output voltage and PZT impedance loading. Without any loading, the driver output is perfectly linear with the input. With PZT loading, the effective impedance is strongly modulated, resulting in the upper frequency limitation. See the answer to question 2 for more details.

Q. What is the power consumption of the PCD-M02?

A. The PCD-M02 in its standard configuration requires a +12V/1.2A power supply and a –12V/0.1A power supply. The maximum peak current per channel is 60 mA when one channel is operated separately, or 20 mA/channel when all 4 channels are operated together.

Q. How can I remote control the driver? Do you provide any operation utilities for remote communication and control?

A. The PCD-M02 can be controlled digitally using TTL levels. It requires a R/W bit, chip select, 2 channel-control bits, and 12 signal bits. A DIO card can be used to generate the control signals. Many DIO cards can be remote-controlled via RS-232 or USB.

Polarization Scramblers

Q. What are the advantages of General Photonics' polarization scramblers?

A. General Photonics (GP) offers a broad line of polarization scrambling products. The major advantages include:

1. extremely low insertion loss (< 0.05 dB w/o connector);
2. low electrical power consumption (< 12 Watts for PCD-005, <9 Watts for PSM-002)
3. ultra broad wavelength range
4. wide operation temperature range (-35 ~70°C case temperature possible for PSM-002);
5. small board size (board <1 inch in height);
6. low cost for wide applications;
7. custom design available. Module can be easily modified to fit OEM requirements.

GP polarization scrambler products include both modules (PCD-003, PCD- 005, PSM-002, PSM-003) and a benchtop instrument (PCD-104). All are suitable for both OEM customers and R&D laboratories. In addition, the multifunction polarization controller and polarization synthesizer products have polarization scrambling functions. GP's microprocessor controlled scrambler allows intelligent scrambling control, including wavelength selection, external communications, and remote on/off switching.

Q. What does DOP stand for?

A. DOP stands for Degree of Polarization; its value shows the portion of light that is polarized during the detection time frame. For example, linearly and circularly polarized light have a DOP of 100%, while natural white light has a DOP of 0%.

Q. If I use a PolaRITE™ II -based scrambler at 980nm, is the fiber single mode or multimode?

A. The fiber used in a scrambler intended for use at 980nm is a single mode fiber that covers a wavelength range from 970nm to 1550 nm. Currently, we test our device at 1550 nm and extrapolate to 980 nm operation conditions in order to keep the DOP (degree of polarization) less than 5% at the output. Standard SMF-28 fiber will be multimode at 980 nm.

Q. What is the typical electrical power consumption of your polarization scramblers?

A. The typical power consumption of the PCD-003 is <10W.
The typical power consumption of the PCD-005 is <12W.
The power consumption of the PSM-002 varies with scrambling speed over a range of 0.5 to 9W.

Q. What is the maximum optical power throughput that your devices can handle?

A. GP's polarization scramblers use continuous fiber in their construction. They can therefore handle more than 1000mW optical power.

Q. Can I change the polarization scrambling frequency?

A. The scrambling frequencies of the PCD-003 and PCD-005 polarization scrambler modules and the PCD-104 instrument are preset during manufacturing for optimized DOP performance. They are based on the scrambler's resonance frequencies, and result in an effective scrambling frequency of >700kHz. The user should not change them without GP's explicit authorization.

The PSM-002 generates random, discontinuous SOPs at a user-controllable rate. The PSM-002's scrambling rate range is 0.01 to 20k points/s.

The PSM-003 scramblers are preset at the factory to a scrambling rate and type (continuous or discrete) corresponding to the configuration ordered by the user and cannot be changed after that.

The MPC-20X and PSY-201 are designed for laboratory testing and can generate various types of scrambling patterns at user-controllable rates.

Q. What are the differences between the different models of scramblers? Can they be remote controlled? What software is needed?

A. The table below summarizes some of the differences between different scrambler models.

Model	Scrambling Type	Scrambling Rate	Remote Control	Software
PSM-003	Continuous or Discrete Depends on model	Fixed (slow) Depends on model	No	NA
PSM-002	Discrete	Variable 0 to 20k points/s	Yes	No
PCD-003	Continuous	Fixed (fast)	No	NA
PCD-005	Continuous	Fixed (fast)	Yes	Yes
PCD-104	Continuous	Fixed (fast)	Yes	Yes
MPC-20X	Continuous -Triangle -Rayleigh -Tornado Discrete	Variable 0 to 2000 x 2π rad/s 0 to 2000 rad/s (mean) Depends on model 0 to 20k points/s	Yes	Yes
PSY-201	Continuous -Triangle -Rayleigh -Tornado Discrete	Variable 0 to 2000 x 2π rad/s 0 to 2000 rad/s (mean) 0 to 2000 rev/s 0 to 20k points/s	Yes	Yes

The PSM-003 is a compact, simple-to-use module suitable for applications that require a fixed, relatively slow (<60π rad/s continuous or <5 points/s discrete) scrambling rate. The scrambling type and rate are determined by the configuration ordered.

The PSM-002 is a miniature polarization scrambler designed for hand held and field instruments. Its size and power consumption are larger than those of the PSM-003, but much smaller than those of the PCD-003/005. It can also have an extremely wide operating temperature range (−35 to 70°C). It operates on a discrete, random scrambling model, in which random sets of control voltages are input to the different channels of the polarization controller at a user-selected frequency. It has a single preset center wavelength and a relatively wide operating wavelength range. It can be controlled via RS-232 using a special cable provided with the module. It can be used to mitigate polarization dependent effects, or to generate random SOPs for measurement applications.

The PCD-003 and 005 are high frequency, resonance based scramblers primarily used to randomize the SOP to average out polarization dependent effects. They are based on continuous sinusoidal waveform scrambling, with each channel driven at a different resonance frequency. The PCD-003 has no remote interface, but the PCD-005 can be remote controlled via an RS-232 communication port on the digital interface adapter board (ADB-001) to turn the module on/off, or change the operating wavelength to any of 6 settings (980nm, 1060nm, 1310nm, 1480nm, 1550nm, 1600nm). Customers who use 980 nm or 1060 nm wavelengths need to specify this during the ordering process. The standard PCD-005 covers only 1310, 1480, 1550, and 1600 center wavelengths. Simple LabView based control software is provided with the PCD-005. With the microprocessor controller, the polarization scrambler performance can be dynamically optimized with the temperature and wavelength.

The PCD-104 provides the same functions as the PCD-005 in an instrument form with RS-232, Ethernet, and GPIB interfaces.

The MPC-20X and PSY-201 are more general purpose polarization control and measurement instruments that include built-in polarization scrambling functions. They can generate multiple types of scrambling patterns for different purposes with user-controllable rates. These include Triangle scrambling (continuous pattern suitable for PDL measurement), Rayleigh scrambling (continuous pattern that emulates SOP variation in fiber systems), Tornado scrambling (continuous pattern designed for SOP tracking speed testing), and Discrete scrambling (random generation of discrete points; the same function as the PSM-002). These instruments have RS-232, USB, Ethernet, and GPIB interfaces, and come with software.

FAQs: Polarization Scramblers

Q. What are residual phase and amplitude modulation? How are they measured?

A. Residual phase modulation is a constant phase modulation term that exists in addition to the phase difference change between two eigenmodes (e. g., Ex and Ey). The residual phase modulation is independent of input polarization state. Residual amplitude modulation is a modulation-induced insertion loss change, which is also called activation loss. Compared with other, similar products on the market, General Photonics polarization scramblers have the lowest residual phase modulation (~ 0.1π) and amplitude modulation (0.01dB). Residual amplitude modulation can be measured by optical intensity measurements such as insertion loss tests. However, residual phase modulation cannot be determined directly from an intensity sensitive photodetector measurement. A fiber interferometer setup is required. For detailed information, please call General Photonics.

Q. What are some applications of polarization scramblers?

A. Polarization scramblers can be used to mitigate polarization dependent effects, such as polarization dependent gain (PDG) in fiber amplifier systems, polarization dependent loss (PDL) in WDM systems, and polarization mode dispersion at data receivers. In addition to fiber optic transmission systems, polarization scramblers also have wide applications in test and measurement instrumentation. They are used in random polarization generators, PDL meters, OTDRs, and optical spectrum analyzers, to name a few.

Q. What is the difference between a passive depolarizer and a polarization scrambler?

A. Passive depolarizers generally work by removing the phase relationship between orthogonal polarization components of light, resulting in depolarized light. Polarization scramblers generate a pattern that evenly covers the Poincaré sphere over time. The instantaneous output DOP of a polarization scrambler with a fully polarized input is still 100%. However, when averaged over a sufficient period of time for the scrambler to cover most of the sphere, the DOP of the signal drops to close to 0%. General Photonics' polarization scramblers have less wavelength dependence than passive depolarizers; a polarization scrambler can cover a 100nm wavelength range with a DOP of less than 5%. In addition, passive depolarizers are highly dependent on the coherence length of laser output; they operate effectively only when the light source has a short coherence length, while polarization scramblers can work with light sources of any coherence length, including DFB lasers, diode pumped solid state lasers and so on. Due to their all-fiber construction, GP's polarization scramblers also have extremely low insertion loss. On the other hand, polarization scramblers require an electrical power supply, while passive depolarizers have no electrical power requirement.

Q. What are the resonant frequencies of the polarization scrambler?

A. Several resonant frequencies are used in the PCD-003/005/104 polarization scramblers. There is a distribution of these resonant frequencies depending on individual components. Typically, the resonant frequencies are distributed between several bands: 50 ~ 70 kHz, 90 ~ 120 kHz, 125 ~ 146 kHz and 150 ~ 170 kHz. Other types of scramblers (PSM-002/003, MPC-201/2, PSY-201) do not use resonant frequencies.

Q. What are the operating temperature ranges for GP's polarization scramblers? If my condition is slightly out of that range (for example, by 5 °C), what is the result?

A. For the specified DOP of 5% or less, the operating temperature ranges are 10 to 40°C for the PCD-003, 10 to 45°C or −5°C to 65° C for the PCD-005, and 0 to 65°C or −35 to 70°C (case temperature) for the PSM-002. When operation temperatures are outside of these ranges, DOP values may increase gradually, sometimes reaching 10%.

Q. What is the wavelength coverage? If my wavelength is out of the coverage range, how much does the DOP change?

A. Most polarization scramblers consist of multiple sections of birefringent modulators that are sensitive to wavelength changes. A typical polarization scrambler is tuned for minimum DOP operation in a band centered at a specified wavelength. The operation bandwidth in which the DOP is specified is called the wavelength coverage of the polarization scrambler. GP's multiband polarization scrambler (PCD-005/104) covers most popular center wavelengths from 980 nm to 1650 nm in 6 user-selectable bands. The mini-scrambler (PSM-002) covers >±50nm from the center wavelength. If your wavelength is outside the coverage range, the DOP may increase gradually as the differences between the center and actual wavelengths increase.

Q. Can I use a polarization scrambler to measure Polarization Dependent Loss (PDL)?

A. Yes. There are several methods to measure PDL, such as the random scanning (minimum-maximum) method, Mueller Matrix method, Jones-Matrix method, and reference method. The random scanning method employs a polarization scrambler in the measurement. Depending on the speed of the photodetectors and electronic circuits, different scrambling speeds are used to scan polarization states to the DUT. GP offers both fast (>700 KHz) and slow (down to quasi-DC) polarization scramblers to meet customers' measurement needs.

Q. What are the advantages of measuring PDL using GP's polarization scrambler?

A. The extremely low PDL (PDL ≤ 0.05 dB, 0.01 dB typical) of GP's polarization scramblers provides a clean measurement environment for PDL testing. In other words, GP's polarization scrambler assures that the PDL reading error due to scrambler PDL will be much smaller than the test instrument's PDL resolution.

Depolarizers

Q. What is the principle of operation behind the depolarizer?

A. The standard depolarizer works by splitting the input beam into two equally powered beams of orthogonal polarization, delaying one beam with respect to the other, then recombining them into a single output. As long as the relative delay between the orthogonally polarized beams is larger than the coherence length of the light beams, there is no fixed phase relationship between them when they are recombined. The resulting output is, therefore, depolarized.

Q. What kind of fiber can be used to connect to the depolarizer?

A. The input is typically PM fiber, and the output is typically SM fiber. In some cases, devices that can work with SM inputs can be made.

Q. Can the depolarizer be used with a pulsed or modulated signal?

A. The depolarizer is designed for use with cw input light. Because it functions by using DGD to depolarize the light, a depolarizer can have an adverse effect on a modulated signal.

Q: Is the depolarizer bidirectional?

A. No. The standard depolarizer is a unidirectional device.

Q. What kinds of light sources can be depolarized?

A. Depolarizers are generally used with light sources with relatively short coherence lengths. General Photonics' standard depolarizer can depolarize a light source with a coherence length of up to 10m. However, custom depolarizers can be made to work with light sources with longer coherence lengths (up to a few km).

Polarization Stabilizers

Q. What does a polarization stabilizer or tracker do?

A. The function of a polarization stabilizer or tracker is to find a target output state of polarization, and to maintain that SOP against variations in input polarization. A polarization stabilizer generally consists of a polarization controller, polarization monitor, and feedback circuit. It uses the polarization monitor and feedback circuit to detect how far the current SOP is from the target and direct the polarization controller to return it to the target state.

Q. What is the difference between an internal feedback and an external feedback stabilizer?

A. An internal feedback stabilizer has an integrated polarization monitor, and the feedback circuit uses the information from the monitor to control the polarization controller. General Photonics' internal feedback stabilizers and trackers (POS-202, POS-002-I) have a PM output fiber and stabilize the output SOP to linear, aligned to the slow axis of the output PM fiber. This configuration is useful if the stabilizer is being used to align a signal to a PM fiber or simply to provide a linear SOP.

In an external feedback stabilizer, the polarization monitor is decoupled from the polarization controller. The user taps the signal at the point in the system at which the SOP needs to be maintained, and provides either an optical or electrical control signal to the stabilizer. The stabilizer then actively adjusts the polarization to maximize or minimize the control signal. This configuration requires more setup by the user, but is more flexible in that the control signal can be correlated to secondary polarization-related parameters such as output DOP in a PMD compensation system or interference signal strength when used for polarization matching in an interferometer. Also, the tap can be placed at any point in the system, allowing the stabilizer to be used to maintain the SOP at a point far from the location of the controller. One example of this is a laser amplifier system, in which a stabilizer placed between the laser and amplifier can be used to maintain the output polarization of the amplifier by placing the tap after the amplifier. The POS-002-E and POS-203 are examples of external feedback stabilizers. The POS-002-E accepts an electrical control signal, and tunes the polarization state to maximize that signal. The POS-203 can accept either an optical or electrical control signal, and can be set to either maximize or minimize the control signal.

Q. What is the difference between SM and PM output stabilizers?

A. The effect of an SM output stabilizer can be seen directly in the polarization state of the output beam. With stabilization disabled, the stabilizer does not actively modify the SOP of the input beam; any polarization changes to the input will be seen at the output. With stabilization enabled, the output polarization state will remain constant, regardless of changes to the input polarization.

The PM output stabilizer uses a polarizer to align the output to the slow axis of the output PM fiber. Therefore, the output polarization state is always constant (linear, aligned to the slow axis of the PM fiber), and any changes in polarization are translated into changes in output power. Therefore, the output power will fluctuate with changes in input polarization state while the stabilization is disabled, but will remain constant with stabilization enabled.

The internal feedback stabilizers (POS-002-I, POS-202) are PM output. The external feedback stabilizers (POS-002-E, POS-203) are SM at the controller output.

Q. Does the stabilizer affect the DOP of the input light?

A. The POS-002-E or POS-203's main light path consists of a fiber-squeezer polarization controller. Its effect on DOP is negligible. This also means that it can only stabilize the polarized portion of the input light.

Because of its alignment polarizer, a PM output stabilizer's (POS-002-I or POS-202) output is fully polarized.

Q. How do I use the tunable control parameters?

A. For internal feedback stabilizers, in general, the user does not have to adjust control parameters. For external feedback stabilizers, control parameters can be used to optimize the stabilizer response for particular systems. The principal control parameters are:

Step size: This controls the size of the voltage step applied to the polarization controller, and thus the size of the polarization change, during each control cycle. For highly variable signals, a larger step size can provide faster response, while for stable signals, a smaller step size can increase the stability of the output.

Delay offset: The user can insert a controllable delay offset between a polarization step and the next read of the control signal. This is useful if the response of the control signal circuit is slow or if the tap point for the feedback signal is far from the controller. Delay should be set such that the control signal circuit has time to respond to the polarization step before the next readout.

Threshold: The threshold controls the size of the tolerance for deviation from the target state before the stabilizer acts to correct the SOP. In general, the threshold should be set larger than the noise level of the control circuit.

ER Measurement

Q. Which General Photonics instruments can measure polarization extinction ratio (PER)?

A. Several General Photonics instruments can measure the polarization extinction ratio of a light source or PM fiber component or system. The ERM-202 polarization extinction ratio meter is a dedicated PER measurement instrument that uses the rotating polarizer method. The POD-201 and PSY-201 polarimeters and the PSGA-101A polarization measurement system can measure PER using the polarimeter method. The PXA-1000 distributed polarization crosstalk analyzer can also measure PER by measuring all crosstalk events that contribute to the PER.

Q. What is the operating principle of the polarization extinction ratio (PER) meter?

A. The ERM-202 polarization extinction ratio meter is composed of a rotating polarizer with ultra high PER and a photodetector circuit with low polarization dependent responsivity and very high dynamic range. For every polarizer rotation cycle, the PER meter measures the maximum power P_{max} and minimum power P_{min}, and calculates and displays the polarization extinction ratio PER=10 log(P_{max}/P_{min}) and input light power P=P_{max}+P_{min}. The displayed angle is the orientation angle of the internal polarizer, with respect to the connector key, at which maximum power is detected during each polarizer rotation cycle. Looking into the connector, an angle rotated counterclockwise from the key slot is positive. The 2-input version can measure the ER of two light paths at once and can also compare the power ratio of the two outputs, making it a good choice for characterizing PM components such as PM couplers.

Q. What is the operating principle of the polarimeter method?

A. Polarimeters such as those used in the POD-201, PSY-201, and PSGA- 101A measure the PER by measuring the polarization state change while the input wavelength is swept, or while the fiber is stretched or heated/cooled. The PER can be calculated from the size of the circle traced out. In the PSGA-101, which has a free-space input, the position of the rotation axis of the circle also gives information about the slow axis of the PM fiber and whether the connector is stressed.

Q. What are the differences between PER measurements using the different instruments?

A. The ERM-202 directly measures the PER by monitoring the power change during polarizer rotation, and its test results include both the polarization and depolarization information of the device under test. Therefore, the PER meter can provide a more conservative and reliable result for some signals than the polarimeter method. However, because it bases its measurement on the power ratio between orthogonal linear polarization components of light, it cannot distinguish between unpolarized light and circularly polarized light.

PER measurement instruments such as the PER meter and PSGA, for which the input is free space, can accurately measure the PM connector orientation angle.

A fiber-coupled polarimeter like the POD-201 and PSY-201 cannot give PM connector key alignment information because there is single mode fiber between the input connector and the polarimeter optical head. On the other hand, these instruments can measure the PER of a DUT even with SM fiber connected between the DUT and the polarimeter.

Polarimeter based measurements characterize the effects of DUT input connector stress and misalignment, as well as fiber effects, but do not measure the effects of the DUT output connector. The ERM-202 measures the effects of the output connector as well as those of the input connector and the fiber.

For a PM fiber coil or a DUT consisting of multiple PM fibers connected by connectors or splices, the PXA-1000 provides the most detailed information. In addition to a cumulative PER measurement, it can provide information on polarization crosstalk at each location in the system, and allows the user to exclude sections of fiber from the PER calculation.

	ERM-202	POD-201 / PSY-201	PSGA-101A	PXA-1000
Cumulative PER measurement of DUT	X	X	X	X
Can measure very high PER	X			X
Can measure very low PER	X	X	X	
Can distinguish between unpolarized and circularly polarized light		X	X	
Requires stretching/heating fiber or wavelength scanning		X	X	
Measure output connector key alignment	X		X	
Detect stress on output connector			X	
Can measure PER of PM fiber DUT with SM fiber in the measurement path		X	X	
Can exclude sections of fiber from PER calculation				X

FAQs: ER Measurement

Q. Should a narrow band or broadband light source be used for PER measurement?

A. It depends on the measurement instrument.

For the ERM-202, a broadband light source should be used in order to measure the worst-case (minimum) PER of a DUT. The light source coherence length should be shorter than λ_{center} *l_{PM} /beat length, where λ_{center} is the center wavelength of the light source and l_{PM} is the length of PM fiber under test. When a narrow band laser source with a coherence length much longer than λ_{center} *l_{PM} /beat length is used, the polarization components of the light aligned to the slow and fast axes will be coherent. If they are either in phase or antiphase, the output light will be linearly polarized even if the input light is misaligned. Generally, the instantaneous PER values are not stable because of the variable phase difference between the slow and fast axes caused by stress changes in the PM fiber or temperature fluctuations, so the instantaneous PER cannot be used for device performance specification. In this case, the PER meter should be operated in minimum search mode and the performance specification should be the minimum ER measured by the PER meter as the fiber is stretched or heated/cooled.

A polarimeter based system such as the POD-201, PSY-201, or PSGA-101A uses a narrow band laser source. For the POD-201 or PSY-201, the measurement requires stretching or heating the fiber. For the PSGA-101A, the measurement can be done either by stretching/heating the fiber or wavelength scanning the laser.

The PSGA-101A and PXA-1000 generally come with integrated light sources, while the ERM-202, POD-201, and PSY-201 require external light sources.

Q. What is the minimum input power needed to measure high PER values up to 50dB?

A. Only the ERM-202 and the PXA-1000 can measure PER values around 50 dB. For the ERM-202, the power range is limited by the extinction ratio of the internal polarizer and by the dynamic range of the detection circuit. For power levels above −25 dBm, the PER meter can measure PER values up to about 30 dB. For power levels above −5 dBm, the PER meter can measure PER values up to 50 dB.

For the PXA-1000, the attenuation should be adjusted such that the DUT power out is >1mW and the detector does not saturate during measurement.

Polarimeters

Q. What is the main difference between an in-line polarimeter and a terminated polarimeter? What are the advantages of an in-line polarimeter?

A. The main difference between the two types of polarimeters is that an in-line polarimeter allows data traffic to continue along the optical fiber to the next stage, while terminated polarimeters terminate data transmission at the polarimeter. The in-line polarimeter offers direct, accurate measurement of polarization-related properties for the network environment, eliminating errors introduced by fiber splitting or tapping. GP's in-line polarimeter also offers a wider bandwidth than other types of polarimeters, an advantage for fast network response and quick feedback/feedforward control.

Because terminated polarimeters can use all of the light signal for analysis, they can have higher detection sensitivity.

Q. What are the major applications of an in-line polarimenter?

A. GP's in-line polarimeter is designed for polarization-related measurements in fiber optic systems. It is particularly useful for fiber optic networks that carry live data traffic and require accurate state of polarization (SOP) and/or degree of polarization (DOP) measurements. It can be used in a broad range of applications including PMD monitoring, PMD compensation, DOP monitoring, polarization stabilization, coherent optical communications, fiber optic sensors, network performance monitoring, polarization multiplexing/demultiplexing, etc.

Q. What are the insertion loss and PDL of General Photonics' polarimeter?

A. In-line PolaDetect™ devices generally have an insertion loss of less than 1.2 dB and a PDL of less than 0.25 dB, excluding connector contributions.

Q. What is the operation principle of GP's polarimeters?

A. GP's polarimeters are based on the 4-detector polarization measurement approach. Each photodetector measures the optical signal intensity of a particular polarization state. Stokes vector components are a linear combination of these measured intensities. The Stokes vector directly provides the state of polarization (SOP). The degree of polarization (DOP) can be calculated from the Stokes vector components.

Q. What is the measurement speed of GP's polarimeter?

A. It depends on the product. GP's polarimeter optical head (model POD-001) has an analog bandwidth of 1.5 MHz (from DC to 1.5 MHz). The module with a preamplifier board (POD-002) has a bandwidth of 50 kHz. When a data acquisition (DAQ) card is used, the sampling rate of the card may impose additional limits on the measurement speed. The PSY-201 and POD-201 have a measurement bandwidth of 1MHz, and a sampling rate of up to 4Msamples/s.

Q. What is the output data format of GP's polarimeter?

A. It depends on the product. The output of the PolaDetect™ modules (POD-001/002) consists of four analog voltage signals. Each voltage signal is linearly proportional to the optical intensity of a particular polarization state. The maximum output voltage is 10 Volts, which corresponds to an input optical power of 5 mW. Analog to digital conversion is required when a digital computer is used to process the polarimeter measurement data. Analog to digital conversion can be performed with a plug-in DAQ card designed for computers.

The polarimeter instrument (PSY-201 or POD-201) performs the necessary conversions and can display measured SOP in the form of Stokes parameters, azimuth and ellipticity angles, and degree of linearity or circularity, as well as displaying DOP.

Q. Do you have any suggestions on DAQ card selection? What are the card settings?

A. General Photonics' suggested DAQ cards for use with the polarimeter modules POD-001/002 are the NI PCI-6024E for desktop and NI DAQCard-6062E for laptop computers, with an I/O Connector Block and cable. Both cards are manufactured by National Instruments (www.ni.com). Once the hardware and software are installed, users can use NI Measurement & Automation Explorer, which accompanies the delivered card, to set up DAQ card parameters. The Analog Input (AI) should be set to Differential Mode. Please make a note of its device number, which will be used in software parameter setting.

Q. Do you offer an integrated polarization measurement system based on this polarimeter?

A. General Photonics currently offers an integrated system (the PSY-201 or POD-201) which combines the polarimeter, high speed electronics, a USB interface, and the corresponding software for rapid measurement and readout of SOP and DOP, with a trigger mode for synchronization to external equipment and a data logging function for long-term SOP monitoring. SOP properties can be displayed either in real time on the Poincaré Sphere, or on an oscilloscope readout, as shown below. The PSY-201 or POD-201 can also be used for PM fiber extinction ratio measurements.

For those who need in-depth PMD and PDL analysis, General Photonics also makes a polarization measurement system, the PSGA, based on a different technology.

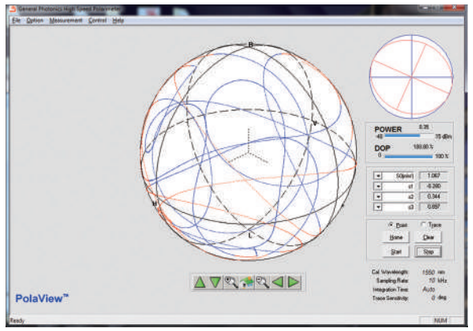

Fig. 1 Poincaré Sphere display of a polarization-scrambled input signal.

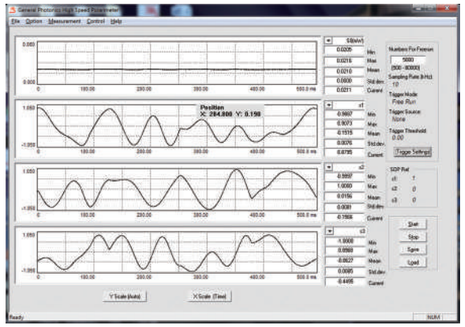

Fig. 2 Oscilloscope display of 4 Stokes parameters, with polarization modulation

---

Q. The SOP of the light may be different at different locations between the input and output fiber connectors. Where does the measured state of polarization apply?

A. The measured data indicates the SOP at the polarimeter optical module location. It is well known that even a short section of optical fiber can transform the input SOP to a different SOP. Therefore, when the in-line polarimeter is connected to an optical fiber path, the measured SOP, in general, will be different from the SOP at the input connector. The fiber pigtail to the polarimeter may alter the input SOP, depending on the fiber mounting.

Q. Is the output polarization state the same as the input polarization state?

A. No. Due to the construction of the polarimeter and the output fiber pigtail, the output SOP is generally different from the input SOP and the measured SOP.

Q. Why do I need a calibration matrix to calculate polarization state?

A. The calibration matrix ensures an accurate mapping between the measured voltages and SOP. Although SOP can be directly calculated from the measured voltage outputs, the fabrication tolerance sometimes affects the accuracy of the direct calculation. The calibration matrix corrects errors induced by fabrication tolerance.

For the PSY-201 and POD-201, the calibration matrices are stored in the instrument's memory. These instruments also include a self-calibration function that can be used to increase the measurement accuracy at the user's wavelength of interest.

Q: What is the optical power range?

A. GP's in-line polarimeter is designed mainly for fiber optic network applications. Therefore, the optical power level is similar to that of data traffic, typically from –23 dBm to +7 dBm at 1550 nm. The POD-201 can accept inputs as low as -35 dBm.

Phase Shifters

Q. What are the key characteristics of the fiber phase shifter? Are there any moving parts?

A. General Photonics' All Fiber Phase Shifters achieve optical phase modulation directly on a section of optical fiber. No optical waveguides or fiber pigtails are used. There is no epoxy in the optical path. The standard model is polarization independent, although polarization-maintaining versions are available. The GP Phase Shifter uses no mechanical moving components.

Q. Is the phase shift independent of the modulation frequency of the input light?

A. The amplitude of the phase shift depends only on the applied voltage. It is independent of the data modulation rate of the optical signal. The dependence on the input light wavelength is very small unless the input light is from a very broadband source.

Q. Can the phase shifter be controlled with a DC drive voltage?

A. A DC control voltage can be used to achieve the desired phase shift. It is recommended that a closed loop feedback system be used for high accuracy phase control.

Q. What is the maximum frequency of operation for your All Fiber Phase Shifter to generate a half-wave phase change at 1550 nm? What are the required drive voltages?

A. The operation frequency range and V_π depend on the model of phase shifter.

Model	Operating Frequency Range	Typical V_π	Maximum Phase Shift
FPS-001	DC-20 kHz	10-20V	8π - 15π
FPS-002	DC-20 kHz	2.5-4.5V	>65 π
FPS-003	DC-60 kHz	1-3V	>55 π

Q. Is the All Fiber Phase Shifter bi-directional?

A: Yes, the fiber phase shifter is bi-directional.

Q. What can I use to drive the phase shifter?

A. For common applications that require small phase shifts, a function generator or standard laboratory DC power supply can often be used to generate the drive voltage.

Q. How accurately can I control the phase?

A. Since the phase shifters are piezo-driven, the phase resolution will depend on the resolution with which the drive voltage can be controlled. For very precise control, it is recommended that the phase shifters be used in a closed-loop system. Because the piezos have some hysteresis, it can be difficult to maintain or return to a particular phase value when using the phase shifter in an open-loop system.

INSTRUMENTS
MODULES
PASSIVE COMPONENTS
ACCESSORIES
APPLICATION GUIDE
FAQS

Delay Lines (MDL/VDL, ODG)

Q. Is there any special gas in the variable delay line package that might influence interferometer applications?

A. There is no special gas in the standard package.

Q. What is the minimum (zero-state) delay of the manual and motorized variable optical delay lines?

A. The minimum delay is on the order of 170 picoseconds, excluding contributions from pigtails. Each meter of the fiber pigtail will add approximately 5 nanoseconds to the delay.

Q. How do I read the delay setting on a delay line?

A. The VDL-001 manual delay line has a scale that reads in millimeters, with a movable vernier. The increments on the vernier correspond to 0.1 mm, which is equivalent to approximately 0.67 ps delay.

The VDL-002 manual delay line has a magnetic pointer that can be used to give an approximate delay readout on the scale, but because of the requirements of the waterproof housing, it is not as accurate as the VDL-001.

The MDL-002 motorized delay line versions with the control box display the delay setting on the LCD display. The MDL-002 with OEM control board does not have an external readout, but the delay setting can be queried via RS-232.

The MDL-003 motorized delay line uses a stepper motor directly driven by the user. The delay state can be derived from the sensor signal and the step count.

Q. What is the delay per turn for the manual delay lines (VDL-001 and VDL-002)?

A. It is about 1.8 ps/turn for single-pass models, and about 3.6 ps/turn for double-pass models.

Q. How much fiber is in the delay line? How much dispersion is expected to occur?

A. The actual optical delay path is mostly free space, so dispersion effects should be minimal. If dispersion is a concern, the fiber pigtail length can be minimized.

Q. Is driver software available for the motorized delay line?

A. For the MDL-002, there is no control program, but a remote control command list is provided in the user manual. Windows HyperTerminal or a similar program can be used to send ASCII code to the RS-232 serial port for delay control.

The MDL-003 does not have a remote control interface.

Q. What is the operating wavelength range for the MDLs and VDLs?

A. Standard single-pass SM MDLs and VDLs are dual-window and function at 1310 ± 50 nm and 1550 ± 50 nm. PM and double-pass versions are single-window and function at either 1550 ± 50 nm or 1310 ± 50 nm. Other wavelengths may also be available by special request.

Q. Is there a separate encoder output enabling tracking of MDL position without using serial commands?

A. This can be done for the MDL-002. Please request it when ordering. The MDL-003 uses a stepper motor, so there is no encoder output.

Q: Are the variable delay lines bidirectional?

A: Yes.

Q. What are the differences between the different models of MDL/ VDLs?

A. The differences are mainly in delay range, control method, and purpose. The VDL-001 is a longer-range delay line designed for lab use. It is easy to adjust and to read out the delay. The VDL-002 is a smaller delay line for OEM applications. It has a durable package and a set screw that allows it to be locked in place after adjustment.

The MDL-002 is a longer range delay line that can be configured for lab or OEM use. It uses a DC motor and encoder and allows the user to set delay values or scan parameters directly from a front panel interface or via remote control commands. The MDL-003 is a more compact, smaller range OEM delay line that uses a stepper motor.

Q. What is the difference between single pass and double pass models of MDL/ VDLs?

A. A single-pass delay line is a transmission device. The light signal enters from an input pigtail, passes through the device, and exits on a separate output pigtail. In a double-pass device, the output collimator is replaced with a Faraday mirror. The light signal enters, passes through the device, is reflected by the Faraday mirror, passes through the device again, and exits on the same pigtail. The double-pass device therefore has twice the range, but half the resolution/accuracy of its single-pass counterpart. In addition, since the input and output beams travel on the same pigtail, a separator may be required to separate them. For SM systems, a 3-port circulator can be used to separate the input and output signals. The input signal should be connected to port 1 of the circulator, the delay line to port 2, and the output to port 3. For PM systems, an SM common port PBS can be used to separate the input and output. The SM common port of the PBS is connected to the delay line. The input can be connected to one of the single-polarization ports of the PBS, and the output to the other single-polarization port of the PBS.

Q. What are the principal differences between the MDL/ VDLs and the programmable optical delay generator (ODG)?

A. The MDLs and VDLs provide continuous optical delay variation of up to 1200 ps, with a free-space optical path. The ODG provides digitally variable optical delay of up to 500µs, single pass, with a fiber delay path.

Fiber Coils

General Questions on Coils

Q. What types of coils does General Photonics offer? What are the differences?

A. General Photonics has developed the capability to produce several types of specialized custom coils.

These include compact, low-loss coils for delay applications; extremely temperature-stable, low-crosstalk fiber gyro coils; and several other types of specialty coils. Our proprietary winding techniques and equipment, potting adhesives, and characterization techniques and equipment enable us to produce high performance coils optimized for different applications.

Time Delay Coils

Q. What is the fiber length tolerance of the compact time delay coils?

A. Fiber length is typically tested by OTDR . The length tolerance is ±2m for coil length up to about 4000m. Tighter tolerances may be possible for shorter coils. Contact General Photonics for more information.

Q. What is the maximum length that can fit in an enclosure?

A. Coils up to about 4km can fit into the standard enclosure. Longer delays can be constructed as multiple coils that can be either spliced together or connected using patchcords. Custom enclosures for nonstandard coils are also possible.

Q. What are typical fiber coil dimensions?

A. The coil enclosure dimensions are 6x6x1.59 inches. For coils without enclosures, the customer typically specifies any size requests or constraints when ordering.

Fiber Gyro Coils

Q. What fibers and winding patterns are available?

A. Gyro coils can be wound with various types and sizes of SM or PM fiber. Customers can request coils made with standard fibers, or can supply fiber for winding. Most coils are wound using either a simple or quadrupole winding pattern, although other patterns are available on request.

Q: What dimensions and lengths are available?

A: Gyro coils are customized to users' needs. Typically, the customer specifies dimensional and length requirements, and General Photonics calculates the closest possible match. Generally, the lengths of simple coils can be very close to requested lengths, while the lengths of quadrupole coils are constrained by the requirements of the winding pattern.

Q: What test data is supplied with gyro coils?

A. For SM coils, test data typically includes fiber length, IL, PMD and PDL, and PMD and PDL variation over temperature. For PM coils, test data typically includes fiber length, IL, PER, and polarization crosstalk vs. position at room temperature. The crosstalk data include a plot of crosstalk vs. position in the fiber, average crosstalk, maximum crosstalk, and a table listing crosstalk peaks >−50 dB.

Additional testing is available as an option. Extended test data for PM coils can include PER vs. temperature, as well as crosstalk data at high and low temperature extremes as well as at room temperature.

Q. What high performance options are available?

A. Various kinds of process modifications and enhanced testing are available. These include special potting adhesive for enhanced temperature stability, testing at different temperatures, and several levels of Shupe effect mitigation.

Other Products

PolaSwitch

Q. What is the difference between switching and latching current/voltage?

A. The PolaSwitch rotates the input polarization state to either of two states which are 45° or 90° apart, depending on the configuration ordered. The switching current and voltage indicate the current and voltage that must be applied to switch the polarization state from one of these two states to the other, while the latching current and voltage are the current and voltage that must be applied to maintain the switch in its current state. Nominally, a voltage of 2.5V between the two pins corresponds to one state, and -2.5V to the other. For example, if the switching voltage is 2.5V, and the latching voltage is 1.5V, then if the switch is initially in the -2.5V state, applying a voltage of +2.5V will switch it to the other state. Once it is switched, the applied voltage must be maintained above 1.5V to maintain the new state.

Q. What happens when 0 volts is applied between the pins?

A. This is essentially an "off" state. The output polarization state can float, and the insertion loss will be higher than when the switch is in one of its two defined states.

Q. Is a driver available for the PolaSwitch?

A. Yes. The driver board requires an 8-15VDC/200 mA power supply, and uses TTL level inputs to specify output state (TTL high for one state, and TTL low for the other). The driver board generates the necessary switching and latching voltages and currents in the proper order in order to control the switch with minimal heating effects. The maximum switching rate with the board is 1 kHz (1ms per state).

NoTail Components

Q. What is the fiber length inside a NoTail™ component?

A. It depends on the product. For a 2-port device like an isolator, fiber length is typically about 2cm on each side, while for a 3 or 4-port device, it is typically about 20cm on each side.

PBC/S vs. PM Coupler

Q. What is the difference between a polarization beam combiner/splitter and a PM coupler?

A. The polarization beam combiner/splitter is used to combine or separate two signals of orthogonal polarization state. The power ratio of the split components depends on the ratio of the two orthogonal polarization components in the combined signal. The PM coupler is used to split a single-polarization signal (usually aligned to the slow axis of the fiber) into two or more paths with a specified power split ratio.

GLOSSARY AND ACRONYMS

Activation Loss: The change in insertion loss caused by activation of the device. It is defined as the difference between the maximum and minimum insertion loss of the device under all possible activation conditions (e.g. different drive voltages in a polarization controller).

ASE: Amplified spontaneous emission- the spontaneous emission component of an amplifier's output (e.g., the output of a pumped EDFA with no signal input). ASE is broadband radiation with a DOP close to 0, and is a major component of amplifier noise.

Birefringence: Also known as double refraction, birefringence refers to anisotropism of the refractive index of a material. Birefringence can be a natural property of a crystalline material, determined by the crystal structure, or it can be induced by mechanical stress in a noncrystalline material. In the former case, the crystal structure determines one or two optical axes, each associated with its own index of refraction. In the latter case, the direction of the mechanical strain determines one optic axis. The component of incoming light polarized along the direction of the optical axis will encounter index of refraction n_e (for extraordinary wave, so called because it does not obey Snell's law), while the component polarized perpendicular to the optical axis will encounter index of refraction n_o (for ordinary wave, which does obey Snell's law).

dB: A unit used to express loss or gain of optical power, expressed as

$$10 \log \left(\frac{Output\ Power}{Input\ Power} \right)$$

where input and output power are expressed in the same units (i.e., mW or W)

dBm: A unit of power referenced to one milliwatt (mW), expressed as

$$Power\ (dBm) = 10 \log \left(\frac{Power\ (mW)}{1\ mW} \right)$$

Degree of Polarization (DOP): The percentage of light that is polarized (has a definable polarization state).

Dense Wavelength Division Multiplexing (DWDM): The transmission of multiple signals using closely spaced wavelengths in the 1550nm region over a single optical fiber. Frequency spacings are usually 100 GHz or 200 GHz, corresponding to wavelength spacings of 0.8 nm or 1.6 nm.

Differential Group Delay (DGD): The relative time delay between the two orthogonally polarized components of light. Same as first order PMD.

Dispersion: The spreading out of a pulse due to the difference in propagation velocities of different components of an electromagnetic wave due to the dependence of the index of refraction of the propagation medium on wavelength (chromatic dispersion) or polarization state (polarization mode dispersion.)

Erbium-Doped Fiber Amplifier (EDFA): An optical amplifier, composed of a length of optical fiber doped with the rare earth element erbium, which can amplify light in the wavelength region 1530-1625nm when pumped by a shorter wavelength pump source. The gain of an EDFA has some polarization dependence.

Extinction Ratio (ER): As used in this catalog, extinction ratio refers to the ratio of the power level of a preferred polarization component of light (for example, for a polarizer or a PM fiber component) to the power level of the orthogonal polarization component. Usually expressed in dB.

Faraday Effect: A phenomenon in which the plane of polarization of linearly polarized light rotates under the influence of a magnetic field applied parallel to the direction of propagation. The direction of rotation is determined by the direction of the magnetic field and the material properties of the propagation medium, and is the same for light propagating forward or backward along the B field direction.

Fast Axis: In a material or component with two defined polarization axes (such as a PM fiber or a wave plate), the axis associated with the faster propagating polarization component.

Half-Wave Voltage (V_π): The amount of applied voltage required to achieve a phase shift of π radians (i.e., for a phase shifter), or to achieve a phase difference of π radians between the two polarization components (polarization controller.)

Index of Refraction (n): The ratio between the speed of light in a vacuum and the phase velocity of light in a material. Index of refraction is a characteristic material property.

Insertion Loss (IL): Total optical power loss caused by insertion of an optical component into a system. Usually expressed in dB.

Jones Matrix: A 2x2 matrix that expresses the effect of an optical component on the Jones vector representation of an electromagnetic wave.

Jones Vector: A vector expression of the polarization state of an electromagnetic wave. The components are the x and y components of the electric field vector: $J = E(t) = [E_x(t)\ \ E_y(t)]^T$

Mueller Matrix: A 4x4 matrix that expresses the effect of an optical component on the Stokes vector representation of an electromagnetic wave.

Multimode Fiber (MMF): An optical fiber with a core large enough to allow multiple modes to propagate.

Optical Add-Drop Multiplier (OADM): A device that adds or drops individual wavelengths from a DWDM system.

Optical Path Length (OPL): A distance traveled by light in an optical system, defined as $\int n(s)ds$. For a medium of constant refractive index, OPL = ns, where s is the thickness of the medium. OPL is equal to the distance in a vacuum that the light beam would traverse in the same amount of time.

Poincaré Sphere: A system for graphical representation of

polarization state. Every polarization state can be represented as a point on the sphere. All linear polarizations are on the equator, with horizontal and vertical polarizations on one axis, and ±45° on the other. Circular polarizations are at the poles of the sphere. A rotation of 2° on the sphere corresponds to a real-space rotation of 1°.

Polarization: An intrinsic property of electromagnetic waves that describes the time-varying amplitude and direction of the electric field vector. A general polarization vector can be expressed as a linear combination of two orthogonal components perpendicular to the direction of propagation of the wave. For more detail, see article "What is Polarization?"

Polarization Dependent Gain (PDG): The phenomenon in which the gain of an optical amplifier is less for the stronger polarization component than for the weaker polarization component of the input signal. See article "Combat Polarization Impairments with Dynamic Polarization Controllers."

Polarization Dependent Loss (PDL): The difference between the maximum and minimum optical power transmission of a component as a function of input polarization state. Usually expressed in dB.

Polarization Dependent Modulation (PDM): The phenomenon in which the depth of modulation of an electro-optical or electroabsorption modulator varies with the polarization of the input signal. See article "Combat Polarization Impairments with Dynamic Polarization Controllers."

PDR: Polarization dependent response

PDS: Polarization dependent sensitivity

PDW: Polarization dependent center wavelength

Polarization Maintaining (PM) fiber (PMF): Optical fiber designed with intentional birefringence such that there are two preferred (fast and slow) polarization axes. Linearly polarized light aligned to one of these axes will maintain its polarization state during transmission through the fiber.

Polarization Mode Dispersion (PMD): A phenomenon in which the different polarization components of light travel at different speeds in a particular physical medium, such as a fiber, because of birefringence caused by asymmetry. First order PMD, or DGD, is the relative time delay between the two polarization components. Second order PMD is the change in DGD with frequency. For more detail, see article "What is Polarization?"

Principal Axes: The preferred polarization axes of a component or fiber section. Any given input polarization is decomposed into polarization components along these axes.

PSP: Principal State of Polarization

Retardation Plate: A component that introduces a defined phase difference (e.g. π radians for a half-wave plate, or π/2 radians for a quarter-wave plate) between polarization components aligned with its fast and slow axis.

Return Loss (RL): A measure of the portion of the optical signal that returns towards the source against the direction of signal propagation. Return loss is caused by Fresnel reflection (back reflection from interfaces at mated connectors and mechanical splices) and Rayleigh back scattering (scattered light due to intrinsic fiber properties). Usually expressed in dB.

Single Mode Fiber (SMF): A small-core fiber in which only the lowest order bound mode can propagate at the wavelength of interest.

Slow Axis: In a material or component with two defined polarization axes (such as a PM fiber or a wave plate), the axis associated with the slower propagating polarization component.

SOP: State of Polarization, expressed in Stokes parameters.

Stokes Parameters: 4 parameters that specify the phase and polarization of a light beam. S_0 represents the intensity of the light beam. S_1 represents the part of the beam linearly polarized in the horizontal plane, S_2 the part of the beam linearly polarized in the +45° direction, and S_3 the circularly polarized part of the beam. S_1, S_2, and S_3 are the coordinates of the SOP in a Poincaré Sphere representation. For fully polarized light, $S_0^2=S_1^2+S_2^2+S_3^2$. For partially polarized light, $S_0^2>S_1^2+S_2^2+S_3^2$, and the ratio of the two sides of the equation gives the DOP.

Stokes Vector: A vector whose components are the 4 Stokes parameters, often normalized to 1.

Temperature Dependent Loss (TDL): Maximum variation in insertion loss of a component with variation in temperature over its operating temperature range.

Time Division Multiplexing (TDM): The process or device by which more than one signal can be sent over one channel by interleaving pulses representing bits from different signals. This may be done by varying the pulse duration, amplitude, and position.

Wavelength Division Multiplexing (WDM): A technique in which multiple signals with different wavelengths can be simultaneously transmitted over one optical fiber.

High-Tech Corporation
www.high-tech.co.jp
sales@high-tech.co.jp

I-Wave Corporation
www.i-waveco.com
sales@i-waveco.com

Japan Laser Corp
www.japanlaser.co.jp
prd@japanlaser.jp

Ainnotech
www.ainnotech.com
Korea@ainnotech.com

Enaco Communication
enaco@sbcglobal.net

China Light
www.clight.com.cn
cl@clight.com.cn

Luster LightTech Corporation
www.lusterinc.com
vincentwang@lusterlighttech.com

Suzhou Optoring Technology Co., Ltd.
www.optoring.com
info@optoring.com

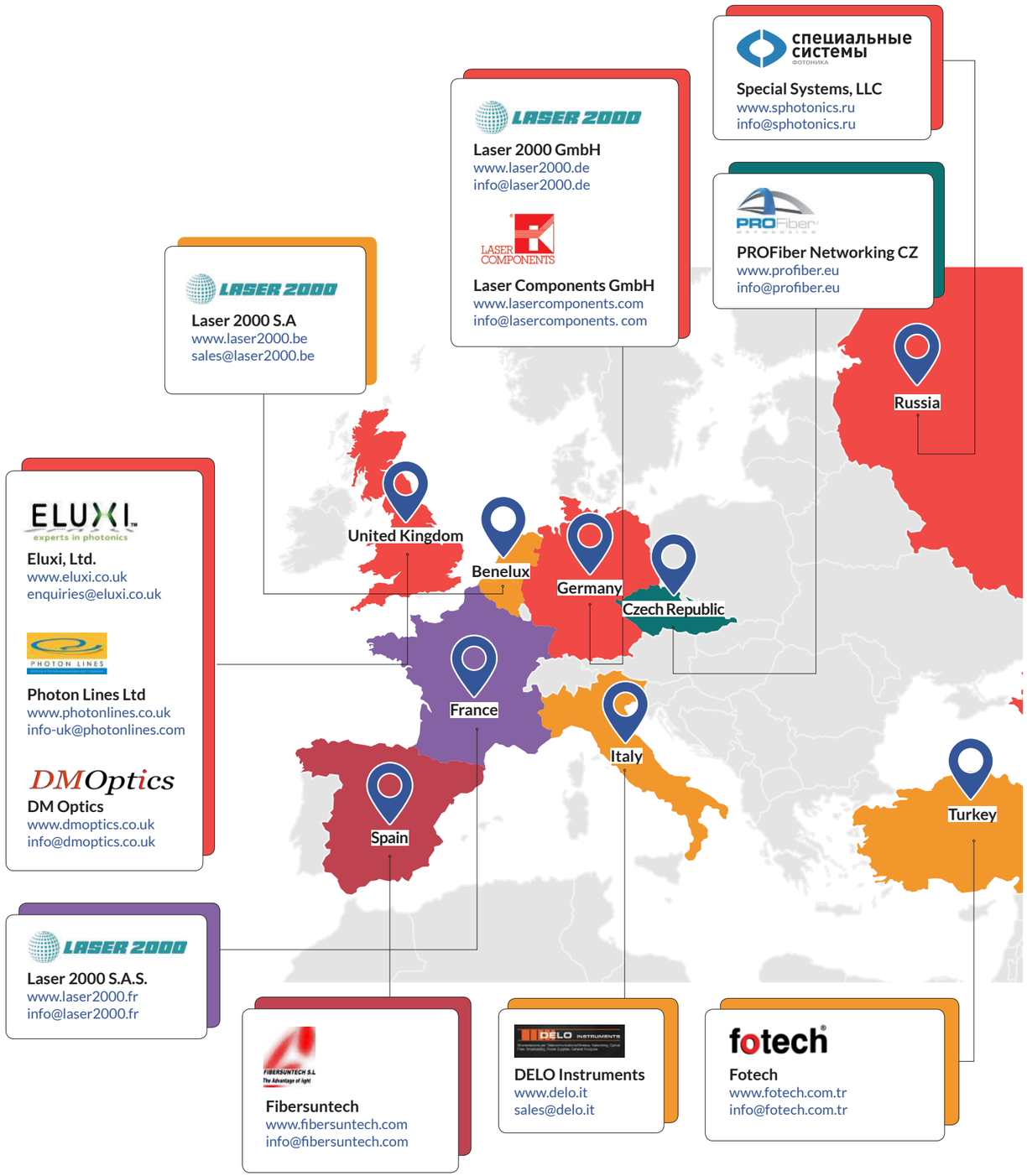
специальные системы
ФОТОНИКА
Special Systems, LLC
www.sphotonics.ru
info@sphotonics.ru
LASER 2000
Laser 2000 GmbH
www.laser2000.de
info@laser2000.de
LASER COMPONENTS
Laser Components GmbH
www.lasercomponents.com
info@lasercomponents. com
PROFiber
PROFiber Networking CZ
www.profiber.eu
info@profiber.eu
LASER 2000
Laser 2000 S.A
www.laser2000.be
sales@laser2000.be
Russia
ELUXI
experts in photonics
Eluxi, Ltd.
www.eluxi.co.uk
enquiries@eluxi.co.uk
United Kingdom
Benelux
Germany
Czech Republic
France
Italy
Spain
Turkey
PHOTON LINES
Photon Lines Ltd
www.photonlines.co.uk
info-uk@photonlines.com
DMOptics
DM Optics
www.dmoptics.co.uk
info@dmoptics.co.uk
LASER 2000
Laser 2000 S.A.S.
www.laser2000.fr
info@laser2000.fr
FIBERSUNTECH S.L.
The Advantage of light
Fibersuntech
www.fibersuntech.com
info@fibersuntech.com
DELO INSTRUMENTS
DELO Instruments
www.delo.it
sales@delo.it
fotech
Fotech
www.fotech.com.tr
info@fotech.com.tr

Canada
TMetrix Inc.
TMetrix Inc.
www.tmetrix.com
Northern California
East Coast
Texas
Kacha Optics
www.kachaoptics.com
kachaoptics@pacbell.net
TeraComm
Test & Measurement and Component Solutions
Teracomm
www.teracomm.com
sales@teracomm.com
PMR Technical, LP
PMR Technical, LP
www.pmrtexas.com
chad@pmrtexas.com

Making Light Work Lighter

General Photonics

Corporation

General Photonics Corporation

Tel: (909) 590-5473 | Fax: (909) 902-5536 | 5228 Edison Ave. Chino, CA 91710 USA
Email: info@generalphotonics.com | www.generalphotonics.com